Faculty of Science

Department of Imaging and Applied Physics

Microstructural Design of High Performance Natural Fibre Reinforced Vinyl-Ester Eco-Nanocomposites

Abdullah Mohammed S. Alhuthali

This thesis is presented for

the degree of Doctor of Philosophy of

Curtin University

July 2013

DECLARATION

"To the best of my knowledge and belief this thesis contains no material previously published by any other person except where due acknowledgment has been made. This thesis contains no material which has been accepted for the award of any other degree or diploma in any university."

Abdullah Alhuthali

Signature: 

Date: 4th July 2013

ABSTRACT

The addition of stiffer and stronger fibres can greatly improve the properties of the polymer. To date, the most common synthetic fibres are based on aramid, glass, and carbon. Nonetheless, the shortcomings of synthetic fibres are fast being recognised due to increasing global concern over the depletion of petroleum resources, the emission of greenhouse gases, and a greater need to recycle and reuse. Recently, cellulose fibre-reinforced polymer composites have been gaining a great attention in several engineering applications due to their desirable properties, which include low cost, low density, renewability and recyclability as well as good mechanical properties. Notwithstanding the promising future of nature fibre composites, inherent incompatibility must be overcome between this category of fibres which are hydrophilic and the matrix components which are hydrophobic. To improve fibre-matrix adhesion and prevent loss of strength, treatment of the natural fibre surface is required. In addition, issues concerning moisture still compromise the fibre-matrix interface integrity which can lead to overall loss in mechanical properties. Addressing these limitations of natural fibre composites is critical to overcoming the existing barriers to research and development in this important field of composite materials.

A novel approach was used to enhance the interfacial bonding between fibre and matrix. The project investigated nano-filler addition to achieve good resistance to water diffusion, better mechanical and thermal properties in cellulose fibre reinforced polymer composites.

The project used vinyl-ester (VER) as the matrix for three categories of composite materials. Firstly, eco-composites were produced by reinforcing VER with thin sheets of recycled cellulose fibre (RCF). Secondly, nano-composites were produced by reinforcing VER with halloysite nanotubes (HNTs) and silicon carbide nanoparticles (n-SiC). Thirdly, eco-nanocomposites were produced by reinforcing VER with sheets of RCFand nano-fillers for multi-scale reinforcement.

The influence of the reinforcement materials - RCF sheets, nano-fillers, and multi-scale reinforcement (RCF/nano-fillers) were investigated. The physical, thermal,

mechanical and fracture properties of the resulting composites were studied in terms of the water absorption, flexural strength, flexural modulus, impact strength, fracture toughness, impact toughness, thermal stability and flammability of each composite. The effect of water soaking on the mechanical properties of composites was also investigated. X-ray diffraction (XRD), synchrotron radiation diffraction (SRD), Fourier transforms infrared spectroscopy (FTIR) transmission electron microscopy (TEM), and scanning electron microscopy (SEM) were used to examine the nano and microstructures of these materials.

The first category of composites, the eco-composites (VER-RCF) were prepared at 20, 30, 40, 50 wt%. An infiltration method was used in the preparation of the eco-composites. Step one involved 10 µm sheets of RCF being fully soaked in the VER system. Step two required the saturated sheets to be laid-up on silicon moulds. Finally, the third step required saturated sheets of RCF be pressed together in vacuum under fixed pressure. During step two and three, low pressure was applied frequently to remove trapped air bubbles. SEM micrographs confirmed that the novel infiltration method of preparation led to composites with good fibre/matrix adhesion, reduced void content and increased fibre–volume fraction. The effect of fibre content on water absorption behaviour in the eco-composites was also investigated. As the fibre content increases, the uptake of moisture was also found to increase. Increasing the fibre content was also found to lead to an increase in the elastic modulus, strength and fracture toughness properties of the eco-composites. Using typical mathematical models for prediction the elastic modulus for the eco-composites was modelled revealing experimental data consistent with Cox–Krenchel model obtained prediction data. Moisture exposure reduced the elastic modulus, strength and toughness of the eco-composites. This reduction was most noticeable at high fibre content and was attributed to compromise interfacial bonding due to the effect of water absorption.

The second category of composites, the nano-composites (VER/HNT and VER/n-SiC), were prepared by reinforcing the matrix with different loadings of nano-filler using a high speed mechanical mixer (30 minutes, 1200 rpm).

The addition of HNTs to VER is a field yet to contain an in-depth repository of information. This project has presented the first characterisation of VER/HNT nano-

composites providing water absorption, fracture, mechanical, thermal properties and flammability behaviours of this group of nano-composites. VER/HNT composites were prepared at 1, 3, and 5 wt% using high-speed mechanical stirring. The intercalation of the HNT by the chains of VER is confirmed in XRD results. For example the d-space of the peak (001) of pure HNT increased from 0.721 to 0.745 nm in VER/HNT with 1 wt%. This intercalation confirms the formation of nanocomposites. TEM observations support that the extent of HNT dispersion is acceptable, notwithstanding the presence of micro-sized HNT clusters. In VER/HNT with 5 wt%, the reduction in the water absorption behaviour was most noticeable.

The addition of HNTs was found to effectively enhance the toughness properties of VER. Crack bridging, deflection, and plastic deformation mechanisms around clusters of HNT are believed to be three toughening mechanisms that HNT provided as confirmed by SEM observations. A large aspect ratio, good interfacial adhesion, good degree of dispersion, and adequate inter-tubular interaction between HNT and VER are believed to be the factors underpinning enhanced strength properties of VER/HNT. The experimental data was consistent with that of both Paul model and Guth model suggesting that the aspect ratios of fillers, their dispersion within the matrix, and the state of interfacial adhesion were all relevant to the prediction of elastic modulus for particulate reinforced composites. HNT's barriers for heat and mass transport, the presence of iron, and their hollow tubular structure are believe to be the factors enhancing thermal stability and decreasing in flammability in the nano-composites.

VER/n-SiC composites were prepared at 1, 3, 5 and 10 wt% using high-speed mechanical stirring. Particularly, the project evaluated the influence of morphological structures such as particle dispersion and particle/matrix interaction on resulting mechanical and fracture properties of these nano-composites. SEM micrographs revealed that at the fracture surfaces of VER/n-SiC there appeared to be no obvious voids at the particle/matrix interface. This is indicative of an absence of n-SiC pull-out from the polymer matrix supporting strong interaction between the n-SiC and VER matrix. The absence of n-SiC agglomeration throughout the nano-composite is also supportive of generally uniform dispersion of n-SiC throughout the matrix. The addition of n-SiC increased elastic modulus and strength but reduced the

toughness of the nano-composites. Good interfacial adhesion and a good degree of dispersion enhanced the strength of the nanocomposites whereas agglomeration of nanoparticles at 10 wt% forming clusters of n-SiC decreased elastic modulus and strength. The experimental data was consistent with that of both the Guth and Kerner model suggesting that good dispersion within the matrix and good interfacial adhesion were both relevant to the prediction of elastic modulus of particulate reinforced composites.

The third category of composites of interest is the eco-nanocomposites. To prepare eco-nano-composites, a two-step process was used. First, three nano-mixtures were produced. The first of these was VER and nanoclay platelets. The second was VER and HNT. The third was VER and n-SiC. Each was prepared at 1, 3, and 5 wt%. The second step of the preparation required that sheets of RCF be used to reinforce the nano-mixtures. The eco-nanocomposites were then studied in terms of their water uptake, mechanical and thermal properties. Concerning water uptake, nano-filler addition was found to decrease water uptake with 5 wt% eco-nanocomposites giving more favourable results than the 1% and 3%. Concerning strength properties, nano-filler addition was also found to enhance these properties most optimally at 3 wt%. These results were attributed to the reinforcing effect of nanofiller with RCF sheets and the enhanced fibre-matrix adhesion observed in the eco-nanocomposites. Concerning toughness properties, compared to pure VER, the composites reinforced with sheets of RCF featured a significantly higher toughness due to the toughening mechanisms provided by cellulose fiber. However, nanofiller addition resulted in samples which were brittle due to the nanofillers's effects on fibre-matrix adhesion limiting the mechanisms of fibre pull-out and fibre de-bonding. Therefore, the toughness properties of the eco-nanocomposites were lower than those of the eco-composites. Concerning thermal stability and flammability, the eco-nanocomposites gave preferable results compared to those of the eco-composites and pure samples. This observed improvement was believed to have occurred by virtue of improved mass and heat barriers and the enhanced fibre-matrix interfacial adhesion provided by the nano-fillers.

The impetus of this project was to develop environmental friendly composite materials with high performance using multi-scale reinforcement. This project is part of a larger movement towards designing for recycling, also referred to as eco-design. Manufacturers are increasingly being asked to assume responsibility for the materials they use in their products. With this is mind, one of the aims of this project was to add to contemporary understanding of best practice eco-design. The results presented in this study suggest that with future investigation the development of fully green materials will be achievable. The project recommends that one such pathway to meet this ends will be through the use of non-petroleum-based biodegradable resins reinforced with cellulose fibres and eco-nanofillers.

ACKNOWLEDGEMENTS

Firstly, I heartily owe my deepest gratitude to Professor Jim Low who has provided exceptionally worthy supervision with great patience and direction. The guidance from Professor Low has fortified me throughout this research work, and I must say that this thesis would have not been completed if it had not been for his friendly and enduring encouragement. I would also like to thank my associate supervisor, Dr. Chunsheng Lu, for his inspiration and timely suggestions.

My sincere appreciation is expressed to Ms. Elaine Miller, Dr. Rob Hart, Mr. Tony Wong and Dr. Cat Kealley from the Applied Physics Department at Curtin University for their support regarding SEM imaging, TEM imaging, and XRD data collection. Mr. Peter Chapman and Ms. Kristy Blyth from the Chemistry Department at Curtin University are acknowledged and sincerely thanked for their support regarding FTIR and TGA experimentation. I would also like to thank Mr. Ross Williams from the Applied Physics Department and Mr. Andreas Viereckl of the Mechanical Engineering Department at Curtin University for their support regarding mechanical testing.

I wish to express my warmest thanks to all my colleagues, in particular, Ramzy Algamdi, Nobuo Tezuka and Wei-Kong Pang for their great friendship and emotional support for the duration of my postgraduate studies in Perth, Western Australia.

I am also grateful to Dr. Brendan McGann, the current chairman of this thesis and Post-graduate Coordinator of the Department of Applied Physics. I take the opportunity here to duly thank Dr. McGann for the extraordinary periods of time that he has made available to support and guide me in both academic and administrative matters over the duration of my postgraduate studies

Last but not least, the most special of all thanks and gratitude must be expressed to my lovely wife Nawal Alhuthali and to my children, Sanad, Hamad, Farah, Moaath and Omar. My family has accompanied and supported me at each stage of this

interesting and challenging time. It has been the great patience of my family that has enabled this thesis to develop to the standard which it has, and I am forever indebted for their support. i have no doubt that without the great help and support of my wife and everlasting love of my children this work thesis would have never be reached these stages of completion.

LIST OF PUBLICATION INCLUDED AS PART OF THE THESIS

(Listed in order as found on this thesis)

ALHUTHALI, A. and LOW, I. M. 2013. Mechanical properties of cellulose fibre reinforced vinyl-ester composites in wet conditions. *Journal of Materials Science*, 48, 6331-6340.

ALHUTHALI, A. and LOW, I. M. and DONG, C. 2012. Characterisation of the water absorption, mechanical and thermal properties of recycled cellulose fibre reinforced vinyl-ester eco-nanocomposites. *Composites Part B: Engineering,* 43, 2772-2781.

ALHUTHALI, A. and LOW, I. M. 2013. Influence of halloysite nanotubes on physical and mechanical properties of cellulose fibres reinforced vinyl ester composites. *Journal of Reinforced Plastics and Composites,* 32, 233-247.

ALHUTHALI, A. and LOW, I. M. 2013. Multi-scale hybrid eco-nanocomposites: synthesis and characterization of nano-SiC-reinforced vinyl-ester eco-composites. *Journal of Materials Science,* 48, 3097-3106.

ALHUTHALI, A. and LOW, I. M. 2013. Water absorption, mechanical, and thermal properties of halloysite nanotube reinforced vinyl-ester nanocomposites. *Journal of Materials Science,* 48, 4260-4273.

ALHUTHALI, A. and LOW, I. M. 2013. Mechanical and fracture properties of halloysite nanotube reinforced vinyl-ester nanocomposites. *Journal of Applied Polymer Science*, DOI: 10.1002/app.39348

ALHUTHALI, A. and LOW, I. M. 2013. Characterization of Mechanical and Fracture Behaviour in Nano-Silicon Carbide-Reinforced Vinyl-Ester Nanocomposites. *Polymer-Plastics Technology and Engineering*, 52, 921-930.

STATEMENT OF CONTRIBUTION OF OTHERS

Abdullah Alhuthali's input into this study and the associated papers included the execution of all the experimental work as well as a dominant contribution to the intellectual input involved in the project. Other scientists made some contributions to the current work, as is almost always the case in the physical sciences. These contributions were significant enough to warrant co-authorship on the resulting journal articles. These are specified below:

Prof. I.M. Low provided project supervision and manuscript editing.

Dr. C. Dong provided mechanical modelling support.

Abdullah Alhuthali

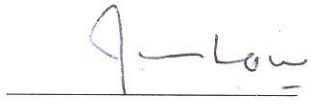

Prof. It-Meng (Jim) Low

LIST OF PUBLICATIONS BY THE CANDIDATE RELEVANT TO THE THESIS BUT NOT FORMING PART OF IT

Conference papers

Presented as a Poster

ALHUTHALI, A., and I.M. LOW. 2009. Physical and Mechanical Properties of Natural Fiber Reinforced Vinyl-Ester Nanocomposites. *Proc. 16th AINSE Conference on Nuclear and Complementary Techniques of Analysis (NCTA)*, Sydney, Australia, 25-27 Nov, 4 pages.

ALHUTHALI, A., and I.M. LOW. 2010. Physical and Mechanical Properties of Polymer Eco-Nanocomposites. *Proc. 7th Asian-Australasian Conference on Composite Materials (ACCM-7)*, Taipei, Taiwan, 15-18 Nov, 4 pages.

Oral presentation

ALHUTHALI, A and I.M. LOW. 2010. Mechanical and Fracture Properties of Recycled Cellulose Fibre Reinforced Vinyl-Ester Nanocomposites. *Proc. 6th Australasian Congress on Applied Mechanics (ACAM-6)*, Perth, Australia, 12-15 Dec, 10 pages.

Book-Chapters

ALAMRI H., **ALHUTHALI, A.,** and I. M. LOW. 2010. Mechanical properties and moisture absorption behaviour of cellulose-fibre reinforced polymer composites. In *Green Composites: Properties, Design and Life Cycle Assessment*, ed. F. Willems and P. Moens, 175-196. New York, USA: Nova Publishers.

ALHUTHALI, A., Alamri, H., and I. M. LOW. 2011. Physical, flammability and mechanical properties of polymer eco-nanocomposites. In *Fibre Reinforced Composites*, ed. Quingzheng (George) Cheng, 105-124. Hauppauge, New York, USA: Nova Science Publishers Inc

TABLE OF CONTENTS

LIST OF FIGURES

LIST OF TABLES

LIST OF ABBREVIATIONS

DTA	Differential Thermal Analysis
FTIR	Fourier Transforms Infrared Spectroscopy
HNT	Halloysite Nanotubes
IROM	Inverse Rule of Mixtures
MEKP	Methyl Ethyl Ketone Peroxide
NC	Nano-Clay
n-SiC	Nano-Silicon Carbide
RCF	Recycled Cellulose Fibre
ROM	Rule of Mixtures
SAXS	Small Angle X-Ray Scattering
SEM	Scanning Electron microscopy
SiC	Silicon Carbide
SRD	Synchrotron Radiation Diffraction
TEM	Transmission Electron Microscopy
TGA	Thermogravimetric Analysis
VER	Vinyl-Ester Resin
XRD	X-Ray Diffraction

1. INTRODUCTION

1.1 Background

Vinyl ester resin (VER) has superior resistance to moisture and chemicals, providing greater hydrolytic stability compared to cheaper polymer resins and allowing greater control over cure rate and reaction conditions compared to epoxy resins (Sultania et al., 2010). VER also has excellent mechanical properties (Guo et al., 2007). The advanced polymer is produced by a reaction between an epoxy and carboxylic acid (Holbery and Houston, 2006, Mallick, 2007). As a thermoset, being produced by a curing process, VER is highly rigid. VERs are believed to combine the best properties of epoxies and unsaturated polyesters (Sultania et al., 2010). Though VERs are already used extensively in electrical components, automobile parts, coatings, adhesives, molding compounds, structural laminates used in mining and chemical operations, and sporting goods, further research is required to better understand the potential of the material (Holbery and Houston, 2006, Ku et al., 2007). The chemistry of VERs is complicated. The substance has carbon double bonds at the end of molecule providing a sole site for cross-linking. The means that the thermoset, i.e. cured, VER has less cross-links which makes it more flexible than other cured polyester resins. These intermolecular forces also give VERs higher facture toughness than other resins. VER tends to have a low viscosity. The reason for this is that it substance is often dissolved in a styrene monomer. When polymerization is occurring, cross-links are formed between the unsaturation points. The two properties which are weaker in VERs compared to epoxy resins and polyester resins are firstly, the volumetric shrinkage is higher which is undesirable, and VERs have lower adhesive strength (Mallick, 2007, Marsh, 2007, Sultania et al., 2010).

In polymer science, a major challenge is broadening the window of application for such materials. This is generally achieved by preparation procedures, treatments, and other techniques that retain desirable features while enhancing features such as modulus, strength, fire performance and heat resistance. As matrices, polymers have relatively poor mechanical, thermal, and electrical properties compared to metal or ceramic.

Homopolymers, co-polymers, blended polymers, modified polymers, and other polymer types, alone, have insufficient property quality to meet the demands of industry. The inclusion of fibre (synthetic/natural), whisker, platelets, or particles are some of the alternative approaches that are used to improve the properties of polymers. Here, the inclusion of natural fibres and nano-particles will be discussed.

The use of cellulose fibres to reinforce the polymeric matrices has been studied for at least a decade. Cellulose fibres, as flax, sisal, oil palm, henequen, jute, banana, wood pulp, stinging nettle, coir, and hemp fibres, are natural fibres (Sreenivasan et al., 2011). Cellulose fibres are environmentally friendly. They are biodegradable, so unlike many plastics, they will not stay on the earth's surface for millions of years. Moreover, the production of cellulose fibres requires less energy than the production of glass or carbon fibres (Venkateshwaran et al., 2011). They are less dense (1.25-1.5 g/cm^3) than for carbon fibre (1.8–2.1 g/cm^3) or E-glass (2.54 g/cm^3), and they are lighter than the synthetic fibres (Sgriccia et al., 2008, Anuar and Zuraida, 2011). Cellulose fibres also have excellent modulus-weight ratio, which makes them successful in stiffness-critical designs. The acoustic damping property of cellulose fibres also makes them preferable to glass or carbon for noise attenuation purposes, an important requirement for automobile interior products (Mallick, 2007). In addition, cellulose fibres possess excellent toughness, flexibility, specific modulus, and specific strength properties (Bax and Mussig, 2008, Monteiro et al., 2009). Compared to most synthetic fibres, cellulose fibres are much more commercially viable (Dhakal et al., 2007).

Recycled cellulose fibre (RCF) refers to cellulose fibre that is extracted from newspapers, printed paper, and/or cardboard (Huda et al., 2006, Low et al., 2007). Newspaper-fibre reinforced composites, for example, have similar properties to wood-fibre reinforced composites. Moreover, newspaper fibre reinforced composites can be more easily produced due to cost advantage, renewability of the resource, greater flexibility and lower wear of processing machinery (Huda et al., 2007). Load bearing roof systems, sub-flooring and framing components as well as residential applications such as doors, windows, and furniture are applications of RCF reinforced materials

(Baroulaki et al., 2006). Composites reinforced with RCF represent a new class of materials with potential to replace wood and other plant composites in the near future (Alhuthali et al., 2012).

Drawbacks exist however. Cellulose fibre reinforced polymeric composites suffer two inherent weaknesses. Firstly, cellulose fibres which are hydrophilic and matrix components which are hydrophobic are inherently incompatible (Dhakal et al., 2007, Athijayamani et al., 2009). This lack of chemical affinity due to the hydrophilic nature of cellulose fibres adversely affects composite strength. Thus, to improve fibre-matrix adhesion and prevent loss of strength, Extensive physical and chemical treatment of the fibre surface is required (Herrera-Franco et al., 2005). Secondly, cellulose fibre reinforced polymeric composites suffer moisture-related problems (Chen et al., 2009). Fibre-matrix interface integrity is compromised on exposure to water which leads to poor stress transfer efficiencies and loss of overall mechanical properties (Bakare et al., 2010). Issues relating to water absorption, are therefore, the predominant deterrent to cellulose fibre reinforced polymeric composites research and development (Joseph et al., 2003, Assarar et al., 2011, Mylsamy and Rajendran, 2011).

The inclusion of nano-particles is another one of the approaches used to improve the properties of polymers. The addition of nano-particles to a polymer creates a multiphase material, known as a nano-composite (Alexandre and Dubois, 2000, Ajayan et al., 2006). In 1987, the first work on polymer/clay nanocomposites was conducted. In the early 1990s, researchers at the Toyota Company made a number of breakthroughs with polymer-layered silicates. These researchers were the first to exfoliate clay with the polymer of nylon-6 (Chen and Evans, 2006). Improvements in strength, modulus, and heat distortion temperature were all reported as due to addition of nanoclay (Hussain et al., 2006, Pavlidou and Papaspyrides, 2008). Since this time, polypropylene, polyethylene, polystyrene, polyvinylchloride, polylactide, polycaprolactone, phenolic resin, poly p-phenylene vinylene, polypyrrole, rubber, starch, polyurethane, polyvinylpyridine and other more common polymers such as nylons, have been included in studies with nano-fillers (Okamoto, 2006, Paul and Robeson, 2008, Davtyan et al.,

2012). Today the most commonly used polymers in nano-composite science are the epoxies, polyurethanes, polyester, and vinyl ester (Hussain et al., 2006).

Nanocomposite science has attracted interest due to the improvements that ~ 5 wt.% of nano-additive can have on the properties of the pre-existing material (Zuiderduin et al., 2003, Cauvin et al. 2010). Typically, moisture barrier, flammability resistance, thermal, and mechanical properties of polymeric composites are improved by virtue of ~ 5 wt.% nano-filler (Haq et al., 2008). The unique properties of polymer nanocomposites arise due to the nanometer size of nano-particles. Having dimensions in the nano-scale, nano-particles have a large surface area per unit volume. Since many essential chemical and physical interactions are governed by surfaces such a large surface area enables dense phase interactions to occur at the matrix/particle interfaces (McNally et al., 2003, Yong and Hahn 2009). Polymer nanocomposites possess superior specific strength and stiffness, good fire retardant and enhanced barrier properties compared to most polymers filled with micron-sized particles (Zuiderduin et al., 2003, Hussain et al., 2006, Zainuddin et al., 2010). Abrasive wear resistance, creep and fatigue performance, and functional properties are other areas where polymer nanocomposites exhibit superior properties, and it is the enhanced mechanical, thermal and physical properties overall that has enabled these materials to find wide application in the packaging, automotive, adhesive, and microelectronics industries (Zhao et al., 2005, Pavlidou and Papaspyrides, 2008, Zainuddin et al., 2010).

In this project, a novel approach for synthesizing eco-nanocomposites was used. The synthesis approach had two-steps. The first step involved nano-fillers (nanoclay platelets, halloysite nanotubes and silicon carbide) being dispersed into VER matrices to prepare nano-mixtures while the second step involved the reinforcement of these nano-mixtures with sheets of RCF obtained from newspaper, cardboard, and printed paper. Particularly, the effect of the sheets of RCF, nano-fillers, and both RCF sheets and nano-fillers dispersion on the microstructure, mechanical, thermal and barrier properties of VER resin was investigated and discussed in terms of X-ray diffraction (XRD), Synchrotron radiation diffraction (SRD), Fourier transforms infrared spectroscopy

(FTIR), transmission electron microscopy (TEM), scanning electron microscopy (SEM), flexural strength, flexural modulus, impact strength, fracture toughness, impact toughness, thermo-gravimetric analysis (TGA) and water absorption. Moreover, numbers of micromechanical models were applied to predict and analysis experimental data of elastic modulus of produced composites. The effect of water absorption on the mechanical properties of these composites was also investigated and discussed.

1.2 Project Significance

This project combines a novel processing method with new materials design concept for improved moisture resistance mechanical and thermal properties in polymer composites. The project opens the door for research and development into cost effective and eco-friendly material design concerning the processing of eco-composites made from natural fibres. When reinforced with natural fibres, polymeric composites can become products that are light-weight, inexpensive, corrosion resistant, impact resistant, and which have high specific strength and modulus. These products have potential applications in the automobile, defence, sporting, and marine industries.

There is a growing need for materials that do not require toxic agents in their production, and which are completely renewable naturally biodegrading where possible. The materials for packaging and agricultural are a prime example where eco-design is increasingly important. Furthermore, natural fibre composite production is a process which is flexible and creates minimal wear on processing machinery. One advantage of natural fibre composites, and one of the secondary objectives of the project, was the investigation of the potential use of cellulose fibres, such as recycled newspaper or waste paper, in materials for construction. Green composites, such as these, could be used as windows, doors, roof systems and framing components in the construction of homes. House construction could occur without the need to draw from timber sources of other finite resource bases at all.

Historically, cellulose fibre reinforced materials have had limited applications due to the inherent incompatibility arising from the hydrophilic nature of the cellulose fibres and the matrix components which are hydrophobic. This challenge exacerbates the other long standing shortcoming of cellulose fibre reinforced materials, their preponderance to absorb water and decay. This project set out to resolve these issues making renewable natural fibres a more attractive option for future applications, and by improving interfacial adhesion and reducing water absorption has achieved these ends. Principally, the project has successfully applied an innovative process and multi-layered RCF /nano-filler reinforced VER eco-nanocomposites have been synthesized. These eco-nanocomposites fabricated were found to gain toughness and strength advantages from the sheets of RCF, and gain thermal and barrier properties from the nano-fillers.

The project describes the process of synthesizing eco-nanocomposites. To construct multi-layered vinyl-ester eco-nanocomposites reinforced with recycled cellulose fibres, 10 μm sheets of RCF and three nano-fillers (nanoclay platelets, halloysite nanotubes and nano-silicon carbide) were used. The approach set out to produce of composites with uniform fibre/nano-filler dispersion into the matrix, controlled microstructure and increased fibre volume fractions as a result of improved fibre packing and fibre/matrix adhesion, and succeeds in meeting this end. As anticipated, the novel structure provided enhanced moisture resistance, mechanical properties and thermal properties. Thus, for materials science, this project builds essential links concerning the use of natural fibres and nano-fillers as multi-scales reinforcements for polymer resins.

1.3 Project Objectives

This project concerned eco-nanocomposites reinforced with nano-fillers (nanoclay platelets, halloysite nanotubes and silico carbide nanoparticles) and sheets of RCF, and in particular, their optimal design and advantages, such as green benefits and enhanced and/or controlled moisture and thermal properties.

The specific objectives of this project were as follows;

- To obtain a fundamental understanding of the processing-nanostructure-property relationships of eco-composites.
- To study the optimum content for nano-fillers and sheets of RCF to achieve desired mechanical fracture properties and thermal stability.
- To study the roles of nano-particles and RCF interfacial properties on the efficiency of strengthening and toughening.
- To investigate and use models for understanding water absorption and water diffusion in VER eco-composites and eco-nanocomposites.
- To identify the underlying mechanisms of eco-composites with nano-fillers additives and micro-fibre dispersions which give rise to enhanced physico-mechanical properties.
- To apply mechanics models for understanding the effect of reinforcement materials (cellulose fibres and nano-sized particles) separately, looking specifically at the nanostructure: shape and size distribution, aspect ratio, degree of dispersion and interfaces adhesion between matrix and fillers.

1.4 Research Plan

The following research plan guided the sequential execution of the project. This research plan was prepared initially pursuant to the objectives of the project:

1) Fabrication of eco-composites by reinforcing VER with sheets of RCF.
2) Fabrication of nanocomposites by reinforcing VER with nano-fillers (nanoclay platelets, halloysite nanotubes and silicon carbide nanoparticles) at different concentrations.

3) Fabrication of eco-nanocomposites by using multi-scale reinforcement of VER with sheets of RCF and nano-fillers (nanoclay platelets, halloysite nanotubes and silicon carbide nanoparticles)

4) Characterization (dispersion, morphology and micro-structure) of the raw materials, composites, and nano-filler using synchrotron radiation diffraction (SRD), Fourier transform infrared (FTIR) and Transmitted electron microscopy (TEM).

5) Investigation of influence of RCF, nano-fillers and RCF/nano-filers dispersion on physical, moisture barrier, mechanical, and thermal properties of produced composites.

6) Determination of the effect of moisture absorption on mechanical properties of produced composites.

7) Observation of fracture surface, failure mechanisms and crack path features by scanning electron microscopy (SEM).

2. LITERATURE REVIEW

2.1 Natural Fibres

Natural fibres can be subdivided into three general categories (Figure 2.1) of derived from animals, derived from mineral, or natural fibres derived from plants. The first category is animal fibre. Animal fibres have been used in bioengineering and orthopaedic applications for some time. Animal fibres are generally biodegradable. Examples of animal fibres which are commonly in use are wool, silk and spiders' web (Akil et al., 2011, Bismarck et al., 2005). Chemically, animal fibres are generally made up of proteins. Due to the hydrophobic nature of these proteins, and further strengthened by extensive hydrogen bonding, these fibres have excellent environmental stability (Cheung et al., 2009). The second group is mineral fibre. Geological materials, such as quarts and asbestos, can provide useful fibres. This fibre type has excellent strength and temperature resistant a property which is why it is readily used in construction and machinery exposed to extreme heat (Riedel and Nickel, 2005).

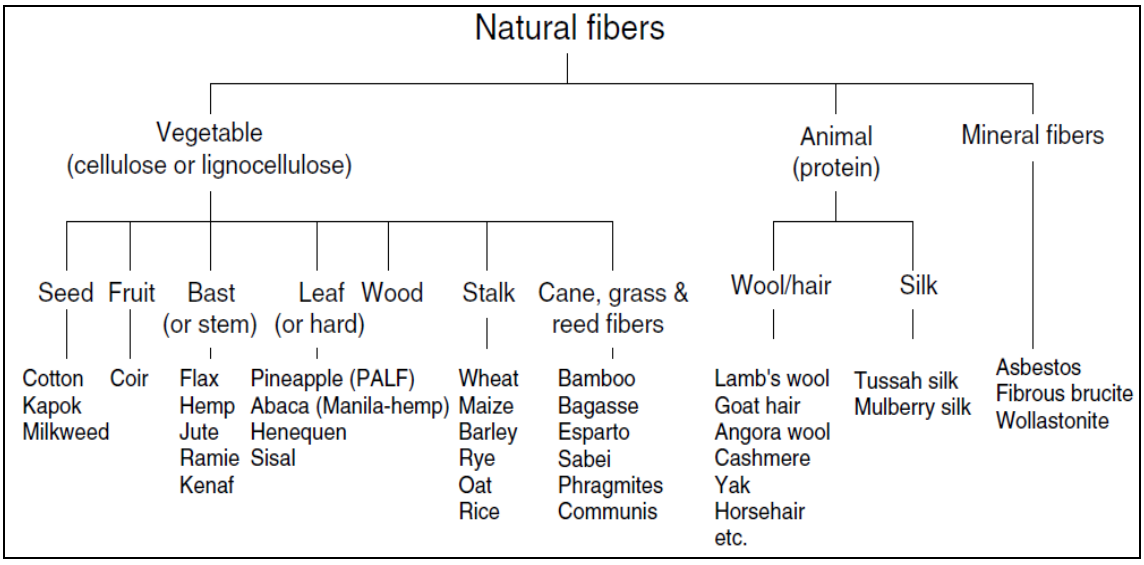

Figure 2.1: Classification of natural fibres (Akil et al., 2011)

The third fibre type, plant fibres, will be the main focus in this review of the literature. Plant fibres include a range of commercially available fibres such as wood fibre, agro-

based bast, stem, fruit, cereal fibres and seed fibres (Bismarck et al., 2005). Some industry names for plant fibres include jute, flax, hemp, ramie, sisal, coconut fibre, and banana fibre (Mallick, 2007). In nature, these fibres are a central ingredient in maintaining the strength of the grasses, plants, and trees in which they are found. When plant fibres are extracted and used in composites, they provide significant structural reinforcement (Clemons and Caulfield, 2005). For this reason, plant fibres are readily used in a range of products such as ropes, carpet, and bags (Mallick, 2007).There has been a surge in public interest in renewable resources in the past fifty years. The two reasons for this are, firstly, the acceptance that fossil fuels are indeed finite non-renewable resources, and secondly, more recently, the increase attention given to the amount of carbon dioxide omitted as a result of fossil fuel combustion (Riedel and Nickel, 2005). Renewable plants fibres are unlikely to be able to provide a complete solution to the limitations of fossil fuels, at least not in the near future. However, these fibres are already playing a big role in the construction industry (Stamboulis et al., 2001). Plant fibres, as some of these fibre types have excellent breaking length mechanical properties, are also highly useful for use as reinforcement products, such as reinforced polymers (Riedel and Nickel, 2005). The largest industry applying these reinforced polymers at the moment is the automobile field, particularly in Europe. When combined with polyester, polypropylene, or polyurethane, plant fibres are particularly flax, which is used in 71% of European automobile applications, can be used to make headrests, doors, interior sunroof shields, and a range of other automobile components (Clemons and Caulfield, 2005, Singha and Thakur, 2008).

2.1.1 Structure of plant fibres

Plant fibres have a very detailed structure. Essentially, plant fibres are a type of composite material. In close up, the fibres are crystalline and unyielding (Mallick, 2007). The substance inside the fibres is cellulose microfibril reinforced amorphous lignin with a hemicelluloses matrix. Cellulose, as well as substances known as hemicelluloses, waxes, lignin, and pectin, are the main constitutes of plant fibres. The main substance of plant fibres is cellulose making up to 80% of the weight of any given

plant fibre. Lignin content usually accounts for up to 20%. Pectin is another common element of most plant fibres. In sisal, it accounts for up to 10% of the weight of the substance. Moisture from water is another element. Plants fibres like sisal can hold up 20% of their weight in water while dryer plant fibres like hemp tend to hold a third of this amount (6%) (Bismarck et al., 2005, Li et al., 2000). Table 2.1 shows the chemical composition including seven variables for seventeen different plant fibres. Four of the main elements of plant fibres, cellulose, hemicelluloses, lignin, and pectin, are discussed in the further detail in the following paragraphs.

Table 2.1: Chemical composition, moisture Content, and microfibrillar angle of vegetable fibres (Bismarck et al., 2005).

Fiber	Cellulose (wt%)	Hemicelluloses (wt%)	Lignin (wt%)	Pectin (wt%)	Moisture Content (wt%)	Waxes (wt%)	Microfibrillar Angle (deg)
Flax	71	18.6–20.6	2.2	2.3	8–12	1.7	5–10
Hemp	70–74	17.9–22.4	3.7–5.7	0.9	6.2–12	0.8	2–6.2
Jute	61–71.5	13.6–20.4	12–13	0.2	12.5–13.7	0.5	8
Kenaf	45–57	21.5	8–13	3–5			
Ramie	68.6–76.2	13.1–16.7	0.6–0.7	1.9	7.5–17	0.3	7.5
Nettle	86				11–17		
Sisal	66–78	10–14	10–14	10	10–22	2	10–22
Henequen	77.6	4–8	13.1				
PALF	70–82		5–12.7		11.8		14
Banana	63–64	10	5		10–12		
Abaca	56–63		12–13	1	5–10		
Oil palm EFB	65		19				42
Oil palm mesocarp	60		11				46
Cotton	85–90	5.7		0–1	7.85–8.5	0.6	—
Coir	32–43	0.15–0.25	40–45	3–4	8		30–49
Cereal straw	38–45	15–31	12–20	8			

2.1.1.1 Cellulose

The most basic building block of cellulose is the polysaccharide, simply, sugar molecules bound in a chain structure. This linear macromolecule is shown below in the image. It can be seen that it consists mainly of D-anhydro glucose ($C_6H_{11}O_5$) units which are repeating and which are joined by linkages of β -1,4-glycosidic (Joseph et al., 2002).

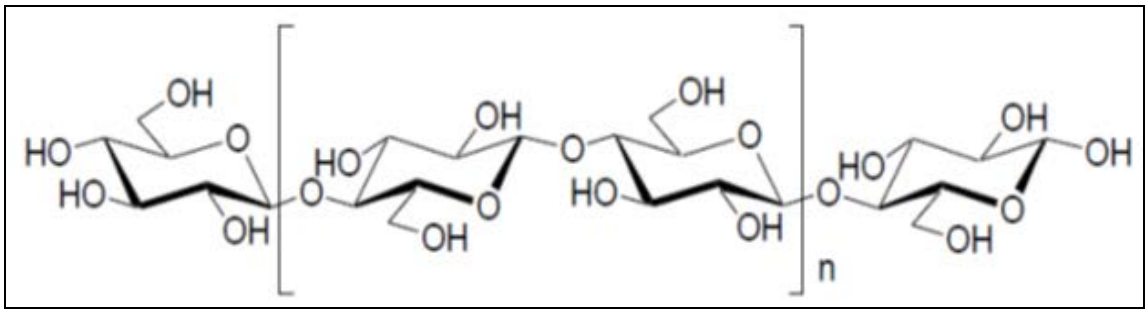

Figure 2.2: Diagrammatic representation of cellulose structure (Mohanty et al., 2004).

The degree of polymerization (DP) of cellulose molecules is approximately 10,000 (de la Luz Reus Medina and Kumar, 2007, Siqueira et al., 2010). This suits the formation of microfibrils (diameter 10 nm and 20 nm) with a high crystallinity (Lu et al., 2008, Rosler et al., 2007). Each basic unit of cellulose has three hydroxyl groups, and it is these groups which enable the extensive hydrogen bonding in the structures. This relates to the hydrophilic nature of plant fibres which can have moisture contents of more than 8% to 13% (Joseph et al., 1999). Concerning other properties of cellulose, the Young's modulus is estimated to be between 130 GPa and 250 GPa (Bledzki and Gassan, 1999, Zimmermann et al., 2004). Cellulose is highly resistant to strong alkali, but can be hydrolyzed into water-soluble sugars by acids Cellulose is partially resistant to oxidizing agents (Bledzki and Gassan, 1999). In wood, cellulose makes almost half of the matter (45%) (Pérez et al., 2002). The ancillary elements are lignin and hemicelluloses making up approximately 20% of the matter. In the plant fibres, cellulose takes the form of long straw-like tubes. The dimensions of these long tube cells are 20 μm and 40 μm in diameter, and 2mm to 4mm in length. These tubes align in an axial position with different layers being evident. Figure 2.3 shows this structure, namely, highlighting the primary cell wall and the secondary cell wall. The difference between the two cell walls is that the first, the primary, is made of irregularly arranged fibres, however, the second, the secondary, is made up of three layers (John and Thomas, 2008). The three layers amongst the secondary cell wall are arranged so that the substance can bear a high amount of tension and stress. It is has been found that the compressive strength of wood, 45% cellulose, is roughly 30 MPa which is one third of its tensile strength (Pérez et al., 2002, Rosler et al., 2007).

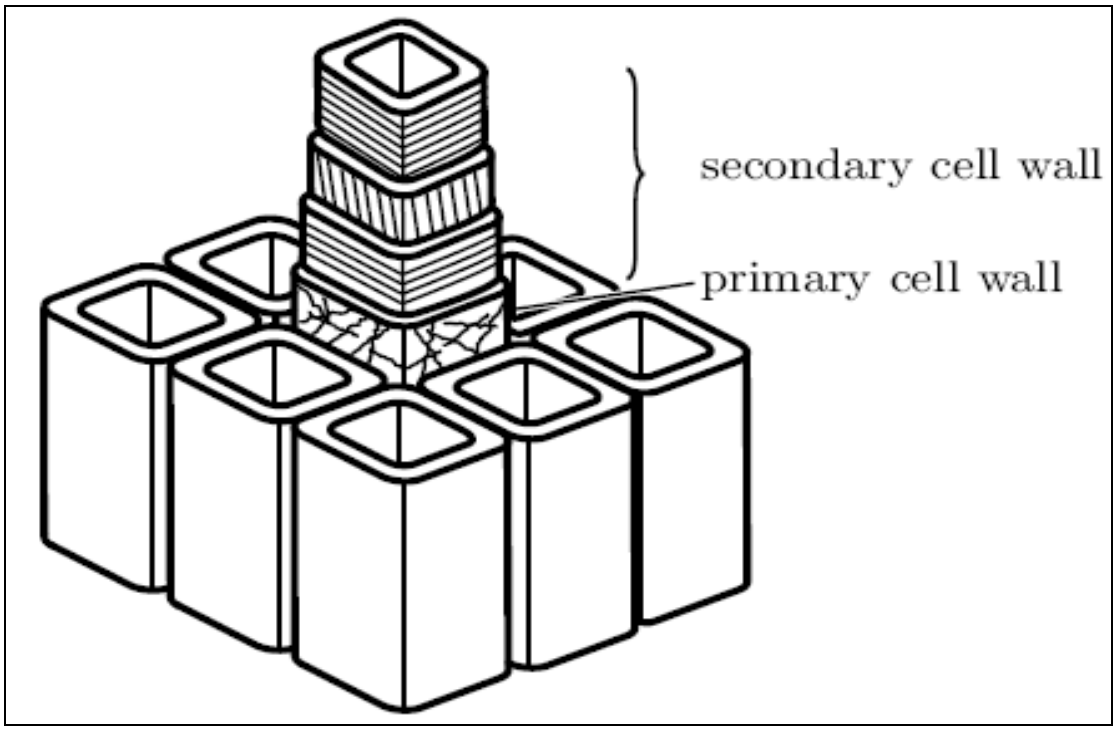

Figure 3.2: The primary and secondary cell wall structure of cellulose (Rosler et al., 2007).

2.1.1.2 Hemicelluloses

Polysaccharides (sugars) made up of 5 and 6 ring carbon ring sugars are known as hemicelluloses. These substances are not celluloses at all, and they have a range of different properties, so the name is clearly a misnomer (Bismarck et al., 2005, Bledzki and Gassan, 1999). Hemicelluloses are non-crystalline, the first difference between these are cellulose. Also, hemicelluloses contain different sugars units however cellulose involves only 1.4-b-d-glucopyranose units. This is because the polymer chains are shorter, the degree of polymerization (DP) less than 300, ten times to one hundred times less than cellulose, and the chains are branched, whereas cellulose is strictly linear. Hemicellulose is highly hydrophilic and in alkali is soluble and in acids readily hydrolyzed (Glasser et al., 2000, Sun and Tomkinson, 2003). Nonetheless, the connection between the two substances is that hemicelluloses remains associated with the celluloses through various interactions such as providing a highly supportive matrix

for cellulose microfibrils. In this way, hemicelluloses contribute to the structural components of wood (Clemons and Caulfield, 2005).

2.1.1.3 Lignin

Lignin is considered the second most important component of plant fibres after cellulose. Lignin is essentially the glue that holds the structure together and for that reason it has a close link with the properties and morphology of plant fibres (Joseph et al., 1999). Chemically, lignin is a cross-linked polymer network, which is amorphous, and consists of an array of hydroxyl- and methoxy- substituted phenylpropane units. While the chief monomers are the phenylpropane units, aliphatic and aromatic add-ons influence the lignin exact properties. Lignin is markedly less polar than cellulose (Clemons and Caulfield, 2005). Lignin tends to have much lower Young's modulus (4 GPa), compared to the stronger and more resilient cellulose. Lignin has a glass transition temperature of 90°C and a melting temperature of 170°C. Also, lignin exposed to phenol is condensable. For these reasons, some references refer to lignin as a thermoplastic polymer (Bismarck et al., 2005, Bledzki and Gassan, 1999).

2.1.1.4 Pectin

Pectin is an essential ingredient for non-woods fibres especially bast. The role of pectin is to act as an adhesive, like lignin, and at the same time provide a matrix, like hemicelluloses, for the cellulose (Clemons and Caulfield, 2005). Structurally, pectin is a complex polysaccharide with chains which consist of glucuronic acid in polymer form and rhannose residues. Rhamnose, galactose, and arabinose sugars are readily found in the side chains of the substance. Improving the strength, i.e. structural integrity of the pectin, and the structure it is supporting are calcium ions which cross-link and bond chains (Mohnen, 2008).

2.1.2 Properties of natural fibres

2.1.2.1 Mechanical properties

The mechanical properties of natural fibres on the whole are not as good as synthetic fibres such as E-glass and S-glass. However, there are a number of advantages of natural fibres nonetheless. The densities of natural fibres are markedly lower (Clemons and Caulfield, 2005). Furthermore, natural fibres tend to have a high reinforcing potential. Still the greatest advantage of natural fibres is their low cost (Beckwith, 2008). These are the reasons why this type of fibre is highly appealing to the automobile and other industries (Clemons and Caulfield, 2005). The exact differences over four properties are listed in Table 2.2. The first eight fibres from flax to cotton are natural, and the last four, E-glass, S-glass, Aramid, and standardized carbon fibres, are synthetic. What can be seen, as mentioned above, is that the strength properties of the artificial fibres are much greater than the natural fibres. However, more and more people are accepting that natural fibres do offer strength and stiffness properties which are workable, i.e. usable in industry (Clemons and Caulfield, 2005). Regarding the density, natural fibres are up to 50% less dense than artificial fibres. This, along with the abundance of natural fibres, and therefore cost advantage, makes natural fibres attractive to scientists and engineers alike (Beckwith, 2008).

Table 2.2: The density, tensile strength, tensile modulus, and range of elongation for 12 natural and synthetic (commercial and aerospace-based) fibres (Beckwith, 2008)

Fiber	*Density (gm/cm^2)*	*Tensile Strength (ksi)*	*Tensile Modulus (msi)*	*Range of Elongation (%)*
Flax	1.50	75 – 215	4	2.7 – 3.2
Hemp	1.47	100	10	2.0 – 4.0
Kenaf	1.45	135	7.7	1.6
Jute	1.30	55 – 110	3.8	1.5 – 1.8
Ramie	1.50	60 – 135	8.9 – 18.6	3.6 – 3.8
Sisal	1.50	75 – 90	1.4 – 3.2	2.0 – 2.5
Coir	1.20	85	0.6 – 0.9	~30
Cotton	1.55	60	0.8 – 1.8	3 – 10
E-Glass	2.56	290 – 350	10	3.0
S-Glass	2.57	665	12.5	2.8
Aramid (Commercial)	1.44	435 – 455	9 – 10	3.3 – 3.7
Carbon (PAN Std. Mod.)	1.67	580	33 – 35	1.4 – 1.8

2.1.2.2 Thermal properties

The thermal properties of natural fibres are characterised by low degradation temperatures and low thermal stability and thus considered to be a limitation to the application of this category of fibres (De Rosa et al., 2010, Jawaid and Abdul Khalil, 2011). For example, Araujo et al (2008) note that the majority natural fibres have degradation temperatures as low as 200°C which makes them inadequate for use in processing with thermoplastics having processing temperatures exceeding this degree of temperature (Araújo et al., 2008). The degradation process results in deterioration of mechanical properties, release of odours, toxins, volatiles, and discoloration from the fibre (Mallick, 2007). Degradation concerns two key steps. The first is called hemicelluloses thermal depolymerisation involving cleavage of glycosidic cellulose linkages, and the second is the decomposition of a-cellulose (Manfredi et al., 2006).

Figure 2.4 shows the temperature versus residual mass, i.e. thermogravimetric analysis (TGA) results, for three natural fibres flax, sisal, and jute. Figure 2.5 shows the derivative of the residual mass percentage (DTG) for the three natural fibres studied. Manfredi et al (2006) found that overall the results for the three are very similar, however, there were a number of points to note. Firstly, lignin decomposes at a range of different temperatures from between 200 and 500°C. In sisal, lignin decomposes first at 215 °C. For sisal, a-cellulose shows the fastest degradation at 340°C. It appears that hemicelluloses decompose at 290 °C in sisal. The first two plant fibres, sisal and jute are highly similar. However, in jute the lignin decomposes at the same time as the hemicelluloses making it difficult to discern any differences exactly. In contrast with sisal and jute, flax burns at the temperature approximately 20°C higher. Precisely, the main peak is at 345°C while at 285°C a shoulder exists, which depicts the hemicelluloses decomposition. As a general rule, hemicelluloses decompose before lignin and before cellulose (Mallick, 2007). This shows the better thermal stability of flax fibres (Manfredi et al., 2006). This is reportedly because of decreased lignin content. High lignin content equals a high decomposition rate and inversely a low proportion of lignin equals thermal stability. Nonetheless, these fibres, flax fibres, have low oxidation resistance (Manfredi et al., 2006).

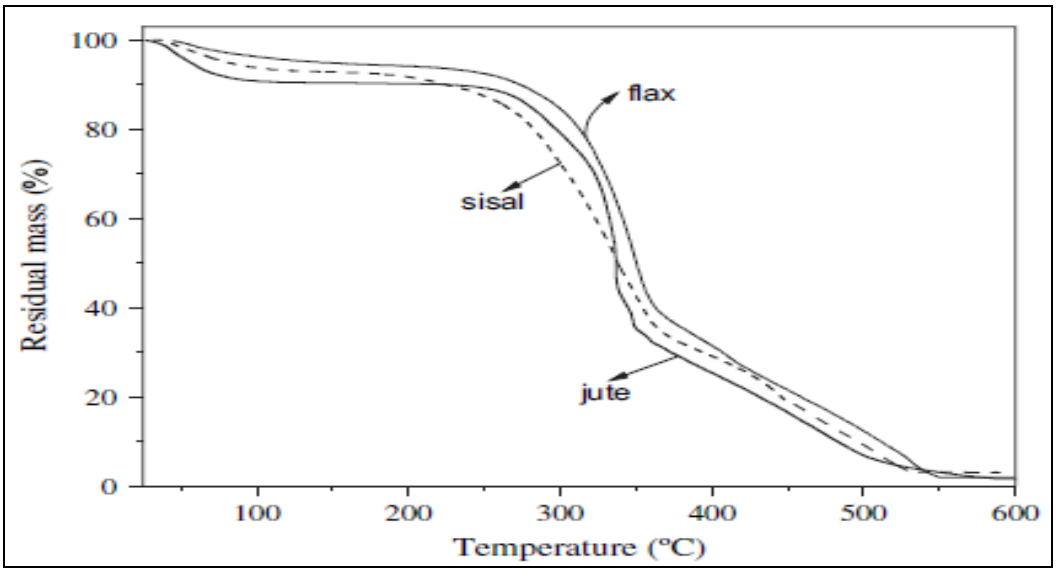

Figure 2.4: Temperature versus residual mass for flax, sisal, and jute (Manfredi et al., 2006).

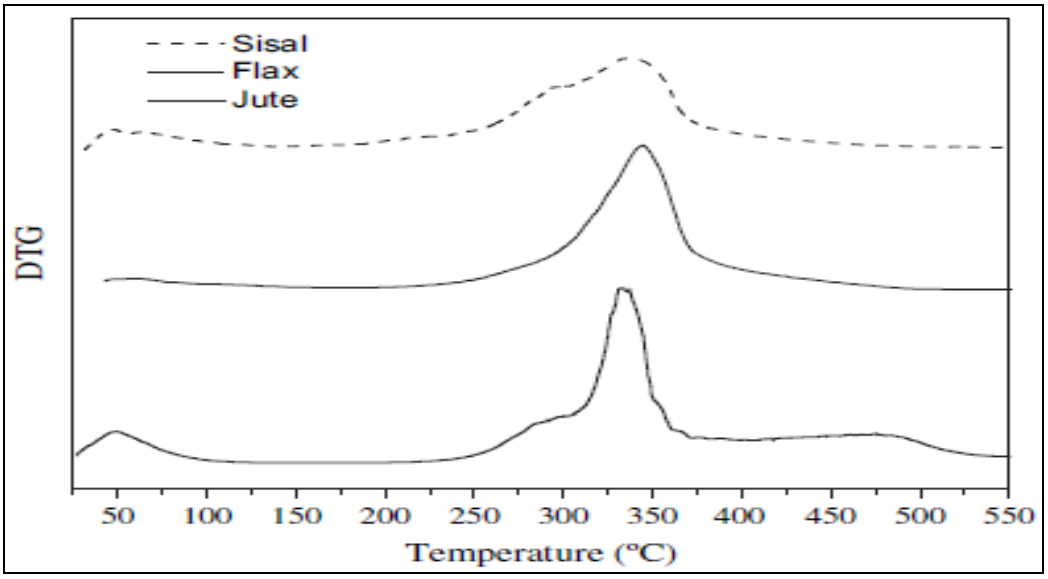

Figure 2.5: The derivative of the residual mass percentage (DTG) for the three natural fibres studied, flax, sisal, and jute (Manfredi et al., 2006).

2.1.2.3 Moisture properties

All plant fibres are hydrophilic naturally. Moisture content in these fibres can reach up to 13% in room conditions. The chemical reason for this is because the hydroxyl and oxygen-containing groups in the cellulose macromolecule strongly promote hydrogen

bonds (Alhuthali et al., 2012, Hong et al., 2008). Moisture is attracted to these hydrogen bonds. Furthermore, the exact nature of the processing of plant fibres can lead to a higher moisture intake and content. Table 2.3 shows the different moisture contents for seven natural fibres over different humidity.

Table 2.3: Moisture content of seven natural fibres over different humidity at 27°C (Clemons and Caulfield, 2005).

Fiber	Equilibrium moisture content (%)		
	30% relative humidity	65% relative humidity	90% relative humidity
Bamboo	4.5	8.9	14.7
Bagasse	4.4	8.8	15.8
Jute	4.6	9.9	16.3
Aspen	4.9	11.1	21.5
Southern pine	5.8	12.0	21.7
Water hyacinth	6.2	16.7	36.2
Pennywort	6.6	18.3	56.8

2.2 Polymers

2.2.1 Introduction

Polymer is formed whenever repeating units of atoms form long chain molecules and these polymers are joined together with strong covalent bonds. The molecular weight of polymers is usually measured in the hundreds of thousands. When a large number of polymers join together a plastic is formed (Mallick, 2007). For this reason, polymers are known as macromolecules (Faruk et al., 2012, Sperling, 2005). The study and production of polymers has now become a branch of science in its own right. Plastics, rubbers, fibres, adhesives, and specialized coatings are polymer-based. From the earliest polymers, the natural polymers, such as, cotton, proteins, starch, and wool, since the turn of the twentieth century, the synthetic polymers such as Bakelite and nylon have been used massively. When a plastic is solid, the molecules are frozen either randomly (amorphous) or orderly (semi-crystalline). These two designs are shown in Figure 2. 6. However, even in orderly polymers, on a submicroscopic scale, these polymer molecules

have areas of instability, i.e. random excitation. Also, as the temperature increases, the number of movements increases (Mallick, 2007, Rosler et al., 2007).

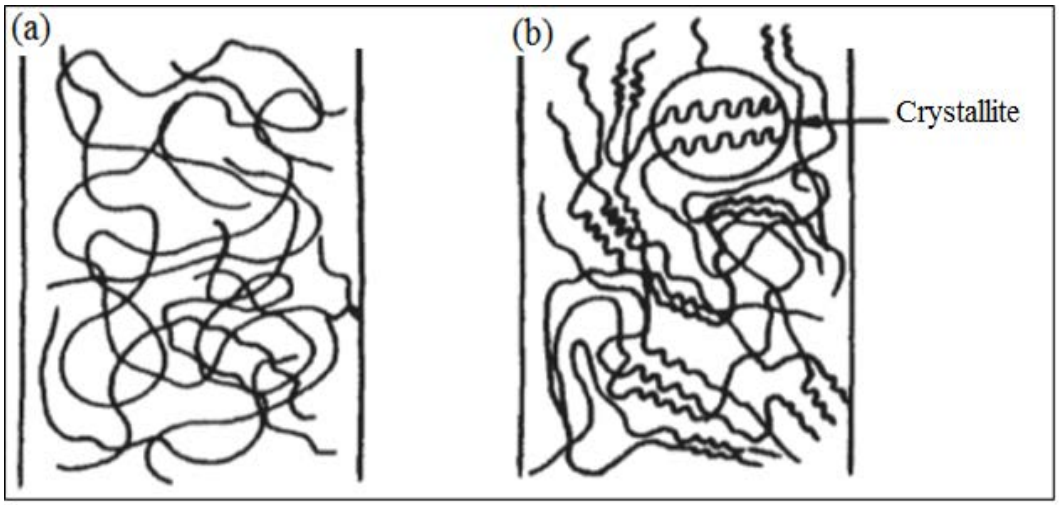

Figure 2. 6: (a) Amorphous versus (b) semi-crystalline polymers (Mallick, 2007).

2.2.3 Categories of polymers

Thermoplastics and thermosetting are the two categories of polymers. Thermoplastics are also known as thermoplasts. The difference between thermoplastics and thermosetting is that thermoplastic polymer does not have chemical joining between individual molecules. In other words, linear polymers with branched structures which have flexible chains are usually thermoplastic (Callister, 2003). Holding thermoplastics together is simply weak secondary bonds and Van der Waals and hydrogen bond intermolecular forces. When thermoplastic polymer receives heat the bonds can be temporarily broken and movement in formation occurs (Callister, 2003). On cooling, the new shape is set. Therefore, the engineering significance is that the polymer can be melted and reshaped as many times as desirable. However, most thermoplasts are soft. On the other hand, Thermosetting polymers (or thermosets) have cross-links which are highly rigid. The substance is made through a curing reaction. The thermoset cannot be melted by heat application. However, there are certain exceptions where there are a low number of cross-links are the substance can be softened (Guilleminot et al., 2008,

Raquez et al., 2010). Figure 2.7 shows the difference between thermoplasts and thermosets.

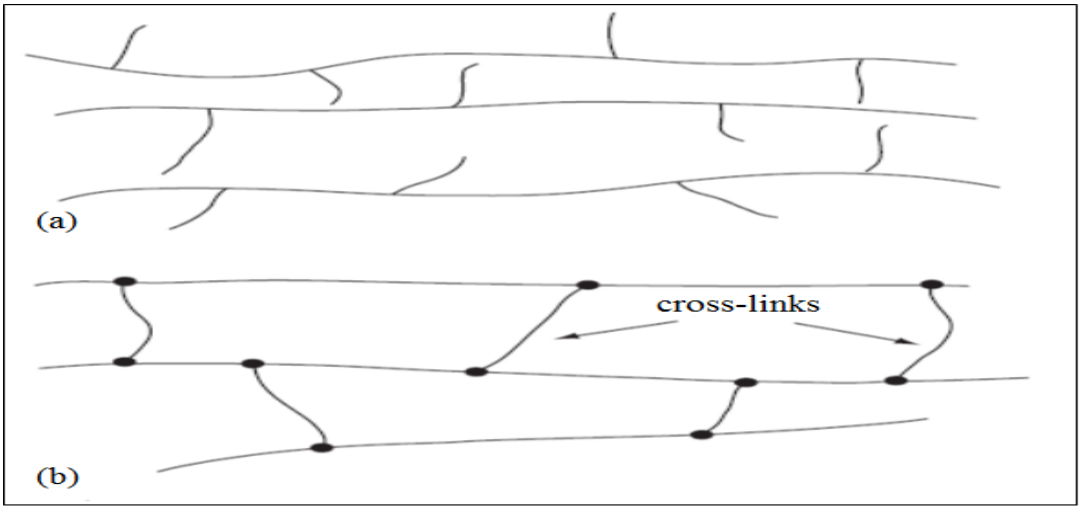

Figure 2.7: Thermoplastic polymer (a) versus thermosetting polymer (b) in diagrammatic representation with cross-linking highlighted (Mallick, 2007).

2.2.4 Vinyl-ester resin

2.2.4.1 Introduction

Vinyl-ester resin (VER) has excellent mechanical properties, superior resistance to chemicals and moisture providing greater hydrolytic stability compared to cheaper polymer resins and providing greater control over cure rate and reaction conditions compared to epoxy resins (Guo et al., 2008, Sultania et al., 2010). As a thermoset, being produced by a curing process, VER is highly rigid. VER are believed to combine the best properties of epoxies and unsaturated polyesters. Though VER is used extensively in the automobile industry, further research is required to better understand the potential of the material (Holbery and Houston, 2006, Sultania et al., 2010). VERs are currently used in electrical components, automobile parts, in the coatings, adhesives, moulding compounds, structural laminates used in mining and chemical operations, and even sporting goods. VERs are also increasingly used as thermoset matrices to fabricate ducts, pipes, tanks, and other reinforced structures and are believed to be a matrix of

great interest for the use the future composite products for infrastructure and transportation applications (Guo et al., 2007, Ku et al., 2007).

2.2.4.2 Chemical structure of vinyl esters

The chemistry of vinyl esters is somewhat complicated. The advanced polymer is produced by a reaction between unsaturated carboxylic acid and an epoxy, this reaction is shown in Figure 2.8. VER has carbon double bonds at the end of molecule. Therefore, this is the only site where cross-linking occurs. The means that the thermoset, i.e. cured, vinyl ester has fewer cross-links (Figure 2.9) which makes it more flexible than other cured polyester resins. These intermolecular forces also give vinyl esters higher facture toughness than other resins. Vinyl ester resin tends to have a low viscosity. The reason for this is that it is a substance that is often dissolved in a styrene monomer. When polymerization is occurring, cross-links formed between the unsaturation points (Guo et al., 2008, Mallick, 2007).

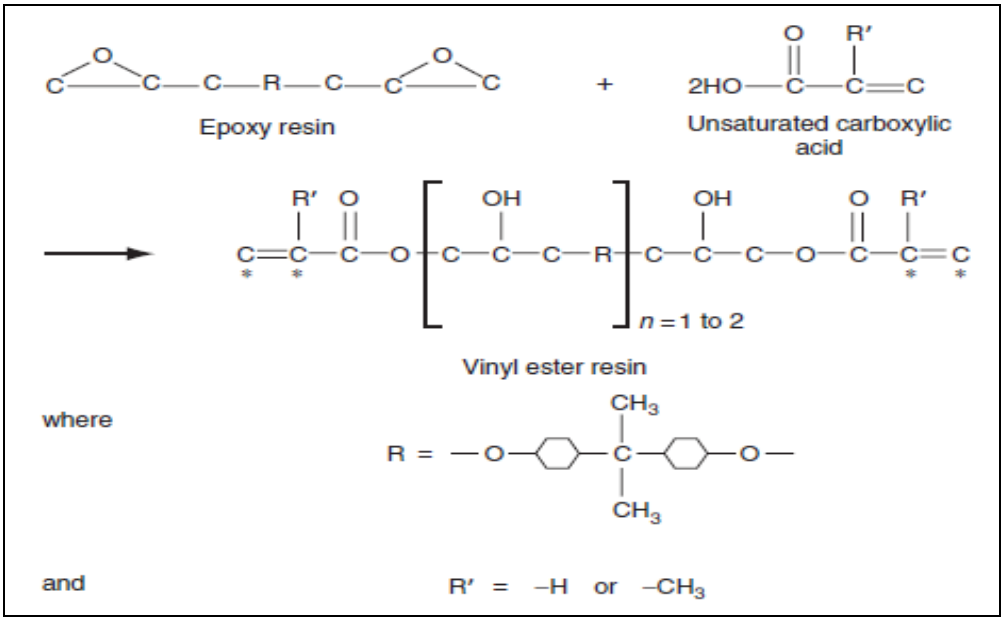

Figure 2.8: The Production of vinyl ester resin, namely, epoxy resin combining with unsaturated carboxylic acid. Unsaturation points are highlighted in the diagram with asterisks (Mallick, 2007).

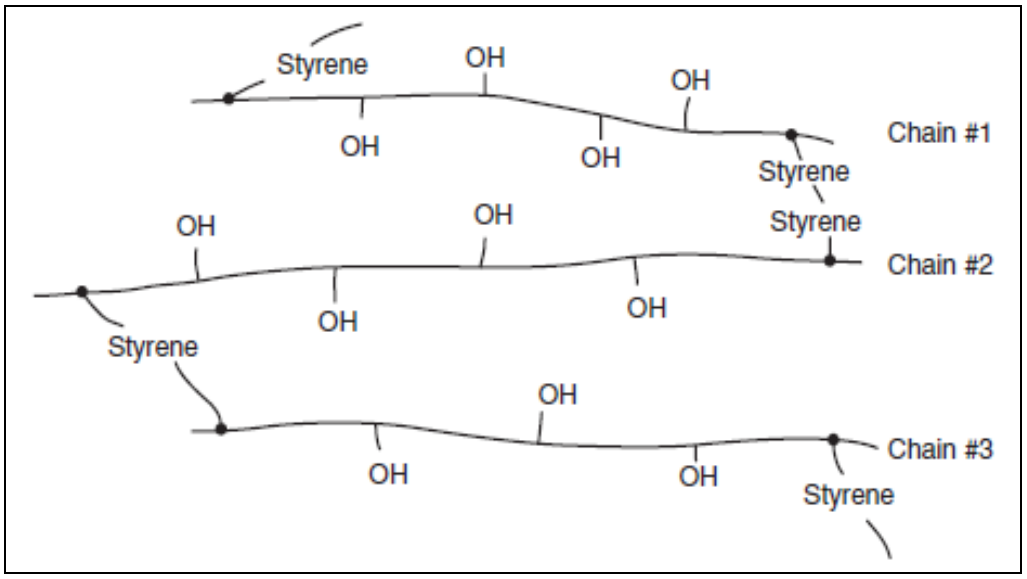

Figure 2.9: Crosslinking shown in vinyl ester resin (VER) Schematic representation of a cross-linked vinyl ester resin (Mallick, 2007).

2.2.4.3 Properties of vinyl ester resin

The interest in vinyl ester resins stems from their exciting properties. Ku et al (2007) found that the polymer has high design flexibility, has high chemical resistance, is easy to install, and is generally very low maintenance over a lengthy time period (Ku et al., 2007). Vinyl ester resins are a newer thermosetting resin compared to alternatives such as polyester and epoxy resins. Although all three are used in the automobile industry (in composite form), vinyl ester resins have a number of desirable property advantages compared to other thermosetting polymers (Table 2.4). Vinyl ester resins when cured at room temperature give better moisture resistance and have greater flexibility compared to the alternatives. This means that they are highly useful in hard-worked hull and deck structures in marine craft. Also, increasingly, the advantages of vinyl ester resins in terms of useable thermal, can withstand without distortion temperatures of up to 200°C (Marsh, 2007), and mechanical properties as well as chemical resistance and ideal curing characteristics are attracting more and more attention to the new polymer (Holbery and Houston, 2006). Furthermore, the location of reactive sites at the ends of molecular chains on the vinyl ester resins means that these chains can absorb energy resulting in a polymer which is overall tougher than the alternatives.

Some of the reason for vinyl ester resins desirable properties is that they maintain the positive characteristics from the substances they are produced from. Vinyl ester resins have similar excellent chemical resistance and tensile strength to epoxy resins. Also, they have the desirable low viscosity and fast curing properties which polyester resins have. Vinyl ester resins have similar tensile and flexural properties to other epoxy resins. The two properties which are weaker in vinyl ester resins compared to epoxy resins and polyester resins are firstly, the volumetric shrinkage higher which is undesirably, and vinyl ester resins can have a lower adhesive strength (Guo et al., 2008, Guo et al., 2007, Mallick, 2007).

Table 2.4: Comparison of eight properties of vinyl ester resins versus two common alternatives, polyester resins, and epoxy resins (Holbery and Houston, 2006).

Property	Polyester Resin	Vinylester Resin	Epoxy
Density (g/cc)	1.2–1.5	1.2–1.4	1.1–1.4
Elastic Modulus (GPa)	2–4.5	3.1–3.8	3–6
Tensile Strength (MPa)	40–90	69–83	35–100
Compressive Strength (MPa)	90–250	100	100–200
Elongation (%)	2	4–7	1–6
Cure Shrinkage (%)	4–8	—	1–2
Water Absorption (24 h @ 20°C)	0.1–0.3	0.1	0.1–0.4
Izod Impact, Notched (J/cm)	0.15–3.2	2.5	0.3

2.3 Natural Fibres Eco-composites

2.3.1 Introduction

The replacement of conventional materials with biodegradable 'green' materials is an important goal articulated in charters of sustainability worldwide. This message of a greater need to recycle and reuse, as well as strong and criteria for cleaner and safer environment, has directed scientific research to materials that can be easily degraded or bio assimilated (Liu and Hughes, 2008). Eco-composites are an important example. Eco-composites are composites materials that contain natural fibres, natural polymers, or a combination of both. These composites derive their name from the environmental and ecological advantages that they have over conventional composites (Bogoeva-Gaceva, et al., 2007, Low, et al., 2009).

Some examples of natural fibres include flax, hemp, jute, pineapple and sisal (Cheung et al., 2009). Part of the reason for the interest in greener substances is that there is growing global concern over the rapid depletion of petroleum resources, greenhouse gases issues, and a greater need to recycle and reuse. Some regions such as the European Union and Japan have legislation which states that a particular percentage of a vehicle must be reused or recycled. This percentage is approximately 80% to date and is set to increase in the coming years. Thus, more and more, scientists are looking to use materials which have a greater compatibility with the environment (Bogoeva-Gaceva et al., 2007, Holbery and Houston, 2006). Developing products with promote a global sustainability message has now become very important for manufacturers. Below is an example of a well-known automobile company, Mercedes-Benz. Figure 2.10 shows the 50 different products which are made from flax, hemp, sisal, and wool natural fibres which are incorporated into the E class series of cars (Hossain et al., 2011, Monteiro et al., 2009).

Figure 2.10: Fifty components made from natural fibres which are part of Mercedes-Benz's E series of cars (Holbery and Houston, 2006).

The below five points are the perceived benefits of using natural fibres over synthetic fibres. Firstly, natural fibres are environmentally friendly. There are two reasons for this – they are biodegradable, so they will not stay on the earth's surface for millions of years unlike some plastics and so on, also the energy required to produce these fibres is low especially compared with the consumption required to produce glass and carbon fibres (Osorio et al., 2011). Secondly, natural fibres have a lower density 1.25-1.5 g/cm^3 compared with 1.8–2.1 g/cm^3 for carbon fibres and 2.54 g/cm^3 for E-glass. What this means is that the final product with reinforced with natural fibres is lighter than a synthetic reinforced product (Sgriccia et al., 2008). Thirdly, natural fibres can have an excellent modulus-weight ratio. This makes them successful in stiffness-critical designs (Arora et al., 2012). Fourthly, natural fibres have excellent acoustic damping properties. This makes them preferable to glass or carbon for noise attenuation which is a requirement for automobile interior products (Anuar and Zuraida, 2011).

2.3.2 Fabrication of natural fibres eco-composites

Natural fibre composite production is, on the whole, similar to the production of synthetic fibre composites. Two basic differences are that the temperature must not exceed 200°C and the time the composites are exposed to the heat must be shorter. The reason for this is to avoid the decomposition of the natural fibres (Bogoeva-Gaceva et al., 2007, Sgriccia et al., 2008). There are a number of areas of consideration manufactures must reflect on before choosing which technique to use to produce natural fibre composites. The production technique will impact on the final product form, the overall cost, the properties of the composite, the overall energy required to produce the composite (Holbery and Houston, 2006). However, there are at least five recognized techniques for natural fibre composite production.

The first is injection molding. This technique is the most commonly applied method for natural fibre synthesis. Injection molding is especially useful when delicate shapes are required in high volume. This technique is reportedly useful in providing dimensional tolerance. However, there have been reports of issues with ensuring consistent quality with this production type. The process to improve this shortcoming is known as direct long fibre thermoplastic (D-LFT) molding. This injection molding technique involves fibres spooled into a heating zone, mixed with thermoplastic, and then cut at the required length. Several companies including BMW are still working to improve D-LFT (Holbery and Houston, 2006, Wan Abdul Rahman et al., 2008).

Compression molding is a second technique for the production of natural fibre composites. Different from injection molding using thermoplastics, compression molding uses thermosets. Compression molding is also a widely used technique is the automobile industry particularly for the production of light and thin structures. The advantage of this technique is that it is a quick process which gives very low fibre attrition. Within this style of fabrication is an associated technique, sheet molding compound (SMC). Both of these techniques work by extruding large thermoplastic bundles of fibres and putting them into a compression mold. The compression is then applied to mold the composite. However, one of the major drawbacks of this technique

is that it has a high initial capital cost to prospective manufacturers (Sreekumar et al., 2007, van Voorn et al., 2001).

Two more recent natural fibre composite production techniques are resin transfer molding and vacuum-assisted resin transfer. The two main benefits of these techniques are that they offer the most effective compounding conditions and that the temperatures required are too high as to damage the natural fibres. For these reasons, these two techniques are useful for creating composites with high fibre content (up to 70 %) and with good devolatilization. Nonetheless, these techniques, resin transfer molding and vacuum-assisted resin transfer, share the same shortcoming as other types of compression molding in that they are expensive to set up (Bogoeva-Gaceva et al., 2007, Holbery and Houston, 2006).

A fifth technique is compounding processes. This technique is straightforward and involves natural fibres being mixed into a thermoplastic matrix. There are a number of compounding processes which are used in laboratories and factories today; the most notable are extrusion compounding process, kneading compounding process, as well as high-shear compounding process. The first, extrusion, involves a heated barrel. What happens is essentially the materials are fed in together, heat is applied, mixing is comprehensive, devolatilization occurs, and finally the material is extruded through a die. The second technique, kneading, requires continuous kneading from mixers which consist of intermeshing rotors in a heated system. The rotors, usually two, are high torque, low speed rotors. A pelletizer is then used to cut off pellet sized products. The third compounding process is high-shear compounding. This technique is similar to kneading; however, the machines used are more robust. (Sun et al., 2009, Thomason, 2005).

2.3.3 Properties of Natural Fibre Eco-composites

2.3.3.1Introduction

Studies on the preparation and characterisation of thermosetting and thermoplastic composites reinforced with flax, sisal, oil palm, henequen, jute, banana, wood pulp, stinging nettle, coir, or hemp natural fibres with and without treatment have been extensively conducted in more recent decades (Ratna Prasad and Mohana Rao, 2011, Sreenivasan et al., 2011). Currently, increasing interest has been drawn to the use of these natural fibres to reinforce polymer composites due the natural fibres' low cost, low density, excellent tensile mechanical properties and most recently the benefits of biodegradability, reduced tool wear (nonabrasive to processing equipment), enhanced energy recovery, and CO_2 neutrality when burned has driven a renewed enthusiasm from academics and industry (Liu and Hughes, 2008, Low et al., 2009). The potential application for natural fibres is replacing the more expensive and denser conventional glass fibres, talc and mica in composite materials. Natural fibres, thus, offer lower cost and density while providing high toughness and acceptable specific strength (Low et al., 2007). Natural fibres are now believed to hold significant potential for the transportation and construction industries and may even be seen increasingly applied in consumer goods many other common applications in the near future (Harish et al., 2009).

2.3.3.2 Mechanical properties

Natural fibres are generally added to polymer matrix composites to produce materials with the desirable mechanical properties of higher specific strength and higher specific modulus while at the same time materials that maintain a low density and low cost. The mechanical performance of these composites is dependent on the type of natural fibre, its treatment, the type of polymer matrix, additives, and processing methods (Clemons and Caulfield, 2005, Low et al., 2009). Fibre orientation has also been recognized as an important determinant. However, most recently, fibre-matrix adhesion is believed to be the primary determinant in mechanical performance and overall composite quality (Herrera-Franco and Valadez-González, 2005). The role of the matrix, in a fibre reinforced composite, is to transfer the load to the stiff fibres through shear stresses at

the interface. A good bond between the polymeric matrix and the fibres is required in this process (Bakare et al., 2010).

Natural fibres can have mechanical properties which are comparable or better than synthesised fibres. For example, flax fibres were found to have a tensile strength of 1340 MPa, Young's modulus of 54 GPa, and a density of around 1500 kg/m^3. In contrast, E-glass fibre were found to have a tensile strength of 2000 MPa, a Young's modulus of 76 GPa and a density around 2560 kg/m3 (Liu and Hughes, 2008). The impact strength, a measure of toughness, of polymers is also reported to be enhanced through the addition of natural fibres and furthermore by the chemical and physical treatment of the natural fibres (de Albuquerque et al., 2000).

Using jowar, sisal, and bamboo fibres, Prasad and Rao (2011) investigated the effect of increasing volume fraction of these fibres on the mechanical properties of polyester composites (Ratna Prasad and Mohana Rao, 2011). The flexural strength and the flexural modulus of all of the composites considered by Prasad and Rao (2011) were found to increase with the addition of jowar, sisal, and bamboo fibres as shown in Table 2.5.

Table 2.5: The flexural properties of jowar fibre composites, along with other natural fibre reinforced composites at 0.40 volume fraction of fibre (Ratna Prasad and Mohana Rao, 2011).

Name of the Composite	**Volume fraction of fibre**	**Ultimate flexural strength (MPa)**	**Flexural modulus (GPa)**
Plain polyester	0.00	55.08	1.53
Jowar	0.407	134	7.87
Sisal	0.40	99.5	2.49
Bamboo	0.40	128.5	3.70

The flexural strength and flexural modulus of the jowar, sisal, and bamboo fibre reinforced composites was also found to increase with an increasing volume fraction of each fibre. As shown in figure 2.11 and figure 2.12.

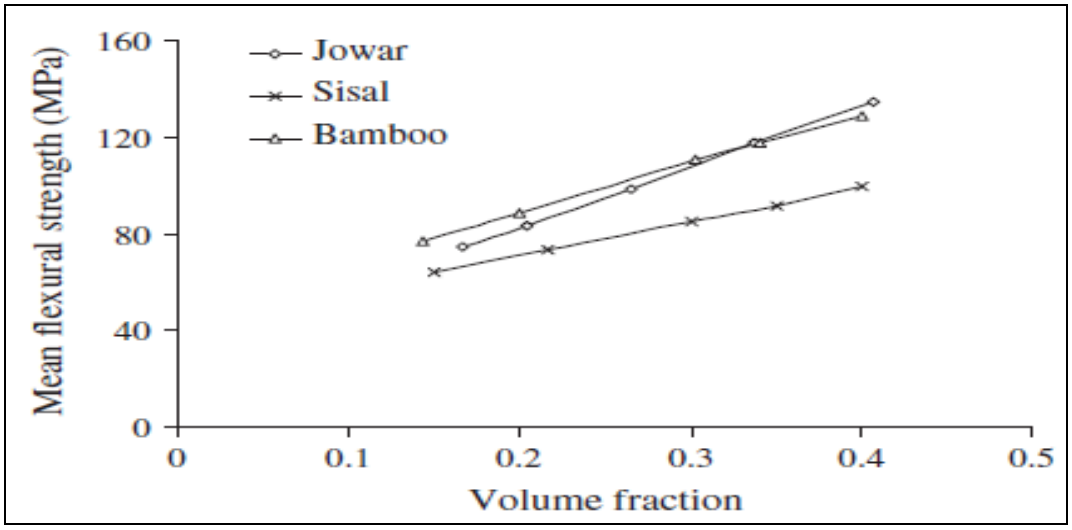

Figure 2.11: Effect of volume fraction of fibre on mean flexural strength of various natural fibre composites (Ratna Prasad and Mohana Rao, 2011).

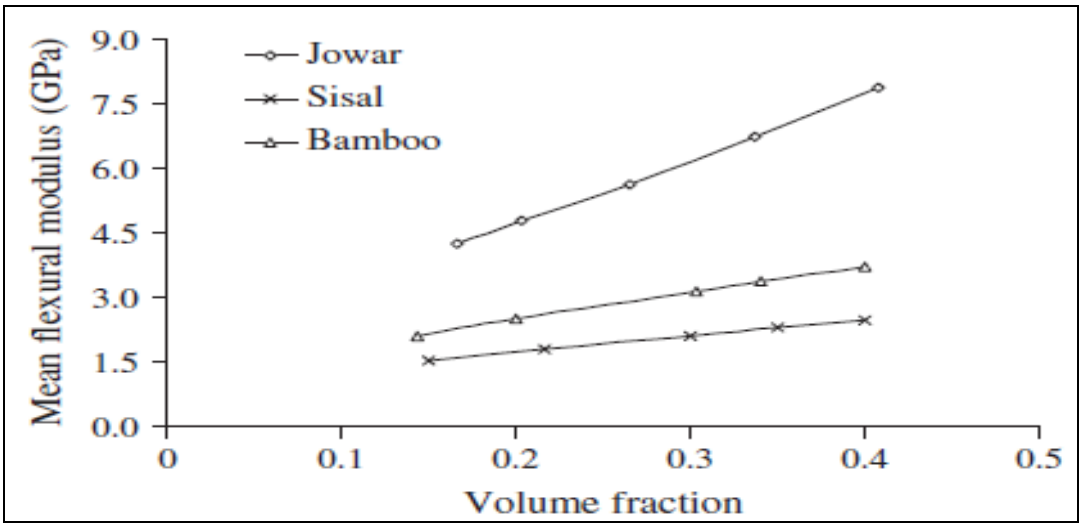

Figure 2.12: Effect of volume fraction of fibre on mean flexural modulus of various natural fibre composites (Ratna Prasad and Mohana Rao, 2011).

In figure 2.11, it can be seen that jowar fibre composites dominate the bamboo and sisal composites in terms of flexural strength beyond the volume fraction of fibre of 0.34. Figure 2.12 shows that the jowar fibre composites also had superior flexural modulus compared to the bamboo and sisal. The researchers believe that this may be due to the stronger bonding of the jowar fibres with the polyester matrix (Ratna Prasad and Mohana Rao, 2011).

Oksman et al. (2009) studied the mechanical properties of sisal, banana, jute, and flax with and without treatment as reinforcement materials for polypropylene (PP). Like Prasad and Rao (2011), Oksman et al. (2009) found that the flexural modulus of all composites increased with fibre content (20, 25, 30, 35, 40 and 45 wt.%). For example, while a flexural modulus of 1.3 GPa was found for pure PP, for composites with 44% jute fibres, the modulus was increased to 4.9 GPa (Oksman et al., 2009). With respect to flexural strength, the table indicates that in this study, the addition of untreated fibres did not enhance this property. The researchers believe this is due to poor adhesion between the untreated fibres and the matrix causing poor stress transfer from the matrix to the stronger fibres (Oksman et al., 2009). The researchers, however, found that flexural strength of the composites was significantly improved in the cases where 2 wt.% maleated polypropylene (MAPP) was used to treat the sisal, jute, and flax fibres. For example, the improvement was most significant for PP–flax where the strength increased from 40 MPa to 79 MPa and PP–sisal composites where strength increased from 46 MPa to 75 MPa (Oksman et al., 2009).

Flax was considered by the researchers to provide most superior mechanical properties of the natural fibres tested when used to reinforce PP. The micrographs for the untreated natural fibres composites, below, figure 13 a, b, c, and d provide explanation for the better performance of this fibre. The flax fibres appear smoother than the sisal and banana fibres which appear coarse. The flax fibres are also the thinnest and the most evenly distributed fibres in the PP compared to sisal, banana, and jute. Furthermore, the flax fibres can be seen as taking single fibre form, which suggests that during the extrusion process the fibres were separated. The lower lignin content of flax compared with other fibres is believed to be a reason causing the favourable dispersion, an important determinant of strong mechanical properties (Oksman et al., 2009). Clean surfaces of the untreated fibres in the composites can be seen in the micrographs below. Oksman et al. (2009) believe these surfaces are indicative of poor adhesion between the fibres and the matrix, which is a major determinant of lower flexural strength.

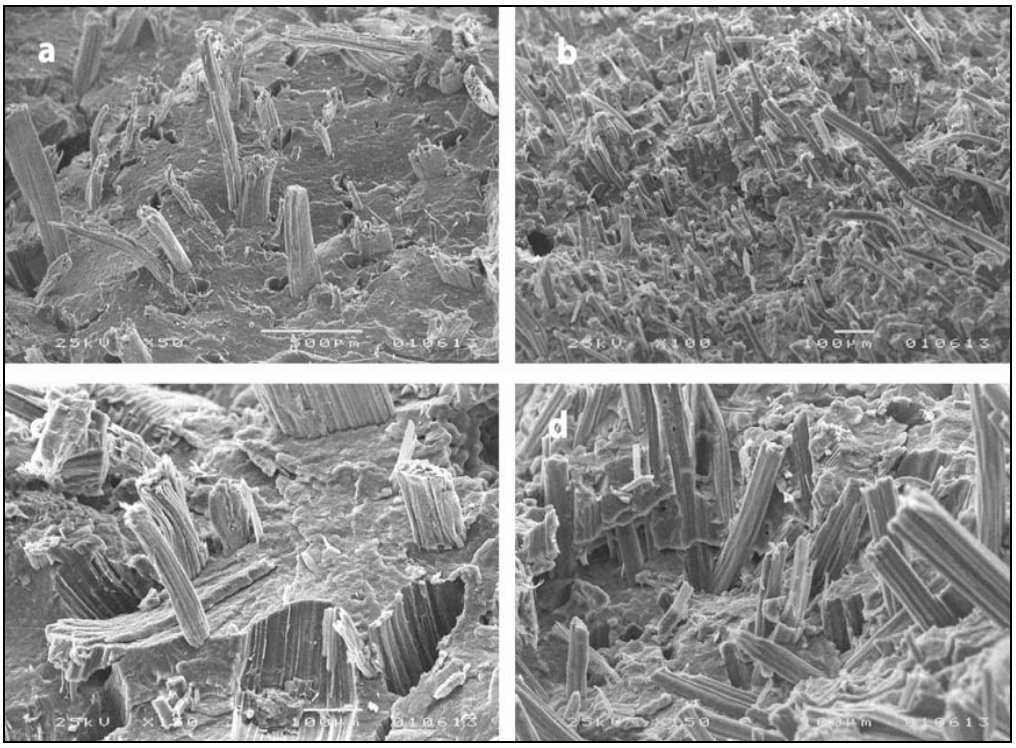

Figure 2.13: Over-view of fractured composite surfaces: (a) PP–sisal, (b) PP–flax, (c) PP–banana and (d) PP–jute (Oksman et al., 2009).

On the other hand, the micrograph below, figure 2.14, shows the fracture surfaces of the treated flax-PP composites. The change in the appearance of the fibre breakages and the decreased number of pull-outs compared to untreated flax-PP indicates improved adhesion between the fibres and matrix according to Oksman, et al. (2009).

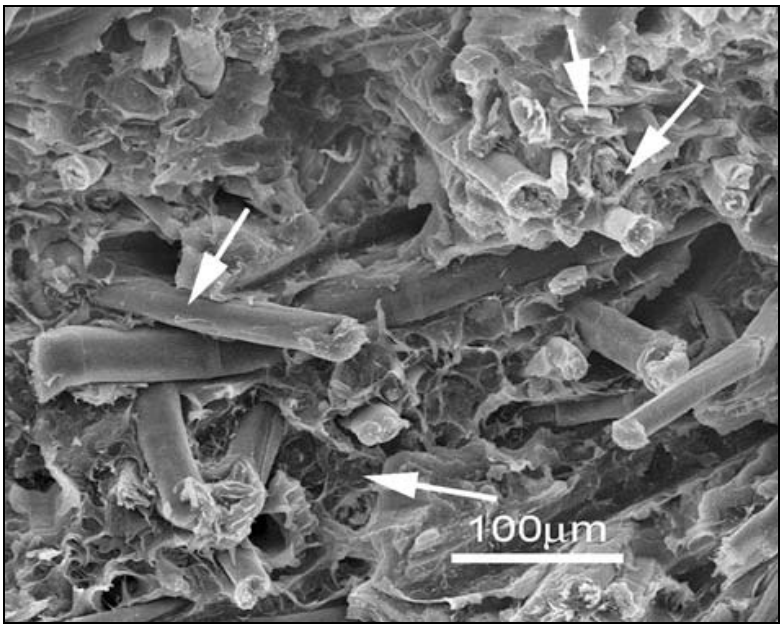

Figure 2.14: Fractured surface of PP–flax composite with 2 wt.% MAPP (Oksman et al., 2009).

Venkateshwaran, et al. (2011) studied the role of fibre length on strength properties of composites. The mechanical properties of composites reinforced with natural fibres in these studies were found to increase to a certain limit due to increasing fibres length and weight percentage (Venkateshwaran et al., 2011). For example, in Venkateshwaran et al.'s (2011) studies, tensile strength, flexural strength and impact strength peaked at 16.39 MPa, 57.53 MPa and 13.25 kJ/m^2 for 5 mm, 15 mm and 15 mm fibre lengths and 12, 16 and 16 weight percentages respectively, but then declined. The decline in properties of strength in composites with natural fibres exceeding optimal fibre length is explained by Venkateshwaran et al. (2011). While the mechanism of pull-out strengthens the composite with increasing fibre length, at a point if fibre length is too long material failure will occur due to an absence of fibre-matrix interaction causing agglomeration and uneven distribution of fibres throughout the matrix (Venkateshwaran et al., 2011). Figure 2.15 from this study shows void creation due to fibre pull-out.

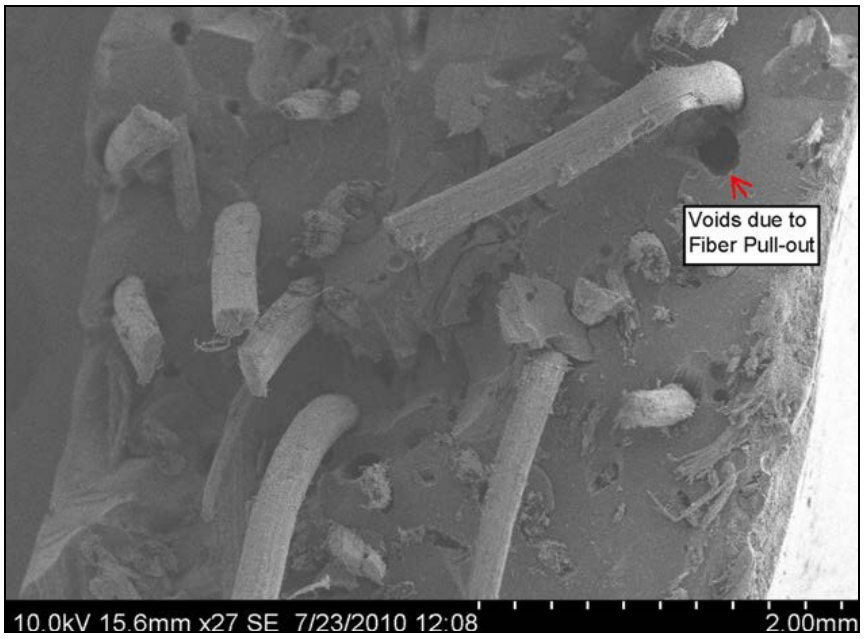

Figure 2.15: SEM micrograph of tensile fractured surface of 50/50 hybrid composite (Venkateshwaran et al., 2011).

Wong et al. (2010) conducted a study on the effect of bamboo fibre length and concentration on the fracture toughness properties of composites. Figure 2.16 shows how composites reinforced with fibre display favourable properties of toughness compared to thermosetting polymers which while rigid are highly brittle. Wong et al. (2010) found that for 4 mm, 7 mm and 10 mm lengths of fibre, 10 vol.%, 40 vol.%, and 50 vol.% concentrations of fibre gave the highest toughness properties. The highest fracture toughness, $K_{IC,}$ attained was 1.73 MPa.$m^{1/2}$ for the 10 mm/50 vol.% composite. This represents a 340% of improvement in fracture toughness compared to neat polyester. The second highest fracture toughness result was obtained by 7 mm/40 vol.% followed by 4 mm/10 vol.%. Wong et al.'s (2010) findings suggest that fibre length is another important parameter in affecting the fracture resistance.

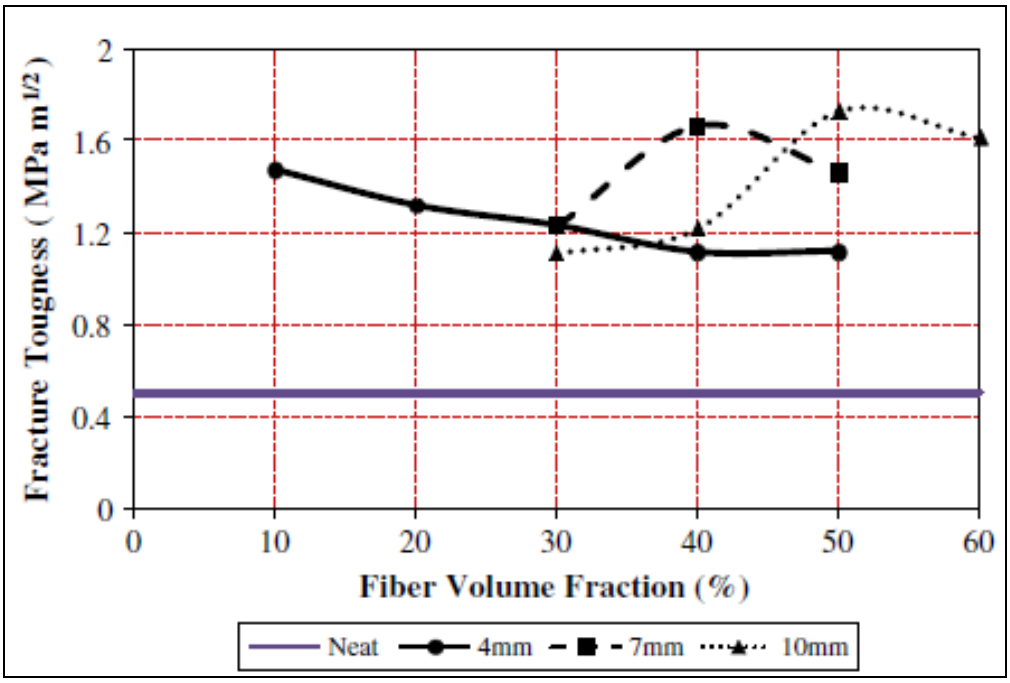

Figure 2.16: Effects of fibre volume fraction on fracture toughness of the composite (Wong et al., 2010).

Wong et al.'s (2010) investigation of fracture surfaces reveals marked difference in the smoothness of fracture surfaces between samples of neat polyester and composites. The comparatively smooth fracture surface is shown in Figure 2.17a. Crack growth propagates unrestrained upon external loading. Plastic deformation present near crack tip exacerbates plastic zone generation (Wong et al. 2010). In contrast, the fracture surface of 7 mm/30 vol% composite displays fibres extruding from the surface evidencing fibre pull out (Figure 17b). These extruding fibres are an indication of the crack deflection mechanism provided by the fibres. Fibre pull out is an indicator of crack fronts having intersected with the interface between matrix and fibre and causing fibre de-bonding. The phenomenon absorbs energy toughening the composite and the dissipation of energy is further evident from fibre end damage and split of fibres (Wong et al. 2010).

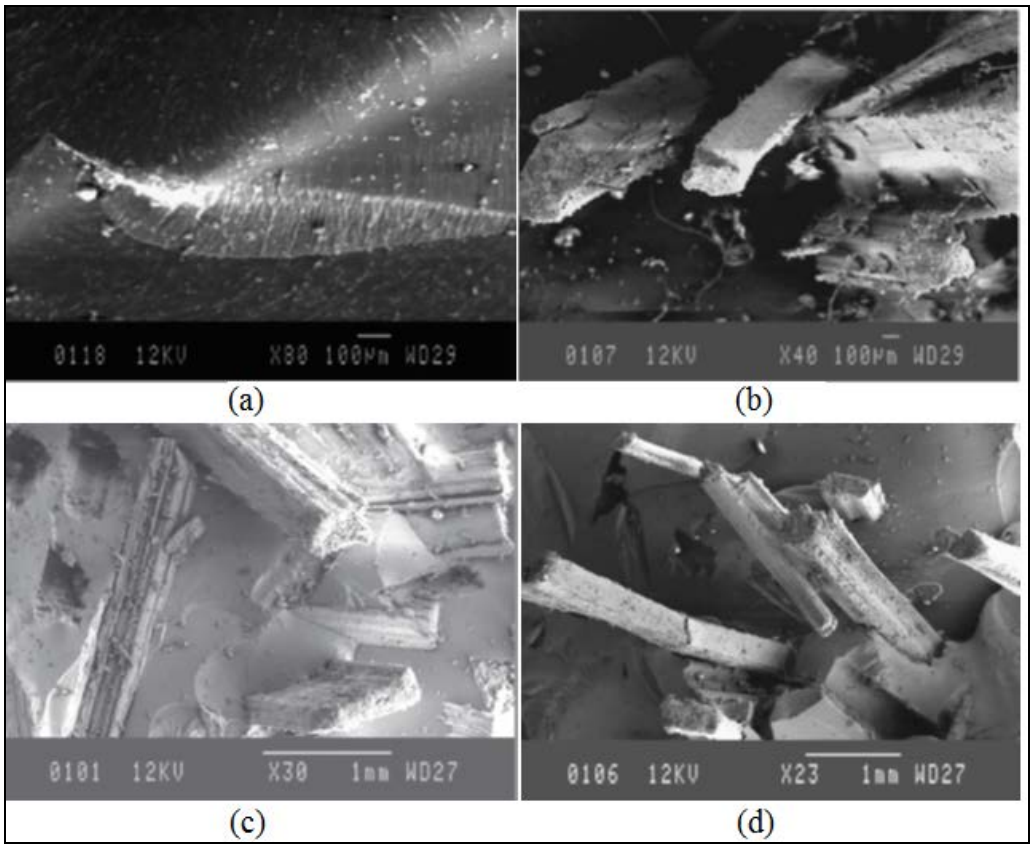

Figure 2.17: (a) Fractured surface morphology of neat polyester, (b) of 7 mm/30 vol.% composite, (c) of 4 mm/40 vol.% composite, (d) of 10 mm/40 vol.% composite (Wong, et al. 2010).

Wong et al. (2010) attribute the lower toughness properties of composites reinforced with shorter fibres (4 mm/40 vol% composite) to the less available fibre surface on shorter fibres (4 mm/40 vol% composite) leading to less absorption of fracture energy during the mechanism of pull-out and the presence of fibres experiencing no damage at all during pull-out indicative of failure of energy dissipation. These observations can be seen in figure 2.17c. Given increases in fibre length, (10 mm/40 vol% composite) highest fracture toughness is obtained at higher fibre volume fraction according to Wong et al. (2010). This postulation confirms further that longer fibres tend to dissipate energy more effectively. Figure 2.17d shows fibre damage of a comparatively severe extent on extruding fibres. With more surface area of fibre available at high fibre content, fracture resistance is increased (Wong, et al. 2010). Wong, et al (2010) concluded that the range

of composite samples demonstrated higher properties of fracture toughness compared to the neat polyester. Energy dissipation, vital for enhancement of fracture toughness, is believed to be caused through matrix plastic deformation, fibre de-bonding, fibre pull-out and fibre damage, all underpinned by the initial mechanisms of crack-tip blunting, crack deflection and crack pinning (Wong, et al. 2010).

Stocchi et al. (2007) conducted a study on the effect of various fibre surface treatments on the properties of strength and toughness of composites. Stocchi et al (2007) found that alkali-treated fibre composites gave the highest flexural strength values most likely attributable interfacial adhesion of a higher level between fibre and matrix. Silicone-treated fibre composite was found to have favourable properties of toughness which is most likely attributable longer pull-out lengths. The mechanical behaviours exhibited by Stocchi and team's composites were in agreement with fracture surface observations. Figure 18(a-c) provides SEM micrographs of the fracture surfaces of the composites with different fibre treatments. The figure shows pull-out length greater for non-treated fibre composites (Figure 18a) and silicone-treated fibre composites (Figure 18b) which were found to have favourable toughness. This can be contrasted with the alkali-treated fibre composites (Figure 18c) in which a greater number of fibres pulled out by a short length. This observation serves as evidence of the stronger adhesion between the fibre and matrix in this composite causing the properties of lower toughness and higher strength (Stocchi, et al. 2007).

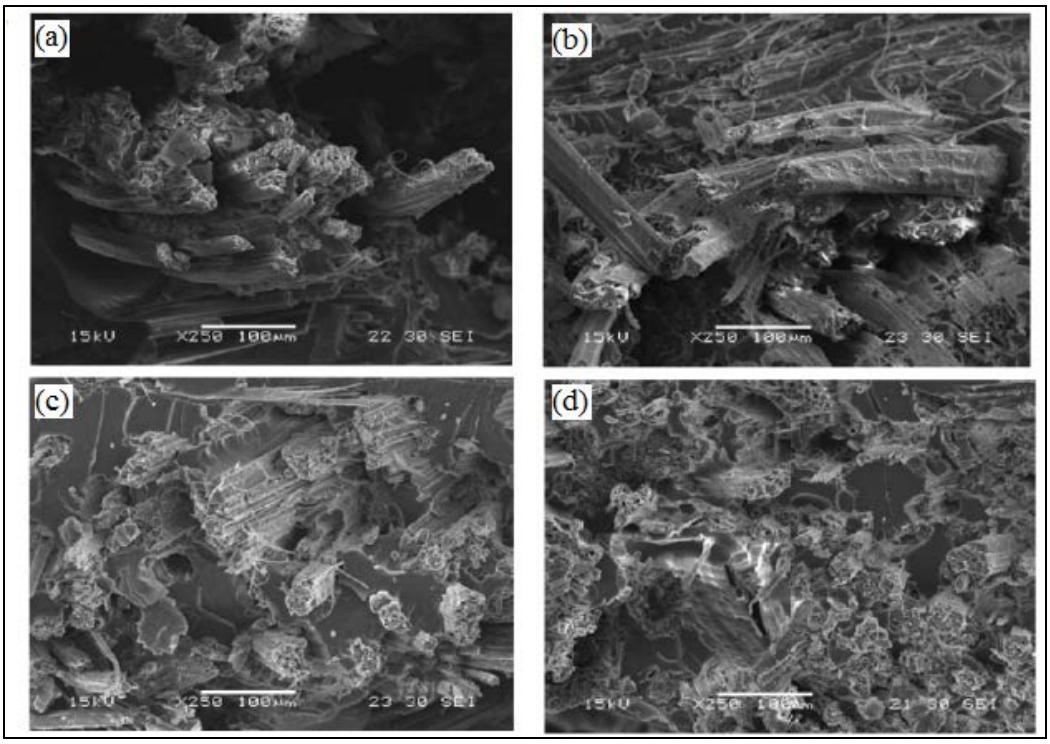

Figure 2.18: SEM micrographs of fracture surfaces of the composites with different fibre treatments broken in tension (a) Composite with non-treated fibre. (b) Composite with silicone-treated fibre (c) Composite with alkali treated fibre. (d) Composite with acetylated fibre (internal view of a pulled-out yarn) (Stocchi et al., 2007)

To sum up, in fibre reinforced composites, the role of the matrix is to transfer the load to the stiff fibres through interfacial shear stresses. Adhesion quality between matrix and fibres is therefore a key determinant in the mechanical properties of composites reinforced with natural fibres (Mylsamy and Rajendran, 2011). The strength properties of the composite will be dependent on the effectiveness of the matrix, once subjected to load, in transferring stress to fibre and the fibre in carrying the load. This effectiveness can be improved through chemical or physical treatment of the surface of natural fibres (Anuar and Zuraida, 2011; Stocchi et al., 2007). It is also necessary to refer to crack deflection, de-bonding between fibre and matrix, pull-out and fibre -bridging, which are also believed to be important mechanisms of energy absorption in composites reinforced with natural fibres. Amongst these it is difficult to determine with accuracy the dominant

mechanisms leading to enhanced toughness (Silva et al., 2006, Venkateshwaran et al., 2011, Wong et al., 2010).

2.3.3.3 Water absorption behaviors

It is generally accepted that the shortcoming of natural fibres is their water absorption behaviors. Increased fibre content tends to result in increased moisture absorption (Dhakal et al., 2007). Wang et al. (2006) refer to this as the hygroscopicity of the fibres. In the long-term, the performance of materials using these fibres is compromised (Wang et al., 2006). The mechanism of water absorption is natural fibres is well understood. On exposure to moisture, the very first molecules of water are directly absorbed by the hydrophilic groups of the natural fibre material (Chen et al., 2009). Then, the second groups of water molecules are attracted to other hydrophilic groups that may be present, or alternatively, the second group of water molecules may be attracted to the top of the already absorbed water molecules. If the conditions of high humidity exist, surface tension forces may be sufficient to hold liquid water in capillary spaces (Athijayamani et al., 2009; Chen et al., 2009).

Similarly, for all general polymer composites, such as polymer/natural fibres composites, conditions of high humidity, or high water content, result in surface absorption of moisture which is instantaneous. Once taken up, the moisture diffuses through the matrix. This process continues, namely, the moisture concentration increases with time, until equilibrium level, also the material's saturation point (Alhuthali et al., 2012; Kim and Seo, 2006). This phenomenon is generally represented with an absorption curve, which compares and contrasts weight gain with exposure time. Generally, absorption rate is rapid initially and then tapers off before reaching a plateau, namely, the point it approaches equilibrium (Doan et al., 2006). This process considered best described generally by Fickian diffusion behavior (Vilay et al., 2008).

The moisture diffusion mechanism for both polymers and polymer composites is also well understood. Fick's second law has been developed to describe non-steady state diffusion. This model is discussed by a number of research teams including Kim et al.

(2005), Liu et al. (2008), and See et al. (2009). Fick's second law, with a constant diffusivity, represented by *D*, using the Cartesian coordinate, *x*, *y*, and *z*, explains moisture diffusion (Kim and Seo, 2006; Liu et al., 2008b):

$$\frac{\partial c}{\partial t} = D\left(\frac{\partial^2 c}{\partial x^2} + \frac{\partial^2 c}{\partial y^2} + \frac{\partial^2 c}{\partial z^2}\right) \tag{2.1}$$

In the above equation, equation 2.1, *c* represents the diffusing substance concentration while *t* represents time. With one-dimensional diffusion moving through a plate of thickness which is infinite, i.e. *h*, the equation 2.1 is reduced to:

$$\frac{\partial c}{\partial t} = D\frac{\partial^2 c}{\partial x^2} \tag{2.2}$$

If the sheet, is isotropic, and has finite thickness, the equation solution, is dependent of time, *t*, and distance, *x*, and is shown as below (See et al., 2009):

$$\frac{c(x,t)}{C_\infty} = 1 - \frac{4}{\pi}\sum_{m=0}^{\infty}\frac{1}{(2m+1)} \times \exp\left[-D\frac{(2m+1)^2\pi^2 t}{h^2}\right] \times \sin\left[\frac{(2m+1)\pi x}{h}\right] \tag{2.3}$$

In the above equation, equation 2.3 C_∞ is the absorbed substance's saturation concentration. Looking at equation 2.3 again when it is solved with boundary conditions, namely, $c = 0$ when $t = 0$ and $0 \le x \le h$; $c = C_\infty$, when $t > 0$, $x = 0$, $x = h$; and $\partial c / \partial x = 0$ when $x = 0$, $t > 0$, therefore the expression for relative moisture uptake is as follows (Dhakal et al., 2007; See et al., 2009):

$$\frac{M_t}{M_\infty} = 1 - \sum_{n=0}^{\infty}\frac{8}{(2n+1)^2\pi^2} \times \exp\left[-D\frac{(2n+1)^2\pi^2 t}{h^2}\right] \tag{2.4}$$

In the above equation, equation 2.4 M_i indicates the mass gain with reduced time and M_∞ indicates the maximum mass gain which is present at saturation point. During the linear relationship, initially, diffusion, as shown in equation 2.4 is approximated by the equation 2.5 (Alhuthali et al., 2012; Kim et al., 2005):

$$\frac{M_t}{M\infty} = 4\left(\frac{D_t}{\pi h^2}\right)^{1/2} \tag{2.5}$$

Then the diffusion quantity from the above equation, equation 2.5 can be drawn out through using the below equation 2.6 (Dhakal et al., 2007):

$$D = \frac{\pi}{16}\left(\frac{M_t / M_\infty}{\sqrt{t}/h}\right)^2 \tag{2.6}$$

While pure polymers have low water absorption properties, which are desirable for materials, polymer/natural fibre composites tend to have higher behaviours of water absorption. Results from experiments show that increasing the natural fibre content results in an increased capacity for water molecules to be absorbed.

Espert et al. (2004) also studied water absorption in polymer/natural fibre composites with ethylene vinyl acetate copolymer and sisal fibres. The group compared dried samples with water exposed samples and found that the water absorption curves displayed the well-established behaviour of rapid absorption then slowing as approaching saturation point. The figure below, figure 2.19, shows the results for three PPEVA/cellulose composites, namely, 10 wt.%, 20 wt.%, and 30 wt.% fibre. Espert et al. (2004) concluded that it was due to the hydrophilic character of the natural fibres that led to greater water absorption.

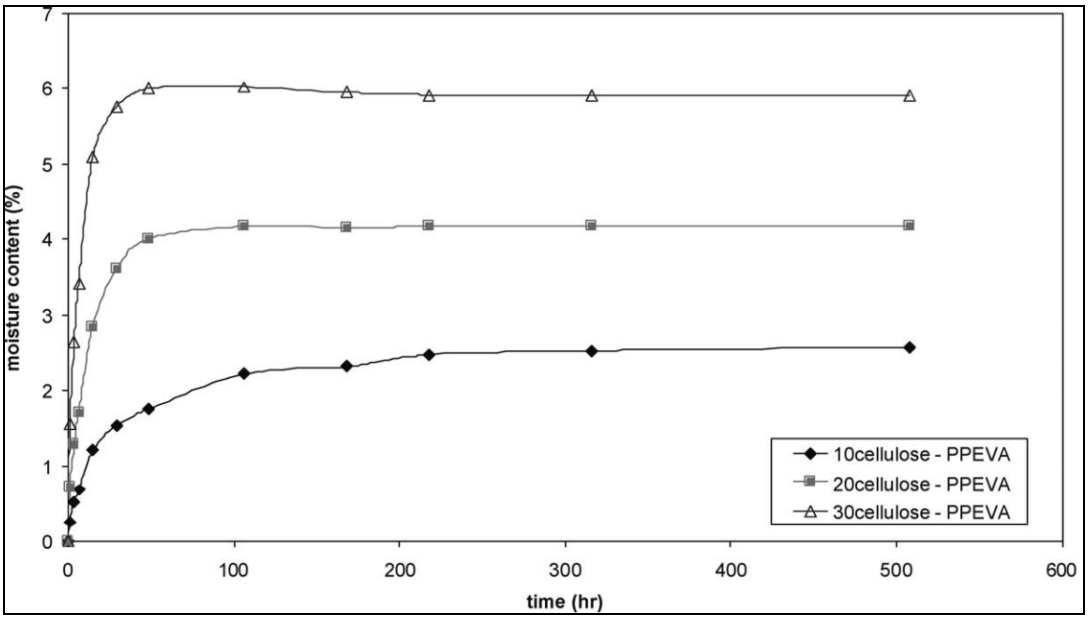

Figure 2.19: Water absorption curve for three PPEVA/cellulose composites, 10 wt.%, 20 wt.%, and 30 wt.% fibres (Espert et al., 2004).

Dhakal et al. (2009) studied the percentage of weight gain with unsaturated polyester known as UPE with hemp fibres. The researchers produced composites with different layered structuring of the hemp fibre. The team reported that four different fibre volume fractions were used in the experiment, namely, 0, 0.15, 0.21 and 0.26. The results are shown in the figure below, figure 2.20. Put simply, the higher the proportion of hemp fibre content, the higher the weight gain of the substance. Dhakal et al. (2009) argued that it was the hemp fibre's water uptake characteristics which led to the increase. They stated that the high cellulose content, 74%, led to swelling and stress creation within the composite. This finding is consistent with earlier studies (Kim and Seo, 2006). The team also added that micro cracking was occurring within the matrix due to fibre swelling leading to water absorption due to allowing increased capillarity mechanism, namely, the flow of water molecules.

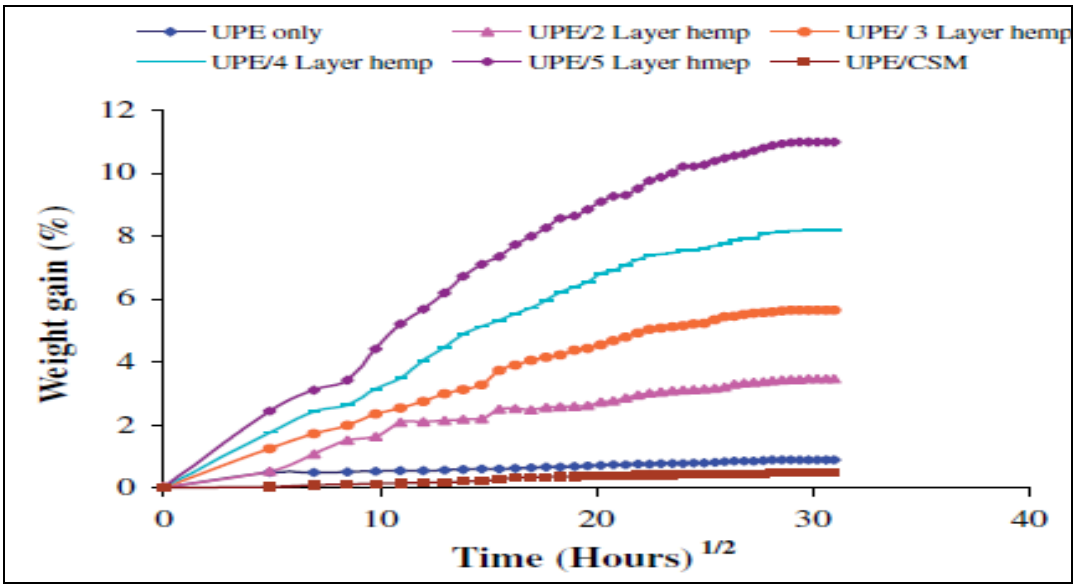

Figure 2.20: Water absorption curves showing weight gain by different polyester and hemp composites at room temperature (Dhakal et al., 2007).

Athijayamania et al. (2009) also conducted similar studies into the effect of fibre content on the water absorption tendencies of composites. The below figure, Figure 2.21, shows the increasing water absorption with larger proportions of fibre.

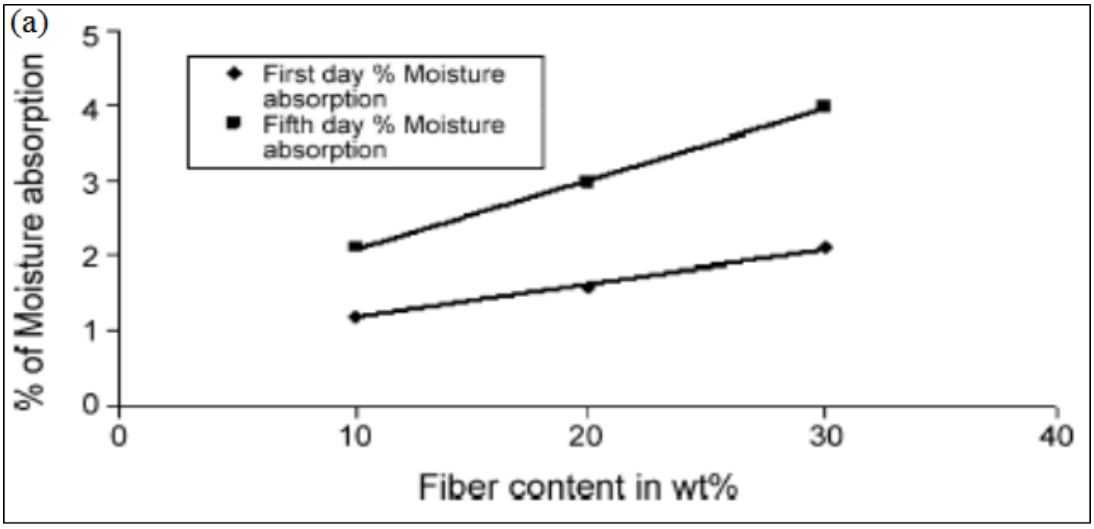

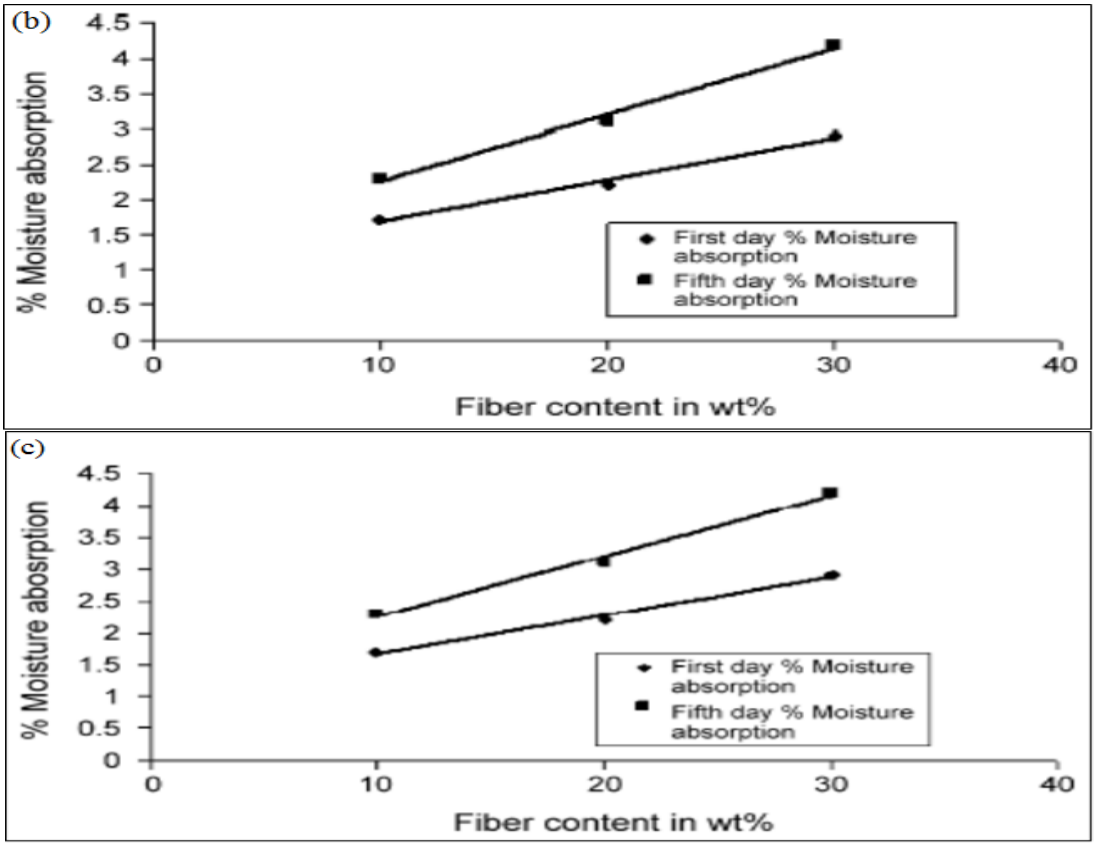

Figure 2.21: the effect of fibre content on water absorption across three fibre lengths (a) 50 mm, (b) 100 mm, and (c) 150 mm (Athijayamani et al., 2009).

The findings shown in the above graphs support the accepted concept that increased fibre content will mean increased water absorption. The team explained the phenomenon as a result of increased microvoid formation in the matrix resin. However, one new finding by Athijayamania et al. (2009) was that increasing the length of fibre, from 50 mm, to 100 mm, to 150 mm, resulted in increased moisture absorption

2.3.3.4 Thermal properties

The thermal properties of polymers and polymer composites are studied to provide information about the structure-property relationship of these materials. The development of thermo-resistant polymers and ablation problems to the stabilization of thermolabile polymers can be better understood through thermal analysis. The investigation of thermal properties is important for the production of natural fibres reinforced composites as it provides information about molecular design and the

mastering of production technology (Joseph et al., 2003). TG is an accepted method for studying the thermal properties of polymeric materials. Thermal breakdown, weight loss of the material in each stage, and threshold temperature can be obtained using TG. Derivative thermogravimetry (DTG) can be used to provide data concerning the nature and extent of degradation of the material. Another one of the methods is differential scanning calorimetry (DSC), which measures the heat flow rate associated with a thermal event as a function of time and temperature. In conducting this assessment, DSC can reveal data in regards to composite system melting and phase transitions (Joseph et al., 2003; Zhang et al., 2006).

Joseph et al. (2003) conducted studies into the thermal properties of isotactic polypropylene /sisal composites containing 30% fibre aiming to detect changes in thermal behaviour on modification by chemicals. A urethane derivative of polypropylene glycol (PPG/TDI) and maleic anhydride modified polypropylene (MAPP) were used to modify sisal fibre. The aim of the modifications was to improve the interfacial adhesion between the fibre and matrix. Joseph et al.'s (2003) thermogravimetric curve results for are shown in Figure 2.22. Using a temperature range of 30–650ºC, dehydration and degradation of the natural fibre, lignin, was found to between temperatures 60–200ºC. The cellulose was almost completely decomposed at 350ºC. The polypropylene (PP) decomposed at a temperature higher than the fibre at 398 ºC. The favourable thermal properties of the composite, compared to isolated fibre or PP, is shown in the following figure. The composite system degrades later than the PP matrix and the fibre alone indicative of a higher thermal stability for the composite. Improved fibre–matrix interaction is believed to be the reason for the increased stability of the composite. Joseph et al.'s (2003) DTG curve results, as can be seen in Figure 2.23, also support the favourable thermal properties of the composite. For sisal fibres, a peak can be observed at 65ºC which represents the heat of vaporisation of water from the fibre. A second peak is observed at 350ºC which is believed to represent thermal depolymerisation of hemicellulose and cleavage of the glycosidic linkage of cellulose. A third peak is observed for sisal at 550ºC is believed to indicative of formation of tar due to further decomposition of products. For PP, at 400ºC a peak is observable believed to be indicative of degradation of PP's saturated and unsaturated carbon atoms. For the

sisal/PP composite, a minor peak at 368ºC is present believed to indicative of the degradation of cellulose, and more significant peak at 476ºC is present believed to correspond to the degradation of de-hydro cellulose. Figure 2.23 clearly shows a shift in the major peak in the sisal-PP composite highlighting the enhancement of thermal stability in composite compared to fibre and neat PP, and showing the favourable effect of the fibre/matrix interaction (Joseph et al., 2003).

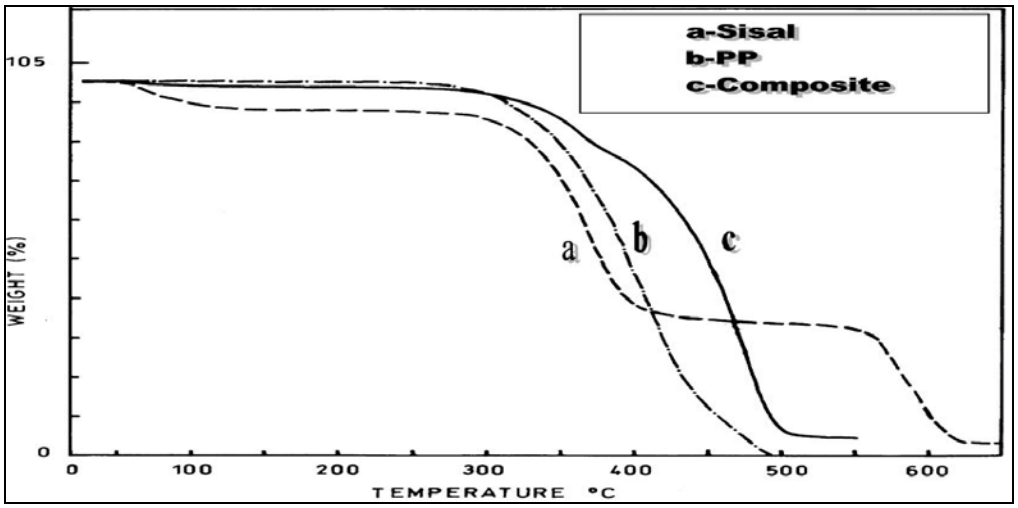

Figure 2.22: Thermogravimetric curves of (a) sisal fibre, (b) PP and (c) sisal fibre/PP composite containing 30% by wt of fibre (Joseph, et al. 2003).

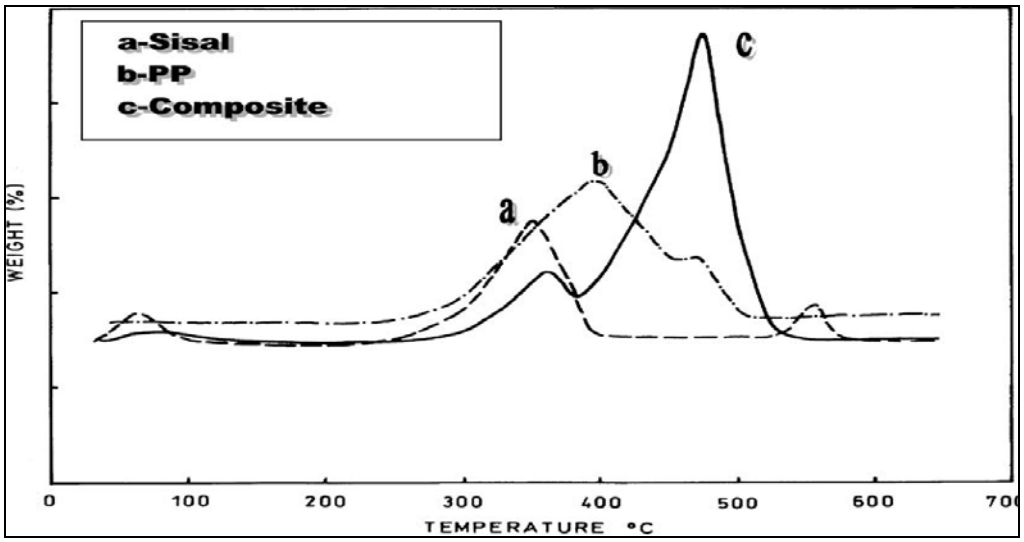

Figure 2.23: DTG curves of (a) sisal fibre, (b) PP and (c) sisal fibre/PP composite containing 30% by wt of fibre (Joseph, et al. 2003).

Joseph et al. (2003) found that the extent of degradation at a given temperature in chemically modified sisal/PP composites (fibre content, 20%) was less than that of untreated sisal/PP composite. This is shown in Figs. 2.24 and 2.25 where the shift in degradation temperature to a slightly higher region can be seen for treated composites. Joseph et al. (2003) believe that coupling agents associated with chemical modification form additional bonds between fibre and matrix and improve fibre/matrix adhesion. The esterification reaction between cellulose fibre hydroxyl groups and anhydride functionality of maleated PP was believed to be one of the reasons underpinning improved fibre/matrix adhesion in MAPP treated sisal fibre/PP composite resulting in enhanced thermal stability compared to the untreated sisal fibre/PP composite (Joseph et al., 2003).

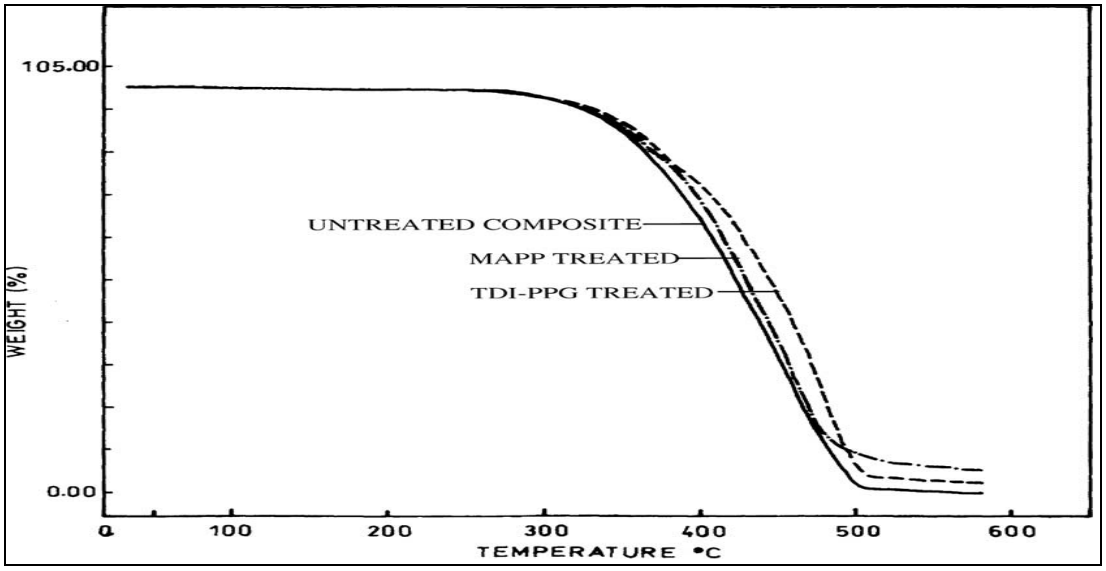

Figure 2.24: TG curves showing the effect of fibre treatment given to sisal fibre in sisal/PP composite; (a) untreated fibre composite, (b) TDI/PPG treated fibre composite and (c) MAPP treated fibre composite, fibre content, 20% by wt (in all cases) (Joseph, et al. 2003).

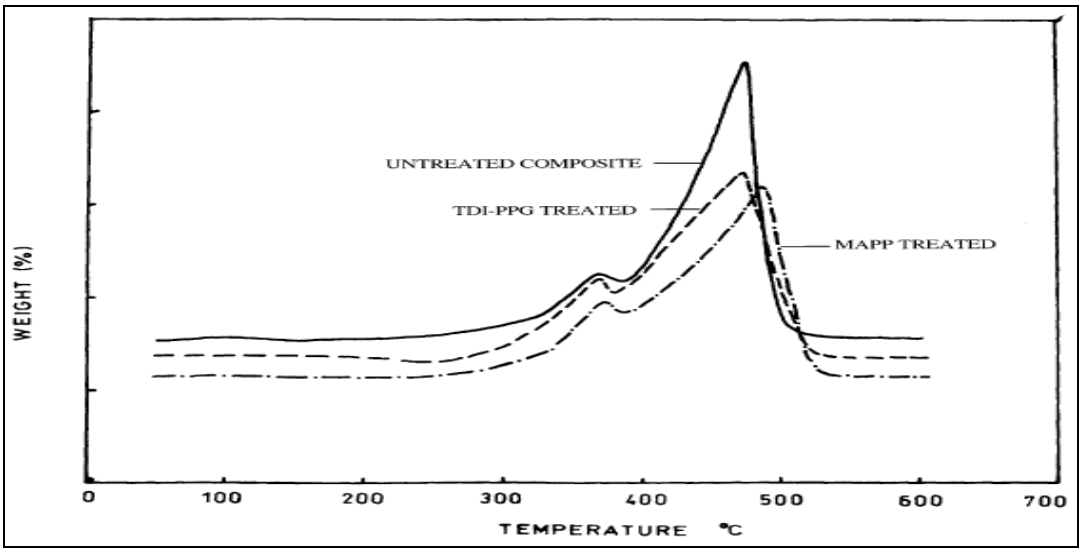

Figure 2.25: DTG curves showing the effect of fibre composite treatment given to sisal fibre in sisal/PP composite; (a) untreated fibre, (b) TDI/PPG treated, fibre composite and (c) MAPP treated fibre composite, fibre content 20% by wt (in all cases) (Joseph, et al. 2003).

De Rosa et al. (2010) investigated the thermal stability of Phormium-tenax fibres, neat epoxy, and Phormium-tenax fibre/epoxy composite containing 20 wt.% fibre. TG curves, in Figure 2.26a, show whilst the initial weight loss (~ 8%) between 37 and 130^{o}C corresponds to vaporization of water from fibres, the onset of thermal degradation for Phormium-tenax fibres occurs slightly after 200^{o}C (De Rosa et al., 2010).

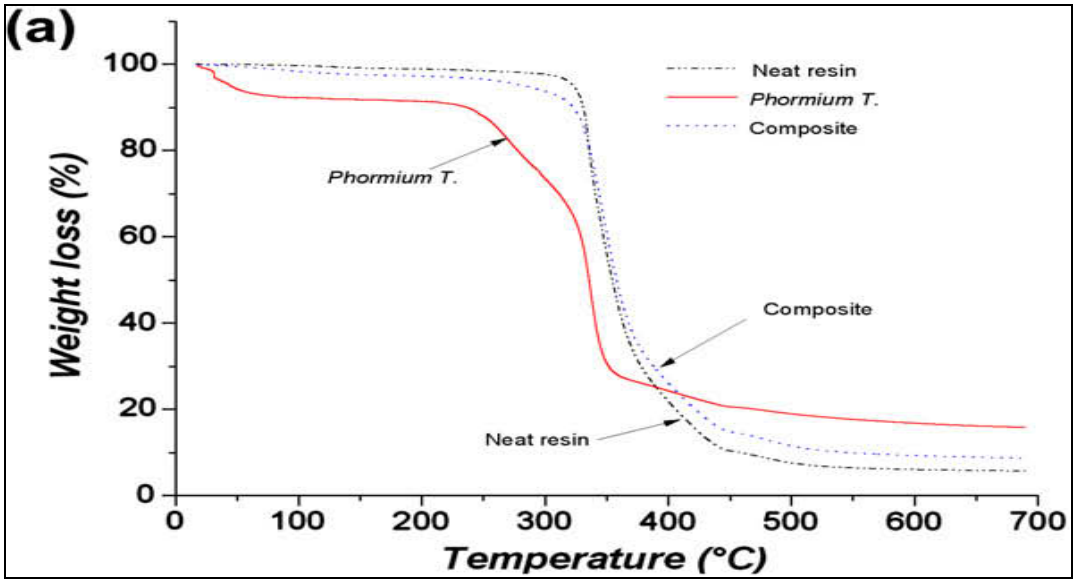

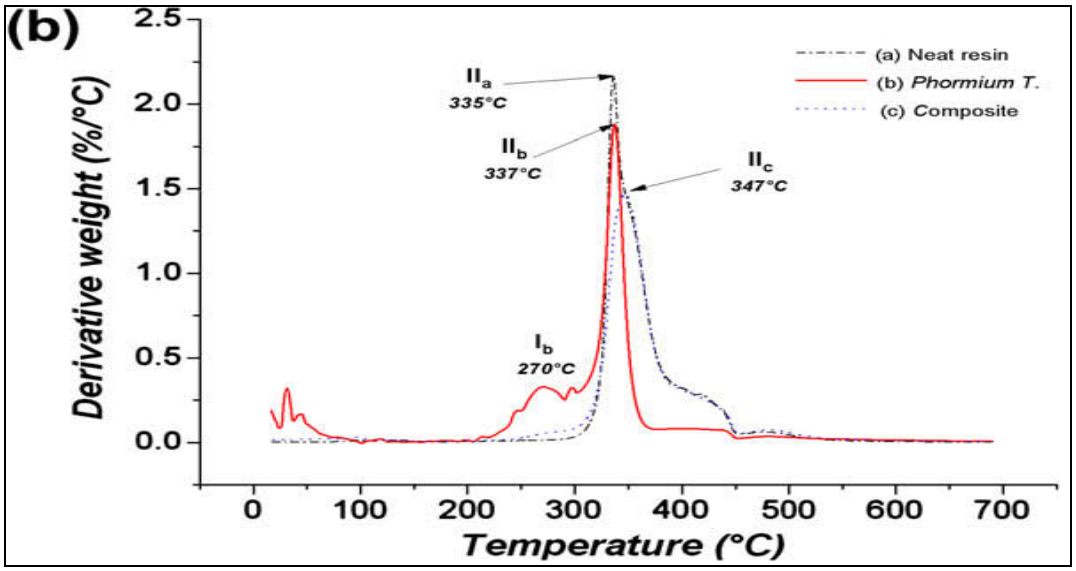

Figure 2.26: (a) TG and (b) DTG curves of neat resin, Phormium-tenax fibres, and Phormium-tenax reinforced composites (De Rosa, et al. 2010).

Thermal depolymerisation of hemicellulose, pectin, and cleavage of glycosidic linkages of cellulose is believed to be indicated in the figure between the temperatures of 200–305°C. Decomposition of a-cellulose occurs between 305-370°C. Decomposition of lignin occurs between the wide temperature ranges of 200 to 900°C. The structure of lignin having an aromatic structure with various branches is believed to be the reason for the wide range of decomposition temperatures. At 700°C, the residual weight of Phormium tenax fibres was equal to 15.7 wt.%. The DTG curves, in Figure 2.26b, reveal that at 335°C, neat epoxy decomposes. At 337°C, most cellulose decomposition occurs. At 347°C, composite decomposition occurs. These results highlight the improved thermal stability of the system fibre–matrix compared to neat epoxy and fibres further emphasising the positive effect of fibre–matrix interaction on thermal stability (De Rosa, et al. 2010).

Bakare et al. (2010) also conducted a thermal stability study with sisal fibre; this time with rubber-seed oil-based polyurethane (RSOPU) composite. The TGA results can be seen in Figure 2.27. For sisal fibre, release of moisture occurs at around 100°C. The decomposition of cellulose, lignin and hemi cellulose occurs at between 250 and 480°C. For the RSOPU, at 215°C, decomposition occurs. For sisal fibre, TGA step analysis

from 30 to 100°C revealed mass drop percentage of 3.6%. Later at 200°C, the mass drop percentage for sisal fibre was 4.2%. For RSOPU and sisal fibre/RSOPU composite, no mass drop occurred before 200°C. At 400°C, 66% of the sisal fibre had undergone degradation while at the same time temperature only 50% of RSOPU had undergone degradation. Sisal fibre/RSOPU composites had undergone 64% degradation at this temperature. At 500°C, sisal fibre had a residual weight of 25% with RSOPU and sisal fibre/RSOPU composites had only 16% and 17%, respectively. Bakare et al. (2010) concluded that the thermal stability of sisal fibre/RSOPU composites was intermediate in relation to the thermal stabilities of the fibre and pure matrix. Given the results of Josepha et al.'s (2003) and De Rosa et al.'s (2010) studies in which thermal stability of composites was greater than fibre and pure matrix attributed to fibre/matrix interaction, it is suggested that the interaction between fibre and matrix in the sisal fibre/RSOPU composite developed in this study was unsatisfactory.

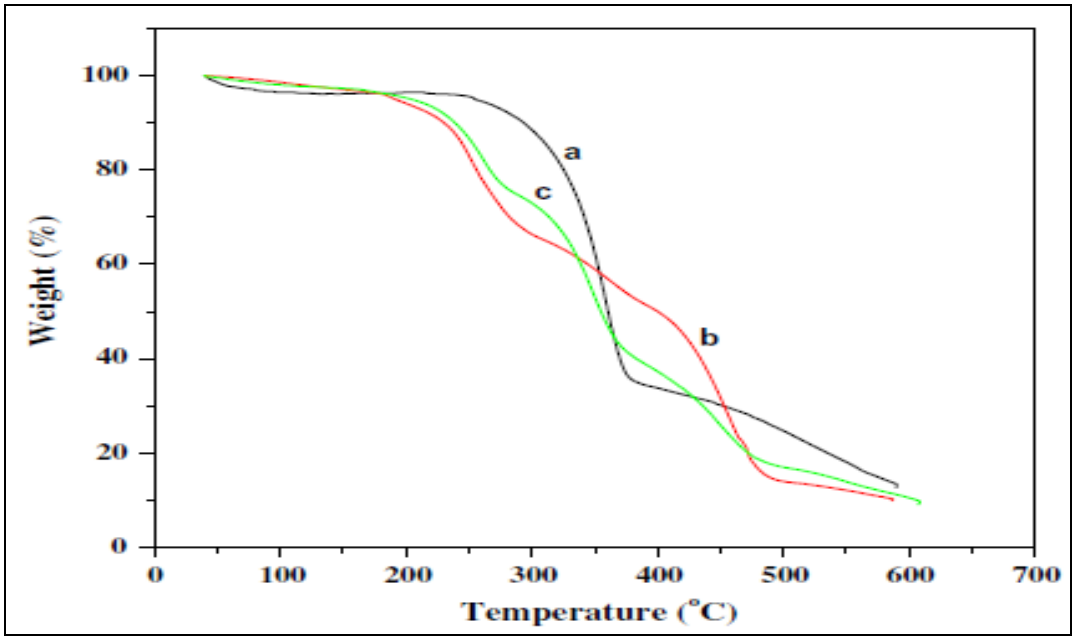

Figure 2.27: TGA curves of (a) sisal fibre (b), RSOPU and (c) sisal fibre/RSOPU composite (Bakare et al., 2010).

Yu et al. (2010) conducted studies into the thermal properties of PLA/ramie composites containing (30 wt.%) fibre aiming to detect changes in thermal behaviour on modification of the surface of ramie by silane and alkali treatments. Figure 2.28 shows

the TGA/DTG reveals at 328^{o}C thermal degradation of PLA is complete. An interesting result is that the PLA/ untreated-ramie composites enter degradation at a lower temperature compared to pure PLA, which may be due to composite process by the two-roll mill. The thermal degradation temperatures of PLA/treated-ramie composites, nonetheless, were found to be higher than the PLA/ untreated-ramie composites. The chemical bond between PLA matrix and ramie fibre is believed to be enhanced by the treatment of the surface of the fibres ultimately improving interfacial adhesion and consequently increasing thermal stability. Composites with silane-treated fibre were found to have higher thermal degradable temperature than those composites with alkali treated fibre suggesting that the chemical bond at the interface between silane-treated ramie fibres and PLA is stronger than the chemical bond formed at the interface between alkali-treated ramie fibre and PLA (Yu et al., 2010).

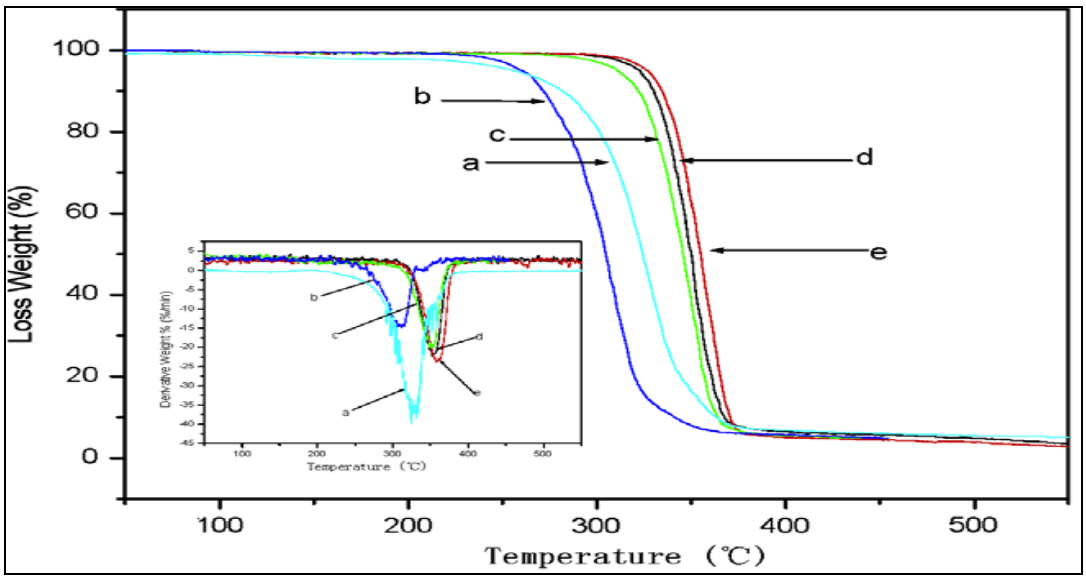

Figure 2.28: Thermogravimetric curves (inset: DTG curves) of PLA and PLA-based composites: (a) neat PLA (by two-roll mill), (b) composite with untreated fibre (c) composite with fibre treated by alkali, (d) composite with fibre treated by silane 1, and (e) composite with fibre treated by silane 2 (Yu et al, 2010).

Yu et al. (2010) also studied the Vicat softening temperature with pure PLA and its composites (Figure 2.29). While the untreated composite was found to have a lower thermal stability in TGA/DTG compared to pure PLA, here, the softening temperature of

untreated composite was found to be higher than that of pure PLA. The role in fibre in reducing polymer deformation is believed to be responsible for this result. However, the remainder of the softening temperature results were found to be in agreement with the results of TGA/DTG with all treated composites give higher softening temperature results compared to the untreated samples and treatment with silane leading to slightly higher softening temperature compared to treatment with alkali (Yu et al, 2010).

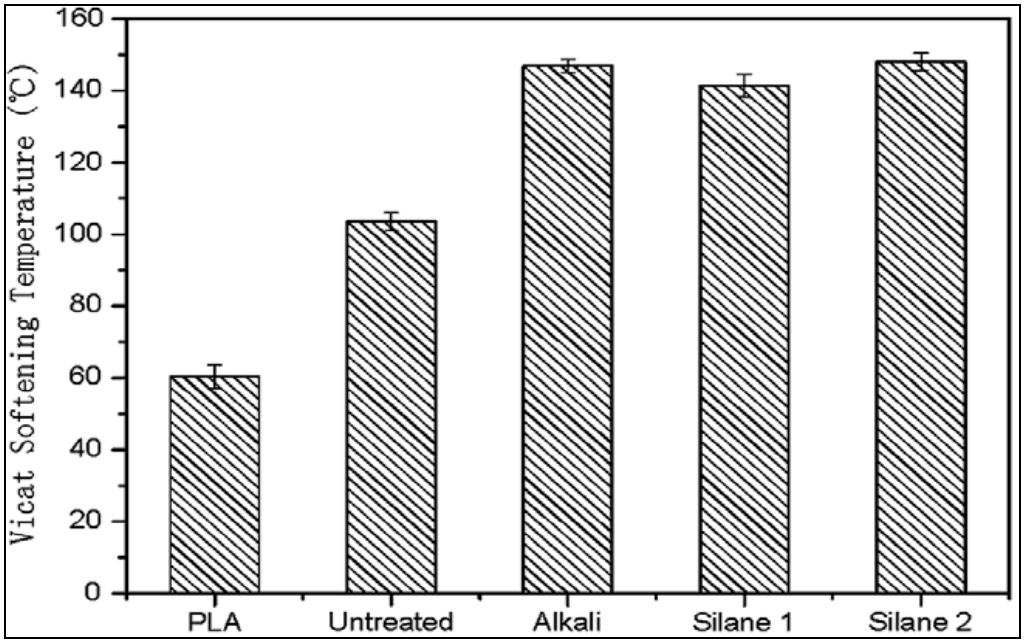

Figure 2.29: Vicat-softening temperature of neat PLA and PLA-based composites (Yu et al, 2010).

In summary, the addition of fibres to polymer matrices is almost always found improve the thermal properties of the resultant composite. Furthermore, treatment of the surface of fibres can be used to enhance the thermal properties of natural fibre polymer composites. Chemical modification using treatment of surface of fibres improves interfacial adhesion between surface of the fibre and matrix which is believe to be a principal factor leading to the enhancement of thermal properties in natural fibre composites.

2.4 Polymer Nanocomposites

2.4.1 Introduction

Polymer nanocomposites are polymer-based hybrids which contain a component with at least one nano-sized (1- 100 nm) dimension (Yong and Hahn, 2006). Nanoparticles have a large surface area to mass and therefore display extraordinary properties. These remarkable properties arise from the phase interactions which occur at the interfaces. As there is a higher surface area, there is a greater interfacial matrix interaction. In other words, polymer nanocomposites offer improved internal adhesion of the components due to a desirable aspect ratio and lesser required amounts of fillers (Rodgers et al., 2005, Yong et al., 2008, Zeng et al., 2005). The interest in polymer nanocomposites comes from the hybrid's excellent mechanical properties as well as its electrical, optical, and thermal advantages (Mallick, 2007, Pavlidou and Papaspyrides, 2008). For this reason, particularly in the past decade, polymer nanocomposites have attracted wide research and development attention. There are a number of categories of substances which can be combined with polymers. Table lists some of these substances that can be used in combination with polymers to form nano-composites.

Table 2.6: Examples of layered host crystals used in this type of composite (Gacitua et al., 2005).

Chemical nature	**Examples**
Element	Graphite
Metal chalcogenides	$(PbS)_{1.18}(TiS_2)_2$, MoS_2
Carbon oxides	Graphite oxide
Metal phosphates	$Zr(HPO_4)_2$
Clays and layered silicates	Montmorillonite, hectorite, saponite, fluoromica, fluorohectorite, vermiculite, kaolinite, magadiite
Layered double hydroxides	$Mg_6Al_2(OH)_{16}CO_3$ nH_2O; M=Mg. Zn

2.4.2. Categories of nanoparticles

All nanoparticles by definition should be less than 100nm in diameter as mentioned previously (Hussain et al., 2006). There are three categories of based on the number of dimensions in the nano-scale. The first are three-dimensional nanoparticles, i.e three dimensions in the nano-scale. Examples of three-dimensional nanoparticles include spherical and polyhedral shapes such as colloidal silica and silicon carbide. Other examples of three-dimensional nanoparticles include carbon black, silica nanoparticle, polyhedral oligomeric sislesquioxanes (POSS) (Thostenson et al., 2005). The second category is two-dimensional nanoparticles, i.e. two dimensions in the nano-scale. Examples of this include nanotubes, nanowhiskers, nanowires, nanofibres and carbon nanotubes. The third category is one-dimensional nanoparticles. These particles are usually disc-shaped, such as, clay platelets and plated-shaped items such as organosilicate (Thostenson et al., 2005, Zeng et al., 2005).

The most common forms of nanoparticles are shown in Figure 2.30. This figure highlights the geometries and surface area-to-volume ratios of each given shape. For fibres, the surface area over volume is dominated by the first terms in the equation. This is especially true for nanomaterials. As can be seen in the figure, $2/l$ and$4/l$, the second term has only a limited influence as opposed to the first term. What this equation tells us is that any change in the diameter, such as the diameter of the particle or the fibrous material, or in the thickness of the layers, moving from micro to nano-scale will result in a dramatic change in surface area-to-volume (Hussain et al., 2006, Okamoto, 2006, Schmidt et al., 2002). To date, the utilization of nanomaterials in nanocomposites most typically involves a wider group of components such as nanoparticles, fullerenes, nanofibres, nanotubes, and nanowires. These nanomaterials are currently being studied in a number of studies worldwide. The properties of the nanocomposites is ultimately influenced by firstly, the size scale of component phases, i.e. the above nanomaterials, and the degree of dispersion of these nanomaterials inside the matrix (Okamoto, 2006, Schmidt et al., 2002).

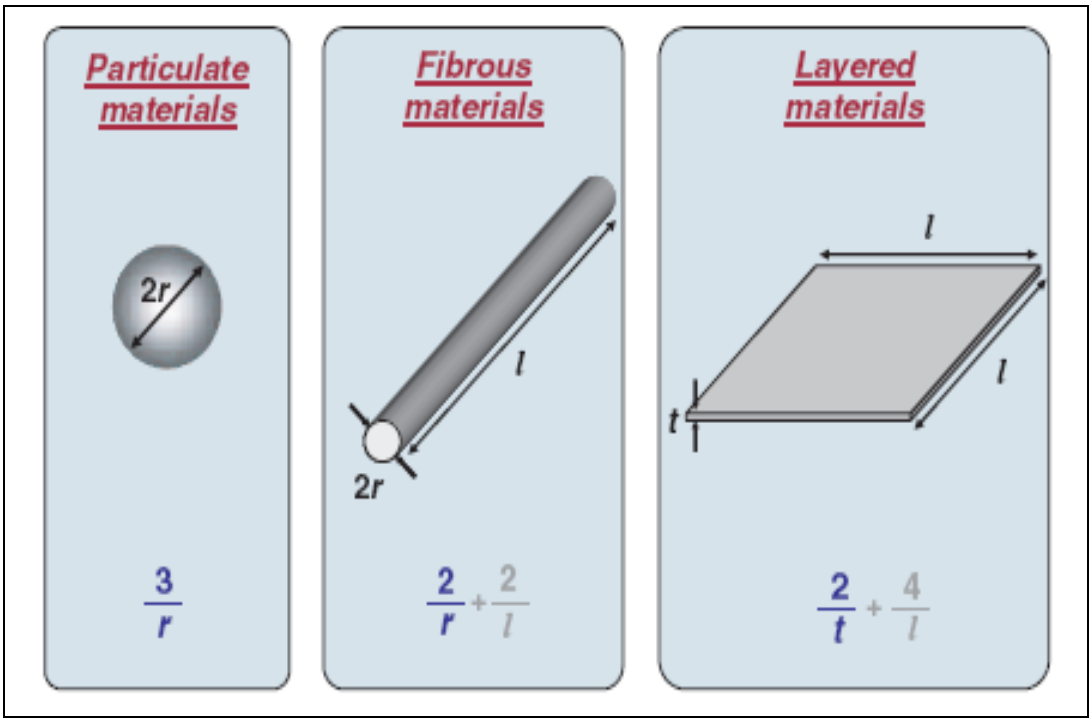

Figure 2.30: the geometries and surface area-to-volume ratios of the three categories of nanomaterials (Hussain et al., 2006).

2.5 Polymer Clay Nanocomposites

2.5.1 Introduction

In 1987, the very first work on polymer/clay nanocomposites was conducted. Soon after in the early 1990s, Toyota researchers made a number of breakthroughs with polymer-layered silicates and were first exfoliated clay with the polymer of nylon-6 (Chen and Evans, 2006). This work by the Toyota research team claiming superior improvement on strength, modulus, and heat distortion temperature, with the additional of nanoclay, led to further interest in these materials in academic, governmental, and industrial laboratories (Hussain et al., 2006, Pavlidou and Papaspyrides, 2008). The types of clays and polymers used in this process has expanded significantly including almost all engineering polymers including polypropylene, polyethylene, polystyrene,

polyvinylchloride, polylactide, polycaprolactone, phenolic resin, poly p-phenylene vinylene, polypyrrole, rubber, starch, polyurethane, polyvinylpyridine also including more commonly known polymers such as nylons (Davtyan et al., 2012, Okamoto, 2006, Paul and Robeson, 2008). Since 2006, it has been most common to use epoxies, polyurethanes, polyester, and vinyl ester (Hussain et al., 2006).

2.5.2 Structure and categories of clay

Not all clays are the same. Some clays are plate-like or disc-like, other clays are in particle-form, and others are made up of small tube-like structures. The term clay originally was used to describe substances made up of inorganic particles smaller than 2 mm with no significant crystalline content (Thostenson et al., 2005). Chemically, the mineral referred to as clay is a layered-like substance which contains hydrous magnesium and aluminium silicates. Each clay mineral contains sheets in two geometries tetrahedral and octahedral. Using this as a basis of categorization, clay minerals are divided into three categories. There is clay 2:1 type, 1:1 type, and Layered silicic acid (Zeng et al., 2005). The 2:1 type, as shown in Figure 2.31, involves only tetrahedral linking, Si-O is one example. In 2:1 type, Van der Waals consideration plays a vital role. One of the most common 2:1 type clays is Montmorillonite (MMT). This clay is considered useful due to its high surface area, which is 750m^2/g, and aspect ratio of 100 to 1000. Taxonomically, MMT is referred to as a hydrous aluminosilicate clay mineral with an expanding layered crystal structure. The layered structure contains aluminium octahedrons within two silicon tetrahedron layers. Each sheet has the thickness of 1nm and has the length of 30nm to 7microns (Choudalakis and Gotsis, 2009, Sinha Ray and Okamoto, 2003). The difference between 2:1 type clays and 1:1 type clays is the number of tetrahedral sheets to the number of octahedral sheets. When there is one tetrahedral sheet to one octahedral sheet, a 1:1 clay results. Type 1:1 clays involve clay layers made up of layers held together by hydrogen bonding. In 1:1 clay types, an aspect ratio of 1000 is possible in well-dispersed samples where no breaking of clay platelets occurs; however, commonly the aspect ratio is between 30 and 300 after shear stress and breaking. The third group as categorised by analysts is layered silicic

acids and there are at least five of these commonly used in clay/polymer composites particularly kanemite (Choudalakis and Gotsis, 2009, Zeng et al., 2005).

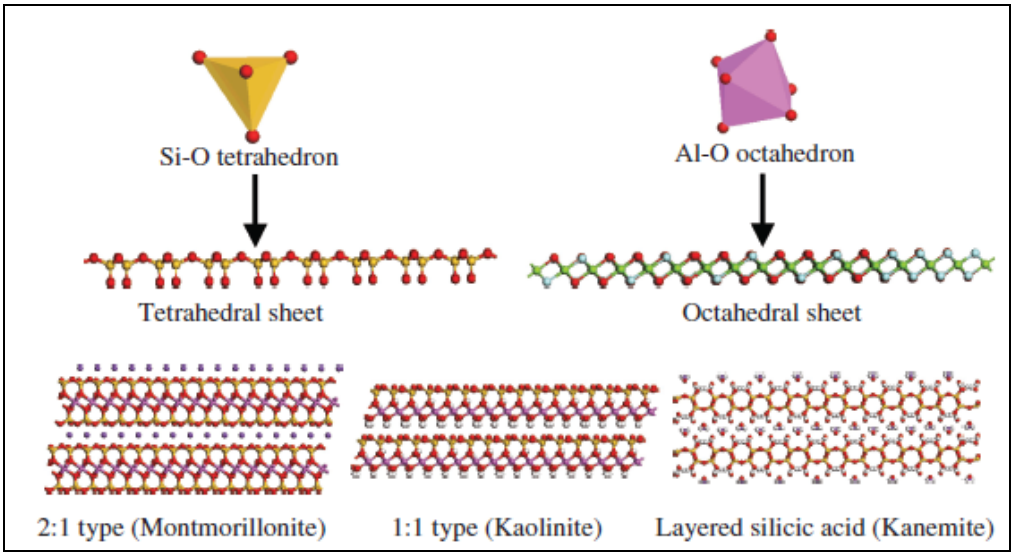

Figure 2.31: Structure of clay minerals showing 2:1 type, 1:1 type, and layered silicic acid (Zeng et al., 2005).

2.5.3 Categories of polymer clay nanocomposites

It is the extent of separation of the internal layers of clay which determines its characterization. One of the first theories of categorization is shown in Figure 2.32.

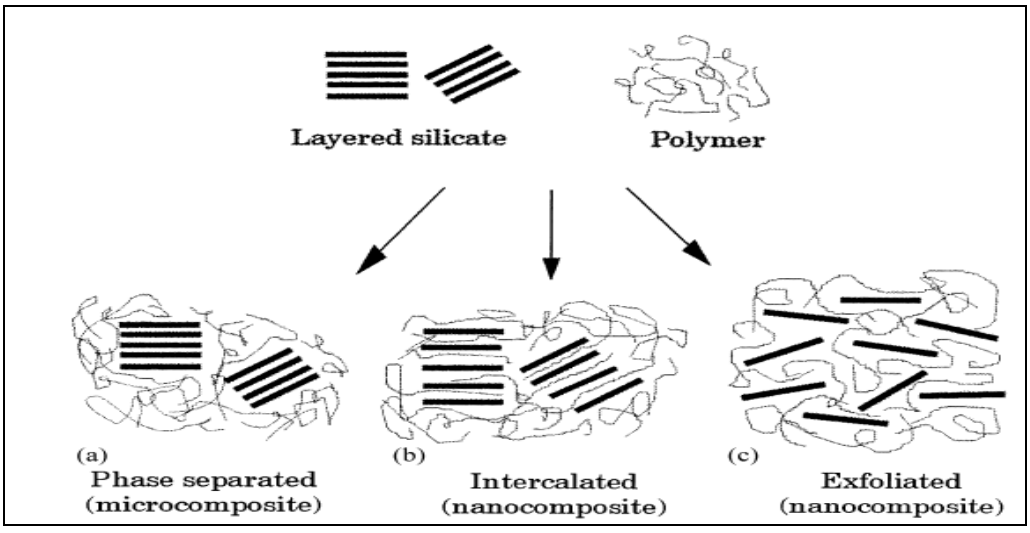

Figure 2.32: The Three hypothesized Categories of Clay-Polymers (Mittal, 2009).

Conventional composites (microcomposite), the first hypothesized group, are the hybrids which contain clay material existing in its original aggregated state with no inserting of the polymer matrix into the clay (as can be seen in the figure above). In other words, the case polymer chains are inserted into layered clays occurring in a regular fashion, a few nano-meters distance, irrespective of the ratio of polymer to layered structure (Gacitua et al., 2005). Secondly, intercalated nanocomposites occur when the mixing of polymer into the clay structure occurs in a crystallographically regular manner. Intercalated nanocomposites are characterised as having good retention of uniform spacing between the platelets, which is less than 2–3 nm separation between the platelets in this case (Powell and Beall, 2006). The third and final group was considered to be exfoliated nanocomposites. In this case, the polymer separates the clay platelets by 8–10 nm or more (Pavlidou and Papaspyrides, 2008). This category, also referred to as full exfoliation, is considered to be the best of the three due to its complete dispersion of clay plates in the polymer matrix giving the maximum improvement in properties through maximum reinforcement. Properties such as high storage modulus, increased tensile and flexural properties, heat distortion temperature, and decrease in gas permeability are noted, as well as seeing unique properties such as self-extinguishing behaviour and biodegradability (Gacitua et al., 2005, Pavlidou and Papaspyrides, 2008, Zeng et al., 2005). However, a number of studies reported that there was a fourth extent of separation, and therefore a fourth category of polymer/clay nanocomposites. This new category has been referred to by many names including partially intercalated (Thostenson et al., 2005), or partially exfoliated nanocomposites (Zeng et al., 2005), or intercalated – flocculated (Hussain et al., 2006). Numerous other researchers have also investigated the nano-structure of intercalated and exfoliated composites and the various levels of intercalation and exfoliation possible (Alexandre and Dubois, 2000). Figure 2.33(a-d) gives more information on the microscopic appearance of the different clay/polymer composite types; conventional composites (Figure 2.33a), Intercalated nanocomposite (Figure 2.33b), exfoliated nanocomposite, (Figure 2.33c), and intercalated –flocculated (Figure 2.33d).

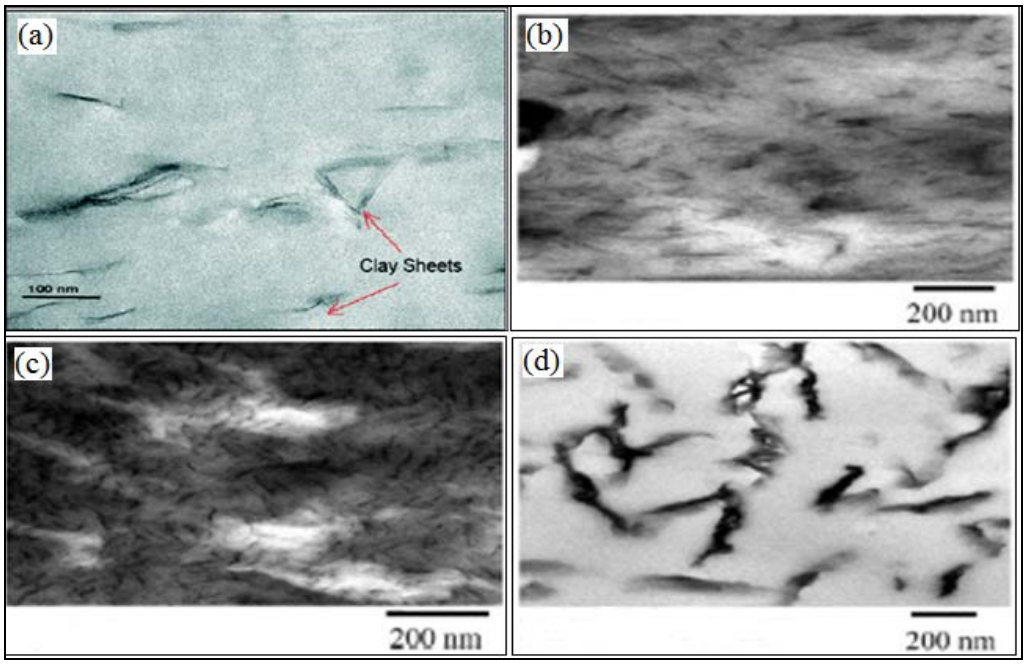

Figure 2.33: TEM image of (a) Conventional Composites (b) Intercalated nanocomposite, (c) exfoliated nanocomposite, and (d) intercalated –flocculated nanocomposite (Gacitua et al., 2005, Hussain et al., 2006).

2.5.5 Properties of polymer clay nanocomposites

2.5.5.1 Mechanical properties

Nanoclay platelets, i.e. layered silicates, are one type of filler used in polymer nanocomposites (PNC). These fillers have high moduli, and are therefore highly resistant to straining. The polymer matrix, on being embedded with these highly resistant nanoclay fillers, itself becomes restricted mechanically. What this means is that the polymer matrix, originally a softer substance, becomes strengthened as a composite, and with the filler is able to carry an increased proportion of the load (Fornes and Paul, 2003). Therefore, this means the larger the surface area of the stronger filler with the softer polymer, the greater the extent of reinforcement. Therefore, nanoclay platelets, which have an extremely high surface area ratio (approximately 800 m^2/g) give remarkable mechanical properties in modulus strength to the polymer, even when added in very small amounts (Sinha Ray and Bousmina, 2005). The first work done on

polymer nanoclay platelet composites was done by the Toyota Central Research Laboratories. The team worked with nylon 6-clay nanocomposites and found mechanical properties never seen before. Specifically, the team added uniformly dispersed nanoclay into the nylon-6 matrix. Hamidi et al. (2008) reported on the team's findings stating that addition of 4wt.% nanoclay led to an 100% increase in stiffness and a 50% increase in strength. The team also found that the tensile strength, flexural strength, tensile modulus, and flexural modulus all improved by 40%, 60%, 68%, and 126% respectively as a result of adding the nanoclay platelets (Hamidi et al., 2008). In addition to the amount of nanoclay platelet added, others have cited the dispersion and exfoliation of these fillers within the matrix as the reason for the improved mechanical properties (He et al., 2006, Hotta and Paul, 2004, Svoboda et al., 2012). Figure 2.34 shows how the tensile strength and tensile modulus both increase as the amount of nanoclay platelets increases initially. However, once the proportion of filler reaches 5%, the increase plateaus (Lee et al., 2005).

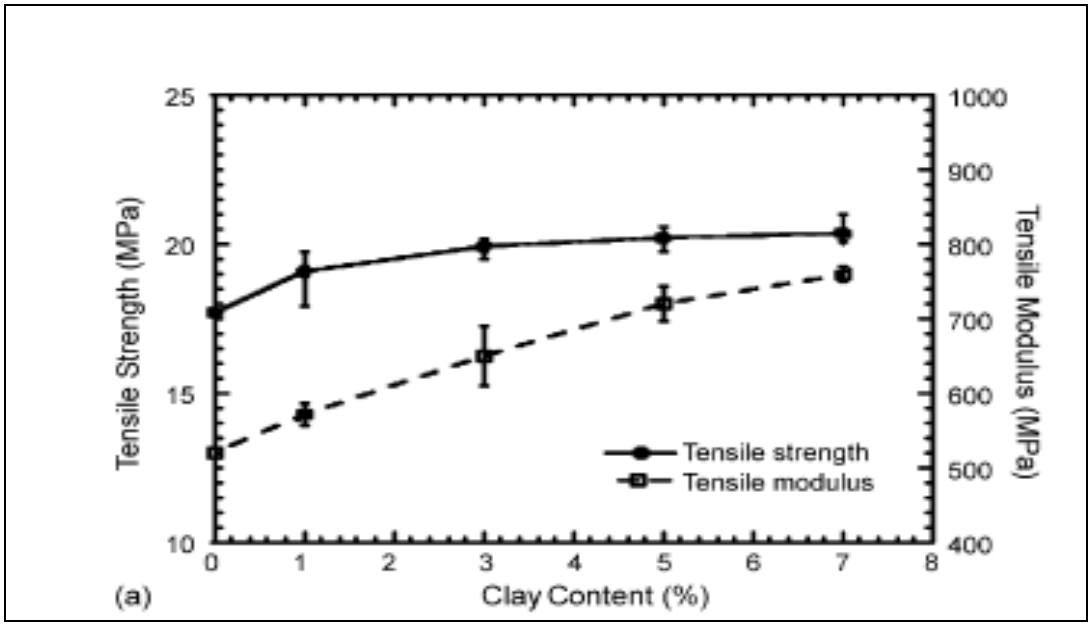

Figure 2.34: Tensile Strength versus clay platelets content (Lee et al., 2005)

Other modified forms of nanoclay platelets, namely, commercially prepared pristine montmorillonite (MMT-Na+), Cloisite 30B, and Nanomer I.30E were tested for tensile properties. It was found that an increase in nanoclay content led to an increase in tensile

properties. At maximum addition of nanoclay 10%, the maximum improvement in the tensile modules of the nanocomposites was found to be 26.9% on addition of montmorillonite (MMT-Na+), 15.1% with Cloisite 30B addition, and 12.2% with Nanomer I.30E. The improved modulus is explained by the strong stiffening effect of the clay fillers which themselves have a higher modulus than epoxy (Oi et al., 2006). Improvements in Young's modulus as result of adding nanoclay platelets to polymer matrix have also been reported by Tortora et al. (2002). The team found an increase nearly four-fold from 120 to 445MPa for a poly(ε-caprolactone) (PCL) nanocomposite on the addition of 8% ammonium-treated MMT (Tortora et al., 2002). In another study reported by Gorrasi et al. (2003), Young's modulus increased from 216 to 390MPa with the 10% addition of ammonium treated clay to the same matrix PCL (Gorrasi et al., 2003).

Another property of interest is the stress-strain behavior of reinforced nanocomposites. One study by Yasmin et al. (2006) compared the stress-strain behavior of nanocomposites reinforced with two types of nanoclay platelets commercially named Nanomer I.28E and Cloisite 30B by testing tensile loading at room temperature. What is shown in the two graphs below is that when the clay content increases, the loading of stress that the sample can withstand increases. This is shown in the two graphs below highlighting stress-strain behavior (Figure 2.35)

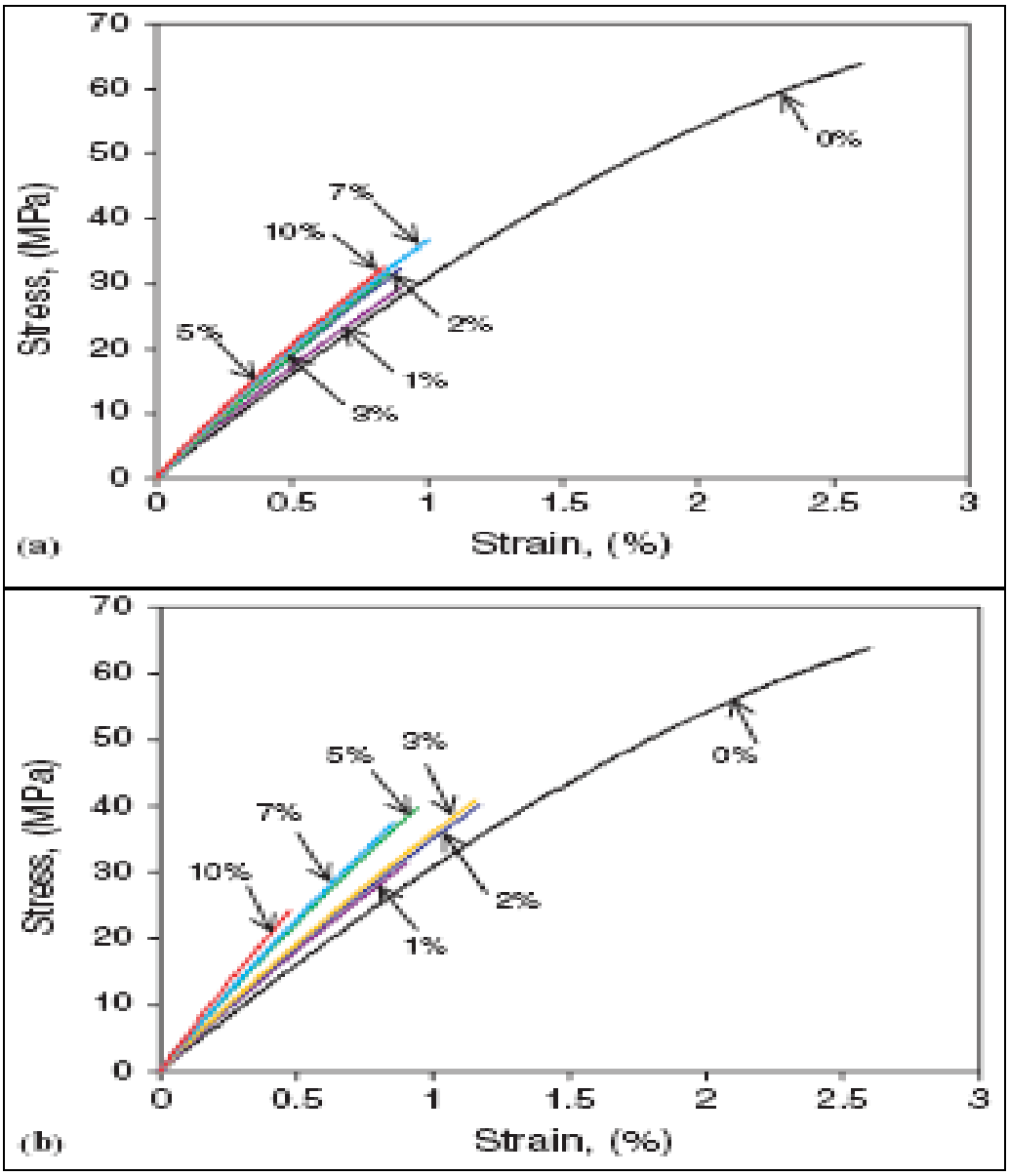

Figure 2.35: Stress- strain behaviors of two nanocomposites, (a) Nanomer I.28E/epoxy and (b) Cloisite30B/epoxy (Yasmin et al., 2006).

Yasmin et al. also studied the elastic modulus of these nanocomposites. It was found that as the clay content is increased, the elastic modulus also increased gradually as seen in figure 2.36. Yasmin and co-workers found that at lower levels such as 2wt.% clay content both Nanomer I.28E/ and Cloisite 30B/epoxy nanocomposites presented similar elastic modulus values, however, on increasing the clay content, Cloisite 30B showed a more rapid increase in elastic modulus. According to the team these results can be

attributed to a number of factors. They expect that the better mechanical properties of Cloisite 30B/epoxy over Nanomer I.28E/epoxy composites are due to the better dispersion of the nanoparticles as well as effective interfacial adhesion. In more detail, Yasmin et al. (2006) writes that it is the restricting effect of the nanoclay particles on the polymer chains within the epoxy matrix limiting mobility which leads to an increase in elastic modulus. Furthermore, the orientation of both the silicate layers of the nanoclay particles and the loading direction can contribute to the reinforcement effects, i.e. elastic modulus. Nonetheless, both Nanomer and Cloisite 30B were found to slow down their rate of modulus increase at higher clay levels such as between 8 wt.% and 10 wt.%. It is expected that this is caused by the formation platelets aggregates (Yasmin et al., 2006).

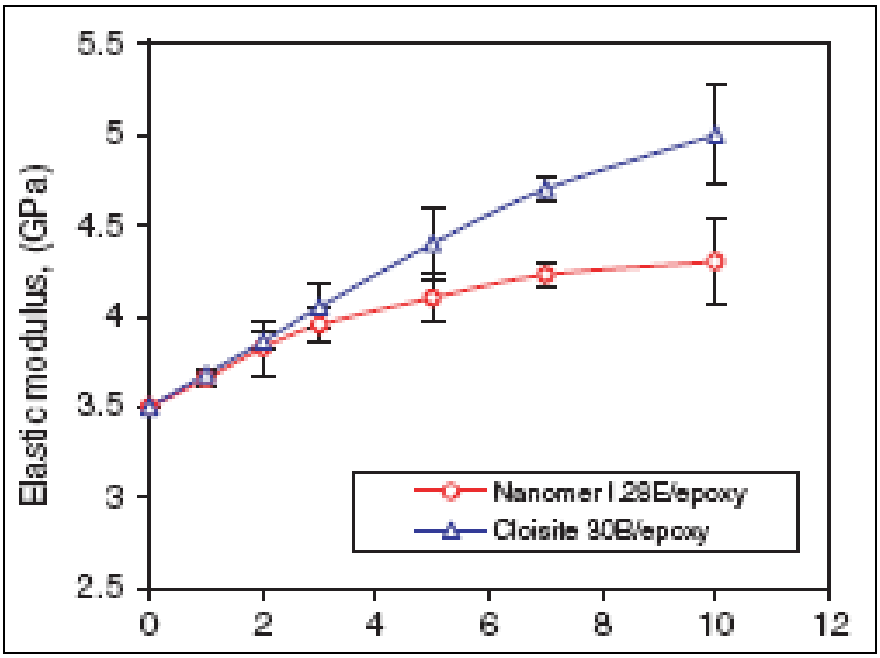

Figure 2.36: Elastic modulus versus clay content (Yasmin et al., 2006).

Thus, the majority of studies agree that the increase in nanoclay content leads to an increase in tensile properties. However, there is a clear point where the increase in modulus plateaus. Early study by Liu et al. in 1999 as shown in Figure 2.37 highlights how the increase in clay content to 10% leads to an increase in tensile strength, however, at 10% and higher, there is only a slight increase in properties. Therefore, the team concluded that 10% was the critical point. The team further explained this commenting

that lower than 10% addition of filler, the nanocomposite is likely to be completely exfoliated, i.e, uniformly dispersed, however, higher than 10%, the nanocomposite is likely to be partially exfoliated and partially intercalated (Liu et al., 1999).

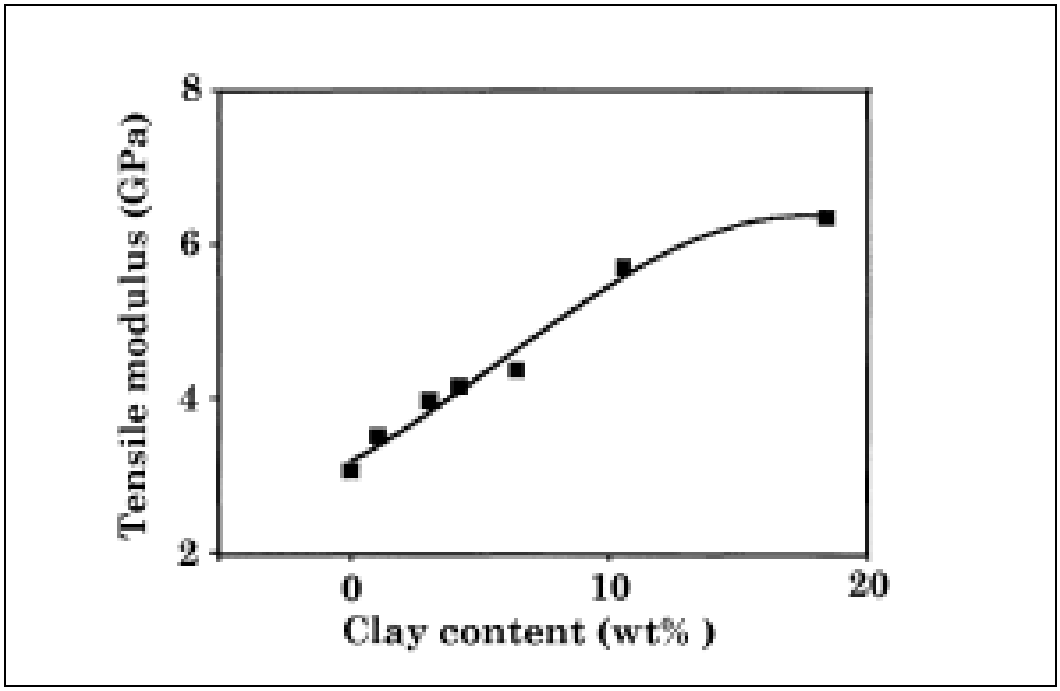

Figure 2.37: Organo-modified montmorillonite nylon-6-based nanocomposite demonstration of effect of increasing clay content on tensile strength (Liu et al., 1999).

A study by Zhao et al. (2005) supported a number of the above findings regarding the effect of increasing the amount of nanoclay platelets on tensile strength; however, it also added information regarding the changes in flexural strength and flexural modulus. Zhao et al. (2005) agreed that not only was the amount of nanoclay platelets significant to improving qualities but also the aspect ratio, and degree of dispersion contributed. Table 2.7 shows the mechanical properties of polyethylene (PE) with different concentrations of two different modified nano-clays, JS and DM. What can be seen is that the increase in nanoclay platelets, from 5%, 10% to 15%, leads to an increase in tensile strength, flexural strength, and flexural modulus. Also, something to be noted is that the overall mechanical properties of the PE/JS composites are higher than the PE/DM composites. According to the team this difference in mechanical properties can be explained by

difference in the degree of dispersion, and therefore PE/JS composites are more effective and more suitable as reinforcing materials (Zhao et al., 2005).

Table 2.7: The mechanical properties of polyethylene nanocomposites (Zhao et al. 2005)

Sample	Tensile strength (MPa)	Flexural strength (MPa)	Flexural modulus (MPa)
PE	22 ± 1.2	26 ± 1.1	710 ± 54
PE/JS5	25 ± 1.4	28 ± 0.8	780 ± 61
PE/JS10	27 ± 1.1	33 ± 2.0	1050 ± 63
PE/JS15	28 ± 1.4	38 ± 1.3	1330 ± 108
PE/DM5	21 ± 2.0	26 ± 2.1	750 ± 65
PE/DM10	23 ± 0.9	31 ± 0.9	980 ± 78
PE/DM15	24 ± 1.8	30 ± 1.2	1030 ± 99

Toughness can be increased by adding nanoclay platelets. Studies by Oi et al. (2006) using different types of silicate layers including MMT-Na+, MMT-30B, MMT-I.30E, and MMT-CPC, all found increases in epoxy toughness. MMT-Na+/epoxy was found to have a 58.3% increase in toughness. The reason for this increase in toughness in linked with the nanoclay particles ability to deflect cracks due to a higher fracture surface area. The reason for this significant increase in fracture surface area is the intercalation of clay particles and resin. According to Oi and team while uniform and complete dispersion and exfoliation leads to improved modulus, it is the stacked structure, i.e. aggregated structure of intercalated clay platelets, which leads to an improvement in toughness (Qi et al., 2006). Early, similar results were found by Liu and Wu (2002) observing toughening results with Polyamide 66 /clay nanocomposites (PA66CN nanocomposite) and the addition of nanoclay. The impact toughness (notched Izod impact strength) of PA66CN was 50% higher than that of PA66 when the clay loading was 5 wt.%. The impact toughness of the nanocomposites still higher than that of PA66, even at 10 wt.% clay content. Liu et al. (2005) also studied the toughness properties of epoxy nanocomposites. The team investigated both fracture toughness (K_{1C}) and impact

toughness (G_{1C}) properties against clay loading (Liu et al., 2005). Similarly to Oi et al. (2006), the team found that the toughness of the samples increased very closely with the clay loading until a point, 4.5 phr clay loading, when further increases in clay loading only resulted in limited increases in fracture and impact toughness.

In summary, while exfoliation is known to lead to a number of improvements in the mechanical properties of nanocomposites, intercalated dispersion of nanoclay platelets can lead to a significant improvement in toughness due to the increase in crack deflection capacity. In other words, there is a specific size range which impacts on toughness properties. The fillers needed to be larger than 0.1 μm in order to be able to deflect cracks and provide toughening through a crack-bridging mechanism. Completely exfoliated nanocomposites contain nanofillers which are not large enough to fulfill this role. Therefore, only nanocomposites with nanoparticles which are intercalated are able to present an improvement in toughness (Pavlidou and Papaspyrides, 2008, Zerda and Lesser, 2001)

2.5.5.2 Thermal properties

When studying the thermal properties of a substance, thermal stability is one of the key measures. It was the work of Toyota researchers in the early 90s which highlighted this possibility for remarkable improvements in thermal and flammability properties for polymers on the addition of nanoclay. In fact, the Toyota team found that the heat distortion temperature, HDT, of nylon 6 increased from 65^{o}C to 145^{o}C for nylon 6/clay nanocomposites (Hussain et al., 2006, Okamoto, 2006). Thermogravimetric analysis (TGA) is the most common assessment used for studying the thermal stability of polymer composites. As the name suggests, weight loss at high temperatures is measured against temperature. The weight loss stems from the production of volatile products at degradation. This degradation can either be oxidative, on exposure to air or oxygen, or non-oxidative. The addition of nanoclay platelets into polymer based samples is, most commonly, found to increase the thermal stability of the samples, as the nanoclay platelets act as an insulator to the heat as well as a barrier to the production of volatile products (Okamoto, 2006, Sinha Ray and Bousmina, 2005). However, a number

of studies have found that the maximum increase in thermal stability is achieved at a clay content of approximately 5 wt.%. On increasing the clay content higher than this, the thermal stability is not increased and can decrease (Zanetti and Costa, 2004, Zhang and Loo, 2009, Zhu et al., 2001).

Paul et al. (2003) reported that the highest thermal stability was found at just 3 wt.% and that the thermal stability decreased from that point. The TGA graph in figure 2.38 shows the weight against temperature for Poly-(L-lactide) (PLA) clay nanocomposites with a pristine sample and with different concentrations, namely, 1%, 3%, 5%, and 10%, of nanoclay platelets. In the study of Paul et al. (2003) it was found that 3 wt.% was optimal addition concentration. The team explained this by pointing to the degree of exfoliation and delamination. It was suggested that at lower filler content, namely, 1 and 2 wt.%, exfoliation occurs however, there is not enough silicate present to promote significant thermal stability improvement. At 3 and 5 wt %, it was said that there are more exfoliated silicate particles therefore providing better thermal stability (Paul et al., 2003). However, past 3 or 5 wt.%, there is too much strain on the composite geometrically, complete exfoliation is hindered, and therefore, thermal stability is reduced (Paul et al. 2003). Similar findings were reported by Phang et al. (2005) with nylon 12/organoclay nanocomposites. The team found that with additions of less than 5 wt.%, only limited thermal stability improvements but with 5% there was an enhancement of 20^{o}C.

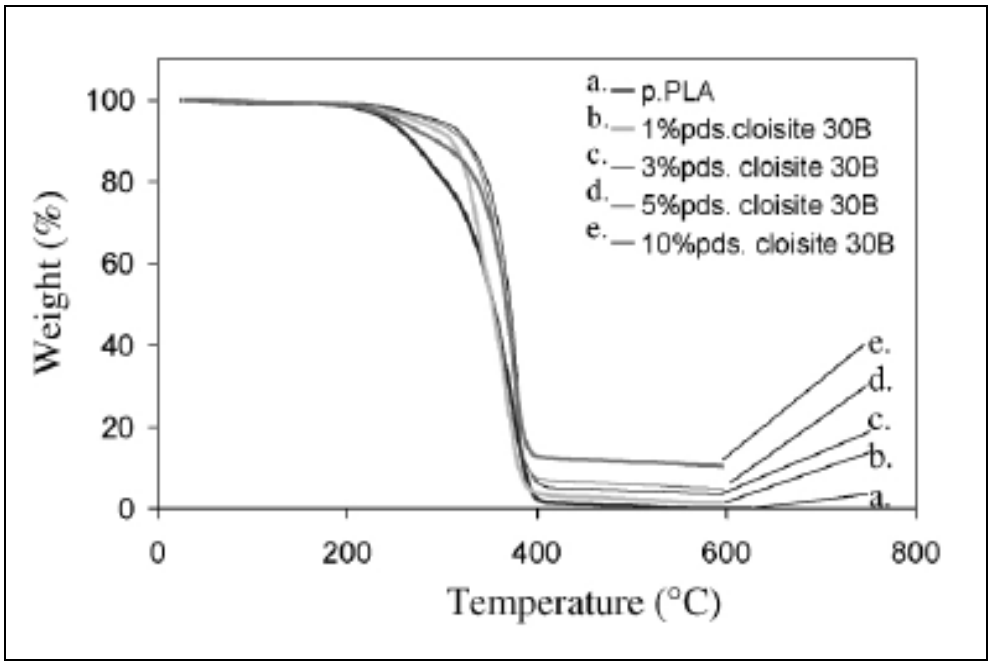

Figure 2.38: TGA (weight versus temperature) graph showing the different thermal stabilities of PLA with different concentrations of commercial nanoclay platelets, namely, Cloisite 30B 1%, 3%, 5% and 10% under exposure to heated air flow (Paul et al. 2003).

In another study by Valera-Zaragoza et al. (2006) using ethylene vinyl acetate (EVA) copolymer and Cloisite 20A it was found that the thermal stability increased as the clay content increased. As can be seen in Figure 2.39, the lower concentration such as 4% and 6% tended to retard thermal degradation more than the higher concentration of 8%. The team commented that the reason the higher concentration did not increase thermal stability was due to compatibility characteristics, morphological changes, and a reversing in layer compactness (Valera-Zaragoza et al., 2006). As aforementioned, it is the barrier properties of clay which improve the thermal stability of polymer/clay nanocomposites.

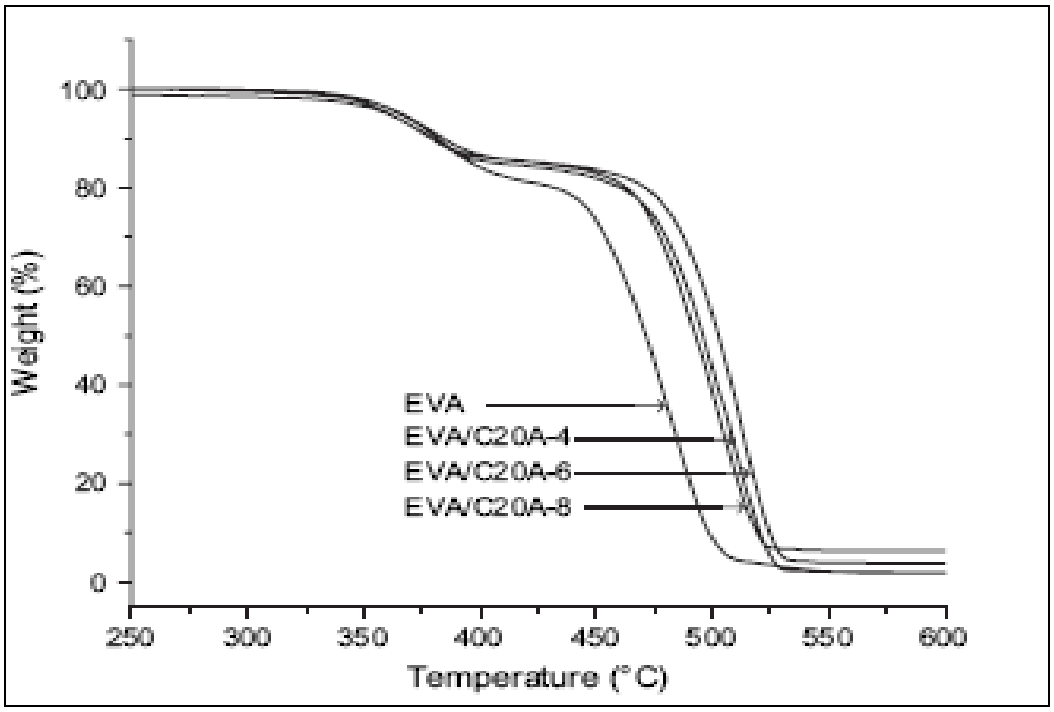

Figure 2.39: TGA curves of EVA and EVA/Cloisite nanocomposites with 4, 6 and 8 wt.% nanoclay (Valera-Zaragoza et al. 2006).

Zhao and research team (2005) studied polyethylene, PE, modified with nanoclay platelets. The team used a nitrogen atmosphere and tested the samples for both TGA and DTG (Figure 2.40). The results are displayed in the figure below. The trials involved using different amounts of nanoclay. What was found was that with temperatures exceeding 400^{o}C, the nanocomposites demonstrated much higher stability than pure polyethylene. The commencement of sample degradation was delayed with the nanocomposite samples showing a higher thermal stability. However, interestingly, Zhao and team (2005) found that it was the 2% that gave the best results. The team discussed the findings saying that while adding nanoclay always gave better results, it was adding only a small fraction, i.e, 2% which gave the best results. The addition of more nanoclay concentration than this was found to give both lower TGA and DTG results. The team explained this by saying that the clay has two effects on the polymer. The first effect is the barrier effect which gives a positive result in terms of thermal stability. However, the second effect is a catalyzing which decreases the resistance to degradation. A low addition of nanoclay gives the best chances of a uniform dispersion

while higher concentrations are more likely to result in aggregate masses amongst the composite (Zhao, et al. 2005).

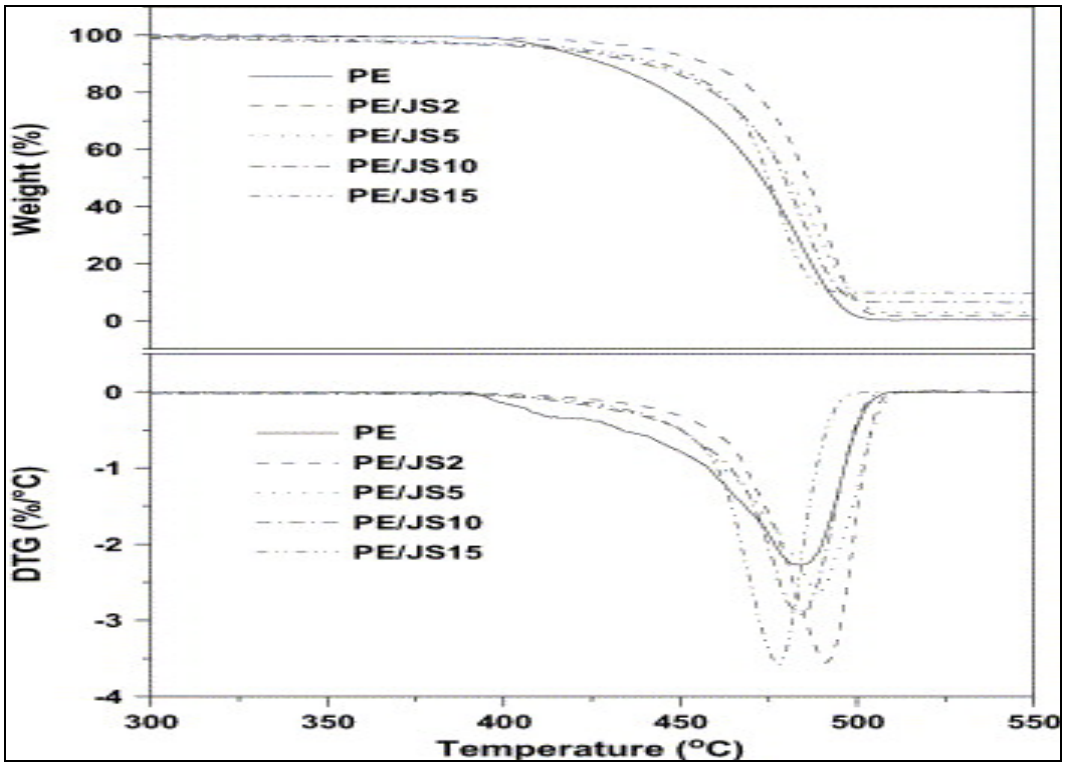

Figure 2.40: Representations (TGA and DTG curves) of the thermal properties of PE and PE/clay nanocomposites under an atmosphere of nitrogen (Zhao et al., 2005).

Another thermal property of polymers is the point of heat where the sample deforms. This measure is referred to as the Heat Distortion Temperature (HDT). Materials can withstand a certain exposure to temperature before they distort. The addition of nanoclay has been found to strengthen samples in that they less readily buckle on exposure to heat. For example, Liu et al. (2002) confirmed this finding with their studies of polyamide 66/clay nanocomposites. The pure polyamide 66 has a HDT of 75°C. Dramatically, with an addition of 1% clay, the HDT increased to 92°C. More interestingly, at a clay loading of 5%, the HDT increased to 142°C. The researchers continued with loadings of up to 10% and found a HDT of roughly 170°C. These results can be seen in Figure 2.41. According to Liu et al. (2002), HDT improvements with polymer/clay nanocomposites can be explained by the stiffness that the silicate layers

provide for the polymer phases. When the silicate is uniformly dispersed at the nano level the results are best. Similarly to the TGA results, HDT improvements in polymer/clay nanocomposites with over 5 wt.% clay loading slow down due to the formation of aggregated masses within the composite (Liu et al. 2002).

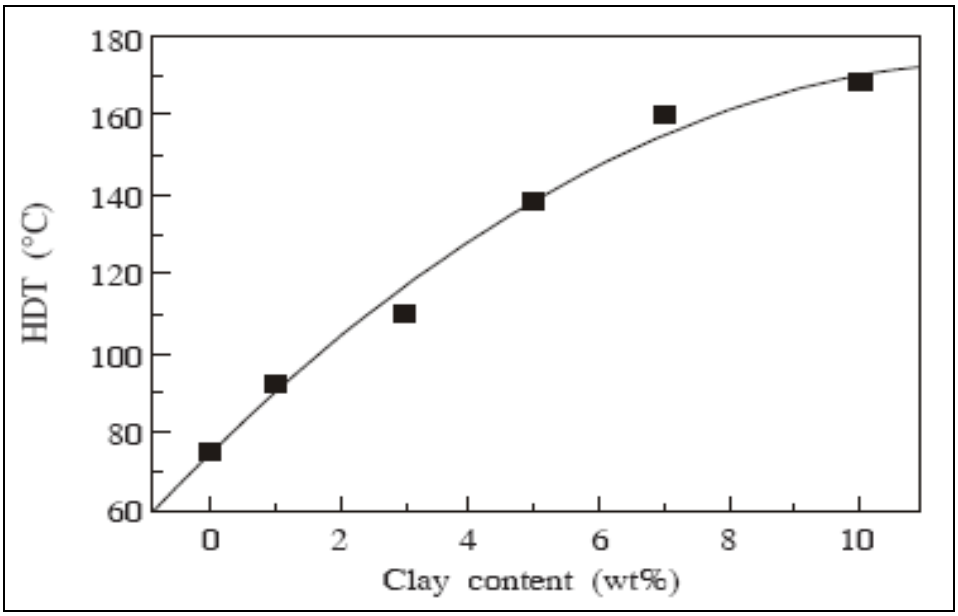

Figure 2.41: Effect of clay loading on heat distortion temperature (HDT) of polyamide 66 (Liu and Wu, 2002).

In sum up, the exfoliation of nanoclay platelets within the nanocomposite at low concentration, i.e. less than 2 wt.% is not sufficient enough to trigger the barrier benefits of clay. However, exceeding 5 wt.%, agglomeration of the nanoclay platelets becomes a problem with both intercalated and exfoliated structures present with lower the stability of the unevenly dispersed composite. Therefore, it seems that a number of studies have concurred that clay loadings between 2.5 and 5 wt.% give the best thermal stability.

2.5.5.3 Flammability properties

Flammability properties include principally flame retardant properties among other qualities. Flame retardant properties refer to the capacity for the material to avoid combustion. Cone calorimetry is method which scientists used to gather data on the flame retardant properties. This technique provides data concerning the behavior of the

material in fire-like conditions. Cone calorimetry also provides data which suggests the actual flame retardancy mechanism of the material. Cone calorimetry operates by measuring oxygen consumption. When a material combusts, there is a relationship between the mass of oxygen consumed and heat released (Beyer, 2002, Zhang et al., 2009). Typically, a cone calorimetry test involves the material being exposed a defined heat, generally, between 35 and 50kW/m^2. From this procedure, scientists measure most importantly, the heat release rate (HRR), as well as numerous other ancillary properties such as mass loss rate (MLR), mean CO yield, mean specific extinction area, peak of heat release (PHRR), time to ignition (TTI), and total heat released (THR). The HRR suggests the likelihood of rapid ignition and flame spread. If the HRR is high flame spread is anticipated to be rapid (Morgan, 2006, Zanetti et al., 2000). Research by Zhao et al. (2005) using polyethylene, PE, and PE/clay nanocomposites found that an increase in nanoclay (JS) content in PE/clay nanocomposites to 2, 5, 10, 15 phr resulted in a decrease in HRR as shown in Figure 2.42. The figure shows that after ignition, the HRR increases rapidly for the composite materials, and then plateaus. However, for the pure PE, the HRR increases more steadily yet sharply to a peak and then drops. These results from Zhao et al. (2005) suggest that the flame resistance shown by the composites is a result of a physical barrier, such as char formation. These results reinforced the assumption that an increase of nanoclay leads to an increase in fire resistance.

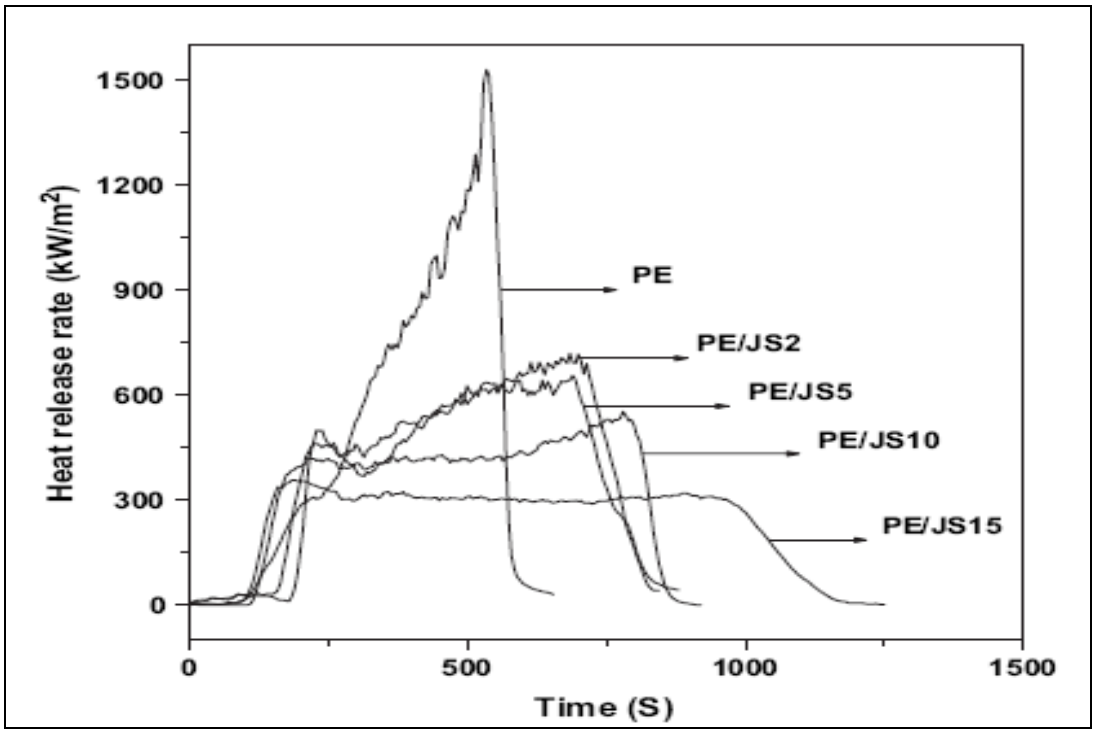

Figure 2. 42: Heat release rate (HRR) (kW/m^2) against time in seconds for five materials, PE, PE/JS2, PE/JS5, PE/JS10, PE/JS15 (Zhao et al. 2005)

Supporting this, Figure 2.43, shows the difference between a copolymer, EVA, and a nanocomposite, EVA/C20A as found in Valera-Zaragoza et al.'s (2006) study. The team found that the copolymer, EVA, alone, shown in (a.) and (b.), is more likely to drip after ignition, however, in contrast, the nanocomposite, EVA/C20A, shown in (c.) and (d.), displays no dripping after one minute of burning. This and other differences in the burning behavior of the two copolymers versus nanocomposites are said to be expected due to the flammability retardation process of the dispersed nanoclay materials (Valera-Zaragoza et al., 2006).

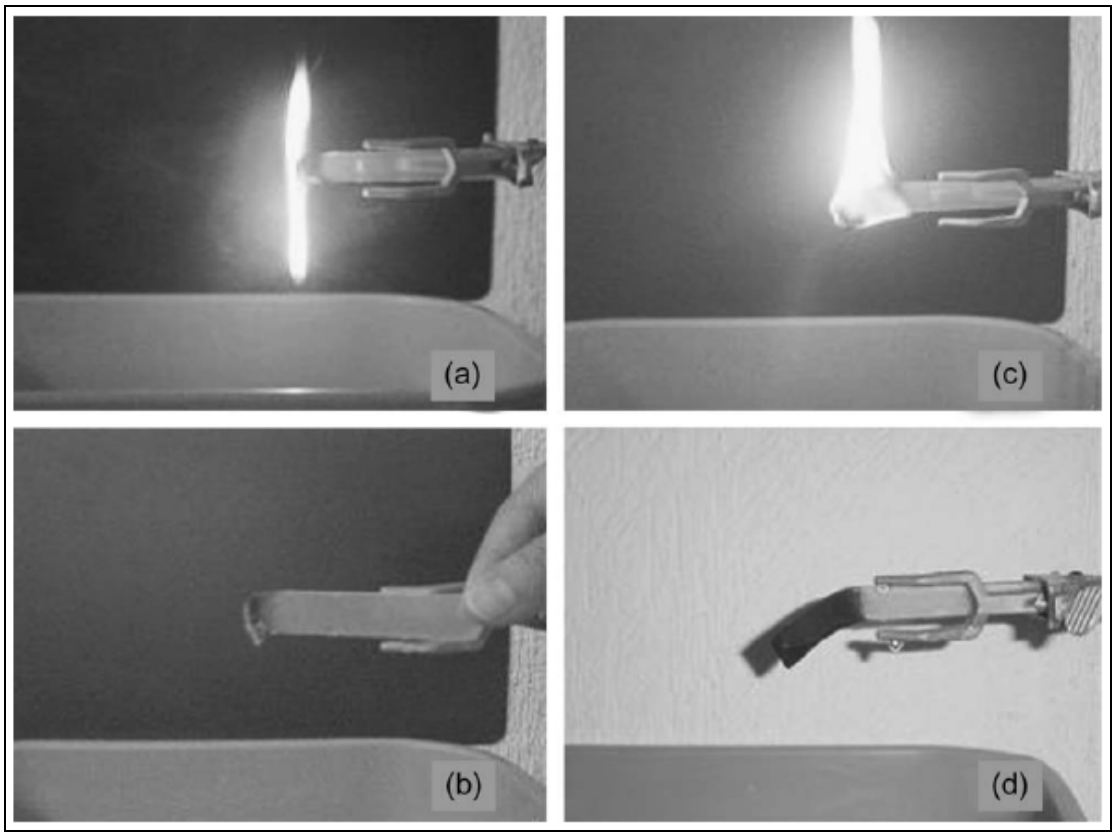

Figure 2.43, Flame retardant properties. The copolymer, EVA, alone, shown in (a.) (after 1 min burning) and (b.) (after flame extinguished), is more likely to drip after ignition, than the nanocomposite, EVA/C20A 6 wt.% organoclay, shown in (c.) (after 1 min burning) and (d.) (after flame extinguished) (Valera-Zaragoza et al., 2006).

Another example of nanoclay addition leading to decreasing burning rate is Lee et al.'s (2005) study. The effect of dispersion was discussed in this study. This study highlighted the importance of relative orientation. It was found that exfoliated nanocomposites had higher flammability resistance than intercalated nanocomposites. The researcher achieved exfoliated dispersion by adding a coupling agent. Figure 2.44, shows the burning rate versus the clay content. NC represents to the intercalated nanocomposites produced without coupling agents while WC indicates exfoliated nanocomposites. Lee et al. (2005) explain that reduction of burning rate is due to the production of char, in the exfoliated WC, which insulates the material. The specific mechanism that the researchers refer to is the building up of char on the surface of the material after ignition.

This build up creates a barrier, and this barrier, through its insulating properties, limits the diffusion of oxygen and greatly reduces the mass loss rate of the products of decomposition explain Lee et al. (2005).The researchers further explain that the char produced is of a high performance carbonaceous-silicate composition. Therefore, the researchers stress that these nanocomposites are suitable materials for use as containers of flammable materials.

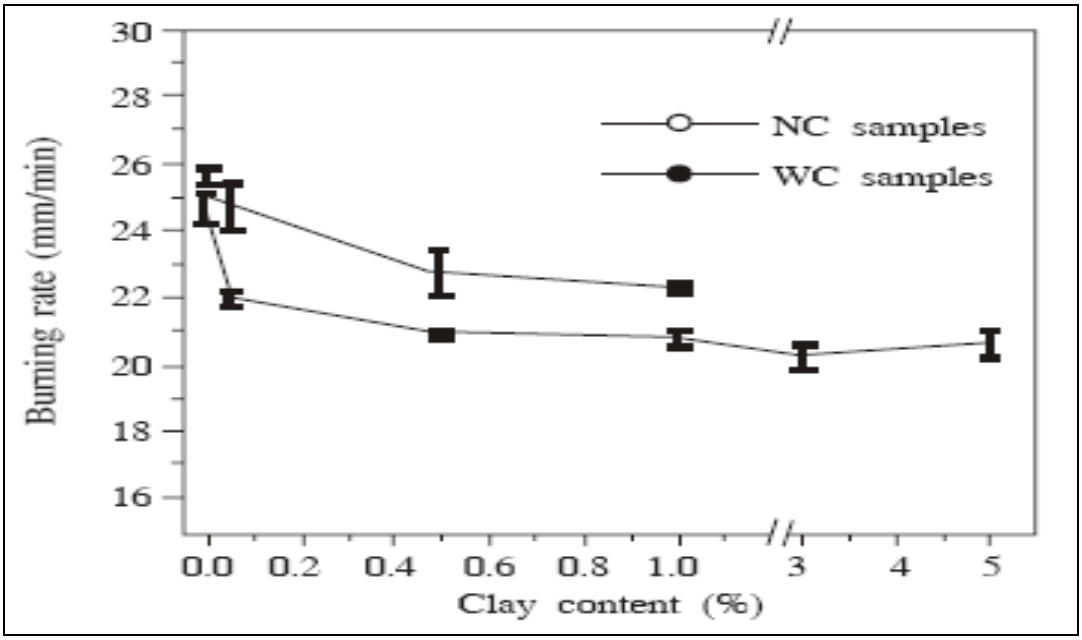

Figure 2.44: the burning rate against the clay content. NC = intercalated nanocomposites produced without coupling agents; WC = exfoliated nanocomposites produced with coupling agents (Lee et al., 2005).

2.5.5.3 Water absorption properties

The water absorption resistance of polymer clay nanocomposites is generally described as excellent. Favourable water absorption properties are due to the enhancement of moisture barriers properties provided by nanoclay platelets. Thus, excellent barrier properties of nanocaly allow the filler to have application in protective coatings, matrices for fibre-reinforced plastics used in off-shore construction, moulding compounds, electronic applications and adhesives. Still for polymer clay nanocompositets, their water absorption properties are yet to be fully exploited by

industry (Kim et al., 2005, Zeng et al., 2005). Nanoclay content, aspect ratio, and degree of silicate layer dispersion are determinants of permeability performance of polymer clay nanocomposites. As nano-clay platelets have an extremely high aspect ratio, their addition to polymer clay nanocomposites generally leads to a reduction in moisture permeability (Becker et al., 2005, Magaraphan et al., 2001). The explanation generally provided for this is that the high aspect ratio increases the tortuosity of the path of water molecules diffusing into the polymer clay nanocomposites. The tortuous path model provides that permeability is a function of nano-clay content and aspect ratio of the nano-clay platelets (Lange and Wyser, 2003, Sinha Ray and Okamoto, 2003).

In addition, the degree of dispersion of the nano-clay platelets directly affects tortuosity (Figure 2.45). In order for the degree of dispersion to be maximized, the clay itself must be highly delaminated (exfoliated). There is a positive relationship between the degree of delamination and both the aspect ratio of nano-clay platelets and the tortuosity of the path of water molecules diffusing into the polymer. In line, exfoliated (fully delaminated) polymer clay nanocomposites are preferred for their more favourable barrier properties compared to conventional or intercalated (partially delaminated) composites in terms of their barrier (Bharadwaj, 2001, Choudalakis and Gotsis, 2009).

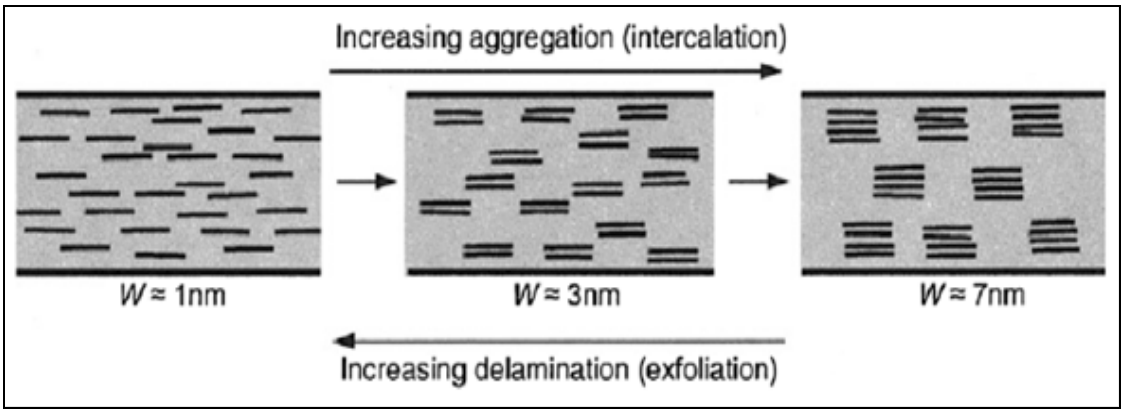

Figure 2.45: Effect of the degree of delamination on the tortuosity factor and the aspect ratio of nanoplatelets, W is the thickness of the stacks (Bharadwaj, 2001).

The concept of tortuous path is used to explain the improvement of barrier properties in polymer clay nanocomposites (Figure 2.46). The presence of impermeable nano-clay

platelets to a polymer clay nanocomposite forces permeating water molecules to wiggle around these platelets. Thus, the formerly straight path becomes tortuous

.

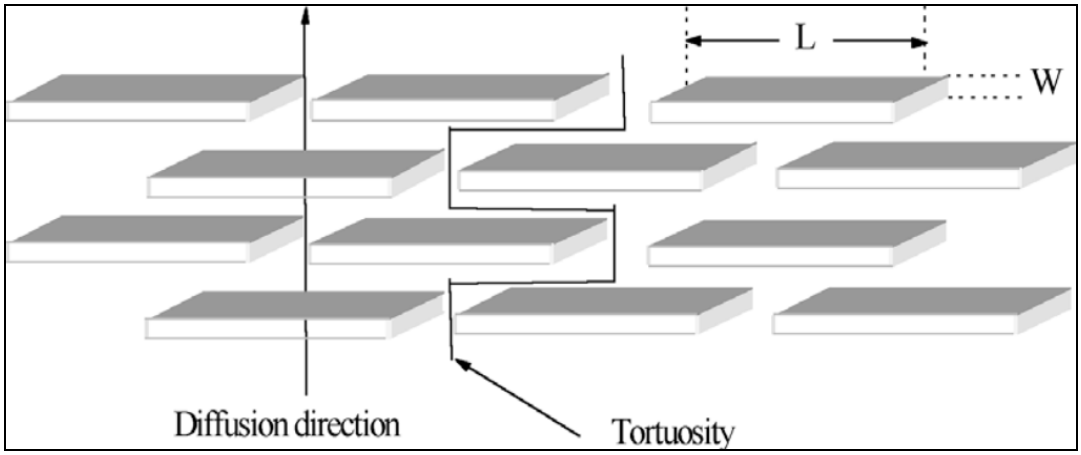

Figure 2.46: The torturous diffusion path in an exfoliated polymer–clay nanocomposite (Choudalakis and Gotsis, 2009).

Tortuosity factor can be defined as the ratio of actual distance, *d*', that a penetrant must travel against the shortest distance *d* travelled in the absence of barriers. Tortuosity factor is expressed in terms of length *L*, width *W* and volume fraction of nanoplatelets ϕ_s as follows (Sinha Ray and Okamoto, 2003):

$$\tau = \frac{d'}{d} = 1 + \frac{L}{2W}\phi_s \tag{2.7}$$

From the expression the advantage of a sheet-like morphology is its efficiency in maximizing the path length, due to its larger length-to-width ratio compared to other filler designs. The effect of tortuosity on permeability, according to the model proposed by Nielsen can be expressed as (Pavlidou and Papaspyrides, 2008):

$$\frac{P_{PCN}}{P_P} = \frac{1-\phi_s}{\tau} \tag{2.8}$$

where P_{PCN} represents the permeability of the nanocomposite, and P_P represents the permeability of the pure polymer, and ϕ_s is the clay content (Sinha Ray and Bousmina, 2005). The equations were developed to model the diffusion of small molecules in conventional composites. Nonetheless, they have also been used effectively in reproducing experimental results for relative permeability in polymer layer silicate nanocomposites. Discrepancies between experimental data and theoretical lines are attributed either to model inadequacies or to incomplete particle orientation within the nanocomposite film plane. The assumption of the Nielsen model is that the sheets are placed in an arrangement so that the direction of diffusion is consistent to the direction of the sheets. This arrangement results in the highest tortuosity, and therefore any deviation would lead to deterioration of barrier properties (Hotta and Paul, 2004, Pavlidou and Papaspyrides, 2008).

The Nielsen equation, the Cussler formula, the Barrel formula, the power law equation, and the other phenomenological relations that are based on the tortuous path theory are all grounded on the assumption that the presence of nanoparticles does not affect the diffusivity of the polymer matrix. Experimental observations do not necessarily support this. They often demonstrate that molecular mobility in a polymer matrix, closely connected to mass transport properties, is diminished by clay incorporation. Such reduction should be accompanied by a decrease in diffusivity of small molecules. This is not considered in the concept of tortuous paths (Pavlidou and Papaspyrides, 2008).

As discussed in section 2.3.3.3, moisture diffusion experimental data for neat polymer resin suggests behavior is almost Fickian. Nonetheless, it is erroneous to make generalizations based on Fick's law, as in situations diffusion behaviour is anomalous. In other words, moisture mobility within the composite material obeys neither Ficks law coefficient nor the exponent value. Glassy polymers are one example where this behaviour is observed. Ficks law predicts that diffusion rate will be small compared to the mobility of the polymer segment. In the non-Fickian state, viscosity of polymers, microcracks, and leaching from composites can all lead to a higher rate of polymer

segment mobility. This is when compared with the diffusion rate into the composites (Alhuthali et al., 2012, Liu et al., 2008a, See et al., 2009).

There are other models that take into consideration those variables to obtain valid diffusion behaviour predictions. The Langmuir Model for diffusion (LMD) is one of these models. This model assumes that diffusion of water molecules inside composite materials consist of both mobile and bound phases (Liu et al., 2008b). The Langmuir Model equation is as follows:

$$\frac{M_t}{M_\infty} = 1 - \frac{\gamma}{\gamma+\alpha} e^{-\alpha t} - \frac{8}{\pi^2} \frac{\alpha}{\alpha+\gamma} \sum_0^\infty \frac{1}{(2n+1)^2} \exp\left\{ -\left[\frac{\pi(2n+1)}{2l} \right]^2 Dt \right\} \tag{2.9}$$

The key variables for this model are (γ), the trapped molecules probability per unit volume at a given time and place in a polymer (c_t) and (α) the mobile molecules probability per unit volume, at a certain time and place in the polymer (C_t) (Gurtin and Yatomi, 1979). At the equilibrium, when trapped molecules become mobile molecules, the relation is as follows:

$$\gamma c_\infty = \alpha C_\infty \tag{2.10}$$

The Diffusion with Time Varying Diffusivity (DTVD) is another model (LaPlante et al., 2008). In this model, diffusion can be obtained by analogy of a relaxation modulus for the viscoelastic model. Comparing the DTVD model with Fick's model, the time decreasing function replaces a diffusion coefficient constant, and can be expressed as follows:

$$\frac{M_t}{M_\infty} = 1 - \sum_0^\infty \frac{8}{(2n+1)^2 \pi^2} \exp\left\{ \frac{-(2n+1)^2 \pi^2}{4l^2} \left[D_0 t + \sum_{r=1}^m D_r \left[t + \tau_r \left(e^{-t/\tau_r} - 1 \right) \right] \right] \right\} \tag{2.11}$$

To study the kinetics of moisture absorption in composite materials, other models have been proposed. The Barrier Model assumes diffusion in fillers is parallel to the surface, and that composite permeability is dependent on the aspect ratio of the filler consisting

of an average face length (L) and an average thickness (W). At a certain clay loading, other parameters are related to volume fraction of the polymer (υ_p) and the fibre (υ_f). This model gives the permeability ratio between the polymer (P_u) and the filler (P_f) (Alexandre and Dubois, 2000, Pavlidou and Papaspyrides, 2008):

$$\frac{P_f}{P_u} = \upsilon_p + \left(\frac{L}{2W}\right)\upsilon_f \tag{2.12}$$

From the previously described formulae and assuming a uniform distribution of aligned and exfoliated clay platelets, another model, the Diffusion Model for Exfoliated Nanocomposite (DMEN), is written as follows (Liu et al., 2008b, Sun et al., 2008):

$$\frac{D_n}{D_m} = \frac{1}{\left(1 + \frac{2\xi\upsilon_c}{3\pi}\right)^2} \tag{2.13}$$

where D_n is the diffusivity of the nanocomposite at random orientation, D_m the diffusivity of the matrix, and υ_c is the volume fraction of the composite. When nanocomposites are considered to be intercalated nanocomposites, they will consist of agglomerates with n platelets. This diffusion model is based on a similar formula as equation (2.13), but includes the number of platelets, n, as follows (Liu et al., 2008b, Sun et al., 2008):

$$\frac{D_n}{D_m} = \frac{1}{\left(1 + \frac{2\xi\upsilon_c}{3n\pi}\right)^2} \tag{2.14}$$

A number of studies have investigated the water absorption behaviours of polymer clay nanocomposites. For example, Liu and Wu (2002) recorded the water absorption curves of pure Polyamide 66 (PA66) and corresponding nanocomposites. The pair found that with increasing clay content, water absorption at saturation decreases from 7.6% for pure PA66 to 5.2% for 5 wt.% clay nanocomposite. This reduction was attributed to the presence of immobilized polymer in the amorphous phase. However, at loadings greater

than 5 wt.%, decreases in saturation amounts of water were less clear. The team attributed this to the aggregation of silicate layers. Moreover, with increasing clay loading, the diffusion coefficient values were found to decrease. Again, the amplitude of the decrease was slower when clay loading exceeded 5 wt.% (Liu and Wu, 2002)

Becker et al. (2004) studied the water uptake of nanocomposites made by the direct mixing. Three different epoxy resins, diglycidyl, ether of bisphenol A (DGERA), triglycidyl p-amino phenol (TGAP), and tetrafunctional tetraglycidyldyldiamino (TGDDM) were used in the study. The epoxy resins of three different functionalities were mixed with I.30E organoclay to prepare the sample nanocomposites. While clay loading of 2.5% and 5% reduced the equilibrium water uptake at 80 ºC for all samples, at 10% loading no further reduction was observed. This change can be attributed to aggregation of the nanoclay. The results revealed that compared to the pure epoxy system, at 10% clay loading, the equilibrium water uptake at 80ºC was reduced by 4.76% for DGEBA, 9.74% for TGAP, and 4.76% for TGDDM. Therefore, nanoclay concentration did not correlate proportionally with the reduction in equilibrium water uptake, or the increase of diffusivity; thus, this may depend on the type of epoxy systems (Becker et al., 2004).

Liu, et al. 2005 studied the water uptake properties of epoxy/clay nanocomposites fabricated with direct mixing (DM) and high pressure mixing (HPM). Tested in different temperatures (23, 50, and 80 ºC), and different clay loadings (0, 1.5, 3, 4.5, 6, and 7.5 phr) the results revealed that all curves exhibit a similar trend and demonstrated good agreement with Fick's Law. The maximum water absorption results of the nanocomposites decreased with increasing clay loading for all nanocomposites at the three environment temperatures. However, at 23 ºC, the HPM fabricated nanocomposites at high clay loading did not reach full saturation. Moreover, as the environment temperature rose, the curves did not completely obey Fick's law. At lower temperatures the diffusion coefficients of materials are lower than those at higher temperatures. At lower temperatures, the nanocomposites did not reach full saturation. This is due to the tortuosity effect caused by impermeable clay platelets being coupled with a low diffusion coefficient mandating a tortuous pathway for slower moving water

particles to enter the nanocomposites. In contrast, at higher temperatures, water particles move more readily and thus the result is nanocomposites much closer to full saturation. Furthermore, the results show nanocomposites fabricated with HPM exhibit lower water absorption than nanocomposites fabricated with DM. This suggests that nanocomposites fabricated with the HPM method have preferable dispersion of nanoclay. This favourable dispersion mandates higher tortuosity, and thus lower water absorption is observed (Liu et al., 2005).

2.6 Polymers Halloysite Nanotube Nanocomposites

2.6.1 Introduction

Halloysite nanotubes (HNTs) are a naturally-occurring clay mineral. In 1826, Berthier first reported HNTs as a dioctahedral 1:1 clay mineral of the kaolin group (Du et al., 2010). Structurally, HNTs have a unique crystal structure which is primarily in the form of hollow tubular nano-structures giving HNTs useful low density of hydroxyl functional groups (Ismail et al., 2008). HNT's structure means that they are highly applicable as a filler not requiring exfoliation, dispersing easily in polymer matrices even at high loading. Epoxy resins, polypropylene, polyamide polyvinyl alcohol, styrene rubber, and other polymers tend to demonstrate marked improvements in mechanical and thermal properties as a result of reinforcement effect of HNTs addition. Despite rapid commercial interest, HNTs can be inexpensively mined as a raw material from soils in most countries (Pasbakhsh et al., 2010).

2.6.2 Structure and categorized of halloysite nanotubes

HNTs are alumino-silicate clays ($Al_2Si_2O_5(OH)4.2H_2O$). While HNTs are similar to kaolin with the latter having a stacked plate-like structure, HNTs' unique structure provides a higher aspect ratio (Joussein et al., 2005). The presence of interlayer water in HNTs, whether current or historical, is an important feature differentiating HNTs from kaolinite. During the process of dehydration, d_{001} spacing of HNTs irreversibly shifts from 10 to 7 Å (Marney et al., 2008). Thus, HNTs can be classified into hydrated HNTs, those with a crystalline structure of 10 Å d_{001} spacing, and dehydrated HNTs, those with

7 Å d_{001} spacing (Hashemifard et al., 2011). HNTs contain inner and outer hydroxyl groups. Due to HNTs' multilayer structure, inner hydroxyl groups are more numerous than hydroxyl groups located on the HNT's outer surface. This outer surface is composed of O–Si–O groups predominantly as is shown in Figure 2.47.

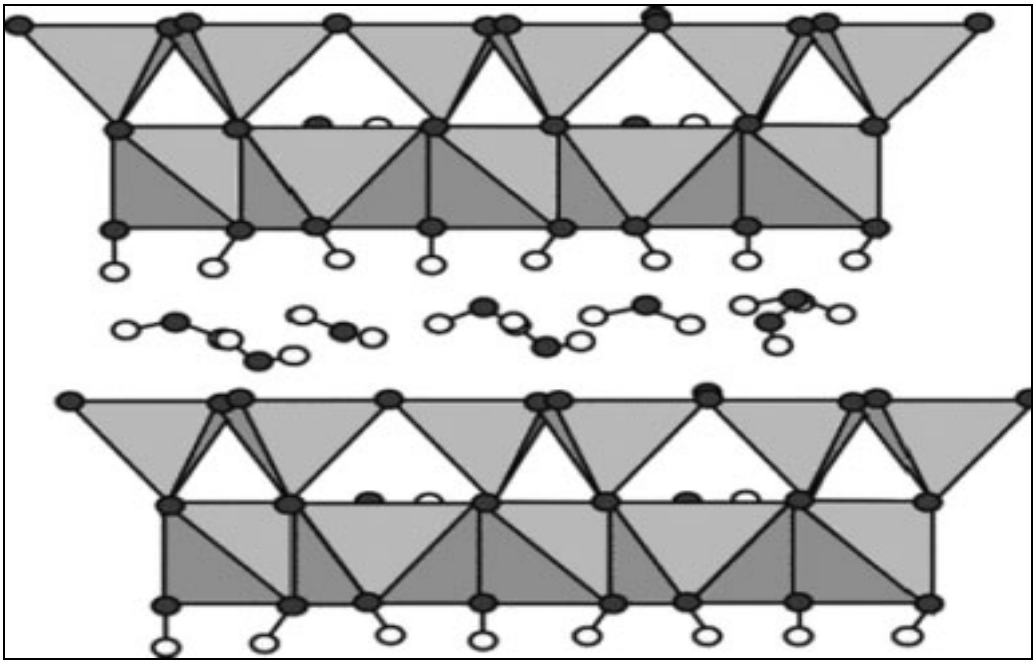

Figure 2.47: Crystalline structure of HNTs (Du et al., 2010).

A Fourier transform infrared spectrum confirms this surface due to the characteristic strong absorption of O–Si–O (1030 cm^{-1}). Thus, the density of surface hydroxyl groups of HNTs is much smaller compared with kaolinite and montmorillonites (Du et al., 2008). The average thickness of the walls of the HNTs is between 10 and 40 nm with 0.725nm basal spacing. The interlayer surfaces of HNTs are the Al–OH group inside tubes and the Si-O (siloxane) group of external surfaces as can be seen in figure 2.48 (Pasbakhsh et al., 2010).

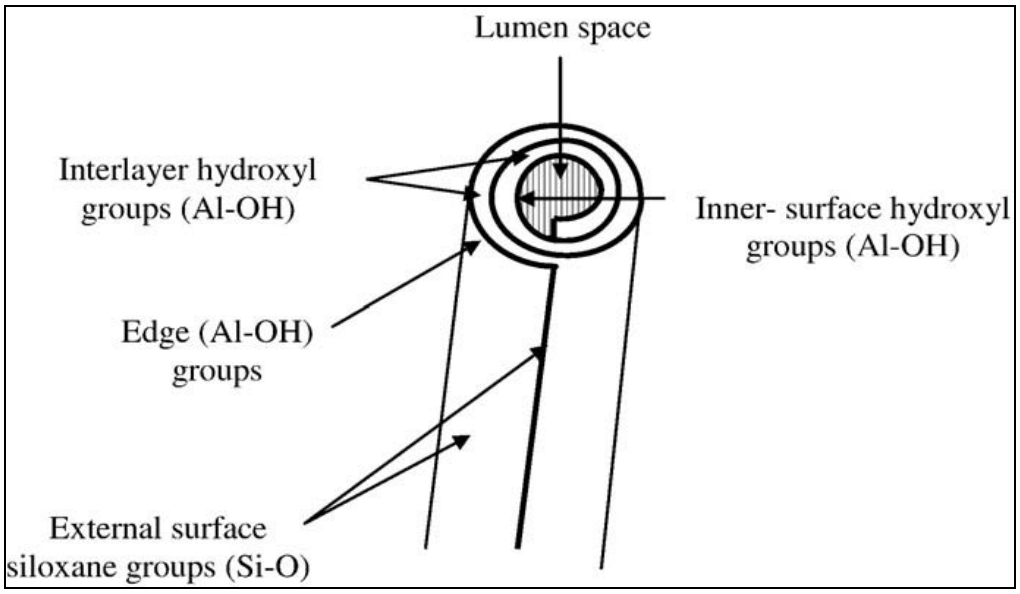

Figure2.48: Schematic structure of a halloysite nanotube (Pasbakhsh et al., 2010).

Short-tube tubular, large-tube tubular and spheroidal morphologies are adopted by HNTs depending on the geological occurrence and conditions of crystallization of the HNTs (Figure 2.49). The tubular structure while most common is also most valuable. HNTs' inner diameter is typically between 10 and 30 nm, outer diameter between 30 and 70 nm and length from 100 up to 2000 nm (Du et al., 2010, Liu et al., 2007).

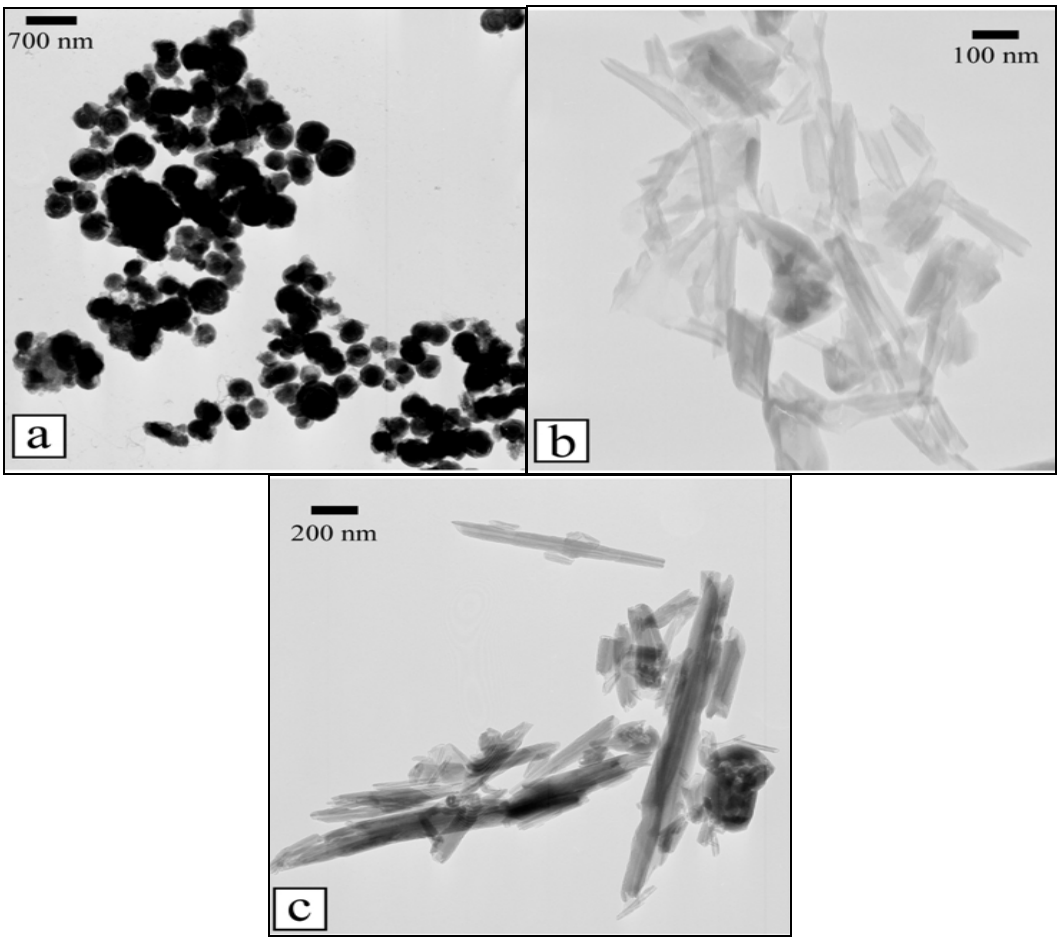

Figure 2.49: TEM images of the three main morphologies of halloysite nanoclay (a) spheroidal, (b) short-tubes and (c) large-tubes (Joussein et al., 2005).

2.6.3Properties of polymer halloysite nanotube nanocomposites

2.6.3.1 Mechanical properties

HNTs can be used to effectively improve mechanical properties. Polymers, typically brittle materials, have been found to demonstrate enhancement in mechanical properties after reinforcement with HNTs. The rod-like and high aspect ratio structures as well as the unique surface chemical properties of HNTs are believed to be the reasons behind the noticeable improvement in flexural properties, tensile strength and impact strength for polymers, such as, PA (polyamide) and PBT (poly(butylene terephthalate) (Deng et al., 2008, Ye et al., 2007) as shown in Table 2.8.

Table 2.8: Mechanical properties of engineering plastics and their HNTs/nanocomposites (Du et al., 2010).

Material	Flexural modulus (GPa)	Flexural strength (MPa)	Tensile strength (MPa)	Impact strength (kJ m^{-2})
Neat PA	2.71	110.0	77.0	5.25
PA/HNT (100/5)	3.23	118.5	82.1	5.75
PA/HNT (100/8)	3.85	127.4	77.5	5.25
PA/HNT (100/10)	4.13	130.9	84.4	5.75
PA/HNT (100/13)	4.56	135.5	84.1	6.50
Neat PBT	2.3	79.7	52.3	5.65
PBT/HNT (100/5)	2.6	82.7	54.9	4.65
PBT/HNT (100/10)	3.0	90.1	58.0	3.78
PBT/HNT (100/20)	3.9	92.9	56.0	3.46
PBT/HNT (100/30)	4.7	82.7	45.2	3.20

Ye et al. (2007) investigated impact strength of pure epoxy and epoxy /HNT nanocomposites. Addition of 2.3 wt.% HNTs to the epoxy matrix increased the impact strength from 0.54 kJ/m^2 for the pure epoxy to 2.77 kJ/m^2 for the nanocomposite. The toughening effect of HNTs is remarkable compared with other inorganic nanofiller modified epoxy nanocomposites (Figure 2.50). Here, an approximate 400% increase in impact strength was recorded whereas for 3 wt.% MMT in epoxy/MMT nanocomposites only a 60% increase was recorded, and using 4 vol% TiO2 nanoparticles in epoxy/TiO2 nanocomposites a 35% improvement was recorded (Ye, et al. 2007).

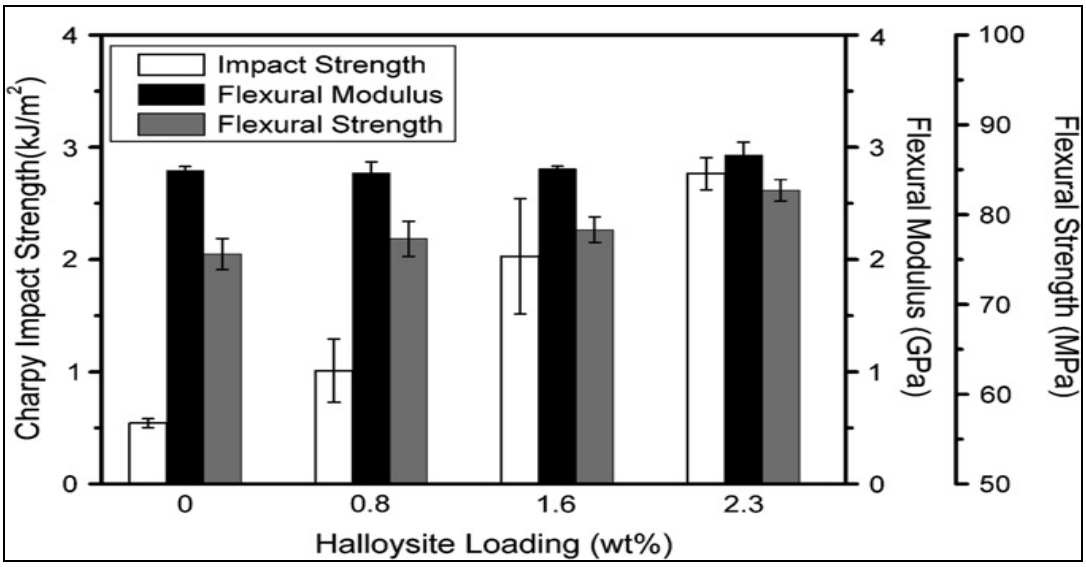

Figure 2.50: Mechanical properties of neat epoxy and the nanocomposites with different halloysite loadings (Ye et al., 2007).

Ye et al. (2007) used high resolution SEM to view fracture surfaces of broken specimens after impact tests to investigate toughening mechanisms as shown in Figure 2.51 (a-c). Nanotube debonding/pull-out in the crack initiation region of the fracture surface is noticeable in Figure 2.51a. Nanotubes can bridge micro-cracks. For example, a micro-crack with a gap of about 600 nm can be seen to have nanotubes bridging its two surfaces in Figure 2.51b. The mechanism of nanotube bridging stabilizes micro-cracks and prevents the development of larger and more harmful cracks. Figure 2.51c shows that some of the bridging HNTs broke when crack opening force exceeded fracture strength of the HNTs. Ye et al. (2007) believed that strong adhesion between HNTs and matrix led to the breakage of bridging HNTs. Nanotube breakage was considered to be an additional mechanism consuming energy and leading to enhancement of toughness properties.

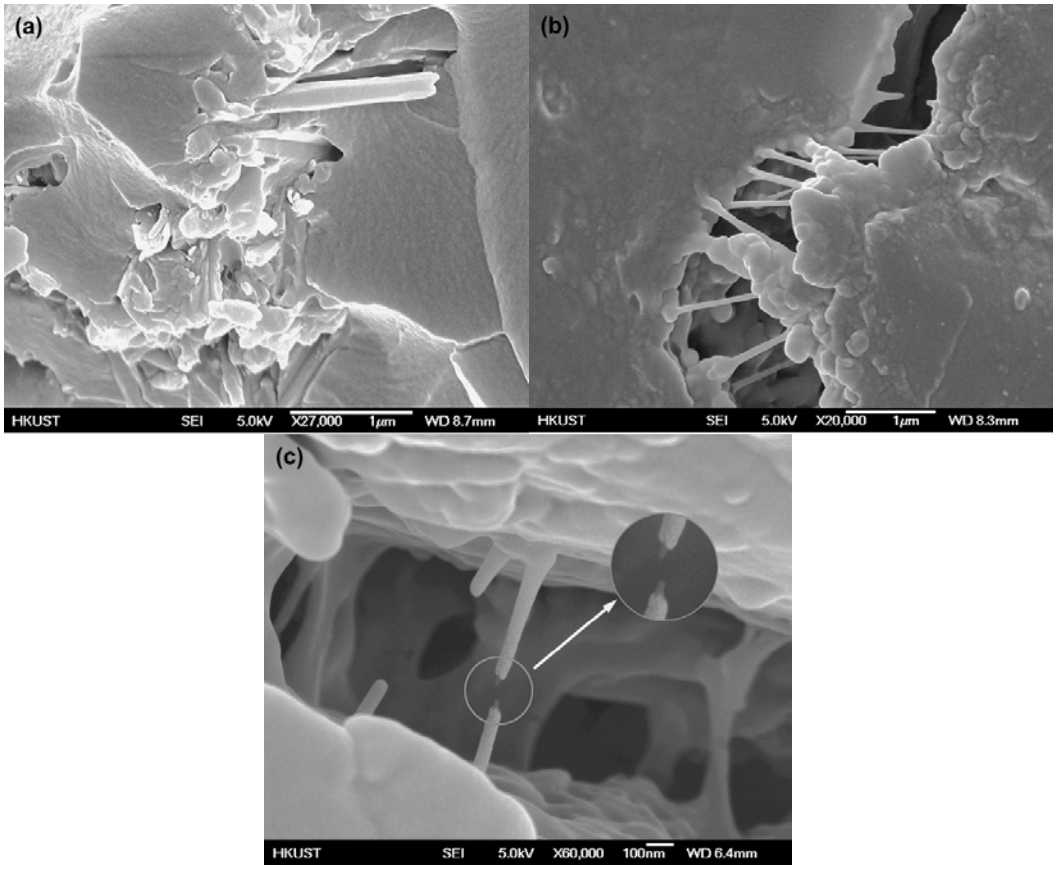

Figure 2.51: SEM micrographs taken on the fracture surfaces of the nanocomposites with 2.3 wt.% halloysite showing: (a) nanotube debonding/pull-out, (b) nanotube bridging, and (c) nanotube fracture (Ye, et al. 2007).

Another study using epoxy and HNTs, was conducted by Deng et al. (2008) who attempted to characterize the fracture behaviour of epoxies reinforced with HNTs and specifically investigate toughening mechanisms provided by HNTs. Load–crack opening displacement (COD) curves from CT tests for pure epoxy and epoxy/HNT nanocomposites with 5 wt.% and 10 wt.% content are shown in Figure 2.52.

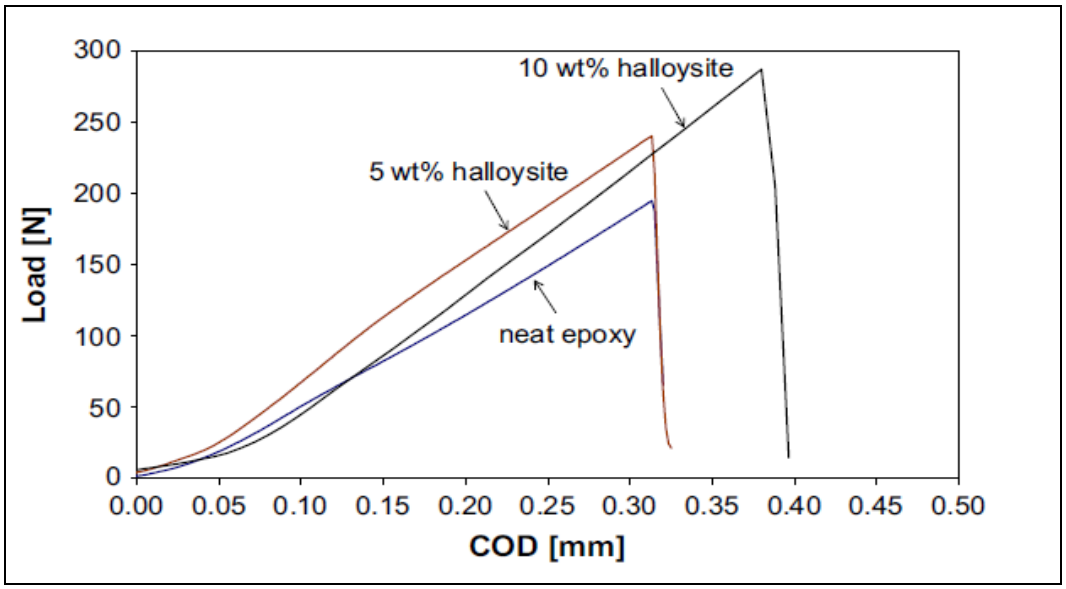

Figure 2.52: Typical load vs. crack opening displacement (COD) curves obtained from CT tests (crack length =19 mm) (Deng et al., 2008).

When maximum load is reached, pure epoxy and epoxy/HNTs nanocomposites with 5 wt.% and 10 wt.% all undergo unstable crack propagation. However, noticeably, when crack length of specimens is the same, the maximum load for epoxy/HNTs nanocomposites is higher. Figure 2.53 shows values obtained at ambient temperature for critical stress intensity factor K_{IC} and the critical stain energy release rate $G_{IC.}$

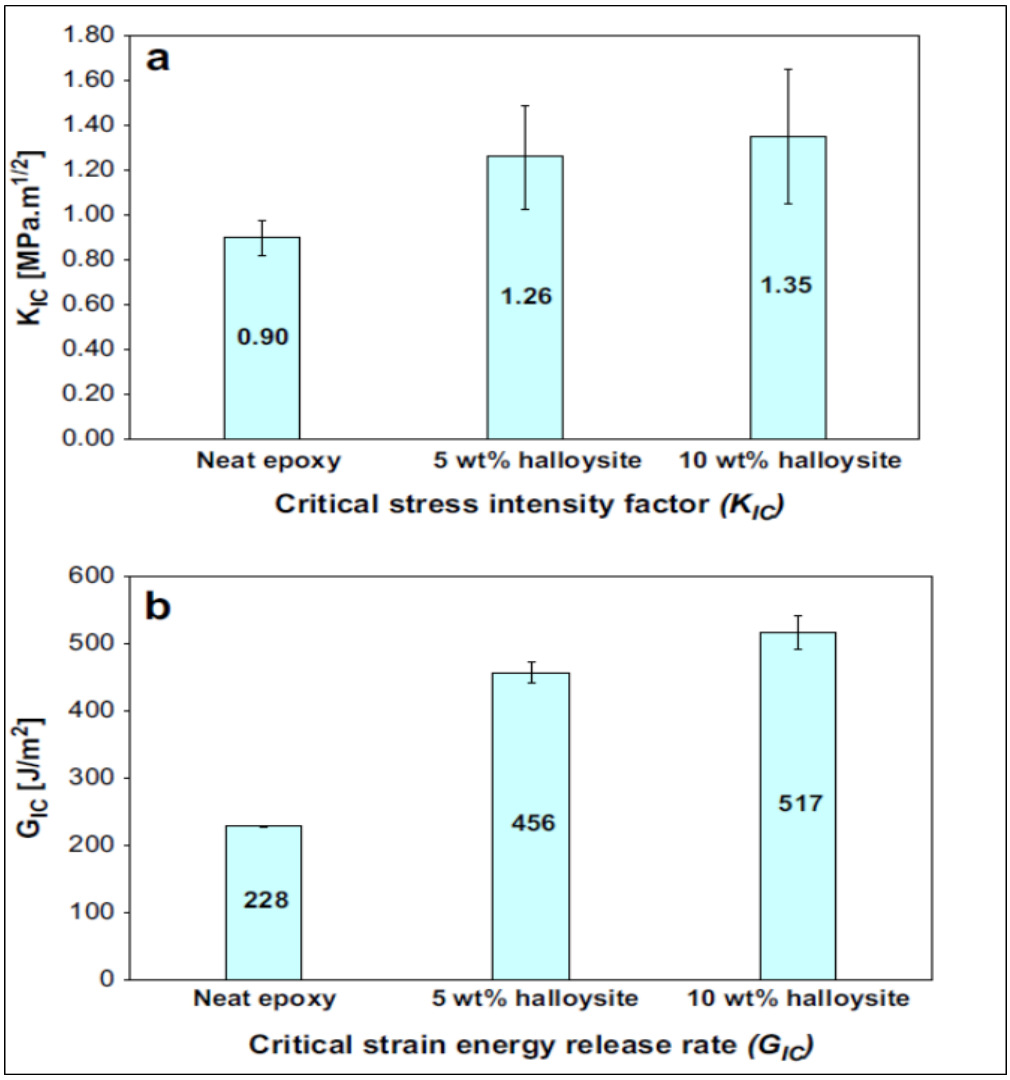

Figure 2.53: Plane-strain fracture toughness of halloysite-epoxy nanocomposites (Deng, et al. 2008).

After HNT reinforcement, the epoxy/HNTs nanocomposites with 5 wt.% and 10 wt.%, magnitudes of K_{IC} were significantly improved. For example, for pure epoxy K_{IC} was 0.90 MPa.m$^{1/2}$ while epoxy/HNTs nanocomposite with 5 wt.% K_{IC} was 1.26 MPa.m$^{1/2}$ indicating a 39% improvement. For epoxy/HNTs nanocomposite with 10 wt.%, the increase in K_{IC} was even greater at 1.35 MPa.m$^{1/2}$ indicating an almost 50% improvement. The increases in the critical strain energy release rate (G_{IC}) for epoxy/HNTs nanocomposite with 5 wt.% and 10 wt.% were 100% and 127% respectively (Deng et al., 2008). Figure 2.54 (a-c) shows the appearance of fracture surfaces of CT specimens near the crack tip. For pure epoxy Figure 2.54a flatness and

smoothness characterise the fracture surface indicative of brittle cleavage failure. In contrast, for epoxy/HNTs nanocomposites at 5 wt.% (Figure 2.54b) and 10 wt.% (Figure 2.54c) roughened fracture surfaces and the presence of dispersed particles clusters are noticeable.

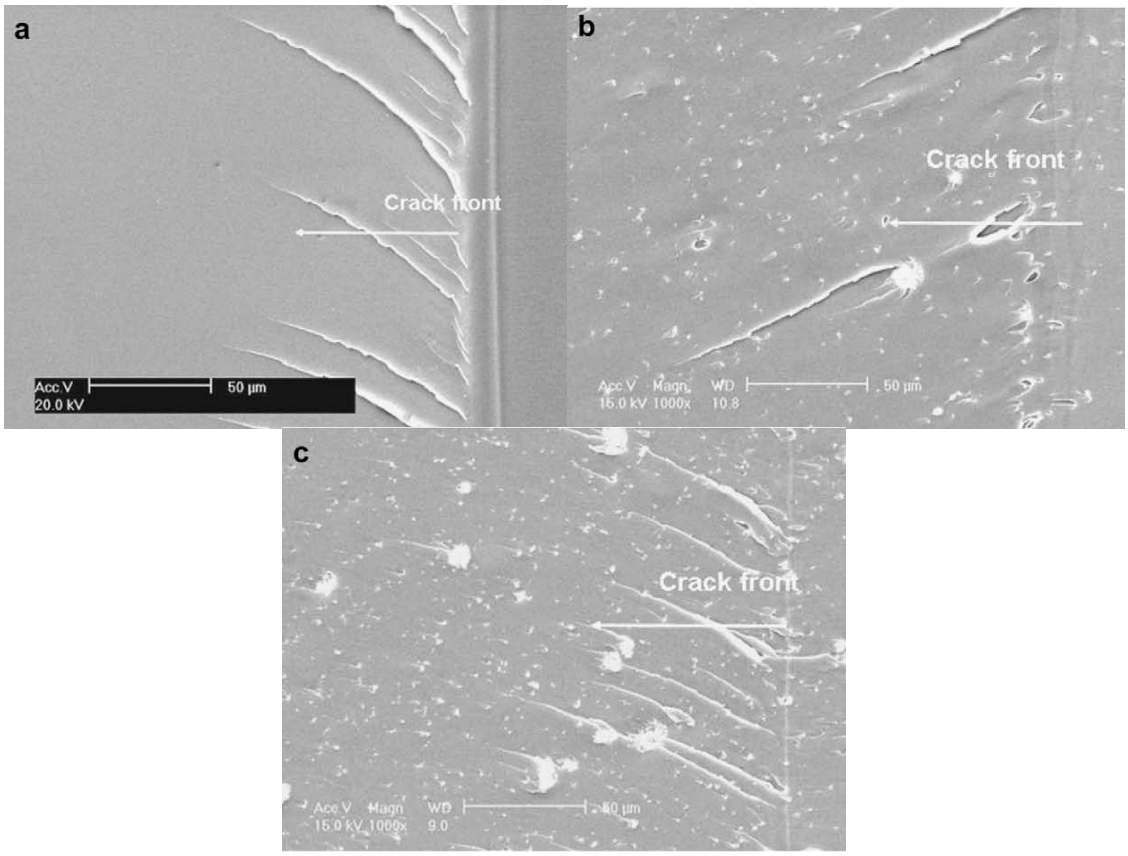

Figure 2.54: SEM micrographs of fracture surfaces near crack tip, (a) pure epoxy, (b) 5 wt.% halloysite, and (c) 10 wt.% halloysite (Deng, et al. 2008).

Plastic deformation of the epoxy around the particle clusters, crack bridging, and crack deflection are believed to be toughness mechanisms provided by the addition of HNTs. Particle clusters of HNTs are believed to be able to interact with cracks at the crack front, effectively resisting crack advancement and thus increasing fracture toughness (Deng, et al. 2008). The team also investigated the tensile and flexural properties of pure epoxy and epoxy/HNTs nanocomposite samples finding that epoxy when reinforced with HNTs demonstrates improvements in strength and modulus properties. This

enhancement of properties is believed to be due to the large aspect ratio of HNTs (Deng, et al. 2008).

2.6.3.2 Thermal properties

HNTs can be used effectively as flame-retardants. Investigations have shown that the thermal stability and flame retardancy of polymer composites, such as epoxy nanocomposites, are increased markedly with an increase of loading of HNTs (Ismail et al., 2008, Rooj et al., 2010). Du et al. (2006) conducted studies into the thermal stability and flammability of polypropylene (PP)/HNTs composites. The data revealed in TGA curves in Figure 2.55 and characteristic weight loss temperatures results summarized in Table 2.9 give an indication of the drastic impact loading of HNTs and surface modification of HNTs has on the thermal stability of nanocomposites. For pure PP, 5% weight loss occurs at 384ºC. For PP/HNT nanocomposite with 10 phr unmodified HNTs, 5% weight loss occurs at 414ºC. For PP/HNT nanocomposite with 10 phr modified HNTs, 5% weight loss occurs at 444ºC. While compared to pure PP, the 10 phr PP/HNT nanocomposites demonstrate superior thermal stability, at 30 phr loading of HNTs thermal stability declines. The results shown in the following table for temperature at 5% weight loss, 10% weight loss, and at maximum weight loss highlight 10 phr loading giving favourable thermal stability compared to 30 phr (Du et al., 2006).

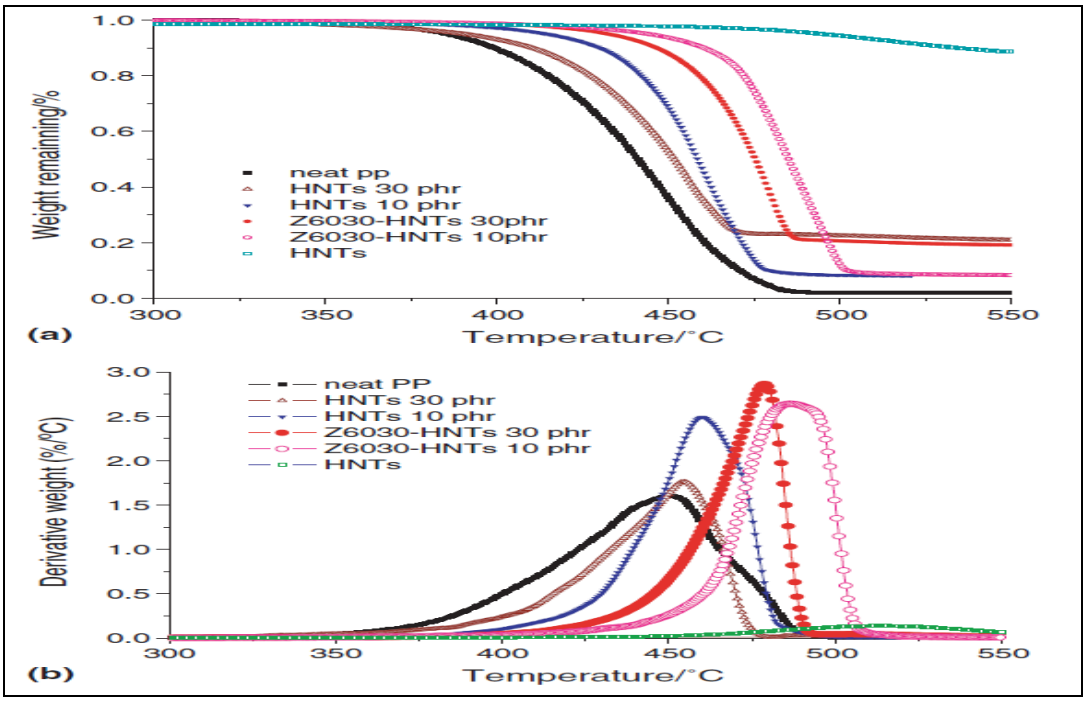

Figure 2.55: TGA curves of neat PP, HNTs, and PP/HNTs nanocomposites in nitrogen. (Du, et al. 2006)

Table 2.9: TGA data of PP/HNTs nanocomposites in nitrogen (Du, et al. 2006)

Nanocomposites	HNTs content	Temperature at 5% weight loss/°C	Temperature at 10% weight loss/°C	Temperature at maximum weight loss rate/°C
Neat PP	–	384	400	450
PP/HNTs	10	414	430	460
PP/modified HNTs	10	**444**	**460**	**487**
PP/HNTs	30	390	410	454
PP/modified HNTs	30	432	446	478
HNTs	–	495	535	–

Du et al. (2006) used a cone calorimeter to investigate the flammability of PP and PP/HNTs nanocomposites. Figure 2.56 and Table 2.10 highlight that incorporation of HNTs led to PP/HNTs nanocomposites' peak of heat release rate (PHHR), peak of specific extinction area (PSEA), and peak mass loss rate (PMLR) to each be substantially lower than the corresponding peaks in pure PP indicative of a reduction in the flammability from PP to PP/HNTs nanocomposites (Du, et al. 2006). Loading of 30 phr HNTs led to greater reduction of flammability in PP compared to loading of 10 phr. Specifically, PHHR, PSEA and PMLR of nanocomposites reduced to almost half of

those of the pure PP, at 30 phr loading of HNTs. For pure PP, the curve of HRR is very sharp indicative of furious burning and quick heat release. Increasing loading of HNTs in PP to 30 phr, however, flattens the HRR curve and noticeably increases the time to burn out (Du, et al. 2006).

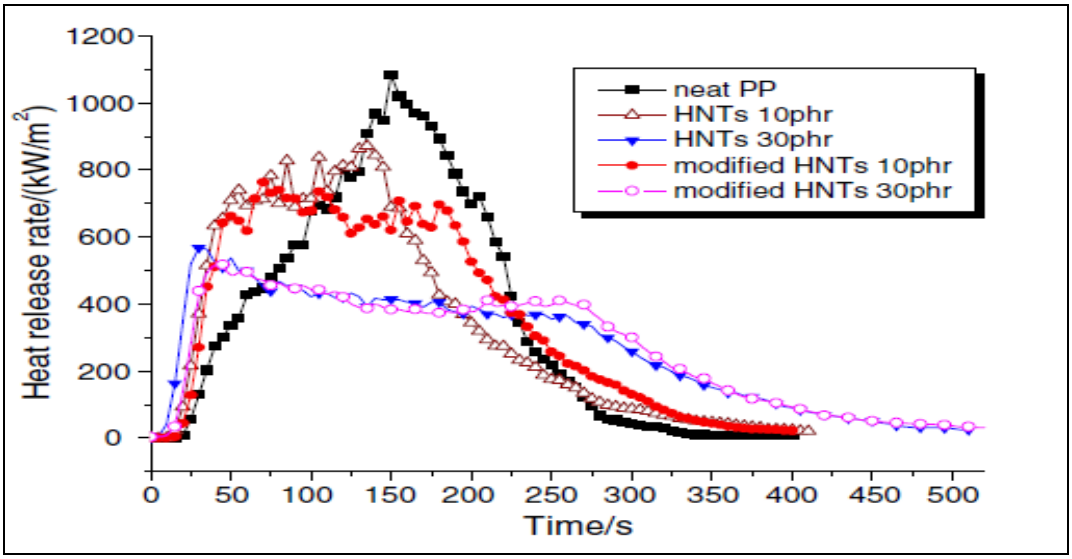

Figure 2.56: Heat release rate of neat PP and PP/HNTs nanocomposites (Du, et al. 2006).

Table 2.10: Cone calorimeter data of neat PP and PP/HNTs nanocomposites (Du, et al. 2006).

Nanocomposites	Neat PP	PP/HNTs-10	PP/HNTs-30	PP/modified HNTs-10	PP/modified HNTs-30
Time to ignition, s	8.8	11.6	5.0	15.3	19.5
PHRR, kW/m^2	1083	871	567	763	519
Time to PHRR, s	150	135	30	70	40
Time to burn out, s	319	376	478	370	511
Average HRR, kW/m^2	388	359	277	386	272
Peak specific extinction area, m^2/kg	2035	1297	1444	1221	1021
Peak mass loss rate, $g/(sm)^2$	0.3129	0.2296	0.1988	0.2149	0.1606

The hollow tubular structures of HNTs, heat and mass transport barriers, and iron presence in HNTs (0.29 wt.% Fe_2O_3) are suggested to be the principal factors leading to the favourable thermal stability and flame retardant effects of HNTs addition (Du et al. 2006).

Ismail et al. (2008) investigated the thermal stability and flammability properties of Ethylene propylene diene monomer (EPDM) and EPDM/HNTs nanocomposites. Figure 2.57 and Table 2.11 provide TGA results for the EPDM/HNT nanocomposites showing with increasing HNTs at 5 and 10 phr HNT loading the temperature at 5% weight loss decreased. In contrast, when increasing HNTs at 15 to 100 phr HNT loading, the temperature at 5% weight loss increased. Compared to pure EPDM, the temperature at 5% weight loss for EPDM/HNTs nanocomposites at 70 phr loading was 15ºC higher and at 100 phr loading 20ºC higher. Maximum weight loss as a percentage was highest for pure EPDM and decreased at 0 to 100 phr loading as HNTs content was added. The improved thermal stability of the composites compared to the pure EPDM is believed to be due to the formation of char residue which hinders the diffusion of volatile decomposition products. In Ismail et al. (2008)'s comparative study of the rate of maximum weight loss, even the slightest increase in HNTs content, was found to enhance the composites' thermal stability. Good dispersion of HNTs, entrapment of degradation products of EPDM within the tubule's lumen structure, interfacial and inter-tubular interactions between EPDM and HNTs, and formation of zigzag structures are believed to be the mechanisms responsible for the enhanced thermal properties in EPDM/HNTs composites over 15 phr HNT loading (Ismail et al., 2008).

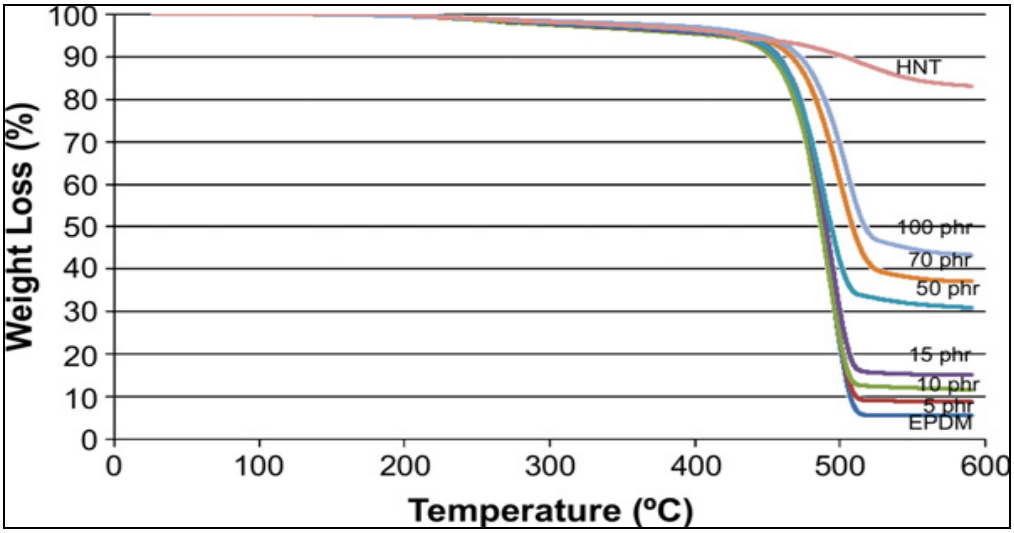

Figure 2.57: TGA curve of EPDM, HNT and EPDM/HNT nanocomposites (Ismail et al. 2008).

Table 2.11: Thermal stability parameters of EPDM/HNT nanocomposites (Ismail et al., 2008).

Composites	Loading (phr)	Temperature at 5% weight loss	Maximum weight loss (%)	Temperature at maximum weight loss rate (°C)
C.1	0	423	94.4	488
C.2	5	417	91.2	492
C.3	10	413	88.3	491
C.4	15	425	84.9	492
C.5	30	426	77.8	493
C.6	50	428	69.0	494
C.7	70	438	63.0	497
C.8	100	443	56.7	503
HNT	–	491	19.1	524

For the investigation of flammability, Ismail et al. (2008) used the UL-94 vertical burn test to conduct a ranking of flammability. Table 2.12 shows pure EPDM as 'Unclassified', as specified by the standard, with 5 specimens having a total ignition of over 250 s. Addition of 5–15 phr of HNT decreased dripping and total ignition time, and EPDM/HNT composite was also still 'Unclassified' with flame still reaching specimen top. HNTs loading from 0 to 100 phr reduced flammability of EPDM/HNT nanocomposites.

Table 2.12: Classification of flammability of EPDM/HNT nanocomposites according to UL-94 test (Ismail et al., 2008).

Composites	Classification	Dripping observed	Specimen burns up to holding clamp	Total flaming combustion for all 5 specimens (s)
C.1	Unclassified	Yes	Yes	396
C.2	Unclassified	Yes	Yes	342
C.3	Unclassified	No	Yes	288
C.4	Unclassified	No	Yes	231
C.5	V-2	No	No	191
C.6	V-1	No	No	154
C.7	V-1	No	No	99
C.8	V-0	No	No	46

Lecouvet et al. (2011) investigated the thermal stability and flammability properties of pure polyamide 12 (PA12), PA12/HNTs nanocomposites prepared by Batch Internal Mixing (BIM) and PA12/HNTs composites prepared by Twin-Screw Mini-Compounding (TSMC) in order to study the influence of dispersion of HNTs on physical properties of the resulting nanocomposites. Table 2.13 shows temperatures at 5 and 10% weight loss for BIM PA12/HNTs nanocomposites increased with HNTs loading. Compared to pure PA12, at 10 wt.% BIM PA12/HNTs nanocomposite temperature was 31ºC higher. Table 2.14 reveals the better thermal properties for the BIM PA12/HNTs nanocomposite compared to the TSMC PA12/HNTs. For example, the increase in temperature at 10% weight loss for PA12/HNTs at 10% HNTs content is 12ºC greater for samples prepared using the BIM method compared to those samples prepared using the TSMC method. The team postulated that the random orientation of HNTs, a result of BIM preparation, provides better barrier properties and consequently better thermal stability, compared to preferential orientation of HNTs, a result of TSMC preparation method. This postulation was supported by observations using TEM as shown in Figure 2.58. Based on this postulation, the team believed that the internal structure and presence of iron in HNTs were important factors leading to the result of increased thermal stability in PA12/HNTs nanocomposites.

Table 2.13: TGA data of Batch internal mixed (BIM) PA12/HNTs nanocomposites in air atmosphere at a constant heating rate of 10ºC /min (Lecouvet et al., 2011).

HNTs Content [wt%]	Temperature at 5% weight loss [°C]	Temperature at 10% weight loss [°C]	Temperature at maximum rate of weight loss [°C]
0	391	403	460
2	404	421	466
5	406	425	468
10	422	434	471

Table 2.14: TGA data of twin-screw compounded (TSMC) PA12/HNTs nanocomposites in air atmosphere at a constant heating rate of 10ºC /min (Lecouvet et al., 2011).

HNTs Content [wt%]	Temperature at 5% weight loss [°C]	Temperature at 10% weight loss [°C]	Temperature at maximum rate of weight loss [°C]
0	404	419	461
2	408	426	463
5	420	436	466
10	426	438	463

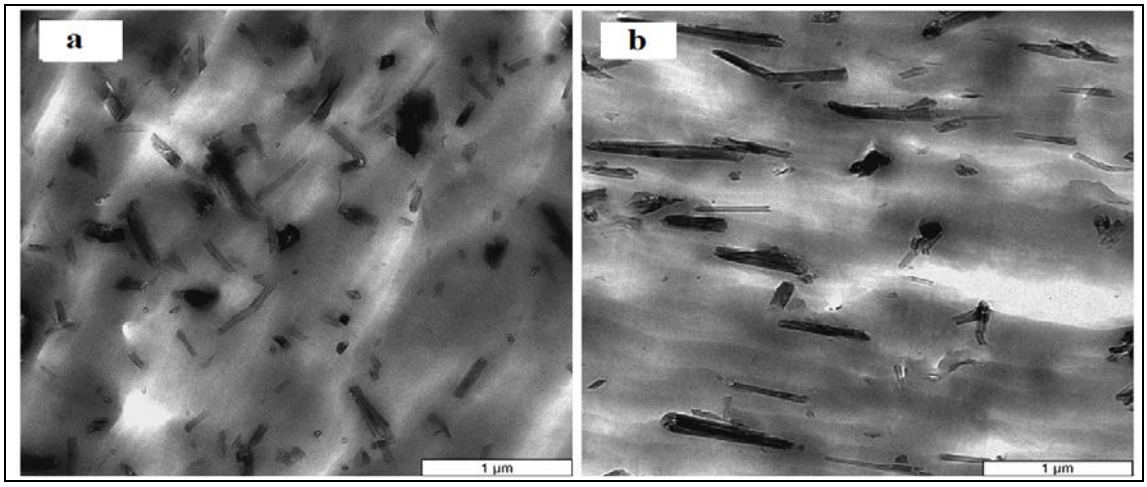

Figure 2.58: TEM micrograph of PA12/HNTs nanocomposites with 10 wt.% of HNTs (a) prepared using BIM and (b) prepared using TSMC (Lecouvet et al., 2011).

In summary, the structure of HNTs is believed to a principal factor underpinning enhancement of thermal properties often reported when polymers are modified with this type of nano-particle. It is this microstructure of HNTs which promotes favourable dispersion and orientation of HNTs within the matrix allowing effective interfacial interaction between HNTs and matrix. This microstructure entraps degradation products of composites within tubules on heating and provides heat and mass transport barriers which enhance thermal stability in polymer/HNTs composites. The chemical components of HNTs are also believed to underpin enhancement of thermal properties. A layer of thermal insulation is provided through the formation of char in

polymer/HNTs composites leads to improvement in thermal stability while and the presence of iron from HNTs in composites is considered to be a flame-retardant.

2.7 Polymers Nano-Silicon Carbide Nanocomposites

2.7.1 Introduction

Silicon carbide (SiC) exhibits outstanding mechanical and physical properties (Majewski et al., 2006). With these properties, SiC is a promising material for both high temperature and superior abrasion resistant applications (Zhi-min et al., 2007). Accordingly, in recent years, the nano-powder of silicon carbide (n-SiC), has been identified as a promising filler to enhance the properties of polymer composites (Liao et al., 2011).

2.7.2 Structure and categorized of silicon carbide

The name silicon carbide describes a range of materials that are in fact structurally distinct. Mechanical engineers often describe ceramics fabricated from impure SiC crystallites bonded with binders under temperature and/or pressure as silicon carbide while electrical engineers describe high purity single crystal wafers as SiC. Nonetheless, the layered crystal structure of silicon carbide occurs in different polytypes. SiC crystal is composed of equal amounts of carbon and silicon. Each atom of SiC ctystal bonds to four opposite atoms in a tetrahedral bonding configuration. A, B and C positions are three possible arrangements of atoms in each SiC crystal layer. Each polytype has similar layers but different stacking sequence (Figure 2.59). As a given layer may be stacked on top of another layer in a variety of orientations with lateral translations and rotations being feasible, silicon carbide occurs in a variety of stacking sequences. Each stacking sequence is unique and generates a different polytype. Cubic, hexagonal and rhombohedral structures are all possible. Hexagonal and rhombohedral structures, designated as α-form (noncubic), crystallize in a large number of polytypes. In contrast, only one form of cubic structure, designated as β-form, has been recorded to date. Nonetheless, although a limited number forms are of interest technologically, over 215

polytypes have been recorded. Commercial availability of substrates and low mobility anisotropy for certain polytypes drives high demand for these materials (Saddow, 2012, Shaffer, 1969, Wright, 2000).

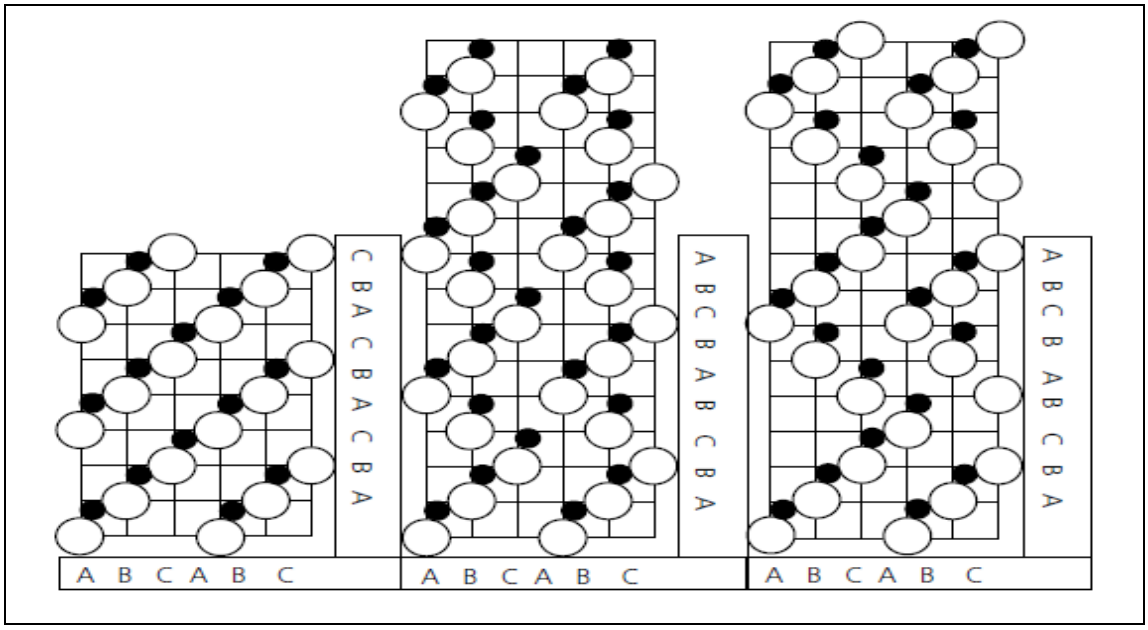

Figure 2.59: Comparison of stacking sequences of (a) 3C SiC, (b) 4H SiC, and (c) 6H SiC (Wright and Horsfall, 2011).

2.7.3 Properties of polymer nano-silicon carbide nanocomposites

2.7.3.1 Mechanical properties

Nano-sized ceramic composites, for some time, have been known to provide higher fracture toughness and strength compared to conventional ceramic composites Niihara. Nano-SiC retains its strength at high temperatures and provides good creep properties. For example, a 30% increase in tension and flexure properties was observed when only 1.5 wt.% n-SiC was added to pure epoxy (Kueseng and Jacob, 2006, Zhou et al., 2008).

Concerning elastic modulus and flexural strength, Yong and Hahn (2004) studied effect of addition of n-SiC to vinyl-ester with and without the coupling agent/dispersant,

gamma methacryloxy propyl trimethoxy silane (MPS). The pair found that elastic modulus and flexural strength of vinyl-ester increased with increases in volume fraction of SiC (Table 2.15). Changes to the interface and dispersion quality at constant volume fraction were not found to have a significant influence on elastic modulus. However, these variables are essential in determining composite strength and toughness. There was a positive relationship between use of coupling agent (MPS) and strength properties. Yong and Hahn (2004) concluded that the increase in strength was attributable to better dispersion quality, lower porosity, and stronger particle/matrix interfacial bonding as a result of MPS. In contrast, without dispersant, the pair believed that higher particle loading introduced larger and more loosely assembled nanoparticle agglomerates, which acted as stress concentrators, and caused a decrease in strength (Yong and Hahn, 2004).

Table 2.15: Mechanical properties of pure vinyl-ester and vinyl-ester/n-SiC nanocomposites (Yong and Hahn, 2004).

SiC (vol%)	Mixing condition	Ultimate flexural stress σ_{max} (MPa)		Flexural modulus E (GPa)	
		Mean	SD	Mean	SD
0	Neat resin	116	16	2.9	0.11
1	Without MPS	63	4	3.6	0.07
2		53	1	3.7	0.07
1	With MPS	126	11	3.5	0.28

Rodgers et al. (2005) studied the elastic modulus and flexural strength properties of epoxy/n-SiC nanocomposites. Rodgers et al. (2005) aimed to study the effect of adding 0.5, 1, and 1.5 wt.% n-SiC on the mechanical properties of epoxy (SC-15 epoxy) matrix. The researchers performed flexural tests to evaluate bulk stiffness and strength for each nanocomposite. The results revealed that addition of 1 wt.% n-SiC led to the most favourable enhancements with a 36% increase in elastic modulus and a 21% increase in strength (Table 2.16).

Table 2.16: Flexural test data for pure epoxy and epoxy/n-SiC nanocomposites (Rodgers et al., 2005).

Material	Flexural modulus	Gain/loss in modulus	Flexural strength	Gain/loss in strength
	GPa	%	MPa	%
SC-15 epoxy, neat (unsonicated)	2.45 ± 0.09		91.87 ± 5.13	
SC-15 epoxy, neat (sonicated)	3.09 ± 0.10	26.12	104.79 ± 6.65	14.06
0.5 wt.-% SiC/SC-15	3.26 ± 0.21	33.06	111.73 ± 9.35	21.62
1.0 wt.-% SiC/SC-15	3.33 ± 0.21	35.92	111.53 ± 6.97	21.40
1.5 wt.-% SiC/SC-15	3.32 ± 0.10	35.51	95.86 ± 4.01	4.34

Interestingly, the team found that there was almost negligible difference in enhancement between 0.5 wt.% and 1 wt.% addition. Moreover, the researchers noted that mechanical properties began to degrade at 1.5 wt.% loading as shown in Figure 2.60 (Rodgers et al., 2005).

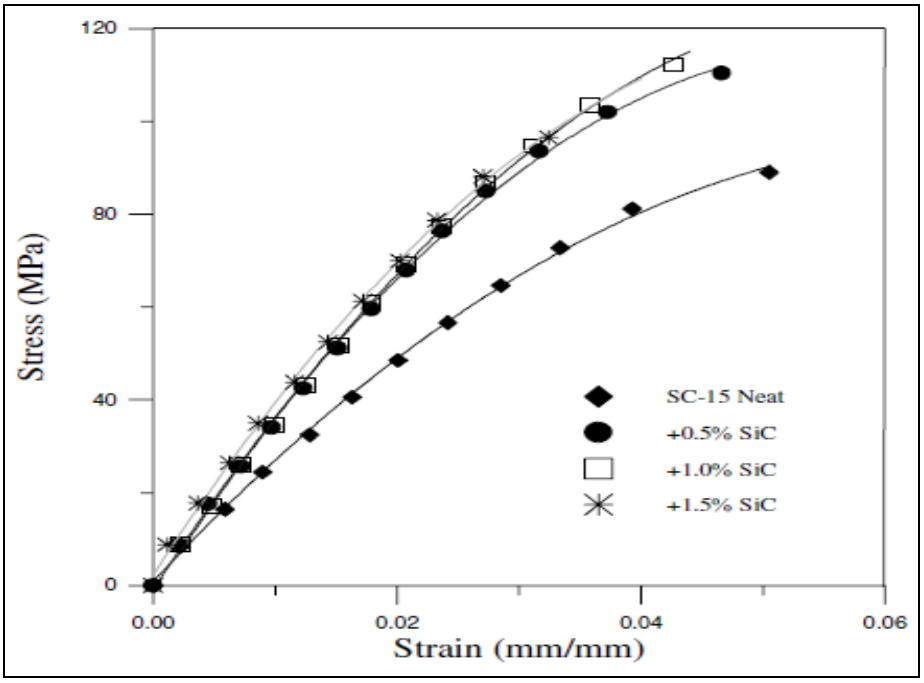

Figure 2.60: Stress/strain curves from flexural tests for pure epoxy and epoxy/n-SiC nanocomposites (Rodgers et al. 2005).

Rodgers et al. (2005) noted that 21% enhancement in strength during flexure was surprising compared to the results of previous studies with nanoclays. The researchers attributed the enhancement to better dispersion of spherical n-SiC compared to the dispersion of nanoclay particles with micron size planar dimensions providing less interaction with polymer chains. The team suggested that if the centres of the nanoparticles were close to the radius of gyration of the polymer coils, a significant increase in the number of atoms at the surface would occur. This increase would enhance reactivity between particle and polymer leading to improved mechanical properties. The degradation of strength beginning at 1.5 wt.% was believed to be due to particle agglomeration (Rodgers et al., 2005).

Liao et al. (2011) studied the elastic modulus, the strength, and the impact strength of maleated high density polyethylene (mPE) reinforced with 2, 4, 6 and 8 wt.% n-SiC. Liao et al. (2011) aimed to investigate the impact fractography, deformation, and other structural factors relevant to the properties of such nanocomposites. The researchers found that all specimens exhibited cold drawing and necking behavior which can be seen in the typical tensile stress–strain curves for mPE and its nanocomposites (Figure 2.61). The team found the reinforcement of 2 wt.% n-SiC led to substantial improvements in strength and elastic modulus results (Table 2.17). The researchers noted that mechanical properties began to degrade at 4 wt.% loading due to agglomeration of n-SiC at high filler content. Liao et al. (2011) attributed the favourable tensile strengths and stiffness of their nanocomposites to the higher degree of crystallinity (Xc). While pure mPE has a Xc value of 61.0%, adding 2 wt.% n-SiC increased this value to 65.8%, and 8 wt.% to 67.1%. In addition to degree of crystallinity, the researchers referred to the reinforcing effect of n-SiC (Liao et al., 2011).

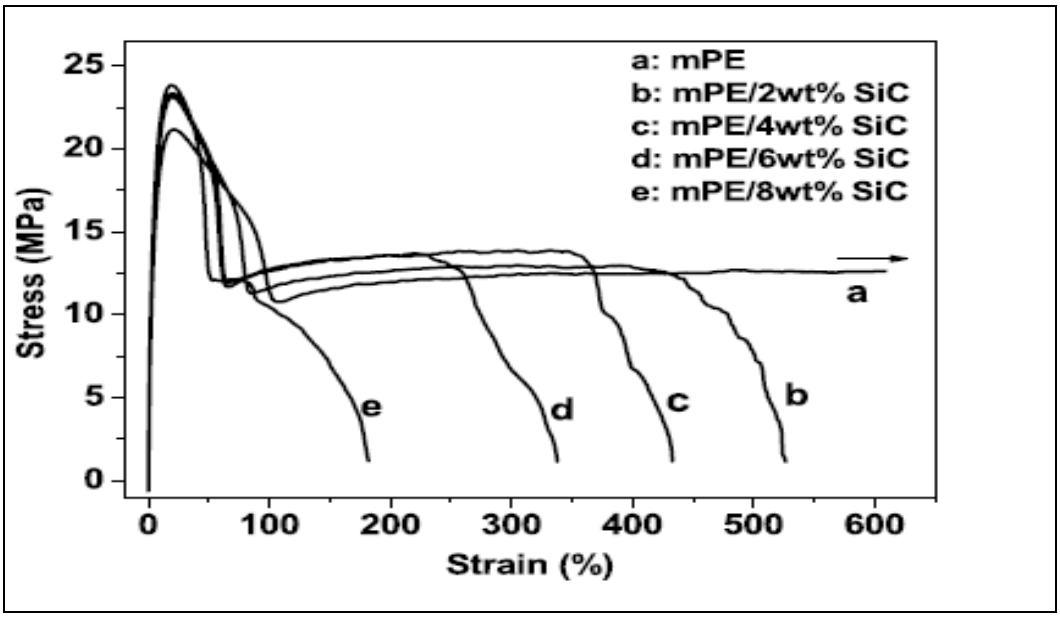

Figure 2.61: Tensile stress/strain curves of mPE reinforced with 2, 4, 6 and 8 wt.% n-SiC at a 10 mm/min crosshead speed (Liao et al. 2011).

Table 2.17: Mechanical properties of pure mPE and Mpe/n-SiC nanocomposites (Liao et al., 2011).

Sample	HDT (°C)	Young's modulus (MPa)	Yield strength (MPa)	Elongation at break (%)	Impact strength (kJ/m^2)
mPE	83.92	1084 ± 10	20.96 ± 0.36	>600	2.86 ± 0.03
mPE/2 wt% SiC	91.79	1218 ± 18	23.07 ± 0.15	530	2.54 ± 0.08
mPE/4 wt% SiC	92.84	1246 ± 11	23.24 ± 0.20	430	2.52 ± 0.11
mPE/6 wt% SiC	94.24	1274 ± 20	23.25 ± 0.12	337	2.49 ± 0.11
mPE/8 wt% SiC	94.42	1286 ± 17	23.82 ± 0.19	182	2.30 ± 0.12

Liao et al. (2011) investigated the effect of n-SiC addition on the notched impact strength (toughness) of the pure mPE (Figure 2.62). Notch testing revealed a negative relationship between impact toughness and n-SiC content (Table 2.16). The researchers attributed the low impact toughness in the composites to the absence of particle cavitation and matrix fibrillation, and the extreme hardness of the n-SiC (2840-3320 kg/mm2) compared to the hardness of mPE, which compromises the mechanism of plastic deformation in the mPE matrix (Liao et al., 2011).

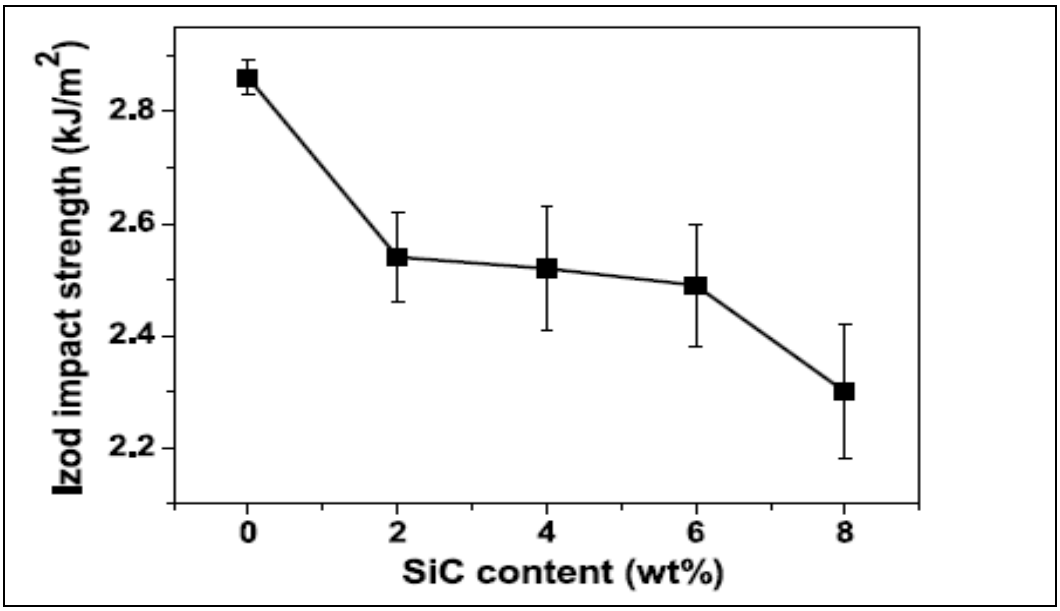

Figure 2.62: Notched impact strength (toughness) of pure mPE, and mPE/n-SiC nanocomposites (Liao et al., 2011).

2.7.3.2 Thermal properties

Rogers et al. (2005) studied the thermal stability and the reinforcement of epoxy with n-SiC. To measure changes in heat flow associated with material transitions for various volume fractions of n-SiC nanocomposites, the researchers used modulated differential scanning calorimetry (DSC) analyses. The researchers also used DSC to determine the effect of SiC nanoparticle addition on glass transition temperatures (T_g) of nanocomposite systems. Typical heat flows versus temperature curves of this study are shown in Figure 2.63. The team described that the broad endothermic peak detected in Figure 2.63 at 73ºC was assigned to the T_g of the neat epoxy resin system, and that peak is meant to indicate a depression in the curve. The researchers determined glass transition temperatures as inflection points of heat flow curves. Rogers et al. (2005) reported that for 0.5, 1.0, and 1.5 wt.% epoxy/n-SiC glass transition temperatures (T_g) measured were 80ºC, 85, and 65.8ºC respectively. The researchers attributed the 12.8ºC increase in T_g from neat epoxy (73ºC) to 1.0 wt.% (85ºC) to increased cross-linking of epoxy resin, due to the presence of n-SiC. This restriction of molecular mobility decreases free volume However, Rogers et al. (2005) reported the addition of 1.5 wt.%

led to a 20ºC decrease in T_g from 1.0 wt.% (85ºC) to 1.5 wt.% (65ºC). The researchers attributed this decrease to n-SiC agglomeration and the subsequent increased in particle/particle interaction as opposed to particle/polymer interaction. Rogers et al. (2005) concluded that particles agglomerated began to act as impurities in polymer, and these agglomerations with a much larger volume could no longer occupy free space nor restrict molecular mobility. Moreover, particle agglomerations lower T_g by reducing cross-linking density of the polymer (Rodgers, et al. 2005).

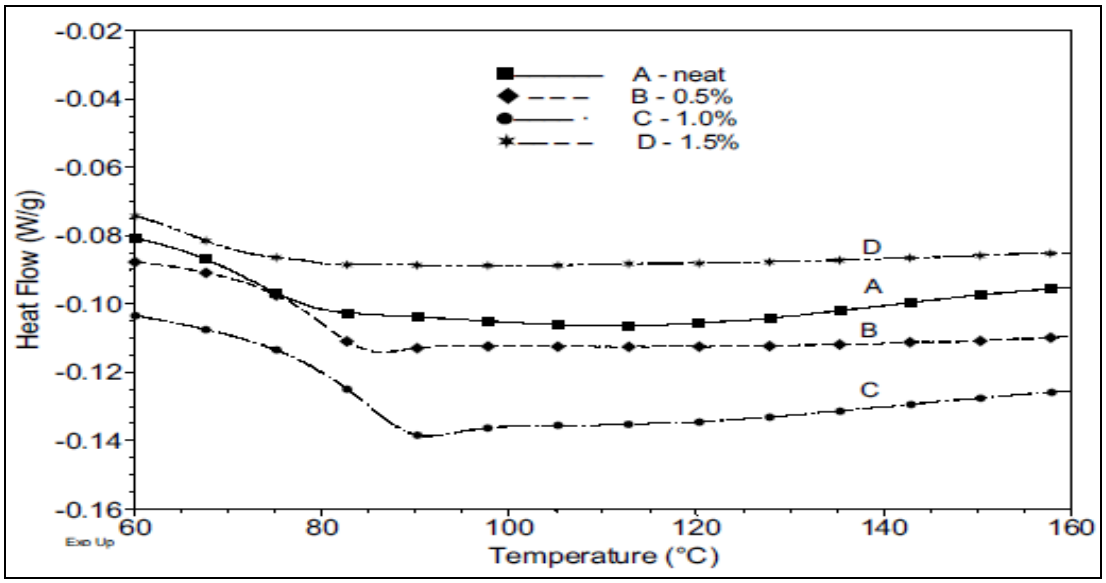

Figure 2.63: Modulated differential scanning calorimetry (MDSC) curves for pure epoxy (A), 0.5 (B), 1.0 (C), 1.5 wt.% (D) epoxy/n-SiC nanocomposites (Rodgers et al. 2005).

Rogers et al. (2005) also compared the TGA decomposition temperatures of 0.5, 1.0, and 1.5 wt.% epoxy/n-SiC with that of pure epoxy (Table 2.18). The researchers reported structural decomposition temperatures of 356ºC, 378ºC, and 385.8ºC for neat, 0.5 and 1.0 wt.% systems respectively. The researchers found that at 1.5 wt.% structural decomposition temperature was reduced to 358.8ºC. Rogers et al. (2005) attributed this decrease in properties to agglomeration of n-SiC at 1.5wt.% perturbing the microscopic integrity of the polymer by weakening the Van der Waals forces that bind polymer chains (Rodgers et al., 2005).

Table 2.18: DSC and TGA data for pure epoxy and epoxy/n-SiC nanoomposites (Rodgers et al. 2005).

Material	DSC glass transition temperature (T_g)	T_g increase	TGA decomposition temperature
	°C	%	°C
SC-15 epoxy, neat	73	–	356
+0.5 wt.-% SiC	80	10	378
+1.0 wt.-% SiC	85	16	385
+1.5 wt.-% SiC	65	–	358

Majewski et al. (2006) also studied the thermal stability of solution blending a styrene ethylene butylenes (SEBS) star-polymer reinforced with n-SiC. The TGA curves of various composite materials and the polymer with temperature are shown Figure 2.64. The researchers found a positive relationship between decomposition temperature and fraction volume of the composites. For example, for the pure polymer (SEBS) the decomposition temperature was 458ºC while for 35 wt.% n-SiC, 468ºC. The team attributed the enhancement of thermal stability in the nanocomposites to the existence of inorganic materials in polymer matrix, which generally enhances the thermal stability of the composite. Majewski et al. (2006) also plotted temperature against the residual weight of pure polymer and polymer reinforced with n-SiC. The researchers reported a positive relationship between n-SiC content and degradation temperature (DT) of samples (Figure 2.65). For example, increasing n-SiC content to 35 wt.%, resulted in an approximate 30ºC increase in DT. The researchers noted that saturation value of polymer by n-SiC powder was attained at 35 wt.%, as further increase in n-SiC content did not result in an increase of the DT. Majewski et al. (2006) concluded that the quality of particle dispersion was an important determinant of thermal stability of particle reinforced polymer composites (Majewski et al., 2006).

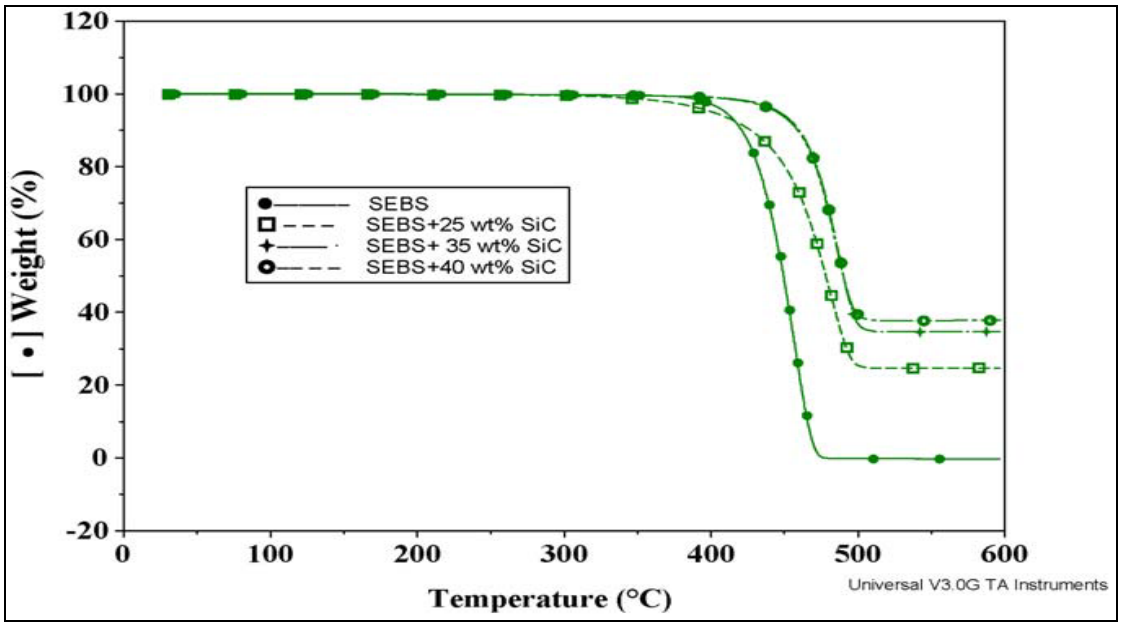

Figure 2.64: TGA of the sample containing up to 40 wt.% n-SiC (Majewski et al., 2006).

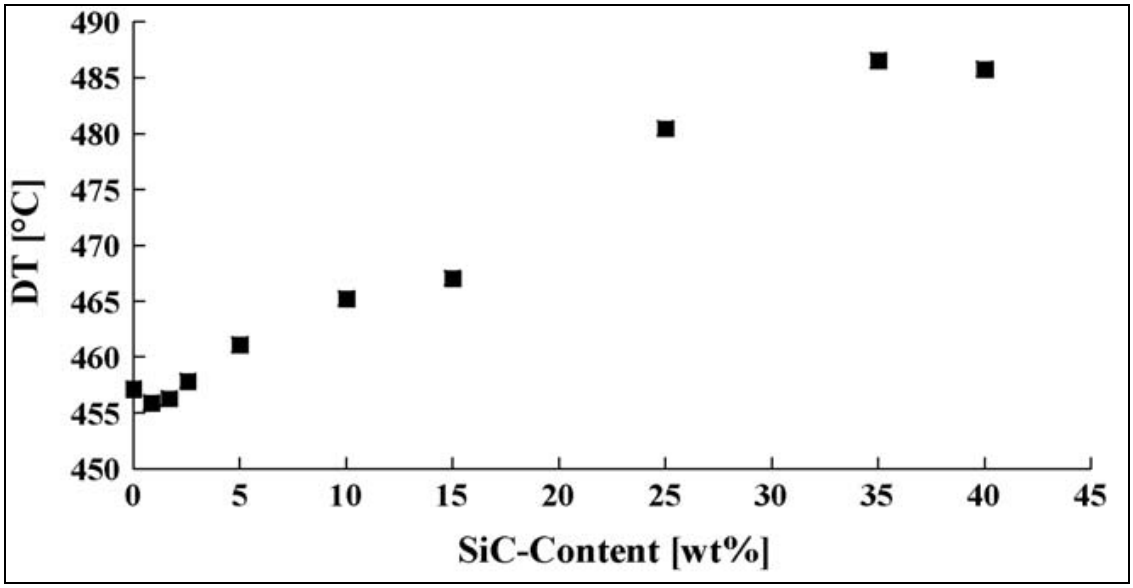

Figure 2.65: Degradation temperature (DT) vs. different SiC containing composites (Majewski et al., 2006).

2.8 Toughening Mechanisms in Polymer Nanocomposites

The toughness of polymers is believed to be primarily underpinned by mechanisms of plastic deformation. The plastic deformation zone is located ahead of the crack tip and it is a zone that is typically under plane strain condition. It is important to note that when polymers are tested for toughness they are typically subjected to high plastic constraint (Lim et al., 2007, Silva et al., 2006). If materials do not have constraint relief mechanisms, under this triaxial stress, materials such as polymers often are fractured in brittle mode exhibiting low toughness. Reinforcing polymers with toughening agents such as rubber particles or other flexibilizers, is one way to improve the toughness properties of these materials (Bagheri and Pearson, 1996, Kaynak et al., 2001). The problem with these traditional fillers, however, is that they, while improving the fracture toughness, generally compromise important mechanical properties (Johnsen et al., 2007, Robinette et al., 2004). Recent developments have shown by simultaneously improving the toughness polymer materials, without sacrificing other mechanical properties, nanoparticles can overcome the drawbacks of traditional toughening agents (Balakrishnan et al., 2005, Deng et al., 2008, Kitey and Tippur, 2005). This section discusses the relationships between nano-filler addition and the mechanisms of plastic deformation, crack pinning, crack deflection, de-bonding and plastic void growth, micro-cracking and crack bridging and how these relationships lead to increases of fracture toughness in polymer nanocomposites.

2.8.1 Plastic deformation of matrix

Due to the cross-linked molecular network architecture of thermosetting polymers, these polymers have a higher resistance to plastic deformation (i.e. shear banding and crazing) compared to thermoplasts. Nevertheless, plastic shear yielding can occur in thermosets polymers such as vinyl ester, epoxy and polyester. Plastic shear yielding is believed to represent an important toughening mechanism in neat polymers and particle-filled composites (Argon and Cohen, 2003, Lee and Yee, 2001). The addition of rigid-particulate fillers is believed to contribute to enhanced localized plastic deformation of

the polymer matrix (Wetzel et al., 2006). This enhanced shear banding and crazing causes enhanced fracture toughness. Formation and propagation of shear zones initiate at stress levels below the tensile strength, and causes partial orientation of the polymer chains (Kausch et al., 1973, Kawaguchi and Pearson, 2003). Shear banding formation will depend on the temperature and the local stress states. Microscopic regions of highly localized plastic deformation called crazes occurring in regions of high hydrostatic tension, cause the formation of micro-voids and fibrils oriented parallel to the tensile direction. When tensile load is sufficient, crazed regions elongate and break, causing the micro-voids to grow and unite and crack formation begins (Gloaguen and Lefebvre, 2001, Tanniru et al., 2006). More plastic deformation may exist in nanocomposites leading to higher fracture toughness. This is due to the large number of particles in these systems as compared to unfilled polymers

Deng et al. (2007) modified epoxy with 0, 4 and 8 wt.% silica nano-particles (with a narrow size distribution centred on 20nm) at different temperatures, - 50, 0, 23, 50 and 70 °C to evaluate fracture toughness. The silica nano-particles, with a narrow size distribution centred on 20nm, in this study were found to provide increased fracture toughness for epoxy resins without sacrificing strength, modulus and glass transition temperature properties. The study results showed that fracture toughness of the nano-silica modified epoxies, especially at room temperature and 50 °C, was noticeably increased. The greatest improvement was found in the systems of around 4 wt.% nano-silica. However, in a plasticised matrix at 70 °C, the nano-silica particles do not promote any mechanism to increase fracture energy. At low temperatures, the fracture mechanisms are similar to those at room temperature, although the influence of nano-silica in increasing fracture toughness is less pronounced at low temperatures. The increases in plastic deformation, as well as the crack deflection were the main toughening mechanisms observed on the fracture surfaces (Deng et al., 2007).

Zerda and Lesser (2001) reported that clay-filled glassy epoxy, upon compression, yields in shear with the evolution of a diffuse but visible shear-banding zone (Figure 2.66 a-b). The scattering of visible light in the band indicates the creation of new surface area in this region. When compression further applied past the yield point, the shear-

banding zone consumes the entire sample. The authors used SEM to further examine the shear-banding zone. In compression, the unfilled system exhibits a gross yielding behavior with no apparent void formation. However, in the filled systems (7 wt.% clay), void development was confined mostly within the large clay domains (figure 2.66 c). The clay particles, upon fracture, serve as stress concentration sites causing debonding at the clay-matrix interface or cleavage of clay tactoids leading to the formation of micro- or nano-voids. Before final fracture, these voids may be able to initiate shear yielding (plastic deformation) of the epoxy matrix at the crack and micro-crack tips throughout the entire volume, thus absorbing a significant amount of energy. The shear yielding of the matrix manifests in a step structure which contributes to surface roughness (Zerda and Lesser, 2001).

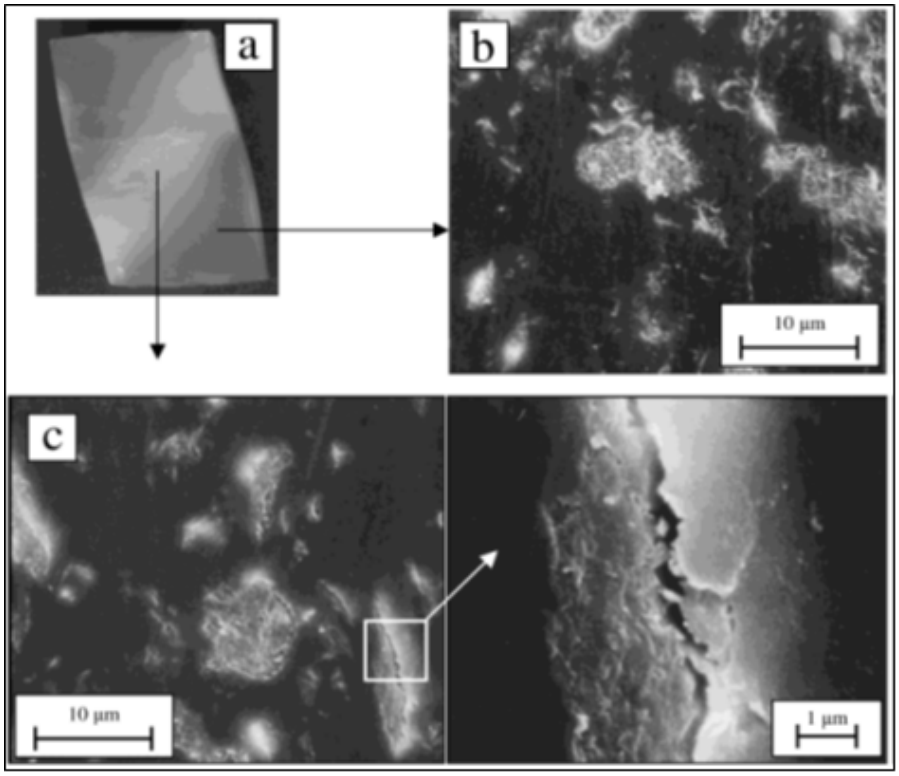

Figure 2.66: Micrographs showing compressive deformation in a 7 wt % clay sample: (a) macroscopic deformation showing diffuse shear band, (b) SEM micrograph of region outside shear band, and (c) SEM micrograph of region within shear band with void detail (Zerda and Lesser, 2001).

2.8.2 Crack pinning

Lange proposed that crack pinning was a useful mechanism for limiting the advancement of cracks in composite materials (Lange, 1970). Evans and Green further added to the theory by stating that rigid particles can act as arresting and pinning points during crack propagation (Wetzel et al., 2002). More specifically, as a crack starts to propagate within a composite material, the front of the crack encounters particle fillers and bows out between the rigid particles. The front of the crack remains pinned at all the positions where it has encountered filler particles. This is the initial stage of crack propagation. At this point, distortion of the crack front by pinning particles increases the length of the crack front. As this process of pinning generates secondary cracks as well as new fracture surfaces, stored strain energy can be alleviated. After passing particles, these secondary cracks unify after passing these obstacle and a fracture step may then be formed which occurs as a 'tail' (Liu et al., 2005, Park and Jana, 2003). When increases is strain energy are sufficient, local step fracture occurs. This causes the pinned points to be released. Figure 2.67 shows "tail-like" appearance at fracture surfaces caused by local step fracture. During the crack-pinning process, energy is absorbed and dissipated leading to increases in fracture toughness (Wetzel et al., 2006, Zhang et al., 2006).

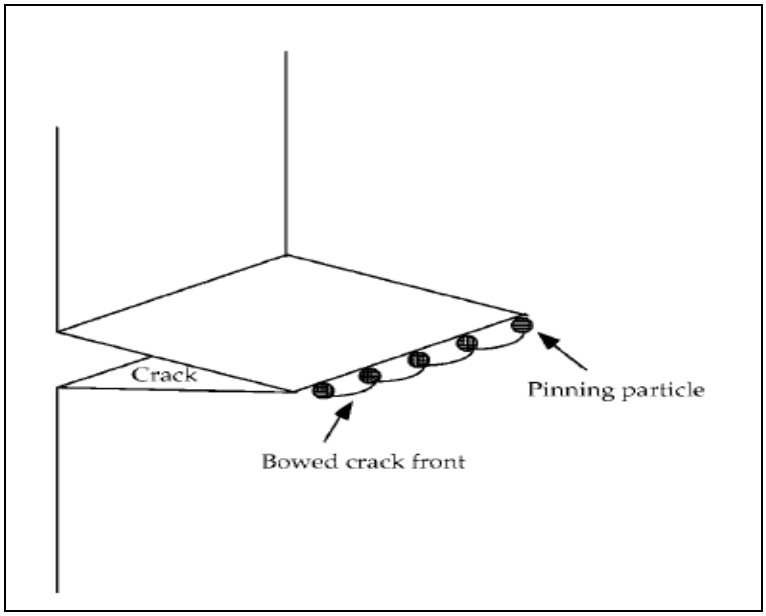

Figure 2.67: Diagrammatic representation of crack pinning in nanocomposites (Park and Jana, 2003).

Higher toughness is believed to be derived from crack-particle interactions as well as the interactions of a propagating crack front with impenetrable obstacles in brittle composites (Liu et al., 2005, Park and Jana, 2003). As mentioned previously, a crack propagating through a particle-filled matrix will encounter the particles as obstacles and these particles may pin the crack. As the front of the crack continues to move between these obstacles, the crack is bowing causes extension which leads to increase crack length. This phenomenon is believed to cause a higher 'line energy' which enhances crack resistance (Kinloch et al., 1985, Wetzel et al., 2006). Tail and crack bowing can be seen in Figure 2.68, obtained from the study of Wetzel et al. (2006). In this study, TiO_2 particles were added to epoxy. On the fracture surfaces of the epoxy/TiO_2 composites, tail features can be seen (Figure 2.68 item A). The magnification of the image (item B) provide evidence of crack pinning by showing bowing of the crack front between particles.

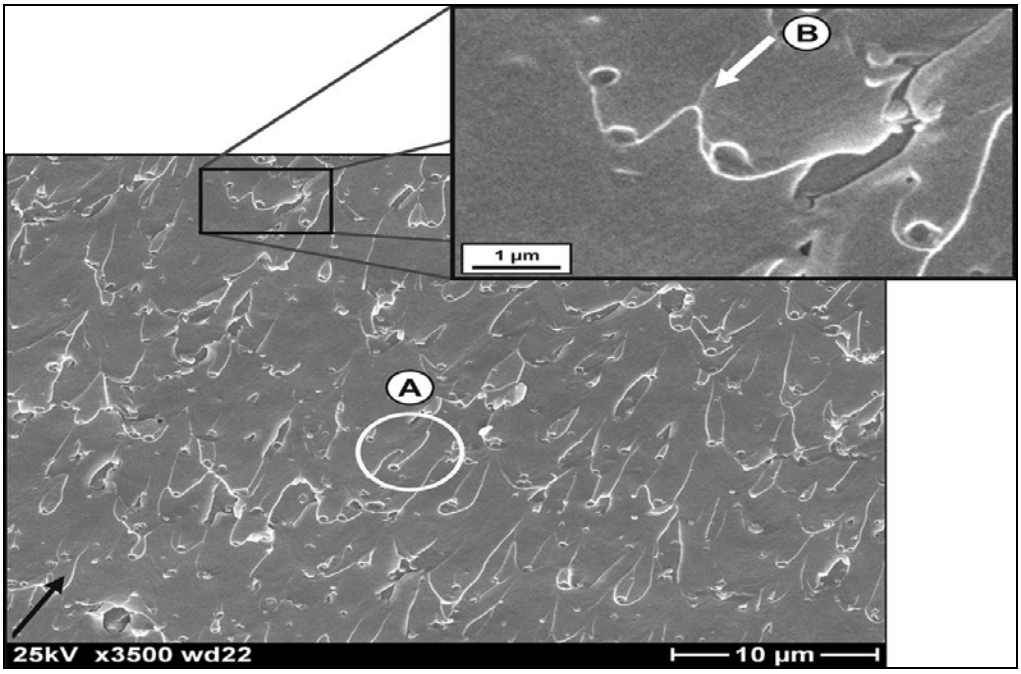

Figure 2.68: Crack pinning (item A) and crack front bowing (item B) in epoxy/TiO_2 (300 nm) nanocomposites (Wetzel et al., 2006).

The phenomenon of bowing results in increased absorption of energy. However, crack pinning in composites is only observed when the bonding between filler and matrix is

sufficient. This difference between good bonding and weak bonding is shown in Figure 2.69. In the study of Kawaguchi and Pearson, (2004) it was found that interfacial bonding with bisphenol-A epoxy resin was superior for glass spheres (GS) functionalized with aminopropyltrimethoxysilane (APS) as opposed to those functionalized with n-butylrimethoxysilane (nBS). As seen in Figure 2.69a, toughening by crack pinning is detectable from the tails behind the glass spheres in the case of treated glass spheres. However, there were no observable traces of crack pinning in the case of nBS-treated glass spheres which showed poor adhesion (Figure 2.69b).

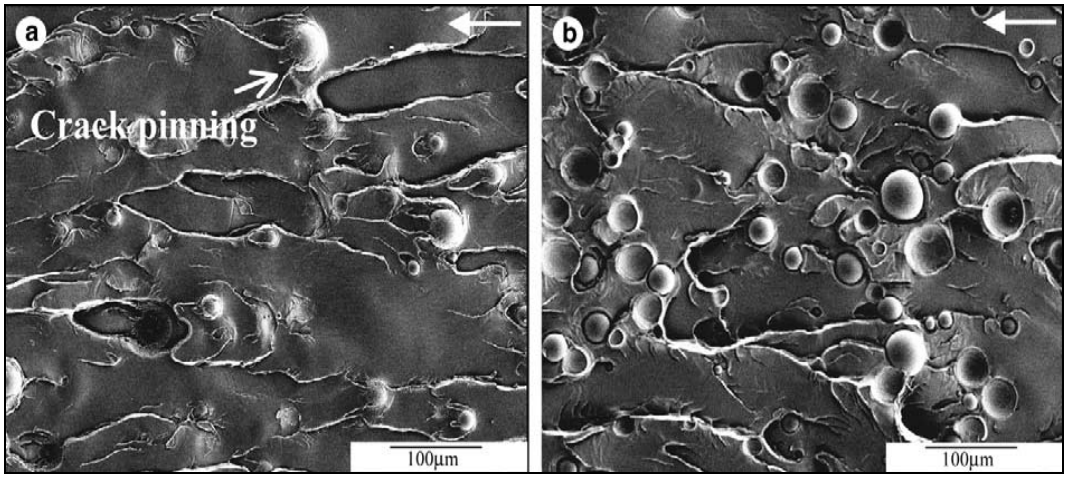

Figure 2.69: SEM images of fracture surfaces of fatigue for (a) the GS-APS-A epoxy (representing good bonding) and (b) the GS-nBS-A epoxy (representing weak bonding) (Kawaguchi and Pearson, 2004).

Crack pinning, however, appears to be rarely observed in nanoparticle filled resin systems (Becker et al., 2002, Ratna et al., 2003). A number of researchers such as Zerda et al. (2001) and Johnsen, et al. (2007) have called the effectiveness of nano-fillers as pinning agents into question. These authors believe is that typical crack surface displacement occurs on a length scale, and being larger than the nano-scale filler, so that the nano-scale filler does not generate a crack pinning pattern on the fracture surface. It is generally accepted that toughening occurs over a specific size range. It is also believed that effective toughening, at nanolength scales, might not be energetically favourable. Nanoparticles feature dimensions that are generally too small to provide the crack-pinning mechanism (Zerda and Lesser, 2001, Pavlidou and Papaspyrides, 2008).

Moreover, this may be the same reason why nanoparticles cannot effectively enhance crack-trajectory tortuosity. Without these mechanisms toughening is not observed. Therefore, fully exfoliated nanocomposites might not be suitable for the purposes of material toughening (Balakrishnan et al., 2005, Kaneko et al., 2013).

2.8.3 Crack deflection

During crack propagation in a particle-filled polymer, crack deflection at, or near, the interface of particles and polymers is a source of energy dissipation. As the front of a crack approaches the interface between a polymer and a particle, the front is presumed to potentially deflect by obstacles and that forces the front, through tilting and twisting, to move out of the initial propagation plane (Wang et al., 2011, Zhao et al., 2008b). This deflection causes a stress state change, from mode I to mixed-mode. For instance, mode I/II (tensile/in-plane shear) are in the case that the crack tilts, and mode I/III (tensile/anti-plane shear) if the crack twists (Chao and Liu, 1997, Gao and Shih, 1998, Liu et al., 2004). Compared to the driving force to propagate a crack in pure mode I, the driving force required to propagate a crack under mixed mode conditions is much higher. When crack deflection occurs, the total fracture surface area also increases as the crack front follows a tortuous path around particles. These events caused more energy to be absorbed during propagation in filled materials compared to propagation in unfilled materials (Liu et al., 2004, Wang et al., 2011, Zhao et al., 2008a).

Zerda and Lesser (2001) used a double-notched four-point bend technique (DN-4PB) to investigate epoxy-clay nanocomposites fracture behaviour. To perform this technique, two cracks of equal length are introduced into a specimen and identically loaded. One crack propagates to failure while the other another propagates sub-critically. Using optical microscopy (OM), cracks that survive can be used to study toughening mechanisms. The following figure, Figure 2.70, shows optical micrographs in which a straight crack with a smooth surface can be seen in the neat epoxy (Figure 2.70a), and a tortuous crack trajectory and exhibits evidence of crack branching along the crack path, can be seen in the intercalated nanocomposite (Figure 2.70b).

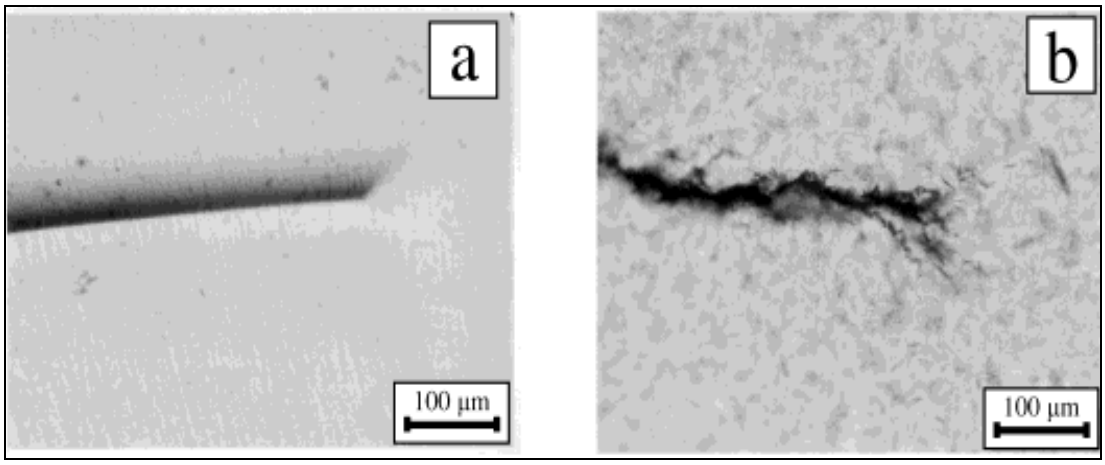

Figure 2.70: Optical micrographs showing DN-4PB specimen crack tip in (a) neat epoxy sample and (b) 10 wt.% clay sample (Zerda and Lesser, 2001)

Liu et al. (2004) investigated nanoclay addition effect epoxy-nanocomposite fracture behaviour and morphology. In this study, transmitted optical microscopy (TOM) was used to investigate arrested crack tip damage zone of the DEN-4PB specimens. Figure 2.71a shows that the unfilled epoxy contains a large crack tip damage zone. A sharp and straight crack path (with almost no deflection) is evident running through the material. Therefore, where there are featureless crack paths, running almost parallel to the direction of crack propagation, it is expected that any significant plastic shear deformation is absent. However, Figure 2.71b shows how small-size crack trajectories that are deflected and meandering through the matrix manifest in the nanocomposite containing 2 wt.% clay.

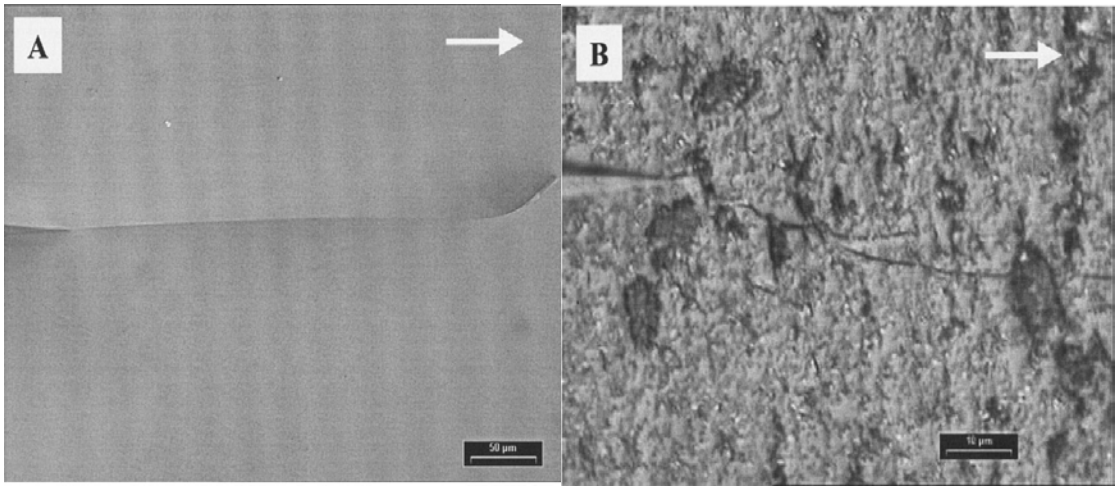

Figure 2.71: TOM images showing crack tip damage zones in (a) neat epoxy and (b) epoxy/clay nanocomposite (containing 2 wt.% nanoclay). Crack propagation direction indicated by arrows (Liu et al., 2004).

Using SEM, as shown in Figure 2.72, the researchers compared neat epoxy fracture surfaces with nanocomposite fracture surfaces (Li et al. 2004). A relatively smooth fracture surface with cracks in different planes but almost parallel to the crack-propagation direction is observable in the neat epoxy resin as indicated by a white arrow (Figure 2.72 a). This fracture surface appearance is a typical fractography feature of brittle fracture behaviour. In contrast, the fracture surfaces of the nanocomposites show considerably different fractographic features. The failure surface of the nanocomposite containing 2 wt.% clay is shown in Figure 72b. Upon adding clay into the epoxy matrix, a much rougher fracture surface is generally seen. Clay platelets make crack propagation more difficult, and this is believed to cause the crack tip to be deflected. Increased surface roughness observable on the sample is believed to be evidence of this. Liu et al. (2004) believe that increasing nanoclay content, past 2 wt.% clay, leads to an increasingly deflected crack path. The distance between the intercalated clay particles decreases as the clay concentration increases, which most likely accounts for the crack taking a more tortuous path around the clay particles (Liu et al., 2004).

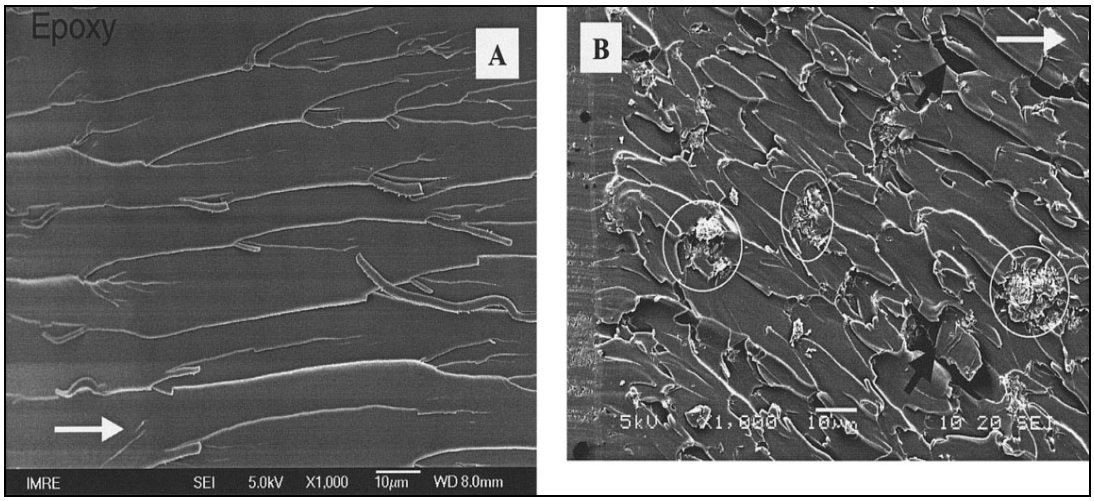

Figure 2.72: Fracture morphologies within the crack initiation region observed by SEM (a) neat epoxy and (b) epoxy/clay with 2 wt.% nanoclay (Liu et al., 2004)

Wetzel et al. (2002) studied the reinforcement of epoxy polymer with varying amounts of calcium silicate $CaSiO_3$ microparticles as well as the the reinforcement of epoxy polymer with varying amounts of titanium dioxide TiO_2 nanoparticles. The objective of the study was to compare the effect of different filler size addition on mechanical properties. The results showed that the mechanical properties of the composites using nano-size filler are better than those using micron size fillers. Optimum filler loading level was found to be 4vol% TiO_2 nanoparticles. The rougher and more textured fracture surface of the nanocomposites suggests that these materials exhibit more ductile fracture behaviour than the corresponding neat resin exhibit. The team indicated that the increase in ductile fracture behaviour was due to the activation of additional energy dissipating fracture mechanisms such crack deflection (Wetzel et al., 2002).

2.8.4 Particles/matrix de-bonding and plastic void growth

Another effective toughening mechanism for particle filled composites is particles/matrix de-bonding. This mechanism occurs when rigid particles from the polymer matrix de-bond. Typically, de-bonding occurs when interface local tensile stress is greater than thermal mismatch stress and interfacial cohesive strength (Wetzel

et al., 2003, Zuiderduin et al., 2003). This void growth toughening mechanism is frequently observed for rubber toughened polymer systems. For nanocomposites, interface-dominated materials, there can be large energy dissipation if significant de-bonding occurs at the interfaces. In addition, the de-bonding of the particles allows another key energy dissipation mechanism, the subsequent plastic void growth within the polymer (Figure 2.73).

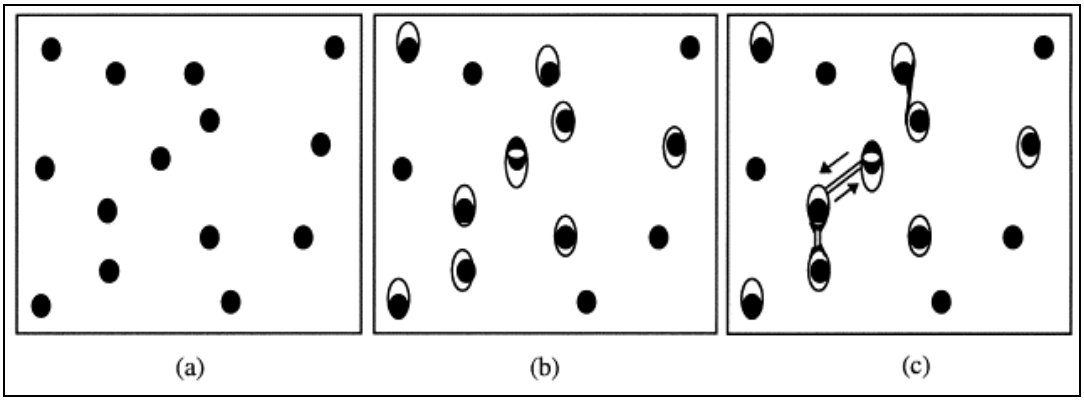

Figure 2.73: (a) distribution of hard particles, (b) particle/matrix de-bonding, and (c) void-growth mechanism (Chevrier and Klepaczko, 1999).

It is generally accepted that, compared to the plastic deformation of the matrix, the de-bonding process absorbs little energy. De-bonding, nonetheless, is essential because it reduces constraint at crack tip allowing the matrix to deform plastically via a void growth mechanism (Hsieh et al., 2010, Norman and Robertson, 2003).

Johnsen et al. (2007) attributed the majority of the toughness increment seen in nanocomposites to the plastic void growth mechanism. The team found a mean fracture toughness, K_{Ic}, of 0.59 MN m $^{-3/2}$ for unmodified epoxy polymer. This measured toughness was increased by the addition of nanosilica. A maximum K_{Ic} of 1.42 MN m$^{-3/2}$ was measured for the polymer at 13.4 vol% nanosilica. The fracture energy increased from 100 J/m^2 for the unmodified epoxy polymer to 460 J/m^2 for the epoxy polymer with 13 vol% of nanosilica. SEM and atomic force microscopy (AFM) micrographs of the fracture surfaces revealed nanoparticles surrounded by voids providing evidence of de-bonding of the nanoparticles and subsequent plastic void growth (Figure 2.74).

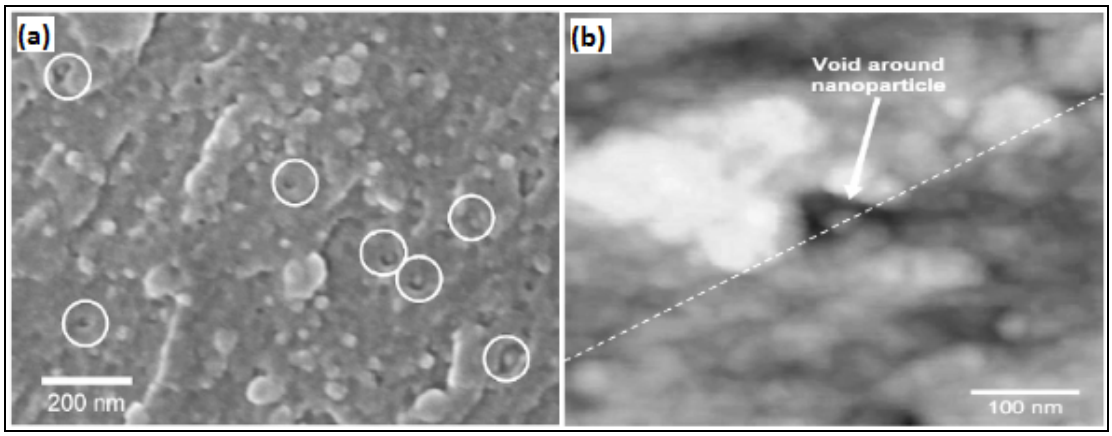

Figure 2.74: (a) SEM micrograph and (b) AFM micrograph of a fracture surface of the epoxy polymer containing 9.6 vol% nanosilica, voids with nanoparticles are circled (Johnsen et al., 2007).

Hsieh et al. (2010) evaluated fracture properties of four epoxy polymers reinforced with silica nanoparticles at concentrations of 0, 10 and 20 wt.%. The silica nanoparticles were characterised as being well dispersed amongst the matrices. The team concluded that localised shear bands initiated by the stress concentrations around the periphery of the silica nanoparticles, and de-bonding of the silica nanoparticles followed by subsequent plastic void growth of the epoxy polymer were two important toughening mechanisms (Hsieh et al., 2010).

The energy absorbed during the process, primarily through particle de-bonding and plastic void growth is believed to be dependent on adhesion, particle-matrix interface interfacial properties, and far-field applied stress (Hsieh et al., 2010, Pukánszky and Maurer, 1995). Nano-size particles are believed to have the advantage of being able to create a higher number of voids when compared to micron sized fillers at the same filler weight percentage. This means that the polymeric material is more involved in the plastic deformation process. Moreover, voids created by nano-fillers are smaller and more stable than those created by a micro-filler, avoiding early brittle fracture.

2.8.5 Micro-cracking and crack bridging

When micro-cracking is observed near to the crack tip, it reduces stress intensity and improves overall fracture toughness. Zones of micro cracking reduce local modulus and lead to local stress reduction. Micro-cracking, as a result of differential thermal shrinkage between polymer and fillers, also releases residual stress present in composites. Particular size and spatial distributions of micro-cracks near the main crack tip may be able to shield the crack and slow further crack advancement (Wouterson et al., 2007, Ye et al., 2007).

Wang et al. (2005) studied the vicinity of an arrested crack tip of an epoxy/clay nanocomposite using a DN-4PB specimen (Figure 2.75). Incipient cracks were found that consist of several discontinuous cavities which were believed to be closely associated with clay platelets (Figure 2.75a). In the region ahead of the arrested crack tip, long, narrow micro-cracks associated with clay were also found (Figure 2.75b). It can be seen that most of the micro-cracks are formed either along the matrix-clay interface or on the delaminated clay platelets.

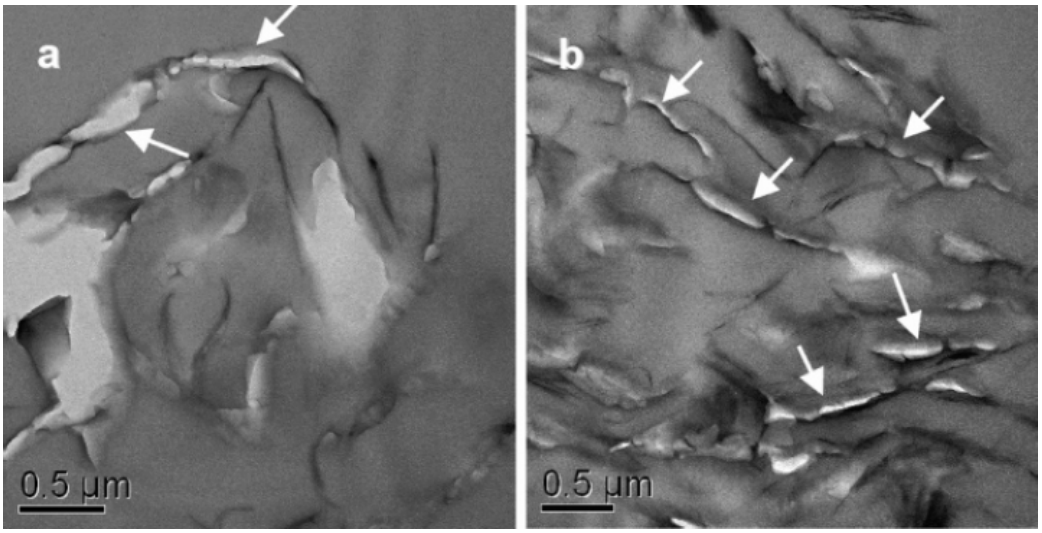

Figure 2.75: TEM micrographs of thin sections taken from the region in front of arrested crack tip in epoxy/clay nanocomposites (Wang et al., 2005).

TEM was used to study the crack propagation of a double-cantilever-beam specimen, as shown in Figure 2.76. Micro-cracks can be seen (Figure 2.76 a and b) to develop into a main crack with a multitude of secondary cracks formed perpendicular to the main crack. Figure 2.76 c shows how these secondary cracks cease after a short crack extension, and their tips are blunted. Wang et al. (2005) concluded that the initiation and development of a large number of micro-cracks due to the delamination of clay layers and the increase of fracture surface area due to crack deflections (Figure 2.76), led to the improvement in toughness. In accounting for the events, the team described, compared to the fracture toughness from 0.70 MPa.m$^{1/2}$ in neat epoxy, the addition of 2.5 wt.% of clay increase fracture toughness to 1.26 MPa.m$^{1/2}$ in the epoxy nanocomposites.

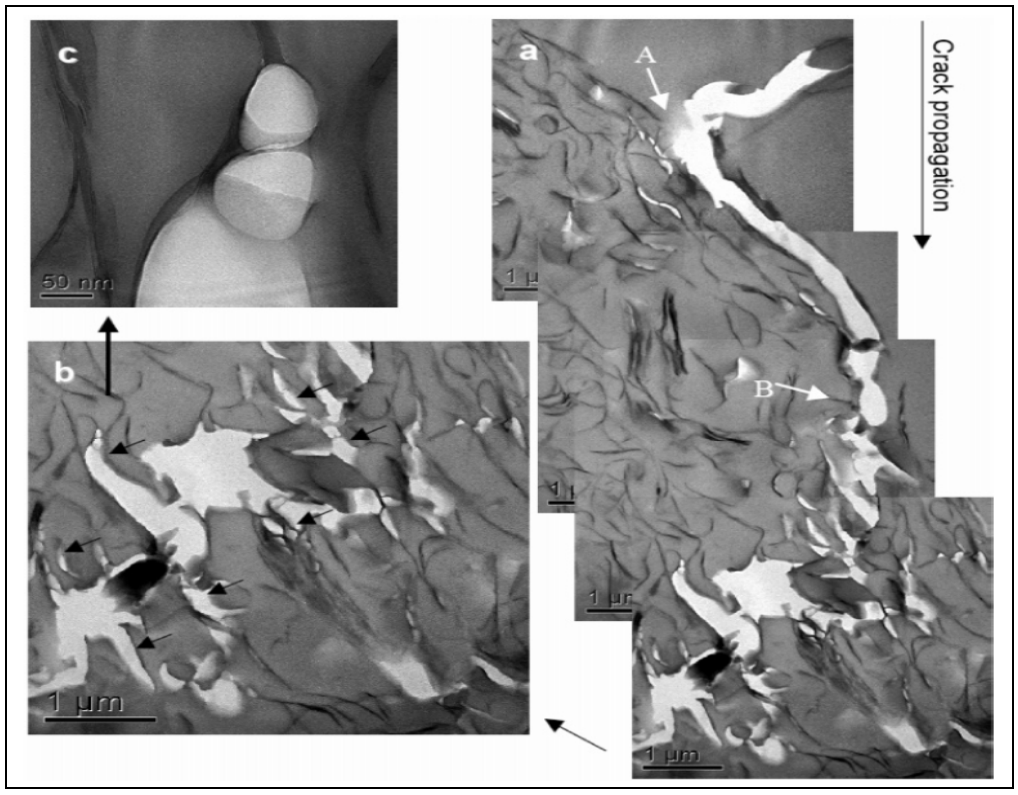

Figure 2.76: TEM micrographs showing crack propagation in epoxy-clay nanocomposites (Wang et al., 2005).

Similarly, multiple cracking was also reported by Sue et al. (2004) to be a primary reason for the increased toughness in epoxy/α-ZrP nanocomposites where α-ZrP layers

partially exfoliated. In this study, voiding, from the delamination of the intercalated α-ZrP platelets (Figure 2.77), along the crack path in the crack tip region caused the formation of micro-cracks.

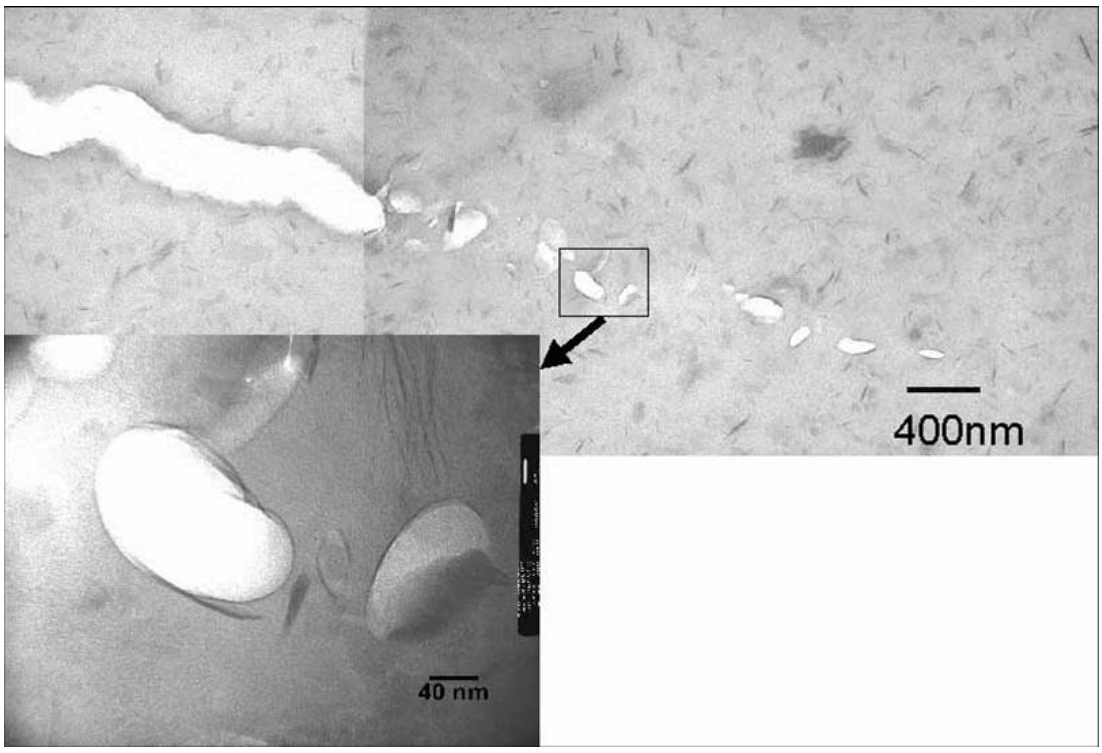

Figure 2.77: TEM showing epoxy/α-ZrP nanocomposite crack tip damage zone. The delaminated micro-cracks are observable at the crack tip region (Sue et al., 2004).

Crack bridging is also reported to be an effective toughening mechanism for particle reinforced composite materials. Nanotubes, near the crack tip, bridge the crack tip and slow down the crack growth. As the stress increases, nanotube pull-out or breakage occur leading to partial dissipation of strain energy near the crack tip. Thus, the quantum of toughness increase is dependent on the filler's length, aspect ratio, and surface properties. Studies by Ye et al. (2007) and Deng et al. (2008) have showed that micro-cracks were spanned by halloysite nanotubes causing enhanced resistance to the crack propagation (Figure 2.53 b).

2.9 Natural fibre Reinforced Polymer Nano-composites

The use of synthetic fibre to reinforce nanocomposite matrices has been studied by a number of researchers (Bozkurt et al., 2007, Gojny et al., 2005, Kinloch et al., 2006, Tsai and Wu, 2008, Xu and Hoa, 2008). However, investigation of the reinforcement of nanocomposite matrices with natural fibres is yet to be widely explored.

For example, Faruk and Matuana (2008) investigated the mechanical properties of wood/epoxy nanocomposites. The study conducted to investigate the effect of using different preparation methods, and different nanoclays, on the flexural and tensile properties of wood/epoxy nanocomposites. Melt blending process and direct dry blending process wood/epoxy nanocomposite fabrication methods were compared. Similarly, the effects of five nanoclays (Cloisite 10A, 15A, 20A, 25A, and 30B) were compared. Concerning the different preparation methods, melt blending process involved clay reinforced epoxy being used as a matrix for the wood/epoxy nanocomposites. In contrast, direct dry blending process involved nanoclay being directly added into the wood/epoxy composites. Using the melt blending method, the researchers found that the addition of nanoclay enhanced both flexural and tensile properties. The results also indicated that Cloisite 10A provided markedly superior mechanical properties. Faruk and Matuana (2008) attributed this to the favourable intercalation of this nanoclay. The team then investigated the effect of using different preparation methods on the flexural properties of wood/Cloisite10A/epoxy nanocomposites. Compared to the unfilled wood/epoxy composites, the flexural strength and flexural modulus of wood/Cloisite10A/epoxy nanocomposites fabricated using the melt blending process were superior (Table 2.19). However, when the direct dry blending process was used to fabricate wood/Cloisite10A/epoxy nanocomposites the resulting flexural strength was lower than that of the unfilled wood/epoxy composites, and while the flexural modulus had increased, the increase was not as significant as the increase observed using the melt blending process (Table 2.19).

Table 2.19: The effect of the direct dry blending process compared to the melt blending process on the flexural properties of wood/Cloisite 10A/epoxy nanocomposites (Faruk and Matuana, 2008).

Blending process	Flexural properties	
	Strength (MPa)	Modulus (MPa)
Control (no nanoclay)	28.9 ± 1.4	1919.7 ± 112
Direct dry blending (direct mix)	27.1 ± 1.4	2233.8 ± 144
Melt blending (HDPE/nanoclay as matrix)	33.5 ± 0.4	2726.9 ± 196

Satapathy et al. (2009) studied the physical and mechanical properties of jute fibre reinforced epoxy/ nano-silicon carbide (n-SiC) nanocomposites. The researchers investigated the effect n-SiC addition on these properties for the resultant jute fibre reinforced epoxy/nSiC nanocomposites. Satapathy et al. (2009) prepared 40 wt.% jute fibre reinforced epoxy nanocomposites filled with either 10 or 20 wt.% n-SiC. The results revealed that after the addition of SiC, tensile and flexural strength of unfilled composites increased as jute fibre content increased. However, the addition of SiC into composites led to a reduction in both tensile and flexural strength as seen in Figure 2.78. Authors claimed that the incorporation of SiC particles could reduce the stress transfer at the matrix/fibres interface resulted in low tensile strength.

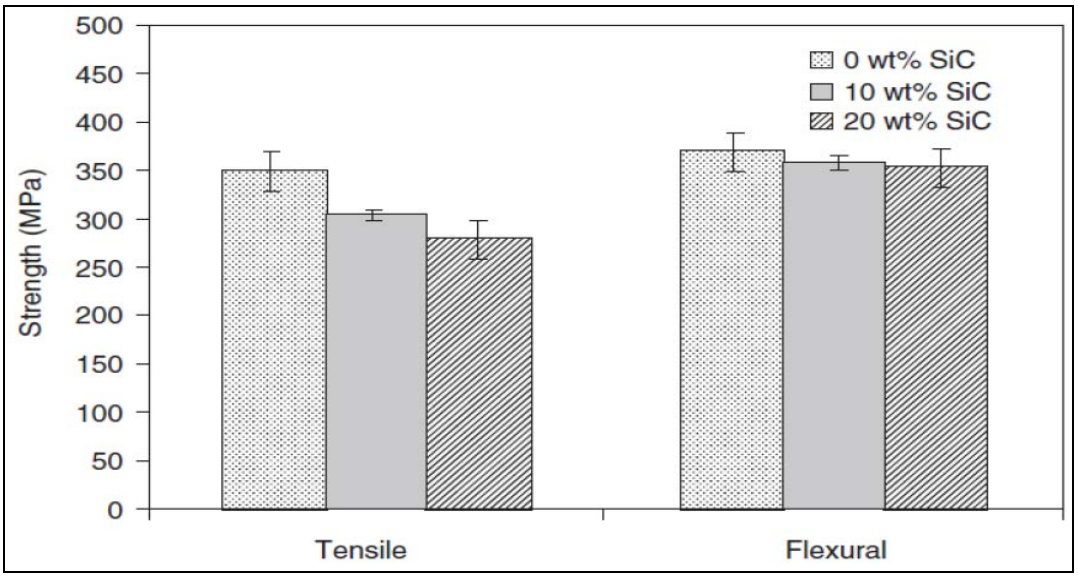

Figure 2.78: Tensile and flexural strength of jute fibre/epoxy composites as a function of SiC content. (Satapathy et al., 2010).

Mohan and Kanny (2011) studied the water absorption behaviour of sisal fibre reinforced epoxy/clay nanocomposites. The team investigated the effect on water uptake of nanoclay addition to sisal fibre/epoxy composites at three weight fractions (1%, 3%, 5% wt.%). Included in the study was microclay addition at 5%. The results revealed the dramatic reduction in water content that was associated with clay addition at each of the concentrations to sisal fibre/epoxy composites. By reducing water mass uptake, the presence of nanoclay improved the water barrier properties of the sisal fibre/epoxy nanocomposites as shown in Figure 2.79. As the clay content increased, water mass uptake decreased, and the maximum reduction of water mass uptake occurring with 5 wt.% nanoclay. A useful finding of the study was the comparison of the barrier properties of sisal fibre/epoxy composites filled with 5 wt.% microclay and sisal fibre/epoxy composites filled with 5 wt.% nanoclay. The latter was found to provide superior barrier properties to the resultant sisal fibre reinforced epoxy/clay nanocomposites.

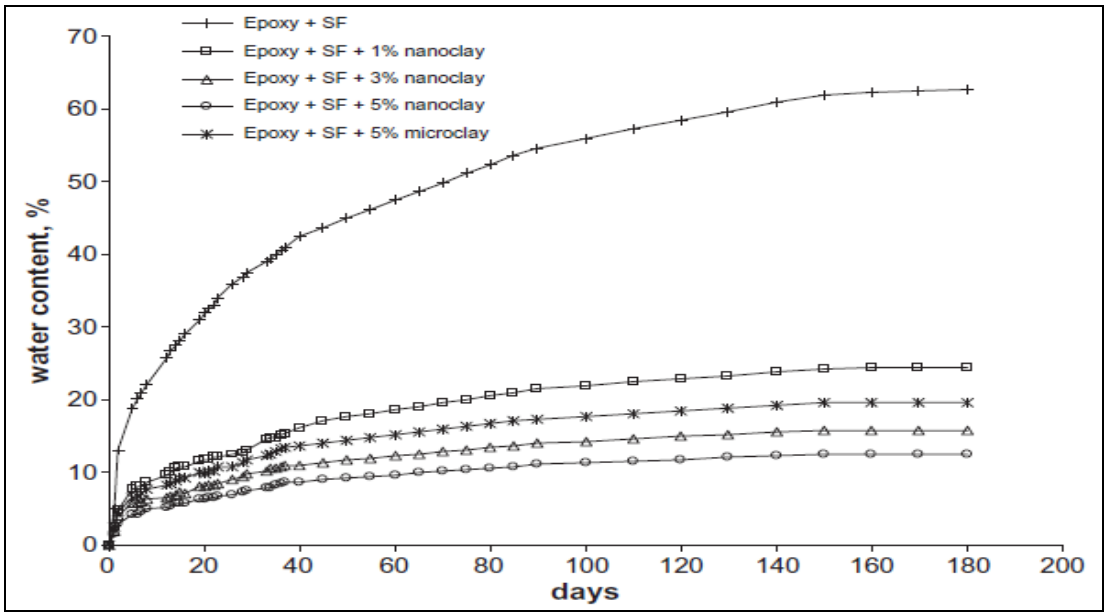

Figure 2.79: The effect on water uptake of nanoclay addition to sisal fibre/epoxy composites at 1%, 3%, 5%, and 5% microclay (Mohan and Kanny, 2011).

LIST OF PUBLICATION INCLUDED AS PART OF THE THESIS

(Listed in order as found on this thesis)

ALHUTHALI, A. and LOW, I. M. 2013. Mechanical properties of cellulose fibre reinforced vinyl-ester composites in wet conditions. *Journal of Materials Science*, 48, 6331-6340.

ALHUTHALI, A. and LOW, I. M. and DONG, C. 2012. Characterisation of the water absorption, mechanical and thermal properties of recycled cellulose fibre reinforced vinyl-ester eco-nanocomposites. *Composites Part B: Engineering,* 43, 2772-2781.

ALHUTHALI, A. and LOW, I. M. 2013. Influence of halloysite nanotubes on physical and mechanical properties of cellulose fibres reinforced vinyl ester composites. *Journal of Reinforced Plastics and Composites,* 32, 233-247.

ALHUTHALI, A. and LOW, I. M. 2013. Multi-scale hybrid eco-nanocomposites: synthesis and characterization of nano-SiC-reinforced vinyl-ester eco-composites. *Journal of Materials Science,* 48, 3097-3106.

ALHUTHALI, A. and LOW, I. M. 2013. Water absorption, mechanical, and thermal properties of halloysite nanotube reinforced vinyl-ester nanocomposites. *Journal of Materials Science,* 48, 4260-4273.

ALHUTHALI, A. and LOW, I. M. 2013. Mechanical and fracture properties of halloysite nanotube reinforced vinyl-ester nanocomposites. *Journal of Applied Polymer Science*, DOI: 10.1002/app.39348

ALHUTHALI, A. and LOW, I. M. 2013. Characterization of Mechanical and Fracture Behaviour in Nano-Silicon Carbide-Reinforced Vinyl-Ester Nanocomposites. *Polymer-Plastics Technology and Engineering*, 52, 921-930.

3.1. Mechanical properties of cellulose fibre reinforced vinyl-ester composites in wet conditions

---

ALHUTHALI, A. and LOW, I. M. 2013. Mechanical properties of cellulose fibre reinforced vinyl-ester composites in wet conditions. *Journal of Materials Science*, 48, 6331-6340.

J Mater Sci (2013) 48:6331–6340
DOI 10.1007/s10853-013-7432-4

Mechanical properties of cellulose fibre reinforced vinyl-ester composites in wet conditions

A. Alhuthali · I. M. Low

Received: 19 February 2013 / Accepted: 6 May 2013 / Published online: 21 May 2013

Abstract The effect of prolonged water absorption on the physical and mechanical properties has been investigated for vinyl-ester composites reinforced with natural fibres. The elastic modulus of these composites was measured and the data were validated with various mathematical models. The modelling results revealed that the experimental data matched the data predicted by the Cox–Krenchel model. Prolonged exposure of these composites to water absorption caused a reduction in elastic modulus and strength.

Introduction

The rationale underpinning the synthesis of polymer–matrix composites is that the lower stiffness and strength of polymers is generally improved through the addition of stiffer and stronger fibres. Aramid, glass, polyethylene and carbon are commonly used for fabricating polymer composites. As a result of growing global concern over greenhouse gas emissions, the depletion of petroleum resources, natural fibres are now increasingly used which include flax, hemp, jute, coconut, cotton, kenaf and sisal [1]. Unlike most synthetic fibres, natural fibres are completely biodegradable; they will not remain in the environment for millions of years, as synthetic fibres are likely to do. Moreover, natural fibres require less energy to produce than glass and carbon fibres if the life cycle assessment of these fibres is taken into consideration [2].

Natural fibres have a lower density (1.25–1.5 g/cm^3) than carbon fibres (1.8–2.1 g/cm^3) and E-glass (2.54 g/cm^3) [8]. In addition, products reinforced with natural fibres are lighter than those that are reinforced with synthetics. With an excellent modulus–weight ratio, natural fibres are successful in stiffness-critical designs [3]. The favourable acoustic damping properties of natural fibres over glass and carbon fibres also make them suitable for noise attenuation purposes a requirement for many automobile interior products [4].

Newspapers, printed paper and cardboard are recognised as useful sources from which cellulose fibres can be extracted [5]. Composites reinforced with cellulose fibres from newspaper have comparable properties to those reinforced with wood fibres [6]. Most importantly, cellulose fibres reinforced composites are easily produced with lower cost, greater renewability of the resource, greater flexibility and lower wear on processing machinery [7].

However, natural fibre reinforced polymeric composites still must overcome inherent incompatibility issues. For example, natural fibres are hydrophilic and matrix components are hydrophobic, which negatively affects the strength of composites. Thus, to improve fibre–matrix adhesion and prevent this loss of strength, physical and chemical treatment of the fibre surface is required [8]. Moisture-related problems must also be considered, as climatic conditions influence water absorption mechanisms [9]. For example, at high levels, humidity enables water to diffuse into polymeric composites primarily via inter-polymer chain microgaps. This also occurs to a lesser degree via the fibre–matrix interfaces, by using capillary transport to trace any gaps or flaws caused by incomplete wettability and impregnation. Lastly, it also occurs via microcracks in the matrix that result from swelling of the natural fibres [10]. The volume fraction of fibre, the presence of voids, the viscosity of the matrix, the humidity, and the temperature are all relevant when determining the extent to which moisture diffusion will occur in a composite [11].

A. Alhuthali · I. M. Low (✉)
Department of Imaging & Applied Physics, Curtin University, GPO Box U1987, Perth, WA 6845, Australia
e-mail: j.low@curtin.edu.au

In this article, an infiltration method was used to prepare vinyl-ester composites reinforced with cellulose fibres. This approach enabled the fabrication of polymer composites with minimum voids and large fibre–volume fraction. High fibre content is generally desired to achieve high performance in short fibre reinforced polymer (SFRP) composites as is the case in this study. The effect of prolonged water absorption on the flexural strength and modulus of these composites was investigated.

Experimental

Materials

RCF sheets of grade 80 GSM and 100-μm thickness were supplied by Todae Company, New South Wales, Australia. A general purpose vinyl-ester resin was supplied by Fibreglass and Aesin Sales Pty Ltd, Perth, Western Australia.

Samples preparation

To provide the baseline data, pure vinyl-ester resin (VER) samples were made as controls. Preparation of these samples required the VER to be mixed with a 1.0 wt% catalyst (MEKP). To ensure that no air bubbles were formed within the matrix, the system was slowly and thoroughly mixed. The resultant mixture was then poured into silicon moulds and left under low vacuum (20 kPa) for 2 h, then left at room temperature for 24 h to cure. To prepare the VER/RCF composites, it was necessary to remove stored moisture in RCF. To do this, the RCF sheets were dried at 150 °C in a fan-assisted oven for 60 min. Storage moisture was recorded to be approximately 10 %. The RCF sheets were then fully soaked in the vinyl-ester system and laid-up in the mould. During the laying-up of the RCF sheets, low pressure was applied frequently to remove trapped air bubbles. The moulds were placed under compressive pressure and in a vacuum of 60 kPa for 2 h. The composites were then left at room temperature to cure for 24 h. To investigate the effect of the fibre content on the physical and mechanical properties of the VER/RCF composites, samples with 20, 30, 40 and 50 wt% fibre were fabricated. These composites were then labelled VER/20 % RCF, VER/30 % RCF, VER/40 % RCF and VER/50 % RCF, respectively.

Density and void content

The fibre volume fraction, the density and void content of the composites were determined according to ASTM D2734-94 standard [12] by using the following equations:

$$V_v = [(p_{ct} - p_{ce})/p_{ct}] \times 100 \quad (1a)$$

$$p_{ct} = 1/[W_f/p_f + W_m/p_m] \quad (1b)$$

$$p_{ce} = M/V \quad (1c)$$

$$V_f = (W_f/p_f)/[W_f/p_f + W_m/p_m] \quad (1d)$$

where V_v is the void fraction percentage, p_{ct} and p_{ce} are the theoretical density and the experimental density of the composites, respectively. W_f and W_m are the weight fractions, and p_f and p_m are the densities of the fibre and matrix, respectively. V_f is the fibre volume fraction (where there are no voids). M and V are mass and volume, respectively.

Water uptake test

The water absorption of the composites was determined as a percentage by using the difference in weight between dry samples and samples immersed in water. This is shown in the following equation [13]:

$$W_A = \frac{M_T - M_D}{M_D} \times 100 \quad (2)$$

where W_A is water uptake, M_D is dry mass and M_T is mass of the sample soaked, within time, T.

Different models to describe the moisture absorption behaviour of materials have been developed over time [13]. For moisture absorption that is one-dimensional, each sample is exposed on two sides to the same environment. The following equation can be used to express total moisture content (G) [14]:

$$G = \frac{m - m_i}{m_s - m_i} = 1 - \frac{8}{\pi^2}\sum_{j=0}^{\infty}\frac{1}{(2j+1)^2}\exp\left[-\frac{(2j+1)^2\pi^2 D_x t}{h^2}\right] \quad (3)$$

where m_i is the initial weight of moisture in the material and m_s is the weight of moisture in the fully saturated material in equilibrium with its environment. D is the mass diffusivity in the composite, which represents effective diffusivity as heterogeneities of the composites have been neglected. t is time, h is thickness of the specimen and j represents the summation index. The diffusion coefficient is an important constraint of Fick's law [15]. The following equation [14] shows how the diffusion equation for the weight of moisture can be determined and then rearranged in terms of moisture content (W):

$$W = \frac{4M_m}{h}\left(\frac{t}{\pi}\right)^{0.5} D_x^{0.5} \quad (4)$$

where M_m is the moisture content of the sample at equilibrium or when no more moisture is absorbed. The value of M_m corresponds to the maximum absorption of

moisture. A graph of weight gain versus time can be plotted by using the weight gain data of the material with respect to time. Using the following equation, by considering the slope of the first part of the weight gain curve versus the square root of time, the diffusion properties of the composites described by Fick's laws were evaluated by using the weight gain measurements of the pre-dried specimens immersed in water. The diffusion coefficient (D) can be defined as the slope of the normalised mass uptake set against the square of time. This takes the form [15]:

$$D = \pi\left(\frac{kh}{4M_m}\right)^2 \quad (5)$$

where k is the initial slope of the plot of $M(t)$ versus $t^{1/2}$, M_m is the weight gain maximum, and h is composite thickness.

Elastic modulus and flexural strength

Rectangular bars of 60 mm × 10 mm × 10 mm were cut from the fully cured samples for three-point bend tests, with a span of 40 mm, to evaluate the elastic modulus and flexural strength. A LLOYD material testing machine (5–50 kN) with a displacement rate of 1.0 mm/min was used to perform the test. Five samples of each group were used to evaluate elastic modulus and flexural strength. The values of each measurement were recorded and analysed with machine software (NEXYGENPlus), and averages values were calculated.

Microstructure examination

A NEON 40ESB, scanning electron microscope, SEM, (ZEISS, UK) operating at accelerating voltage of 5 kV, under secondary electrons mode was used to examine the microstructure of the RCF and fracture surfaces of the samples. In order to avoid charging, all samples were coated with platinum.

Theoretical models

Theoretical models have been proposed for modelling the elastic modulus properties of composite material based on the parameters of the composites. Thus, it is the properties of components, as well as their arrangement, that determine the outcomes of the models of mechanical properties. Elastic modulus, Poisson's ratio and the relative volume fractions of the fibre and matrix are the inputs used in mathematical modelling. To a lesser extent, fibre aspect ratio and fibre orientation are also used. In this study, the experimental results for the elastic modulus were compared with the theoretical values obtained from micromechanical modelling, based on the following models.

Rule of mixtures (ROM) and inverse rule of mixtures (IROM) models

The ROM is one of the simplest models for the prediction of the elastic properties of composite materials. Presuming that the matrix and fibre experience the same strain, and that this strain is a result of uniform stress applied over a uniform cross-sectional area, the elastic modulus of the composite material in one direction (E_1) can be determined according to the ROM and the IROM equations. For apparent elastic modulus in the fibre direction, the ROM equation is [16]:

$$E_1 = E_f V_f + E_m V_m \quad (6)$$

where E_f, E_m, V_f and V_m are the respective moduli and volume fractions for the fibre and matrix materials.

The ROM is useful for aligned continuous fibre composites, particularly when there is the correct assumption of equal strain in the two components. Elastic modulus of a composite in the two directions (E_2) is calculated, presuming that the applied transverse stress is equal in the fibre and matrix. This means that E_2 is determined using the IROM, as given by [16]:

$$E_2 = \frac{E_f E_m}{V_m E_f + V_f E_m} \quad (7)$$

When composites have well-bonded reinforcements, the values predicted by the ROM mixtures or the IROM equations serve as the upper and lower bounds for elastic modulus in the principal fibre direction [17].

Halpin–Tsai model

Halpin and Tsai developed a semi-empirical model that is widely used for modelling the elastic properties of short fibre reinforced composites. For short fibre reinforced composites, the Halpin–Tsai equation, in the following form, is used to predict the elastic modulus [18]:

$$E = E_m\left(\frac{1 + \xi\eta V_f}{1 - \eta V_f}\right) \quad (8)$$

The parameter η, which depends on various characteristics of the reinforcing phase, such as the shape and aspect ratio of the fibres, is given as:

$$\eta = \frac{(E_f/E_m) - 1}{(E_f/E_m) + \xi} \quad (9)$$

where ξ in Eqs. 11 and 12 is a shape fitting parameter to fit the Halpin–Tsai model to experimental data. This parameter considers the packing arrangements and

geometry of the reinforcing fibre. The following equation [19] gives ξ when the elastic modulus in the principal fibre direction is required, and the fibres are circular in shape:

$$\xi = 2(l/d) \tag{10}$$

where l is the length of the fibre in one direction and d is the diameter of the fibre.

Tsai–Pagano model

Tsai and Pagano developed a method to model elastic modulus in those composites containing short fibres with random orientation [20]. This model has similarities to Halpin and Tsai's equation. It is given as:

$$E = \frac{3}{8}E_1 + \frac{5}{8}E_2 \tag{11}$$

where E is the elastic modulus of the composite, and E_1 and E_2 are the elastic moduli of fibre reinforced composites containing short fibres with random orientation, as given by the Halpin–Tsai model [21]:

$$E_i = E_m\left(\frac{1 + \xi_i\eta_i V_f}{1 - \eta_i V_f}\right) \tag{12}$$

$$\eta_i = \frac{(E_f/E_m) - 1}{(E_f/E_m) + \xi_i} \tag{13}$$

$$\xi_i = 2(l_f/d_f) \quad \text{for } i = 1 \quad \text{or} \quad \xi_i = 0.5 \quad \text{for } i = 2 \tag{14}$$

Cox–Krenchel model

The Cox–Krenchel model is a relatively simple mathematical equation for modelling. This yielded good agreement with the experimental elastic modulus values for a range of glass fibre lengths and volume fractions. The model also performed acceptably well for certain natural fibre composites [22]. The composite elastic modulus, E, is related to the fibre and matrix moduli, E_f and E_m, and the fibre volume fraction, V_f, by using a ROM type of relationship [23]:

$$E = \eta_{0E}\eta_{lE}E_fV_f + (1 - V_f)E_m \tag{15}$$

where η_{0E} is the orientation factor and η_{lE} is the fibre length efficiency factor. In the case of reinforcing fibres of length, l, the fibre length efficiency factor is given by [22].

$$\eta_{lE} = 1 - \frac{\tanh(\beta l/2)}{\beta l/2} \tag{16}$$

where the value of β, which represents the orientation of fibres, can be expressed as:

$$\beta = \frac{1}{r_f}\sqrt{\frac{2E_m/(1+v)}{E_f \ln(\pi/4V_f)}} \tag{17}$$

where r_f is the fibre radius and v is Poisson's ratio of the matrix.

Results and discussion

Density and void content results

Table 1 provides results for the density, fibre volume fraction and void content of the samples. As the weight fraction of the fibre increased, the theoretical and experimental composite densities also rose. This was due to the presence of fibrous material (1.54 g/cm^3) within the composites, which was denser than the matrix (1.14 g/cm^3). A plausible explanation for the increase in densities in these composites may be the efficient packing of fibres and favourable fibre–matrix adhesion [24].

The experimental density values of the composites were lower than the theoretically predicted values (Table 1). This discrepancy suggests some void formation in the composites of this study. Despite this, as the weight fraction of the fibre increased, there was a clear reduction in void content. This reduction could be linked to the preparation method. First, soaking the thin RCF sheets allowed for more contact of the fibre–matrix surfaces, thus leading to better adhesion. Second, formation of the composite using compression moulding forced the air to be expelled from specimens more readily during the composite processing. Thus, these processes minimise void content and increase the densities of the resultant composites.

These results agree with other earlier studies. For instance, Sreekala et al. [24] found that, as oil palm fibre volume fraction increased from 0.24 to 0.40 in phenol formaldehyde/glass fibre composites reinforced by oil palm fibres, the void content in these composites decreased from 3.33 to 2.83 %. In another study, Facca et al. [17] used a

Table 1 Fibre volume fraction and void content of VER/RCF composites

Sample	Fibre weight fraction (wt%)	Fibre volume fraction (%)	Theoretical density (g/cm^3)	Experimental density (g/cm^3)	Void content (%)
VER/20 % RCF	20	0.16	1.21	1.18 ± 0.03	5.6 ± 0.3
VER/30 % RCF	30	0.24	1.24	1.21 ± 0.02	4.8 ± 0.2
VER/40 % RCF	40	0.33	1.27	1.24 ± 0.05	3.3 ± 0.5
VER/50 % RCF	50	0.43	1.31	1.27 ± 0.02	2.7 ± 0.2

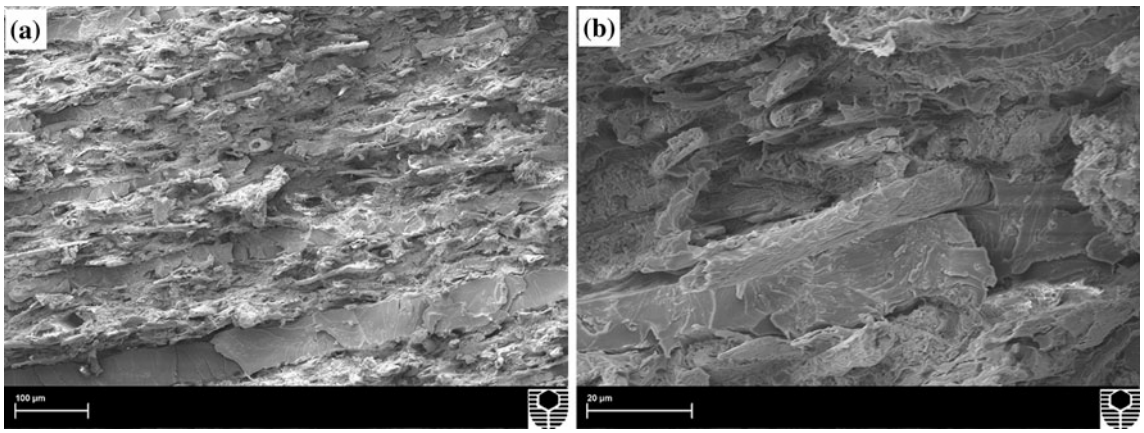

Fig. 1 **a** Low and **b** high magnification SEM micrographs of fracture surfaces for 40 wt% RCF reinforced VER

range of fibres to reinforce high-density polyethylene (HDP) composites. They found that void content reduced, in most cases, as the weight fraction of the fibre increased. In their study, as the weight fraction of hemp fibre was increased from 10 to 50 wt%, the void content dropped from 9 to 3 %. The fracture surfaces of composites with 40 wt% RCF at low and high magnification are shown in Fig. 1(a, b). From these images, no noticeable voids can be detected within the composites and the appearance of good adhesion between the fibre and matrix is clearly observed.

Water absorption behaviour

Figure 2 shows the percentage of water uptake as a function of the square root of time for pure VER and RCF reinforced samples at 20, 30, 40 and 50 wt% addition, immersed in tap water at room temperature. The maximum water uptake for VER and the composites immersed for 2500 h at room temperature was 0.76, 6.52, 9.56, 12.37 and 14.62 %, respectively.

All the composites that were immersed in water for a prolonged period demonstrated Fickian diffusion behaviour. When first exposed to water, absorption occurred

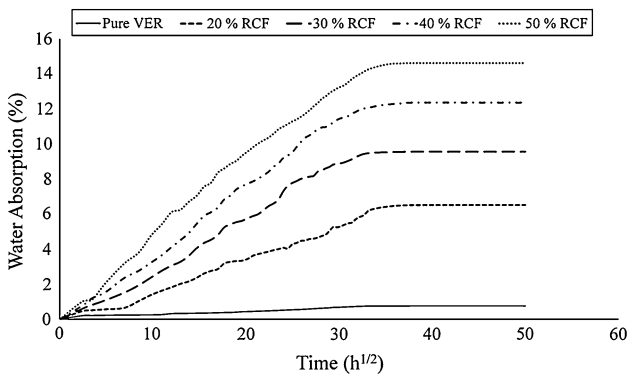

Fig. 2 Water absorption curves of VER and VER/RCF composites

rapidly. However, the rate of moisture absorption slowed as time progressed, until reaching the point of equilibrium [25]. An increase in content of cellulose fibres led to an increase in water uptake, as would be expected. It is worth noting that, for the composites, in the first 250 h, the rate of water uptake was rapid, and thereafter steadied. In natural fibres, the mechanism of water absorption is well understood. When exposed to moisture, the first molecules of water are absorbed by the hydrophilic groups of the natural fibres. After this, a second group of water molecules is attracted to the other hydrophilic groups present. A third group of water molecules may also be attracted to the top molecules already absorbed. When humidity is high, surface tension forces may hold liquid water in capillary spaces [9, 11]. The presence of hydroxyl groups on natural fibres gives the fibres a hydrophilic nature. This causes water molecules to be attracted and bound to the natural fibres by forming hydrogen bonds [26]. The addition of cellulose fibre to the polymer composites increases the size of the interfacial area, thereby allowing more water to be absorbed as a result of the capillary effect [27, 28]. Hence, the higher the content of cellulose fibres in the composites, the higher the rate of water absorption [29].

Moreover, when these composites are exposed to environments of extreme moisture, swelling of the cellulose fibres occurs. For brittle thermosetting resins, such as vinyl-ester, fibre swelling causes microcracking. These microcracks can create swelling stresses that lead to composite failure [27, 30]. As the composite cracks, the damage facilitates capillarity and transport that uses microcracks. Capillarity is a mechanism that involves the flow of water molecules along fibre–matrix interfaces, and diffusion through the bulk matrix. The water molecules attack the interface, causing degradation of the fibre–matrix interface areas [26, 29].

The microstructures of composites reinforced with 30 and 50 wt% RCF, after water absorption experiment are

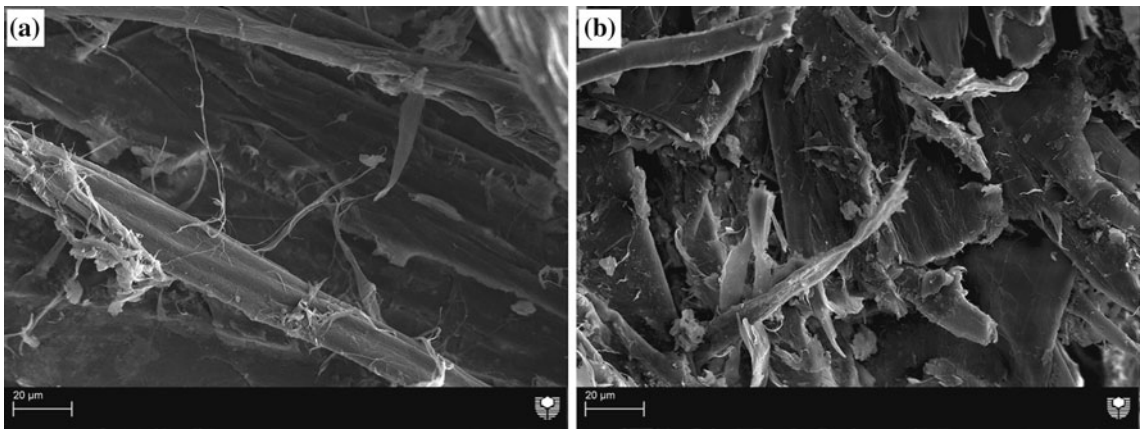

Fig. 3 SEM micrographs showing the degradation of the fibre–matrix interface due to moisture attacked composites with **a** 30 wt% RCF and **b** 50 wt% RCF

Table 2 Maximum water uptake, M_∞, and diffusion coefficients, D, of VER and VER/RCF composites

Sample	Fibres weight fraction (wt%)	Fibres volume fraction (%)	M_∞ (%)	D (mm^2/sec)
VER	0	0	0.76	3.72×10^{-6}
VER/20 % RCF	20	0.16	6.52	2.71×10^{-7}
VER/30 % RCF	30	0.24	9.56	6.66×10^{-7}
VER/40 % RCF	40	0.33	12.36	1.19×10^{-6}
VER/50 % RCF	50	0.43	14.62	2.01×10^{-6}

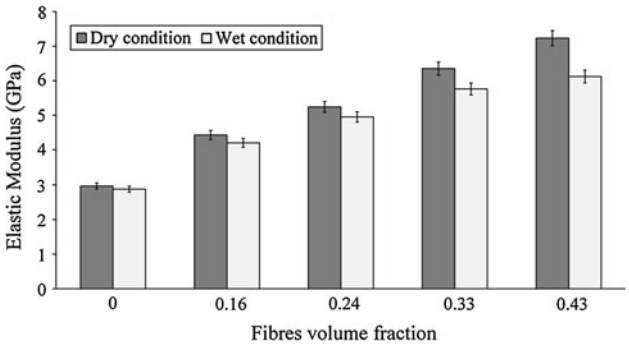

Fig. 4 Elastic modulus versus fibre volume fraction in dry and wet conditions

shown in Fig. 3. The loss of adhesion between fibre and matrix can be seen. The fibres appear degraded with absence of a covering matrix layer on them, and the microfibrils can be observed.

An increase in the fibre volume fraction of composites caused gradual increases in maximum water content and diffusion coefficient values (Table 2). As mentioned earlier, composites with higher fibre loading contain a higher content of cellulose fibres and have greater interfacial area, each of which leads to greater diffusivity.

Elastic modulus

Figure 4 shows the elastic modulus versus RCF volume fraction for VER/RCF composites in dry and wet conditions. For the dry samples, the elastic modulus increased as the fibre volume fraction increased. The addition of 20, 30, 40 and 50 wt% RCF, corresponding to 0.16, 0.24, 0.33 and 0.43 fibre volume fractions, increased the elastic modulus by 49.2 76.4, 113.8 and 143.4 %, respectively, compared to pure VER (2.97 GPa). Thus, an increase in the fibre content of the composite material resulted in an increase in the elastic modulus. The improvement in elastic modulus is believed to be due to the higher initial modulus of the cellulose fibres acting as backbones in the composites [21, 29]. This is supported by earlier studies, which have reported significant increases in the elastic modulus of natural fibre reinforced polymer composites. For example, Ma et al. [31] investigated winceyette fibres reinforced thermoplastic starch composites with increasing fibres content from 0 to 20 %. In this study, the elastic modulus increased from 45 MPa for neat resin to approximately 140 GPa as the fibre content increased. Hajnalka et al. [32] studied the elastic modulus for hemp fibre reinforced polypropylene with zero to 70 wt% fibre loading. Compared with an elastic modulus of 2.7 GPa for the matrix, at 50 % fibre loading, the result was nearly 2.5 times greater. However, after the elastic modulus peaked at 50 %, it was found to be lower at 70 % fibre loading. Similarly, Khoathane et al. [33] studied the effect of fibre contents on the elastic modulus of polypropylene copolymer composites reinforced with bleached hemp fibre. In this study, the elastic modulus for neat resin was 1.3 GPa, and it was

found that increasing the amount of fibre to 30 wt% increased the elastic modulus to 4.4 GPa.

For wet samples, water absorption reduced elastic modulus (see Fig. 4). For example, RFC reinforced composites with 0.16 and 0.43 fibre volume fractions were found to show 5.2 and 15.4 % reductions in elastic modulus, when compared with the results for the dry samples with equivalent fibre volume fractions. A reduction in elastic modulus as a result of water absorption has also been found in earlier studies [11, 26]. In the current study, the reduction in elastic modulus was found to be most noticeable for composites with high fibre content. The most likely reason for this is that moisture absorption reduces the integrity of bonding between the fibre and matrix, which degrades the interfacial stress transfer capability, thereby leading to reduced elastic modulus.

Analysis of elastic modulus

As there are no theoretical or experimental data available for the elastic modulus of RCF, as used in this study, the elastic modulus of RCF was assumed to be 39 GPa. This assumption was based on the earlier investigations of Lamy and Baley[38], which found a close relationship between the diameter and elastic modulus for natural fibres. Lamy and Baley found that, where fibres were approximately 35 μm in diameter, elastic moduli were around 39 GPa, whereas a diameter of approximately 5 μm had elastic moduli at around 79 GPa. They attributed these variations in elastic moduli to changes in lumen size among fibres of different diameters. Another important parameter is the fibre orientation factor, η_{0E}. This value is determined by using fibre orientation distribution. The η_{0E} value for random in-plane orientation of the fibres is theoretically 0.375 [22, 28]. The value of 0.375 neglects the influence of transverse deformations. Nonetheless, it is expected that in-plane orientation would be approximately based on the arrangement of fibres in the RCF sheets.

Using the presumptions of the fibre's elastic modulus and orientation factor, the four models mentioned earlier could be applied to the data listed in Tables 1 and 3.

Table 3 Material properties required for micromechanical models

Material property	Value
Poisson's ratio of VER	0.35
VER density[a]	1.14
Elastic modulus of VER[a]	2.97 GPa
RCF density[a]	1.54 g/cm^3
RCF diameter and length[b]	30 μm, 1500 μm

[a] This study's experimental data

[b] Measured based on 50 different fibres (SEM observation)

A plot of predicted elastic moduli against fibre volume fraction is shown in Fig. 5. All values of elastic modulus for both the prediction data and the experimental data fell between the upper bounds (ROM) and lower bounds (IROM). However, when compared to other models, the ROM-IROM models offer the least validity of results in this study.

The Halpin–Tsai model greatly overestimated elastic modulus for composites. This is because this model relies upon the use of a fitting parameter, ξ which is determined using Eq. 13. This equation was based on observations of synthetic fibres primarily glass fibres. Synthetic fibres have lengths and cross-sections that are well defined; thus, this model produces good prediction of the elastic modulus for composites reinforced with synthetic fibres. However, natural fibres do not possess the same uniformity of dimensions; they have complex, irregular lengths and cross-sections (see Fig. 6).

The initial overestimation of elastic modulus using the Halpin–Tsai model with values of ξ computed using equation 13 indicated large discrepancies between the

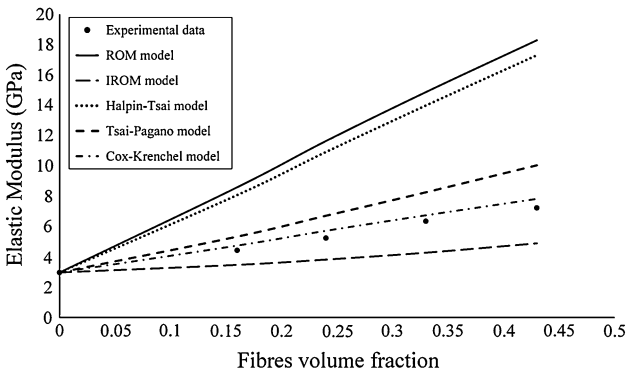

Fig. 5 Experimental and prediction data of elastic modulus against fibre volume fraction

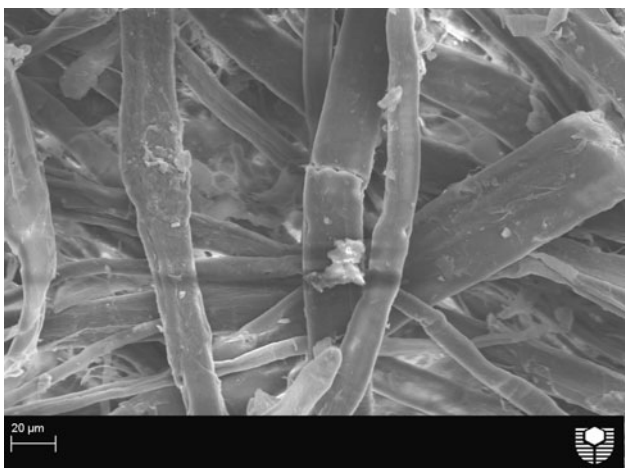

Fig. 6 SEM micrograph showing irregularly shaped fibres

values of ξ computed using Eq. 13 and the best-fit value of ξ. The calculations revealed that a value of ξ adjusted to 2.3 gave the best fit to the experimental data of this current study. The Tsai–Pagano model, similar to the Halpin–Tsai model, also overestimated the elastic modulus of experimental data. The explanation made earlier is also relevant here. The discrepancy between experimental data for the elastic modulus of natural fibre reinforced composites and prediction data based on the Halpin–Tsai model and the Tsai–Pagano model has been found in other studies [21, 34].

The Cox–Krenchel model prediction data gave the best agreement with the experimental data. The values obtained from the model were consistent with the experiment data, despite being slightly higher. A plausible explanation for the marginally greater elastic modulus results based on the prediction data is that the Cox–Krenchel model relies on an orientation factor (η_{0E}) of 0.375 a value based on two-dimensional random orientation synthetic fibre composites that is not necessary suitable for natural fibre composites.

Unlike glass fibres, which are stiff and remain straight, natural fibres exhibit curvature and may readily bend or curl in the mat after processing [35]. Thus, composites reinforced with natural fibres are more compliant than comparable composites reinforced with synthetic fibres [23]. This highlights that the orientation factor (η_{0E}) of 0.375 that the Cox–Krenchel model relies on needs to be adjusted to provide a better fit with the experiment data for the elastic modulus of natural fibre reinforced composites.

The inaccuracy of predicted values obtained using elastic modulus modelling based on Cox–Krenchel has been reported in earlier studies by Bos et al. [36] and Andersons et al. (2006) [23]. Bos et al. used an orientation factor (η_{0E}) of 0.62 to obtain best fit between the prediction and experimental data for polypropylene composites reinforced with short flax fibres. Andersons et al. used an adjusted orientation factor (η_{0E}) of 0.2 to obtain best fit between the prediction and experimental data for polypropylene composites reinforced with extruded flax fibres.

Interestingly, for the present study, the best-fit orientation factor (η_{0E}) was found to be 0.333. This value is close to the theoretical orientation factor value of 0.375 that was taken to predict data with the Cox–Krenchel model. This may be due to the use of thin fibre sheets (mats) with fibre lengths (1500 μm) much greater than the thickness of the sheets (100 μm). It may also be because the fibres were expected to be mainly oriented in two directions.

Flexural strength

Figure 7 provides the flexural strength results for dry and wet conditions as a function of fibre volume fraction. For the dry samples, increasing fibre content improved significantly flexural strength. Specifically, the addition of 20, 30, 40 and 50 wt% RCF led to 173.7, 216.5, 254.2 and 295.7 % increases in flexural strength, respectively. These significant enhancements in strength were attributed to a reinforcing effect caused by cellulose fibres, which are of high strength and modulus [37]. Moreover, the ability of RCF to resist bending force is also believed to improve composite flexural strength as the fraction volume of fibre is increased in composites [38]. Increasing RCF content also provided increased resistance to shearing during the three-point flexure test [24].

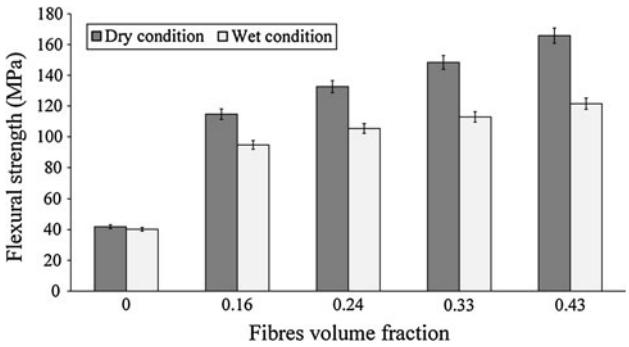

Fig. 7 Flexural strength versus fibre volume fraction in dry and wet conditions

At lower RCF content, lower values of flexural strength were observed. This was attributed to a reduction in load transfer from matrix to fibre, resulting in lower load carrying by fibres. In general, the reinforcement provided by fibres in composites was not served where the volume fraction of fibre was insufficient [39]. In contrast, at higher RCF content; there was an increase in flexural strength. This is believed to be due to the increase in stress transferred from matrix to fibres. The level of stress transfer from the matrix to the fibre is dependent on fibre–matrix interactions [40]. A good bond between the fibres and matrix is required in this process. Where good bonding is present, the fibres will provide uniform stress distribution from the continuous polymer matrix phase to the dispersed fibres phase, which gives the composite its strength. In this study, the enhancement of flexural strength with increasing fibre content suggests good bonding between the fibre and matrix. In general, blending higher fibre content (>40 wt%) with polymer matrix leads to poor fibre–matrix bonding, which promotes microcrack formation [41]. This poor bonding is due to limited wettability, in which the fibres are not completely surrounded by the matrix material [42]. Limited wettability can increase fibre–fibre interaction, thereby reducing effective stress transfer from the matrix to the fibres and lowering the composite strength [24].

Figure 7 also reveals the effect of moisture absorption on flexural strength. The flexural strength for the samples

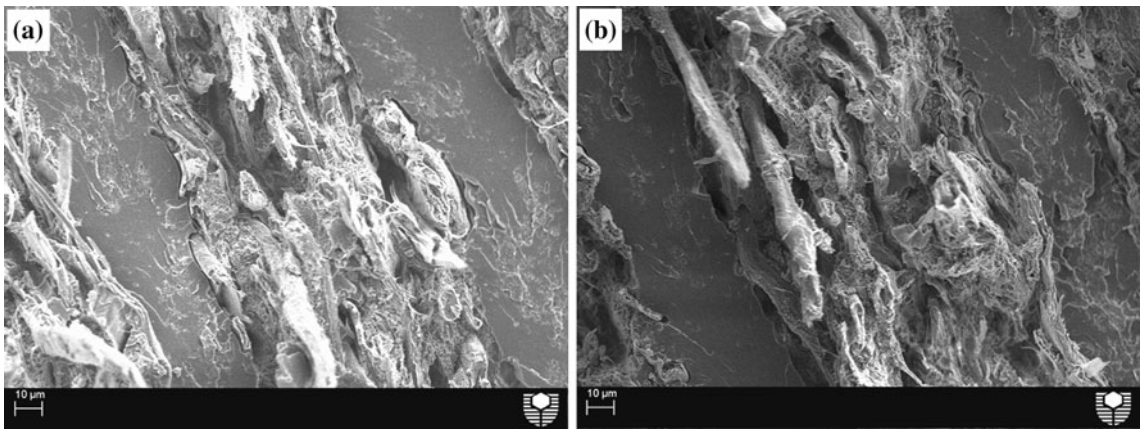

Fig. 8 Effect of water absorption on the fibre–matrix interface for composites reinforced with **a** 20wt% RCF and **b** 50wt% RCF

decreased markedly after water absorption. Compared to the dry samples, the reductions in flexural strength of the samples reinforced with 20, 30, 40 and 50 wt% RCF were 17.4, 20.5, 23.9 and 26.7 %, respectively. Espert et al. [14] and Zamri et al. [43] published similar reports that highlighted a negative effect of water uptake on the flexural strength of natural fibre composites. The reduction in flexural strength was due to the weakening of the fibre–matrix interface. As water content increased in the composite, the absorbed water formed intermolecular hydrogen bonding with the cellulose fibres. This occurrence reduced interfacial adhesion between the fibre and matrix, and the strength was subsequently reduced [44, 45]. In environments with high percentages of hydroxyl groups, natural fibres exhibit low resistance to moisture [46]. This leads to dimensional variations of the composite products (the matrix and fibres) and poor bonding between the matrix and fibres. It also causes lower stress transfer from the matrix to the fibres. Again, these factors cause a decrease in the composite's mechanical properties [26, 47]. Moreover, higher fibre content also leads to increased water absorption, which negatively affects the fibre–matrix bonding [13, 41].

Figure 8 shows the adverse effects of water uptake on the fibre–matrix interface reinforced with 20 and 50 wt%. As the content of RCF increased, the effect of water uptake on interfacial bonding became more evident.

Conclusions

An infiltration method was used to prepare RCF-reinforced polymer composites. The composites produced were measured for their elastic modulus and strength with various fibre volume fractions. The effect of varying fibre contents on water absorption behaviour was also investigated. The water absorption followed a Fickian behaviour, and that higher fibre content led to greater moisture absorption. Elastic modulus for the composites was modelled using a number of typical mathematical models for prediction. The modelling results revealed that the experimental data matched the prediction data best with the Cox–Krenchel model. Exposure of composites to moisture caused reductions in elastic modulus and strength.

Acknowledgements The authors are grateful to Mr. Andreas Viereckl from Mechanical Engineering at Curtin University for assistance with mechanical tests. The authors would also like to thank Elaine Miller for her assistance with SEM.

References

1. Netravali AN, Chabba S (2003) Mater Today 6:22
2. Dissanayake NPJ, Summerscales J, Grove SM, Singh MM (2009) J Natural Fibers 6:331
3. Meredith J, Coles SR, Powe R, Collings E, Cozien-Cazuc S, Weager B, Müssig J, Kirwan K (2013) Compos Sci Technol 81:31
4. Di Landro L, Lorenzi W (2009) J Biobased Mater Bioenergy 3:238
5. Huda MS, Drzal LT, Mohanty AK, Misra M (2007) Compos B 38:367
6. Low IM, Somers J, Kho HS, Davies IJ, Latella BA (2009) Compos Interfaces 16:659
7. Hussain F, Hojjati M, Okamoto M, Gorga RE (2006) J Compos Mater 40:1511
8. Low IM, McGrath M, Lawrence D, Schmidt P, Lane J, Latella BA (2007) Compos A 38:963
9. Chen H, Miao M, Ding X (2009) Compos A 40:2013
10. Espert A, Vilaplana F, Karlsson S (2004) Compos A 35:1267
11. Dhakal HN, Zhang ZY, Richardson MOW (2007) Compos Sci Technol 67:1674
12. ASTM D 2734-94 (1997). Standard methods for void content of reinforced specimen plastics, American society for testing and materials
13. Wang W, Sain M, Cooper PA (2006) Compos Sci Technol 66:379
14. Espert A, Vilaplana F, Karlsson S (2004) Compos A 35:1267
15. Liu W, Hoa SV, Pugh M (2008) Compos Sci Technol 68:156

16. Ku H, Wang H, Pattarachaiyakoop N, Trada M (2011) Compos B 42:856
17. Facca AG, Kortschot MT, Yan N (2006) Compos A 37:1660
18. Tucker ICL, Liang E (1999) Compos Sci Technol 59:655
19. Bourmaud A, Baley C (2009) Polym Degrad Stab 94:297
20. Esfandiari A (2008) Fibers Polym 9:48
21. Lee BH, Kim HJ, Yu WR (2009) Fibers Polym 10:83
22. Garkhail SK, Heijenrath RWH, Peijs T (2000) Appl Compos Mater 7:351
23. Andersons J, Spārniņs E, Joffe R (2006) Polym Compos 27:221
24. Sreekala MS, George J, Kumaran MG, Thomas S (2002) Compos Sci Technol 62:339
25. Assarar M, Scida D, Mahi A, Poilâne C, Ayad R (2011) Mater Des 32:788
26. Athijayamani A, Thiruchitrambalam M, Natarajan U, Pazhanivel B (2009) Mater Sci Eng A 517:344
27. Stamboulis A, Baillie CA, Peijs T (2001) Compos A 32:1105
28. Thomason JL, Vlug MA (1996) Compos A 27:477
29. Kim HJ, Seo DW (2006) Inter J Fatigue 28:1307
30. Bismarck A, Aranberri-Askargorta I, Springer J, Lampke T, Wielage B, Stamboulis A (2002) Polym Compos 23:872
31. Ma X, Yu J, Kennedy JF (2005) Carbohyd Polym 62:19
32. Hargitai H, Rácz I, Anandjiwala RD (2008) J Thermoplast Compos Mater 21:165
33. Khoathane MC, Vorster OC, Sadiku ER (2008) J Rein Plast Compos 27:1533
34. Conzatti L, Giunco F, Stagnaro P, Capobianco M, Castellano M, Marsano E (2012) Compos A 43:1113
35. Herrera-Franco PJ, Valadez-González A (2005) Compos B 36:597
36. Bos HL, Müssig J, van den Oever MJA (2006) Compos A 37:1591
37. Alhuthali A, Low IM, Dong C (2012) Compos B 43:2772
38. Colom X, Carrasco F, Pagès P, Cañavate J (2003) Compos Sci Technol 63:161
39. Ghosh RKA, Reena G, Raju BL (2011) Int J Adv Eng Sci Technol 4:89
40. Araújo JR, Waldman WR, De Paoli MA (2008) Polym Degrad Stab 93:1770
41. Thwe MM, Liao K (2003) J Mater Sci 38:363
42. Bax B, Müssig J (2008) Compos Sci Technol 68:1601
43. Zamri MH, Akil HM, Bakar AA, Ishak ZAM, Cheng LW (2012) J Compos Mater 46:51
44. Aquino EMF, Sarmento LPS, Oliveira W, Silva RV (2007) J Reinf Plast Compos 26:219
45. Bessadok A, Marais S, Roudesli S, Lixon C, Métayer M (2008) Compos A 39:29
46. Sombatsompop N, Chaochanchaikul K (2004) Polym Int 53:1210
47. Mishra S, Mohanty AK, Drzal LT, Misra M, Parija S, Nayak SK (2003) Compos Sci Technol 63:1377

3.2. Characterisation of the water absorption, mechanical and thermal properties of recycled cellulose fibre reinforced vinyl-ester eco-nanocomposites

---

ALHUTHALI, A. LOW, I. M. and DONG, C. 2012. Characterisation of the water absorption, mechanical and thermal properties of recycled cellulose fibre reinforced vinyl-ester eco-nanocomposites. *Composites Part B: Engineering*, 43, 2772-2781.

Composites: Part B 43 (2012) 2772–2781

Contents lists available at SciVerse ScienceDirect

Composites: Part B

journal homepage: www.elsevier.com/locate/compositesb

Characterisation of the water absorption, mechanical and thermal properties of recycled cellulose fibre reinforced vinyl-ester eco-nanocomposites

A. Alhuthali, I.M. Low *, C. Dong

Department of Imaging & Applied Physics, Curtin University of Technology, GPO Box U1987, Perth, WA 6845, Australia

ARTICLE INFO

Article history:
Received 30 June 2011
Received in revised form 15 December 2011
Accepted 28 December 2011
Available online 6 May 2012

Keywords:
A. Recycled cellulose fibres sheets (RCFs)
A. Nanoclay platelets (30B)
A. Vinyl-ester resin (VER)
B. Flexural strength
B. Impact strength

ABSTRACT

Natural fibres are cheaper and have a lower density compared to synthetic reinforcement products and therefore offer benefits for use in commercial applications. The physical and mechanical properties of these 'eco-composites' can be further enhanced through the addition of nanoclay. This paper reports on the fabrication of vinyl ester, eco-composites and eco-nanocomposites and characterises these samples in terms of water absorption, strength, toughness, and thermal properties. Weight gain and FTIR spectrum analysis indicated that 5% nanoclay addition gave favourable reduction in the water absorption behaviours of the samples. Nanoclay addition strengthened fibre–matrix adhesion leading to improved strength properties in the eco-nanocomposites. However, SEM images of fracture surfaces revealed that nanoclay addition limited toughness mechanisms of fibre pull-out and fibre debonding leading to sample brittleness. Eco-nanocomposites were still found to have favourable thermal stability and flammability results.

1. Introduction

There has been increasing attention into the study of materials of a composite nature. In contrast to monolithic materials, these composite materials usually involve a matrix, such as polymers, and fillers such as fibres [1]. The rationale behind creating a polymer matrix composite is that the lower stiffness and strength of polymer can be improved through the addition of stiffer and stronger fibres. The most common synthetic or human made fibres include aramid, glass, polyethylene, and carbon [2]. Glass is the most common form of the reinforcing fibres because it is cheap and has good mechanical properties. The resultant composites are used in a range of industries including aerospace, leisure, sporting, automotive, and construction [1].

However, increasingly the scientific community is recognising the shortcomings of synthetic fibres and is paying more attention to natural fibres [3]. Some examples of natural fibres include flax, hemp, jute, pineapple wood, coconut, cotton, kenaf, abaca, banana leaf fibres, bamboo, wheat straw and sisal [4,5]. Part of the reason for the interest in greener substances is that there is growing global concern over the rapid depletion of petroleum resources, greenhouse gases issues, and a greater need to recycle and reuse. Some regions such as the European Union and Japan have legislation which states that a particular percentage of a vehicle must be reused or recycled [6]. This percentage is currently approximately 80% but is expected to increase in the coming years. More and more, scientists are looking to use materials which have a greater compatibility with the environment [7]. Developing products which promote a global sustainability message has now become very important for manufactures. For example, Mercedes-Benz has developed fifty polymer–natural fibre composites products for its E class series of automobiles [6].

Natural fibres are environmentally friendly. They are biodegradable, so they will not stay on the earth's surface for millions of years unlike some plastics and the energy required to produce these fibres is low especially compared with the consumption required to produce glass and carbon fibres [5–8]. Natural fibres have a lower density 1.25–1.5 g/cm^3 compared with 1.8–2.1 g/cm^3 for carbon fibres and 2.54 g/cm^3 for E-glass [9]. Products reinforced with natural fibres are lighter than synthetic reinforced [8]. Natural fibres also can have an excellent modulus-weight ratio. This makes them successful in stiffness-critical designs [10]. The acoustic damping property of natural fibres makes them preferable to glass or carbon for noise attenuation which is a requirement for automobile interior products [10]. Natural fibres are also more commercially viable than most synthetic fibres [9–11].

Researchers can now extract cellulose fibres from newspapers, printed paper, and cardboard [3]. Newspaper fibre reinforced composites, for example, have similar properties to wood fibre reinforced composites. Moreover, newspaper fibre reinforced composites can be more easily produced due to cost advantage, renewability of the resource, greater flexibility and a lower wear on processing machinery [12]. Load bearing roof systems, sub-flooring

* Corresponding author.
E-mail address: j.low@curtin.edu.au (I.M. Low).

1359-8368/$ - see front matter Crown Copyright © 2012 Published by Elsevier Ltd. All rights reserved.
http://dx.doi.org/10.1016/j.compositesb.2012.04.038

and framing components as well as residential applications such as doors, windows, and furniture are applications for recycled waste paper fibre reinforced materials [3,12–14].

Drawbacks for natural fibre reinforced polymeric composites exist however. Inherent incompatibility must be overcome between natural fibres which are hydrophilic and the matrix components which are hydrophobic [11]. The hydrophilic nature of natural fibres adversely affects the strength of the composites. Extensive physical and chemical treatment of the fibre surface is required to improve fibre–matrix adhesion and prevent loss of strength [15]. Moisture-related problems also must also be taken into account. The mechanism of water absorption is based on the climatic conditions [16]. Humidity at high levels will mean that water is able to diffuse into polymeric composites in three ways; primarily via the inter-polymer chain micro-gaps, to a lesser degree, via the fibre and matrix interfaces through capillary transport tracing any gaps and/or flaws caused by incomplete wettability and impregnation [17], and finally, via micro-cracks in matrix which result from natural fibre swelling [11].

Implications of natural fibre reinforced polymeric composites' adhesion incompatibility and moisture-related problems are a significant loss in mechanical properties and overall properties in general. Moisture compromises fibre–matrix interface integrity. This leads to poor stress transfer efficiencies and overall loss in mechanical properties [16–18]. Water absorption is, thus, is key deterrent to research and development in natural fibre reinforced polymeric composites due to degrading mechanical properties in wet conditions [19]. In addition to this, adhesion between the matrix and fibre can affect the thermal properties. Initiatives to improve adhesion have resulted in an improvement of thermal stability [20]. In general, the composite properties will be a result of the nature of the matrix, the fibre, the interfacial bonding involved, and the adhesion quality of the finalised composite [21].

Nanoclay addition enhances polymer performance. Organically modified layered silicate nanocomposites demonstrate barrier properties, mechanical properties, flammability resistance, and thermal stability properties which are superior to the unmodified polymer [22]. Silicate content of lower than 5 wt.% provides the desirable material properties while at the same time allowing for a lighter composite. Such a product reconciles earlier shortcomings and can thus compete in the material market for specific applications [23]. Silicate clay nanolayers possess high particle aspect ratios and can be further enhanced through modification of the interlayer surface using ion-exchange reaction and the formation of stable Si—O bonds [24,25].

The aim of this study, thus, was to combine knowledge on natural fibre reinforced polymeric composites, their strengths and weaknesses, namely, adhesion incompatibility and moisture-related problems, with knowledge of nanoclay addition, in order to reconcile the shortcomings and possibilities from both areas of study. In essence, this study aimed to investigate the effect of nanoclay on water absorption, mechanical, flammability and thermal properties of vinyl-ester reinforced with recycled cellulose fibre sheets.

2. Experimental methods

2.1. Materials

Recycled cellulose fibre sheets (RCFs) of grade 80GSM, 100 μm thickness, were supplied by Todae Company, NSW, Australia. In addition to the RCFs, general purpose vinyl ester resin was used in this study. The resin was supplied by Fibreglass & Aesin Sales Pty Ltd, WA, Perth, Australia. A third material used in the study was organoclay (Cloisite 30B), supplied by Southern Clay Products in the USA. Cloisite 30B is organically-modified clay with physical properties shown in Table 1.

2.2. Samples preparation

2.2.1. Preparation of pure samples

Pure polymer samples (VER) were the first samples made. These samples were needed as a control to provide baseline data of the properties of pure vinyl ester resin. The vinyl ester resin was mixed with 1.0 wt.% catalyst (MEKP) in order to prepare the samples. The mixture was slowly and thoroughly mixed to ensure that no air bubbles formed within the matrix. The resultant mixture was poured into silicon moulds and left under low vacuum (70 kPa) for 2 h and later left at room temperature for 24 h to cure.

2.2.2. Preparation of eco-composites

The second group samples were the eco-composites (VER/RCF). Here, recycled cellulose-fibre sheets (RCFs) were dried for 60 min at 150 °C. RCFs ware fully soaked in the vinyl-ester system and then laid up in close silicon mould under 20 kg load and under vacuum of (150 kPa) for 2 h. Then samples left to cure for 24 h at room temperature. The weight percentage of fibres in these eco-composites was 40%.

2.2.3. Preparation of eco-nanocomposites

The third group of samples was eco-nanocomposites. Here, nanocomposite mixtures containing different concentrations (wt.%), namely, 1%, 3%, and 5%, of Cloisite 30B were prepared. Nanoclay was first dried for 60 min at 150 °C, and then mixed with vinyl ester resin for 30 min using high speed electrical-mixer. The mixtures were then left under (150 kPa) to remove air bubbles. After that, catalyst was added and mixed manually to void creating air-bubbles inside the composites. Next, the mixtures were then reinforced with the same percentage of RCFs sheets (40 wt.%). The sheets were also dried for 60 min at 150 °C. The sheets then were fully soaked in the mixtures and pressed together under 20 kg and under vacuum of (150 kPa) for 2 h. Finally, the samples were left to cure at room temperature for 24 h. The resultant eco-nanocomposites were labelled as VER/RCF/1%NC, VER/RCF/3%NC and VER/RCF/5%NC.

2.3. 3. Microstructure examination

The samples were measured on a D8 Advance Diffractometer (Bruker-AXS) using copper radiation and a LynxEye position sensitive detector. The diffract metre were scanned from 3° to 50° (2θ) in steps of 0.02° using a scanning rate of 0.5°/min XRD patterns obtained by using Cu Kα lines (λ = 1.5406 Å). A knife edge collimator was fitted to reduce air scatter.

The fracture surfaces of the samples were examined using a NEON 40ESB, ZEISS scanning electron microscope (SEM), operating at accelerating voltage of 5 kV, under secondary image mode. All samples were coated with platinum before the analysis to avoid charging.

Table 1
The physical properties of the nanoclay (Cloisite 30B).

Physical properties of Cloisite 30B	
Color	Off white
Density (g/cm^3)	1.98
Aspect ratio	200–1000
Surface area (m^2/g)	750
Mean particle size (μm)	6

2.4. Water uptake test

2.4.1. Weight gain study

Rectangular bar samples with dimensions of 20 mm × 20 mm × 6 mm were used. The researcher soak individual sample with tap water at room temperature. At prescribed intervals, the researcher removed individual samples, removed excess water, weighed the samples, and immediately returned the samples to the water. A digital scale (AA-200, Denver Instrument Company, USA) with a 0.0001 g weighing precision was used to determine weight change. The following equation was used to determine the amount of moisture uptake or absorbed (M_A) by the samples over a period of 120 days [11].

$$M_A = \frac{M_t - M_D}{M_D} \times 100 \tag{1}$$

where M_D is the dry mass and M_t is the mass of sample soaked for time t.

Diffusion coefficient behaviour of all samples have been calculated by using following equation [11]:

$$D = \frac{\pi}{16}\left(\frac{M_t/M_\infty}{\sqrt{t}/h}\right)^2 \tag{2}$$

where M_∞ is maximum water uptake, M_t is water uptake at time t, h is sample thickness, and D is diffusion coefficient.

2.4.2. FTIR analyses

The Fourier transform infrared spectroscopy (FTIR) was performed in the transmission-mode with a Perkin Elmer Spectrum 100 FTIR spectrometer. The device is fitted with a single-bounce diamond/ZnSe ATR accessory and a room temperature detector. Four background and four sample scans were performed and were co-averaged and ratios determined to produce the transmittance spectrum. The spectral resolution was four wavenumbers. To compensate for the wavelength dependence on penetration depth, an ATR correction was performed. The rationale for applying FTIR was to study water content in all composites after placed in water, as well as the gathering data on the effect of nanoclay addition on water absorption behaviour of all samples.

2.5. Mechanical tests

2.5.1. Impact toughness

To determine the impact toughness (G_{IC}), a Zwick Charpy-impact tester with a 2.0 J pendulum hammer was used. Five 40 mm-span bar samples with varying notch lengths and razor-cracks were used. The impact toughness value was calculated using the equation [3]:

$$U = G_{IC}BD\phi + U_0 \tag{3}$$

where U is the measured energy, U_0 is the kinetic energy, D is the specimen thickness, B is the specimen breadth, and ϕ is the calibration factor for the geometry used [3].

2.5.2. Impact strength

To determine the impact strength (σ_i), a Zwick Charpy impact tester with a 2.0 J pendulum hammer was used. Five 40 mm-span bar samples were assessed. Impact strength was calculated using the following equation [3]:

$$\sigma_i = \frac{E}{A} \tag{4}$$

where E is the impact energy to break a sample with a ligament of area A.

2.5.3. Flexural strength

To evaluate the flexural strength (σ_F), rectangular bars of 60 mm × 10 mm × 6 mm were cut from the fully cured samples for three-point bend tests with a span of 40 mm. This test was performed with a LLOYD Material Testing Machine using a displacement rate of 1.0 mm/min. Five samples of each of the four composition groups were used for the measurements. The value of σ_F was computed using the following equation [3]:

$$\sigma_F = \frac{3}{2}\frac{P_m S}{WD^2} \tag{5}$$

where P_m is the maximum load, S is the span of the sample, D is the specimen thickness and W is the specimen width.

2.5.4. Fracture toughness

For the fracture toughness (K_{IC}) measurement, the ratio of notch length to width of sample (a/w) used was 0.4 and a sharp razor blade was used to initiate a sharp crack. The flexural tests were performed with a LLOYD Material Testing Machine using a displacement rate of 1.0 mm/min; five samples of each composition were used for the measurements. The value of K_{IC} was computed using the following equation [3]:

$$K_{IC} = \frac{p_m S}{WD^{2/3}} f\left(\frac{a}{w}\right) \tag{6}$$

where p_m is the load at crack extension, S is the span of the sample, D is the specimen thickness, W is the specimen width, and a is the crack length, and $f(a/w)$ is the polynomial geometrical correction factor given as [3]:

$$f\left(\frac{a}{W}\right) = \frac{3(a/W)^{1/2}[1.99 - (a/W)(1-a/W)\times(2.15 - 3.93a/W + 2.7a^2/W^2)]}{2(1+2a/W)(1-a/W)^{2/3}} \tag{7}$$

2.6. Thermal and flammability test

Thermal behaviours composites were examined using a thermogravimetric analyser (TGA-DTA; Instrument: 2960 SDT V3.0F). Each composite was heated from room temperature to 800 °C, at a rate of 20 °C/min. Thermal decomposition temperatures of the composites were examined under20 ml/min of nitrogen using platinum pans.

Flammability was determined through horizontal burning testing using three measures, ignition time, burning out time and fire velocity. Three samples, with the dimensions of 100 mm × 10 mm × 10 mm were prepared for each composite and hung on a retort stand. A stop watch was used to record times and a constant flam source was applied.

3. Results and discussion

3.1. Structure and morphology of composites

XRD patterns for both nanoclay and VER/clay nanocomposites are shown in Fig. 1. A sharp reflection peak is demonstrated at 4.74° at 2θ for Cloisite 30B corresponding to interlaying spacing of 1.8 nm. Different results were revealed in the XRD of nanocomposites with 5 wt.% nanoclay which is shifting to a broad and weak lower diffraction peak at 4.42°. This shifting is corresponding to the interlaying spacing of 2.1 nm. An intercalated nanocomposite structure was the result evident from entrance of matrix polymer into nanoclay interlayer spacing and increased d-spacing. However, at 1 wt.% and 3 wt.% nanoclay there was no reflection peak for the XRD patterns of the composites. The result could suggest an exfoliated structure with uniform dispersion of nanoclay within

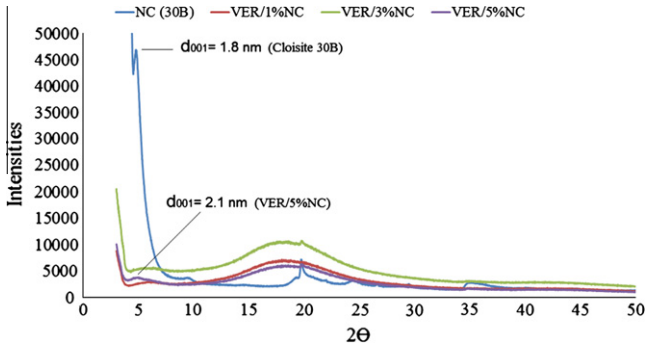

Fig. 1. XRD pattern of nanoclay (Cloisite 30B) and VER/nanoclay composites.

the matrix. Alternatively, the absence of this peak may be due to the lower nanoclay concentration in composites then that XRD reflection is absent or due to the exciting of an aggregated arrangement of clay nanolayers which indicates there is no nanocomposites formation.

3.2. Water uptake properties

3.2.1. Weight gain

Water absorption curves of the eco-composites and eco-nanocomposites are shown in Fig. 2. Results showed that samples followed typical Fickian diffusion behaviours. Water absorption, according to the theory, occurs rapidly at the beginning of exposure of the matter with water, however, after time, the absorption rate slows down until reaching the point of equilibrium. Nanoclay addition reduces the uptake of water. Nanoclay platelets cause this behaviour as they have a high aspect ratio [26] where the water molecules path is distributed. The presence of the nanoclay platelets means that the water molecules path is altered from the direct-fast diffusion into the polymer matrix to a maze-like obstacle-ridden path decreasing the overall uptake of water [27,28]. Table 2 shows the maximum water uptake M_∞ and diffusion coefficient D values of all composite.

Table 2 shows that as nanoclay loading is increased, the amount of water absorbed is decreased. This shows that nanoclay limits water absorption in composites. This is a desirable property for commercial applications. However, as the nanoclay loading is increased, there is no statistically significant change in the diffusion behaviours of the composites as per the diffusion coefficient. In other words, no trend between the nanoclay content and the water's diffusivity values is observed [29,30].

3.2.2. FTIR

The following FTIR spectrums of eco-composite and nanocomposites identify the main absorbance peaks of water sensitive

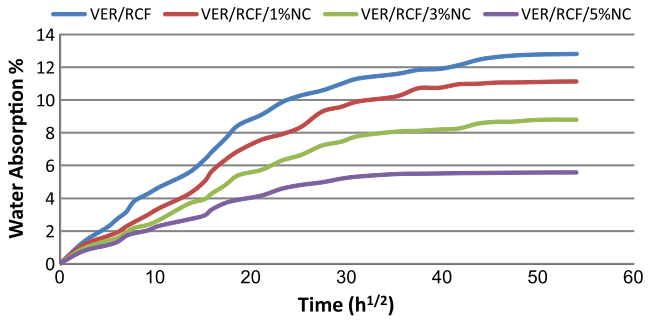

Fig. 2. Water absorption behaviour of VER, VER/RCF, VER/RCF/1%NC, VER/RCF/3 and VER/RCF/5%NC.

Table 2
Maximum water uptake M_∞ and diffusion coefficients D of VER-eco and eco-nanocomposites.

Samples	M_∞ (%)	D (mm^2/s)
VER/RCF	12.81	0.989×10^{-6}
VER/RCF/1%NC	11.13	0.832×10^{-6}
VER/RCF/3%NC	8.78	0.827×10^{-6}
VER/RCF/5%NC	5.57	1.16×10^{-6}

bands. The FTIR spectrums in both dry and wet conditions are presented (Fig. 3).

The main peak in each of the figures represents the hydroxyl (OH) stretching that occurs between 3000 and 3700 cm^{-1}. This hydroxyl stretching at this higher frequency is a fundamental phenomenon which corresponds to the hydroxyl peak of liquid water and is often assigned to unassociated water alternatively with loosely bound water, and indirectly bonded water bonded to the hydroxyl groups using other water molecules. Moreover, the lower frequency region peak is associated with strongly bound water as characterised by water bound directly by hydrogen bonds to hydroxyl groups of composite components [31,32].

When these hydroxyl groups interact with water, water adsorption occurs. Evidence for this is the hydroxyl groups which are part of the water molecules displaying in-plane bending at 1650 cm^{-1} [33]. Out-of-plane vibrations of the hydroxyl groups cause the broad band which is evident at 700 cm^{-1}. These vibration are referred to as librations – a collective normal multiple water molecule mode [31].

In addition to these peaks, there are peaks arising between 1000 and1110 cm^{-1} due to Si—O stretching, peaks at around 915 cm^{-1} due to Al—O/Al—OH stretching, and peaks at around 851 cm^{-1} due to Al—Mg—OH deformation. CH_2 bending vibration causes peaks around 1460 cm^{-1} and CH_3 bending vibration causes peaks 1350 cm^{-1}. These peaks are due to nanoclay vibrations [34,35]. All composites displayed peaks at around 2900 cm^{-1}. It is expected that these peaks are due to CH stretching, as CH is present in the chemical structures of vinyl-ester and cellulose fibres stretching [36,37]. The benzene ring of vinyl-ester is believed to cause the exhibited absorptions between 1607 cm^{-1} and 1510 cm^{-1} [38]. Out-of-plane bending of carbon—hydrogen bonds in the vinyl group of the vinyl-ester monomer is believed to cause the absorbance at 945 cm^{-1} [39]. As well as, a specific absorption band from vinyl-ester at around 1030 cm^{-1} is a resulting from C—O—C bending vibrations [36,37]. Finally, the C=O stretching of the acetyl groups of hemicellulose is believed to cause the peak at around 1730 cm^{-1} [36].

The peak of interest in this study is the peak centred at 3350 cm^{-1} (Fig. 4). This peak indicates the water content. Even in dry conditions, this peak is still present due to the HO groups which are part of the chemical structure of cellulose fibres (see Fig. 5). After the water absorption experiment, the peak was found to increase in response to immersion in water for 120 days. The FTIR spectrums for the different composite samples included in the study indicated that water immersion led to an increase in the quantities of moisture absorbed and that these quantities were different for each composite.

The peak due to water content which centred at 3350 cm^{-1}, was studied to identify the effect of nanoclay addition on water uptake behaviours of eco-composites and eco-nanocomposites. Nanoclay addition decreases the amount of water absorption in composites. In particular, the addition of 5 wt.% nanoclay provided substantial water absorption resistance to composites as evidenced by both the weight gain study and FTIR analysis.

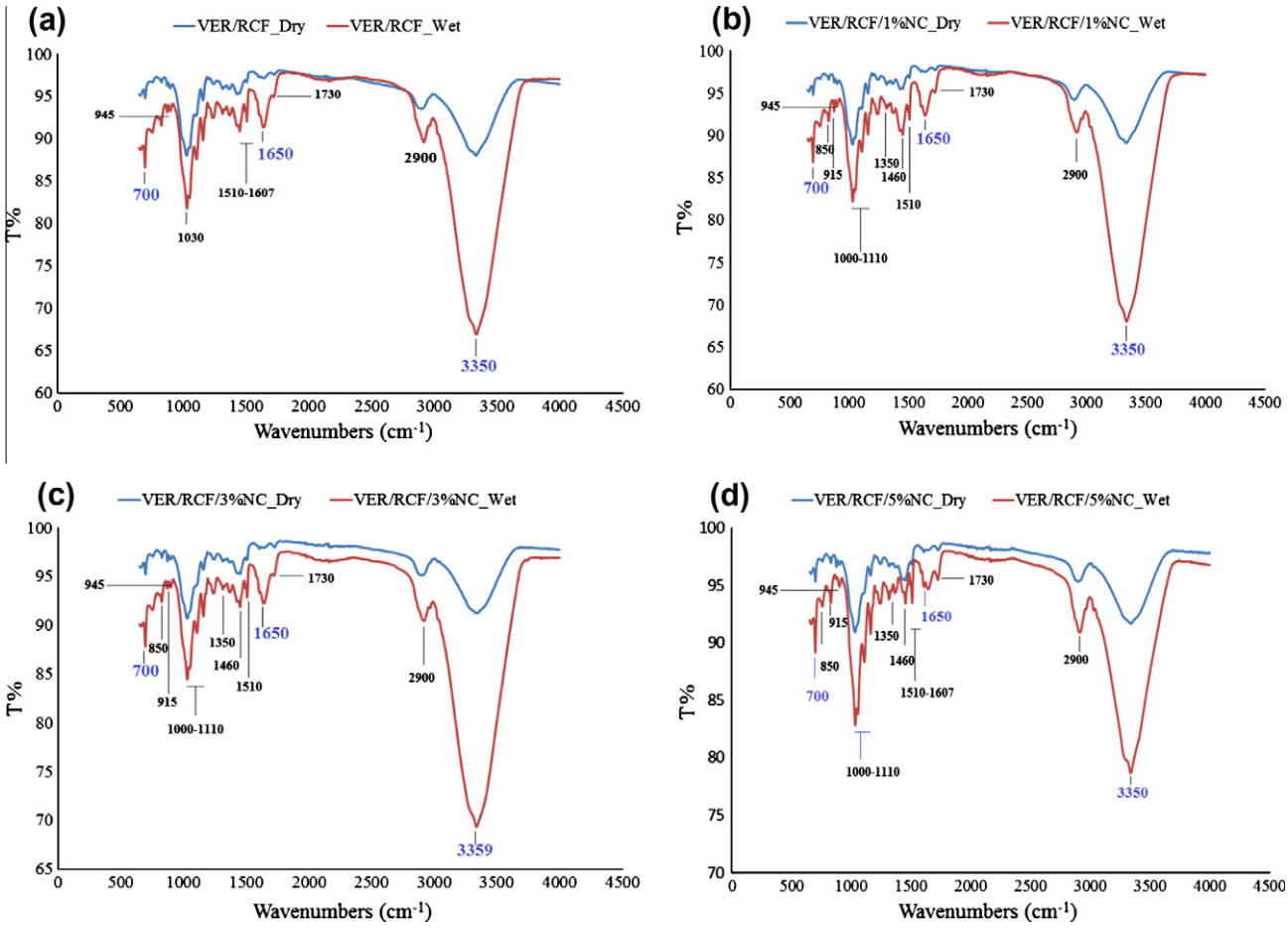

Fig. 3. FTIR Dry and Wet spectrums of (a) VER/RCF eco-composites (b) VER/RCF/1%NC eco-nanocomposites (c) VER/RCF/3%NC eco-nanocomposites and (d) VER/RCF/5%NC eco-nanocomposites.

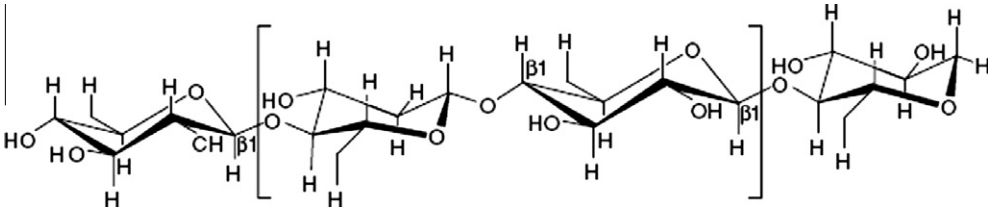

Fig. 4. Diagrammatic representation of cellulose structure [40].

3.3. Mechanical properties

3.3.1. Strengths

Flexural strength and impact strength are measures of strength properties. Results for flexural strength (Fig. 6) revealed that eco-composites and eco-nanocomposite had greater strength than pure samples. Results for impact strength (Fig. 7) also indicated that ecocomposites and eco-nanocomposite were stronger than the pure samples. Specifically, compared to the pure sample, the eco-composite's flexural strength was greater by approximately 33.98%. Cellulose fibres' high strength and modulus and the strong matrix–fibre interfacial adhesion contribute to the observed enhanced flexural properties [8,16,18]. The improved strength properties of polymer reinforced with natural fibres composites have also been also documented in other studies [41–43]. The addition of 1 wt.%, 3 wt.% nanoclay showed 38.43% and 41.42% respective increase in flexural strength.

The addition of 5 wt.% nanoclay reduced flexural strength however. The failure of 5 wt.% nanoclay addition to further enhance strength properties is because of the processing events. At higher clay content, viscosity increases during mixing of resin and nanoclay rendering degassing insufficient before curing. A complete degassing process is essential for the composite to minimise void formation. For nanocomposites containing 5 wt.% of clay, the degassing process is particularly critical as the formation of voids causes specimen failure even on exposure to very low strains. The highly viscous mixture that results when 5 wt.% nanoclay is added to polymer also has further undesirable effects on fibre–matrix adhesion. Since high viscosity causes a reduction in wettability, interfacial adhesion between matrix and fibres are more likely which also reduce the resultant material's strength [44,45].

The pure sample impact strength was 2.6 kJ/m^2. Eco-composites were found to be many magnitudes stronger at 15.9 kJ/m^2. The addition of 1 wt.% and 3 wt.% nanoclay gave impact strength

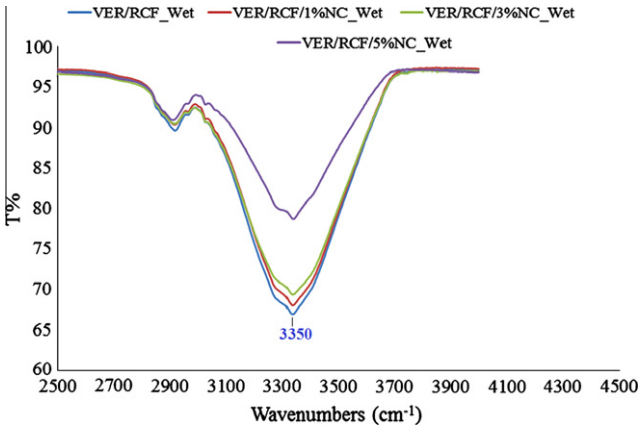

Fig. 5. Comparison between FTIR spectrums peaks of water content of eco and eco-nanocomposites.

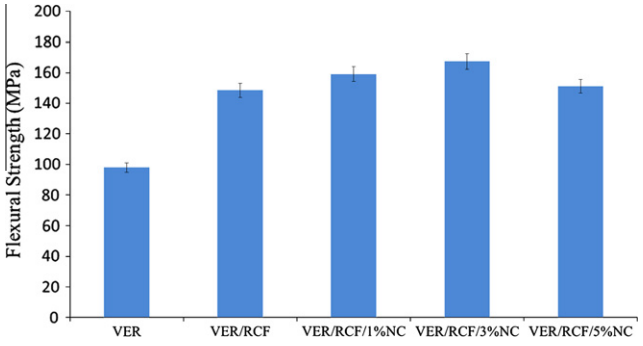

Fig. 6. Flexural strength of vinyl-ester eco and nano-eco composites.

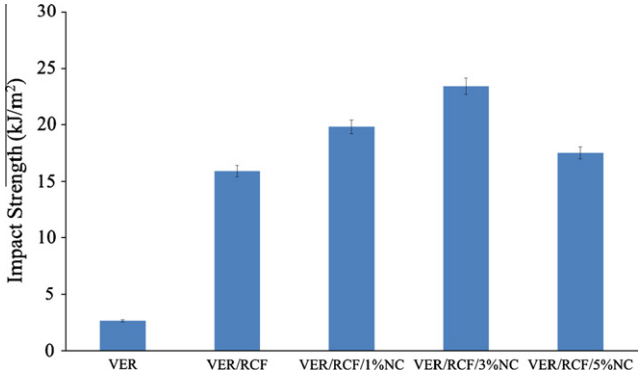

Fig. 7. Impact strength of vinyl ester eco and eco-nanocomposites.

results of 17.9 kJ/m^2 and 20.0 kJ/m^2 respectively. The addition of 5 wt.% nanoclay did not give a higher impact strength result. The high viscosity of the mixture reduced interfacial adhesion of matrix and fibre reducing strength properties.

Impact strength and flexural strength results, as seen in Figs. 5 and 6, all indicate improved values due to nanoclay addition. Despite the problems described above regarding the addition of 5 wt.% nanoclay, strength property results in both impact strength and flexural strength were greater than the unmodified eco-composites. The fibre–matrix adhesion is a primary determinant in composite quality. In a fibre reinforced composite, the role of the matrix is to transfer the load to the stiff fibres through shear stresses at the interface, this process requires a good bond between the polymeric matrix and the fibres [15,16,18]. Studying the fracture surfaces of modified samples (eco-nanocomposites) and unmodified samples eco-composites using SEM reveals the effect of nanoclay addition on fibre–matrix adhesion.

Fig. 8 shows the fracture surfaces of all samples using SEM. The images display fibres pull-outs from the matrix. The disparity in the length of fibres, the fibre surfaces and matrix–fibre gaps is apparent in each of the composites. The pull-out lengths, the extent that individual fibres are isolated, was greater for in the unmodified composites (Fig. 8a) in comparison to the modified composites (Fig. 8b–d). Also, the number of fibres that were pulled out was greater in the unmodified sample. This phenomenon is a result of poor adhesion between the fibres and the matrix materials [46,47].

The fibre surfaces in unmodified eco-composite appear clean. This suggests poor adhesion as no matrix materials have adhered to the fibres [48,49]. In contrast, the modified eco-nanocomposite fibres surfaces are rough indicating better adhesion between the fibres and the matrix materials. Finally, the matrix–fibre gaps appear larger in the unmodified composites compared to the small gaps of the modified composites. The fracture surface images are indicative of nanoclay addition's positive effect on matrix–fibre adhesion [50,51].

3.3.2. Toughness

The RCF composites feature fracture toughness and impact toughness greater than those of the pure samples (Figs. 9 and 10). Cellulose fibres interact with the matrix to provide a composite which has better crack deflection, energy dissipation, and fracture resistance properties. [41–43].

Typically, natural fibre–polymer composites display crack deflection, de-bonding between fibre and matrix, pull-out effect and a fibre-bridging mechanism, which all contribute to fracture toughness. In terms of the matrix alone, plastic deformation provides toughness using an energy dissipation mechanism [46,52]. However, this mechanism is hindered by the addition of fibres. Nonetheless, the overall material is tougher due to the toughness mechanisms provided by natural fibres.

In this study, eco-composites' fracture toughness (Fig. 9) was, at its highest, 60% greater than the baseline pure matrix. Increasing nanoclay addition, however, led to a reduction in fracture toughness. It was previously discussed that nanoclay addition results in desirable strength properties due to fibre–matrix adhesion improvement. However, this improvement of fibre–matrix adhesion makes the eco-nanocomposite brittle as indicated in the lower fracture toughness results for the samples. The addition of nanoclay causes fibre–matrix adhesion to be high which prevents the materials energy absorption mechanisms provided by fibre pull-outs and fibre de-bonding [46]. The images in Fig. 8 reveal how without nanoclay, the fibres in the eco-composite slide out from the matrix in a greater length and number (Fig. 8a), however, with nanoclay, the fibres pulled-out are shorter and in less number (Fig. 8b–d) indicating the strong interfacial adhesion of the eco-nanocomposites [49].

For this reason, a similar trend was observed with impact toughness (Fig. 10). Eco-composite impact toughness was markedly greater than the baseline pure matrix sample with 42.3 kJ m^2 and 1.5 kJ/m^2 as respective results. Increasing of the loading of nanoclay decreased impact toughness properties again. Fibre pull-outs and fibre fracture were determined the dominant toughness mechanisms as evidenced by the images in (Fig. 8).

3.4. Calculation of flexural strength and modulus

From the load–deflection data obtained from testing, flexural strength (σ_F), modulus (E_F) and strain to failure (ε_F) can be calculated by [53]:

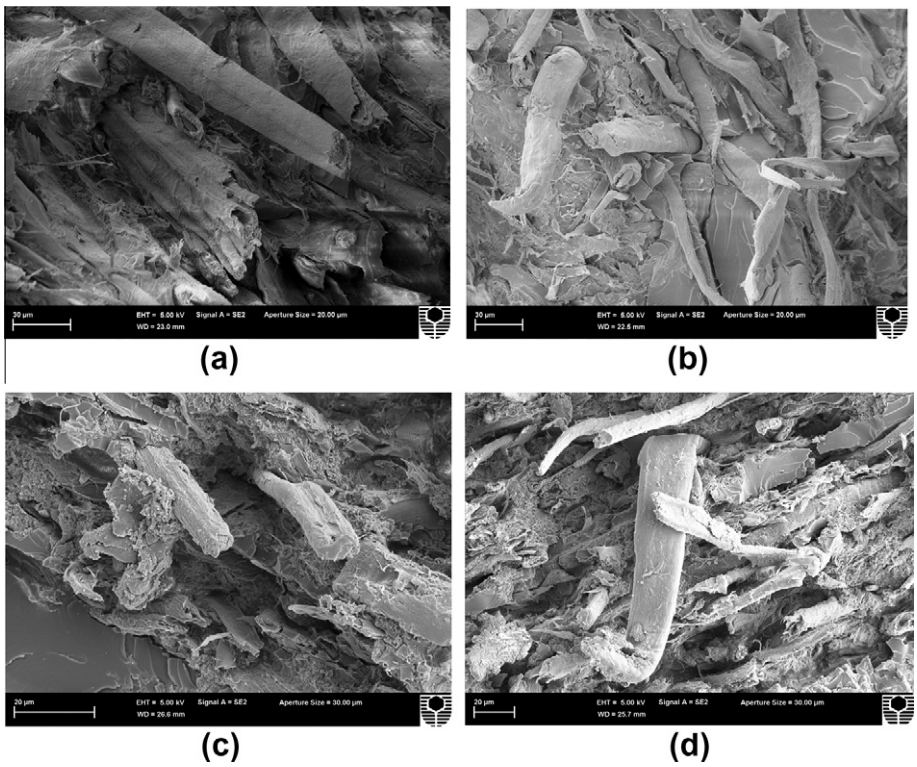

Fig. 8. SEM images of fracture surfaces of (a) eco-composite, (b) eco-nanocomposite with 1 wt.% nanoclay loading, (c) eco-nanocomposite with 3 wt.% nanoclay loading (d) eco-nanocomposite with 5 wt.% nanoclay loading all samples were subjected to fracture toughness test.

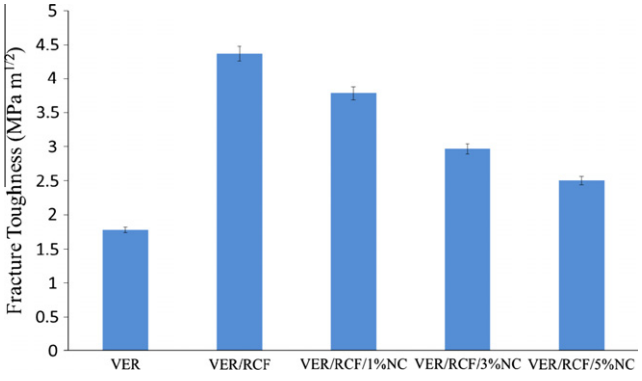

Fig. 9. Fracture toughness of eco-composite and eco-nanocomposites.

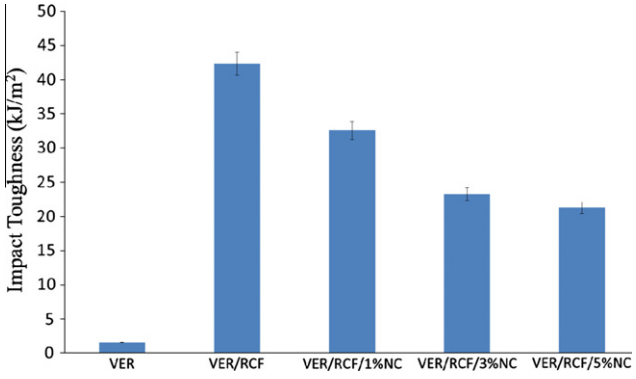

Fig. 10. Impact toughness of eco-composite and eco-nanocomposites.

$$\sigma_F = \frac{3P_{\max}L}{2bh^2}\left[1 + 6\left(\frac{D}{L}\right)^2 - 4\left(\frac{h}{L}\right)\left(\frac{D}{L}\right)\right] \tag{8}$$

$$E_F = \frac{mL^3}{4bh^3} \tag{9}$$

$$\varepsilon_F = \frac{6Dh}{L^2} \tag{10}$$

where L, b and h are the span, width and depth of the specimen, m is the slope of the tangent to the initial straight-line portion of the load–deflection curve, D is the maximum deflection before failure, and $P_{\max}$ is the maximum load encountered before failure.

For each weight loading, five tests were conducted for each configuration, and the average values and variations were determined and presented. Following the testing, specimens were also inspected under an optical microscope in order to investigate any anomalies in flexural performance.

3.4.1. Void content

If voids exist in a composite, the fibre weight fraction w_f is given by

$$w_f = \frac{\rho_f V_f}{\rho_f V_f + \rho_m(1 - V_f - V_v)} \tag{11}$$

where ρ_c, ρ_f and ρ_m are the densities of composite, fibre and matrix, respectively, and V_f and V_v are the volume fractions of fibre and voids, respectively.

If the fibre weight fraction is known, the fibre volume fraction can be found by

$$V_f = \frac{1 - V_v}{1 + \frac{\rho_f}{\rho_m}\left(\frac{1}{w_f} - 1\right)} \tag{12}$$

The density of composite can be obtained using the rule of mixtures as given below.

$$\rho_c = \rho_f V_f + \rho(1 - V_f - V_v) \tag{13}$$

When a composite is void-free, Eqs. (12) and (13) become

$$V_f = \frac{1}{1 + \frac{\rho_f}{\rho_m}\left(\frac{1}{w_f} - 1\right)} \tag{14}$$

$$\rho_c = \rho_f V_f + \rho_m(1 - V_f) \tag{15}$$

Substituting Eqs. (14) into (15) yields

$$\rho_c = \rho_m + \frac{\rho_f - \rho_m}{1 + \frac{\rho_f}{\rho_m}\left(\frac{1}{w_f} - 1\right)} \tag{16}$$

First, the VER/RCF composites are assumed to be void-free, and the density of RCF sheets was derived to be ρ_{RCF} = 1.542 g/cm^3 from the densities of VER/RCF composites and VER (Table 3) using Eq. (16). The fibre volume fraction is 32.76%.

3.4.2. Flexural modulus and flexural strength

Since the eco-composites contain voids, they are three-phase materials and modulus is given by [54]:

$$E_{VER/RCF/NC} = E_{VER/ROF}\left(\frac{1 - V_v^{2/3}}{1 - V_v^{2/3} + V_v}\right)\left[\frac{1 + (E_{NC}/E_{VER/RCF} - 1)V_{NC}^{2/3}}{1 + (E_{NC}/E_{VER/RCF} - 1)(V_{NC}^{2/3} - V_{NC})}\right] \tag{17}$$

where $E_{VER/RCF/NC}$, E_{NC} and $E_{VER/RCF}$ are the elastic moduli of the composite, nanoclay particles and matrix, respectively. The tensile modulus and tensile strength of Cloisite 30B are 170 GPa and 1 GPa, respectively [55].

Because of the linear load–displacement relationships, the elastic modulus and the flexural modulus are very close. The flexural moduli from the experiments and calculation are shown in Fig. 11. It is seen that good agreement is found. The general trend is flexural modulus increases with weight percentage of nanoclay particles except the 5%NC specimens, where their decreased flexural modulus is due to their highest void content. The flexural strengths from the experiments are shown in Fig. 12. It is also seen that the flexural strength of the 5%NC specimens decreases due to their highest void content.

3.5. Thermal and flammability properties

Fig. 13 shows the TGA curves for vinyl-ester, eco-composites and eco-nanocomposites. The temperature range used for the analysis was room temperature to 800 °C. For vinyl-ester Thermal degradation occurred in a single stage at around 370 °C. Compared with the pure samples, the samples reinforced with RCF sheets showed a slightly higher thermal stability. This is due to the higher and longer thermal resistance of the cellulose fibres [56]. In all composites, the release of moisture led to a slight weight loss between 60 °C and 100 °C. At approximately 230–260 °C, the degradation profile of the composites started according to thermogravimetric analysis. Between 270 °C and 480 °C degradation of the eco-composites followed relating to constituent decomposition. Continued decomposition was evident from 380 °C until the temperature reached near 500 °C at which point a constant mass was achieved. Eco-nanocomposite thermal stability results followed a similar trend however the temperature required for decomposition were slightly higher (Fig. 13). Eco-nanocomposites with 1 wt.%, 3 wt.%, and 5 wt.% of nanoclay required 387.1 °C, 399.76 °C, and 404.3 °C temperatures respectively to start constituent decomposition.

In terms of weight loss, from 60 to 250 °C, eco-composites gave a percentage mass drop of 1.85% according to TGA analysis. At 350 °C, a 23.3% drop in mass was recorded. However, at the same temperature the eco-nanocomposites gave about 22.9%, 21.9% 18.9% degradation for composites with 1%NC, 3%NC and 5%NC

Table 3
Measured thicknesses, densities and void contents.

Samples	NC wt.%	Measured density (g/cm^3)	Void content (%)
VER/RCF	0	1.263	0
VER/RCF/1%NC	1	1.273	0
VER/RCF/3%NC	3	1.277	0.12
VER/RCF/5%NC	5	1.269	1.17

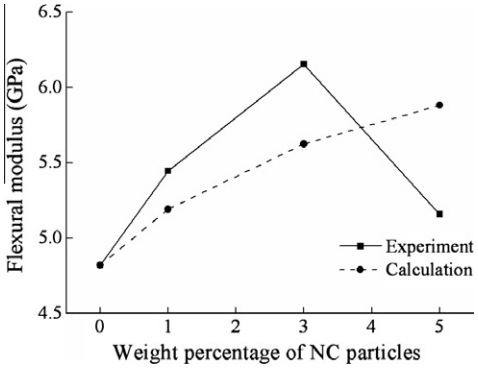

Fig. 11. Comparison between flexural moduli from the experiment and calculations.

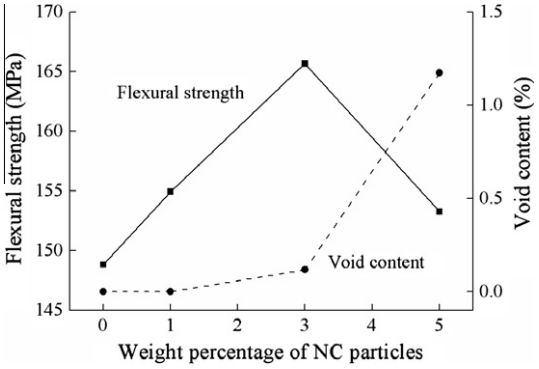

Fig. 12. Effect of void content on flexural strength.

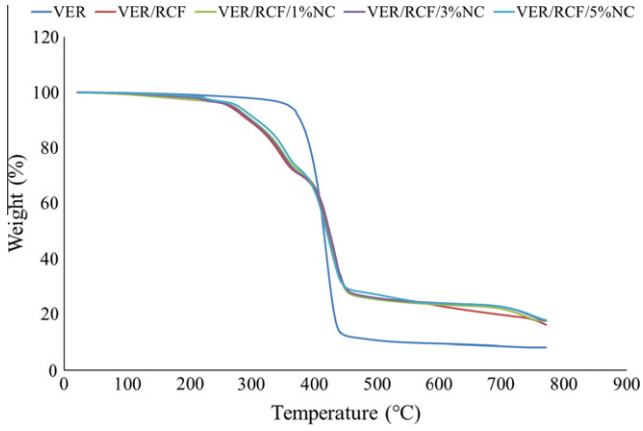

Fig. 13. TGA curves of eco-composites and eco-nanocomposites.

Table 4
Flammability properties of vinyl ester resin and its composites.

Sample	Burning out time (s)	Ignition time (s)	Fire spreading speed (mm/s)
VER	92	3.2	0.109
VER/RCF	98	3.53	0.097
VER/RCF/1%NC	102	4.03	0.102
VER/RCF/3%NC	104	4.24	0.098
VER/RCF/5%NC	110	4.6	0.091

respectively. Above 700 °C, the residual weight of eco-composites was 16.3% of the original. While the pure samples, only 8.3% remained. For the eco-nanocomposites at 1%NC, 3%NC and 5%NC, 17.6%, 17.8% and 18% of the starting weight remained respectively. The quantities of residual weights were only slightly higher due the addition of the nanoclay silicate [28,29].

Flammability tests simulate the realistic fire action and therefore were conducted at ambient conditions. Time of burning out and ignition time were determined and the fire spreading speed was calculated. Pure samples were found to burn out and ignite faster than eco-composites and eco-nanocomposites as seen in Table 4.

As previously described in terms of thermal stability, cellulose fibres provide more favourable thermal properties. Nanoclay addition was found to further reduce the flammability of the composites due to its insulating mechanism and action as a mass transport barrier for volatile products of decomposition [29,57,58]. Nanoclay addition also promotes the formation of char which acts as a fire-retardant [28,59].

4. Conclusions

Vinyl-ester eco-composites and vinyl-ester eco-nanocomposites have been fabricated and studied in terms of water uptake, mechanical and thermal properties. Nanoclay was found to effectively decrease the water uptake in eco-nanocomposites with 5% loading giving more favourable results compared to 1% and 3%. Strength properties were also found to be enhanced due to the reinforcing effect of both RCF and nanoclay. In particular, nanoclay addition improved fibre–matrix adhesion giving greater strength property results for the eco-nanocomposites. A good agreement was found between the experiment and calculations regarding flexural modulus. With weight percentage of nanoclay particles, flexural modulus increases except for the 5%NC specimens in which high void content leads to a decreased flexural modulus. Due to the toughness mechanism of cellulose fibres, the presence of cellulose fibre found to increase the toughness properties of samples. However, nanoclay addition resulted in samples which were brittle due to the nanoclay's effect on the fibre–matrix adhesion limiting the mechanisms of fibre pull-out and fibre debonding. Therefore, the toughness properties of the eco-nanocomposites were lower than those of the eco-composites. The thermal properties, both thermal stability and flammability, of the eco-nanocomposites were preferable to those of the eco-composites or pure samples. Nanoclay addition increased both the thermal stability and fire-resisting properties of the composites.

Acknowledgements

We thank Mr. Charles Hrubos of NichePlas for providing the organoclay (30B) and Mr. Andreas Viereckl for assistance with Charpy impact tests. We also thank Peter Chapman and Kristy Blyth assistance in FTIR and TGA measurements.

References

[1] Singha AS, Thakur VK. Mechanical properties of natural fibre reinforced. Polymer Composites Bull Mater Sci 2008;31(5):791–9.
[2] Lei Y, Wu Q, Clemons CM, Yao F, Xu 1 Y. Influence of nanoclay on properties of HDPE/wood composites. J Appl Polym Sci 2007;106:3958–66.
[3] Low IM, McGrath M, Lawrence D, Schmidt P, Lane J, Latella BA, et al. Mechanical and fracture properties of cellulose-fibre-reinforced epoxy laminates. Composites: Part A 2007;38:963–74.
[4] Cheung H, Ho M, Lau K, Cardona F, Hui D. Natural fibre-reinforced composites for bioengineering and environmental engineering applications. Composites: Part B 2009;40:655–63.
[5] Venkateshwaran N, Elayaperumal A, Alavudeen A, Thiruchitrambalam M. Mechanical and water absorption behaviour of banana/sisal reinforced hybrid composites. Mater Des 2011;32:4017–21.
[6] Halberd J, Houston D. Natural-fibre-reinforced polymer composites in automotive applications: low-cost composites in vehicle manufacture. JOM 2006:80–6.
[7] Monteiro SN, Lopes FPD, Ferreira AS, Nascimento DO. Natural-fibre polymer–matrix composites: cheaper, tougher, and environmentally friendly. JOM 2009;61(1):17–22.
[8] Anuar H, Zuraida A. Improvement in mechanical properties of reinforced thermoplastic elastomer composite with kenaf bast fibre. Composites: Part B 2011;42:462–5.
[9] Sgriccia N, Hawley MC, Misra M. Characterization of natural fibre surfaces and natural fibre composites. Composites: Part A 2008;39:1632–7.
[10] Mallick P. Fibre-reinforced composites: materials, manufacturing, and designs. 3rd ed. New York: CRC Press, Taylor & Francis Group; 2007.
[11] Dhakal HN, Zhang ZY, Richardson MOW. Effect of water absorption on the mechanical properties of hemp fibre reinforced unsaturated polyester composites. Compos Sci Technol 2007;67:1674–83.
[12] Huda MS, Drzal LT, Mohanty AK, Misra M. Chopped glass and recycled newspaper as reinforcement fibres in injection molded poly(lactic acid) (PLA) composites: A comparative study. Compos Sci Technol 2006;66:1813–24.
[13] Huda M, Drzal L, Mohanty A, Misra M. The effect of silane treated- and untreated-talc on the mechanical and physico-mechanical properties of poly (lactic acid)/newspaper fibres/talc hybrid composites. Composites: Part B 2007;38:367–79.
[14] Baroulaki I, Karakasi B, Pappa G, Tarantili P, Economides D, Magoulas K. Preparation and study of plastic compounds containing polyolefins and post used newspaper fibres. Composites: Part A 2006;37:1613–25.
[15] Herrera-Franco PJ, Valadez-Gonzalez A. Study of the mechanical properties of short natural-fibre reinforced composites. Composites: Part B 2005;36:597–608.
[16] Chen H, Miao M, Ding X. Influence of moisture absorption on the interfacial strength of bamboo/vinyl ester composites. Composites: Part A 2009;40:2013–9.
[17] Espert A, Vilaplana F, Karlsson S. Comparison of water absorption in natural cellulosic fibres from wood and one-year crops in polypropylene composites and its influence on their mechanical properties. Composites: Part A 2004;35:1267–76.
[18] Bakare IO, Okieimen FE, Pavithran C, Abdul-Khalil HPS, Brahmakumar M. Mechanical and thermal properties of sisal fiber-reinforced rubber seed oil-based polyurethane composites. Mater Des 2010;31:4274–80.
[19] Assarar M, Scida D, El Mahi A, Poilâne C, Ayad S. Influence of water ageing on mechanical properties and damage events of two reinforced composite materials: flax–fibres and glass–fibres. Mater Des 2011;32:788–95.
[20] Joseph PV, Joseph K, Thomas S, Pillai CKS, Prasad VS, Groeninckx G, et al. The thermal and crystallisation studies of short sisal fibre reinforced polypropylene composites. Composites: Part A 2003;34:253–66.
[21] Mylsamy K, Rajendran I. The mechanical properties, deformation and thermomechanical properties of alkali treated and untreated Agave continuous fibre reinforced epoxy composites. Mater Des 2011;32:3076–84.
[22] Pavlidoua S, Papaspyrides CD. A review on polymer-layered silicate nanocomposites. Progress Polym Sci 2008;33:1119–98.
[23] Hussaain F, Hojjat M. Review article: polymer-matrix nanocomposites, processing, manufacturing, and application: an overview. J Compos Mater 2006;40(17):1511–75.
[24] Pfaendner R. Nanocomposites: industrial opportunity or challenge. Polym Degrad Stab 2010;95:369–73.
[25] Sancaktar E, Kuznicki J. Nanocomposite adhesives: mechanical behavior with nanoclay. Int J Adhes Adhes 2011;31:286–300.
[26] Kim J, Hu C, Woo RSC, Sham ML. Moisture barrier characteristics of organoclay-epoxy nanocomposites. Compos Sci Technol 2005;65:805–13.
[27] Ray SS, Okamoto M. Polymer/layered silicate nanocomposites: a review from preparation to processing. Progress Polym Sci 2003;28:1539–641.
[28] Zeng QH, Yu AB, Lu GQ, Paul DR. Clay-based polymer nanocomposities: research and commercial development. J Nanosci Nanotechnol 2005;5:1574–92.
[29] Becker O, Varley RJ, Simon GP. Thermal stability and water uptake of high performance epoxy layered silicate nanocomposites. Eur Polym J 2004;2004(40):187–95.
[30] Mohan P, Kanny K. Water barrier properties of nanoclay filled sisal fibre reinforced epoxy composites. Composites: Part A 2011;42:385–93.

[31] Lasagabaster A, Abad MJ, Barral L, Ares A. FTIR study on the nature of water sorbed in polypropylene (PP)/ethylene alcohol vinyl (EVOH) films. Eur Polym J 2006;42:3121–32.
[32] Lasagabaster A, Abad MJ, Barral L, Ares A, Bouza R. Application of FTIR spectroscopy to determine transport properties and water– polymer interactions in polypropylene (PP)/poly(ethylene-co-vinyl alcohol) (EVOH) blend films: effect of poly(ethylene-co-vinyl alcohol) content and water activity. Polymer 2009;50:2981–9.
[33] Karbowiak T, Ferret E, Debeaufort F, Voilley A, Cayot P. Investigation of water transfer across thin layer biopolymer films by infrared spectroscopy. J Membr Sci 2011;370:82–90.
[34] Leslie SL, Karen KG. Investigation of polymer and nanoclay orientation distribution in nylon6/montmorillonite nanocomposite. Polymer 2004;45:5933–9.
[35] Sonawane SH, Chaudhari PL, Ghodke SA, Parande MG, Bhandari VM, Mishra S, et al. Ultrasound assisted synthesis of polyacrylic acid–nanoclay nanocomposite and its application in sonosorption studies of malachite green dye. Ultrason Sonochem 2009;16:351–5.
[36] Sgriccia N, Hawley MC, Misra M. Characterization of natural fiber surfaces and natural fiber composites. Composites: Part A 2008;39:1632–7.
[37] Oh SY, Yoo DI, Shin Y, Seo G. FTIR analysis of cellulose treated with sodium hydroxide and carbon dioxide. Carbohydr Res 2005;340:417–28.
[38] Scott TF, Cook WD, Forsythe JS. Kinetics and network structure of thermally cured vinyl ester resins. Eur Polym J 2002;38:705–16.
[39] Brill RP, Palmese GR. An investigation of vinyl–ester-styrene bulk copolymerization cure kinetics using Fourier transform infrared spectroscopy. J Appl Polym Sci 2000;76:1572–82.
[40] Mohanty AK, Misra M, Drzal LT. Natural fibres, biopolymers, and biocomposites. New York: CRC Press Taylor & Francis; 2005.
[41] Low IM, Somers J, Kho HS, Davies IJ, Latella BA. Fabrication and properties of recycled cellulose fibre-reinforced epoxy composites. Compos Interfaces 2009;16(7–9):659–69.
[42] Wambua P, Ivens J, Verpoest I. Natural fibres: can they replace glass in fibre reinforced plastics? Compos Sci Technol 2003;63:1259–64.
[43] Benjamin B, Jorg M. Review: impact and tensile properties of PLA/Cordenka and PLA/flax composites. Compos Sci Technol 2007;68:1601–7.
[44] Ashori A, Nourbakhsh A. Characteristics of wood–fiber plastic composites made of recycled materials. Waste Manage 2009;29:1291–5.
[45] Avella M, Buzarovska A, Errico ME, Gentile G, Grozdanov A. Review: eco-challenges of bio-based polymer composites. Materials 2009;2:911–25.
[46] Silva RV, Spinelli D, Bose WW, Filho S, Neto C, Chierice GO, et al. Fracture toughness of natural fibers/castor oil polyurethane composites. Composites Sci Technol 2006;66:1328–35.
[47] Stocchi A, Bernal C, Vazquez A, Biagotti J, Kenny J. A silicone treatment compared to traditional natural fiber treatments: effect on the mechanical and viscoelastic properties of jute–vinyl ester laminates. J Compos Mater 2007;41(16):2005–24.
[48] De Rosa IM, Santali C, Sarasini F. Mechanical and thermal characterization of epoxy composites reinforced with random and quasi-unidirectional untreated phormium tenax leaf fibers. Mater Des 2010;31:2397–405.
[49] Mylsamy K, Rajendran I. The mechanical properties, deformation and thermomechanical properties of alkali treated and untreated agave continuous fibre reinforced epoxy composites. Mater Des 2011;32:3076–84.
[50] Suppakarn N, Jarukumjorn K. Mechanical properties and flammability of sisal/PP composites: effect of flame retardant type and content. Composites: Part B 2009;40:613–8.
[51] Franco-Marquès E, Méndez JA, Pèlach MA, Vilaseca F, Bayer J, Mutjé P. Influence of coupling agents in the preparation of polypropylene composites reinforced with recycled fibers. Chem Eng J 2011;166:1170–8.
[52] Wong KJ, Zahi S, Low KO, Lim CC. Fracture characterisation of short bamboo fibre reinforced polyester composites. Mater Des 2010;31:4147–54.
[53] ASTM International, Standard test methods for flexural properties of unreinforced and reinforced plastics and electrical insulating materials, in D790. 2007, ASTM International: West Conshohocken.
[54] Cohen LJ, Ishai O. The elastic properties of three-phase composites. J Compos Mater 1967;1(4):390–403.
[55] Yasmin A, Luo JJ, Abbot JL, Daniel IM. Mechanical and thermal behavior of clay/epoxy nanocomposites. Compos Sci Technol 2006;66(14):2415–22.
[56] Ma X, Yu J, Kennedy JF. Studies on the properties of natural fibers-reinforced thermoplastic starch composites. Carbohydr Polym 2005;62:19–24.
[57] Paul MA, Alexandre M, Degee P, Henrist C, Rulmont A, Dubois P. New nanocomposite materials based on plasticized poly (L-lactide) and organo-modified montmorillonites: Thermal and morphological study. Polymer 2003;44:443–50.
[58] Vyazovkin S, Dranka I, Fan X, Advincula R. Kinetics of the thermal and thermo-oxidative degradation of a polystyrene–clay nanocomposite. Macromol Rapid Commun 2004;25:498–503.
[59] Pavlidou S, Papaspyrides CD. A review on polymer-layered silicate nanocomposites. Progress Polym Sci 2008;33:119–1198.

3.3. Influence of halloysite nanotubes on physical and mechanical properties of cellulose fibres reinforced vinyl ester composites

---

ALHUTHALI, A. and LOW, I. M. 2013. Influence of halloysite nanotubes on physical and mechanical properties of cellulose fibres reinforced vinyl ester composites. *Journal of Reinforced Plastics and Composites*, 32, 233-247

Article

JOURNAL OF REINFORCED PLASTICS & COMPOSITES

Journal of Reinforced Plastics and Composites
32(4) 233–247

DOI: 10.1177/0731684412467392
jrp.sagepub.com
SAGE

Influence of halloysite nanotubes on physical and mechanical properties of cellulose fibres reinforced vinyl ester composites

AM Alhuthali and IM Low

Abstract

Natural fibres are generally added to polymer matrix composites to produce materials with the desirable mechanical properties of higher specific strength and higher specific modulus while at the same time to maintain a low density and low cost. The physical and mechanical properties of polymer composites can be enhanced through the addition of nanofillers such as halloysite nanotubes. This article describes the fabrication of vinyl ester eco-composites and eco-nanocomposites and characterizes these samples in terms of water absorption, mechanical and thermal properties. Weight gain test and Fourier transform infrared analysis indicated that 5% halloysite nanotube addition gave favourable reduction in the water absorption and increased the fibre–matrix adhesion leading to improved strength properties in the eco-nanocomposites. However, halloysite nanotube addition resulted in reduced toughness but improved thermal stability.

Keywords

Vinyl ester, halloysite nanotubes, recycled cellulose fibre, water uptake, mechanical properties, thermal properties

Introduction

Halloysite nanotubes (HNTs) are derived from naturally deposited alumino-silicate ($Al_2Si_2O_5$ $(OH)_4 \bullet H_2O$) and are chemically similar to kaolin.[1] Structurally, due to mismatch between tetrahedral and octahedral internal components, HNTs take on a cylindrical shape forming the tubes which are typically between 1 and 15 μm in length.[2] These tubes have dimensions of between 50 and 70 nm for the outer diameters and between 10 and 30 nm for the inner diameters. As the tubes are hollow, they allow HNTs to have very high surface area with a high aspect which promotes excellent interaction between the filler and matrix.[3] Tensile, fracture and impact strength as well as other mechanical and thermal properties are believed to be dramatically improved when HNTs are added to epoxy, polystyrene, polypropylene, polyvinyl alcohol and other polymers.[4]

Natural fibres are eco-friendly, commercially viable fillers, that have excellent modulus to weight ratios and are capable of forming polymer composites with excellent toughness properties.[5] Natural fibres are biodegradable, unlike plastics, and are energy efficient and often less expensive than the synthetic counterparts.[6,7] Natural fibres are lighter than synthetic materials, and having an excellent modulus to weight ratio, are ideal for stiffness-critical designs needed in construction, automotive and even aerospace industries.[7] Acoustic damping properties of natural fibres make them suitable for use in components in the internal areas of automobiles.[8] Compared to synthetic fibres,

Department of Imaging and Applied Physics, Curtin University, Perth, Australia

Corresponding author:
IM Low, Department of Imaging and Applied Physics, Curtin University, GPO Box U1987, Perth, WA 6845, Australia.
Email: j.low@curtin.edu.au

many natural fibres have elastic modulus and specific modulus comparable or better than synthetic fibre composites.[7,8]

Vinyl ester (VER) resins are a newer thermosetting resin compared to alternatives such as polyester and epoxy resins. In terms of industrial applications, the desirable properties of VER resins make them suitable for adhesives, coatings, electrical applications, moulding compounds and structural laminates. Thus, VER resins that combine the most sought-after properties of epoxies and unsaturated polyesters are favoured by the industry.[9]

So far, studies have established that the addition of natural fibres to polymer matrices as a micro-scale reinforcement material provides toughness and strength to these composites.[10] Barrier, thermal and mechanical properties of polymeric composites can also be improved by adding a low concentration of nanofiller particles as a nanoscale reinforcement material.[11] The combination of multi-scale reinforcement materials in polymer matrix can provide the reinforcements properties at two scales. However, incorporation nanofillers to natural fibre polymer composites, is an area that has not been widely investigated.

The selection of HNTs as the nanofiller to be incorporated in natural fibre polymer composites for the purposes of development and characterization is a novel proposition and one which it seems has yet to be attempted by the scientific community at this time. This study, therefore, aimed to investigate this addition of HNTs to VER reinforced with recycled cellulose fibre (RCF) and to characterize the resulting composite's properties in terms of water absorption, mechanical, thermal and flammability. A novel finding on the functions of HNT particles was revealed by the water uptake behaviours and fibres–matrix adhesion.

Experimental

Materials

RCF in sheets form, grade 80 GSM, 100 μm thickness, supplied by Todae Company, NSW, Australia; a general purpose VER resin, supplied by Fibreglass & Aesin Sales Pty Ltd, WA, Perth, Australia and ultrafine HNTs with 50.4% SiO_2, 35.5% Al_2O_3, 0.25 Fe_2O_3 and 0.05 TiO_2 (wt%), supplied by NZCC, New Zealand, were used in this study.

Preparation of samples

Preparation of pure samples. VER samples were first made as a control to provide the baseline data of the properties of pure VER resin. The VER resin was mixed with 1.0 wt% methyl ethyl ketone peroxide in order to prepare the samples. The mixture was slowly and thoroughly mixed to ensure that no air bubbles formed within the matrix. The resultant mixture was poured into silicon moulds and left under low vacuum (20 kPa) for 2 h and later left at room temperature for 24 h to cure.

Preparation of eco-composites. RCF sheets were dried for 60 min at 150°C. RCF sheets were then fully soaked in the VER system. Next, the sheets were laid up in a silicon mould under compressive pressure (10.2 kPa) and then placed under vacuum (60 kPa) for 2 h. Then, samples left to cure for 24 h at room temperature. The weight percentage of fibres in these eco-composites was 40%.

Preparation of eco-nanocomposites. Nanocomposites containing different concentrations, namely, 1, 3 and 5 wt% HNTs were prepared. HNTs were first dried for 60 min at 150°C, and then mixed with VER resin for 30 min using high-speed electrical mixer. The mixtures were then left under vacuum of 60 kPa to remove air bubbles. After that, catalyst was added and mixed manually to avoid creating air bubbles inside the composites. Next, the mixtures were then reinforced with the same percentage of RCF sheets (40 wt%). The sheets were also dried for 60 min at 150°C. The sheets were then fully soaked in the mixtures and pressed together under compressive pressure of 10.2 kPa and under vacuum of 60 kPa for 2 h. Finally, the samples were left to cure at room temperature for 24 h. The resultant eco-nanocomposites were labelled as VER/RCF/1%HNTs, VER/RCF/3%HNTs and VER/RCF/5%HNTs, respectively.

Characterization

Microstructure examination

Samples were measured on a D8 Advance Diffractometer (Bruker-AXS) using copper radiation and a LynxEye position sensitive detector. The diffract meter were scanned from 3° to 50° (2θ) in steps of 0.02° using a scanning rate of 0.5°/min X-ray diffraction analysis (XRD) patterns obtained using Cu-Kα lines ($\lambda = 1.5406$ Å). A knife edge collimator was fitted to reduce air scatter.

To study the morphologies of the HNTs and their dispersion inside the VER matrix, a transmission electron microscope (TEM; JEOL JEM2011, Japan) was used. A NEON 40ESB, scanning electron microscope (SEM; ZEISS, UK) operating at accelerating voltage of 5 kV, under secondary electrons mode was used to examine the microstructure of HNTs and fracture surfaces of the samples. In order to avoid charging, all samples were coated with platinum.

Water uptake properties

Samples with rectangular-shaped dimensions ($10 \times 10 \times 6\,mm^3$) were used. Individual samples were soaked in tap water at room temperature. At prescribed intervals, samples were removed from water. After excess water was removed, they were weighed and immediately returned to the water. The amount of moisture uptake or absorbed (M_A) by the samples over a period of 120 days, was determined using the following equation[9]

$$M_A = \frac{M_T - M_D}{M_D} \times 100 \quad (1)$$

where M_D is the dry mass and M_T the mass of sample soaked for time t.

Diffusion coefficient of samples have been calculated using the following equation[12]

$$D = \frac{\pi}{16}\left(\frac{M_t/M_\infty}{\sqrt{t}/h}\right)^2 \quad (2)$$

where M_∞ is the maximum water uptake, M_t the water uptake at time t, h the sample thickness and D the diffusion coefficient.

Fourier transform infrared analysis

A Perkin Elmer Spectrum 100 Fourier transform infrared analysis (FT-IR; Perkin Elmer, MA, USA) infrared spectrometer was used for the Fourier transform spectroscopy analysis (FT-IR). The spectral resolution was four wavenumbers. The FT-IR analysis was conducted to determine the water content of the samples after the water absorption experiment. An ATR correction was performed to compensate for the wavelength dependence on penetration depth. Thin slice samples with dimensions $5 \times 5 \times 1\,mm^3$ for both the dry- and wet-condition specimens were prepared. The dry condition samples were dried for 15 min at 100°C prior to FT-IR analysis to remove existing moisture. The wet-condition samples were immersed in water for 120 days, and immediately prior to FT-IR analysis, these samples were left at room temperature (~25°C) for 5 min to remove surface moisture.

Flexural strength

Rectangular bars of $60 \times 10 \times 6\,mm^3$ were cut from the fully cured samples for three-point bend tests with a span of 40 mm to evaluate the flexural strength. A LLOYD Material Testing Machine (5–50 kN) with a displacement rate of 1.0 mm/min was used to perform the test. Five samples of each batch were used to evaluate flexural strength. The values were recorded and analysed with the machine software (NEXYGENPlus) and average values were calculated.

Impact strength

To determine impact strength σ_i, a Zwick Charpy impact tester with a 2.0 J pendulum hammer was used. Five 40 mm span bar samples in edgewise position were assessed. Impact strength was calculated using the following equation[13]

$$\sigma_i = \frac{E}{A} \quad (3)$$

where E is the impact energy to break a sample with a ligament of area A.

Fracture toughness

For the fracture toughness (K_{IC}) measurement, the ratio of notch length to width of sample (a/w) used was 0.4 and a sharp razor blade was used to initiate a sharp crack. The flexural tests were performed with a LLOYD Material Testing Machine using a displacement rate of 1.0 mm/min; five samples of each composition were used for the measurements. The value of (K_{IC}) was computed using the following equation[14]

$$K_{IC} = \frac{p_m S}{WD^{2/3}} f\left(\frac{a}{w}\right) \quad (4)$$

where p_m is the maximum load, S the span of the sample, D the specimen thickness, w the specimen width and a the crack length, and $f(a/w)$ is the polynomial geometrical correction factor given as[14]

$$f(a/w) = \frac{\left(\begin{array}{c} 3(a/w)^{1/2}[1.99 - (a/w)(1 - a/w) \\ (2.15 - 3.93a/w + 2.7a^2/w^2)] \end{array}\right)}{2(1 + 2a/w)(1 - a/w)^{2/3}} \quad (5)$$

Impact toughness

To determine the impact toughness (G_{IC}), a Zwick Charpy impact tester with a 2.0 J pendulum hammer was used. Five 40 mm span bar samples in edgewise position with varying notch lengths and razor sharp cracks were used. The value of impact toughness was calculated using the equation[14]

$$U = G_{IC} BD\phi + U_0 \quad (6)$$

where U is the measured energy, U_0 the kinetic energy, D the specimen thickness, B the specimen breadth and ϕ the calibration factor for the geometry used.

Thermal and flammability test

A differential thermo-gravimetric analyser (TGA; Instrument: 2960 SDT V3.0 F) was used to examine thermal behaviours of composites. At a rate of 20°C/min, composites were heated from room temperature to 800°C. Thermal decomposition temperatures of the composites were examined under 20 mL/min of nitrogen using platinum pans. Horizontal burning testing determined flammability in terms of ignition time, burning-out time and fire velocity. For each composite, three samples ($100 \times 10 \times 10\,mm^3$) were prepared and hung on a retort stand and a constant flame source was applied.

Results and discussions

X-ray diffraction analysis

XRD patterns for pure HNTs and VER/RCF/HNTs composites with 1, 3 and 5 wt% of HNTs are shown in Figure 1. A diffraction peak at 2θ at around 12.27° related to the (0 0 1) plane can be seen in XRD pattern of pure HNTs. A highly disordered tubular morphology featuring inter-stratification of layers with various hydration states and small crystal size is indicated by this basal reflection.[15] Two additional diffraction peaks at $2\theta \approx 20.15°$ and $2\theta \approx 24.95°$ which relate to the (0 2 0) and (0 0 2) basal reflections are noticeable.[1,16] Trace amounts of quartz and feldspar in powders are also evident and are represented by (*) and (+), respectively. The presence of these minerals in HNT samples has been noted by other researchers.[15,17] For pure HNT samples, a diffraction peak at $2\theta = 12.27°$ corresponds to a basal spacing of 0.721 nm. For VER/HNT composites, the diffraction peak has shifted towards lower 2θ values. The diffraction peaks, with the corresponding basal spacing shown in parenthesis, for VER/1%HNTs, VER/3%HNTs and VER/5%HNTs were 11.87° (0.745 nm), 12.07° (0.733 nm) and 12.15° (0.728 nm), respectively (Table 1). The evidence of intercalation between VER chains and the HNTs is strongly supported by the 2θ reductions or the increases in the basal spacing of the HNTs in these composites, which further confirms the formation of nanocomposites as found in other studies.[1,4] In relation to the two additional diffraction peaks displayed in the XRD pattern for pure HNTs, the subsequent XRD patterns for the composites samples revealed that the pure HNTs peak at 2θ at around 20.15°, for the composites, had shifted markedly lower, and the pure HNTs peak at 2θ at around 24.95°, for the composites, had almost completely vanished. These results support the existence of intercalation of the VER chain into the structure of the HNTs.

Microstructure of HNTs and VER/RCF/HNT composites

The SEM and TEM images of HNTs reveal that the majority of HNTs exist in a tubular shape and this is evidenced in Figure 2. The presence of short tubular

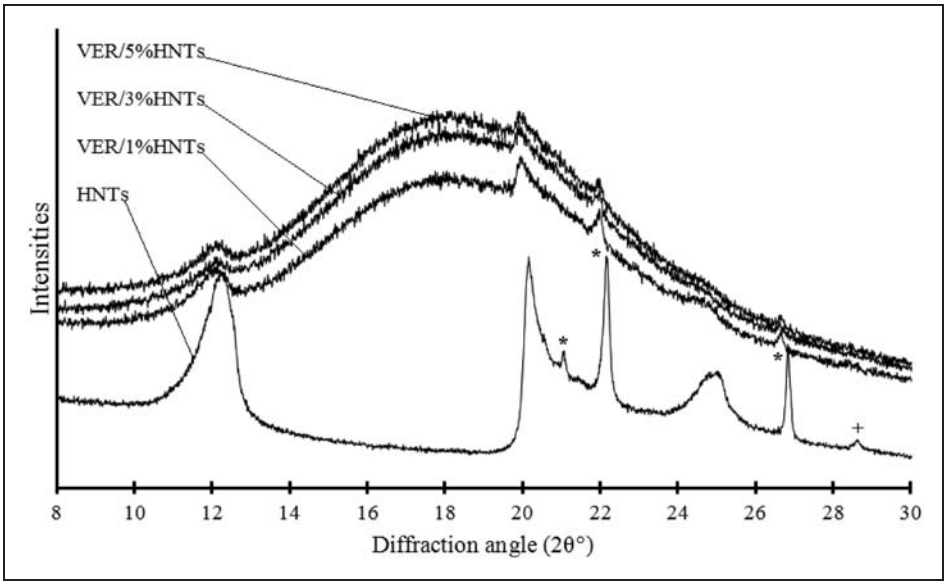

Figure 1. XRD pattern of pure HNTs and VER/HNT composites.
XRD: X-ray diffraction analysis; VER: vinyl ester; and HNTs: halloysite nanotubes.

Table 1. XRD results of HNTs and VER/HNTs composites

Specific plane	(001)		(020)		(002)	
2θ/*d*-spacing	2θ	*d* (nm)	2θ	*d* (nm)	2θ	*d* (nm)
HNTs	12.27	0.721	20.15	0.44	24.95	0.357
VER/1%HNTs	11.87	0.745	19.85	0.447	–	–
VER/3%HNTs	12.07	0.733	19.92	0.445	–	–
VER/5%HNTs	12.15	0.728	19.98	0.444	–	–

XRD: X-ray diffraction analysis; VER: vinyl ester; and HNTs: halloysite nanotubes.

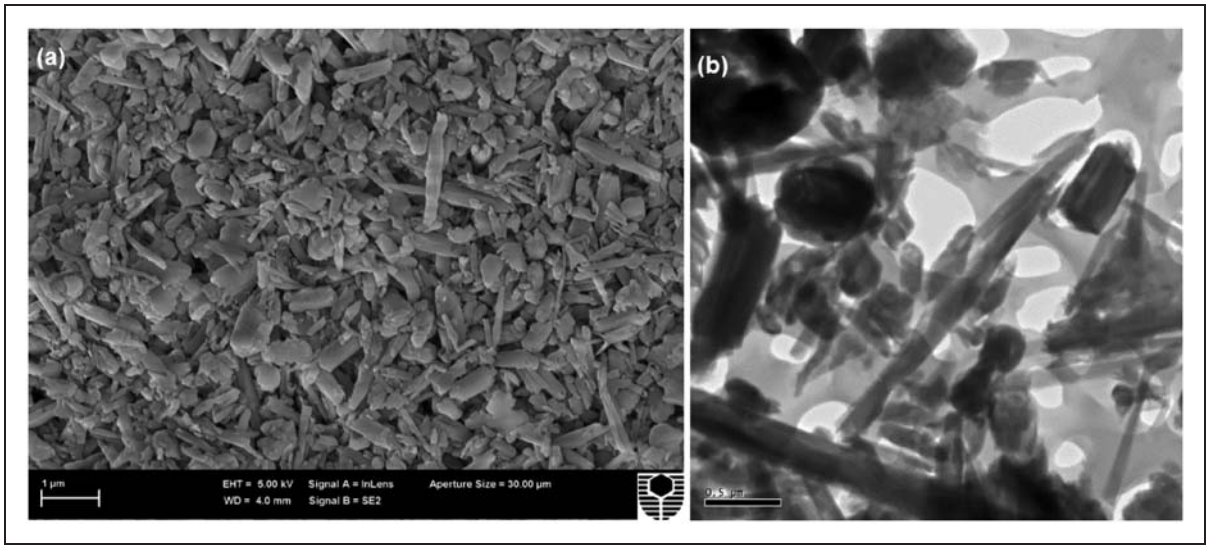

Figure 2. (a) SEM micrograph of HNT particles and (b) TEM micrograph of HNT particles.
SEM: scanning electron microscope; HNT: halloysite nanotube; and TEM: transmission electron microscope.

HNTs, semi-rolled HNTs and pseudo-spherical HNTs is evident. A mean particle size of 2 µm and a length of HNTs ranging from 400 nm to 3 µm were determined. The aspect ratio of HNTs varies between 1.5, 3 and 10. The inner diameters range from 50 to 150 nm while the outer diameters of the HNTs range from 150 to 500 nm. The TEM micrographs (Figure 3) show that there is an acceptable degree of dispersion of HNT particles or clusters within the composites for 1, 3 and 5 wt% HNTs.

Water uptake properties

Weight gain test. Water absorption curves of the eco-composites and eco-nanocomposites are shown in Figure 4. When the samples were first exposed to water, the process of water absorption occurred rapidly then gradually the absorption rate slowed down until equilibrium, these behaviours follow the Fickian diffusion behaviour.[12] Clearly, increasing the HNT addition to the system has resulted in a reduction in the uptake of water. The most plausible explanation for this is that HNTs interfere with the transfer paths of water molecule by transforming the original path of direct-fast diffusion into a torturous or maze-like path which slows water absorption and reduces the overall uptake of water. The impermeability of nanocomposites provided by HNTs prevents their complete saturation and causes maximum water uptake to be lower.[18,19] The maximum water uptake M_∞ and diffusion coefficient D values for all composites are presented in Table 2. The amount of water absorbed decreased as the HNT loading increased, thus indicating the desirable effect of HNTs in reducing water absorption in the composites.

FT-IR analysis. The FT-IR spectra of eco-composites and eco-nanocomposites in dry- and wet-conditions are shown in Figure 5(a) and (b). A broad peak representing the stretching of hydroxyl groups between 3000 and 3700 cm^{-1} can be seen for each spectrum in dry

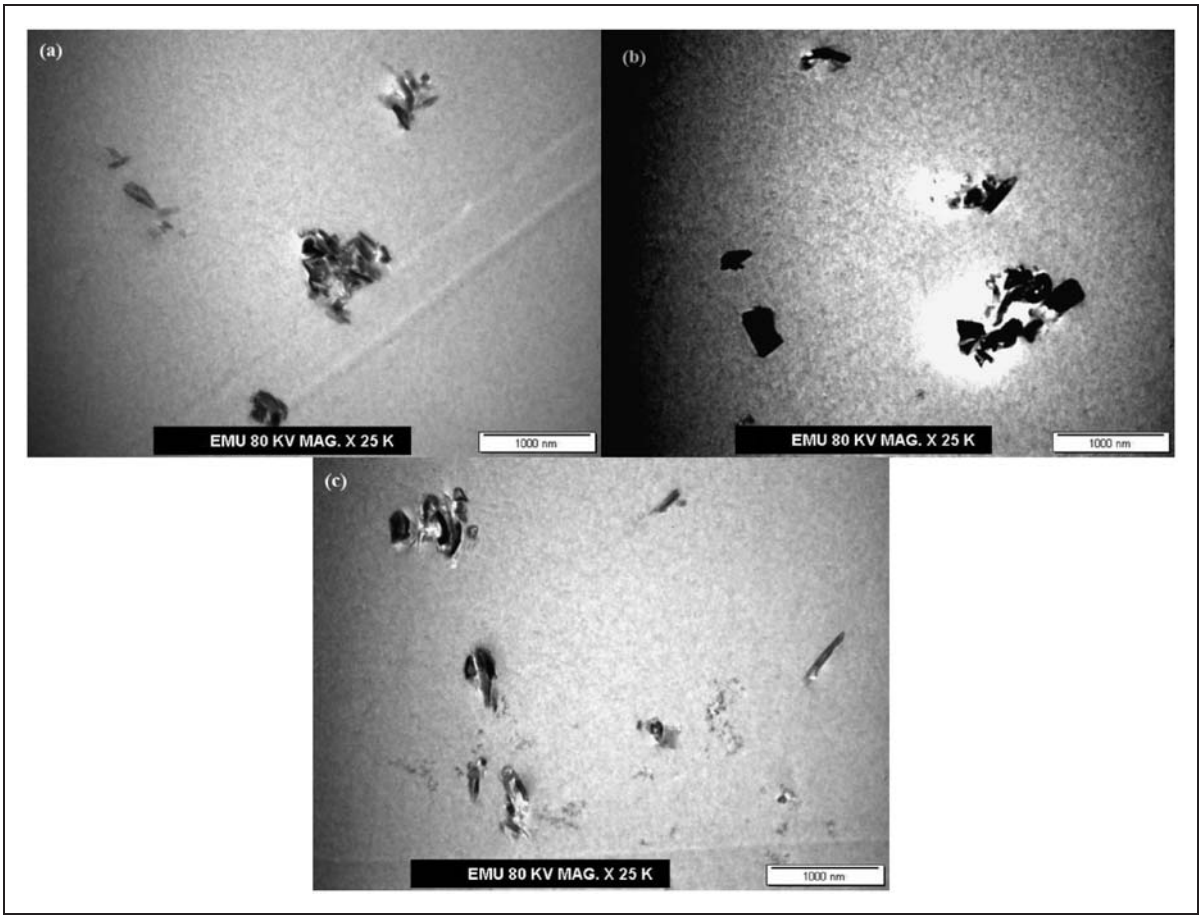

Figure 3. Dispersion of HNTs particles within composites: (a) 1 wt% of HNTs, (b) 3 wt% of HNTs and (c) 5 wt% of HNTs. HNTs: halloysite nanotubes.

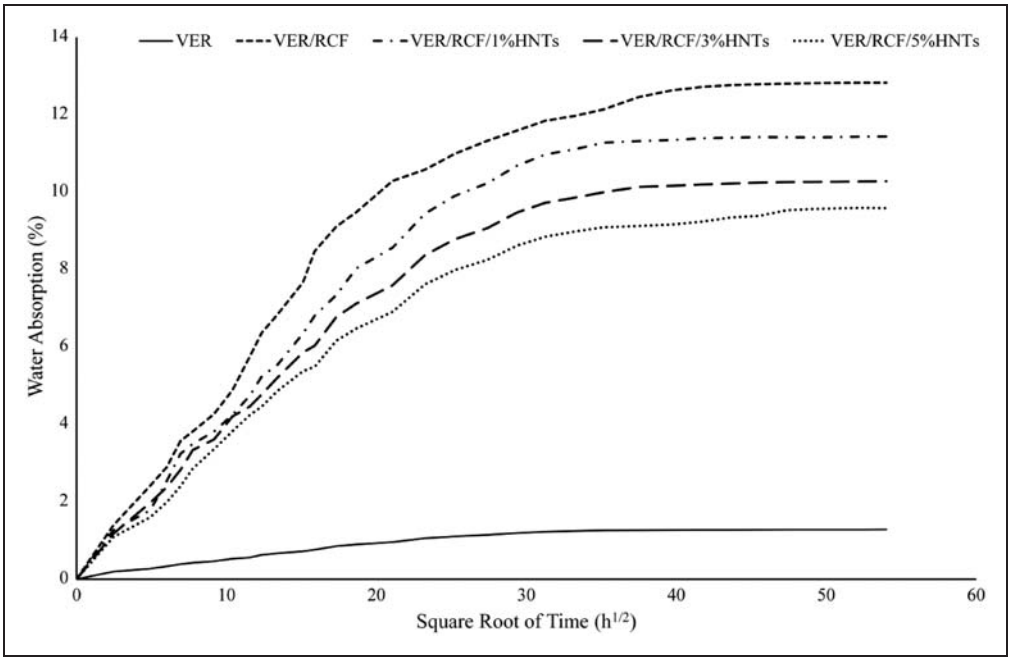

Figure 4. Water absorption behaviour of VER, VER/RCF, VER/RCF/1%HNTs, VER/RCF/3%HNTs and VER/RCF/5%HNTs. VER: vinyl ester; HNTs: halloysite nanotubes; and RCF: recycled cellulose fibre.

Table 2. Maximum water uptake M_∞ and diffusion coefficients D of VER-eco and eco-nanocomposites

Samples	RCF content (%)	HNTs content (%)	M_∞ (%)	D (mm^2/s)
VER	0	0	1.29	2.72×10^{-6}
VER/RCF	40	0	12.83	2.81×10^{-6}
VER/RCF/1%HNTs	40	1	11.44	2.56×10^{-6}
VER/RCF/3%HNTs	40	3	10.28	2.16×10^{-6}
VER/RCF/5%HNTs	40	5	9.58	2.99×10^{-6}

VER: vinyl ester; HNTs: halloysite nanotubes; and RCF: recycled cellulose fibre.

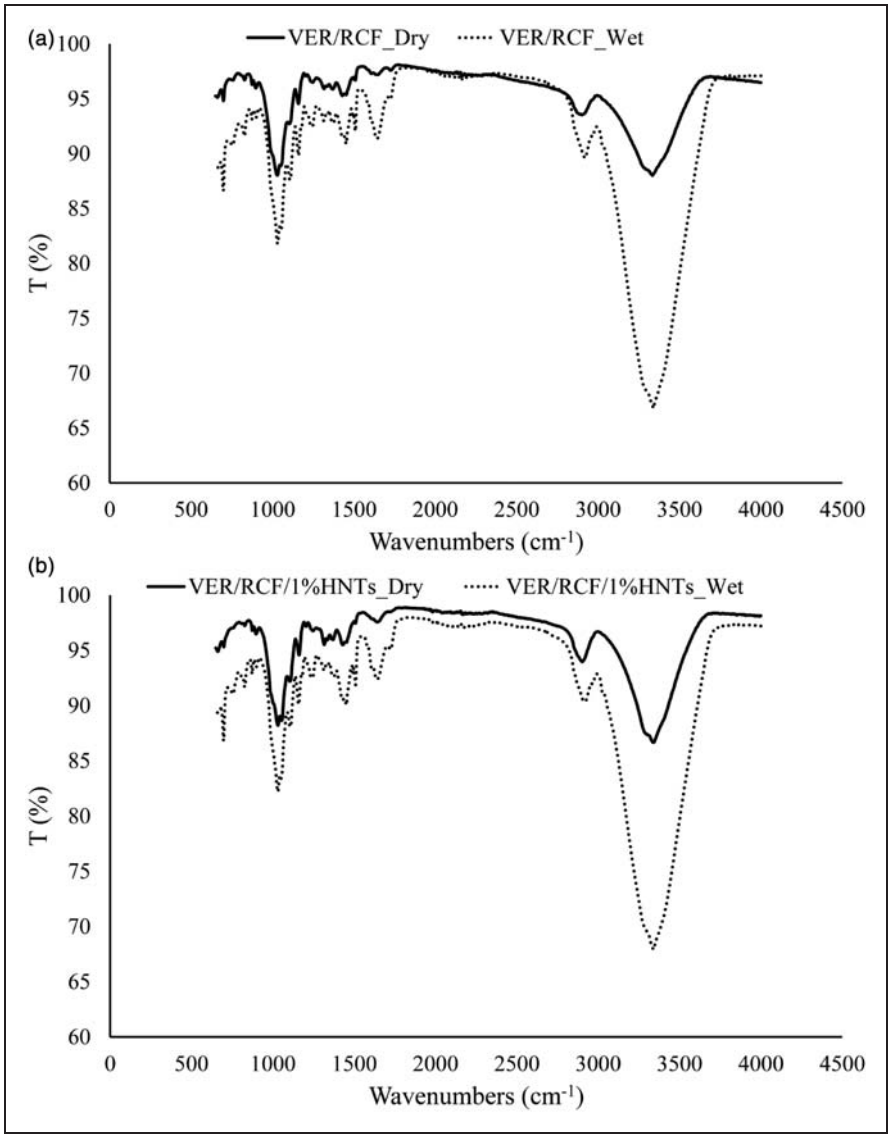

Figure 5. FT-IR dry and wet spectrums of: (a) VER/RCF eco-composites, (b) VER/RCF/1%HNT eco-nanocomposites, (c) VER/RCF/3%HNT eco-nanocomposites and (d) VER/RCF/5%HNT eco-nanocomposites.
FT-IR: Fourier transform infrared analysis; VER: vinyl ester; HNT: halloysite nanotube; and RCF: recycled cellulose fibre.

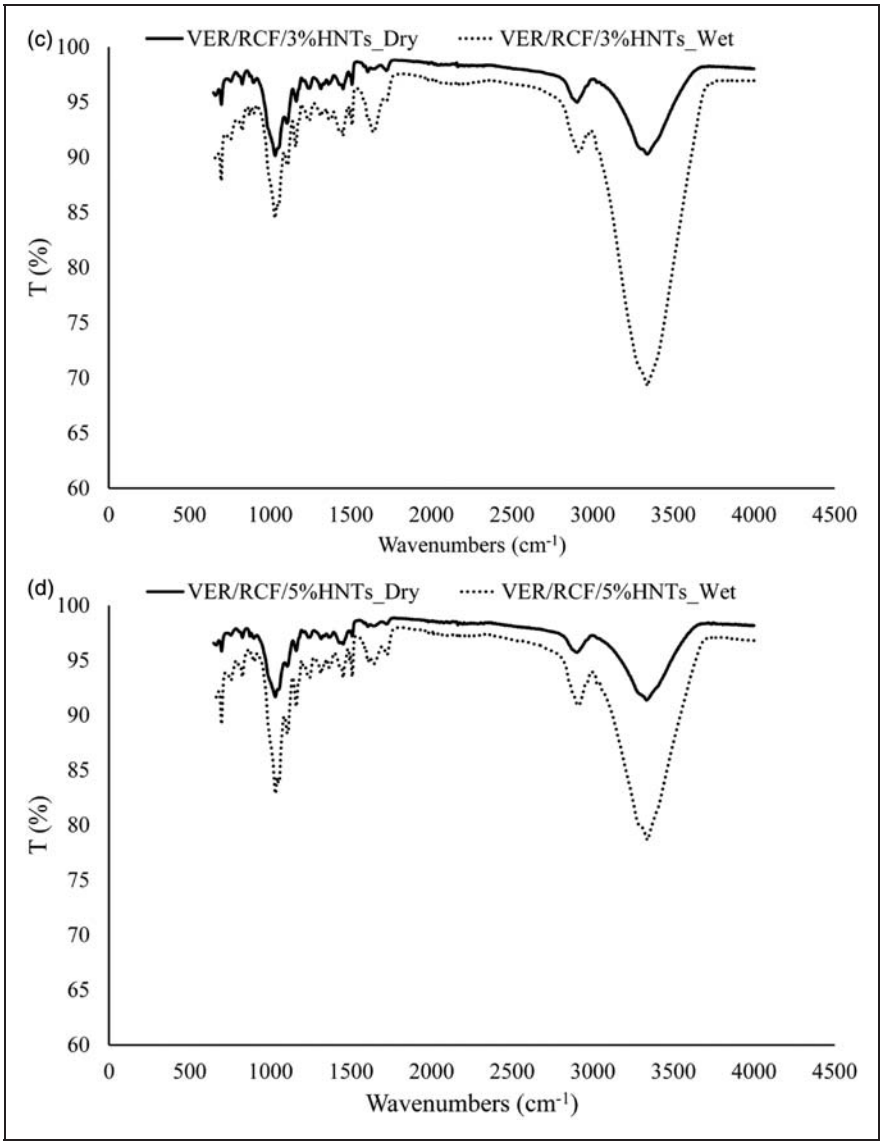

Figure 5. Continued.

conditions due to OH ions present in VER, RCF and HNTs.[20–22] This broad peak will be reference for the description of water absorption behaviour.

Additional peaks also caused by presence of VER, RCF and HNTs can be seen in addition to this broad peak. A strong peak at ~2924 cm^{-1} and weaker peak at around 2870 cm^{-1} caused by the presence of VER and RCF can be seen in all spectra displayed. It is expected that these peaks are due to symmetric and asymmetric vibration from CH.[16] The absorption peak at 830 cm^{-1} is believed to be caused by bending vibrations of the vinylic group in VER whereas the peak near 947 cm^{-1} is believed to be caused by out-of-plane bending of VER monomer.[23] The bending vibration peak at ~1450 cm^{-1} for methyl groups and 1350 and 1380 cm^{-1} for methylene groups are due to symmetric and asymmetric vibration from CH.[24] Absorption peaks seen at 1607 and 1510 cm^{-1} are attributed to the benzene ring of VER while peaks at ~1720 and 1180 cm^{-1} are due to the carbonyl groups of the ester linkage.[25] The presence of HNTs is believed to cause at least three more peaks. The peak at around 1030 cm^{-1} is caused by perpendicular Si–O stretching whereas the peak at 1113 cm^{-1} is caused by apical Si–O vibration. The stretching of the Al–O/Al–OH bonds is responsible for the peak at ~912 cm^{-1}.[23]

The water absorption of composites for 120 days caused an increase in the broad peak of hydroxyl stretching. The higher frequency region of the peak is due to hydroxyl stretching which is caused by the hydroxyl peak of absorbed liquid water. The effects of absorbed liquid water are considered to include

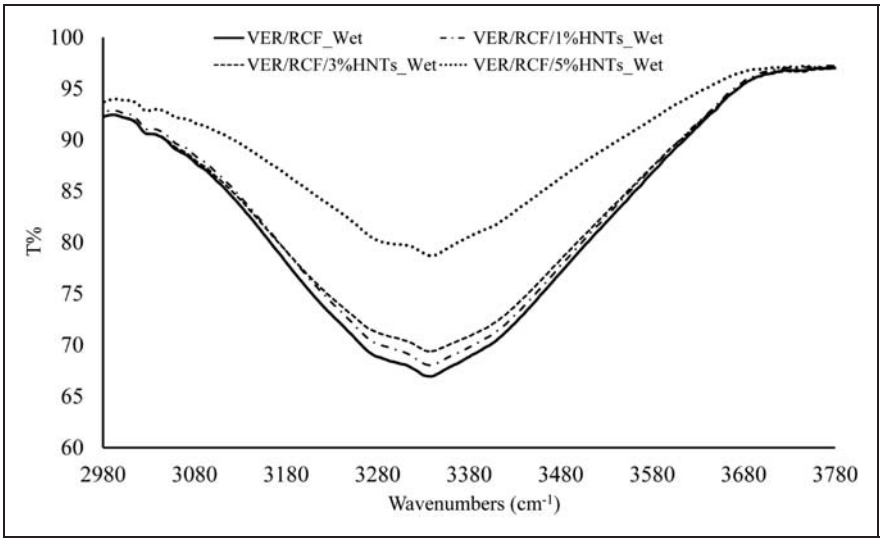

Figure 6. Comparison between FT-IR spectrum peaks of water content of eco-composites and eco-nanocomposites.
FT-IR: Fourier transform infrared analysis.

Table 3. Elastic modulus and strength properties of pure VER, VER/RCF eco-composites and VER/RCF/HNTs eco-nanocomposites

Samples	RCF content (%)	HNTs content (%)	Elastic modulus (GPa)	Flexural strength (MPa)	Impact strength (kJ/m^2)
VER	0	0	2.97 ± 0.2	41.9 ± 1.4	2.6 ± 0.2
VER/RCF	40	0	4.82 ± 1.1	148.4 ± 1.7	15.9 ± 1.2
VER/RCF/1%HNTs	40	1	5.11 ± 1.3	156.1 ± 1.5	16.81 ± 1.5
VER/RCF/3%HNTs	40	3	$5.75.1 \pm 1.2$	161.2 ± 1.7	18.86 ± 1.3
VER/RCF/5%HNTs	40	5	5.24 ± 0.9	150.2 ± 1.3	16.12 ± 1.2

VER: vinyl ester; HNTs: halloysite nanotubes; and RCF: recycled cellulose fibre.

the effects of unassociated water, loosely bound water, as well as the indirectly bonded water which may be bonded to the hydroxyl groups using other water molecules. The lower frequency region of the peak is a result of hydroxyl stretching caused by hydroxyl stretching of strongly bound water. Strongly bound water is produced when direct hydrogen bonds are formed between the hydroxyl groups of absorbed water and the composite components.[26]

The broad peaks, centred at around 3340 cm^{-1}, are shown in Figure 6. These peaks increased after 120 days of immersion in water. The respective FT-IR spectra reveal that there were differing quantities of moisture absorbed for each composite. The addition of HNTs was found to lead to a decrease in water uptake behaviours. This provides further support for the premise that HNT addition increases the resistance to water absorption. When compared to 1 and 3 wt% HNTs, the addition of 5 wt% HNTs led to the greatest resistance to water absorption as evidenced by the studies on weight gain and FT-IR.

Elastic modulus and strength properties

Table 3 presents the results for elastic modulus, flexural strength and impact strength. Compared to pure VER, eco-composites and eco-nanocomposites had greater elastic modulus. In particular, the elastic modulus of eco-composites VER/RCF increased by 162.3%. The improvement in elastic modulus is due to the higher initial modulus of the cellulose fibres acting as backbones in the composites.[27]

The flexural strength of eco-composite (148.4 MPa) was more than three times that of the pure sample (41.9 MPa). These significant enhancements in strength properties are attributed to the reinforcing effect imparted by cellulose fibres which are of high strength and modulus. Moreover, the ability of cellulose fibres in resisting bending force is also a contributor in the

improved flexural strength.[28] Since, the role of matrix is to transfer the load to the stiff fibres through shear stresses at the interface, a good bond between the polymeric matrix and the fibres is required in this process.[29]

When compared to pure VER, the impact strength of eco-composites was found to be six times larger at 15.9 kJ/m^2. As impact strength is defined as the ability of a material to resist fracture under conditions of stress applied at high speed, the marked enhancement of impact strength in the eco-composites can be attributed to cellulose fibres having a superior ability to absorb impact energy compared to pure polymer.[30] Similarly, good interfacial bonding is required for composites to exhibit enhanced impact strength. This is because when there is good bonding between fibres and matrix, the load requires for debonding or fibre pull-outs will be high and thus high impact resistance can be expected.[31] Previous studies have documented these improvements in elastic modulus and strength properties in polymer composites reinforced with natural fibres.[30,32]

The addition of HNTs to VER/RCF composites resulted in eco-nanocomposites with increased elastic modulus. Compared to unfilled eco-composites, eco-nanocomposites reinforced with 1, 3 and 5 wt% of HNTs exhibited enhanced elastic moduli of 5.1, 5.8 and 5.2 GPa, respectively. HNTs have a high specific surface area which is favourable for interfacial interaction with the polymer matrix, thus promoting stronger bonding at the interfaces. Hence, HNTs are expected to hinder the mobility of surrounding chains in the polymer matrix, thus increasing the matrix stiffness.[9,33] Moreover, HNTs have a higher elastic modulus (i.e. 10.1 GPa) when compared to pure VER (2.97 GPa) or VER/RCF eco-composites (4.8 GPa).

The addition of HNTs imparted a moderate increase in both flexural and impact strengths. When eco-composites were reinforced with 1, 3 and 5 wt% HNTs, the flexural strength of eco-nanocomposites increased from 148.4 to 156.1, 161.2 and 150.2 MPa, respectively. Similarly, the addition of HNTs at 1, 3 and 5 wt% increased the impact strength from 15.9 to 16.8, 18.9 and 16.1 kJ/m^2, respectively.

The SEM micrographs in Figure 7 show the fracture surfaces of all samples. The investigation of the quality of fibre–matrix adhesion is based on fibre pull-outs, disparity in fibre lengths, fibre surfaces and fibre–matrix gaps. Figure 7(a) shows that the pull-out lengths, the extent that individual fibres are debonded, were greater in the eco-composites when compared to eco-nanocomposites shown in Figure 7(b) to (d). Moreover, Figure 7(a) shows that the number of fibres that were pulled out was greater in the eco-composites when compared to eco-nanocomposites. Th greater pull-out lengths and greater number of fibres pulled-out in eco-composites is a consequence of poor interfacial adhesion and can be contrasted with the stronger fibres–matrix adhesion in eco-nanocomposites.[31,34] In the case of weak fibre–matrix adhesion, cracks propagate along the debonded fibre–matrix interfaces and result in greater fibre pull-out length and number. In contrast, when fibre–matrix adhesion is strong, the propagation of cracks along the debonded interfaces is less and thus less fibre pull-outs.

Interestingly, with loading of HNTs the length and number of fibres pulled out was clearly reduced compared to eco-composites. In eco-nanocomposites with 3 wt% HNTs, almost no fibre pull-outs are observed and the fibres can be seen to be fractured instead due to strong interfacial bonding. Another distinguishing feature of the eco-composites is the clean appearance of the fibre surfaces. This clean appearance is another indicator of poor adhesion between the matrix and fibres. This contrasts with the rough appearance of fibre surfaces in eco-nanocomposites as a result of strong fibre–matrix adhesion.[35] Finally, the matrix–fibre gaps appear larger in the eco-composites compared to the eco-nanocomposites. These observations indicate that the addition of HNTs leads to stronger adhesion between fibre–matrix with concomitant strength improvements. The high surface area of HNTs increases the contact area within the matrix and thereby increases the interfacial bonding between the fibre and the polymer matrix.[36,37] In addition; HNTs can provide strong attractive forces to further enhance adhesion between the fibres and the matrix.[38]

With regards to the addition of 5 wt% HNTs, it was found that this concentration led to less improvement in strengths when compared 1 and 3 wt% HNTs. Processing events are believed to underpin the failure of 5 wt% HNTs addition to further improve the strength. When there is a high loading of HNTs, the viscosity increases during mixing of resin and HNTs rendering insufficient degassing before curing. It is vital that during processing, a complete degassing process is ensured for the composite to minimize void formation. The formation of voids in composites can act as stress-concentrators to reduce the strength.[39] The SEM images in Figure 8 compares the fracture surfaces due to void formation in sample with 5 wt% HNTs with void-free samples with 1 and 3 wt% HNTs.

The ASTM D2734-94 standard[40] was used to determine void content or porosity of the composite samples. The void contents for eco-composites and 1, 3 and 5 wt% eco-nanocomposites were determined to be 3.3% and 1.1%, 0.57% and 3.1%, respectively. Eco-nanocomposites exhibited a lower void content when compared to eco-composites. Eco-nanocomposites with 3 wt% exhibited the lowest void content (0.57%). However, the void content for 5 wt% (3.1%) was almost the same as the unfilled eco-composites (3.3%).

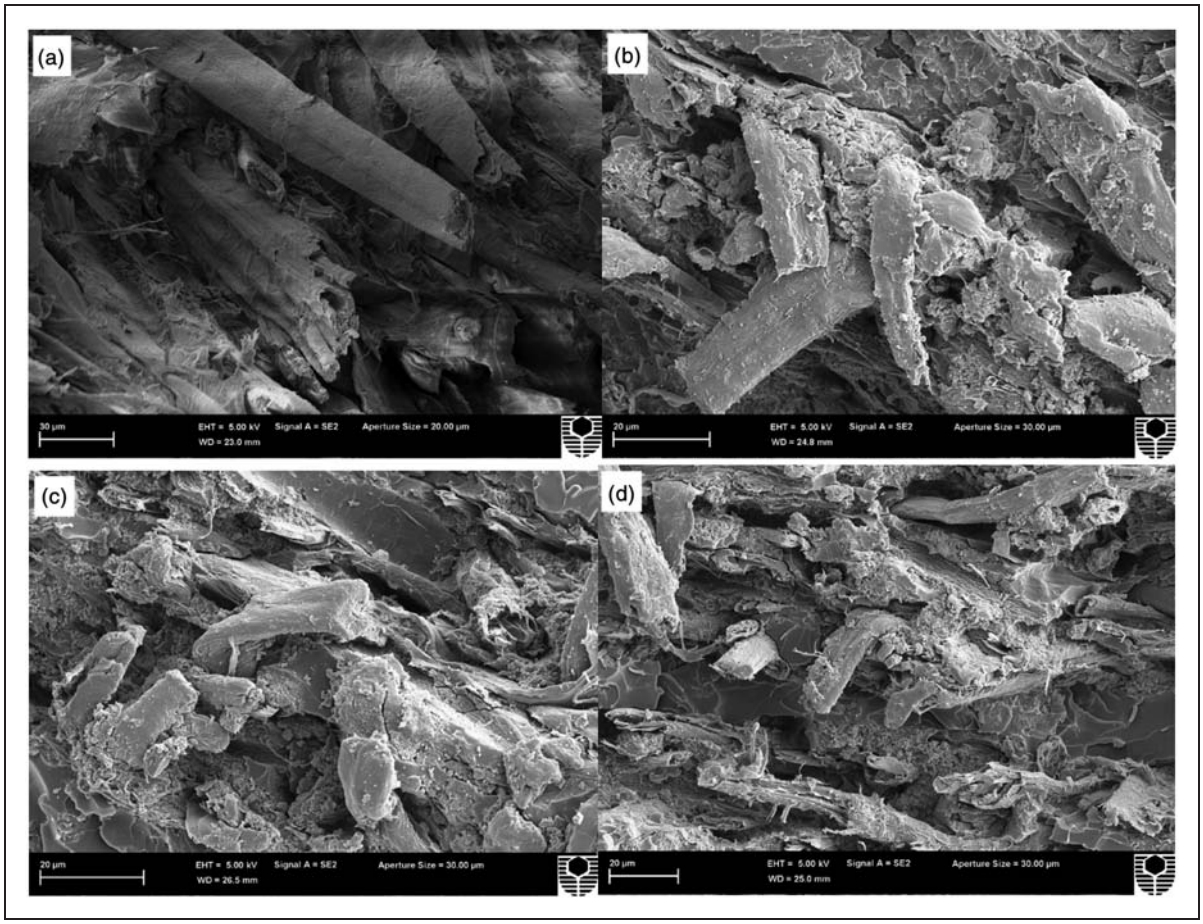

Figure 7. SEM images showing the fracture surfaces of: (a) eco-composite, (b) eco-nanocomposite with 1 wt% HNT loading, (c) eco-nanocomposite with 3 wt% HNTs loading and (d) eco-nanocomposite with 5 wt% HNTs loading.
SEM: scanning electron microscope; HNTs: halloysite nanotubes.

A plausible explanation is that the addition of 5 wt% HNTs caused an increase in the resin viscosity, thus resulting in a reduction of fibre wettability by the matrix or interfacial adhesion.

SEM observations of fibre/matrix adhesion combined with the calculation values of void content support the observed strength results. Thus, the higher strengths exhibited by 3 wt% eco-nanocomposites are attributed to strong fibre/matrix adhesion and low void content. In contrast, weaker fibre/matrix adhesion and higher void contents resulted in lower strength.

Toughness properties

Table 4 presents that, compared to pure samples, the eco-composites have greater fracture toughness and impact toughness. The improved fracture toughness may be attributed to the pronounced display of crack-deflection, interfacial debonding, fibre-bridging and pull-outs in these materials.[29,31] When compared to pure VER samples which are quite brittle like all thermosetting resins[9] (1.8 MPa·m$^{1/2}$), eco-composites are much tougher with 4.4 MPa·m$^{1/2}$. Similarly, compared to pure samples, with an impact toughness of 1.5 kJ/m^2, eco-composites are also much tougher with an impact toughness of 42.3 kJ/m^2. However, toughness properties were reduced on increasing the loading of HNTs. Addition of 1, 3 and 5 wt% HNTs reduced the fracture toughness to 3.8, 3.1 and 3.1 MPa·m$^{1/2}$, respectively. Similar reductions in impact toughness were observed impact toughness.

Thermal and flammability properties

The TGA curves for VER, eco-composites and eco-nanocomposites are shown in Figure 9 and summarized in Table 5. Here, the temperature range used was from room temperature to 800°C. Thermal degradation, for VER, occurred in a single stage at around 430°C. Across all composites, the release of moisture led to slight weight loss between 60°C and 100°C.

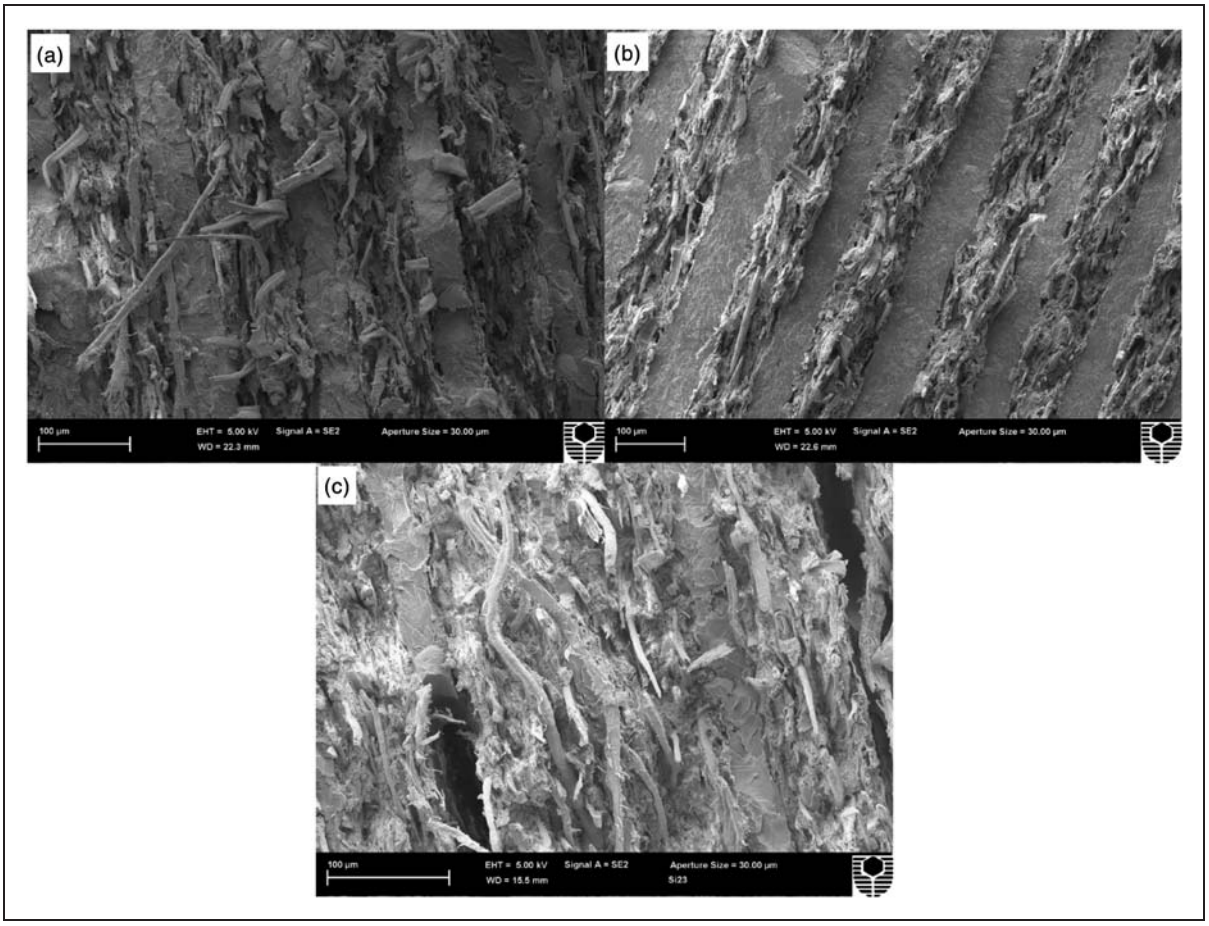

Figure 8. SEM images showing the fracture surfaces of eco-nanocomposites contain: (a) 1 wt% HNTs, (b) 3 wt% HNTs and (c) 5 wt% HNTs with existing of voids.
SEM: scanning electron microscope; HNTs: halloysite nanotubes.

Table 4. Toughness properties of pure VER, VER/RCF eco-composites and VER/RCF/HNTs eco-nanocomposites

Samples	RCF content (%)	HNTs content (%)	Fracture toughness ($MPa \cdot m^{1/2}$)	Impact toughness (kJ/m^2)
VER	0	0	1.8 ± 0.2	1.5 ± 0.2
VER/RCF	40	0	4.4 ± 0.5	42.3 ± 2.1
VER/RCF/1%n-SiC	40	1	3.84 ± 0.3	36.5 ± 1.5
VER/RCF/3%n-SiC	40	3	3.06 ± 0.2	26.2 ± 1.3
VER/RCF/5%n-SiC	40	5	3.12 ± 0.9	29.3 ± 1.2

VER: vinyl ester; HNTs: halloysite nanotubes; and RCF: recycled cellulose fibre.

In eco-composites, decomposition occurred in two stages with complete degradation occurring at approximately 445°C. These results also support that the eco-composites, fibre-filled polymer matrix, decompose at higher temperatures compared to pure samples. The present results are in agreement with previous studies on the thermal properties of lingo-cellulosic fibre composites. The thermal resistance of the cellulose fibres, and the ability of these natural fibres to increase char formation are responsible for the improved thermal stability.[41]

For eco-nanocomposites, the thermal stability followed a similar trend albeit requiring a marginally higher temperature whereby eco-nanocomposites of 1, 3 and 5 wt% HNTs required 392°C, 394°C and 395°C, respectively. In terms of weight loss, from 100°C

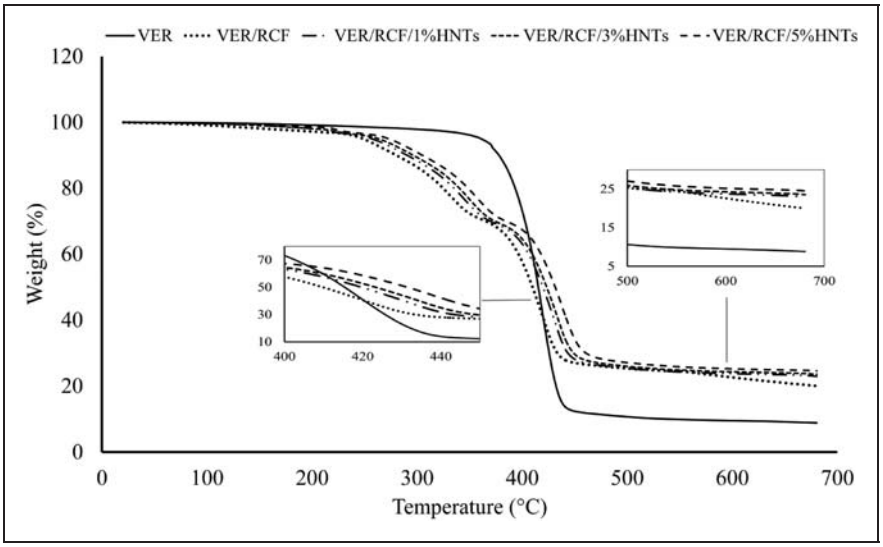

Figure 9. TGA curves of VER, VER/RCF, VER/RCF/1%HNTs, VER/RCF/3%HNTs and VER/RCF/5%HNTs.
TGA: thermo-gravimetric analyser; VER: vinyl ester; HNTs: halloysite nanotubes; and RCF: recycled cellulose fibre.

Table 5. TGA data of pure VER, VER/RCF eco-composites and VER/RCF/HNTs eco-nanocomposites

Sample	Temperature at 50% weight loss (°C)	Temperature at maximum weight loss (°C)	Residual weight (%)
VER	418	430	8.7
VER/RCF	409	445	19.7
VER/RCF/1%HNTs	423	448	23.1
VER/RCF/3%HNTs	429	453	23.6
VER/RCF/5%HNTs	431	460	24.7

TGA: thermo-gravimetric analyser; VER: vinyl ester; HNTs: halloysite nanotubes; and RCF: recycled cellulose fibre.

to 200°C, eco-composites and eco-nanocomposites gave a weight loss of about 2% according to TGA analysis. At 300°C, in eco-composites a weight loss of 11.7% was recorded. However, at the same temperature the eco-nanocomposites gave a weight loss of 11.7%, 10.1% and 9.2% for loading of 1, 3 and 5 wt% HNTs, respectively. Above 700°C, the residual weight of eco-composites was 19.7% of the original. In contrast, only 8.7% remained in the control sample. For the eco-nanocomposites with 1%, 3% and 5% HNTs, the residual weight was 23.1%, 23.6% and 24.7%, respectively.

The improvement of interfacial adhesion between RCF and VER as a result of HNTs addition can lead to the enhancement of thermal stability.[16] Nanofillers such as HNTs are believed to provide, first, a thermal barrier which prevents heat transfer inside the polymer matrix, and second a mass transport barrier which during the process of degradation forms a char which hinders the escape of the volatile products.[42,43] The hollow tubular structure of HNTs is also reported to be another factor that leads to enhanced thermal stability. The hollow tubular structure of HNTs enables the entrapment of degradation products inside the lumens, causing effective delay in mass transfer which leads to improved thermal stability.[1,2] The presence of iron oxides, Fe_2O_3, in silicate fillers is also a possible flame retardant which serve to enhance the thermal stability of composites by trapping radicals during the process of degradation.[43]

Flammability tests conducted at ambient conditions included time of burning out, ignition time and fire velocity determinations. Pure VER samples were found to burn out and ignite faster than VER/HNT composites, as indicated in Table 6. Calculations imply that fire spreads through pure VER at nearly twice the rate of 5 wt% VER/HNT composite, thus highlighting the favourable flammability resistance of the composites. The presence of HNTs within composites provides a mechanism of insulation which protects the composites from contacting with fire. Furthermore, char formation of HNTs acts as a heat and fire-retardant.

Table 6. Flammability properties of VER resin and its composites

Sample	Burning out rate (g/min)	Ignition time (s)	Fire velocity (mm/min)
VER	0.67 ± 0.06	10.8 ± 1.6	31.5 ± 1.7
VER/RCF	0.54 ± 0.03	17.2 ± 1.5	25.7 ± 1.6
VER/RCF/1%HNTs	0.49 ± 0.02	18.7 ± 1.4	23.2 ± 1.2
VER/RCF/3%HNTs	0.46 ± 0.04	22.8 ± 1.2	19.1 ± 1.8
VER/RCF/5%HNTs	0.41 ± 0.05	25.4 ± 1.8	17.5 ± 1.4

VER: vinyl ester; HNTs: halloysite nanotubes; and RCF: recycled cellulose fibre.

Conclusions

VER eco-composites and VER eco-nanocomposites have been fabricated and studied in terms of water uptake, thermal and mechanical properties. The addition of 5 wt% HNTs led to the greatest water absorption resistance compared to 1 and 3 wt% HNTs as evidenced by both the weight gain study and FT-IR analysis. Elastic modulus and strengths properties were also found to be enhanced due to the reinforcing effect of both RCF and HNTs. In particular, HNT addition improved fibre–matrix adhesion in eco-nanocomposites and gave greater strength properties. Due to the toughness mechanism provided by cellulose fibres, the presence of cellulose fibres increased the fracture toughness of all composites. However, the HNT addition led to a reduction in fracture toughness due to the improvement of fibre–matrix adhesion. The HNT addition increased both the thermal stability and fire-resisting properties of the eco-nanocomposites.

Funding

This study received no specific grant from any funding agency in the public, commercial, or not-for-profit sectors.

Acknowledgements

The authors are grateful to Dr Nobuo Tezuka for providing HNTs for this study and they thank Mr Andreas Viereckl from Mechanical Engineering at Curtin University for assistance with mechanical tests. They also thank Elaine Miller and Dr Cat Kealley for their assistance with SEM imaging and XRD data collection. Peter Chapman and Kristy Blyth from the Chemistry Department are thanked for their help in FT-IR and TGA measurements.

References

1. Ismail H, Pasbakhsh P, Fauzi MNA, et al. Morphological, thermal and tensile properties of halloysite nanotubes filled ethylene propylene diene monomer (EPDM) nanocomposites. *Polym Test* 2008; 27(7): 841–850.
2. Lecouvet B, Gutierrez JG, Sclavons M, et al. Structure–property relationships in polyamide 12/halloysite nanotube nanocomposites. *Polym Degrad Stab* 2011; 96(2): 226–235.
3. Handge UA, Hedicke-Höchstötter K and Altstädt V. Composites of polyamide 6 and silicate nanotubes of the mineral halloysite: influence of molecular weight on thermal, mechanical and rheological properties. *Polymer* 2010; 51(12): 2690–2699.
4. Rooj S, Das A, Thakur V, et al. Preparation and properties of natural nanocomposites based on natural rubber and naturally occurring halloysite nanotubes. *Mater Des* 2010; 31(4): 2151–2156.
5. Jawaid M and Abdul Khalil HPS. Cellulosic/synthetic fibre reinforced polymer hybrid composites: a review. *Carbohydr Polym* 2011; 86(1): 1–18.
6. Arora S, Kumar M and Kumar M. Flammability and thermal degradation studies of PVA/rice husk composites. *J Reinf Plast Compos* 2012; 31(2): 85–93.
7. Osorio L, Trujillo E, Van Vuure AW, et al. Morphological aspects and mechanical properties of single bamboo fibers and flexural characterization of bamboo/epoxy composites. *J Reinf Plast Compos* 2011; 30(5): 396–408.
8. Anuar H and Zuraida A. Improvement in mechanical properties of reinforced thermoplastic elastomer composite with kenaf bast fibre. *Composites Part B* 2011; 42(3): 462–465.
9. Grishchuk S, Castellà N, Apostolov AA, et al. Structure and properties of vinyl ester resins modified with organophilic synthetic layered silicates bearing non- and co-reactive intercalants. *J Compos Mater* 2012; 46: 941–947.
10. Ku H, Wang H, Pattarachaiyakoop N, et al. A review on the tensile properties of natural fiber reinforced polymer composites. *Composites Part B* 2011; 42(4): 856–873.
11. Hossain MK, Dewan MW, Hosur M, et al. Mechanical performances of surface modified jute fiber reinforced biopol nanophased green composites. *Composites Part B* 2011; 42(6): 1701–1707.
12. Dhakal HN, Zhang ZY and Richardson MOW. Effect of water absorption on the mechanical properties of hemp fibre reinforced unsaturated polyester composites. *Compos Sci Technol* 2007; 67(7–8): 1674–1683.
13. Low IM, Somers J, Kho HS, et al. Fabrication and properties of recycled cellulose fibre-reinforced epoxy composites. *Compos Interfaces* 2009; 16(7–9): 659–669.
14. Low IM, McGrath M, Lawrence D, et al. Mechanical and fracture properties of cellulose-fibre-reinforced epoxy laminates. *Composites Part A* 2007; 38(3): 963–974.

15. Joussen E, Petit S, Churchman J, et al. Halloysite clay minerals: a review. *Clay Miner* 2005; 40(4): 383–426.
16. De Rosa IM, Kenny JM, Maniruzzaman M, et al. Effect of chemical treatments on the mechanical and thermal behaviour of okra (Abelmoschus esculentus) fibres. *Compos Sci Technol* 2011; 71(2): 246–254.
17. Deng S, Zhang J, Ye L, et al. Toughening epoxies with halloysite nanotubes. *Polymer* 2008; 49(23): 5119–5127.
18. Ladhari A, Ben Daly H, Belhadjsalah H, et al. Investigation of water absorption in clay-reinforced polypropylene nanocomposites. *Polym Degrad Stab* 2010; 95(4): 429–439.
19. Corobea MC, Donescu D, Grishchuk S, et al. Organophilic layered silicate modified vinylester-urethane hybrid resins: structure and properties. *Polym Polym Compos* 2008; 16(8): 547–554.
20. Baiardo M, Frisoni G, Scandola M, et al. Surface chemical modification of natural cellulose fibers. *J Appl Polym Sci* 2002; 83(1): 38–45.
21. Du M, Guo B, Lei Y, et al. Carboxylated butadiene–styrene rubber/halloysite nanotube nanocomposites: interfacial interaction and performance. *Polymer* 2008; 49(22): 4871–4876.
22. Jinhua W, Xiang Z, Bing Z, et al. Rapid adsorption of Cr (VI) on modified halloysite nanotubes. *Desalination* 2010; 259(1–3): 22–28.
23. Sultania M, Yadaw SB, Rai JSP, et al. Laminates based on vinyl ester resin and glass fabric: a study on the thermal, mechanical and morphological characteristics. *Mater Sci Eng A* 2010; 527(18–19): 4560–4570.
24. Jebrane M and Sèbe G. A new process for the esterification of wood by reaction with vinyl esters. *Carbohydr Polym* 2008; 72(4): 657–663.
25. Scott TF, Cook WD and Forsythe JS. Kinetics and network structure of thermally cured vinyl ester resins. *Eur Polym J* 2002; 38(4): 705–716.
26. Lasagabáster A, Abad MJ, Barral L, et al. Application of FTIR spectroscopy to determine transport properties and water–polymer interactions in polypropylene (PP)/poly(-ethylene-co-vinyl alcohol) (EVOH) blend films: effect of poly(ethylene-co-vinyl alcohol) content and water activity. *Polymer* 2009; 50(13): 2981–2989.
27. Guo Q, Cheng B, Kortschot M, et al. Performance of long Canadian natural fibers as reinforcements in polymers. *J Reinf Plast Compos* 2010; 29(21): 3197–3207.
28. Chen H, Miao M and Ding X. Influence of moisture absorption on the interfacial strength of bamboo/vinyl ester composites. *Composites Part A* 2009; 40(12): 2013–2019.
29. Alhuthali A, Low IM and Dong C. Characterisation of the water absorption, mechanical and thermal properties of recycled cellulose fibre reinforced vinyl-ester eco-nanocomposites. *Composites Part B* 2012; 43(7): 2772–2781.
30. Bax B and Müssig J. Impact and tensile properties of PLA/Cordenka and PLA/flax composites. *Compos Sci Technol* 2008; 68(7–8): 1601–1607.
31. Kim HJ and Seo DW. Effect of water absorption fatigue on mechanical properties of sisal textile-reinforced composites. *Int J Fatigue* 2006; 28(10): 1307–1314.
32. Facca AG, Kortschot MT and Yan N. Predicting the elastic modulus of natural fibre reinforced thermoplastics. *Composites Part A* 2006; 37(10): 1660–1671.
33. Zuiderduin WCJ, Westzaan C, Huétink J, et al. Toughening of polypropylene with calcium carbonate particles. *Polymer* 2003; 44(1): 261–275.
34. Stocchi A, Bernal C, Vázquez A, et al. A silicone treatment compared to traditional natural fiber treatments: effect on the mechanical and viscoelastic properties of jute—vinylester laminates. *J Compos Mater* 2007; 41(16): 2005–2024.
35. Deng S and Tang Y. Increasing load-bearing capacity of wood-plastic composites by sandwiching natural and glass fabrics. *J Reinf Plast Compos* 2010; 29(20): 3133–3148.
36. Chandradass J, Ramesh Kumar M and Velmurugan R. Effect of clay dispersion on mechanical, thermal and vibration properties of glass fiber-reinforced vinyl ester composites. *J Reinf Plast Compos* 2008; 27(15): 1585–1601.
37. Avilés F, Cauich-Rodríguez JV, Rodríguez-González JA, et al. Oxidation and silanization of MWCNTs for MWCNT/vinyl ester composites. *eXPRESS Polym Lett* 2011; 5(9): 766–776.
38. Sun L-H, Yang Z-G and Li X-H. Tensile and tribological properties of PTFE and nanoparticles modified epoxy-based polyester fabric composites. *Mater Sci Eng A* 2008; 497(1–2): 487–494.
39. Fu S-Y, Feng X-Q, Lauke B, et al. Effects of particle size, particle/matrix interface adhesion and particle loading on mechanical properties of particulate–polymer composites. *Composites Part B* 2008; 39(6): 933–961.
40. ASTM D 2734-94. *Standard methods for void content of reinforced specimen plastics*. West Conshohocken, PA: American Society for Testing and Materials, 1997.
41. Curvelo AAS, De Carvalho AJF and Agnelli JAM. Thermoplastic starch–cellulosic fibers composites: preliminary results. *Carbohydr Polym* 2001; 45(2): 183–188.
42. Du M, Guo B and Jia D. Thermal stability and flame retardant effects of halloysite nanotubes on poly(propylene). *Eur Polym J* 2006; 42(6): 1362–1369.
43. Rahman NA, Hassan A, Yahya R, et al. Micro-structural, thermal, and mechanical properties of injection-molded glass fiber/nanoclay/polypropylene composites. *J Reinf Plast Compos* 2012; 31(4): 269–281.

3.4. Multi-scale hybrid eco-nanocomposites: synthesis and characterization of nano-SiC-reinforced vinyl-ester eco-composites

---

ALHUTHALI, A. and LOW, I. M. 2013. Multi-scale hybrid eco-nanocomposites: synthesis and characterization of nano-SiC-reinforced vinyl-ester eco-composites. *Journal of Materials Science*, 48, 3097-3106.

J Mater Sci (2013) 48:3097–3106
DOI 10.1007/s10853-012-7084-9

Multi-scale hybrid eco-nanocomposites: synthesis and characterization of nano-SiC-reinforced vinyl-ester eco-composites

A. Alhuthali · I. M. Low

Received: 12 July 2012 / Accepted: 10 December 2012 / Published online: 19 December 2012

Abstract Polymer eco-nanocomposites based on vinyl-ester, recycled cellulose fibre and nano-silicon carbide (n-SiC) have been synthesized and characterized in terms of porosity, water-absorption behaviour, thermal and mechanical properties. The addition of n-SiC led to reduced porosity and water uptake because of enhanced fibre–matrix adhesion which permitted efficient load transfer and thus strength improvement. However, n-SiC addition reduced the prevalence of fibre debonding and pull-outs, thus causing sample brittleness and inferior fracture toughness. In terms of thermal properties, n-SiC addition facilitated improved mass transport and heat barriers, thus improving thermal stability and fire resistance.

Introduction

Studies on the preparation and characterization of thermosetting and thermoplastic composites reinforced with flax, sisal, oil palm, henequen, jute, banana, wood pulp, stinging nettle, coir, or hemp natural fibres with and without treatment have been extensively conducted in more recent decades [1, 2]. Currently, increasing interest has been drawn to the use of these natural fibres to reinforce polymer composites because of the low cost of natural fibres, their low density, excellent modulus–weight ratio properties and benefits of biodegradability [3, 4]. Fibre–matrix adhesion is believed to be the primary determinant in mechanical performance and overall composite quality [5]. The role of the matrix in a fibre-reinforced polymer composite is to transfer the load to the fibres through shear stresses at the interface. Strong bond between the polymeric matrix and the fibres is required in this process [5, 6]. Various physical and chemical methods have been proposed to improve the compatibility between the natural fibres and the polymer matrix [3, 7]. In general, the properties of composites depend on the nature of matrix, fibre, interfacial bonding, and quality of adhesion [8]. Polymer nanocomposites are composites that contain particles in which one or more dimensions of the particles are at the nano-scale level [9]. The very large surface area of nanoparticles can facilitate rapid phase interactions within the polymer matrix [10, 11]. The use of nanofillers for improving the physical and mechanical properties of polymers is not new where numerous investigations polymers reinforced with nanoclay and carbon nanotubes have been reported since the 1990s [12, 13]. Studies on the characteristics of natural fibre–polymer composites containing nanofillers appear to be limited [14–16]. The introduction of fibres into the polymer/nanoclay system is well known to improve the mechanical and thermal properties. The incorporation of nanofillers and natural fibres in a polymer matrix can also provide multi-scale reinforcement effects to the matrix [17]. For example, while the dominant effect on the stiffness of natural fibre–polymer composites is due to the natural fibres, nanofillers can also stiffen the matrix and influence the overall stiffness of these composites. Thus, the nanofillers enhance stiffness, thermal and barrier properties, while the natural fibres provide the main stiffness and strength [18–20]. In this study, multi-scale hybrid eco-nanocomposites from vinyl-ester, recycled cellulose fibres and nano-SiC have been synthesized and characterized. The influence of the multi-scale reinforcements on the physical, water absorption,

A. Alhuthali · I. M. Low (✉)
Department of Imaging & Applied Physics, Curtin University, GPO Box U1987, Perth, WA 6845, Australia
e-mail: j.low@curtin.edu.au

thermal and mechanical properties has been studied and discussed.

Experimental

Materials

The materials used in this study were recycled cellulose fibre sheets (RCF) of grade 80GSM, 100-μm thickness, supplied by Todae Pty Ltd; a general-purpose vinyl ester resin (VER), supplied by Fibreglass & Aesin Sales Pty Ltd; and nano-silicon carbide (n-SiC)—a spherical-shaped filler with a purity: >95 %; specific surface area: 70–90 m^2/g; a particles size <100 nm; and elastic modulus of 470 GPa—supplied by Sigma-Aldrich.

Samples preparation

Three groups of samples were prepared: pure vinyl ester resin (VER), eco-composites (VER/RCF), and eco-nano-composites (VER/RCF/n-SiC). First, pure VER samples were prepared as controls. The VER was mixed with 1.0 wt% catalyst, methyl ethyl ketone peroxide (MEKP), slowly and thoroughly to ensure that no air bubbles are formed within the matrix. The mixture was left under low vacuum (20 kPa) for 2 h and then left at room temperature for 24 h for curing. To prepare eco-composite samples, recycled cellulose–fibre sheets (RCF) were dried for 60 min at 150 °C, prior to soaking in VER and then laid up in closed silicon mould under 20-kg load and vacuum of (60 kPa) for 2 h. Then the samples were left to cure for 24 h at room temperature. To prepare eco-nanocomposites, mixtures containing different concentrations (1, 3 and 5 wt%) of n-SiC were prepared. Nano-SiC was first dried for 60 min at 150 °C, and then mixed with VER for 30 min using a high-speed electrical mixer. The mixtures were then left under vacuum (60 kPa) to remove air bubbles. A catalyst was then added and mixed manually to minimize formation of air bubbles. The mixtures were then reinforced with the same wt% of RCFs sheets which were initially dried for 60 min at 150 °C and then fully soaked in the resin mixtures and pressed together under 20-kg load in vacuum of (60 kPa) for 2 h. Finally, the samples were left to cure at room temperature for 24 h.

Microstructure examination

A NEON scanning electron microscope (ZEISS) operating at accelerating voltage of 5 kV, under secondary image mode was used to examine the microstructures of the fracture surfaces. Samples were coated with platinum to avoid charging during examination.

Density and porosity measurements

The dry mass of each sample (M_d) was measured after oven drying to a constant weight. The samples were then immersed in deionized water for 24 h. After removal from water and removal of excess water, the mass of the saturated samples in air was measured (M_s). Then, the saturated samples were suspended in water, and the mass of the saturated samples in water was measured (M_i). According to the Australia Standard 1774.5 (2001), the density (D_b) and porosity (P_a) of the samples were determined using Eqs. (1) and (2), respectively.

$$D_b = \frac{M_d}{M_s - M_i} \times (\mathrm{g/cm^3}) \quad (1)$$

$$P_a = \frac{M_s - M_d}{M_s - M_i} \times 100 \quad (2)$$

Water uptake test

Three samples with dimensions of 20 mm × 20 mm × 6 mm were used. Individual samples were soaked in tap water at room temperature. At prescribed intervals, individual samples were removed from water, and the excess water was gently removed before they were weighed and immediately returned to the water. A digital scale with a 0.0001-g weighing precision was used to determine weight change. The following equation was used to determine the amount of water uptake or absorbed by the samples over a period of 120 days [21].

$$W_A = \frac{M_t - M_d}{M_d} \times 100 \quad (3)$$

where W_A is water uptake, M_d is the dry mass and M_t is the mass of sample soaked for time t.

The following equation can be used to calculate relevant Diffusion Coefficients for each of the samples [21]:

$$D = \frac{\pi}{16}\left(\frac{M_t/M_\infty}{\sqrt{t/h}}\right)^2 \quad (4)$$

where M_∞ is maximum water uptake, M_t is water uptake at time t, h is sample thickness, and D is diffusion coefficient.

Elastic modulus and flexural strength measurements

Rectangular bars were cut from the fully cured samples for three-point bend tests with a span of 40 mm to evaluate the flexural strength and modulus. A LLOYD Material Testing Machine (5–50 kN) with a displacement rate of 1.0 mm/min was used to perform the test. Five samples of each group were used to evaluate elastic modulus and flexural strength. The values of were recorded and analysed using the machine software (NEXYGENPlus), and their average values were calculated

Impact strength measurements

A Zwick Charpy impact tester with a 2.0-J pendulum hammer was used to determine the impact strength. Five bar samples of each group with 40 mm span were used, and the impact strength was calculated using the following equation [4]:

$$\sigma_i = \frac{E}{A} \tag{5}$$

where σ_i is impact strength, E is the impact energy to break a sample with a ligament area A.

Fracture toughness measurements

Rectangular single edge notch bend (SENB) samples of dimensions 10 mm × 10 mm × 60 mm were used in fracture toughness testing. A sharp razor blade (with a notch-tip radius of 0.25 mm) was used to initiate a sharp crack on samples with the ratio of notch length to width of sample (a/w) at 0.45–0.55 for the measurements.

The flexural tests were performed using a LLOYD Material Testing Machine using a displacement rate of 1.0 mm/min. Five samples with 40-mm span of each group were used, and the value of fracture toughness was calculated using the following equation [22]:

$$K_{IC} = \frac{P_m S}{WD^{2/3}} f\left(\frac{a}{w}\right) \tag{6}$$

where K_{IC} is fracture toughness, P_m is the maximum load, S is the span of the sample, D is the specimen thickness, W is the specimen width, and a is the crack length, and $f(a/w)$ is the polynomial geometrical correction factor given as [22]

$$f(a/w) = \frac{3(a/w)^{1/2}[1.99 - (a/w)(1 - a/w)(2.15 - 3.93a/w + 2.7a^2/w^2)]}{2(1 + 2a/w)(1 - a/w)^{2/3}} \tag{7}$$

Impact toughness measurements

A Zwick Charpy-impact tester with a 2.0-J pendulum hammer was used to determine the impact toughness. Five 40-mm-span bar samples with varying notch lengths and razor-cracks were used. The impact toughness was calculated using the following equation [4]:

$$U = G_{IC} BD\varphi + U_0 \tag{8}$$

where G_{IC} is impact toughness, U is the measured energy, U_0 is the kinetic energy, D is the specimen thickness, B is the specimen breadth, and ϕ is the calibration factor for the geometry used [3].

Thermal and flammability tests

A thermogravimetric analyser (TGA-DTA; Instrument: 2960 SDT V3.0F) was used to characterize the thermal behaviour. Samples were powdered by abrasion, and approximately 50 mg of each sample was prepared for TGA. The heating rate was 20 °C/min over a temperature range of ambient to 800 °C. The thermal decomposition temperatures were measured under 20 ml/min of nitrogen using platinum pans. The flammability of samples was determined through horizontal burning using three measures, namely the ignition time, burning out time and fire velocity.

Results and discussion

Density and porosity

Table 1 shows the values of density and porosity for pure, eco-composite and eco-nanocomposite samples. The addition of RCF and n-SiC was found to increase the density of the composites. The porosities in eco-composites and eco-nanocomposites were found to be much higher compared with the pure samples. Owing to the incompatibility between the hydrophilic natural fibres and hydrophobic polymer matrices, the presence of natural fibres in the composite samples has created voids at the interfacial areas between RCF and matrices [21, 23]. However, the addition of n-SiC has reduced the porosities of the eco-nanocomposite samples which can be attributed to the improvement of RCF–VER interfacial adhesion. The high specific surface area and high surface energy of n-SiC due to its nano-sized dimension can facilitate rapid phase interactions within the polymer matrix. Therefore, RCF–VER interfacial adhesion can be improved. Furthermore, n-SiC provides strong electrostatic attractive forces at the fibre–matrix interfaces serving to impart additional adhesion between the fibres and the matrix [24, 25].

Table 1 Density and porosity results of pure, eco-composite and eco-nanocomposite samples

Sample	RCF content (wt%)	n-SiC content (wt%)	Density (g/cm^3)	Porosity (%)
VER	0	0	1.14 ± 0.01	0.52 ± 0.01
VER/RCF	40	0	1.26 ± 0.02	3.97 ± 0.03
VER/RCF/1 %n-SiC	40	1	1.28 ± 0.01	3.32 ± 0.01
VER/RCF/3 %n-SiC	40	3	1.29 ± 0.01	2.99 ± 0.02
VER/RCF/5 %n-SiC	40	5	1.32 ± 0.02	2.88 ± 0.03

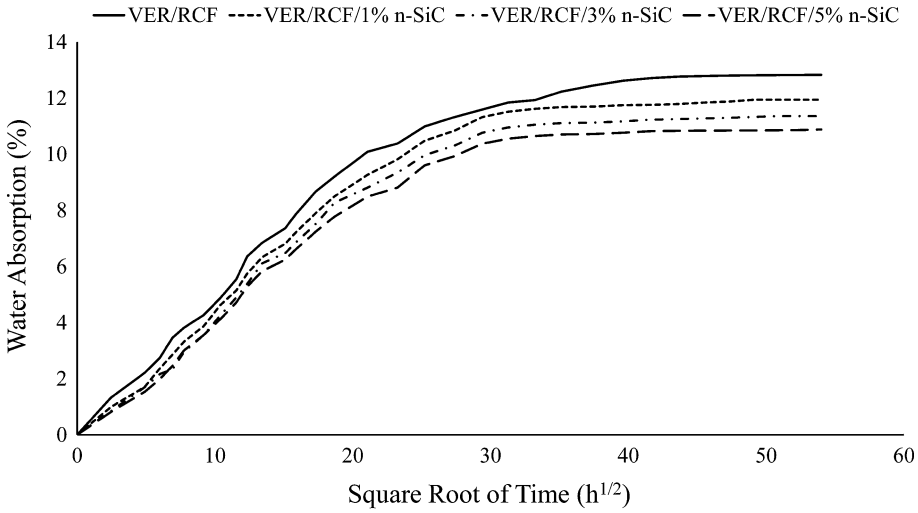

Fig. 1 Water absorption behaviour of eco-composites and eco-nanocomposites

Water uptake behaviour

Figure 1 shows the water absorption curves of the eco-composites and eco-nanocomposites. The Fickian diffusion behaviour was observed for each of the samples immersed in water for prolonged period with water absorption occurring rapidly in the beginning and then slowing down prior to reaching equilibrium [21]. The addition of n-SiC has led to a slight reduction in the overall uptake of water in each of the eco-nanocomposite samples. Table 2 shows that as n-SiC loading is increased, and the amount of water uptake is decreased. This indicates that n-SiC addition inhibits water absorption in eco-nanocomposites. As the equilibrium water content reduces; however, there is no statistically significant change in the diffusion behaviours of the composites. This finding supports the view that there is no direct relationship between water content and diffusivity value as was reported by previous studies [26, 27]. These findings imply that a critical determinant of water uptake may be the rate of water flow into the immersed composite. The following equation provides a method for measuring water transmission rate [27]:

$$\mathrm{WTR} = \frac{M_\infty(g)}{\mathrm{TSA}(\mathrm{m}^2) \times T(\mathrm{days})} \tag{9}$$

Table 2 Maximum water uptake M_∞ and diffusion coefficients D of eco-composites and eco-nanocomposites

Sample	RCF (wt%)	n-SiC (wt%)	M_∞ (%)	D (mm^2/s)
VER/RCF	0	0	12.8	2.86×10^{-6}
VER/RCF/1 % n-SiC	40	1	11.9	2.76×10^{-6}
VER/RCF/3 % n-SiC	40	3	11.4	2.75×10^{-6}
VER/RCF/5 % n-SiC	40	5	10.9	2.77×10^{-6}

where WTR is the water transmission rate, M_∞ is the maximum of water uptake, TSA is total surface area of specimen since the specimen was exposed to the water in all directions and T is the time to reach the maximum water uptake.

Figure 2 shows that with the increasing n-SiC content, there is a slight reduction in WTR. This measurement (i.e. WTR) provides a better understanding of water uptake behaviours of composites as it is representative of water flow in three dimensions of the samples. In contrast, diffusivity is the measurement of one-dimensional water flow along the thickness of the samples.

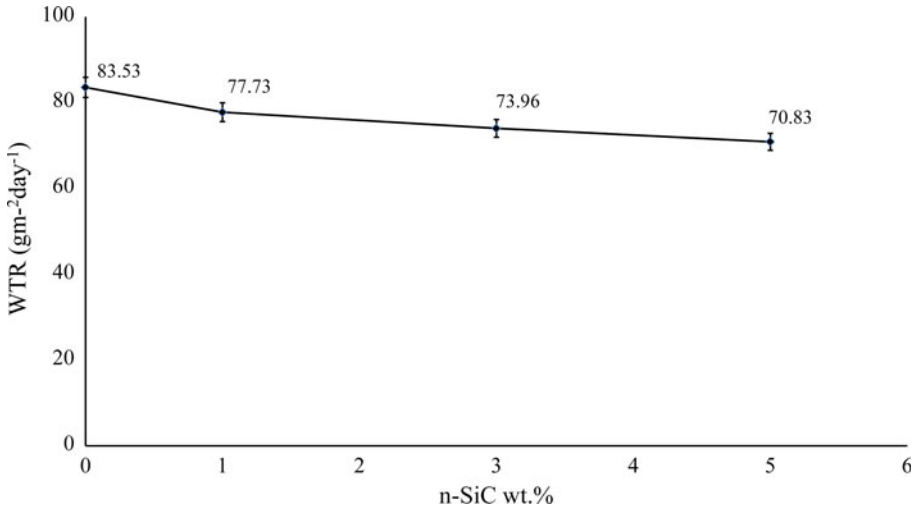

Fig. 2 Water transmission rate for pure VER, eco-composites and eco-nanocomposites

Table 3 Elastic modulus and strength properties of pure VER, VER/RCF eco-composites and VER/RCF/n-SiC eco-nanocomposites

Samples	RCF Content (%)	n-SiC content (%)	Elastic modulus (GPa)	Flexural strength (MPa)	Impact strength (kJ/m^2)
VER	0	0	2.9 ± 0.2	41.9 ± 1.4	2.6 ± 0.2
VER/RCF	40	0	4.8 ± 1.1	148.4 ± 1.7	15.9 ± 1.2
VER/RCF/1 % n-SiC	40	1	5.8 ± 1.2	173.1 ± 1.5	21.8 ± 1.4
VER/RCF/3 % n-SiC	40	3	6.2 ± 1.2	176.1 ± 1.7	24.6 ± 1.3
VER/RCF/5 % n-SiC	40	5	6.9 ± 1.4	179.4 ± 1.3	27.4 ± 1.1

In general, reinforcing composites with nanoparticles can lead to dramatic improvements in the barrier properties of the resultant samples by virtue of the need for the permeating molecules to wiggle around the nanoparticles. Also, the pathway tortuosity of diffusion depends strongly on the aspect ratio or length/width ratio of the nanoparticles. Hence, particles with large aspect ratios will be more likely to form composites with high barrier properties [23, 28]. The low aspect ratio of n-SiC because of its spherical shape suggests that its addition will only impart moderate barrier properties. As mentioned previously, the reduction of water uptake in eco-nanocomposites may be attributed to the improvement of fibres/matrix interfacial bonding as a result of n-SiC addition. Better interfacial adhesion can reduce the width of the interface areas existing between fibres and matrix, thus causing a reduction in the amount of water absorption [29].

Elastic modulus and strength properties

The results for the elastic modulus, flexural strength and impact strength are provided (Table 3). Compared with neat VER (2.97 GPa), the elastic moduli of the eco-composites and eco-nanocomposites were found to be greater. There was a 162.3 % increase in the elastic modulus of VER/RCF eco-composite (4.81 GPa). This enhancement is believed to be attributable to the higher initial modulus of the cellulose fibres [30].

Compared with neat VER (41.9 MPa), the flexural strength of eco-composites was significantly greater (148.4 MPa). The enhancement in strength is believed to be attributable to a reinforcing effect imparted by the high-strength and high-modulus cellulose fibres as well as the resistance to bending force that the fibres provide [5, 15]. Fibres–matrix interaction is also critical to composite strength. Good bonding between polymeric matrix and the fibres facilitates the role of the matrix in transferring load to stiff fibres through shear stresses at the interface [4, 22, 29].

Compared with neat VER (2.6 kJ/m^2), the impact strength of the eco-composites was significantly greater (15.9 kJ/m^2). This increase in strength is attributed to the superior ability of cellulose fibres in terms of impact energy absorption compared to that of the pure polymer.

Energy absorption in fibre–polymer composite materials occurs through the energy dissipation mechanisms of fibre pull-out and fibre debonding. Favourable fibre–matrix interaction promotes good interfacial bonding, which also is a significant factor for enhancing impact strength [15, 23, 31]. These improvements in elastic modulus and

strength properties in polymer composites reinforced with natural fibres have been reported by earlier studies [4, 31, 32].

The addition of n-SiC was found to enhance the elastic moduli of the samples. The elastic modulus of the unfilled eco-composites was 4.8 GPa, whereas addition of 1, 3 and 5 wt% of n-SiC led to eco-nanocomposites with elastic moduli of 5.8, 6.2 and 6.9 GPa, respectively. The n-SiC used in this study, as in the case of other nanofillers, has a high specific surface area, which is believed to provide dense interfacial interaction with polymer matrix. It is believed that the presence of n-SiC affects the mobility of surrounding chains in the polymer matrix, which leads to increased matrix stiffness. Another reason believed to be leading to the increased matrix stiffness is the very high initial elastic modulus of the n-SiC (470 GPa) compared to those of pure VER (2.9 GPa) and the VER/RCF eco-composites (4.8 GPa). By virtue of the rule of mixtures, this high initial elastic modulus is believed to be also contributing to the increased elastic modulus of each of the eco-nanocomposites observed in this study [33, 34]. These two effects of n-SiC are believed to be contributing to the overall stiffness of the composite.

The addition of n-SiC was also found to enhance the flexural strength and impact strength of the samples. The flexural strength of the unfilled eco-composites was 148.4 MPa, whereas addition of 1, 3 and 5 wt% n-SiC led to eco-nanocomposites with flexural strengths of 173.1, 176.1 and 179.4 MPa, respectively. The addition of 1, 3, and 5 wt% of n-SiC also increased the impact strengths of the samples from 15.9 kJ/m^2 for the unfilled eco-composite to 21.8, 24.6 and 27.4 kJ/m^2, respectively for the eco-nanocomposites. Fibre–matrix adhesion, as mentioned, is an important determinant of composite quality. In fibre-reinforced composites, the matrix has the role of transferring load from the matrix to the fibres. This occurs through shear stresses at the interface. Effective transfer of load requires a strong bond to be formed between the polymeric matrix and the fibres [35, 36]. SEM is a useful technique for investigation of the effects of n-SiC addition on the interaction between the cellulose fibre and the VER matrix at the fracture surfaces of eco-composites and eco-nanocomposites.

The fracture surfaces of all composites are shown in Fig. 3 which reveals an extensive occurrence of fibre pull-outs. In addition, these micrographs also reveal useful information about the fibre surfaces and interfacial debondings. It is worth noting that the pull-out lengths and the number of pull-outs were greater in eco-composites (see Fig. 3a) compared with eco-nanocomposites (see Fig. 3b–d). This supports the notion that the strength of interfacial adhesion is stronger in eco-nanocomposites compared with eco-composites. In the presence of weak interfacial adhesion, cracks tend to propagate through the fibre–matrix interfaces and result in greater fibre pull-out lengths and numbers. In contrast, when fibre–matrix adhesion is strong, propagation of cracks through the fibre–matrix interfaces is less, and thus less fibre pull-outs are observed. Interestingly, as the loading of n-SiC increased from 1 to 3 % and then to 5 %, the lengths and numbers of fibre pull-outs were reduced. For example, in eco-nanocomposites with 5 wt% n-SiC, almost no fibre pull-outs were observed, and the fibres were broken off with no interfacial debonding. These observations are the result of strong adhesion between the fibres and the matrix [37, 38]. The micrographs also show that the roughness of the fibre surface increases with the increasing n-SiC loading. In particular, eco-composites with no n-SiC addition have fibre surfaces which appear smooth, which indicate poor interfacial adhesion [8, 39]. In addition, the interfacial gaps due to debonding appear larger in eco-composites compared with eco-nanocomposites. These fracture surface images indicate that the addition of n-SiC has led to the display of a stronger matrix–fibre adhesion.

The notion of thermal expansion mismatch may explain the improvements in the observed interfacial adhesion for eco-nanocomposites. As a result of thermal expansion mismatch, stresses can develop at the interface between matrix and filler of composite materials. The magnitude of radial (σ_r) and tangential (σ_t) stresses induced as a result of thermal expansion mismatch can be estimated from the following equation [40, 41]:

$$-\sigma_r = 2\sigma_t = \frac{\Delta\alpha\Delta T}{(1+\nu_m/2E_m)+(1-2\nu_f/E_f)} \quad (10a)$$

$$\approx \Delta\alpha\Delta T E_m \quad (10b)$$

where α, T, ν and E represent the linear thermal expansion coefficient, temperature, Poisson's ratio and elastic modulus, respectively. The matrix is referred to as (m), and dispersed filler is (f). The thermal expansion characteristics of the phases at the interface play a dominant role in determining the nature of these stresses.

In this study, the polymer matrix is reinforced with RCF and n-SiC. These two phases have lower thermal expansion coefficients (1×10^{-6} °C^{-1} and 2.77×10^{-6} °C^{-1}, respectively) [42, 43] compared with VER (56.8×10^{-6} °C^{-1}). Therefore, $\Delta\alpha$ for the two systems, RCF/VER and n-SiC/VER, is negative. In the case of RCF/VER, and according to Eq. (9), a compressive radial stress of approximately 3.24 MPa is induced at the RCF/VER interface with the production of tensile tangential stresses in the matrix. Compressive radial stresses of about 3.47 MPa are generated at the n-SiC/VER interface in concert with the production of tensile tangential stresses in the matrix. These stresses serve to increase the intrinsic bond developed at the interfaces between VER and both fillers (i.e. RCF and n-SiC) [40, 41]. Under this circumstance, and due to the presence of these lower thermal

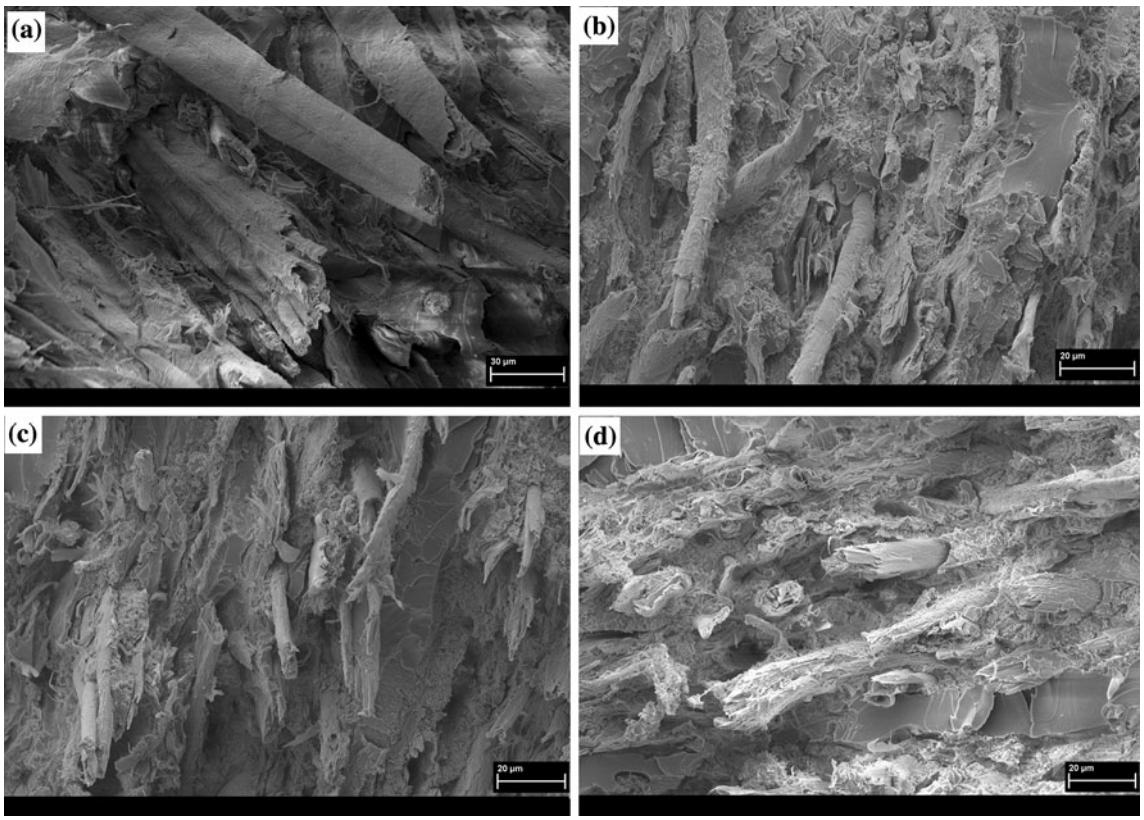

Fig. 3 SEM images of fracture surfaces of **a** eco-composite, **b** eco-nanocomposite with 1 wt% n-SiC loading, **c** eco-nanocomposite with 3 wt% n-SiC loading, and **d** eco-nanocomposite with 5 wt% n-SiC loading; all samples were subjected to three-points bending test

Table 4 Toughness properties of pure VER, VER/RCF eco-composites and VER/RCF/n-SiC eco-nanocomposites

Samples	RCF Content (%)	n-SiC content (%)	Fracture toughness (MPa $m^{1/2}$)	Impact toughness (kJ/m^2)
VER	0	0	1.8 ± 0.2	1.5 ± 0.2
VER/RCF	40	0	4.4 ± 0.5	42.3 ± 2.1
VER/RCF/1 %n-SiC	40	1	2.9 ± 0.1	28.7 ± 1.7
VER/RCF/3 %n-SiC	40	3	2.7 ± 0.2	26.4 ± 1.2
VER/RCF/5 %n-SiC	40	5	2.5 ± 0.1	23.1 ± 1.3

expansion fillers, extra compressive stresses can be induced at the filler/VER interfaces which serve to improve the interfacial adhesion. Thus, the improved strengths of eco-nanocomposites can be attributed to enhanced adhesion at the fibre–matrix interfaces due to the addition of n-SiC as discussed previously.

Toughness

The eco-composites had significantly greater fracture toughness and impact toughness compared with the pure samples (Table 4). As expected, eco-composites displayed greater values of fracture toughness and impact toughness relative to the control. It is the interaction of cellulose fibres with the polymer matrix that is believed to enable eco-composites to exhibit the preferable energy-dissipating, crack-deflection and fracture-resistance properties [33]. In this study, the fracture toughness and impact toughness of eco-composites were significantly enhanced comared with the control. The favourable fracture toughness properties that natural fibre–polymer composites typically display are believed to be determined through crack-deflection, debonding between fibre and matrix, the pull-out effect and a fibre-bridging mechanism [4, 34].

A plausible explanation for the enhanced toughness properties found for the eco-composites in this study is the effect of toughness mechanisms provided by RCF. Pure samples had a fracture toughness of 1.8 MPa $m^{1/2}$, whereas

eco-composites had a fracture toughness of 4.4 MPa $m^{1/2}$. Similarly, the impact toughness of eco-composites (42.3 kJ/m^2) was significantly higher than the impact toughness of the pure samples (1.5 kJ/m^2). However, the increasing loading of n-SiC reduced the toughness properties of the sample. For example, the addition of 5 wt% n-SiC reduced the fracture toughness from 4.4 to 2.5 MPa $m^{1/2}$ and the impact toughness from 42.3 to 23.1 kJ/m^2. The addition of n-SiC, as mentioned, resulted in strength improvements by virtue of enhanced interfacial adhesion. However, fibre–matrix adhesion enhancement causes the eco-nanocomposites to become more brittle inhibiting fibre debonding and fibre pull-out and ultimately leading to lower fracture toughness [8, 33, 38].

Figure 4 displays the load–displacement curves for fracture testing of VER, eco-composites and eco-nanocomposites. For the composite samples, it can be seen that after the initial rise, nonlinearity occurs until the peak fracture load. This shift from linearity to nonlinearity is indicative of improved toughness in the composite samples. For pure VER, the figure shows catastrophic failure at a lower fracture load. In contrast, for eco-composite samples, the results suggest better durability with these materials initially resisting fracture and failing only at a much higher fracture load. Moreover, the eco-composites failed in a graceful manner exhibiting a discontinuous fracture or multiple 'stick–slip' fracture [4]. Repeated occurrence of crack initiation, arrests and fibres debonding at the RCF sheet/epoxy interfaces is the most plausible explanation for the observed nonlinearity. SEM images of the fracture surfaces support this explanation (see Fig. 3a). For the eco-nanocomposites, these samples exhibited a dramatic failure at fracture load lower than that by the eco-composites.

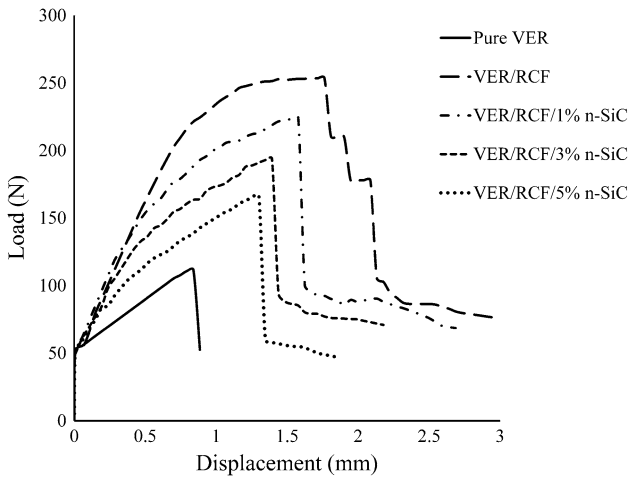

Fig. 4 Load–displacement curves of pure VER, VER/RCF eco-composites and VER/RCF/n-SiC eco-nanocomposites during flexural toughness testing

The dramatic failures of eco-nanocomposites are indicative of simultaneous fracture of the matrix and the fibres. This explanation is consistent with the appearance of the fracture surfaces of these samples (see Fig. 3b–d). However, it should be noted that the pronounced display of nonlinear fracture behaviour in both eco-composites and eco-nanocomposites implies that the principles of linear elastic fracture mechanics are invalid for the measured K_{IC} values, and these quoted values are apparent but not 'true' fracture toughness values. As such, these materials will invariably exhibit an *R*-curve fracture behaviour by virtue of extensive slow crack growth and fibre-bridging at the crack wake.

Thermal and flammability properties

The thermal degradation behaviours of VER, eco-composites, and eco-nanocomposites were investigated using TGA, and the results are shown in Fig. 5 and summarized in Table 5. The results show that thermal degradation of pure VER occurred in a single stage starting at ~260 °C with complete degradation at ~430 °C. However, in all composite samples, the release of moisture has led to a slight weight loss at 60–100 °C. In eco-composite samples, decomposition occurred in two stages with complete degradation occurring at ~445 °C. These results further support that eco-composites decompose at higher temperatures compared with pure VER. This is due to the thermal resistance of cellulose fibres, and the ability of these natural fibres to increase char formation leading to improved thermal stability [44–46]. These results are in agreement with previous studies on thermal properties of lingo-cellulosic fibre composites [47, 48]. In all eco-composite samples thermal depolymerization of hemicellulose, pectin, and cleavage of glycosidic linkages of cellulose are believed to occur at 200–300 °C, and the decomposition of cellulose occurs at 300–370 °C. The decomposition of lignin occurs over a wide range of temperatures, i.e. 200–700 °C because of the aromatic and highly branched structure of lignin [49, 50].

In a manner similar to eco-composites, the decomposition of eco-nanocomposites followed the same trend, albeit the temperatures required for complete decomposition of the eco-nanocomposites were slightly higher, with 1, 3, and 5 wt% loading of n-SiC showing complete decomposition at 456, 471, and 484 °C, respectively. While the residual weight of the pure sample was only 8.7 % of the original, the residual weights of eco-composites and eco-nanocomposites with 1, 3, and 5 wt% loading of n-SiC were found to be greater with 19.8, 22.8, 23.7 and 24.6 % of the starting weight remaining, respectively. Nano-fillers (n-SiC) provide a thermal barrier which prevents heat transfer inside the matrix and a barrier to mass transport by forming a char

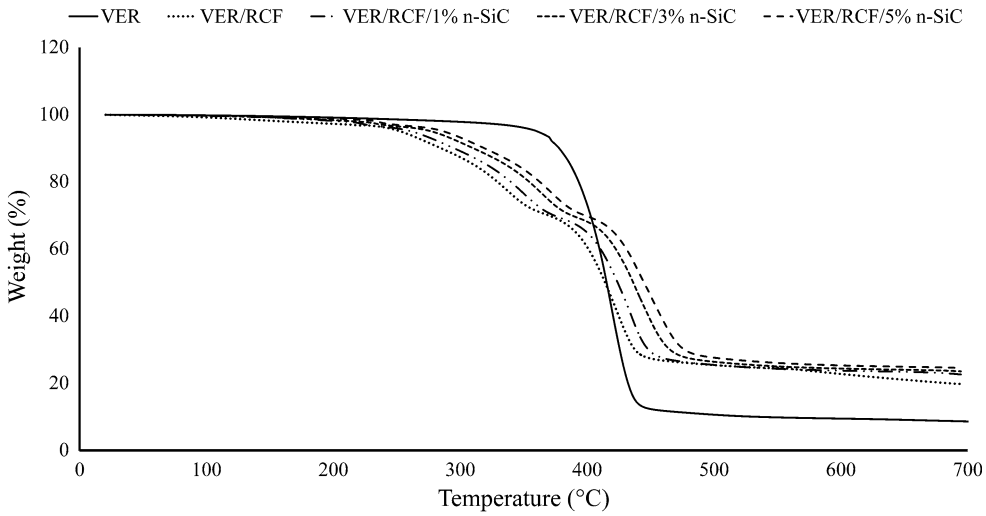

Fig. 5 TGA curves of pure VER, VER/RCF eco-composites and VER/RCF/n-SiC eco-nanocomposites

during the process of degradation. This char formation can hinder the escape of volatile products out of the composites [51]. In addition, the improvement of the adhesion between RCF and VER due to the presence of n-SiC can lead to enhanced thermal stability [44, 52].

Burning out rate, ignition time and fire velocity were determined as part of our investigation into the flammability properties of the pure, eco-composite and eco-nanocomposite samples. Flammability tests were conducted at room temperature to simulate realistic fire action. Table 6 shows that pure VER samples are burnt out and ignited faster than the eco-composite and eco-nanocomposite samples. During flammability test, the burning characteristics of the pure, eco-composites and eco-nanocomposites were clearly different. When the test commenced, pure VER immediately started dripping and continued with fast burning rate, until total loss of material observed at the end of the test. In contrast, the eco-composites showed a different behaviour; when the test commenced, the samples maintained a constant flame with much less burning rate, no dripping, and at the end of the test, it became completely charred. The eco-nanocomposites also displayed similar burning characteristics with longer ignition time, no dripping and slower burning rate.

As previously mentioned, cellulose fibres provide preferable thermal properties. The addition of n-SiC addition, due to its insulating and mass transport barrier capabilities, was found to further reduce the flammability of the composites. The further formation of a fire-retardant char due to addition of n-SiC serves to impart enhanced flammability [26, 53]. Char formation has been found to be directly correlated to the potency of flame retardation for polymer composites [54]. Hence, the use of both RCF and n-SiC has resulted in the observed improved thermal stability and reduced flammability.

Table 5 TGA data of pure VER, VER/RCF eco-composites and VER/RCF/n-SiC eco-nanocomposites

Sample	Temperature at 50 % weight loss (°C)	Temperature at maximum weight loss (°C)	Residual weight (%)
VER	418	430	8.7
VER/RCF	420	445	19.8
VER/RCF/1 %n-SiC	429	456	22.8
VER/RCF/3 %n-SiC	441	471	23.7
VER/RCF/5 %n-SiC	451	484	24.6

Table 6 Flammability properties of pure VER, VER/RCF eco-composites and VER/RCF/n-SiC eco-nanocomposites

Sample	Burning out rate (g/min)	Ignition time (s)	fire velocity (mm/min)
VER	0.67 ± 0.06	10.8 ± 1.6	31.5 ± 1.7
VER/RCF	0.54 ± 0.02	17.2 ± 1.5	19.7 ± 1.3
VER/RCF/1 %n-SiC	0.49 ± 0.02	23.6 ± 1.4	16.3 ± 1.8
VER/RCF/3 %n-SiC	0.42 ± 0.05	27.4 ± 1.2	15.2 ± 1.2
VER/RCF/5 %n-SiC	0.29 ± 0.06	37.7 ± 1.8	14.4 ± 1.6

Conclusions

Pure VER, eco-composite and eco-nanocomposite samples were synthesized and investigated in terms of porosity, water absorption behaviour, mechanical and thermal properties. The addition of n-SiC has led to reduced porosity and water uptake but improved mechanical strength by virtue of an improvement in fibre–matrix interfacial adhesion. The presence of

cellulose fibre increased the fracture toughness significantly, but the addition of n-SiC resulted in reduced fracture toughness. The fracture toughness of eco-nanocomposites was lower than eco-composites, but they showed better thermal stability and flammability by virtue of improved mass and heat barriers and the enhanced fibre–matrix interfacial adhesion provided by n-SiC.

Acknowledgements The authors are grateful to Elaine Miller for her assistance with SEM imaging, and Peter Chapman for his assistance with the collection of TGA data.

References

1. Ratna Prasad AV, Mohana Rao K (2011) Mater Des 32(8–9): 4658
2. Sreenivasan VS, Ravindran D, Manikandan V, Narayanasamy R (2011) Mater Des 32(4):2444
3. Liu Q, Hughes M (2008) Compos A Appl Sci Manuf 39(10):1644
4. Low IM, Somers J, Kho HS, Davies IJ, Latella BA (2009) Compos Interfaces 16(7–9):659
5. Bakare IO, Okieimen FE, Pavithran C, Abdul Khalil HPS, Brahmakumar M (2010) Mater Des 31(9):4274
6. Sangthong S, Pongprayoon T, Yanumet N (2009) Compos A Appl Sci Manuf 40(6–7):687
7. Aziz SH, Ansell MP, Clarke SJ, Panteny SR (2005) Compos Sci Technol 65(3–4):525
8. Mylsamy K, Rajendran I (2011) Mater Des 32(5):3076
9. Yong V, Hahn HT (2004) Nanotechnology 15:1338
10. Shokuhfar A, Zare-Shahabadi A, Atai A-A, Ebrahimi-Nejad S, Termeh M (2012) Polym Testing 31(2):345
11. Pavlidou S, Papaspyrides CD (2008) Prog Polym Sci 33(12):1119
12. Rooj S, Das A, Thakur V, Mahaling RN, Bhowmick AK, Heinrich G (2010) Mater Des 31(4):2151
13. Handge UA, Hedicke-Höchstötter K, Altstädt V (2010) Polymer 51(12):2690
14. Haq M, Burgueno R, Mohanty AK, Misra M (2008) Compos Sci Technol 68(15–16):3344
15. Hossain MK, Dewan MW, Hosur M, Jeelani S (2011) Compos B Eng 42(6):1701
16. Kumar R, Yakabu MK, Anandjiwala RD (2010) Compos A Appl Sci Manuf 41(11):1620
17. Okubo K, Fujii T, Thostenson ET (2009) Compos A Appl Sci Manuf 40(4):469
18. Biswal M, Mohanty S, Nayak SK (2012) J Appl Polym Sci 125(S2):E432–E443
19. Huang X, Netravali A (2007) Compos Sci Technol 67(10):2005
20. Lei Y, Wu Q, Clemons CM, Yao F, Xu Y (2007) J Appl Polym Sci 106(6):3958
21. Dhakal HN, Zhang ZY, Richardson MOW (2007) Compos Sci Technol 67(7–8):1674
22. Low IM, McGrath M, Lawrence D, Schmidt P, Lane J, Latella BA, Sim KS (2007) Compos A Appl Sci Manuf 38(3):963
23. Kim J-K, Hu C, Woo RSC, Sham M-L (2005) Compos Sci Technol 65(5):805
24. Sun L-H, Yang Z-G, Li X-H (2008) Mater Sci Eng, A 497(1–2): 487
25. Shi J, Shi SQ, Barnes HM, Horstemeyer MF, Wang G (2011) Int J Polym Sci. doi:10.1155/2011/736474
26. Becker O, Varley RJ, Simon GP (2004) Eur Polymer J 40(1):187
27. Mohan TP, Kanny K (2011) Compos A Appl Sci Manuf 42(4):385
28. Liu W, Hoa SV, Pugh M (2008) Compos Sci Technol 68(1):156
29. Qin L, Qiu J, Liu M, Ding S, Shao L, Lü S, Zhang G, Zhao Y, Fu X (2011) Chem Eng J 166(2):772
30. Espert A, Vilaplana F, Karlsson S (2004) Compos A Appl Sci Manuf 35(11):1267
31. Bax B, Müssig J (2008) Compos Sci Technol 68(7–8):1601
32. Wambua P, Ivens J, Verpoest I (2003) Compos Sci Technol 63(9):1259
33. Ma J, Mo M-S, Du X-S, Rosso P, Friedrich K, Kuan H-C (2008) Polymer 49(16):3510
34. Zuiderduin WCJ, Westzaan C, Huétink J, Gaymans RJ (2003) Polymer 44(1):261
35. Chen H, Miao M, Ding X (2009) Compos A Appl Sci Manuf 40(12):2013
36. Herrera-Franco PJ, Valadez-González A (2005) Compos B Eng 36(8):597
37. Abdelmouleh M, Boufi S, Belgacem MN, Dufresne A (2007) Compos Sci Technol 67(7–8):1627
38. Stocchi A, Bernal C, Vázquez A, Biagotti J, Kenny J (2007) J Compos Mater 41(16):2005
39. De Rosa IM, Kenny JM, Maniruzzaman M, Moniruzzaman M, Monti M, Puglia D, Santulli C, Sarasini F (2011) Compos Sci Technol 71(2):246
40. Low IM (1990) J Mater Sci 25(4):2144. doi:10.1007/BF01045780
41. Low IM (1990) J Appl Polym Sci 39:759
42. Le Duigou A, Davies P, Baley C (2010) Compos Sci Technol 70(2):231
43. Slack GA, Bartram SF (1975) J Appl Phys 46(1):89
44. Curvelo AAS, de Carvalho AJF, Agnelli JAM (2001) Carbohydr Polym 45(2):183
45. Ma X, Yu J, Kennedy JF (2005) Carbohydr Polym 62(1):19
46. Manfredi LB, Rodríguez ES, Wladyka-Przybylak M, Vázquez A (2006) Polym Degrad Stab 91(2):255
47. Joseph PV, Joseph K, Thomas S, Pillai CKS, Prasad VS, Groeninckx G, Sarkissova M (2003) Compos A Appl Sci Manuf 34(3):253
48. Liu W, Mohanty AK, Drzal LT, Askel P, Misra M (2004) J Mater Sci 39(3):1051. doi:10.1023/B:JMSC.0000012942.83614.75
49. Araújo JR, Waldman WR, De Paoli MA (2008) Polym Degrad Stab 93(10):1770
50. Yang H, Yan R, Chen H, Lee DH, Zheng C (2007) Fuel 86(12–13):1781
51. Leszczyńska A, Njuguna J, Pielichowski K, Banerjee JR (2007) Thermochim Acta 453(2):75
52. Yu T, Ren J, Li S, Yuan H, Li Y (2010) Compos A Appl Sci Manuf 41(4):499
53. Vyazovkin S, Dranca I, Fan X, Advincula R (2004) Macromol Rapid Commun 25(3):498
54. Shih Y-F (2007) Mater Sci Eng, A 445–446:289

3.5. Water absorption, mechanical, and thermal properties of halloysite nanotube reinforced vinyl-ester nanocomposites

---

ALHUTHALI, A. and LOW, I. M. 2013. Water absorption, mechanical, and thermal properties of halloysite nanotube reinforced vinyl-ester nanocomposites. *Journal of Materials Science,* 48, 4260-4273.

J Mater Sci (2013) 48:4260–4273
DOI 10.1007/s10853-013-7240-x

Water absorption, mechanical, and thermal properties of halloysite nanotube reinforced vinyl-ester nanocomposites

A. Alhuthali · I. M. Low

Received: 22 November 2012 / Accepted: 13 February 2013 / Published online: 22 February 2013

Abstract Halloysite nanotube (HNT) addition to vinyl-ester resin (VER) is a field yet to contain an in-depth repository of information. This work represents the first study on the development and characterisation of HNT-reinforced VER nanocomposites, and presents findings on their water absorption, mechanical, and thermal properties. VER composites reinforced with HNTs (1, 3, and 5 wt%) were fabricated using high speed mechanical stirring. Weight gain and FTIR spectrum analysis indicated that the addition of 5 wt% HNTs gave perceptible reduction in the water absorption behavior of the samples. Results showed that elastic modulus increased with increasing HNT content. Strength and toughness were also found to steadily increase with increasing HNT content. Favorable strength can be attributable to the large aspect ratio of HNTs, favorable adhesion and dispersion, and the suitable extent of inter-tubular interaction while enhancements to toughness can be attributable to crack bridging, deflection, and plastic deformation mechanisms. Thermal stability of nanocomposites was found remarkably enhanced by the incorporation of HNTs. The thermal stability enhancement and decrease in flammability are attributable to HNT's barriers for heat and mass transport, presence of iron, and hollow tubular structure.

Introduction

Polymer nanocomposites are blended polymer-based materials that contain one or more dimensions at the nano-scale level [1]. The presence of nano-particles gives the material an extremely large surface area, which is an attribute facilitating rapid phase interactions, and greater interfacial matrix interaction overall. The increased surface area is a key determinant behind the properties of an extraordinary nature that polymer nanocomposites demonstrate [2–4]. The mechanical, electrical, barrier and thermal properties of polymer nanocomposites have aroused research and development attention due to their noted advantages over pure and conventional composites [5, 6]. The science of nano-filler addition to polymers, however, is not new. Polymer engineering has involved investigations of clay mineral and carbon nanotube acting as fillers since the 1990s [7]. Conventional plastics engineering has also involved inquiry into the behavior of nano-fillers infused into polymers and research has described desirable properties of material transparency, surface advantages, flame retardance, heat resistance, gas permeability reduction, wear and barrier protection [8–10].

Vinyl-ester resins (VERs) are used in the fabrication of reinforced pipes, tanks, scrubbers, as well as hard-worked hull and deck structures in marine craft [11]. They are the prime thermoset matrix candidate with mechanical properties suitable for coatings, adhesives, molding compounds, structural laminates, and electrical applications [12]. With higher design flexibility, better moisture resistance, better chemical resistance compared with cheaper polyester resins, VERs combining the best properties of epoxies and unsaturated polyesters are favored and provide industry with control over cure rate and reaction conditions [13–15].

Halloysite nanotubes (HNTs) are derived from naturally deposited aluminosilicate ($Al_2Si_2O_5(OH)_4{\cdot}H_2O$) and are chemically similar to kaolin [16]. A two-layered aluminosilicate structure, which the hollow tubular morphology is formed by layer rolling, constitutes HNTs [17]. The external and internal structures and features of the nanotubes can be distinguished. The external surface of a

A. Alhuthali · I. M. Low (✉)
Department of Imaging & Applied Physics, Curtin University, GPO Box U1987, Perth, WA 6845, Australia
e-mail: j.low@curtin.edu.au

nanotube is constituted by a tetrahedral sheet structure primarily made up of siloxane groups (Si–O–Si), whereas the internal surface of a nanotube is formed by aluminol groups (Al–OH) existing in octahedral structures. The mismatch between the external tetrahedral structures of silica and the internal octahedral structures of alumina gives rise to the HNTs' cylindrical shape [18, 19].

The physical characteristics of HNTs will be determined by the deposit source [20, 21]. HNTs, however, have a hollow tubular structure in the sub-micrometer range, with a length of between 1 and 15 μm. The inner diameter of HNTs is between 10 and 30 nm and the outer diameter is between 50 and 70 nm. The structural characteristics of HNTs give the materials a high aspect ratio and a very high surface area which promote filler and matrix interaction and ultimately provide the materials with advantages over other fillers [7, 8]. In recent years, HNTs have been used as fillers for matrices of epoxy, polypropylene, polyamide, styrene rubber, and polyvinyl alcohol [22, 23].

Due to the hollow tubular structure of HNTs, they do not require exfoliation like other fillers such as nanoclay platelets; they can easily be dispersed in a polymer matrix, even at high weight fraction [16, 24]. It is the rod-like geometry of HNTs that never intertwines which makes the dispersion of the HNT filler amongst the polymer even easier [17]. While reports of polymeric nanocomposite development and characterization have featured in scientific publications for a number of years, the field of study on HNT nanocomposites is yet to contain an in-depth repository of information on the addition of HNTs in vinyl-ester. This study aims to be a pioneering investigation in the field of vinyl-ester/HNT nanocomposite development and characterisation the effect of HNT on water absorption, mechanical, thermal, and flammability properties of vinyl-ester filled by halloysite nanotubes.

Experimental

Materials

A general purpose VER was supplied by Fiberglass & Aesin Sales Pty Ltd, Perth, WA, Australia, and ultrafine halloysite nanotubes (HNTs) were supplied by NZCC, New Zealand. According to the supplier, the elemental compositions (wt%) of HNTs were 50.4 % SiO_2, 35.5 %; Al_2O_3, 0.25; Fe_2O_3, and 0.05; TiO_2. After drying processes to remove existing moisture, a density of 2.14 g/cm^3 was recorded for the HNTs.

Samples preparation

As a control to provide the baseline data of the properties of pure VER, pure vinyl-ester samples (VER) were first made. The VER was mixed with 1.0 wt% methyl ethyl ketone peroxide (MEKP) in order to prepare the control samples. Air bubble formation within the matrix was minimized through slow and thorough mixing of the mixture. The resultant mixture was poured into silicon molds and kept for 2 h under low vacuum (20 kPa) and later for 24 h at room temperature to cure. The nanocomposite samples were prepared with a dispersion of HNTs at concentrations of 1, 3, and 5 %. To remove the pre-existed moisture, HNTs were dried for 60 min at 150 °C, followed by mixing with a high speed electrical-mixer (1200 rpm) for 30 min. Then a catalyst (MEKP) was added to the mixture and to avoid the creation of air bubbles within the sample was hand-mixed slowly. The resultant mixtures were poured into silicon molds, de-gassed in vacuum of 60 kPa for 2 h, and cured at room temperature for 24 h. The samples were labeled as VER/1 %HNTs, VER/3 %HNTs, and VER/5 %HNTs.

Microstructure examination

X-ray diffraction analysis (XRD)

A D8 Advance Diffractometer (Bruker-AXS), using copper radiation and a LynxEye position sensitive detector, was used to study the samples. The diffract meter was scanned from 5° to 30° (2θ) in steps of 0.02° using a scanning rate of 0.5°/min XRD patterns obtained by using Cu Kα lines ($\lambda = 1.5406$ Å). To reduce air scatter, a knife edge collimator was fitted. The d-spacing of the layered particle was then calculated from Bragg's equation, $n\lambda = 2d \sin\theta$, where λ is the wavelength of the X-ray, d is the interlayer distance, and θ is the angle of incident X-ray radiation.

Transmission electron microscopy (TEM)

To study the morphologies of the HNTs and their dispersion inside the vinyl-ester matrix, a transmission electron microscope (TEM; JEOL JEM2011, Japan) was used. The HNTs were suspended in ethanol for 1 min, and then placed in ultra-sonic path for 30 min. Then a droplet of suspension sprayed on a carbon thin film coated 400 mesh copper grid. Ultra-thin specimens ($\sim$170 nm) were prepared using ultra microtome, in order to investigate the microstructures of vinyl-ester/HNTs composites. TEM operating acceleration voltage was 80 kV.

Scanning electron microscopy (SEM)

A NEON 40ESB, scanning electron microscope, (SEM; ZEISS, UK)) operating at accelerating voltage of 5 kV, under secondary image mode was used to examine the microstructure of HNTs and fracture surfaces of the

samples. To prepare non-aggregated clusters, HNTs were stirred first in methanol and the suspension was placed in ultra-sonic path for 5 min. In order to avoid charging, all samples were coated with platinum.

Water uptake measurements

Weight gain study

Samples with rectangular-shaped dimensions (10 × 10 × 6 mm^3) were used for the study. Individual samples were soaked in tap water at room temperature. At prescribed intervals, samples were removed from water. After excess water was removed, they were weighed and immediately returned to the water. The amount of moisture uptake or absorbed (M_a) by the samples over a period of 120 days, was determined using the following equation [25]:

$$M_a = \frac{M_t - M_d}{M_d} \times 100, \quad (1)$$

where M_d is the dry mass and M_t is the mass of sample soaked for time t.

The coefficient of water diffusion (D) was calculated by using the following equation [25]:

$$D = \frac{\pi}{16}\left(\frac{M_t/M_\infty}{\sqrt{t}/h}\right)^2, \quad (2)$$

where M_∞ is the maximum water uptake, M_t is the water uptake at time t, h is the sample thickness, and D is the diffusion coefficient.

FTIR analyses

A Perkin Elmer Spectrum 100 FTIR (FTIR; Perkin Elmer, MA, USA) infrared spectrometer was used for the Fourier transform spectroscopy analysis (FTIR). The spectral resolution was four wavenumbers. The FTIR analysis was conducted to determine the water content of the samples after the water absorption experiment. An ATR correction was performed to compensate for the wavelength dependence on penetration depth. Thin slice samples with the dimensions 5 × 5 × 1 mm^3 for both the dry- and wet-condition samples were prepared. The dry condition samples were dried for 15 min at 100 °C prior to FTIR analysis to remove existing moisture. The wet-condition samples were immersed in water for 120 days, and immediately prior to FTIR analysis, these samples were left at room temperature (~25 °C) for 5 min to remove surface moisture.

Mechanical tests

Fracture toughness

Rectangular single edge notch bend (SENB) samples of 10 × 10 × 60 mm^3 dimensions were used in fracture toughness testing. A sharp razor blade (with a notch-tip radius of 0.25 mm) was used to initiate a sharp crack with the ratio of notch length to width of sample (a/w) at 0.45–0.55 to obtain a fracture toughness (K_{IC}) measurement. The flexural tests were performed at room temperature with a LLOYD Material Testing Machine using a displacement rate of 1.0 mm/min; for the measurements, five samples of each composition were used. The value of K_{IC} was calculated according to ASTM D5045-99 using the following equation [26]:

$$K_{IC} = \frac{P_m S}{WD^{2/3}} f\left(\frac{a}{w}\right), \quad (3)$$

where P_m is the load at fracture, S is the span of the sample, D is the specimen thickness, W is the specimen width, and a is the crack length, and $f(a/w)$ is the polynomial geometrical correction factor given as [26]:

$$f(a/w) = \frac{3(a/w)^{1/2}[1.99-(a/w)(1-a/w)(2.15-3.93a/w+2.7a^2/w^2)]}{2(1+2a/w)(1-a/w)^{2/3}}. \quad (4)$$

Impact toughness

A Zwick Charpy-impact tester with a 2.0 J pendulum hammer was used to determine the impact toughness G_{IC} at room temperature. At least five 40-mm span bar samples with varying notch lengths and razor-cracks were used. Values of fracture toughness were determined according to the method of Plati and Williams [27] with using the following equation:

$$U = G_{IC} BD\phi + U_0, \quad (5)$$

where G_{IC} is impact toughness, U is the measured energy, U_0 is the kinetic energy, D is the specimen thickness, B is the specimen breadth, and ϕ is the calibration factor for the geometry used.

Elastic modulus and flexural strength

Rectangular bars of 60 × 10 × 6 mm^3 were cut from the fully cured samples for three-point bend tests with a span of 40 mm to evaluate elastic modulus and flexural strength according to ASTM D790-86. A LLOYD Material Testing Machine (5–50 kN) with a displacement rate of 1.0 mm/min

was used to perform the test at room temperature. Five samples of each batch were used to evaluate elastic modulus and flexural strength. The values were recorded and analysed with the machine software (NEXYGENPlus) and the mean values were calculated.

Impact strength

A Zwick Charpy-impact tester with a 2.0 J pendulum hammer was used to determine the impact strength at room temperature according to ASTM D 256-06. At least five bar samples of each group with 40 mm span were used and the mean impact strength was calculated using the following equation [26]:

$$\sigma_{\mathrm{i}} = \frac{E}{A}, \tag{6}$$

where σ_{i} is the impact strength, E is the impact energy to break a sample with a ligament area A.

Thermal test

A thermogravimetric analyser (TGA–DTA; Instrument: 2960 SDT V3.0F) was used to examine the thermal behaviors of the composites. Samples were powdered by abrasion and $\sim$50 mg of each sample prepared for TGA. At a rate of 20 °C/min, composites were heated from room temperature to 800 °C. Using platinum pans, thermal decomposition temperatures of the composites were examined under 20 ml/min of nitrogen flow.

Flammability test

Horizontal-burning testing was used to perform flammability test according to the ASTM 635 standard method. In this study, at least three samples with dimensions of $100 \times 10 \times 6$ mm^3 were prepared for each composite. The samples were held horizontally at one end, and a standard constant natural gas fuelled flame was used to ignite the free end of the specimens. The values of burning rate, burning-out rate, and ignition time were determined as follows:

$$\text{Burning rate} = L/t \ (\text{mm/min}), \tag{7}$$

where L is the burnt length in mm, and t is the time it took to burn the length L in min. More specifically t is the time required for the flame to travel between two reference marks, the first 20 mm from the free end and the second 80 mm from the free end

$$\text{Burning-out rate} = M/t \ (\text{g/min}), \tag{8}$$

where M is the burnt mass in g, and t is the time it took to burn the mass M in min. Finally, the time of ignition was recorded for each sample.

Results and discussion

X-ray diffraction analysis (XRD)

XRD patterns for pure HNTs and VER/RCF/HNTs composites with 1, 3, and 5 wt% of HNTs are shown in Fig. 1 and the XRD results summarized in Table 1. A diffraction peak at 2θ at around 12.27° related to the (001) plane can be seen in XRD pattern of pure HNTs. Tubular morphology featuring, inter-stratification of layers with various hydration states and small crystal size is indicated by this basal reflection [19]. Two additional diffraction peaks at 2θ at around 20.15° and around 24.95° relating (020) and (002) basal reflection are noticeable [16]. Trace amounts of quartz and feldspar in powders are also evident and are represented by (*) and (+), respectively. The presence of these minerals in HNT samples has been noted by other researchers [28, 29].

For pure HNT samples, a diffraction peak at a $2\theta = 12.27°$ corresponds to a basal spacing of 0.721 nm. For VER/HNT composites, the diffraction peak shifted towards lower 2θ values. The diffraction peaks, with corresponding basal spacing shown in parenthesis, for VER/1 %HNTs, VER/3 %HNTs, and VER/5 %HNTs were 11.87° (0.745 nm), 12.07° (0.733 nm), and 12.15° (0.728 nm), respectively.

Intercalation between VER chains and the HNTs is strongly supported by the 2θ reductions for composites, the increases in the basal spacing of the HNTs in these composites, which confirms the formation of nanocomposites as found in other studies [7, 16]. In relation to the two additional diffraction peaks displayed in the XRD pattern for pure HNTs the subsequent XRD patterns for the composites samples revealed that the pure HNTs peak at 2θ at around 20.15°, for the composites, had shifted markedly lower, and the pure HNTs peak at 2θ at around 24.95°, for the composites, had almost completely vanished. These results moreover support the existence of intercalation of the VER chain into the structure of the HNTs.

Microstructure of HNTs

SEM and TEM images of HNTS are shown in Fig. 2. The images show that the majority of HNTs exist in a tubular shape, however, short tubular HNTs, and semi-rolled HNTs can also be seen. The image indicates that HNTs have a length range from 500 nm to 3 μm. From the image, the averages of the outer diameters of the HNTs appear to range from 100 to 300 nm whereas the averages of the inner diameters range from 50 to 150 nm. The length/diameter ratio (aspect ratio) of HNTs varies between 3, 5, and 15. In general, the size distribution of halloysite nanotube is quite large, since it is a natural product.

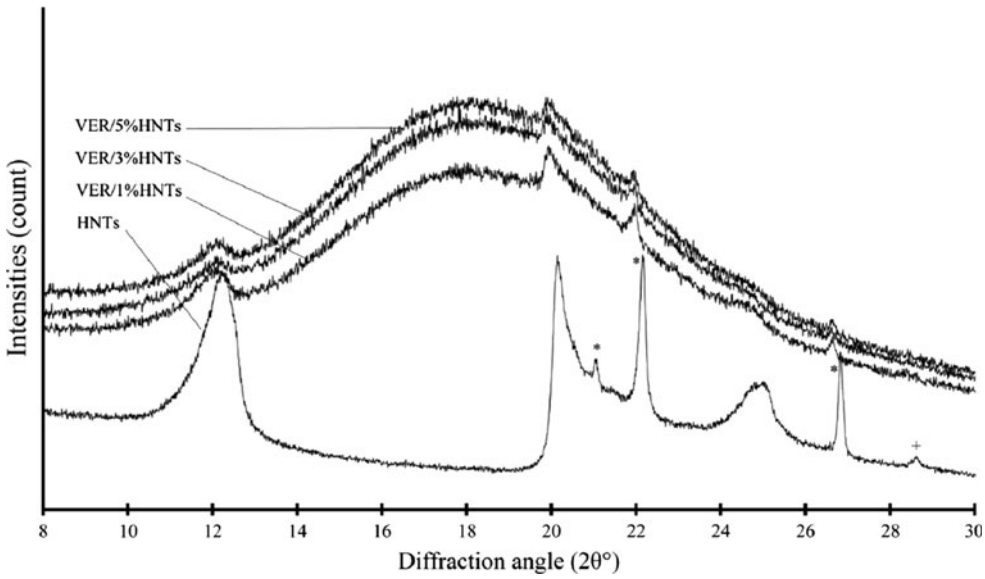

Fig. 1 XRD pattern of HNTs and VER/HNT nanocomposites

Table 1 XRD results of HNTs and VER/HNT nanocomposites

Specific plane	(001)		(020)		(002)	
2θ/*d*-spacing	2θ	*d* (nm)	2θ	*d* (nm)	2θ	*d* (nm)
HNTs	12.27	0.721	20.15	0.44	24.95	0.357
VER/1 %HNTs	11.87	0.745	19.85	0.447	–	–
VER/3 %HNTs	12.07	0.733	19.92	0.445	–	–
VER/5 %HNTs	12.15	0.728	19.98	0.444	–	–

Microstructure of VER/HNTs composites

TEM micrographs in Fig. 3a–c and 4a–c show the dispersion of HNT clusters at low and high magnification, respectively. Based on these images, the degree of dispersion of HNT clusters within the matrix is acceptable as verified by XRD results which indicate the existence of intercalation to form a nanocomposites. Generally, HNTs were found to be evenly randomly dispersed in the matrix with short inter-tube distances resulting in HNT-rich region formation and long inter-tube distances resulting in VER-rich region formation as seen in Fig. 5a. The HNT-rich regions give the appearance of being clusters of solely HNTs. However, a closer examination reveals that VER has filled spaces between these clusters (Fig. 5b).

In other words, as identified by other researchers [29, 30], the morphology of the HNT/VER composites displays a continuous phase and a discontinuous phase. The continuous phase is the VER-rich regions in which a good dispersion of individual clusters is clear. In contrast, the agglomeration of HNT clusters embedded in this continuous phase forms the rigid discontinuous phase, in which a high concentration of HNT clusters is clear.

Water uptake properties

Weight gain

Figure 6 shows the water absorption curves for pure VER samples and VER/HNTs nanocomposites samples. The

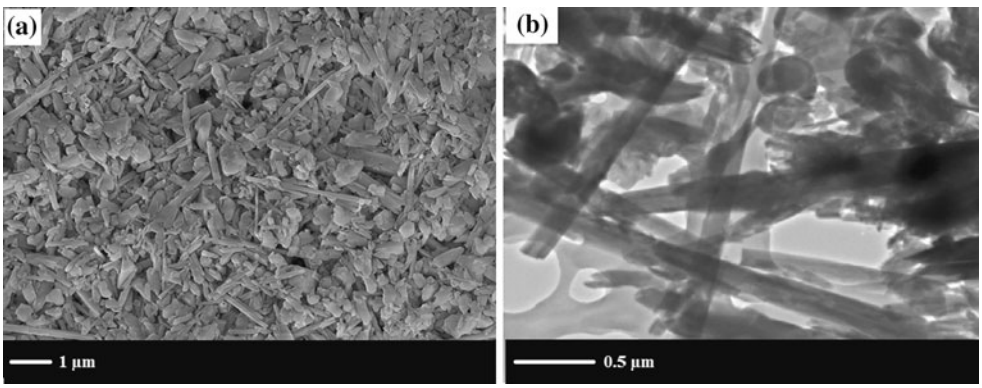

Fig. 2 HNT particles as observed under **a** SEM and **b** TEM

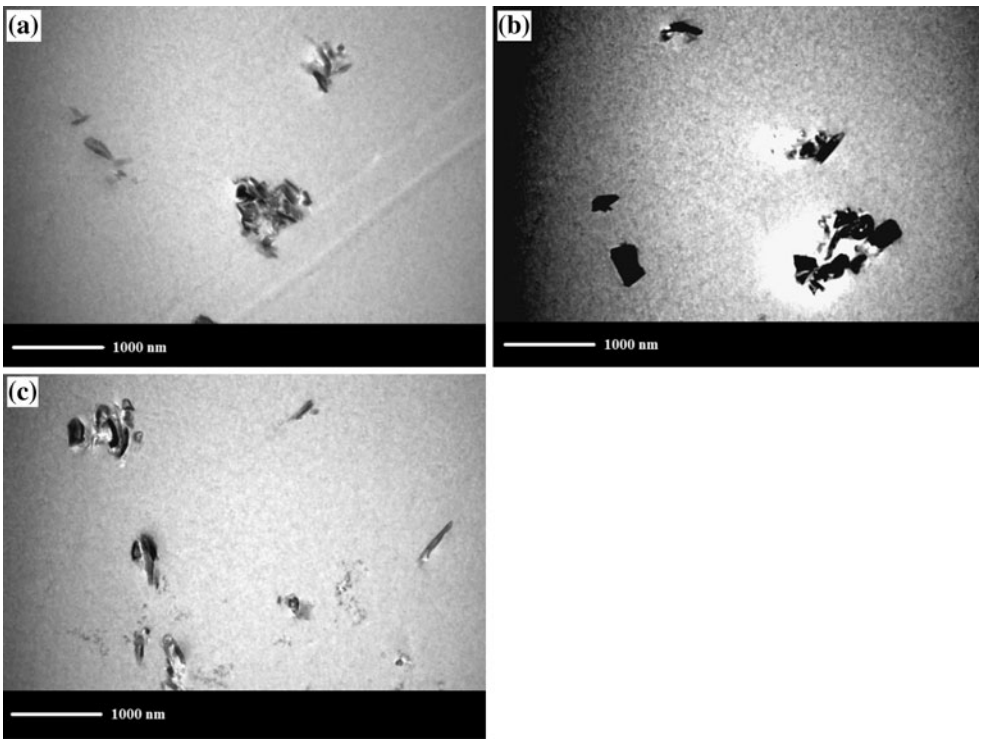

Fig. 3 Low magnification TEM images showing the dispersion of HNT clusters within the matrix of VER containing various amounts of HNTs: **a** 1 wt%, **b** 3 wt%, and **c** 5 wt%

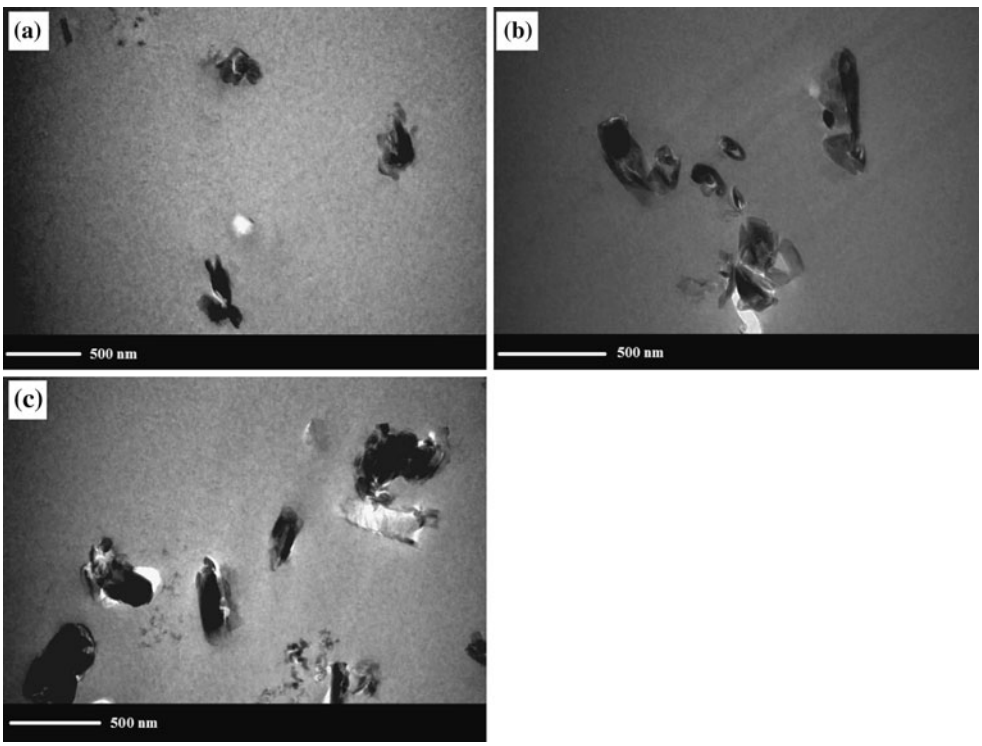

Fig. 4 High magnification TEM images showing the dispersion of HNT clusters within the matrix of VER containing various amounts of HNTs: **a** 1 wt%, **b** 3 wt%, and **c** 5 wt%

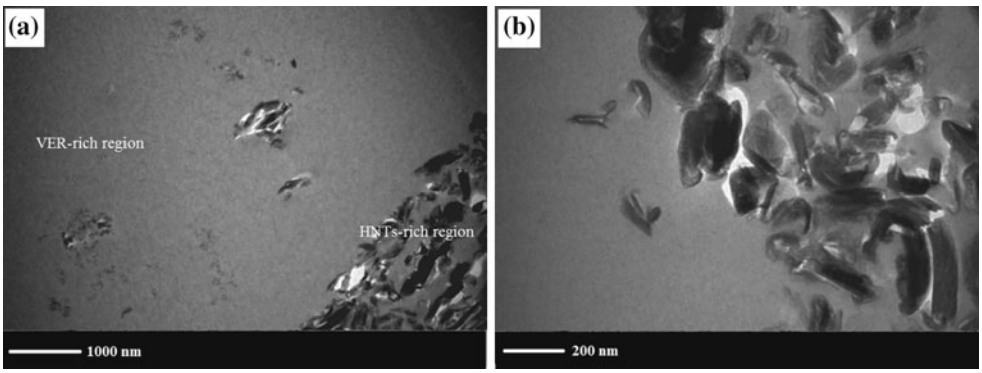

Fig. 5 TEM micrographs of VER/HNT nanocomposites showing **a** VER-rich region and HNT-rich region and **b** spaces between HNT clusters filled by VER

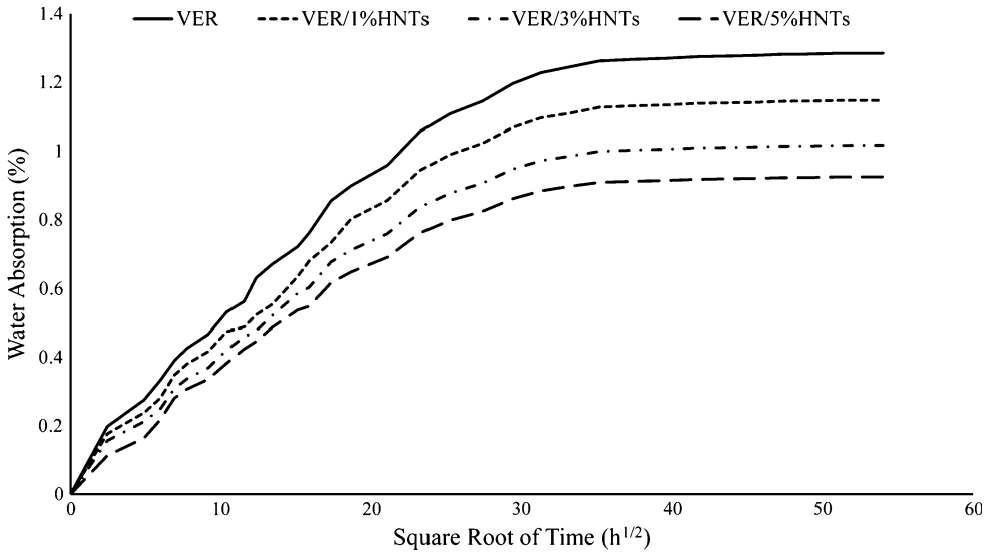

Fig. 6 Water absorption behavior of VER and VER/HNT nanocomposites

curves show for all samples, water absorption increases with time, and that with increasing HNTs content, there is a decrease in the water transmission rate as indicated by the change in slope of the curves. Typical Fickian diffusion behaviors are demonstrated in all composites. As the theory purports, at the beginning of exposure of the matter with water [29], water absorption occurs rapidly, however, after time, the rate of absorption slows down until reaching the point of equilibrium [25].

It is worth-noting that the rates of water absorption of all nanocomposites were quite rapid in the first 225 h. During the time between 225 and 625 h, the rate of water absorption had slowed down. After 625 h of immersion, all composite samples had almost reached complete saturation. There were no significant changes in moisture absorption data even after immersion for 1500 or more hours.

HNTs addition reduces the uptake of water. HNTs cause this behavior as they have a high aspect ratio, where the water molecules path is distributed [31]. The presence of the HNTs means that the water molecules path is altered from the direct-fast diffusion into the polymer matrix to a maze-like or even tortuous path for water molecule to pass through which decreasing the overall uptake of water [17, 32]. This effect is due to the impermeability of the HNTs and implies that nanocomposites will have lower maximum water absorption and tend not to reach full saturation [33].

Table 2 shows that the amount of water absorbed is decreased as the loading of HNTs is increased. HNTs presence in composites limits the composite's water

Table 2 Maximum water uptake M_∞ and diffusion coefficients D of VER and VER/HNT nanocomposites

Samples	HNTs (wt%)	Slope	M_∞ (%)	D (mm^2/s)
VER	0	0.048	1.29	2.66×10^{-6}
VER/1 %HNTs	1	0.042	1.15	2.59×10^{-6}
VER/3 %HNTs	3	0.038	1.02	2.67×10^{-6}
VER/5 %HNTs	5	0.034	0.93	2.67×10^{-6}

absorption. For commercial applications, this is a desirable property. As loading of HNTs is increased, however, statistically significant change in the diffusion coefficient is not observed. The HNT content and diffusivity values do not produce any observable trend [34, 35].

FTIR

Dry condition FTIR spectra and wet-condition FTIR spectra of pure VER and VER/HTs composites are presented in Fig. 7. In dry conditions, each spectrum shows a broad peak which represents the stretching of hydroxyl (OH) groups between 3000 and 3700 cm^{-1}. This peak exists due to the chemical structure of the composite components, VER and HNTs, which contain hydroxyl (OH) groups [36, 37]. For the purposes of this study, this broad peak will be a principal point of focus to assist in the description and explanation of the water absorption behavior.

In addition to this broad peak, the presence of vinyl-ester and HNTs gives rise to additional peaks. Due to the use of VER as the matrix all spectra displayed strong peaks at $\sim$2924 cm^{-1} and weaker peaks at around 2870 cm^{-1}. As CH is present in the chemical structures of vinyl-ester, it is expected that these peaks are due to symmetric and asymmetric vibration from CH stretching [38, 39]. Bending vibrations of the vinylic group in vinyl-ester are assumed to cause the absorption peak at 830 cm^{-1} and the out-of-plane bending of vinyl-ester monomer is reported to cause the peak near 947 cm^{-1} [12]. Methyl groups, CH_3, and methylene groups, CH_2, of vinyl-ester also cause bending vibration peaks around 1450 cm^{-1} for the former and 1350 and 1380 cm^{-1} for the latter [40]. The benzene ring of vinyl-ester is also believed to cause absorptions peaks and these are seen at 1607 and at 1510 cm^{-1}, as well as peaks due to the carbonyl groups of the ester linkage were observed at $\sim$1720 and 1180 cm^{-1} [41]. Perpendicular Si–O stretching causes the peak at around 1030 cm^{-1} and apical Si–O vibration causes the peak at 1113 cm^{-1}. As well as, peak at $\sim$912 cm^{-1} is attributed to the stretching of the Al–O/Al–OH bonds. These peaks are due to the presence of HNT [42, 43].

In wet conditions, the broad peak caused by hydroxyl (OH) stretching was found to increase in response to immersion in water for 120 days. The higher frequency region of the peak is believed to arise from hydroxyl stretching which is caused by the hydroxyl peak of absorbed liquid water. The effects of absorbed liquid water are considered to include the effects of the un-associated water present, the loosely bound water present, as well as the indirectly bonded water which may be bonded to the hydroxyl groups using other water molecules [44, 45]. The lower frequency region of the peak is believed to be a result of hydroxyl stretching caused by hydroxyl stretching of strongly bound water. Strongly bound water is produced when direct hydrogen bonds are formed between the hydroxyl groups of absorbed water and the composite components [46, 47].

Figure 8 highlights results for the broad peak caused by hydroxyl (OH) stretching. This peak is centered at

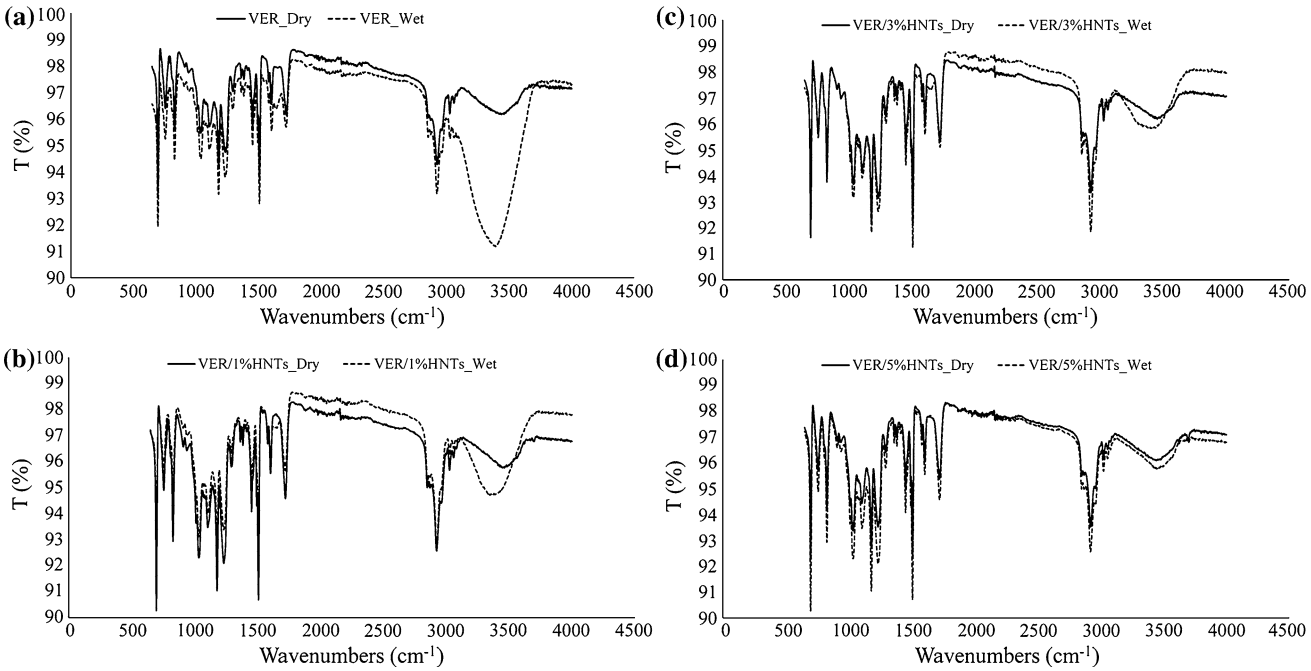

Fig. 7 Dry and wet FTIR spectra of VER/HNT samples containing various amounts of HNTs: **a** 0 wt%, **b** 1.0 wt%, **c** 3.0 wt%, and **d** 5.0 wt%

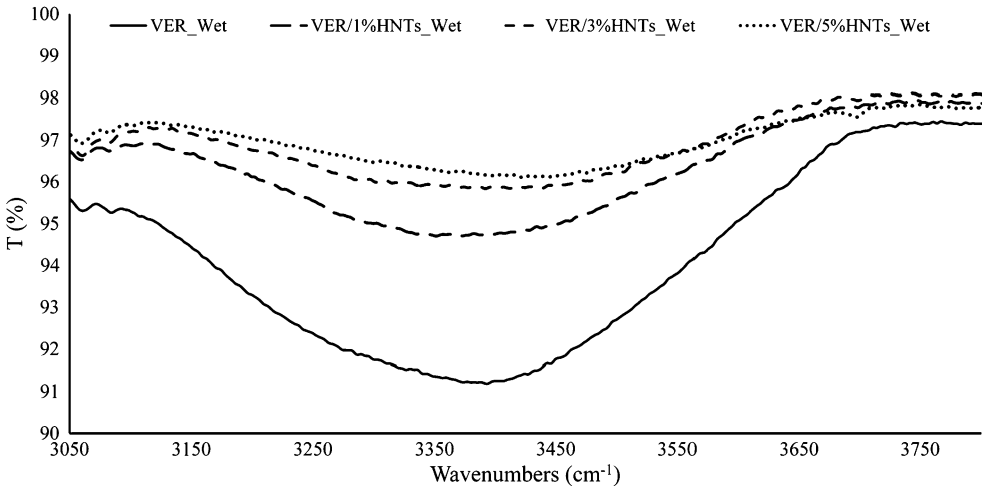

Fig. 8 Comparisons between FTIR spectrum peaks of water content in various VER/HNT nanocomposites

3360 cm^{-1}, as mentioned above, the peak was found to increase as a result of water absorption experiment. The quantity of moisture absorbed for each composite was found to be different as indicated in the respective FTIR spectrum. The FTIR spectrums for the different composites included in this study indicated that water immersion led to an increase in the quantities of moisture absorbed and these quantities were different for each composite. Clearly, HNT addition decreases the amount of water absorption in composites. This reduction in the peak as shown has proven to be one of the most interesting findings of the study and is evidence of the potential of HNTs to increase the water absorption resistance of materials. Addition of 5 wt% HNTs to the matrix resulted in substantial resistance to water absorption as evidenced by weight gain results and FTIR analyses.

Mechanical properties

Fracture toughness

The results of fracture toughness and impact toughness are shown in Table 3. The results show that the addition of HNTs led to enhanced toughness values for all VER/HNT composites samples. Fracture toughness increased from 1.81 MPa $m^{1/2}$ for pure VER to 2.12, 2.43, and 2.64 MPa $m^{1/2}$ for VER/1 %HNTs, VER/3 %HNTs, and VER/5 %HNTs, respectively. Similarly, the addition of HNTs at 1, 3, and 5 wt% increased the impact toughness from 1.52 kJ/m^2 for unfilled VER to 2.93, 3.34, and 4.14 kJ/m^2, respectively. To study the effect of addition of HNTs on toughness properties, SEM was used in this study to make a comparative examination of the various fracture surfaces. The fracture surface of each sample is clearly different between the samples with different amounts of HNTs as shown in Fig. 9a–d.

Table 3 Fracture properties of VER and VER/HNT nanocomposites

Samples	HNTs content (wt%)	Fracture toughness (MPa $m^{1/2}$)	Impact toughness (kJ/m^2)
VER	0	1.81 ± 0.05	1.52 ± 0.08
VER/1 %HNTs	1	2.12 ± 0.16	2.93 ± 0.16
VER/3 %HNTs	3	2.43 ± 0.07	3.34 ± 0.13
VER/5 %HNTs	5	2.64 ± 0.12	4.14 ± 0.15

In pure VER (Fig. 9a), the fracture surface is flat and smooth except for some river line markings near the crack initiation site suggesting typical brittle fracture behavior and thus accounting for the low fracture toughness of VER [48]. Figure 9b–d provide useful evidence on the effect of 1, 3, and 5 wt% HNTs to the toughness properties of VER. These figures depict an increasing roughness of the fracture surfaces with increasing of HNTs. The roughness of the fracture surface is an indicator of the quantity of energy dissipated during fracture [49]. The fracture surfaces of VER/HNT composites exhibit visible and deep crack river-markings. With increasing HNT content, the fracture surfaces of samples are rougher and the crack bifurcation is more evident. Such visual features suggest crack path deflection due to the rigidness of the HNTs hindering crack propagation [33, 50].

SEM image in Fig. 10a–c reveals micro-sized white clusters on the fracture surfaces of the HNT/VER composites. These fine white particles are HNT clusters and are evenly distributed in the matrix. As discussed in previously, these clusters are embedded in the continuous phase and form rigid HNT-rich regions. These clusters can increase toughness by stopping the propagation of cracks. They can interact with passing cracks and resisting crack advancement [24, 25]. Plastic deformation of VER around particle clusters is clearly observed. Plastic deformation and crack deflection by clusters are principal toughening mechanisms in this study [26]. The clusters are believed to

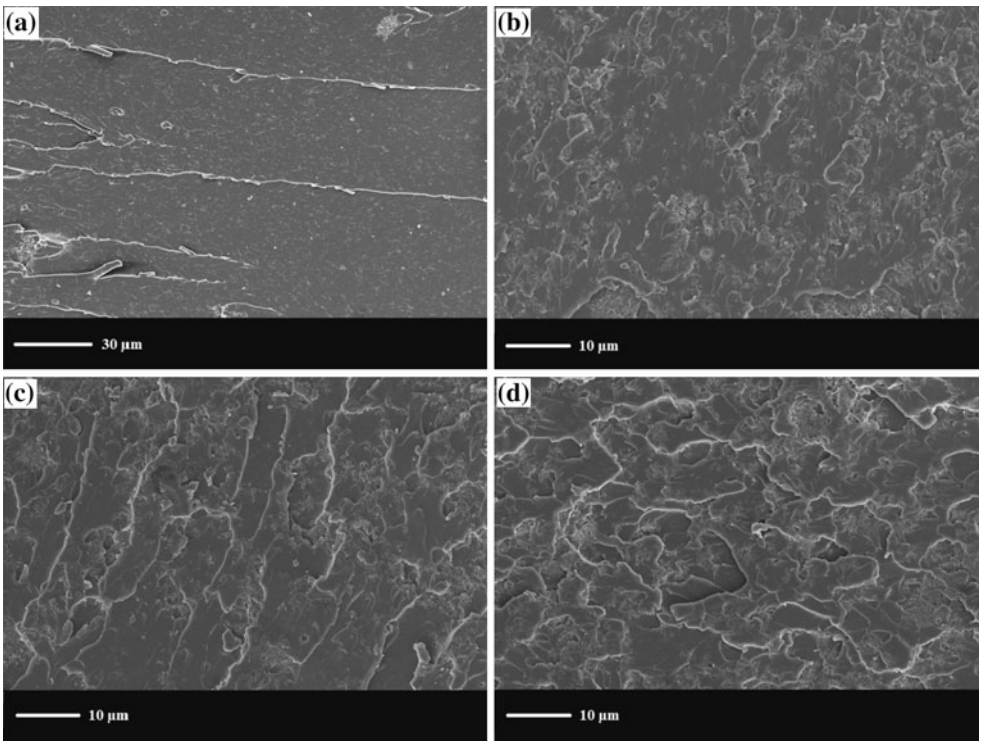

Fig. 9 SEM images showing the fracture surfaces of VER/HNT samples containing various amounts of HNTs: **a** 0 wt%, **b** 1.0 wt%, **c** 3.0 wt%, and **d** 5.0 wt%

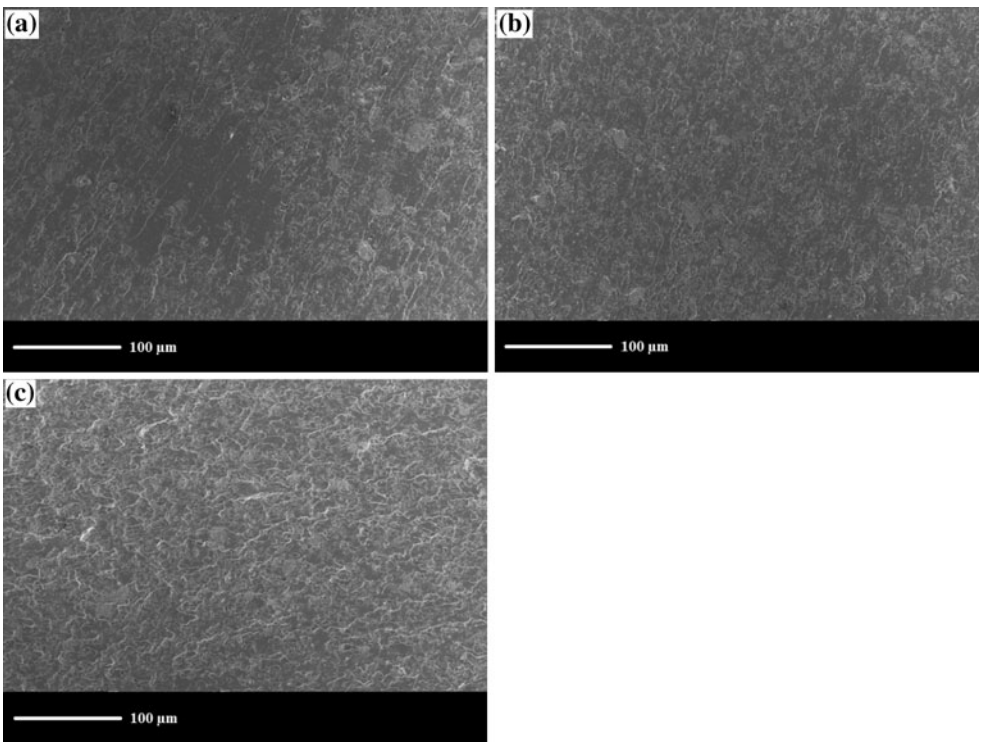

Fig. 10 SEM images showing the evidence of crack deflection and plastic deformation around HNT clusters in VER/HNT samples containing various amounts of HNTs: **a** 1.0 wt%, **b** 3.0 wt%, and **c** 5.0 wt%

resemble micro-sized rigid inorganic particles, which when confronting cracks hinder the crack propagation and cause crack deflection, twisting, and plastic deformation in particulate polymer composite [27, 28].

Individual HNT clusters can provide crack front pinning and bridging effects as a result of their large aspect ratios [1, 29]. In addition, breakage and de-bonding of HNT clusters, which consume extra energy and increase resistance to crack initiation and propagation, are additional mechanisms that individual HNTs provide to enhance toughness properties [30, 31].

Elastic modulus and strength properties

The flexural modulus, flexural strength, and impact strength of VER/HNT composites are summarized in Table 4, and the improvements in these properties due to HNT addition is apparent. With regards to flexural modulus, the addition of HNTs led to enhancement with baseline pure VER, 2.90 GPa, increasing to 3.11, 3.31, and 3.46 GPa after increasing the HNT content to 1, 3, and 5 wt%, respectively. Addition of HNTs achieved a moderate increase in flexural strength and impact strength. When pure VER reinforced with 1, 3, and 5 wt% HNTs, the flexural strength of resultant nanocomposites was found to be increased to 45.9, 51.1, and 56.5 MPa, respectively. Similarly, the addition of HNTs at 1, 3, and 5 wt% increased impact strength to 3.32, 4.15, and 4.45 kJ/m^2 respectively. Based on these results, the composites containing HNTs displayed increased modulus and strength properties compared to those of neat VER.

Table 4 Mechanical properties of VER and VER/HNT nanocomposites

Samples	HNTs content (wt%)	Flexural modulus (GPa)	Flexural strength (MPa)	Impact strength (kJ/m^2)
VER	0	2.90 ± 0.04	42.0 ± 2.4	2.60 ± 0.08
VER/1 %HNTs	1	3.11 ± 0.02	45.9 ± 2.1	3.32 ± 0.14
VER/3 %HNTs	3	3.31 ± 0.05	51.1 ± 1.8	4.15 ± 0.08
VER/5 %HNTs	5	3.46 ± 0.04	56.5 ± 2.0	4.45 ± 0.91

This postulation can be further supported by the fracture mode of three-point bending test samples shown in Fig. 11a–d. Clearly by comparing Fig. 11a of VER with Fig. 11b–d of VER/HNT composites, the roughness and tortuousity of the fracture surfaces can be seen to increase with an increase of HNT loading. Favorable interactions between HNTs and VER explain this difference in appearances [16, 48].

In general, the elastic modulus of a polymer matrix is enhanced by adding fillers that are rigid [8, 29]. Since HNTs have higher elastic modulus (30 GPa) than VER (2.90 GPa) and by virtue of the rule-of-mixtures, an improved elastic modulus was obtained for all VER/HNT composites. On the other hand, with respect to strength of particulate reinforced polymer composites, the size (micro/nano-scale) of particles in relation to the specific surface

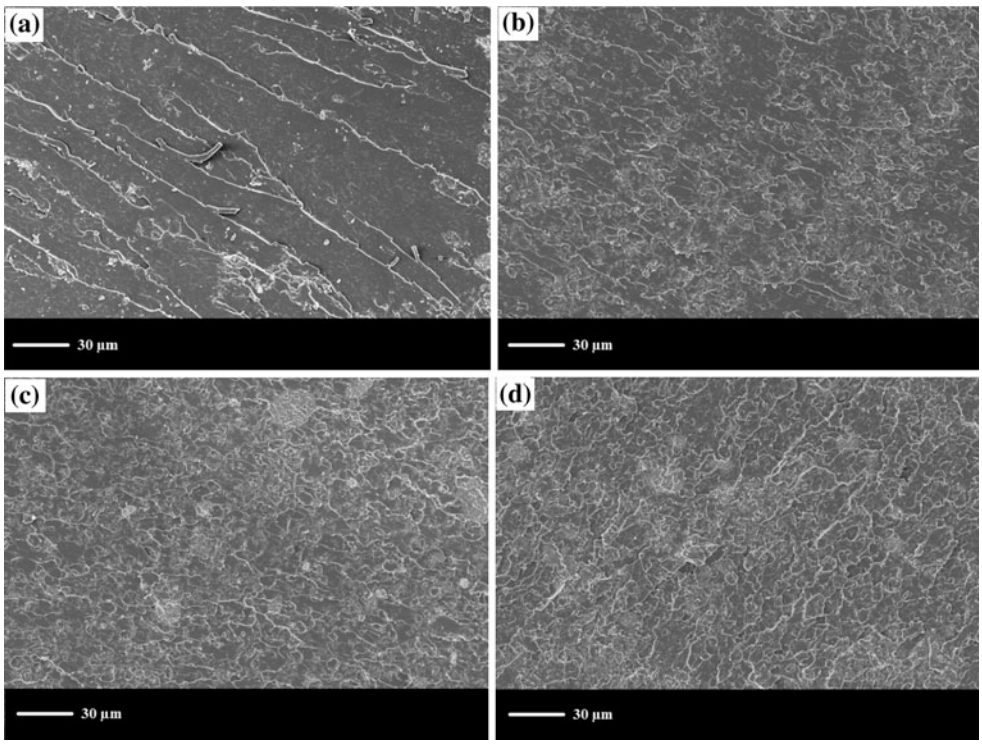

Fig. 11 SEM micrographs showing the fracture surfaces of VER/HNT samples containing various amounts of HNTs: **a** 0 wt%, **b** 1.0 wt%, **c** 3.0 wt%, and **d** 5.0 wt%

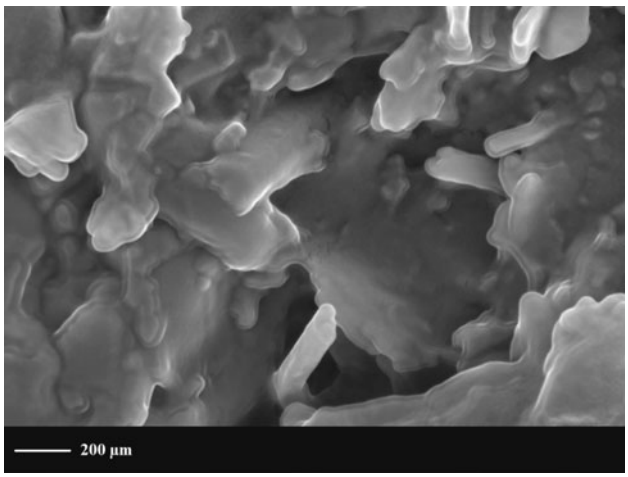

Fig. 12 SEM micrograph showing favorable adhesion between VER and HNTs, as evidence by the lack of obvious cavities at the particle/matrix interface

area [29], interfacial bonding between particles and matrix [24], and degrees of particle dispersion, are factors necessary for enhanced strength properties. These dynamics drive load transfer between reinforcing particles and matrix which is efficient and ultimately results in better strength properties for the composites [16, 29].

Compared to micro-scales fillers, the nano-scales fillers, such as the HNTs used in this study, have a high specific surface area allowing dense interfacial interaction with the polymer matrix. Typically, the specific surface area for this type of halloysite nanotube is about (65 m^2/g) [16]. This large contact surface area can provide a favorable adhesion and bonding between filler and matrix which increases the strength of the composite [7]. The SEM images in Fig. 12 show this favorable adhesion between VER and HNTs, where there are no obvious cavities at the particle/matrix interface. Also, the degree of filler dispersion as seen by TEM in this study is acceptable as discussed previously. Finally, the inter-tubular interaction between HNTs and VER can indicate a good bonding state between filler and matrix, which can be further factor increasing the strength properties [16]. All of these mechanisms mentioned above are believed to underpin the increased strength properties and overall mechanical properties of the composites of this study.

Thermal properties

The TGA curves for the VER and VER/HNTs composites are shown in Fig. 13 and the characteristic weight loss is reported in Table 5. The data reveals that for a temperature range from room temperature to 800 °C, the VER and all composites demonstrated single-stage thermal degradation. Pure VER displayed degradation at ~385 °C. Samples with 1, 3, and 5 wt% HNTs started degradation at ~406, 418, and 422 °C, respectively, thus demonstrating slightly higher thermal stability. The decomposition of samples continued until temperatures rose above 500 °C at which point a constant mass was achieved. At temperatures above 700 °C, the residual weight for pure VER was 8.2 wt% of the original. In contrast, samples modified with 1, 3, and 5 wt% HNTs, at the same temperature, had residual weights of 10, 10.8, and 12.8 wt%, respectively.

According to Table 5, the data highlights that loading of HNTs slightly enhances thermal stability with increases in characteristic weight loss temperatures.

Nonetheless, there is a clear relationship between the addition of HNTs and increases in thermal stability. This influence has been generally attributed to the high barrier properties of nano-fillers [5, 18]. Nano-fillers are believed to provide, first, a thermal barrier which prevents heat transfer inside polymer matrix [51, 52] and second, a mass transport barrier, which during the process of degradation

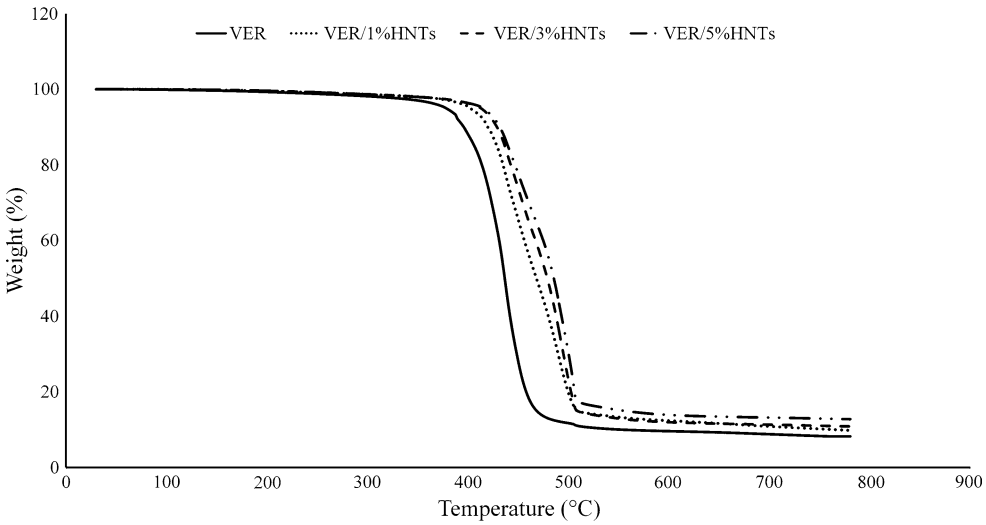

Fig. 13 TGA curves of VER and VER/HNT nanocomposites

Table 5 TGA data of VER and VER/HNT nanocomposites

Samples	HNTs (wt%)	Temperature at 20 % weight loss (°C)	Temperature at 40 % weight loss (°C)	Temperature at 60 % weight loss (°C)	Temperature at 80 % weight loss (°C)
VER	0	423	440	453	474
VER/1 %HNTs	1	435	456	479	503
VER/3 %HNTs	3	444	467	487	505
VER/5 %HNTs	5	446	474	493	507

forms a char which hinders the escape of the volatile products [53, 54]. This char is reported to be a high-performance carbonaceous silicate which provides a layer of insulation to underlying composite material [55]. The presence of iron oxides, Fe_2O_3, in silicate fillers is also believed to be a possible flame retardant enhancing thermal stability of composites by trapping radicals during the process of degradation [56, 57]. Some investigations, however, suggest that this is not a major factor due to the low content of iron oxides, Fe_2O_3, in HNTs [18]. The hollow tubular structure of HNTs is also reported to be another factor that leads to enhanced thermal stability of HNT reinforced composites [7, 51].

Flammability properties

Flammability tests conducted at ambient conditions included burning rate, burning-out rate, and ignition time determinations. Pure VER samples were found to burn out and ignite faster than VER/HNTs composites as seen in Table 6. Calculations imply that burning rate of pure VER at nearly twice the rate of 5 wt% VER/HNTs composite, thus highlighting the favorable flame retardancy properties of the composites.

During flammability test, the burning characteristics of the pure and nanocomposites were clearly different. When the test was started, pure VER immediately started dripping and continued with fast burning rate, until total loss of material in the end of the test. In contrast, the nanocomposites showed a different behavior; when the test started, the samples maintained a constant flame with much less burning rate, less dripping and at the end of the test; nanocomposites samples were completely charred. The barrier effects of HNTs are believed to be the dominant reasons for the reduction in flammability of VER/HNTs composites. First, the presence of HNTs within composites provides a mechanism of insulation which protects the polymer from contacting with fire [58]. Furthermore, char formation of HNTs act as a heat and fire-retardant [59]. However, recent work on flame retardancy of nanocomposites has indicated that flame retardancy may be attributed to a reduction in mass loss rate which in turn results in lower heat release and lower flame spread [60, 61].

Table 6 Flammability properties of VER and VER/HNT nanocomposites

Sample	Burning rate (mm/min)	Burning-out rate (g/min)	Ignition time (s)
VER	31.5 ± 1.7	0.67 ± 0.06	10.8 ± 1.6
VER/RCF/1 %HNT	27.1 ± 1.5	0.57 ± 0.07	12.9 ± 1.3
VER/RCF/3 %HNT	18.7 ± 1.8	0.48 ± 0.04	15.5 ± 1.4
VER/RCF/5 %HNT	16.8 ± 1.2	0.45 ± 0.05	17.9 ± 1.5

Conclusions

Pure VER and VER/HNTs composites have been fabricated and studied in terms of water absorption behaviors, mechanical, and thermal properties. With regards to water uptake, 5 wt% VER/HNTs composites demonstrated the most favorable reduction compared to pure VER, 1 and 3 wt% based on in weight gain and FTIR tests. The noticeable enhancements in strength properties for VER/HNTs composites found to be due to the large aspect ratio of HNT clusters, the good adhesion between HNT clusters and VER, the good degree of dispersion, and the suitable extent of inter-tubular interaction in composites. The HNTs were also found to be effective additives for improving toughness properties. Enhancements in these properties were attributable to crack bridging, deflection, and plastic deformation mechanisms around the HNT cluster. Clusters of HNTs can interact with cracks effectively resisting the advancement of the crack and leading to an increase in fracture toughness properties.

A clear relationship is supported between the addition of HNTs and enhanced thermal stability and flammability. The good thermal stability and flame retardant effects of HNTs can be attributed to the presence of iron and their hollow tubular structure, together with the provision of thermal and mass transport barriers.

Acknowledgements We are grateful to our colleague Dr. Nobuo Tezuka for providing HNTs for this study and we would like to thank Mr. Andreas Viereckl from Mechanical Engineering at Curtin University for assistance with mechanical tests. We would also like to thank Elaine Miller and Dr. Cat Kealley for their assistances with

SEM imaging and XRD data collection. Peter Chapman and Kristy Blyth from the Chemistry Department are thanked for their support in the preparation of the measurements for both FTIR and TGA experiments.

References

1. Yong V, Hahn HT (2004) Nanotechnology 15:1338
2. Mallick P (2007) Fiber-reinforced composites: materials, manufacturing, and design, 3rd edn. CRC Press: Taylor & Francis Group, New York
3. Cauvin L, Kondo D, Brieu M, Bhatnagar N (2010) Polym Test 29(2):245
4. Shokuhfar A, Zare-Shahabadi A, Atai A-A, Ebrahimi-Nejad S, Termeh M (2012) Polym Test 31(2):345
5. Zeng QH, Yu AB, Lu GQ, Paul DR (2005) J Nanosci Nanotechnol 5(10):1574
6. Pavlidou S, Papaspyrides CD (2008) Prog Polym Sci 33(12):1119
7. Rooj S, Das A, Thakur V, Mahaling RN, Bhowmick AK, Heinrich G (2010) Mater Des 31(4):2151
8. Handge UA, Hedicke-Höchstötter K, Altstädt V (2010) Polymer 51(12):2690
9. Meneghetti P, Guimarães L, Enyashin AN, Seifert G, Duarte HA (2010) J Phys Chem C 114(26):11358
10. Koh HC, Park JS, Jeong MA, Hwang HY, Hong YT, Ha SY (2008) Desalination 233(1–3):201
11. Marsh G (2007) Reinf Plast 51(8):20
12. Sultania M, Yadaw SB, Rai JSP, Srivastava D (2010) Mater Sci Eng A 27(18–19):4560
13. Holbery J, Houston D (2006) JOM J Miner Met Mater Soc 58(11):80
14. Ku H, Chan WL, Trada M, Baddeley D (2007) J Mater Eng Perform 16(6):741
15. Guo Z, Liang X, Pereira T, Scaffaro R, Thomas Hahn H (2007) Compos Sci Technol 67(10):2036
16. Ismail H, Pasbakhsh P, Fauzi MNA, Abu Bakar A (2008) Polym Test 27(7):841
17. Xie Y, Chang PR, Wang S, Yu J, Ma X (2011) Carbohydr Polym 83(1):186
18. Lecouvet B, Gutierrez JG, Sclavons M, Bailly C (2011) Polym Degrad Stab 96(2):226
19. Du M, Guo B, Jia D (2010) Polym Int 59(5):574
20. Liu M, Guo B, Du M, Cai X, Jia D (2007) Nanotechnology 18:455703
21. Zhao M, Liu P (2008) J Therm Anal Calorim 94(1):103
22. Marney DCO, Russell LJ, Wu DY, Nguyen T, Cramm D, Rigopoulos N (2008) Polym Degrad Stab 93(10):1971
23. Pasbakhsh P, Ismail H, Fauzi MNA, Bakar AA (2010) Appl Clay Sci 48(3):405
24. Hedicke-Höchstötter K, Lim GT, Altstädt V (2009) Compos Sci Technol 69(3–4):330
25. Dhakal HN, Zhang ZY, Richardson MOW (2007) Compos Sci Technol 67(7–8):1674
26. Low IM, McGrath M, Lawrence D, Schmidt P, Lane J, Latella BA (2007) Compos A Appl Sci Manuf 38(3):963
27. Plati E, Williams JG (1975) Polym Eng Sci 15(6):470
28. Joussein E, Petit S, Churchman J, Theng B, Righi D, Delvaux B (2005) Clay Miner 40(4):383
29. Deng S, Zhang J, Ye L, Wu J (2008) Polymer 49(23):5119
30. Ye Y, Chen H, Wu J, Ye L (2007) Polymer 48(21):6426
31. Kim J-K, Hu C, Woo RSC, Sham M-L (2005) Compos Sci Technol 65(5):805
32. Chang PR, Jian R, Yu J, Ma X (2010) Food Chem 120(3):736
33. Liu W, Hoa SV, Pugh M (2005) Compos Sci Technol 65(15–16):2364
34. Becker O, Varley RJ, Simon GP (2004) Eur Polym J 40(1):187
35. Mohan TP, Kanny K (2011) Compos A Appl Sci Manuf 42(4):385
36. Du M, Guo B, Lei Y, Liu M, Jia D (2008) Polymer 49(22):4871
37. Jinhua W, Xiang Z, Bing Z, Yafei Z, Rui Z, Jindun L (2010) Desalination 259(1–3):22
38. De Rosa IM, Kenny JM, Maniruzzaman M, Moniruzzaman M, Monti M, Puglia D (2011) Compos Sci Technol 71(2):246
39. Kong MJ, Lee SS, Lyubovitsky J, Bent SF (1996) Chem Phys Lett 263(1–2):1
40. Jebrane M, Sèbe G (2008) Carbohydr Polym 72(4):657
41. Scott TF, Cook WD, Forsythe JS (2002) Eur Polym J 38(4):705
42. Chang PR, Xie Y, Wu D, Ma X (2011) Carbohydr Polym 84(4):1426
43. Pasbakhsh P, Ismail H, Fauzi MNA, Bakar AA (2009) Polym Test 28(5):548
44. Karbowiak T, Ferret E, Debeaufort F, Voilley A, Cayot P (2011) J Membr Sci 370(1–2):82
45. Lasagabaster A, Abad MJ, Barral L, Ares A (2006) Eur Polym J 42(11):3121
46. Lasagabáster A, Abad MJ, Barral L, Ares A, Bouza R (2009) Polymer 50(13):2981
47. Muñoz MA, Carmona C, Balón M (2007) Chem Phys 335(1):37
48. Wang K, Chen L, Wu J, Toh ML, He C, Yee AF (2005) Macromolecules 38(3):788
49. Chen B, Evans JRG (2008) Polymer 49(23):5113
50. Tang Y, Deng S, Ye L, Yang C, Yuan Q, Zhang J (2011) Compos A Appl Sci Manuf 42(4):345
51. Du M, Guo B, Jia D (2006) Eur Polym J 42(6):1362
52. Paul DR, Robeson LM (2008) Polymer 49(15):3187
53. Kotsilkova R, Petkova V, Pelovski Y (2001) J Therm Anal Calorim 64(2):591
54. Leszczyńska A, Njuguna J, Pielichowski K, Banerjee JR (2007) Thermochim Acta 453(2):75
55. Chrissafis K, Bikiaris D (2011) Thermochim Acta 523(1–2):1
56. Kashiwagi T, Grulke E, Hilding J, Harris R, Awad W, Douglas J (2002) Macromol Rapid Commun 23(13):761
57. Zhu J, Uhl FM, Morgan AB, Wilkie CA (2001) Chem Mater 13(12):4649
58. Paul M-A, Alexandre M, Degée P, Henrist C, Rulmont A, Dubois P (2003) Polymer 44(2):443
59. Vyazovkin S, Dranca I, Fan X, Advincula R (2004) Macromol Rapid Commun 25(3):498
60. Wang L, He X, Wilkie CA (2010) Materials 3:4580
61. Kiliaris P, Papaspyrides CD (2010) Prog Polym Sci 35:902

3.6. Mechanical and fracture properties of halloysite nanotube reinforced vinyl-ester nanocomposites

---

ALHUTHALI, A. and LOW, I. M. 2013. Mechanical and fracture properties of halloysite nanotube reinforced vinyl-ester nanocomposites. *Journal of Applied Polymer Science,* DOI: 10.1002/app.39348

Journal of Applied Polymer Science

Mechanical and Fracture Properties of Halloysite Nanotube Reinforced Vinyl-Ester Nanocomposites

Abdullah Alhuthali, It-Meng Low
Department of Imaging and Applied Physics, Curtin University, GPO Box U1987, Perth, WA 6845, Australia
Correspondence to: I.-M. Low (E-mail: j.low@curtin.edu.au)

ABSTRACT: The mechanical and fracture properties of vinyl-ester composites reinforced with halloysite nanotubes have been investigated. Enhancements in toughness are attributed to crack bridging, deflection, and localized plastic deformation, while strength improvements can be attributed to the large aspect ratio of fillers, favorable interfacial adhesion and dispersion, and inter-tubular interaction. Comparisons of experimental data on elastic modulus and mathematical models for predicting particulate polymer composites have verified the models of Paul and Guth. The aspect ratio of fillers and the degree of interfacial adhesion are crucial factors in the prediction of elastic modulus in these polymer nanocomposites. © 2013 Wiley Periodicals, Inc. J. Appl. Polym. Sci. 000: 000–000, 2013

KEYWORDS: composites; mechanical properties; nanostructured polymers; nanotubes; graphene and fullerenes

Received 19 November 2012; accepted 10 February 2013; Published online 00 Month 2013
DOI: 10.1002/app.39348

INTRODUCTION

Polymer nanocomposites are blended polymer-based materials that contain one or more dimensions at the nano-scale level.[1] The presence of nano-fillers gives the material an extremely large surface area, an attribute that facilitates both rapid phase interaction and greater interfacial matrix interaction overall. It is this increased surface area that underpins the extraordinary properties of polymer nanocomposites.[2,3] The desirable aspect ratios and reduced pre-requisite for nano-fillers also lead to improved interfacial adhesion with the matrix. As such, polymer nanocomposites have superior advantages over pure and conventional composites in terms of mechanical, electrical, barrier, and thermal properties.[4–6]

Halloysite nanotubes (HNTs) are chemically similar to kaolin[7] and feature a two-layered aluminosilicate structure with hollow tubular morphology formed by rolling of layers.[8] The cylindrical shape of HNTs results from the tetrahedral and octahedral structure mismatch.[9] The lengths of the hollow tubes are between 1–15 μm with 10–30 nm inner and 50–70 nm outer diameters. This structure provides HNTs with a high aspect ratio and a very high surface area to promote a comprehensive filler and matrix interaction.[10] The hollow tubular structure of the fillers means that HNTs do not require exfoliation as in nanoclay platelets. HNTs can be easily dispersed in a polymer matrix, even at high weight fraction.[11] It is the rod-like geometry of HNTs, never intertwining, which makes dispersion of HNTs within the polymer even easier.[8]

In recent years, HNTs have become the subject of research attention as a new type of nano-filler for enhancing physical and mechanical properties of thermosets and thermoplastic polymers.[12] For example, Ye et al.[13] investigated the impact toughness of pure epoxy and epoxy/HNT nanocomposites. The addition of 2.3 wt % HNTs was found to increase the impact toughness from 0.54 kJ/m^2 for pure epoxy to 2.77 kJ/m^2 for the nanocomposite. They further concluded that when compared to montmorillonite (MMT), TiO_2, and other nano-filler modified epoxy nanocomposites, HNTs demonstrated a superior toughening effect. For example, only 35 and 60% increase in impact toughness was observed for epoxy/MMT nanocomposites[14] and epoxy/TiO_2 nanocomposites,[15] respectively. In contrast, a 400% increase in impact toughness was achieved for epoxy/HNTs nanocomposites.[13] In a similar study on epoxy/HNTs nanocomposites by Deng et al.,[16] they reported increases in both impact and fracture toughness without the loss of strength. These results further showed that both fracture toughness and impact toughness increased with an increase in filler content with an optimum loading of 5 wt % HNTs.

Vinyl-ester is a thermosetting polymer that has desirable mechanical properties which are suitable for coatings, adhesives, molding compounds, structural laminates, and electrical applications.[17] They are used in the fabrication of reinforced pipes, tanks, scrubbers, as well as hard-worked hull and deck structures in marine craft.[18] When compared to polyester resins, vinyl-esters higher design flexibility, better moisture resistance, better chemical resistance, excellent tensile, and flexural properties. In

fact, vinyl-ester resins have the best properties of epoxies and unsaturated polyesters. Thus, they are highly favored because of better control over cure rate and reaction conditions.[19–22]

Notwithstanding that HNTs have been used as fillers in matrices of epoxy, polystyrene, polypropylene, nylon-6, polyamide-6 among other[11,23–26], the addition of HNTs to vinyl ester is yet to be studied in depth. Thus, the motivation of this article was to investigate the feasibility of using HNTs to improve the mechanical and fracture properties of vinyl-ester resins. In particular, this study attempts to evaluate the influence of morphological factors of HNTs (i.e., filler dispersion, aspect ratio, and filler/matrix interaction) on the mechanical and fracture behavior of the resultant nanocomposites.

EXPERIMENTAL

Materials and Samples Preparation

Vinyl-ester resin (VER) was supplied by Fibreglass & Aesin Sales Pty, Australia, and ultrafine halloysite nanotubes (HNTs) were supplied by NZCC, New Zealand. According to the supplier, the elemental compositions (wt %) of HNTs were 50.4% SiO_2, 35.5% Al_2O_3, 0.25% Fe_2O_3, and 0.05% TiO_2. Pure samples of vinyl ester were prepared as controls by mixing the resin with 1.0 wt % methyl ethyl ketone peroxide (MEKP). The mixture was slowly and thoroughly mixed to ensure that no air bubbles formed within the matrix. The resultant mixture was poured into silicon moulds and left at room temperature under low vacuum (20 kPa) for 2 h, followed by curing at room temperature for 24 h. The nanocomposite samples were prepared by initially mixing the resin with 1, 3, or 5% of HNTs through the use of a high speed electrical-mixer (1200 rpm), followed by slow addition of MEKP as catalyst. The resultant mixtures were then poured into silicone molds, de-gassed in vacuum of 60 kPa at room temperature for 2 h, and cured under room conditions for 24 h. The samples were labeled as VER/1% HNTs, VER/3% HNTs, and VER/5% HNTs.

Microstructure Examination

The phase compositions of HNTs and HNT-reinforced vinyl-ester nanocomposites were characterized using a D8 Advance Diffractometer (Bruker-AXS) using copper radiations (λ = 1.5406 Å) and a LynxEye position sensitive detector. The XRD patterns of samples were collected by scanning from 3° to 50° (2θ) in steps of 0.02° using a scanning rate of 0.5°/min. The d-spacing of the layered particle was then calculated using Bragg's equation, ($\lambda = 2d \sin \theta$), where λ is the wavelength of X-rays, d is the interplanar distance, and θ is the Bragg angle. A transmission electron microscope (TEM; JEOL JEM2011, Japan) was used to study the morphologies of the HNTs and their dispersion within the matrix of vinyl-ester. Prior to TEM examination, samples of the HNTs were prepared by suspending the nanotubes in ethanol for 1 min, and then placed in ultra-sonic bath for 30 min. Then a droplet of suspension sprayed on a carbon thin film coated 400 mesh copper grid. An ultra microtome was used to prepare thin slices (~170 nm) of vinyl-ester/HNT samples for TEM examination.

A NEON 40ESB, scanning electron microscope (SEM; ZEISS, UK) was used to examine the microstructures of HNTs and fracture surfaces of the nanocomposites samples. All samples were coated with platinum prior to SEM examination to avoid charging.

Fracture Toughness

Rectangular single edge notch bend (SENB) samples of 10 mm × 10 mm × 60 mm dimension were used in fracture toughness testing. A sharp razor blade (with a notch-tip radius of 0.25 mm) was used to initiate a sharp crack on each sample. For all samples, the crack-to-width ratio (a/w) was limited to 0.5 and the span-to-width ratio (S/W) was maintained at 4. The tests were performed at room temperature with a LLOYD Material Testing Machine using a displacement rate of 1.0 mm/min. At least five samples of each batch were used and the mean value of fracture toughness was determined according to ASTM D5045-99 using the following equation:[27]

$$K_{\mathrm{IC}} = \frac{P_m S}{WD^{2/3}} f\left(\frac{a}{w}\right) \tag{1}$$

where K_{IC} is fracture toughness, P_m is the maximum load at fracture, S is the span of the sample, D is the specimen thickness, W is the specimen width, and a is the crack length, and $f(a/w)$ is the polynomial geometrical correction factor given as:[27]

$$f(a/w)=\frac{3(a/w)^{1/2}[1.99-(a/w)(1-a/w)(2.15-3.93a/w+2.7a^2/w^2)]}{2(1+2a/w)(1-a/w)^{2/3}} \tag{2}$$

Impact Toughness

A Zwick Charpy-impact tester with a 2.0 J pendulum hammer was used to determine the impact toughness at room temperature. At least five 40 mm span bar samples with varying notch lengths and razor-cracks were used. Values of impact toughness were determined according to the method of Plati and Williams[28] and calculated using the following equation:[27]

$$U = G_{\mathrm{IC}} BD\,\phi + U_0 \tag{3}$$

where G_{IC} is impact toughness, U is the measured energy, U_0 is the kinetic energy, D is the specimen thickness, B is the specimen breadth, and φ is the calibration factor for the geometry used.

Flexural Strength and Modulus

Rectangular bars with dimensions of (10 mm × 10 mm × 60 mm) were cut from the fully cured samples for three-point bend tests with a span of 40 mm to evaluate the flexural strength and flexural modulus according to ASTM D790-86. A LLOYD Material Testing Machine (5–50 kN) with a displacement rate of 1.0 mm/min was used to perform the test and all the tests were performed at room temperature. At least five samples of each group were used to evaluate flexural strength and flexural modulus. The values were recorded and analyzed with the aid of machine software (NEXYGENPlus) and the mean values were computed.

Impact Strength

A Zwick Charpy impact tester with a 2.0 J pendulum hammer was used to determine the impact strength at room temperature according to ASTM D 256-06. At least five bar samples of each

Table I. Mathematical Models Used to Compare with Experimental Data of This Work

Model Name	Model formula	Nomenclature
Reuss-Voigt[33,34]	$E_c^{Lower} = E_pE_m/[E_p(1-V_p) + E_mV_p]$	E_c = Elastic modulus of composite
	$E_c^{Upper} = E_pV_p + E_m(1-V_p)$	E_m = Elastic modulus of matrix
		V_p = Volume fraction of particles
Kerner[30,31]	$E_c/E_m = 1+\frac{V_p}{(1-V_p)}\frac{15(1-\nu_m)}{(8-10\nu_m)}$	V_m = Poisson ratio of matrix
Paul[30,31]	$E_c/E_m = \frac{1+(\delta-1)V_p^{2/3}}{1+(\delta-1)(V_p^{2/3}-V_p^{2/3})}$	$\delta = E_p/E_m$
Guth[32,33]	*For non-spherical particles* $E_c/E_m = (1 + 0.67\alpha V_p + 1.62\alpha^2V_p)$	α = Aspect ratio of the particles
Frankle-Acrivos[35,36]	$E_c/E_m = 1+\frac{9}{8}\left[\frac{V_p/\phi_{max})^{1/3}}{1-(V_p/V_{max})^{1/3}}\right]$	φ_{max} = *Maximum packing fraction of particles*

group with 40 mm span were used and the mean impact strength (σ_i) was calculated using the following equation:[29]

$$\sigma_i = \frac{E}{A} \quad (4)$$

where E is the impact energy to break a sample with a ligament area A.

Mathematical Modeling of Particulate-Reinforced Composites

There are a number of theoretical frameworks that have been developed to support the prediction of elastic modulus of polymer particulate reinforced composites. These sophisticated theories have been developed according to the requirements of different material or geometric parameters.[30,31] Conventionally, the elastic properties of a particulate–polymer composite's components (particle and matrix), its particle loading and its aspect ratio are used in determining the elastic modulus.[30] For example, for spherical particles, when the aspect ratio of particles equals unity, the elastic modulus of components and particle loading or particle size will be used to provide the composite modulus. The composite modulus is normally enhanced by adding particles to the matrix since the modulus of particles is usually much higher than that of the polymer matrices.[31,32] While the theories used for predicting elastic modulus of polymer particulate reinforced composites are to an extent satisfactory, the theories for predicting the strength and fracture toughness of particulate reinforced systems are less developed.[32,33] From this point, this study will limit the prediction of the mechanical properties of the composites to their elastic modulus. Table I outlines the name, formula, and nomenclature of six mathematical models for predicting elastic modulus. These mathematical models were used to compare experimental data from this study with the models to determine the applicability of the empirical relationships. The parameter values that correspond to the materials properties for mathematical model implementation are presented in Table II.

Table II. Values of Parameters Used in Mathematical Modeling

Parameters	Values	Reference
Average of aspect ratio of HNTs α	7[a]	
Elastic modulus of VER E_m (GPa)	2.9[b]	
Poisson ratio of matrix ν_m	0.35	37
Average of elastic modulus of HNTs E_p (GPa)	30	38,39
Maximum packing fraction ϕ_{max}	0.637	40
Density of VER	1.14[c]	
Density of HNTs	2.11[d]	

[a] Calculated based 50 numbers of HNT particles using SEM and TEM micrographs,

[b–d] Our experimental data.

RESULTS AND DISCUSSION

X-Ray Diffraction Analysis (XRD)

XRD patterns for pure HNTs and VER/HNT composites with 1, 3, and 5 wt % of HNTs are shown in Figure 1. A diffraction peak at 2θ of ~12.27° corresponding to the (001) plane can be seen in XRD pattern for pure HNTs. Two additional diffraction peaks at 2θ at ~20.15° and ~24.95° corresponding to (020) and (002) basal reflections are noticeable.[41,42] Trace amounts of quartz and feldspar are also evident and are represented by (*) and (+) respectively. The presence of these minerals in HNTs has also been noted by other researchers.[16,42]

For pure HNTs, a diffraction peak at a 2θ = 12.27° corresponds to a basal spacing of 0.721 nm. For VER/HNT composites, this diffraction peak has shifted towards lower 2θ values or larger basal spacing. The diffraction peaks, with corresponding basal spacing shown in parenthesis, for samples of VER/1% HNTs, VER/3% HNTs, and VER/5% HNTs were 11.87° (0.745 nm), 12.07° (0.733 nm), and 12.15° (0.728 nm), respectively (Table III). This increase in the basal spacing of HNTs in the composites sample suggests the existence of intercalation between vinyl-ester chains and the HNTs, thus confirming the formation of nanocomposites as also found in other studies.[10,41]

Microstructures of HNTs and Composites

SEM and TEM images of HNTS are shown in Figure 2. The images show that the majority of HNTs exist in a tubular shape, however, short tubular HNTs, and semi-rolled HNTs can also

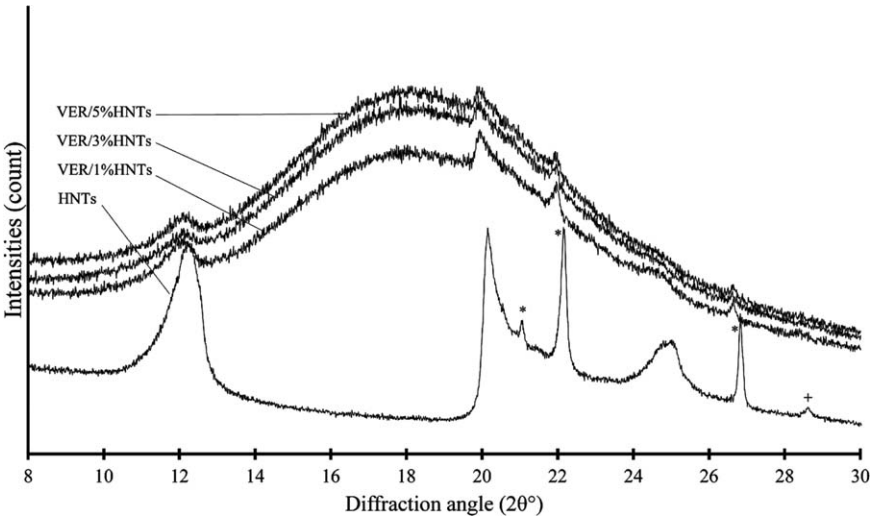

Figure 1. XRD pattern of pure HNTs and VER/HNTs composites.

Table III. XRD Results of HNTs and VER/HNTs Nanocomposites

Specific plane 2θ/d-spacing	(001)		(020)		(002)	
	2θ	d (nm)	2θ	d (nm)	2θ	d (nm)
HNTs	12.27	0.721	20.15	0.44	24.95	0.357
VER/1% HNTs	11.87	0.745	19.85	0.447	-	-
VER/3% HNTs	12.07	0.733	19.92	0.445	-	-
VER/5% HNTs	12.15	0.728	19.98	0.444	-	-

be seen. The image indicates that HNTs have a length ranging from 500 nm to 3 μm. From the image, the average outer diameters of the HNTs ranged from 100 to 300 nm whereas the average inner diameters ranged from 50 to 150 nm. The length/diameter ratio (i.e., aspect ratio) of HNTs varied between 3 and 15. Being a natural product, the size distribution of halloysite nanotubes is expected to be large.

The TEM micrographs in Figure 3(a–c) display the uniform dispersion of HNT fillers in the vinyl-ester (VER) matrix. The extent of dispersion is acceptable even though a number of micro-sized HNT clusters can be found. HNTs were randomly dispersed in the matrix with short inter-tube distances resulting in formation of HNT-rich region and long inter-tube distances resulting in VER-rich region being formed as shown in Figure 4(a). The HNT-rich regions give the appearance of HNT clusters. However, a closer examination reveals that VER has filled spaces between these clusters [Figure 4(b)]. In other words, the morphology of the HNT/VER composites displays a continuous

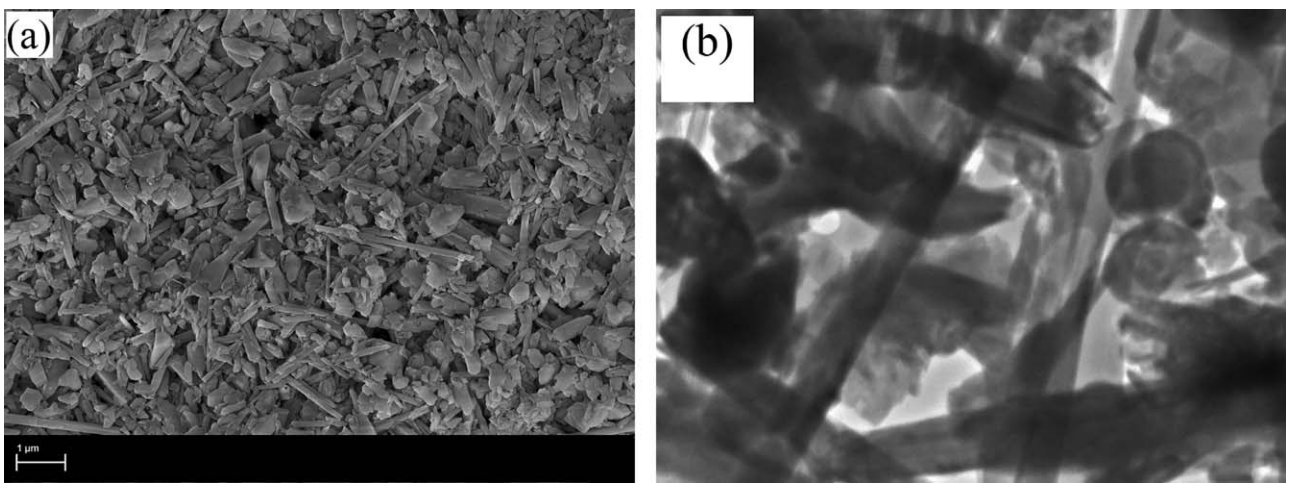

Figure 2. (a) SEM micrograph of HNTs particles and (b) TEM micrograph of HNTs particles.

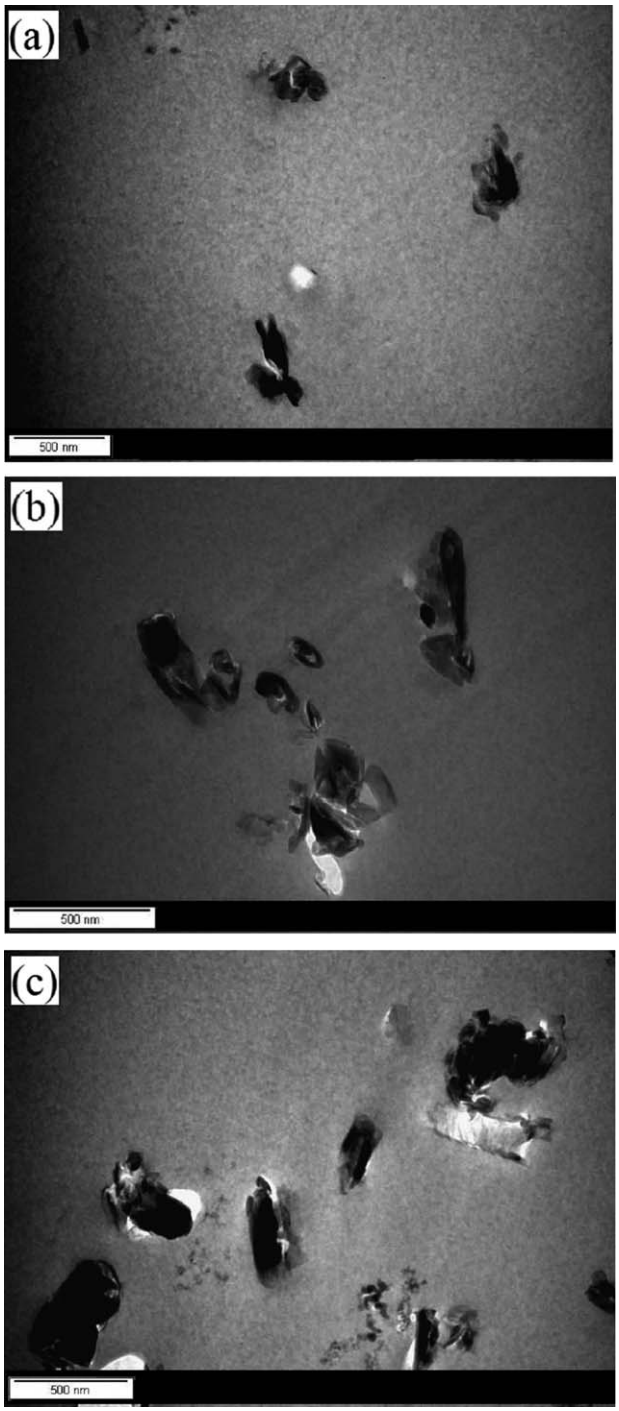

Figure 3. Dispersion of HNTs particles within cured VER (a) 1 wt % of HNTs, (b) 3 wt % of HNTs, and (c) 5 wt % of HNTs.

phase and a discontinuous phase. The continuous phase is the VER-rich regions in which a good dispersion of individual HNT clusters is clear. In contrast, the agglomeration of HNT clusters embedded in this continuous phase forms the rigid discontinuous phase.[13,16]

Toughness Properties

The results of fracture toughness and impact toughness are shown in Table IV. The results show that the addition of HNTs has led to enhanced toughness values for all VER/HNT composites samples. For example, compared to the fracture toughness of pure VER (1.81 MPa $m^{1/2}$), the fracture toughness of VER/HNT samples were higher with 17% increase for HNT loading of 1.0 wt %, 34% increase for 3.0 wt % loading, and 46% increase for 5.0 wt % loading. Similarly, the addition of HNTs at 1, 3, and 5 wt % increased the impact toughness of pure VER (1.52 kJ/m^2) by 93, 118, and 172%, respectively.

Figure 5(a) shows the fracture surface of pure VER which is flat and smooth except for some river line markings near the crack initiation site which indicates typical brittle fracture behavior or low fracture toughness.[43] In contrast, the non-planar fracture surfaces of VER/HNT nanocomposites are shown in Figure 5(b–d). These figures depict an increasing roughness of the fracture surfaces with increasing loading of HNTs. The roughness of the fracture surface is an indicator of the quantity of energy dissipated during fracture.[44] With increasing HNT content, the fracture surfaces of these samples become rougher and the crack bifurcation is more evident. Such visual features suggest crack path deflection due to the rigidness of HNTs in hindering crack propagation.[37,45]

SEM images in Figure 6(a–c) reveal micro-sized white fillers on the fracture surfaces of the VER/HNT nanocomposites. These fine white fillers are HNT clusters and are evenly distributed within the matrix. These clusters can increase toughness by stopping the propagation of cracks through interacting with passing cracks and resisting crack advancement.[13,46] Plastic deformation of VER around clusters is also evident. Plastic deformation and crack deflection by these clusters are the principal toughening mechanisms observed in this study.[16] These clusters are believed to resemble micro-sized rigid inorganic particles, which when confronting cracks hinder the crack propagation and cause crack deflection, twisting, and plastic deformation in particulate polymer composite.[47–49]

The effectiveness of HNTs in imparting toughness needs to be assessed against alternative fillers such as nanoclay or rubbery particles. In an attempt to improve the fracture toughness of vinyl-ester, nanoclay and/or core shell rubber (CSR) particles were used by Subramaniyan and Sun.[4] Their results showed that an improvement in fracture toughness of 12% was achieved by CSR, whereas the addition of nanoclay and nanoclay/CSR caused a reduction in fracture toughness by 16 and 6%, respectively. Therefore, HNTs may be preferable to nanoclay for improving the toughness of vinyl-esters.

Flexural Modulus and Strength Properties

The flexural modulus, flexural strength, and impact strength of VER/HNT composites are summarized in the Table V, and the improvements in these properties due to HNT addition is evident. With regards to flexural modulus, the addition of HNTs has led to an improvement from 2.90 GPa to 3.11, 3.31, and 3.42 GPa for HNT loading of 1, 3, and 5 wt %, respectively. The addition of HNTs caused a moderate increase in flexural strength and impact strength. When pure VER is reinforced with 1, 3, and 5 wt % HNTs, the flexural strength of resultant nanocomposites increased to 45.9, 51.1, and 56.5 MPa,

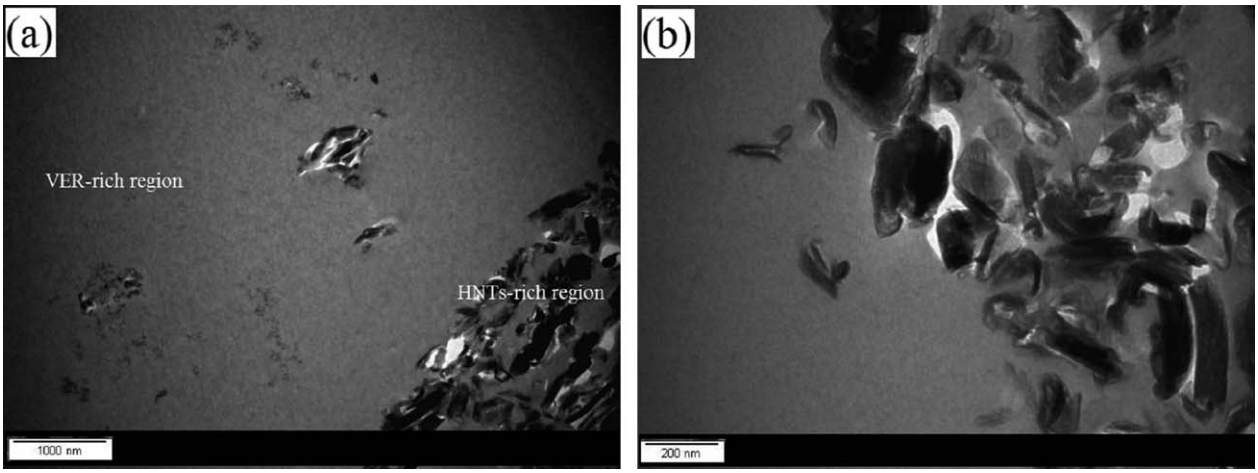

Figure 4. TEM micrographs of VER/HNTs Nanocomposites (a) VER-rich region and HNTs-rich region and (b) Spaces between HNTs particles cluster clearly filled by VER.

Table IV. Fracture Properties of VER and VER/HNTs Nanocomposites

Samples	HNT content (wt %)	Fracture toughness (MPa $m^{1/2}$)	Impact toughness (kJ/m^2)
VER	0	1.8 ± 0.1	1.5 ± 0.1
VER/1% HNTs	1	2.1 ± 0.2	2.9 ± 0.2
VER/3% HNTs	3	2.4 ± 0.1	3.3 ± 0.1
VER/5% HNTs	5	2.6 ± 0.1	4.1 ± 0.2

respectively. Similarly, the addition of HNTs at 1, 3, and 5 wt % increased the impact strength to 3.32, 4.12, and 4.45 kJ/m^2, respectively. Based on these results, the nanocomposites containing HNTs displayed increased modulus and strength properties when compared to neat VER. This observation is further supported by the fracture surface shown in Figure 7(a–d). When comparing Figure 7(a) of VER with Figure 7(b–d) of VER/HNT nanocomposites, the roughness and tortuousity of the fracture surfaces can be seen to increase with increasing HNT loading.

In general, the elastic modulus of a polymer matrix is enhanced by adding fillers that are rigid.[30,35] Since HNTs have higher elastic modulus (30 GPa) than VER (2.90 GPa) and by virtue of the rule-of-mixtures, an improved elastic modulus was obtained for all VER/HNT nanocomposites. On the other hand, with respect to strength of particulate reinforced polymer composites, the size (micro/nanoscale) of particles in relation to the specific

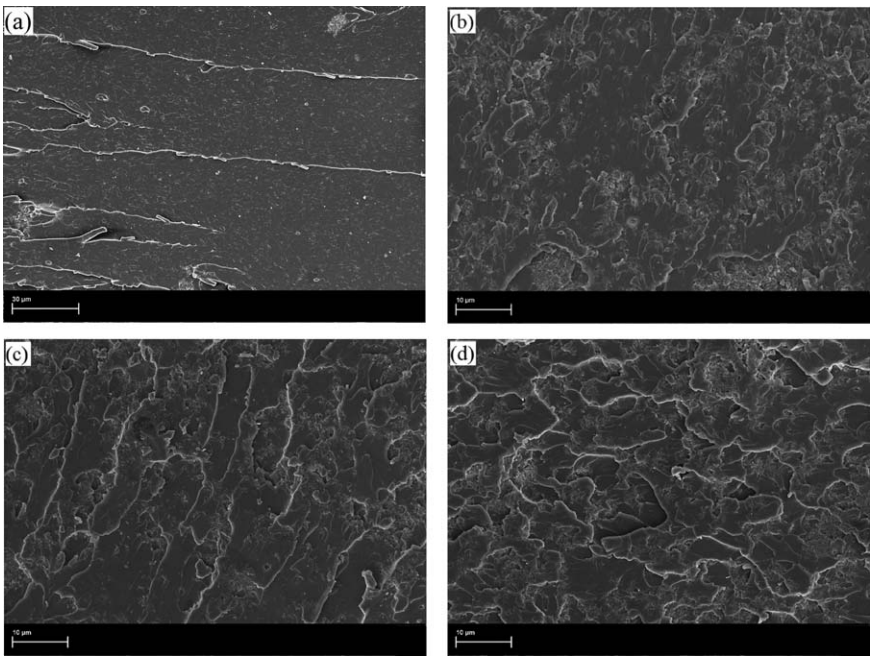

Figure 5. SEM images of fracture surfaces of (a) VER, (b) VER/HNTS composite with 1 wt % HNTs loading, (c) VER/HNTs composite with 3 wt % HNTs loading (d) VER/HNTs composite with 5 wt % HNTs loading. All samples had been subjected to fracture toughness test.

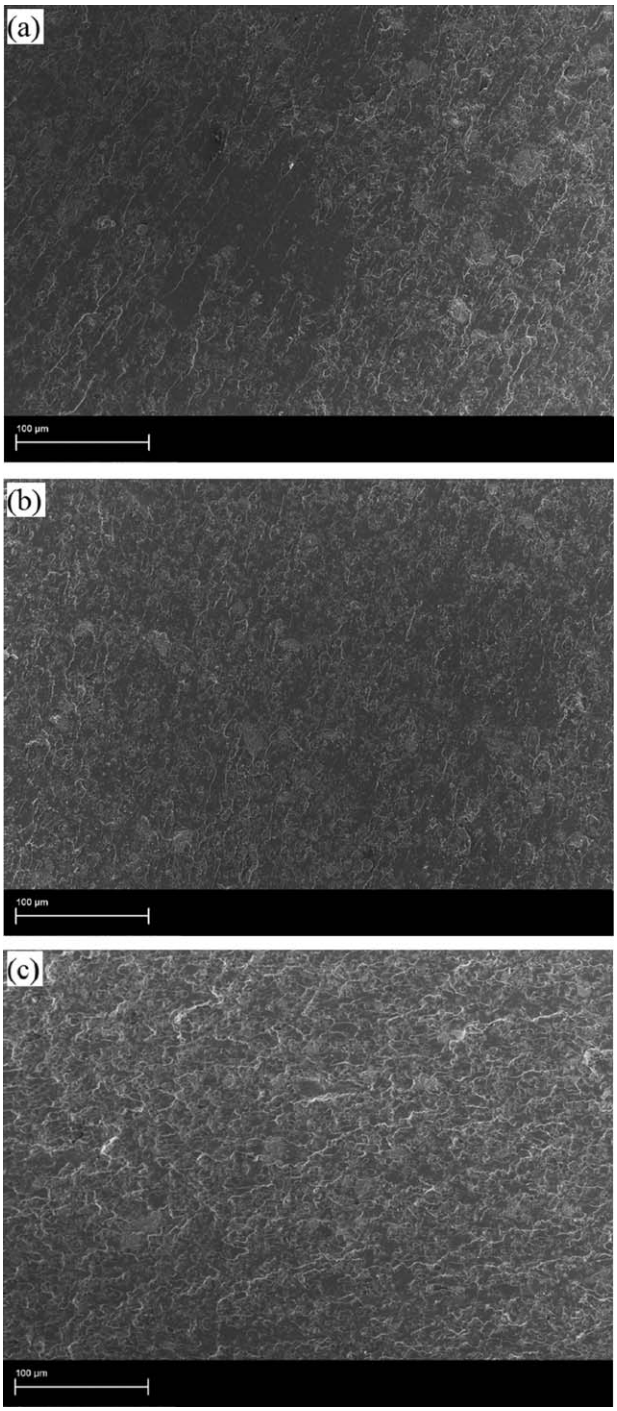

Figure 6. Fracture surfaces of VER/HNTs composites with (a) 1% wt of HNTs loading, (b) 3% wt HNTs loading, and 5% wt HNTs loading, showing crack deflection and plastic deformation around HNTs particle clusters.

surface area,[31] interfacial bonding between particles and matrix,[11] and degrees of particle dispersion,[50] are factors necessary for enhanced strength properties. These dynamics drive the load transfer between reinforcing particles and matrix which is efficient and ultimately results in better strength properties for the composites.[31,41]

Compared to micro-scales fillers the nano-scales fillers, such as the HNTs have a high specific surface area which allows dense interfacial interaction with the polymer matrix. Typically the specific surface area for halloysite nanotubes is about (65 m^2/g).[41] This large contact surface area can provide a favorable adhesion and bonding between filler and matrix which increases the strength of the composite. The SEM images in Figure 8 show this favorable adhesion between VER and HNTs, where there are no obvious cavities at the particle/matrix interfaces. Finally, the inter-tubular interaction between HNTs and VER can indicate a good bonding state between filler and matrix, which can serve to increase the strength properties.[41] All of these mechanisms mentioned above are believed to underpin the increased strength properties and overall mechanical properties of the nanocomposites of this study.

Comparisons with Theoretical Models

The experimental data on flexural modulus in this study were compared with well-known mathematical models of elastic modulus (Figure 9). One test of validity is the Reuss–Voigt model, which is an approximate theory, identifying upper and lower bounds of values for a predicted solution of elastic modulus for particulate reinforced composites. The validity of elastic modulus for most particulate micro- and nano-composites can be tested using the Reuss–Voigt model by comparing experimental data elastic modulus values with the lower and upper bounds provided by this model.[32] Results that fall between the bounds are believed to be valid. In the case of composites reinforced with a filler of large aspect ratio and strong adhesion between filler and matrix, the upper bound of Reuss–Voigt model is appropriate. In the case of rigid spherical fillers, the lower bound is applicable.[34,51] The model supports the validity of elastic modulus results in this study. All experimental and predicted data value fell between the upper bounds and lower bounds. Interestingly, the experimental data lie close to the upper bounds. This can be attributed to the large aspect ratio of HNTs and the good adhesion between HNTs and VER. Both the Paul model and the Guth model agree well with the experimental results. The assumption of a perfect adhesion between the particles and matrix underpins the Paul model.[30,31] Thus the experimental data is believed to support adequate adhesion between the filler and matrix in the nanocomposite samples. The microstructures observed by SEM and TEM also supported adequate interfacial bonding between HNTs and VER. The Guth model also assumes perfect adhesion between filler and matrix, but also assumes perfect dispersion, and large particle aspect ratio.[30,32] Thus the experimental results here support adequate adhesion between the filler and matrix, acceptable dispersion, and that the majority of HNTs were found to exist in a tubular shape with an aspect ratio of between 3 and 15.

Nonetheless, both models of Paul and Guth have over-predicted the modulus of the samples in this study for cases where the volume fraction increased to 5 wt %. This discrepancy is most likely explained by the formation of HNT clusters in the 5 wt % nanocomposites. These clusters within the samples can affect the load bearing capability and result in a lower elastic

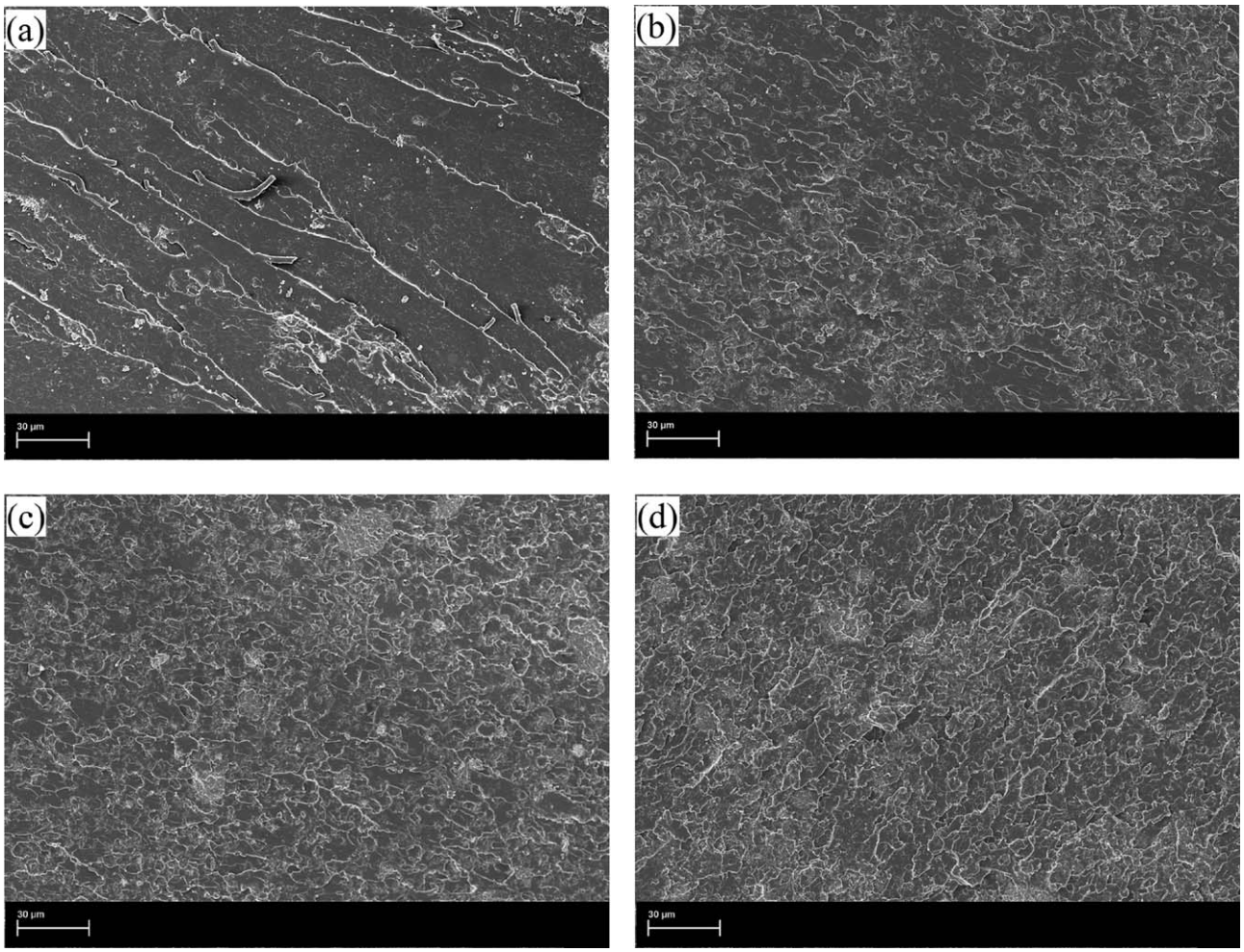

Figure 7. SEM micrographs of fracture surfaces of (a) pure VER/HNTS composite, VER/HNTs composites with 1 wt % HNTs loading, (c) VER/HNTs composite with 3 wt % HNTs loading, and (d) VER/HNTs composite with 5 wt % HNTs loading. All samples had been subjected to flexural strength test.

modulus.[33] At the same time, overall aspect ratio of HNTs can be reduced due to the formation of clusters[52] and also during processing due to the shearing effect which breaks the HNTs.[50] The models of Paul and Guth do not take into consideration the formation of clusters or the reduction in aspect ratio of the fillers. The Kerner model is a measure of validity for composite systems in which the modulus of filler is many times higher than the modulus of the matrix.[31,35] The relative modulus ratio of fillers to matrix in this study is low which explains the lack

Table V. Mechanical Properties of VER and VER/HNTs Nanocomposites

Samples	HNTs content (wt%)	Flexural modulus (GPa)	Flexural strength (MPa)	Impact strength (kJ/m^2)
VER	0	2.90 ± 0.04	42.0 ± 2.4	2.6 ± 0.1
VER/1% HNTs	1	3.11 ± 0.02	45.9 ± 2.1	3.3 ± 0.1
VER/3% HNTs	3	3.31 ± 0.05	51.1 ± 1.8	4.1 ± 0.1
VER/5% HNTs	5	3.46 ± 0.04	56.5 ± 2.0	4.5 ± 0.9

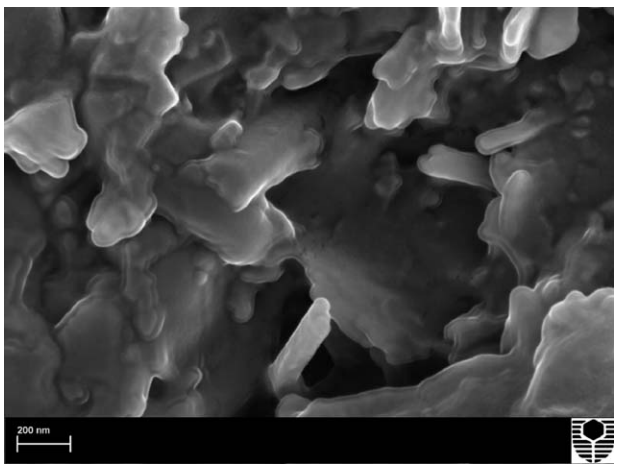

Figure 8. SEM micrograph showing favorable adhesion between VER and HNTs.

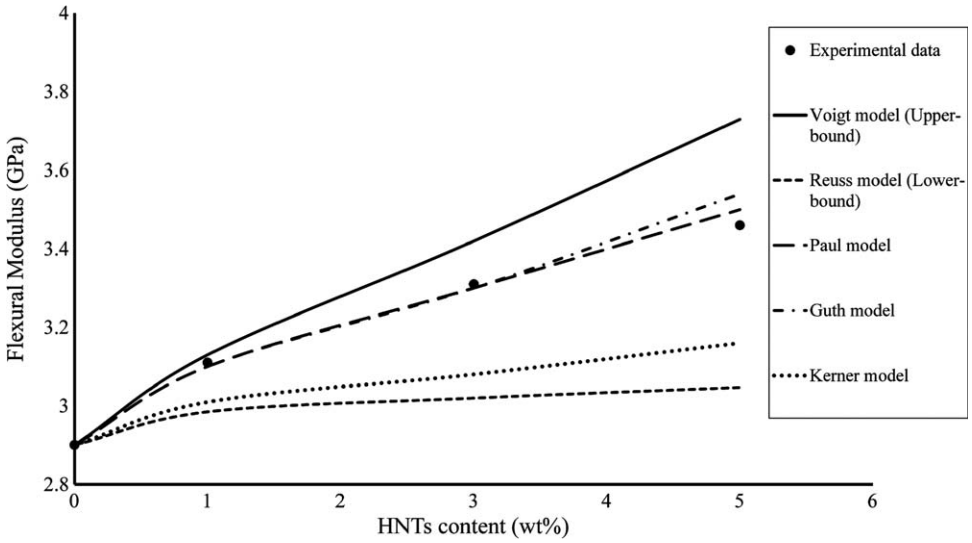

Figure 9. Comparison of experimental data for flexural modulus against HNTs content with results extrapolated from published models.

of agreement between experimental data when compared to the Kerner model. The study parameters applied to Frankle-Acrivos model (not shown) totally over-estimated the modulus of the samples in this study. The model uses the simple relative filler volume fraction (V_p/φ_{max}), thus only takes into consideration a partly dominant effect of particle packing efficiency on the elastic properties. The model neglects particle and matrix interfacial interactions, the Young's modulus and Poisson's ratio effects, which are all important factors that influence the elastic properties of composites.[31,33,34]

In summary, based on current findings and the results of other studies,[16,31,53,54] the aspect ratio of fillers, and, in particular, the state of adhesion between fillers and matrix are both significant factors that should be taken into account when predicting the elastic modulus of particulate-reinforced composites. The postulation that adhesion between fillers and matrix is a significant determinant of elastic modulus contradicts the findings of earlier studies as reviewed by Ahmed and Jones[30] and Fu et al.[32] In contrast to the results of this study, some of the earlier investigations suggested that adhesion between fillers and matrix was an insignificant or irrelevant factor in relation to the prediction of elastic modulus for particulate–polymer composites.

CONCLUSIONS

Pure VER and VER/HNT nanocomposites have been synthesized and characterized in terms of mechanical and fracture properties. HNTs were found to be an effective additive for improving the toughness of vinyl-esters. Enhancements in these properties were attributed to crack bridging, deflection, and plastic deformation in the vicinity of HNT clusters served to interact with cracks effectively to resist the advancement of the crack propagation. The enhancement in strength properties for VER/HNT composites was ascribed to the large aspect ratio of HNTs, good interfacial adhesion, good degree of dispersion, and adequate inter-tubular interaction. The good agreement of experimental data with models of Paul and Guth suggests that the aspect ratios of fillers, their dispersion within the matrix, and the state of interfacial adhesion are relevant to the prediction of elastic modulus for particulate reinforced polymer composites.

ACKNOWLEDGMENTS

We are grateful to our colleague Dr. Nobuo Tezuka for providing HNTs for this study. We would also like to thank Elaine Miller and Dr. Cat Kealley for their assistance with SEM imaging and XRD data collection.

REFERENCES

1. Yong, V.; Hahn, H. T. *Nanotechnology* **2004**, *15*, 1338.
2. Cauvin, L.; Kondo, D.; Brieu, M.; Bhatnagar, N. *Polym. Test.* **2010**, *29*, 245.
3. Shokuhfar, A.; Zare-Shahabadi, A.; Atai, A.-A.; Ebrahimi-Nejad, S.; Termeh, M. *Polym. Test.* **2012**, *31*, 345.
4. Subramaniyan, A. K.; Sun, C. T. *Compos. Part A: Appl. Sci. Manuf.* **2007**, *38*, 34.
5. Zeng, Q. H.; Yu, A. B.; Lu, G. Q.; Paul, D. R. *J. Nanosci. Nanotechnol.* **2005**, *5*, 1574.
6. Pavlidou, S.; Papaspyrides, C. D. *Prog. Polym. Sci.* **2008**, *33*, 1119.
7. Ismail, H.; Salleh, S. Z.; Ahmad, Z. *Int. J. Polym. Mater.* **2012**, *50*, 681.
8. Xie, Y.; Chang, P. R.; Wang, S.; Yu, J.; Ma, X. *Carbohydr. Polym.* **2011**, *83*, 186.
9. Lecouvet, B.; Gutierrez, J. G.; Sclavons, M.; Bailly, C. *Polym. Degrad.Stab.* **2011**, *96*, 226.
10. Rooj, S.; Das, A.; Thakur, V.; Mahaling, R. N.; Bhowmick, A. K.; Heinrich, G. *Mater. Design* **2010**, *31*, 2151.
11. Hedicke-Höchstötter, K.; Lim, G. T.; Altstädt, V. *Compos. Sci. Technol.* **2009**, *69*, 330.

12. Prashantha, K.; Schmitt, H.; Lacrampe, M. F.; Krawczak, P. *Compos. Sci. Technol.* **2011**, *71*, 1859.
13. Ye, Y.; Chen, H.; Wu, J.; Ye, L. *Polymer* **2007**, *48*, 6426.
14. Isik, I.; Yilmazer, U.; Bayram, G. *Polymer* **2003**, *44*, 6371.
15. Wetzel, B.; Haupert, F.; Friedrich, K.; Zhang, M. Q.; Rong, M. Z. *Polym. Eng. Sci.* **2002**, *42*, 1919.
16. Deng, S.; Zhang, J.; Ye, L.; Wu, J. *Polymer* **2008**, *49*, 5119.
17. Sultania, M.; Yadaw, S. B.; Rai, J. S. P.; Srivastava, D. *Mater. Sci. Eng. A* **2010**, *527*, 4560.
18. Marsh, G. *Reinforced Plast.* **2007**, *51*, 20.
19. Alhuthali, A.; Low, I. M.; Dong, C. *Compos. Part B: Eng.* **2012**, *43*, 2772.
20. Guo, Z.; Lei, K.; Li, Y.; Ng, H. W.; Prikhodko, S.; Hahn, H. T. *Compos. Sci. Technol.* **2008**, *68*, 1513.
21. Abdelwahab, M.; Agag, T.; Akelah, A.; Takeichi, T. *Polym. Eng. Sci.* **2012**, *52*, 125.
22. Ratna, D.; Khan, S.; Barman, S.; Chakraborty, B. *Open Macromol. J.* **2012**, *6*, 59.
23. Deng, S.; Zhang, J.; Ye, L. *Compos. Sci. Technol.* **2009**, *69*, 2497.
24. Lecouvet, B.; Sclavons, M.; Bourbigot, S.; Devaux, J.; Bailly, C. *Polymer* **2011**, *52*, 4284.
25. Marney, D. C. O.; Russell, L. J.; Wu, D. Y.; Nguyen, T.; Cramm, D.; Rigopoulos, N.; Wright, N.; Greaves, M. *Polym. Degrad. Stab.* **2008**, *93*, 1971.
26. Zhao, M.; Liu, P. *J. Thermal Anal. Calorim.* **2008**, *94*, 103.
27. Low, I. M.; McGrath, M.; Lawrence, D.; Schmidt, P.; Lane, J.; Latella, B. A.; Sim, K. S. *Compos. Part A: Appl. Sci. Manuf.* **2007**, *38*, 963.
28. Plati, E.; Williams, J. G. *Polym. Eng. Sci.* **1975**, *15*, 470.
29. Low, I. M.; Somers, J.; Kho, H. S.; Davies, I. J.; Latella, B. A. *Compos. Interfaces* **2009**, *16*, 659.
30. Ahmed, S.; Jones, F. R.; *J. Mater. Sci.* **1990**, *25*, 4933.
31. Dong, Y.; Chaudhary, D.; Ploumis, C.; Lau, K.-T. *Compos. Part A: Appl. Sci. Manuf.* **2011**, *42*, 1483.
32. Fu, S.-Y.; Feng, X.-Q.; Lauke, B.; Mai, Y.-W. *Compos. Part B: Eng.* **2008**, *39*, 933.
33. Yan, W.; Lin, R. J. T.; Bhattacharyya, D. *Compos. Sci. Technol.* **2006**, *66*, 2080.
34. Chan, C.-M.; Wu, J.; Li, J.-X.; Cheung, Y.-K. *Polymer* **2002**, *43*, 2981.
35. Kaully, T.; Siegmann, A.; Shacham, D. *Polym. Compos.* **2008**, *29*, 396.
36. Reynaud, E.; Jouen, T.; Gauthier, C.; Vigier, G.; Varlet, J. *Polymer* **2001**, *42*, 8759.
37. Stevanovic, D.; Kalyanasundaram, S.; Lowe, A.; Jar, P. Y. B. *Compos. Sci. Technol.* **2003**, *63*, 1949.
38. Guimarães, L.; Enyashin, A. N.; Seifert, G.; Duarte, H. l. A. *J. Phys. Chem. C* **2010**, *114*, 11358.
39. Handge, U. A.; Hedicke-Höchstötter, K.; Altstädt, V. *Polymer* **2010**, *51*, 2690.
40. Bigg, D. M. *Polym. Compos.* **1987**, *8*, 115.
41. Ismail, H.; Pasbakhsh, P.; Fauzi, M. N. A.; Abu Bakar, A. *Polym. Test.* **2008**, *27*, 841.
42. Joussein, E.; Petit, S.; Churchman, J.; Theng, B.; Righi, D.; Delvaux, B. *Clay Miner.* **2005**, *40*, 383.
43. Wang, K.; Chen, L.; Wu, J.; Toh, M. L.; He, C.; Yee, A. F. *Macromolecules* **2005**, *38*, 788.
44. Chen, B.; Evans, J. R. G. *Scripta Mater.* **2006**, *54*, 1581.
45. Tang, Y.; Deng, S.; Ye, L.; Yang, C.; Yuan, Q.; Zhang, J.; Zhao, C. *Compos. Part A: Appl. Sci. Manuf.* **2011**, *42*, 345.
46. Lee, J.-H.; Jung, D.; Hong, C.-E.; Rhee, K. Y.; Advani, S. G. *Compos. Sci. Technol.* **2005**, *65*, 1996.
47. Meng, J.; Hu, X. *Polymer* **2004**, *45*, 9011.
48. Wetzel, B.; Rosso, P.; Haupert, F.; Friedrich, K. *Eng. Fract. Mech.* **2006**, *73*, 2375.
49. Ye, Y.; Chen, H.; Wu, J.; Chan, C. M. *Compos. Sci. Technol.* **2011**, *71*, 717.
50. Ning, N.-y.; Yin, Q.-j.; Luo, F.; Zhang, Q.; Du, R.; Fu, Q. *Polymer* **2007**, *48*, 7374.
51. Alam, P. *Mech. Res. Commun.* **2010**, *37*, 389.
52. Gantenbein, D.; Schoelkopf, J.; Matthews, G. P.; Gane, P. A. C. *Appl. Clay Sci.* **2011**, *53*, 538.
53. Ahmad, F. N.; Jaafar, M.; Palaniandy, S.; Azizli, K. A. M. *Compos. Sci. Technol.* **2008**, *68*, 346.
54. Masouras, K.; Silikas, N.; Watts, D. C. *Dental Mater.* **2008**, *24*, 932.

3.7. Characterization of Mechanical and Fracture Behaviour in Nano-Silicon Carbide Reinforced Vinyl-Ester Nanocomposites

---

ALHUTHALI, A. and LOW, I. M. 2013. Characterization of Mechanical and Fracture Behaviour in Nano-Silicon Carbide-Reinforced Vinyl-Ester Nanocomposites. *Polymer-Plastics Technology and Engineering*, 52, 921-930.

Polymer-Plastics Technology and Engineering, 52: 921–930, 2013

ISSN: 0360-2559 print/1525-6111 online
DOI: 10.1080/03602559.2013.763372

Taylor & Francis
Taylor & Francis Group

Characterization of Mechanical and Fracture Behaviour in Nano-Silicon Carbide-Reinforced Vinyl-Ester Nanocomposites

Abdullah M. Alhuthali and It-Meng Low
Department of Imaging and Applied Physics, Curtin University, Perth, WA, Australia

Vinyl-ester/nano-silicon carbide nanocomposites were synthesised and investigated in terms of their mechanical and fracture properties. Results show that the addition of nano-SiC particles increases modulus and strength, but reduces toughness. The enhancement in strength for nanocomposites was attributed to good interfacial adhesion and good degree of dispersion. The experimental data for elastic modulus were modelled using several theoretical models. The excellent agreement with the experimental data for elastic modulus given by the Guth and Kerner models indicate that the degree of dispersion and the quality of particle/matrix adhesion were both important considerations for the prediction of elastic modulus.

Keywords Fracture toughness; Mechanical properties; Nano-silicon carbide; Polymer nanocomposites; Transmission electron microscopy

INTRODUCTION

Polymer nanocomposites are materials that have at least one phase with dimension in the nanosize range[1]. Nanoparticles display extraordinary properties due to their large surface area to mass ratio. The phase interactions that occur at the interfaces of polymer matrix give these composites their remarkable properties[2]. The favourable properties of polymer nanocomposites such as mechanical, electrical, optical and thermal have attracted much interest for over 10 years[3]. High elastic modulus, increased strength, favourable heat resistance, decreased gas permeability and decreased flammability are some of the useful properties of polymer nanocomposites[4].

Vinyl ester resins are a newer thermosetting resin compared to alternatives such as polyester and epoxy resins[5]. In terms of industrial applications, the desirable properties of vinyl-ester resins make them suitable for adhesives, coatings, electrical applications, moulding compounds and structural laminates[6]. Thus, vinyl-ester resins that combine the most sought-after properties of epoxies and unsaturated polyesters are favoured by the industry[7]. In recent years, nanoparticles such as carbon nanotubes[8], nanoclay[9–11], iron oxide nanoparticles[12] and cupric-oxide nanoparticles[7] as rigid reinforcements within vinyl-ester matrix have attracted widespread attention. However, few studies have investigated the mechanical properties of vinyl-ester when reinforced with silicon carbide nanoparticles[1,13].

Therefore, this study aims to investigate the mechanical and fracture properties of vinyl ester matrix reinforced with silicon carbide nanoparticles. Particularly, the present work attempts to evaluate the influence of morphological structures such as particle dispersion and particle/matrix interaction on resulting mechanical and fracture properties of vinyl-ester reinforced with nano-silicon carbide.

Address correspondence to It-Meng Low, Department of Imaging and Applied Physics, Curtin University, GPO Box U1987, Perth, WA 6845, Australia. E-mail: j.low@curtin.edu.au

EXPERIMENTAL

Materials

Silicon carbide nano-particles (n-SiC) had a spherical morphology with a phase purity of >95%, specific surface area of 70–90 m^2/g and a particle size of <100 nm. They were purchased from Sigma-Aldrich Co. LLC, Australia. Vinyl-ester resin was supplied by Fibreglass and Aesin Sales Pty Ltd, Australia.

Samples Preparation

Pure vinyl-ester (VER) samples were made as controls to provide the baseline properties. To prepare control samples, 1.0 wt% catalyst (MEKP) was mixed into the vinyl-ester resin and the resultant mixture was then poured into silicon moulds and kept under low vacuum (60 kPa) for 2 h. The resultant mixture was then kept for 24 h at room temperature to cure. Nanocomposite samples were prepared with a dispersion of n-SiC at concentrations of 1, 3, and 5 wt%. First, n-SiC were dried for 60 min at 150°C to remove pre-existing moisture. Then a high-speed electric mixer set at 1200 rpm was used to disperse the n-SiC in the resin for 30 minutes. MEKP was then added to the mixture and stirred slowly to minimise the formation of air-bubbles. The resultant mixture was then poured into silicone moulds, de-gassed for two hours at a vacuum of 60 kPa and then cured at room temperature for 24 h.

Microstructure Examination

A JEM 2011 transmission electron microscope (TEM) was used to study the morphologies of the n-SiC and their dispersion inside the vinyl-ester matrix. A NEON 40ESB scanning electron microscope (SEM) operating at accelerating voltage of 5 kV, under secondary electrons mode was used to examine the dispersion of n-SiC and fracture surfaces. In order to avoid charging, all samples were coated with platinum.

Elastic Modulus and Flexural Strength

Rectangular bars were cut from the fully cured the fully cured samples for three-point bend tests with a span of 40 mm to evaluate the elastic modulus and flexural strength according to ASTM D790-86. A Lloyd Material Testing Machine (5–50 kN) with a displacement rate of 1.0 mm/min was used to perform the test. Five samples of each batch were used to evaluate flexural strength. The values of were recorded and analyzed with the machine software (NEXYGENPlus) and average values were calculated.

Impact Strength

A Zwick Charpy impact tester with a 2.0 J pendulum hammer was used to determine the impact strengths according to ASTM D 256-06. In total, five 40 mm-span bar samples were used for the measurements. The following equation was used to calculate the impact strength[14]:

$$\sigma_i = \frac{E}{A} \tag{1}$$

where σ_i is impact strength and E is the impact energy required to break a sample with a ligament area represented by A.

Fracture Toughness

For fracture toughness (K_{IC}) measurements, the ratio of notch length to width of sample (a/w) used was 0.4 and a sharp razor blade was used to initiate a sharp crack. The flexural tests were performed with a Lloyd Material Testing Machine using a displacement rate of 1.0 mm/min; five samples of each composition were used for the measurements. Five samples of each group were used and the value of fracture toughness was determined according to ASTM D5045-99 using the following equation[15]:

$$K_{IC} = \frac{p_m S}{WD^{2/3}} f\left(\frac{a}{w}\right) \tag{2}$$

where p_m is the maximum load, S is the span of the sample, D is the specimen thickness, w is the specimen width, and a is the crack length, and $f(a/w)$ is the polynomial geometrical correction factor given as[15]:

$$f(a/w) = \frac{3(a/w)^{1/2}\left[1.99 - (a/w)(1-a/w)\left(2.15 - 3.93a/w + 2.7a^2/w^2\right)\right]}{2(1+2a/w)(1-a/w)^{2/3}} \tag{3}$$

Impact Toughness

A Zwick Charpy impact tester with a 2.0 J pendulum hammer was used to determine the impact toughness (G_{IC}). In total, five 40 mm-span bar samples, each with varying notch lengths and razor-cracks, were used. Values of fracture toughness were determined with the following equation[15] according to the method of Plati and Williams[16]:

$$U = G_{IC} BD\phi + U_0 \tag{4}$$

where U is measured energy, U_0 is kinetic energy, D is specimen thickness, B is specimen breadth and ϕ is the calibration factor for the geometry used.

Mathematical Models for Particulate-Reinforced Composites

There are a number of theoretical frameworks that have been developed to support the prediction of elastic modulus of particulate reinforced polymer composites. These sophisticated theories have been developed according to the requirements of different material or geometric parameters. Conventionally, elastic properties of components of particulate–polymer composites, particle loading, and particle aspect ratio are used in determinations of elastic modulus[17,18]. For example, for spherical particles, when the aspect ratio of particles equals unity, the modulus of the components and particle loading or particle size will be used to provide the composite modulus. The composite modulus is enhanced by adding particles to matrix since the modulus of inorganic particles is usually much higher than that of the polymer matrix[17,19].

The theories used for predicting the elastic modulus of particulate-reinforced polymer composites are generally satisfactory. However, theories for predicting the strength and fracture toughness of particulate-reinforced systems are much less developed[19,20]. For theories predicting the strength of particulate-reinforced systems, the largest challenge is to accurately predict how the addition of hard particles will affect a composite's interface adhesion, stress concentration and defect size/spatial distributions[21,22].

There is still a lack of development in the understanding of how the characteristics and concentration of the added hard particles lead to the strength of resultant composite. Current theories do not satisfactorily address whether the addition of hard particles will weaken or reinforce the composite[23,24]. Similar, theories for predicting fracture

TABLE 1
Mathematical models used to compare with experimental data of this work

Model name	Model formula	Nomenclature
Paul (upper-bound)	$E_c/E_m = \dfrac{1+(\delta-1)V_p^{2/3}}{1+(\delta-1)(V_p^{2/3}-V_p^{2/3})}$	E_c = Elastic modulus of composite E_m = Elastic modulus of matrix E_p = Elastic modulus of particles V_p = Volume fraction of particles v_m = Poisson ratio of matrix $\phi_{\max}$ = Maximum packing fraction of particles
Ishai–Cohen (lower-bound)[18,26]	$E_c/E_m = 1 + \dfrac{V_p}{\delta/(\delta-1) - V_p^{1/3}}$	
Kerner[18,19]	$\delta = E_p/E_m$ $E_c/E_m = 1 + \dfrac{V_p}{(1-V_p)}\dfrac{15(1-v_m)}{(8-10\,v_m)}$	
Frankle-Acrivos[21,22]	$E_c/E_m = 1 + \dfrac{9}{8}\left[\dfrac{(V_p/\phi\max)^{1/3}}{1-(V_p/V\max)^{1/3}}\right]$	
Guth[20,23]	*For spherical-shaped particles* $E_c = E_m\,(1 + 2.5V_p + 14.1V_p^2)$	
Counto[17,19]	$\dfrac{1}{E_c} = \dfrac{1-V_p^{1/2}}{E_m} + \dfrac{1}{(1-V_p^{1/2})/V_p^{1/2}E_m + E_p}$	

toughness of particulate-reinforced systems have failed to reach consensus among the scientific community, mainly due to the complexity, inefficiency and lack of reliability that has characterised this group of theories so far[25].

The focus of this study was limited to the prediction of elastic modulus for particulate reinforced composites. Table 1 provides the names, formulas and nomenclatures of seven elastic modulus prediction mathematical models. To determine the applicability of the empirical relationships, these mathematical models were used to compare experimental data from this study with theoretical data generated from these models. Table 2 provides the parameters corresponding to the material properties of the mathematical model implementation.

RESULTS AND DISCUSSION

Mechanical Properties

Table 3 summarises the mechanical properties of the pure VER and VER/n-SiC nanocomposites with different loadings of n-SiC. The addition of n-SiC particles increases elastic modulus and strength but reduces toughness.

The addition of 1 wt% n-SiC particles increased the elastic modulus and strength to 3.05 GPa and 54.9 MPa, respectively, compared with pure VER (2.9 GPa and 42.4 MPa). Similarly, the nanocomposites reinforced with 3 wt% n-SiC particles showed increases to 3.11 GPa and 59.1 MPa in modulus and strength, respectively. Again, the addition of 5 wt% n-SiC was found to increase elastic modulus and flexural strength to 3.17 GPa and 67.2 MPa, respectively. No further improvement in elastic modulus was observed at 10 wt% (3.2 GPa) and the strength decreased at this concentration (63.2 MPa). The results for impact strength were similar. The impact strength for neat VER was 2.6 kJ/m^2. Adding the n-SiC improved the results for impact strength. At 5 wt% impact strength was 3.9 kJ/m^2. No further improvement in impact strength was observed at 10 wt% (3.67 kJ/m^2).

The addition of 1%, 3%, 5% and 10% n-SiC led to lower fracture toughness and impact toughness compared to pure VER. These increases in strength and modulus and decreases in toughness due to n-SiC addition are in agreement with the previous studies of Liao et al.[27] and Rodgers et al.[28]

It is well-accepted that the addition of rigid fillers to a polymer matrix enhances elastic modulus[29,30]. Since n-SiC (457 GPa) has a higher elastic modulus than VER (2.9 GPa), by virtue of the rule of mixtures, an improved elastic modulus was obtained for the resulting nanocomposites. This is believed to be a dominant factor that led to increased elastic modulus in the samples. The enhancement in strength depends on particle size, shape, aspect ratio and degree of dispersion[31] and the quality of interfacial

TABLE 2
Values of parameters used in mathematical modelling

Parameters	Values	Reference
Elastic modulus of VER E_m (GPa)	2.90[a]	
Poisson ratio of matrix v_m	0.39	[17]
Elastic modulus of n-SiC E_p (GPa)	470	[27]
Maximum packing fraction ϕ_{max}	0.637	[18]
Density of VER	1.14[b]	
Density of n-SiC	3.22[c]	

[a,b,c]Our experimental data.

bonding between the particles and matrix[32]. These dynamics can each affect the strength of particulate-reinforced polymer composites by determining the extent to which applied stress is transferred efficiently through the reinforcing particles and matrix[32,33,34].

The SEM and TEM observations, as shown in Figure 1(a–b), confirm that n-SiC particles have a spherical shape and nanoscale size varying from 50 to 150 nm, with an average size of around 100 nm. Thus, n-SiC enables a much higher specific surface area, which provides dense interfacial interaction with the polymer matrix. This high interfacial interaction leads to excellent adhesion and bonding between filler and matrix, thereby increasing composite strength[35,36]. It is well accepted that the nature of bonds in composites will determine how a material responds to load. Thus, when a local stress is applied, and the interfacial interaction is good between the reinforcing particles and matrix, the composite will display favourable strength. In contrast, when the interaction is poor between filler and matrix, artificial defects are more likely to form, which leads to marked reductions in composite strength[37,38].

SEM micrographs in Figure 2 show the fracture surfaces of nanocomposites with 1, 3 and 5 wt% n-SiC. At the particle/matrix interface, there appeared to be no obvious voids, which indicates that nanoparticles had not pull-out from the polymer matrix, thus supporting strong

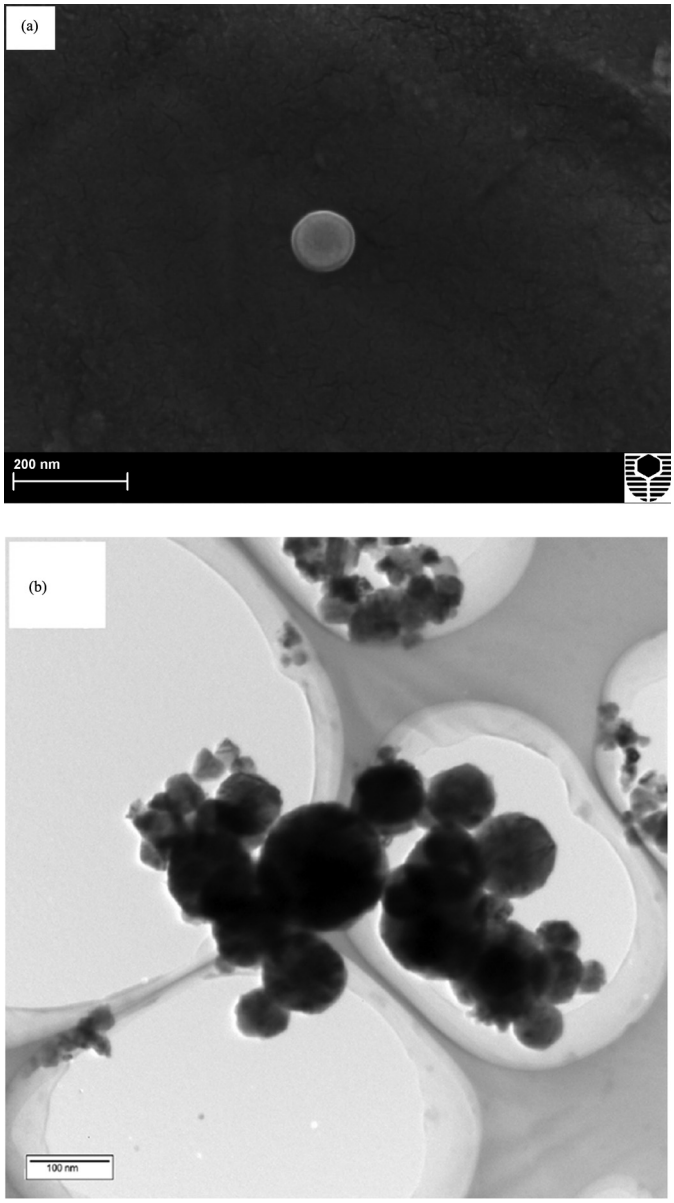

FIG. 1. (a) SEM and (b) TEM micrographs displaying the spherical shape of a n-SiC particle, confirming that the average size of these particles was around 100 nm.

TABLE 3
Mechanical properties of pure VER and VER/n-SiC nanocomposites

Samples	n-SiC content (wt%)	Elastic modulus (GPa)	Flexural strength (MPa)	Impact strength (kJ/m^2)	Fracture toughness ($MPa \cdot m^{1/2}$)	Impact toughness (kJ/m^2)
VER	0	2.90 ± 0.2	42.4 ± 2.4	2.60 ± 0.04	1.81 ± 0.03	1.52 ± 0.04
VER/1% n-SiC	1	3.05 ± 0.08	54.9 ± 2.1	2.91 ± 0.1	1.62 ± 0.02	1.33 ± 0.02
VER/3% n-SiC	3	3.11 ± 0.11	59.1 ± 1.8	3.73 ± 0.08	1.33 ± 0.03	1.12 ± 0.05
VER/5% n-SiC	5	3.17 ± 0.07	67.2 ± 3.0	3.90 ± 0.9	1.12 ± 0.05	0.94 ± 0.03
VER/10% n-SiC	10	3.2 ± 0.05	63.2 ± 2.0	3.67 ± 0.9	1.15 ± 0.05	1.13 ± 0.02

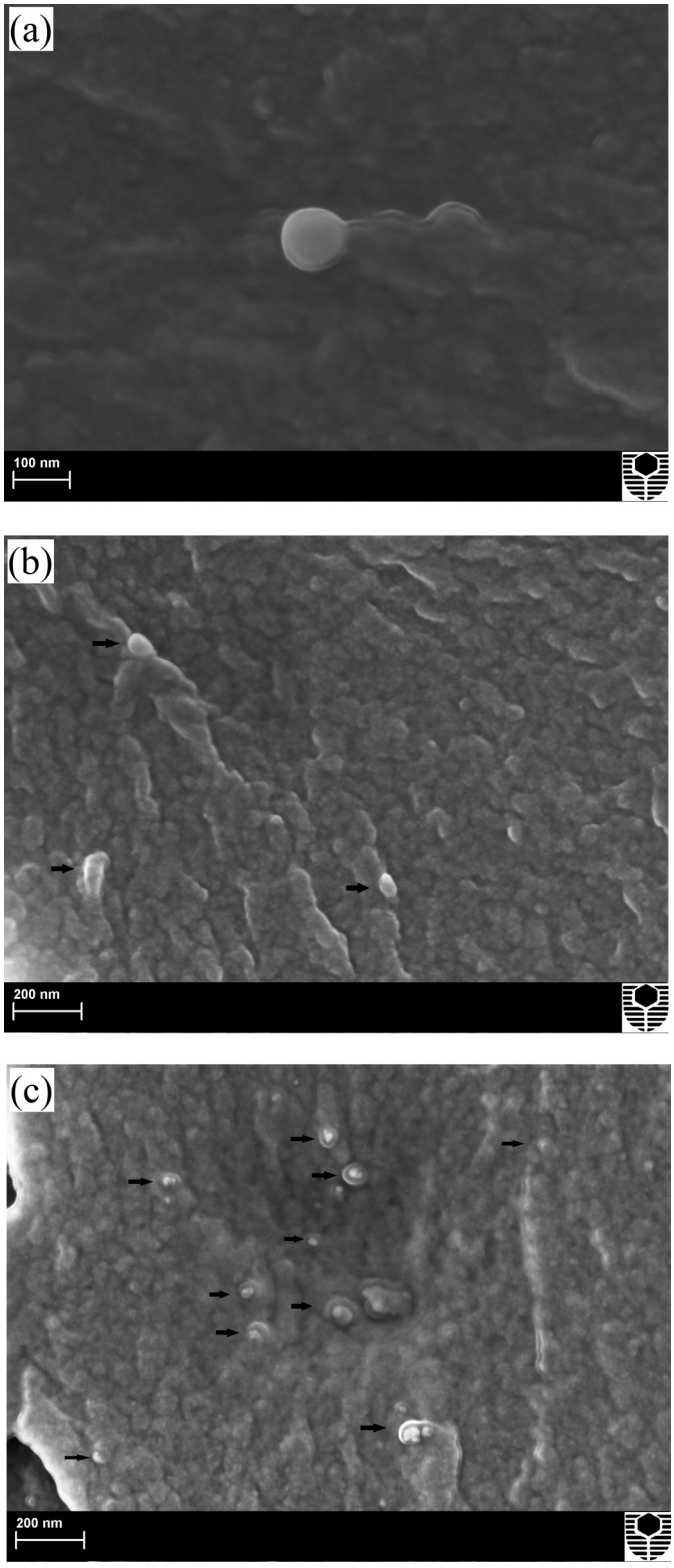

FIG. 2. SEM images of fracture surfaces of VER/n-SiC nanocomposites with (a) 1 wt%, (b) 3 wt%, and (c) 5 wt% (arrows indicate the n-SiC particles).

interaction between the nanoparticles and VER matrix. In addition, the images in Figure 2 (a–c) show no agglomerations thus indicating the dispersion of nanofillers throughout the matrix was quite uniform. Thus, the higher specific surface area inherent with the n-SiC, together with the strong interfacial bonding between n-SiC particles and VER matrix, and the favourable degree of dispersion, effectively facilitate the local stress transfer from VER matrix onto n-SiC particles. Therefore, improved mechanical properties are observed in n-SiC/VER composites.

As previously mentioned, the addition of 10 wt% n-SiC did not lead to further improvements in the modulus and strength properties. The formation of n-SiC agglomerations at this loading is believed to be the reason for lower modulus and strength properties compared to 5 wt% n-SiC/VER nanocomposite. The small size of n-SiC particles, their hydrophilic surface, and their high surface area can act as driving forces for particle agglomeration[13]. When particle agglomeration is present within composites, the load-bearing capability is affected and the elastic modulus is reduced[20].

These larger and more loosely assembled areas of particle agglomerations act as stress concentrators, thus reducing strength and limiting elastic modulus enhancement in the resulting composite[39,40]. Moreover, the presence of particle agglomerations adversely affects adhesion quality between the particles and the matrix, causing further reduction of strength properties[27]. In this study, particle agglomerations were found to exist in the 10 wt% n-SiC/VER nanocomposite (Fig. 3).

TEM micrographs (Fig. 4) show the difference between the 5 wt% and 10 wt% samples. Although the 5 wt%

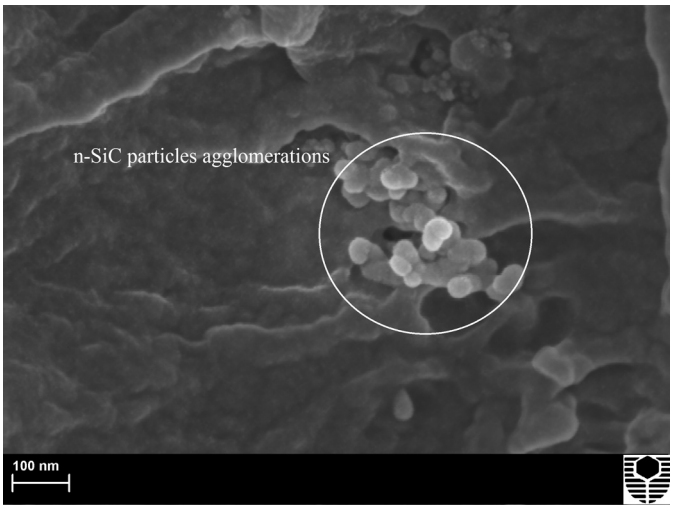

FIG. 3. SEM micrograph displaying n-SiC particle agglomerations within the matrix reinforced with 10 wt% n-SiC.

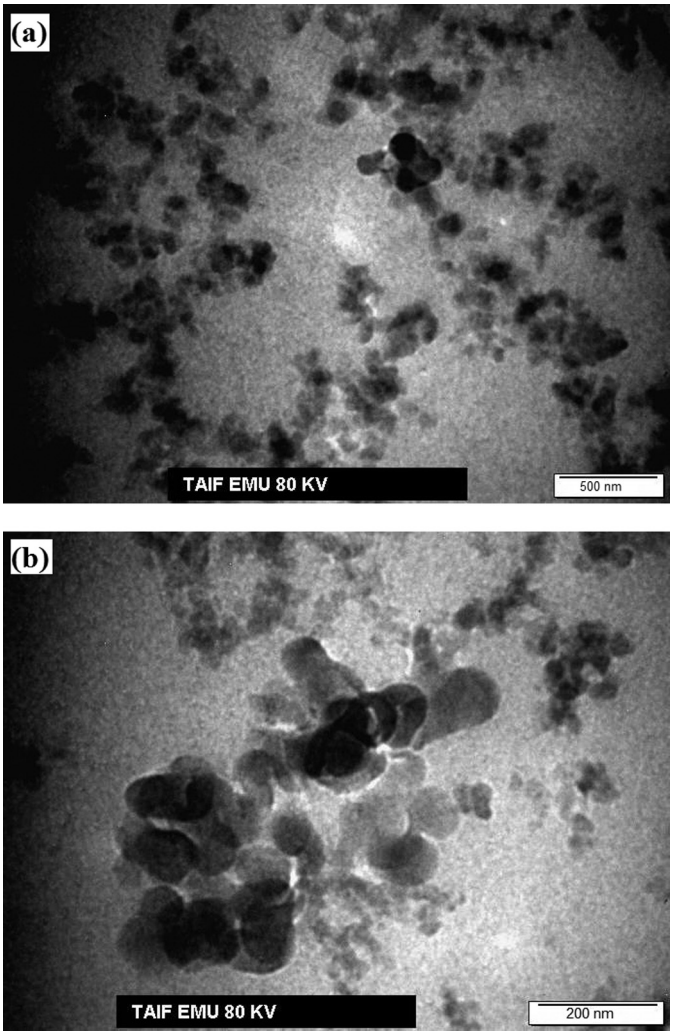

FIG. 4. TEM micrographs of (a) VER/5 wt% n-SiC, and (b) VER/10 wt% n-SiC.

samples show reasonable n-SiC dispersion with minimal agglomerations, the 10 wt% samples exhibit more noticeable agglomeration. Thus, in agreement with previous studies using the direct mixing method for nanoparticle dispersion, this study supports the notion that the addition of nano-fillers beyond 5 wt% is not likely to further improve the overall mechanical properties[18,39,41].

In contrast, with regard to toughness, the addition of 1, 3, 5 and 10 wt% n-SiC led to lower fracture toughness and impact toughness compared to pure VER. Table 3 shows that, while the addition of 1 and 3 wt% led to noticeable reductions in fracture toughness and impact toughness, only slight reductions in fracture toughness and impact toughness were found with 5 and 10 wt%. Plastic deformations are generally accepted as the dominant contributors to the toughness of polymers and polymer composites. It is worth noting that, when investigating toughening mechanisms, the deformation zone ahead of the crack tip is most often under plane strain condition. This means that the materials are subjected to high levels of plastic constraint.

Without vital relief mechanisms, such as plastic deformation, this stress often causes the material to fracture in a brittle mode with low toughness[42,43]. In this study, the addition of stiff n-SiC, is believed to hinder the mobility of surrounding chains in the polymer, consequently limiting the stress relief provided by plastic deformations. The strong filler/matrix interaction is also a hindrance to the mobility of the matrix component. The strong adhesion between the filler and matrix may also have prevented effective de-bonding of n-SiC particles from the VER matrix, thus reducing energy dissipation[44–46].

Therefore, the reduction of toughness is most likely attributed to reduced plastic deformation and the prevention of particle de-bonding. These findings are also supported by previous studies which reported no improvement in toughness in polymer nanocomposites reinforced with nanofillers[29,47,48]. However, It has been suggested that fillers need to be larger than 0.1 μm in order to deflect cracks and to provide the toughening mechanisms of crack bridging, deflection and pinning[4,43].

Figure 5(a–c) shows the fracture surfaces of pure VER and VER/n-SiC nanocomposites with 5 and 10 wt% addition of n-SiC. Inspection of fracture surfaces (Fig.5a) of pure VER shows crack paths spreading in a radial manner, which is indicative of a large zone of plastic deformation. As plastic deformation is an important toughening mechanism in polymers, pure VER was found to have favourable toughness compared to that of the nanocomposites. In contrast, the fracture surfaces of 5 wt% VER/n-SiC nanocomposite (Fig. 5b) reveal more direct crack paths.

The shift from radial cracks, in the pure VER, to direct cracks, in the nanocomposites, is indicative of a shift from ductile to brittle behaviour due to enhanced nanoparticle/matrix adhesion in nanocomposites[27]. The fracture surface of 10 wt% VER/n-SiC nanocomposite (Fig. 5c) reveals evidence of brittle behaviour and the existence of some toughening mechanisms. These mechanisms included plastic deformation around the n-SiC clusters (indicated with circles) and n-SiC cluster pull-out (indicated with squares).

Voids left by the n-SiC cluster pull-out are also clearly noticeable (indicated with diamonds). These clusters act like rigid micro-sized inorganic particles, which when confronting cracks, hinder crack propagation and cause crack deflection, twisting and plastic deformation[49,50]. The results of fracture and impact toughness for the 10 wt% VER/n-SiC nanocomposites were higher than those for

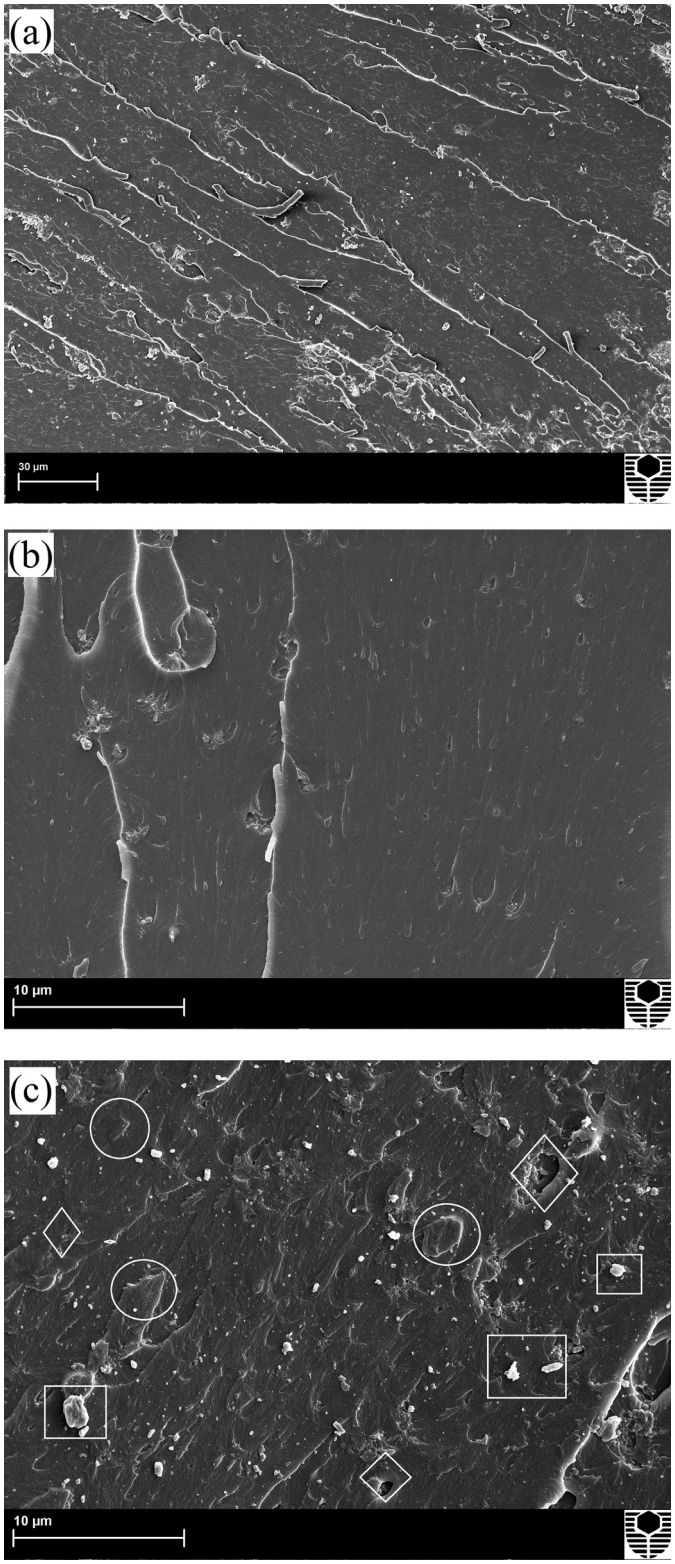

FIG. 5. SEM micrographs showing the fracture surface of (a) pure VER, (b) VER/5% n-SiC nanocomposite, and (c) VER/10% n-SiC nanocomposite.

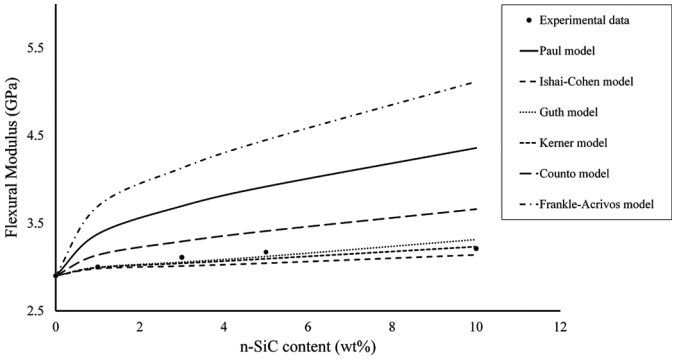

FIG. 6. Comparison of experimental data for flexural modulus against n-SiC content with results extrapolated from published models. (Color figure available online.)

5 wt% samples, which seem to confirm the existence of toughening mechanisms in the former that are not present in the latter.

Comparisons with Theoretical Models

Experimental data for the elastic modulus were compared with typical theoretical models (see Fig. 6). The Paul model and Ishai-Cohen model assume that two phases of the composite are in a macroscopically homogeneous stress state and that interfacial adhesion is perfect. The Paul model gives the elastic modulus of the particulate composite when uniform stress is applied to the boundary. The Ishai-Cohen model is obtained by applying the uniform normal displacement to the boundary in the Paul model. These models, which are accepted tests of validity, form an approximate theory, identifying upper bound values (the Paul model) and lower bound values (the Ishai-Cohen model) of elastic modulus for particulate-reinforced composites. The validity of elastic modulus for most particulate composites can be tested by comparing the experimental data of the elastic modulus values with the upper bound and lower bound values provided by these models. These models provide upper and lower bounds to the elastic modulus of the composite, and all data lie between the two bounds described by these models[17,19].

All experimental and predicted data values in this investigation, with the exception of those obtained using the Frankle-Acrivos model, fell between the upper bounds and lower bounds. This supports the validity of the elastic modulus data for this study. This finding also indicates that the Paul model and Ishai-Cohen model offer reasonable analytical solutions for validity in this study. Although the Paul model and Ishai-Cohen model assume perfect particle/matrix interaction, experimental data in this study lay closer to the lower bound (Ishai-Cohen model), a finding that is in agreement with previous studies[19,51].

The Guth and Kerner models are in excellent agreement with the experimental data. The Guth model is typically applicable to the assumption of perfect adhesion between the spherical particles and matrix, and perfect dispersion of individual filler particles[17,19]. In this study, the microstructure observation has supported strong adhesion between the spherical fillers and matrix, and good dispersion of n-SiC particles within the matrix. The Kerner model is a measure of validity of the composite system in which the modulus of filler is many times higher than that of the matrix[18,21].

In this study, the elastic modulus of n-SiC (470 GPa), was much more rigid than the matrix, VER (2.97 GPa). The relative modulus ratio of filler to matrix was 151.5, which explains the strong agreement between the theoretical models and the experimental data. When the volume fraction increased to 10 wt%, the Guth model over-predicted the elastic modulus of samples. This discrepancy is probably explained by particle agglomerations. As aforementioned, clusters within the composite can affect the load bearing capability, thus reducing its elastic modulus.

The Counto model, a simpler model, assumes perfect particle/matrix bonding. In this study, this model was found to overestimate the elastic modulus. This model predicts the moduli to be in good agreement with a wide range of experimental data. However, the Counto model tends to be used for concrete systems, which may explain the lack of agreement between the theoretical model and the experimental data of this study[16,18]. The overestimation of the Frankle-Acrivos model, the only model with results outside the upper bounds and lower bounds, clearly did not agree with the experimental data. This model uses a simplistic relative filler volume fraction (V_p/Φ_{max}), which implies the particle packing efficiency is dominant, and neglects three important factors that influence the elastic modulus: namely, the effect of particle/matrix interfacial interaction, Young's modulus and Poisson's ratio[18,20,52].

Thus, the degree of dispersion and quality of particle/matrix adhesion seem to be the most important variables in determining composite modulus according to the results of this study and other studies[18,52–55]. However, it is worth noting that some of the earlier studies of particulate polymer composites reviewed by Ahmed and Jones[17] and Fu et al.[19] proposed that the quality of particle/matrix adhesion was irrelevant. The findings of this study on elastic modulus for particulate polymer composites directly contradict those previous studies.

CONCLUSIONS

Pure VER and VER/HNT composites have been synthesised and characterised in terms of mechanical and fracture properties. The addition of n-SiC particles increased elastic modulus and strength but reduced the toughness. The enhancement in strength for VER/HNT composites was attributed to good interfacial adhesion and a good degree of dispersion. Agglomeration of nanoparticles formed clusters that decreased elastic modulus and strength. Experimental data and predicted data were found to fall within the upper and lowers bounds of the Paul model and Ishai-Cohen models supporting the validity of the results of this study. The good agreement of experimental data with Guth and Kerner model suggests that, in addition to dispersion of particles within the matrix, the state of interfacial adhesion between the particles and matrix is a relevant to the prediction of elastic modulus of particulate-reinforced composites.

ACKNOWLEDGMENTS

We are grateful to Dr. Jerry Luo from the Centre for Materials Research at Curtin University for his assistance with SEM imaging and to Mr. Osama Ali from Electron Microscopy Unit at Taif University, Saudi Arabia, for assistance with TEM imaging. This research received no specific grant from any funding agency in the public, commercial, or not-for-profit sectors.

REFERENCES

1. Yong, V.; Hahn, T. Monodisperse SiC/vinyl-ester nanocomposites: Dispersant formulation, synthesis, and characterization. J. Mater. Res. **2009**, *24*, 1553–1558.
2. Chisholm, N.; Mahfuz, H.; Rangari, V.K.; Ashfaq, A.; Jeelani, S. Fabrication and mechanical characterization of carbon/SiC-epoxy nanocomposites. Compos. Struct. **2005**, *67*, 115–124.
3. Zeng, Q.H.; Yu, A.B.; Lu, G.Q.; Paul, D.R. Clay-based polymer nanocomposites: Research and commercial development. J. Nanosci. Nanotechnol. **2005**, *5*, 1574–1592.
4. Balakrishnan, H.; Hassan, A.; Imran, M.; Wahit, M.U. Toughening of polylactic acid nanocomposites: A short review. Polym. Plast. Technol. Eng. **2012**, *51*, 175–192.
5. Pashaei, S.; Siddaramaiah; Syed, A.A. Investigation on mechanical, thermal and morphological behaviors of turmeric spent incorporated vinyl ester green composites. Polym. Plast. Technol. Eng. **2011**, *50*, 1187–1198.
6. Marsh, G. Vinyl ester–The midway boat building resin. Reinf Plast. **2007**, *51*, 20–23.
7. Guo, Z.; Liang, X.; Pereira, T.; Scaffaro; R.; Hahn, HT. CuO nanoparticle filled vinyl-ester resin nanocomposites: Fabrication, characterization and property analysis. Compos Sci Technol. **2007**, *67*, 2036–2044.
8. Seyhan, A.T.; Gojny, F.H.; Tanoğlu, M.; Schulte, K. Rheological and dynamic-mechanical behavior of carbon nanotube/vinyl ester–polyester suspensions and their nanocomposites. Euro. Polym. J. **2007**, *43*, 2836–2847.
9. Chigwada, G.; Jash, P.; Jiang, D.D.; Wilkie, C.A. Fire retardancy of vinyl ester nanocomposites: Synergy with phosphorus-based fire retardants. Polym. Degrad. Stab. **2005**, *89*, 85–100.
10. Ji, G.; Li, G. Effects of nanoclay morphology on the mechanical, thermal, and fire-retardant properties of vinyl ester based nanocomposite. Mater. Sci. Eng. A **2008**, *498*, 327–334.
11. Chandramohan, A.; Vengatesen, M. R.; Devaraju, S.; Dinakaran, K.; Alagar, M. Organoclay filled vinyl ester monomer toughened epoxy–Intercrosslinked matrix materials. Inter. J. Polym. Mater. **2012**, DOI:10.1080/00914037.2012.670818.
12. Guo, Z.; Lei, K.; Li, Y.; Ng, H.W.; Prikhodko, S.; Hahn, H.T. Fabrication and characterization of iron oxide nanoparticles

reinforced vinyl-ester resin nanocomposites. Compos. Sci. Technol. **2008**, *68*, 1513–1520.
13. Yong, V.; Hahn, H.T. Processing and properties of SiC/vinyl ester nanocomposites. Nanotechnol. **2005**, *15*, 1338–1343.
14. Low, I.M.; Somers, J.; Kho, H.S.; Davies, I.J.; Latella, B.A. Fabrication and properties of recycled cellulose fibre-reinforced epoxy composites. Compos. Interf. **2009**, *16*, 659–669.
15. Low, I.M.; McGrath, M.; Lawrence, D.; Schmidt, P.; Lane, J.; Latella, B.A.; Sim, K.S. Mechanical and fracture properties of cellulose-fibre-reinforced epoxy laminates. Compos. Pt. A. **2007**, *38*, 963–974.
16. Plati, E.; Williams, J.G. The Determination of the Fracture Parameters for Polymers in Impact. Polym. Eng. Sci. **1975**, *15* (6), 470–477.
17. Ahmed, S.; Jones, F.R. A review of particulate reinforcement theories for polymer composites. J. Mater. Sci. **1990**, *25*, 4933–4942.
18. Dong, Y.; Chaudhary, D.; Ploumis, C.; Lau, K.T. Correlation of mechanical performance and morphological structures of epoxy micro/nanoparticulate composites. Compos. Pt. A **2011**, *42*, 1483–1492.
19. Fu, S.Y.; Feng, X.Q.; Lauke, B.; Mai, Y.W. Effects of particle size, particle/matrix interface adhesion and particle loading on mechanical properties of particulate–polymer composites. Compos. Pt. B **2008**, *39*, 933–961.
20. Yan, W.; Lin, R.J.T.; Bhattacharyya, D. Particulate reinforced rotationally moulded polyethylene composites: Mixing methods and mechanical properties. Compos. Sci. Technol. **2006**, *66*, 2080–2088.
21. Kaully, T.; Siegmann, A. Shacham, D. Mechanical behavior of highly filled natural $CaCO_3$ composites: Effect of particle size distribution and interface interactions. Polym Compos. **2008**, *29*, 396–408.
22. Tohgo, K.; Itoh, Y.; Shimamura, Y. A constitutive model of particulate-reinforced composites taking account of particle size effects and damage evolution. Compos. Pt. A **2010**, *41*, 313–321.
23. Bigg, D.M. Mechanical properties of particulate filled polymers. Polym Compos. **1987**, *8*, 115–122.
24. Chen, B.; Evans, J.R.G. Impact strength of polymer-clay nanocomposites. Soft Matter. **2009**, *5*, 3572–3584.
25. Pukánszky, B.; Maurer, F.H. Composition dependence of the fracture toughness of heterogeneous polymer systems. Polym. **1995**, *36*, 1617–1625.
26. Chakraborty, P.; Ganguly, S.; Mitra, S.; Bhowmick, A.K. Influence of phase modifiers on morphology and properties of thermoplastic elastomers prepared from ethylene propylene diene rubber and isotactic polypropylene. Polym. Eng. Sci. **2008**, *48*, 477–489.
27. Liao, C.Z.; Bao, S.P.; Tjong, S.C. Effect of silicon carbide nanoparticle additions on microstructure and mechanical behavior of maleic anhydride compatibilized high density polyethylene composites. Compos. Interf. **2011**, *18*, 107–120.
28. Rodgers, R.M.; Mahfuz, H.; Rangari, V.K.; Chisholm; N. Jeelani, S. Infusion of SiC nanoparticles into SC-15 epoxy: An investigation of thermal and mechanical response. Macromol. Mater. Eng. **2005**, *290*, 423–429.
29. Zhao, L.D.; Zhang, B.P.; Li, J.F.; Zhou, M.; Liu, W.S.; Liu, J. Thermoelectric and mechanical properties of nano-SiC-dispersed Bi2Te3 fabricated by mechanical alloying and spark plasma sintering. J. Alloy Compd. **2008**, *455*, 259–264.
30. Handge, U.A.; Hedicke-Höchstötter, K.; Altstädt, V. Composites of polyamide 6 and silicate nanotubes of the mineral halloysite: Influence of molecular weight on thermal, mechanical and rheological properties. Polymer **2010**, *51*, 2690–2699.
31. Ning, N.Y.; Yin, Q.J.; Luo, F.; Zhang, Q.; Du, R.; Fu, Q. Crystallization behavior and mechanical properties of polypropylene/halloysite composites. Polymer **2007**, *48*, 7374–7384.
32. Hedicke-Höchstötter, K.; Lim, G.T.; Altstädt, V. Novel polyamide nanocomposites based on silicate nanotubes of the mineral halloysite. Compos Sci Technol. **2009**, *69*, 330–334.
33. Ismail, H.; Pasbakhsh, P.; Fauzi, M.N.A.; Abu-Bakar, A. Morphological, thermal and tensile properties of halloysite nanotubes filled ethylene propylene diene monomer (EPDM) nanocomposites. Polym Test. **2008**, *27*, 841–850.
34. Ataeefard, M.; Moradian, S. Polypropylene/organoclay nanocomposites: Effects of clay content on properties. Polym. Plast. Technol. Eng. **2011**, *50*, 732–739.
35. Klaysom, C.; Moon, S.H.; Ladewig, B.P.; Lu, G.Q.M.; Wang, L. The effects of aspect ratio of inorganic fillers on the structure and property of composite ion-exchange membranes. J. Coll. Interf. Sci. **2011**, *363*, 431–439.
36. Rooj, S.; Das, A.; Thakur, V.; Mahaling, R.N.; Bhowmick, A.K.; Heinrich, G. Preparation and properties of natural nanocomposites based on natural rubber and naturally occurring halloysite nanotubes. Mater. Des. **2010**, *31*, 2151–2156.
37. Guo, Z.; Kim, T.Y.; Lei, K.; Pereira, T.; Sugar, J.G.; Hahn, H.T. Strengthening and thermal stabilization of polyurethane nanocomposites with silicon carbide nanoparticles by a surface-initiated-polymerization approach. Compos Sci Technol. **2008**, *68*, 164–170.
38. Mammeri, F.; Bourhis, E.L.; Rozes, L.; Sanchez, C. Mechanical properties of hybrid organic-inorganic materials. J. Mater. Chem. **2005**, *15*, 3787–3811.
39. Qi, B.; Zhang, Q.X.; Bannister, M.; Mai, Y.W. Investigation of the mechanical properties of DGEBA-based epoxy resin with nanoclay additives. Compos. Struct. **2006**, *75*, 514–519.
40. Zhou, T.; Wang, X.; Mingyuan, G.U.; Liu, X. Study of the thermal conduction mechanism of nano-SiC/DGEBA/EMI-2,4 composites. Polymer **2008**, *49*, 4666–4672.
41. Liu, W.; Hoa, S.V.; Pugh, M. Fracture toughness and water uptake of high-performance epoxy/nanoclay nanocomposites. Compos. Sci. Technol. **2005**, *65*, 2364–2373.
42. Lim, S.H.; Dasari, A.; Yu, Z.Z.; Mai, Y.W.; Liu, S.; Yong, M.S. Fracture toughness of nylon 6/organoclay/elastomer nanocomposites. Compos. Sci. Technol. **2007**, *67*, 2914–2923.
43. Silva, R.V.; Spinelli, D.; Filho, W.W.B.; Neto, S.C.; Chierice, G.C.; Tarpani, JR. Fracture toughness of natural fibers/castor oil polyurethane composites. Compos. Sci. Technol. **2006**, *66*, 1328–1335.
44. Ma, J.; Mo, M.S.; Du, X.S.; Rosso, P.; Friedrich, K.; Kuan, H.C. Effect of inorganic nanoparticles on mechanical property, fracture toughness and toughening mechanism of two epoxy systems. Polymer **2008**, *49*, 3510–3523.
45. Sue, H.J.; Gam, K.T.; Bestaoui, N.; Spurr, N.; Clearfield, A. Epoxy nanocomposites based on the synthetic α-zirconium phosphate layer structure. Chem. Mater. **2003**, *16*, 242–249.
46. Zuiderduin, W.C.J.; Westzaan, C.; Huétink, J.; Gaymans, R.J. Toughening of polypropylene with calcium carbonate particles. Polymer **2003**, *44*, 261–275.
47. Phang, I.Y.; Liu, T.; Mohamed, A.; Pramoda, K.P.; Chen, L.; Shen, L.; Chow, S.Y.; He, C.; Lu, X.; Hu, X. Morphology, thermal and mechanical properties of nylon 12/organoclay nanocomposites prepared by melt compounding. Polym. Int. **2005**, *54*, 456–464.
48. Meng, J.; Hu, X. Synthesis and exfoliation of bismaleimide–organoclay nanocomposites. Polymer **2004**, *45*, 9011–9018.
49. Wetzel, B.; Rosso, P.; Haupert, F.; Friedrich, K. Epoxy nanocomposites – fracture and toughening mechanisms. Eng. Fract. Mech. **2006**, *73*, 2375–2398.
50. Young, R.J.; Maxwell, D.L.; Kinloch, A.J. The deformation of hybrid-particulate composites. J. Mater. Sci. **1986**, *21*, 380–388.
51. Chan, C.M.; Wu, J.; Li, J.X.; Cheung, Y.K. Polypropylene/calcium carbonate nanocomposites. Polymer **2002**, *43*, 2981–2992.

52. Ahmad, F.N.; Jaafar, M.; Palaniandy, S.; Azizli, K.A.M. Effect of particle shape of silica mineral on the properties of epoxy composites. Compos. Sci. Technol. **2008**, *68*, 346–353.
53. Deng, S.; Zhang, J.; Ye, L.; Wu, J. Toughening epoxies with halloysite nanotubes. Polymer **2008**, *49*, 5119–5127.
54. Masouras, K.; Silikas, N.; Watts, D.C. Correlation of filler content and elastic properties of resin-composites. Dental Mater. **2008**, *24*, 932–939.
55. Giannakas, A.; Ladavos, A. Preparation and characterization of polystyrene/organolaponite nanocomposites. Polym. Plast. Technol. Eng. **2012**, *51*, 1411–1415.

4. CONCLUSIONS AND FUTURE WORK

4.1 Conclusions

4.1.1 VER Eco-composites

RCF-reinforced polymer composites were prepared with a range of fibre contents (0-50 wt%). A new infiltration method was used for the development of natural fibre reinforced polymer composites, which involved very thin sheets of RCF being fully soaked in vinyl ester resin. This method led to the development of composite materials with lower void contents and good fibre–matrix adhesion. The composites produced were investigated to identify and assess the effect of fibre reinforcement and water uptake on elastic modulus, flexural strength, impact strength and fracture toughness of the VER/RCF composites. The effect of varying fibre contents on water absorption behaviours was also investigated, and it was found that moisture uptake increased with fibre volume fraction. This was attributed to the increased cellulose fibre content and specifically the presence of hydroxyl groups on the natural fibres causing the fibres to be hydrophilic. At room temperature, maximum water uptake for VER, and its composites, immersed for 2,500 hours was 0.76, 6.52, 9.56, 12.37 and 14.62% respectively.

The elastic modulus was found to increase with fibre volume fraction with the addition of 20, 30, 40 and 50 wt.% RCF corresponding to 0.16, 0.24, 0.33 and 0.43 fibre volume fractions, increased elastic modulus by 49 76 114 and 143 %, respectively. Elastic modulus improvement is attributed to the higher initial modulus of the cellulose fibres acting as backbones in the composites. Typical mathematical models for prediction were used to model composite elastic modulus, and results revealed consistency between experimental data and prediction data obtained using the Cox–Krenchel model.

Flexural strength was also found to increase with fibre volume fraction. Specifically, the addition of 20, 30, 40 and 50 wt% RCF led to 173.7, 216.5, 254.2 and 295.7 % increases in flexural strength, respectively. These enhancements were attributed to a reinforcing effect caused by the high strength and modulus cellulose fibres as well as the ability of the fibres to resist bending force. Impact strength increased

significantly with fibre content with the addition of 20, 30, 40 and 50 wt.% RCF increasing impact strength by 312, 440, 656 and 1048 % respectively. This enhancement in impact strength is believed to be due to the ability of the cellulose fibres to transfer impact stress using energy dissipation mechanisms, primarily fibre pull-out, fibre fracture, and matrix deformation.

Fracture toughness increased with fibre content with 20, 30, 40 and 50 wt% RCF increasing fracture toughness by 35, 113, 153 and 231 % respectively. This improvement in fracture toughness was attributed to enhanced crack deflection, energy dissipation, and fracture resistance properties provided when cellulose fibres interact with the VER matrix.

Concerning thermal properties, eco-composites were found to decompose at higher temperatures than pure samples. TGA data revealed that above 700°C, the residual weight of eco-composites was 19.7 % of the original whereas for pure VER only 8.7% remained. The thermal resistance of the cellulose fibres and the ability of these natural fibres to increase char formation are believed to be principal factors leading to enhanced thermal stability.

On prolonged exposure to water (i.e., 2500 hours), the elastic modulus, strength, and toughness of all composites were dramatically reduced. For example, composites reinforced with 50 wt% RCF, exposure to moisture resulted in a 15 % reduction in elastic modulus, a 27 % reduction in flexural strength, a 25 % reduction in impact strength and a 9 % reduction in fracture toughness compared to the corresponding dry samples. This drop in mechanical properties was attributed to the degradation of bonding at the fibre–matrix interfaces due to the effect of water absorption. At high fibre content, the adverse effect of water absorption on mechanical properties was more pronounced. SEM micrographs showed severe damage of cellulose fibres and degradation of bonding along fibres-matrix interfaces in wet composites. In addition, prior to exposure to water, SEM micrographs indicated almost no fibre pull-out and that fibres had broken off near surfaces. The observation is indicative of strong bonding between the fibres and the matrix materials. In contrast, after exposure to water, increased fibre pull-out was clearly observed, in SEM micrographs, suggesting of poor fibre/matrix bonding due to the effect of water absorption.

4.1.2 Viny-ester Nanocomposites

Vinyl-ester nanocomposites reinforced with halloysite nanotubes (HNT) and nano-silicon carbide (n-SiC) were fabricated. The effect of nano-filler addition on the morphology, structure, water absorption, fracture, mechanical, thermal and flammability properties of vinyl-ester nanocomposites was investigated.

4.1.2.1 Viny-ester/HNT Nanocomposites

Pure VER and VER/HNTs composites were fabricated. The latter were prepared by dispersion of HNTs at 1%, 3%, and 5wt%. To remove pre-existing moisture, the HNTs were dried for 60 minutes at 150°C. The HNTs were then mixed with the VER by high speed electrical-mixer (1200 rpm) for 30 minutes.

The development and characterization of polymeric nano-composites are often featured in scientific publications. However, concerning the investigation of HNT nano-composites development and characterization, to date, there appears to be no in-depth repository with regards to the addition of HNTs in vinyl ester. Therefore, an aim of study was to gather and present information concerning vinyl-ester/HNT nano-composite development and characterisation, and specifically, the effect of HNT addition on water absorption, fracture, mechanical, thermal and flammability properties of vinyl-ester filled by halloysite nanotubes.

XRD results confirmed intercalation of the HNTs by chains of VER. The d-spacing of the peak (001) of pure HNT increased from 0.721 to 0.745 nm for the 1 wt% VER/HNT which serves to indicate successful formation of nanocomposites. TEM observations suggest HNTs have a length ranging from 500 nm to 3 μm with averages for HNTs outer diameters ranging from 100-300 nm and averages for inner diameters ranging between 50-150 nm. The aspect ratio of HNTs varies between 3 and 15. Though different-sized HNT clusters can be found, the extent of dispersion is acceptable. HNTs were generally well dispersed in the matrix with short inter-tube distances resulting in the formation of HNT-rich regions, and in contrast, long inter-tube distances resulting in the formation of VER-rich regions.

Concerning water uptake, the most favourable reduction was demonstrated by 5 wt% VER/HNTs composites. Compared to pure VER, 1 wt%, and 3 wt%, the 5 wt%

composites, on weight gain and FTIR tests, gave the best results. The high aspect ratio of HNTs is believed to underpin the favourable reduction in water uptake demonstrated by these composites. The presence of HNTs forces water molecules to alter their path from direct-fast polymer matrix diffusion to a tortuous path. This maze-like path effectively decreases the overall uptake of water molecules.

The addition of HNTs also improved toughness. Enhanced toughness values for all VER/HNT composites samples were observed on the addition of HNTs. From 1.8 MPa.$m^{1/2}$ for pure VER, fracture toughness increased to 2.1 MPa.$m^{1/2}$, 2.4 MPa.$m^{1/2}$ and 2.6 MPa.$m^{1/2}$ for 1 wt%, 3 wt% and 5 wt% VER/HNTs respectively. Similarly, from 1.5 kJ/m^2 for unfilled VER, the addition of HNTs at 1, 3, and 5 wt% increased the impact toughness to 2.9, 3.3 and 4.1 kJ/m^2 respectively. Crack bridging, deflection, and plastic deformation around HNT clusters were believed to be the mechanisms underpinning enhancement in toughness. An increase in fracture toughness was also attributed to the interaction of clusters of HNTs and cracks. This interaction was believed to effectively resisting crack advancement.

SEM micrographs of pure VER surfaces revealed flatness and smoothness notwithstanding this presence of river line markings near crack initiation sites. These river line markings suggested typical brittle fracture behavior and thereby provided an explanation for the low fracture toughness of VER. This roughness at the surface is believed to be an indicator of the quantity of energy dissipated during fracture. VER/HNT composite micrographs depicted increasing fracture surface roughness with increasing HNT content. The fracture surfaces are rougher and the crack bifurcation more evident amongst the samples with greater HNT content. These visual features suggest crack path deflection due to the rigid HNTs which are believed to hinder crack propagation.

HNTs addition enhanced flexural modulus. After increasing the HNTs content to 1, 3 and 5 wt%, flexural modulus increased from 2.90 GPa for pure VER, to 3.11, 3.31 and 3.46 GPa respectively. HNTs addition also increased both flexural strength and impact strength albeit moderately. From 42 MPa for pure VER, reinforcement with 1, 3 and 5 wt% HNTs, increased flexural strength to 45.9, 51.1, and 56.5 MPa respectively. Similarly, the addition of HNTs at 1, 3, and 5 wt% increased impact strength, from 2.60 kJ/m^2 for pure VER, to 3.32, 4.15 and 4.45 kJ/m^2 respectively.

The significant enhancements in flexural modulus of the VER/HNT nanocomposites, compared to the pure VER samples, are believed to be due the higher initial elastic modulus of HNTs (30 GPa) compared to the VER (2.90 GPa). By virtue of the rule-of-mixtures, VER/HNT composites thereby demonstrated improved elastic modulus. Strength property enhancements for the VER/HNT composites are believed to be due to the HNT particles large aspect ratio, good adhesion between HNTs particles and VER, good degree of dispersion, and suitable extent of inter-tubular interaction in composites as supported by SEM, TEM and XRD investigations.

The aspect ratio of particles, dispersion of particles within the matrix, and state of adhesion between particles and matrix were found to be each influential to the elastic modulus of the particulate reinforced composites fabricated in this study. This conclusion was supported by agreement of the experimental data with Paul model and Guth model.

A positive relationship existed between HNT additions and enhanced thermal properties. TGA curve data reveals that for a temperature range from room temperature to 800 °C, the VER and all composites demonstrated single-stage thermal degradation. Pure VER displayed degradation at approximately 385 °C. Samples with 1 wt%, 3 wt%, and 5 wt.% HNTs started degradation at ~ 406 °C, 418 °C, and 422 °C respectively, thus demonstrating slightly higher thermal stability. Sample decomposition continued until temperatures rose above 500°C at which point a constant mass was achieved. Above 700 °C, the residual weight for pure VER was 8.2 wt% whereas samples modified with 1 wt%, 3 wt%, and 5 wt.% HNTs, at the same temperature, had residual weights of 10 wt%, 10.8 wt% and 12.8 wt.% respectively. Calculations imply that the burning rate of pure VER at nearly twice the rate of 5 wt% VER/HNT composite, thus highlighting the favourable flammability resistance properties of the composites. The good thermal stability and flame retardant effects of HNTs are resulted from the HNTs hollow tubular structure, provision of thermal and mass transport barriers and presence of iron in HNTs.

4.1.2.2 Viny-ester/n-SiC Nanocomposites

VER/n-SiC composites were prepared at 1, 3, 5 and 10 wt. % using high-speed mechanical stirring. In particular, particle dispersion and particle/matrix interaction

were investigated concerning their effects on the resulting mechanical and fracture properties of these nano-composites.

The addition of n-SiC increased the elastic modulus and strength of the resulting materials. For example, compared with pure VER (2.9 GPa and 42.4 MPa), the elastic modulus and strength of VER/1 wt% n-SiC were greater (3.05 GPa and 54.9 MPa) respectively. Similarly, the nanocomposites reinforced with 3 wt% n-SiC particles had favourable elastic modulus and strength (3.1 GPa and 59.1 MPa) respectively. The greatest increase in elastic modulus and strength was observed at 5 wt% n-SiC (3.1 GPa and 67.2 MPa) respectively. At 10 wt%, no further improvement in elastic modulus was observed (3.2 GPa) and the strength decreased at this concentration (63.2 MPa). Concerning impact strength, the results were similar. For neat VER, impact strength was 2.6 kJ/m^2. While increasing n-SiC content increase impact strength to a point, (at 5 wt% impact strength was 3.9 kJ/m^2), there was no further improvement in impact strength at 10wt% (3.6 kJ/m^2).

By virtue of the rule of mixtures, the higher initial elastic modulus of n-SiC, compared to VER, meant that an improved elastic modulus was obtained for the resulting nano-composites. Good interfacial adhesion and a good degree of dispersion enhanced the strength of the nanocomposites content 1, 3, and 5 wt. %, whereas agglomeration of nanoparticles at 10 wt% forming clusters of n-SiC (as confirmed with SEM and TEM micrographs) decreased elastic modulus and strength. SEM micrographs of the VER/n-SiC fracture surfaces revealed no obvious voids at the particle/matrix interface. This is indicative of an absence of n-SiC pull-out from the polymer matrix supporting strong interaction between the n-SiC and VER matrix. Also supportive of generally uniform dispersion of n-SiC throughout the matrix is the absence of n-SiC agglomeration throughout the nano-composite.

Concerning toughness, n-SiC addition led to lower fracture toughness and lower impact toughness. For example, while fracture toughness for pure VER was 1.8 $MPa.m^{1/2}$, addition of 1 wt% reduced it to 1.6, and addition of 10 wt% of n-SiC reduced it even more dramatically to 1.2 $MPa.m^{1/2}$. Similarly while impact toughness for pure VER was 1.5 kJ/m^2, addition of 1 and 10 wt% of n-SiC reduced to impact toughness to 1.3 to 1.1 kJ/m^2 respectively. Addition of stiff n-SiC is believed to hinder the mobility of surrounding chains in the polymer, consequently

limiting the stress relief provided by plastic deformations. Strong filler/matrix interaction further hinders matrix component mobility. Strong fibre/matrix adhesion may also have prevented effective de-bonding of n-SiC particles from the VER matrix, thus reducing energy dissipation. Therefore, the reduction of toughness is most likely attributed to reduced plastic deformation and the prevention of particle de-bonding.

The experimental data consistent with that of both the Guth and the Kerner model suggested good dispersion within the matrix and good interfacial adhesion were both relevant to the prediction of elastic modulus of particulate reinforced composites.

4.1.3 Vinyl-ester Eco-nanocomposites

A novel two-step approach was used to synthesize eco-nanocomposites. The first step was the dispersion of nano-fillers such as nanoclay platelets, halloysite nanotubes (HNTs) and silicon carbide (n-SiC) into VER matrices to prepare nano-mixtures. The second step was the reinforcement of these nano-mixtures with sheets of RCF. The effects of these RCF/nano-fillers on the physical, water absorption, mechanical, thermal and flammability properties are investigated

4.1.3.1 Viny-ester/RCF/Nanoclay Eco-nanocomposites

Nanoclay effectively decreased the water uptake in eco-nanocomposites. The addition of 5 wt% nanoclay provided substantial water absorption resistance to composites as evidenced by weight gain study and FTIR analysis.

Strength properties were also enhanced. The addition of 1 wt%, 3 wt% nanoclay showed 38.4% and 41.4% respective increase in flexural strength. The addition of 1 wt% and 3 wt% nanoclay gave impact strength results of 17.9 kJ/m^2 and 20.0 kJ/m^2 respectively. The addition of 5 wt% nanoclay did not give further enhancement in flexural and impact strength properties. The reinforcing effect of RCF and nanoclay, and the improvement of fibre-matrix adhesion on nanoclay addition give greater strength properties to eco-nanocomposites. The SEM micrographs displayed fibres pull-outs from the matrix. The disparity in the length of fibres, the fibre surfaces and matrix-fibre gaps is apparent in each of the composites. The pull-out lengths were greater for in the unfilled composites when compared to those of the filled

composites. The number of fibres pulled out was also greater in the unmodified sample. This phenomenon is a result of poor fibre/matrix adhesion. The fibre surfaces in unmodified eco-composite appear clean. This suggests poor adhesion with matrix materials failing to adhere to the fibres. In contrast, the fibre surfaces of modified eco-nanocomposite are rough indicating better adhesion between the fibres and the matrix materials. Finally, the matrix-fibre gaps appear larger in the unmodified composites compared to the small gaps of the modified composites. The fracture surface images are indicative of nanoclay addition's positive effect on matrix-fibre adhesion.

Processing events are believed to underpin the failure of 5 wt% nanoclay addition further enhancing strength properties. At higher clay content, viscosity increases during mixing of resin. This renders degassing insufficient before curing leading to void formation. Ultimately, specimen failure occurs at even on exposure to very low strains. Moreover, highly viscous mixtures can cause reduction in wettability, interfacial adhesion between matrix and fibres are more likely further reducing the material strength.

Concerning flexural modulus, there was good agreement between the experimental data and predictive calculations. Flexural modulus was found to increase with the weight content of nanoclay up to a point. The 5% nanoclay specimens with high void content featured reduced flexural modulus.

The presence of cellulose fibre was found to increase the toughness properties of all composites compared to pure VER. However, nanoclay addition resulted in samples which were brittle due to the nanoclay's effect on the fibre-matrix adhesion limiting the mechanisms of fibre pull-out and fibre de-bonding. Therefore, the toughness properties of the eco-nanocomposites were lower than those of the eco-composites.

The eco-nanocomposites were found to have superior thermal properties. Both thermal stability and flammability results for the eco-nanocomposites were preferable to those of the eco-composites or pure samples. The temperature required for decomposition for eco-nanocomposites with 1 wt%, 3 wt%, and 5wt% of nanoclay was 387.1 °C, 399.76 °C, and 404.3°C temperatures respectively. For the eco-composites, constituent decomposition started at a lower temperature (380 °C). The superior thermal properties are believed to arise from the insulating mechanism

of nanoclay and the fact that the nanoclay acts as a mass transport barrier for volatile products of decomposition features. Nanoclay addition also promotes the formation of char which acts as a fire-retardant.

4.1.3.2 Viny-ester/RCF/HNT eco-nanocomposites

The greatest resistance to water absorption was achieved in the 5 wt% HNTs samples. The addition of 5 wt% HNTs reduced water absorption of unfiled eco-composites from 12.83 % to 9.58 %. It is believed that HNTs, as nano-fillers, interfere with the transfer paths of the water molecules transforming the original path of direct-fast polymer matrix diffusion into a torturous path reducing overall uptake of water

Compared unfilled eco-composites (4.82 GPa), eco-nanocomposites reinforced with 1, 3 and 5 wt% of HNTs exhibited enhancements in elastic moduli of 5.1, 5.8 and 5.2 GPa respectively. A moderate increase in flexural strength and impact strength was demonstrated on HNT addition. Reinforcement with 1, 3 and 5 wt% HNTs increased flexural strength from 148.4 MPa for unfilled eco-composites, to 156.1, 161.2 and 150.2 MPa respectively. Similarly, impact strength increased to 16.8, 18.9 and 16.1 kJ/m^2 respectively for 1, 3, and 5 wt% eco-nanocomposites. The observed enhancements in elastic modulus and strength properties are believed to arise from the reinforcing effect of both RCF and HNTs. In particular, HNT addition improved fibre–matrix adhesion in eco-nanocomposites and gave greater strength properties.

The presence of cellulose fibres increased the fracture toughness of all composites. This enhancement in fracture toughness is attributed to the toughness mechanism provided by cellulose fibres. While HNTs addition improves in fibre-matrix adhesion leading to increased eco-nanocomposites strength properties, as previously described, these improvements in fibre-matrix adhesion make the eco-nanocomposites brittle and prevent fibre pull-outs and fibre de-bonding. As these are major energy absorption mechanisms of the material, prevention of their action causes the composite to become brittle, and thereby, without mechanisms to absorb energy, the toughness properties of the eco-nanocomposites are reduced.

HNT addition increased thermal stability and fire-resisting properties of the eco-nanocomposites. Nano-fillers such as HNTs are believed to provide, firstly, a thermal barrier which prevents heat transfer inside the polymer matrix, and secondly a mass transport barrier which during the process of degradation forms a char which hinders the escape of the volatile products. The hollow tubular structure of HNTs is also reported to lead to enhanced thermal stability by enabling the entrapment of degradation products inside the lumens, causing effective delay in mass transfer leading to improved thermal stability. The presence of iron oxides, Fe_2O_3, in silicate fillers is believed to be flame retardant enhancing thermal stability of composites by trapping radicals during the process of degradation. The dominant reasons for the reduction in flammability of VER/HNT composites are believed to the barrier effects of HNTs and the char formation caused by HNTs. These mechanisms each provide insulation for the composites and act as heat and fire-retardants.

4.1.3.3 Viny-ester/RCF/n-SiC eco-nanocomposites

The addition of n-SiC reduced the porosity and the water uptake. The presence of n-SiC was found to enhance the elastic moduli of the samples. While the elastic modulus of the unfilled eco-composites was 4.8 GPa, the addition of 1, 3 and 5 wt% of n-SiC increased elastic moduli to 5.8, 6.2 and 6.9 GPa respectively. The n-SiC used in this study, as other nano-fillers, has a high specific surface area, which is believed to provide dense interfacial interaction with polymer matrix. The presence of n-SiC is believed to affect the mobility of surrounding chains in the polymer matrix which leads to increased matrix stiffness. Another reason believed to lead to increased matrix stiffness is the very high initial elastic modulus of the n-SiC (470 GPa) compared to that of pure VER (2.9 GPa) and the VER/RCF eco-composites (4.8 GPa). By virtue of the rule of mixtures, this high initial elastic modulus is believed to also contribute to the increased elastic modulus of each the eco-nanocomposites observed in this study. These two effects of n-SiC are believed to contribute to the overall stiffness of the composite.

Flexural strength and impact strength of the samples was also increased on the addition of n-SiC. While the flexural strength of unfilled eco-composites was 148.4

MPa, 1, 3 and 5 wt% n-SiC addition gave eco-nanocomposites with flexural strengths of 173.1, 176.1 and 179.4 MPa respectively. The addition of 1, 3, and 5 wt% of n-SiC also increased the impact strength of the samples from 15.9 kJ/m^2 for unfilled eco-composite to 21.8, 24.6 and 27.4 kJ/m^2 respectively for the eco-nanocomposites. These results support the belief that fibre-matrix adhesion is an important determinant of composite quality.

Improvement of fibre-matrix adhesion is confirmed by SEM micrographs. The pull-out lengths and the number of pull-outs appear notably greater in the eco-composites when compared to eco-nanocomposites. This supports the notion that the strength of interfacial adhesion is stronger in eco-nanocomposites compared to eco-composites. The improvements in interfacial adhesion for eco-nanocomposites may be explained by the notion of thermal expansion mismatch. Stress can develop at the interface between matrix and filler of composite materials as a result of thermal expansion mismatch. Due to the presence of lower thermal expansion fillers (RCF and n-SiC) extra compressive stresses can be induced at the filler/VER interfaces which serve to improve the interfacial adhesion.

In addition, the high specific surface area and high surface energy of n-SiC due to its nano-sized dimension can facilitate rapid phase interactions within the polymer matrix. Therefore, RCF-VER interfacial adhesion can be improved. Furthermore, n-SiC provides strong electrostatic attractive forces at the fibre-matrix interfaces serving to impart additional adhesion between the fibres and the matrix

The fracture toughness and impact toughness of eco-composites and eco-nanocomposites were significantly enhanced when compared to the control. The favourable toughness mechanisms that natural fibre-polymer composites provide such as crack-deflection, de-bonding between fibre and matrix, the pull-out effect and a fibre-bridging are believed to underpin these significant improvements. However, n-SiC addition resulted in reduced fracture toughness. The addition of 5 wt% n-SiC reduced the fracture toughness from 4.4 to 2.5 MPa.m$^{1/2}$ and the impact toughness from 42.3 to 23.1 kJ/m^2. The addition of n-SiC, as mentioned, resulted in strength improvements by virtue of enhanced interfacial adhesion. However, fibre-matrix adhesion enhancement causes the eco-nanocomposites to become more brittle

inhibiting fibre de-bonding and fibre pull-out and ultimately leading to lower fracture toughness.

The fracture toughness of eco-nanocomposites was lower than eco-composites. Notwithstanding this, the eco-nanocomposites showed better thermal stability and flammability by virtue of improved mass and heat barriers and the enhanced fibre-matrix interfacial adhesion provided by n-SiC.

4.2 Recommendations for Future Work

The primary objectives of this research have been achieved. The effects of recycled cellulose-fibre sheets, nano-fillers and multi-scale reinforcement (RCF/nano-fillers) dispersion on the microstructure, water absorption, fracture, mechanical, thermal and flammability properties of vinyl-ester resin were investigated and discussed.

The results of this research project have provided fundamental knowledge on the mechanism and performance of a new class of polymer eco-nanocomposites reinforced with nano-fillers and recycled cellulose fibres. Significant improvements in mechanical properties for RCF/vinyl-ester composites as a results of the new infiltration method, noticeable improvement in all properties of nano-filler reinforced vinyl-ester nanocomposites, and interesting improvement in all properties for nano-fillers filled RCF/vinyl-ester eco-nanocomposites compared to unfilled RCF/vinyl-ester composites successfully were achieved. For future work, there is a need to continue research and development in this field of materials science. Thus, the following recommendations have been formulated to help guide the future study:

1. In general, producing eco-composites with high fibre content and good fibre/matrix adhesion without chemical treatment is still challenging. Here, an infiltration method introduced in this project was successful in fabricating eco-composites with these qualities. This method significantly improved the mechanical properties (elastic modulus by 150 %), (flexural strength by 300 %), (impact strength by 1000 %) and (fracture toughness by 230 %) of VER as result of 50 wt. % RCF addition. Therefore, by adopting this method the

quantity of fibres that can be added may be able to be increased (> 50 wt%), which would lead to greater reinforcement effect.

2. In this project matrix reinforced with fixed concentrations of nano-filers (1, 3, 5 wt%) and fixed fibre content (40 wt. %) clearly displayed improved interfacial adhesion between fibre and the matrix which results to noticeable mechanical and thermal properties. Therefore, to obtain the optimum content of reinforcements, further investigation is required.

3. Nano-filler dispersion in this research was fairly homogenous with some particle agglomerations with the use of a high speed mixer for 30 minutes. Further work is required to achieve optimal dispersion for nano-fillers in polymer matrices. Therefore, different techniques and treatments are required to be investigated further to improve the nano-filler dispersion.

4. Advanced models are required to investigate the influence of nanostructures, such as shape and size distribution, orientation, aspect ratio, degree of spatial and interfaces on the physicomechanical properties of eco-nanocomposites. Multi-scale mechanics models and numerical methods should be developed for better understanding of the enhanced mechanisms of eco-nanocomposites materials.

5. Here, interesting results concerning the effect of nano-filler addition in enhancing water absorption resistance in RCF/vinyl-ester composites immersed in water. This study, however, did not investigate the effect of water absorption on the mechanical properties of the eco-nancomposites. Thus, experiments are required to study the effect of water diffusion on the mechanical properties of these eco-nanocomposites.

6. The primary aim of this project was to synthesize green eco-nanocomposites reinforced with nano-fillers and recycled cellulose fibres. It must be

conceded, however, that the use of vinyl-ester as a matrix means that the resulting composites is not entirely environmentally-friendly. Instead of 100% biodegradability, the biodegradability for the resulting ecocomposites in this study was estimated at 50% and even less for the eco-nanocomposites (~ 40%). Thus, there is a need to study the properties of non-petroleum-based or 100% biodegradable resins reinforced with cellulose fibres and eco-nanofillers.

5. APPENDICES

5.1APPENDIX I: Supplementary Information for Publication

5.1APPENDIX I-1: Supplementary Information for "Mechanical properties of cellulose fibre reinforced vinyl-ester composites in wet conditions"

ALHUTHALI, A. and LOW, I. M. 2013. Mechanical properties of cellulose fibre reinforced vinyl-ester composites in wet conditions. *Journal of Materials Science*, 48, 6331-6340.

5.1.1 Supporting Information

Impact Strength

Figure 5.1 shows the impact strength of VER/RCF composites in dry and wet conditions. For the dry samples, the addition of fibre content increased the impact strength markedly. Compared to the impact strength of pure VER (2.5 kJ/m^2), the addition of 20, 30, 40 and 50 wt% RCF increased impact strength to 10.3, 13.5, 18.9 and 28.7 kJ/m^2 respectively. Interestingly, the impact strength obtained in this study with 50 wt% RCF (28.7 kJ/m^2) was comparable to the impact strength of flax reinforced with polypropylene or maleated polypropylene, both of which have an impact strength of approximately 30 kJ/m^2. These are natural fibre reinforced composites commonly used in the automotive industry (Bos et al., 2006; Bax and Müssig, 2008).

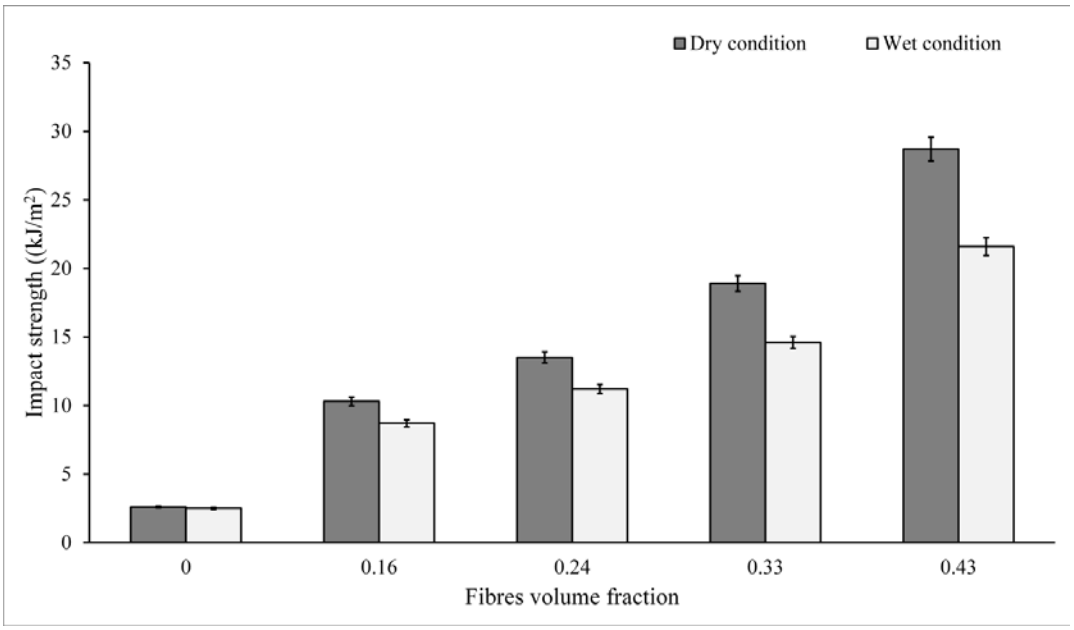

Figure 5.1: Impact strength versus fibre volume fraction in dry and wet conditions.

Impact strength is the ability of a material to resist fracture when experiencing high-speed stress. Fibres play an important role in impact resistance by transferring the stress of impact through energy dissipation mechanisms [(Mishra et al., 2003; Wambua et al., 2003]. Fibre pull-out, fibre fracture, and matrix deformation are believed to be important energy dissipation mechanisms that occur within fibre reinforced composites during impact [(Bax and Müssig, 2008)]. By increasing the fibre content, fibre reinforced composites with high impact strength can be fabricated (Bax and Müssig, 2008). Figure 5.1 also reveals a reduction in impact strength due to moisture absorption. Compared to the dry samples, the reductions of impact strength in the samples reinforced with 20, 30, 40 and 50 wt% RCF were 15.5, 17, 22.8 and 24.7 %, respectively. Water absorption also reduced the impact strength of composites by compromising the fibre–matrix bonding. For un-notched samples, the impact strength depended on the quality of the fibre–matrix adhesion. During the impact tests, good fibre–matrix adhesion enhanced the resistance of the composite to the fracture (Kim and Seo, 2006). Fig. 10 shows the fracture surfaces of composites

reinforced with 50wt% RCF in dry and wet conditions. For dry composite (see Fig. 5.1a) almost no fibre pull-out is observed and the fibres can be seen to be broken off near the surface. This observation is a result of strong bonding between the fibres and the matrix materials. However, in wet condition (see Fig. 5.1b) more fibre pull-out clearly observed as a result of poor fibre–matrix bonding due to the effect of water absorption. This supports the notion that, when composites are exposed to water absorption, impact strength will decrease.

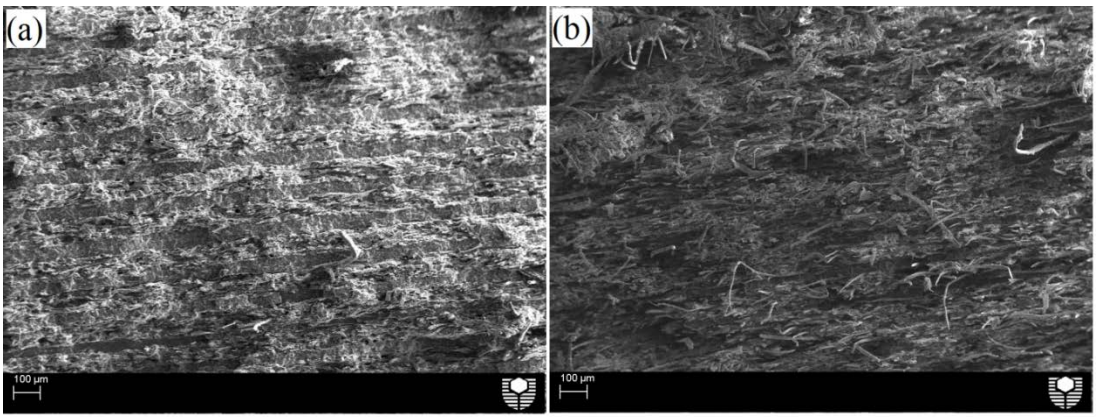

Figure 5.2: SEM micrographs showing the fracture surfaces of composites with 50 wt% RCF are shown (a) before and (b) after water absorption.

Fracture toughness

Figure 5.3 shows fracture toughness results as a function of fibre volume fraction for both dry and wet samples. The addition of RCF leads to enhancement in fracture toughness properties. Compared to that of the pure sample (1.78 $MPam^{1/2}$), adding 20, 30, 40 and 50 wt% RCF improved fracture toughness to 2.4, 3.8, 4.5 and 5.9 $MPam^{1/2}$, respectively. Interaction between the cellulose fibres and the matrix provided the composites with enhanced crack deflection, energy dissipation, and fracture resistance properties (Low et al., 2009; Bax and Müssig, 2008). Crack deflection, fibre–matrix de-bonding, fibre pull-out and fibre-bridging are believed to contribute to the fracture toughness of natural fibre reinforced polymer composites.

In the case of neat polymers, plastic deformation is an important energy dissipation mechanism (Venkateshwaran et al., 2011; Alhuthali et al., 2012); however, this mechanism is undermined by the addition of fibres. Nonetheless, overall material toughness is enhanced in composites by the mechanisms provided by natural fibre addition. High RCF content provided enhanced fracture toughness in the composites, which is believed to be a result of increased fibre pull-out, fibre fracture and fibre-bridging mechanisms.

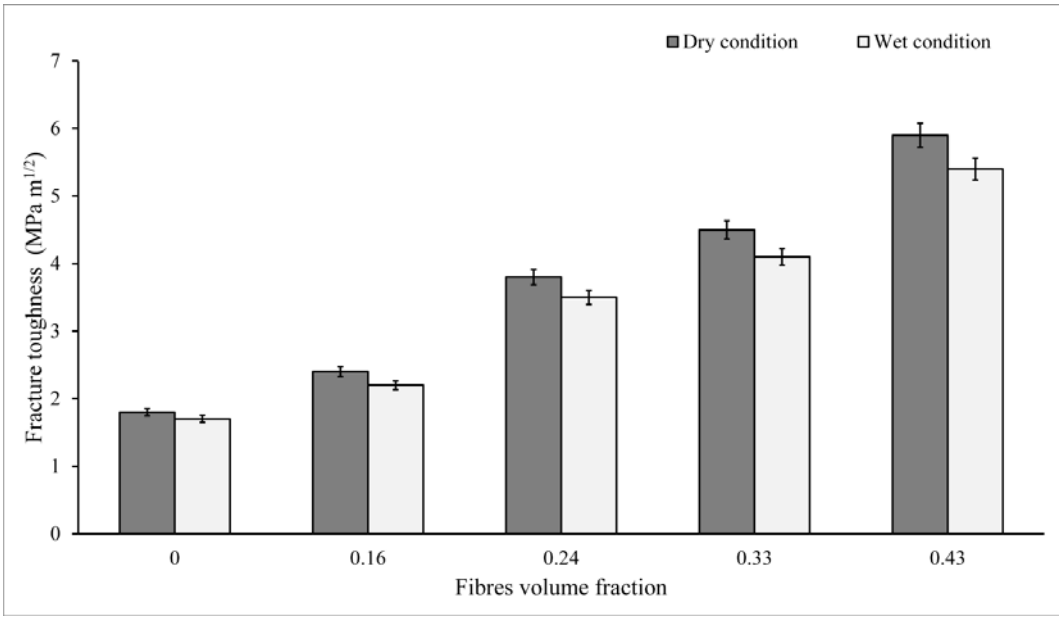

Figure 5.3: Fracture toughness versus fibre volume fraction in dry and wet conditions.

While composites can be prepared with high fracture toughness by adding natural fibre, this enhancement is dependent on interfacial adhesion. If the fibre–matrix adhesion is excessive, the composite will become brittle and exhibit poor toughness results. If the fibre–matrix adhesion is poor, fibre pull-out occurs readily and composites will again exhibit poor toughness results (Venkateshwaran at al., 2011; Bax and Müssig, 2008). Thus, achieving optimal fibre–matrix adhesion is paramount. The results of this study reveal a suitable level of fibre–matrix adhesion

that is supported by enhanced fracture toughness and strength. In this study, exposure to wet conditions caused a slight reduction in fracture toughness for the composite samples (see Fig. 5.3). Moisture absorption exposed the composites to water, which compromised the fibre–matrix interface. By weakening the fibre–matrix interface and causing poor fibre–matrix adhesion, fibre de-bonding and pull-out occur without substantial resistance. Thus, insufficient amount of energy will be dissipated by these mechanisms during the fracture test, leading to lower toughness values (Alhuthali et al., 2012)

5.2 APPENDIX II: Statement of Contributions of Other

5. 2 APPENDIX II-1: Statement of Contribution of Others for “Mechanical properties of cellulose fibre reinforced vinyl-ester composites in wet conditions”.

Statement of Contribution of Others for "Mechanical properties of cellulose fibre reinforced vinyl-ester composites in wet conditions".

3rd July 2013

To Whom It May Concern

I, Prof. It-Meng (Jim) Low, contributed by project supervision and manuscript editing to the paper/publication entitled

ALHUTHALI, A. and LOW, I. M. 2013. Mechanical properties of cellulose fibre reinforced vinyl-ester composites in wet conditions. *Journal of Materials Science,* DOI: 10.1007/s10853-013-7432-4

Undertaken with Abdullah Alhuthali

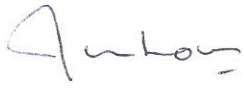

(Signature of Co-Author)

I. M. Low

(Signature of First Author)

Abdullah Alhuthali

5. 2 APPENDIX II-2: Statement of Contribution of Others for "Characterisation of the Water Absorption, Mechanical and Thermal Properties of Recycled Cellulose Fibre Reinforced Vinyl-ester Eco-nanocomposites".

Statement of Contribution of Others for "Characterisation of the Water Absorption, Mechanical and Thermal Properties of Recycled Cellulose Fibre Reinforced Vinyl-ester Eco-nanocomposites".

3rd July 2013

To Whom It May Concern

I, Prof. It-Meng (Jim) Low, contributed by project supervision and manuscript editing to the paper/publication entitled

ALHUTHALI, A., LOW, I. M. and DONG, C. 2012. Characterisation of the water absorption, mechanical and thermal properties of recycled cellulose fibre reinforced vinyl-ester eco-nanocomposites. *Composites Part B: Engineering*, 43, 2772-2781.

Undertaken with Abdullah Alhuthali

(Signature of Co-Author)
I. M. Low

(Signature of First Author)
Abdullah Alhuthali

Statement of Contribution of Others for "Characterisation of the Water Absorption, Mechanical and Thermal Properties of Recycled Cellulose Fibre Reinforced Vinyl-ester Eco-nanocomposites".

16th June 2012

To Whom It May Concern

I, Dr. C. Dong provided mechanical modelling to the paper/publication entitled

ALHUTHALI, A. LOW, I. M. and DONG, C. 2012. Characterisation of the water absorption, mechanical and thermal properties of recycled cellulose fibre reinforced vinyl-ester eco-nanocomposites. *Composites Part B: Engineering*, 43, 2772-2781.

Undertaken with Abdullah Alhuthali

(Signature of Co-Author)
C. Dong

(Signature of First Author)
Abdullah Alhuthali

5.2 APPENDIX II-3: Statement of Contribution of Others for “Influence of halloysite nanotubes on physical and mechanical properties of cellulose fibres reinforced vinyl ester composites”.

Statement of Contribution of Others for "Influence of halloysite nanotubes on physical and mechanical properties of cellulose fibres reinforced vinyl ester composites".

3rd July 2013

To Whom It May Concern

I, Prof. It-Meng (Jim) Low, contributed by project supervision and manuscript editing to the paper/publication entitled

ALHUTHALI, A. and LOW, I. M. 2013. Influence of halloysite nanotubes on physical and mechanical properties of cellulose fibres reinforced vinyl ester composites. *Journal of Reinforced Plastics and Composites,* 32, 233-247.

Undertaken with Abdullah Alhuthali

(Signature of Co-Author)

I. M. Low

(Signature of First Author)

Abdullah Alhuthali

5.3 APPENDIX II-4: Statement of Contribution of Others for “Multi-scale Hybrid Eco-nanocomposites: Synthesis and Characterization of Nano-SiC Reinforced Viny-ester Eco-composites”.

Statement of Contribution of Others for "Multi-scale Hybrid Eco-nanocomposites: Synthesis and Characterization of Nano-SiC Reinforced Viny-ester Eco-composites".

3rd July 2013

To Whom It May Concern

I, Prof. It-Meng (Jim) Low, contributed by project supervision and manuscript editing to the paper/publication entitled

ALHUTHALI, A. and LOW, I. M. 2013. Multi-scale hybrid eco-nanocomposites: synthesis and characterization of nano-SiC-reinforced vinyl-ester eco-composites. *Journal of Materials Science,* 48, 3097-3106.

Undertaken with Abdullah Alhuthali

(Signature of Co-Author)
Prof. It-Meng (Jim) Low

(Signature of First Author)
Abdullah Alhuthali

5.2 APPENDIX II-5: Statement of Contribution of Others for “Water Absorption, Mechanical, and Thermal Properties of Halloysite Nanotube Reinforced Vinyl-ester Nanocomposites”.

Statement of Contribution of Others for "Water Absorption, Mechanical, and Thermal Properties of Halloysite Nanotube Reinforced Vinyl-ester Nanocomposites".

3rd July 2013

To Whom It May Concern

I, Prof. It-Meng (Jim) Low, contributed by project supervision and manuscript editing to the paper/publication entitled

ALHUTHALI, A. and LOW, I. M. 2013. Water absorption, mechanical, and thermal properties of halloysite nanotube reinforced vinyl-ester nanocomposites. *Journal of Materials Science,* 48, 4260-4273.

Undertaken with Abdullah Alhuthali

(Signature of Co-Author)
Prof. It-Meng (Jim) Low

(Signature of First Author)
Abdullah Alhuthali

5.2 APPENDIX II-6: Statement of Contribution of Others for "Mechanical and Fracture Properties of Halloysite Nanotube Reinforced Vinyl-ester Nanocomposites".

Statement of Contribution of Others for "Mechanical and Fracture Properties of Halloysite Nanotube Reinforced Vinyl-ester Nanocomposites".

3rd July 2013

To Whom It May Concern

I, Prof. It-Meng (Jim) Low, contributed by project supervision and manuscript editing to the paper/publication entitled

ALHUTHALI, A. and LOW, I.M. 2013. Mechanical and fracture properties of halloysite nanotube reinforced vinyl-ester nanocomposites. *Journal of Applied Polymer Science*, DOI: 10.1002/app.39348

Undertaken with Abdullah Alhuthali

(Signature of Co-Author)
Prof. It-Meng (Jim) Low

(Signature of First Author)
Abdullah Alhuthali

5.2 APPENDIX II-7: Statement of Contribution of Others for "Characterisation of Mechanical and Fracture Behaviour in Nano-Silicon Carbide Reinforced Vinyl-Ester Nanocomposites".

Statement of Contribution of Others for "Characterisation of Mechanical and Fracture Behaviour in Nano-Silicon Carbide Reinforced Vinyl-Ester Nanocomposites".

3rd July 2013

To Whom It May Concern

I, Prof. It-Meng (Jim) Low, contributed by project supervision and manuscript editing to the paper/publication entitled

ALHUTHALI, A. M. and LOW, I. M. 2013. Characterisation of Mechanical and Fracture Behaviour in Nano-Silicon Carbide Reinforced Vinyl-Ester Nanocomposites. *Polymer-Plastics Technology and Engineering*, DOI:10.1080/03602559.2013.763372

Undertaken with Abdullah Alhuthali

(Signature of Co-Author)
Prof. It-Meng (Jim) Low

(Signature of First Author)
Abdullah Alhuthali

5.3 APPENDIX III: Copyright Forms

5.3 APPENDIX III-1: Copyright information relating to;

ALHUTHALI, A. and LOW, I. M. 2013. Mechanical properties of cellulose fibre reinforced vinyl-ester composites in wet conditions. *Journal of Materials Science*, DOI: 10.1007/s10853-013-7432-4

SPRINGER LICENSE
TERMS AND CONDITIONS

May 29, 2013

This is a License Agreement between Abdullah Alhuthali ("You") and Springer ("Springer") provided by Copyright Clearance Center ("CCC"). The license consists of your order details, the terms and conditions provided by Springer, and the payment terms and conditions.

All payments must be made in full to CCC. For payment instructions, please see information listed at the bottom of this form.

License Number	3158151370356
License date	May 29, 2013
Licensed content publisher	Springer
Licensed content publication	Journal of Materials Science (full set)
Licensed content title	Mechanical properties of cellulose fibre reinforced vinyl-ester composites in wet conditions
Licensed content author	A. Alhuthali
Licensed content date	Jan 1, 2013
Type of Use	Thesis/Dissertation
Portion	Full text
Number of copies	1
Author of this Springer article	Yes and you are the sole author of the new work
Order reference number	
Title of your thesis / dissertation	Microstructural Design of High Performance Natural Fibre Reinforced Vinyl-Ester Eco-Nanocomposites
Expected completion date	Jun 2013
Estimated size(pages)	250
Total	0.00 USD
Terms and Conditions	

The publisher for this copyrighted material is Springer Science + Business Media. By clicking "accept" in connection with completing this licensing transaction, you agree that the following terms and conditions apply to this transaction (along with the Billing and Payment terms and conditions established by Copyright Clearance Center, Inc. ("CCC"), at the time that you opened your Rightslink account and that are available at any time at http://myaccount.copyright.com).

5.3 APPENDIX III-2: Copyright information relating to;

ALHUTHALI, A. LOW, I. M. and DONG, C. 2012. Characterisation of the water absorption, mechanical and thermal properties of recycled cellulose fibre reinforced vinyl-ester eco-nanocomposites. *Composites Part B: Engineering*, 43, 2772-2781.

License Agreement with Elsevier

This is a License Agreement between Abdullah Alhuthali ("You") and Elsevier ("Elsevier") provided by Copyright Clearance Center ("CCC"). The license consists of your order details, the terms and conditions provided by Elsevier, and the payment terms and conditions.

All payments must be made in full to CCC. For payment instructions, please see information listed at the bottom of this form.

Supplier	Elsevier Limited The Boulevard,Langford Lane Kidlington,Oxford,OX5 1GB,UK
Registered Company Number	1982084
Customer name	Abdullah Alhuthali
Customer address	4/44 Armstrong Road, WILSON Perth, WA 6107
License number	3015810600023
License date	Oct 25, 2012
Licensed content publisher	Elsevier
Licensed content publication	Composites Part B: Engineering
Licensed content title	Characterisation of the water absorption, mechanical and thermal properties of recycled cellulose fibre reinforced vinyl-ester eco-nanocomposites
Licensed content author	A. Alhuthali,I.M. Low,C. Dong
Licensed content date	October 2012
Licensed content volume number	43
Licensed content issue number	7
Number of pages	10
Start Page	2772
End Page	2781
Type of Use	reuse in a thesis/dissertation
Portion	full article
Format	electronic

Are you the author of this Elsevier article?	Yes
Will you be translating?	No
Order reference number	
Title of your thesis/dissertation	Microstructural Design of High Performance Natural Fibre Reinforced Vinyl-Ester Eco-Nanocomposites
Expected completion date	Nov 2012
Estimated size (number of pages)	200
Elsevier VAT number	GB 494 6272 12
Permissions price	0.00 USD
VAT/Local Sales Tax	0.0 USD / 0.0 GBP
Total	0.00 USD

Terms and Conditions

Available on

http://www.elsevier.com/wps/find/authorsview.authors/rights

5.3 APPENDIX III-3: Copyright information relating to;

ALHUTHALI, A. and LOW, I. M. 2013. Influence of halloysite nanotubes on physical and mechanical properties of cellulose fibres reinforced vinyl ester composites. *Journal of Reinforced Plastics and Composites,* 32, 233-247.

Title: Influence of halloysite nanotubes on physical and mechanical properties of cellulose fibres reinforced vinyl ester composites:
Author: AM Alhuthali, IM Low
Publication: Journal of Reinforced Plastics and Composites
Publisher: Sage Publications
Date: Nov 13, 2012

Redirected Request

If you are an **Author** inquiring about the re-use of your journal article, please note that after publication of the journal article, Authors may re-use their content in any later work written or edited by the Author or for the Author's classroom use, without seeking permission from SAGE. For any other use of your work, please contact the publisher. For additional information see

www.sagepub.com/repository/binaries/journals/permissions/author_use.doc.

Journal Authors

Under the terms of your contributor agreement, without seeking permission, you may:

- At any time, distribute on a not-for-profit basis photocopies of the published article for your own teaching needs or to supply on an individual basis to research colleagues.
- At any time, circulate or post on any repository or website the version of the article that you submitted to the journal (i.e. the version before peer-review) or an abstract of the article.
- At least 12 months after publication, post on any non-commercial repository or website the version of your article that was accepted for publication.
- At least 12 months after publication, re-publish the whole or any part of the Contribution in a printed work written, edited or compiled by you provided reference is made to first publication by SAGE/SOCIETY.

When posting or re-using the article, please provide a link/URL from the article posted to the SAGE Journals Online where the article is published: http://online.sagepub.com and please make the following acknowledgment **'The final, definitive version of this paper has been published in <journal>, Vol/Issue, Month/Year by <<SAGE Publications Ltd.>>/<<SAGE Publications, Inc.>>, All rights reserved. © [as appropriate]**

The licenses granted above in this paragraph are expressly made subject to and limited by the following restrictions:

- The SAGE-created PDF of the published Contribution may not be posted at any time.
- In each instance of use of the Contribution, or any part of it, must include the copyright notice that appears on the issue of the Journal in which the Contribution is first published and a full bibliographic citation to the Journal as published by SAGE;
- Copies of the Contribution, or any part of it, shall not be sold, distributed, or reproduced for commercial purposes (i.e., for monetary gain on Contributor's own account or on that of a third party, or for indirect financial gain by a commercial entity);
- The Contribution, or any part of it, shall not be used for any systematic external distribution by a third party (e.g., a listserve or database connected to a public access server).

*All commercial requests and any other requests to re-use the article must be forwarded to SAGE.

UK Authors You may wish to register with the ALCS: http://www.alcs.co.uk/ so that you will receive royalties due to you from any reprographic rights income.

For any use of your work not stated above, please request permission using the instructions on the Journals permissions webpage at www.sagepub.com/journalspermissions.nav.

5.3 APPENDIX III-4: Copyright information relating to;

ALHUTHALI, A. and LOW, I. M. 2013. Multi-scale hybrid eco-nanocomposites: synthesis and characterization of nano-SiC-reinforced vinyl-ester eco-composites. *Journal of Materials Science,* 48, 3097-3106.

SPRINGER LICENSE
TERMS AND CONDITIONS

Dec 25, 2012

This is a License Agreement between Abdullah Alhuthali ("You") and Springer ("Springer") provided by Copyright Clearance Center ("CCC"). The license consists of your order details, the terms and conditions provided by Springer, and the payment terms and conditions.

All payments must be made in full to CCC. For payment instructions, please see information listed at the bottom of this form.

License Number	3055961435042
License date	Dec 25, 2012
Licensed content publisher	Springer
Licensed content publication	Journal of Materials Science (full set)
Licensed content title	Multi-scale hybrid eco-nanocomposites: synthesis and characterization of nano-SiC-reinforced vinyl-ester eco-composites
Licensed content author	A. Alhuthali
Licensed content date	Jan 1, 2012
Type of Use	Thesis/Dissertation
Portion	Full text
Number of copies	1
Author of this Springer article	Yes and you are the sole author of the new work
Order reference number	
Title of your thesis / dissertation	Microstructural Design of High Performance Natural Fibre Reinforced Vinyl-Ester Eco-Nanocomposites
Expected completion date	Feb 2013
Estimated size(pages)	250
Total	0.00 USD
Terms and Conditions	

The publisher for this copyrighted material is Springer Science + Business Media. By clicking "accept" in connection with completing this licensing transaction, you agree that the following terms and conditions apply to this transaction (along with the Billing and Payment terms and conditions established by Copyright Clearance Center, Inc. ("CCC"), at the time that you opened your Rightslink account and that are available at any time at http://myaccount.copyright.com).

5.3 APPENDIX III-5: Copyright information relating to;

ALHUTHALI, A. and LOW, I. M. 2013. Water absorption, mechanical, and thermal properties of halloysite nanotube reinforced vinyl-ester nanocomposites. *Journal of Materials Science,* 48, 4260-4273.

SPRINGER LICENSE
TERMS AND CONDITIONS

Mar 03, 2013

This is a License Agreement between Abdullah Alhuthali ("You") and Springer ("Springer") provided by Copyright Clearance Center ("CCC"). The license consists of your order details, the terms and conditions provided by Springer, and the payment terms and conditions.

All payments must be made in full to CCC. For payment instructions, please see information listed at the bottom of this form.

License Number	3101400061547
License date	Mar 03, 2013
Licensed content publisher	Springer
Licensed content publication	Journal of Materials Science (full set)
Licensed content title	Water absorption, mechanical, and thermal properties of halloysite nanotube reinforced vinyl-ester nanocomposites
Licensed content author	A. Alhuthali
Licensed content date	Jan 1, 2013
Type of Use	Thesis/Dissertation
Portion	Full text
Number of copies	1
Author of this Springer article	Yes and you are the sole author of the new work
Order reference number	
Title of your thesis / dissertation	Microstructural Design of High Performance Natural Fibre Reinforced Vinyl-Ester Eco-Nanocomposites
Expected completion date	Mar 2013
Estimated size(pages)	250
Total	0.00 USD
Terms and Conditions	

The publisher for this copyrighted material is Springer Science + Business Media. By clicking "accept" in connection with completing this licensing transaction, you agree that the following terms and conditions apply to this transaction (along with the Billing and Payment terms and conditions established by Copyright Clearance Center, Inc. ("CCC"), at the time that you opened your Rightslink account and that are available at any time at http://myaccount.copyright.com).

5.3 APPENDIX III-6: Copyright information relating to;

ALHUTHALI, A. and LOW, I.M. 2013. Mechanical and fracture properties of halloysite nanotube reinforced vinyl-ester nanocomposites. *Journal of Applied Polymer Science*, DOI: 10.1002/app.39348.

JOHN WILEY AND SONS LICENSE
TERMS AND CONDITIONS

May 19, 2013

This is a License Agreement between Abdullah Alhuthali ("You") and John Wiley and Sons ("John Wiley and Sons") provided by Copyright Clearance Center ("CCC"). The license consists of your order details, the terms and conditions provided by John Wiley and Sons, and the payment terms and conditions.

All payments must be made in full to CCC. For payment instructions, please see information listed at the bottom of this form.

License Number	3152721471430
License date	May 19, 2013
Licensed content publisher	John Wiley and Sons
Licensed content publication	Journal of Applied Polymer Science
Licensed content title	Mechanical and fracture properties of halloysite nanotube reinforced vinyl-ester nanocomposites
Licensed copyright line	Copyright © 2013 Wiley Periodicals, Inc.
Licensed content author	Abdullah Alhuthali,It-Meng Low
Licensed content date	May 6, 2013
Start page	n/a
End page	n/a
Type of use	Dissertation/Thesis
Requestor type	Author of this Wiley article
Format	Print and electronic
Portion	Full article
Will you be translating?	No
Total	0.00 USD

Terms and Conditions

TERMS AND CONDITIONS

This copyrighted material is owned by or exclusively licensed to John Wiley &

5.2 APPENDIX B-7: Copyright information relating to;

ALHUTHALI, A. M. and LOW, I. M. 2013. Characterisation of Mechanical and Fracture Behaviour in Nano-Silicon Carbide Reinforced Vinyl-Ester Nanocomposites. *Polymer-Plastics Technology and Engineering*, DOI:10.1080/03602559.2013.763372

BIBLIOGRAPHY

ABDELMOULEH, M., BOUFI, S., BELGACEM, M. N. & DUFRESNE, A. 2007. Short natural-fibre reinforced polyethylene and natural rubber composites: Effect of silane coupling agents and fibres loading. *Composites Science and Technology,* 67**,** 1627-1639.

AHMAD, F. N., JAAFAR, M., PALANIANDY, S. & AZIZLI, K. A. M. 2008. Effect of particle shape of silica mineral on the properties of epoxy composites. *Composites Science and Technology,* 68**,** 346-353.

AHMED, S. & JONES, F. R. 1990. A review of particulate reinforcement theories for polymer composites. *Journal of Materials Science,* 25**,** 4933-4942.

AJAYAN, P. M., SCHADLER, L. S. & BRAUN, P. V. 2006. *Nanocomposite science and technology,* Wiley-Vch.

AKIL, H. M., OMAR, M. F., MAZUKI, A. A. M., SAFIEE, S., ISHAK, Z. A. M. & ABU BAKAR, A. 2011. Kenaf fiber reinforced composites: A review. *Materials and Design,* 32**,** 4107-4121.

ALAM, P. 2010. A mixtures' model for porous particle–polymer composites. *Mechanics Research Communications,* 37**,** 389-393.

ALEXANDRE, M. & DUBOIS, P. 2000. Polymer-layered silicate nanocomposites: preparation, properties and uses of a new class of materials. *Materials Science and Engineering: R: Reports,* 28**,** 1-63.

ALHUTHALI, A., LOW, I. M. & DONG, C. 2012. Characterisation of the water absorption, mechanical and thermal properties of recycled cellulose fibre reinforced vinyl-ester eco-nanocomposites. *Composites Part B: Engineering,* 43**,** 2772-2781.

ANDERSONS, J., SPĀRNIŅŠ, E. & JOFFE, R. 2006. Stiffness and strength of flax fiber/polymer matrix composites. *Polymer Composites,* 27**,** 221-229.

ANUAR, H. & ZURAIDA, A. 2011. Improvement in mechanical properties of reinforced thermoplastic elastomer composite with kenaf bast fibre. *Composites Part B: Engineering,* 42**,** 462-465.

AQUINO, E. M. F., SARMENTO, L. P. S., OLIVEIRA, W. & SILVA, R. V. 2007. Moisture effect on degradation of jute/glass hybrid composites. *Journal of Reinforced Plastics and Composites,* 26**,** 219-233.

ARAÚJO, J. R., WALDMAN, W. R. & DE PAOLI, M. A. 2008. Thermal properties of high density polyethylene composites with natural fibres: Coupling agent effect. *Polymer Degradation and Stability,* 93**,** 1770-1775.

ARGON, A. S. & COHEN, R. E. 2003. Toughenability of polymers. *Polymer,* 44**,** 6013-6032.

ARORA, S., KUMAR, M. & KUMAR, M. 2012. Flammability and thermal degradation studies of PVA/rice husk composites. *Journal of Reinforced Plastics and Composites,* 31**,** 85-93.

ASHORI, A. & NOURBAKHSH, A. 2009. Characteristics of wood–fiber plastic composites made of recycled materials. *Waste Management,* 29**,** 1291-1295.

ASSARAR, M., SCIDA, D., EL MAHI, A., POILÂNE, C. & AYAD, R. 2011. Influence of water ageing on mechanical properties and damage events of two reinforced composite materials: Flax–fibres and glass–fibres. *Materials and Design,* 32**,** 788-795.

ATAEEFARD, M. & MORADIAN, S. 2011. Polypropylene/Organoclay Nanocomposites: Effects of Clay Content on Properties. *Polymer-Plastics Technology and Engineering,* 50**,** 732-739.

ATHIJAYAMANI, A., THIRUCHITRAMBALAM, M., NATARAJAN, U. & PAZHANIVEL, B. 2009. Effect of moisture absorption on the mechanical properties of randomly oriented natural fibers/polyester hybrid composite. *Materials Science and Engineering: A,* 517**,** 344-353.

AVELLA, M., BUZAROVSKA, A., ERRICO, M., GENTILE, G. & GROZDANOV, A. 2009. Eco-Challenges of Bio-Based Polymer Composites. *Materials,* 2**,** 911-925.

AVILÉS, F., CAUICH-RODRÍGUEZ, J., RODRÍGUEZ-GONZÁLEZ, J. & MAY-PAT, A. 2011. Oxidation and silanization of MWCNTs for MWCNT/vinyl ester composites. *Express Polymer Letters,* 5**,** 766-776.

AZIZ, S. H., ANSELL, M. P., CLARKE, S. J. & PANTENY, S. R. 2005. Modified polyester resins for natural fibre composites. *Composites Science and Technology,* 65**,** 525-535.

BAIARDO, M., FRISONI, G., SCANDOLA, M. & LICCIARDELLO, A. 2002. Surface chemical modification of natural cellulose fibers. *Journal of Applied Polymer Science,* 83**,** 38-45.

BAGHERI, R. & PEARSON, R. A. 1996. Role of particle cavitation in rubber-toughened epoxies: 1. Microvoid toughening. *Polymer,* 37**,** 4529-4538.

BAKARE, I. O., OKIEIMEN, F. E., PAVITHRAN, C., ABDUL KHALIL, H. P. S. & BRAHMAKUMAR, M. 2010. Mechanical and thermal properties of sisal fiber-reinforced rubber seed oil-based polyurethane composites. *Materials and Design,* 31**,** 4274-4280.

BALAKRISHNAN, H., HASSAN, A., IMRAN, M. & WAHIT, M. U. 2012. Toughening of Polylactic Acid Nanocomposites: A Short Review. *Polymer-Plastics Technology and Engineering,* 51**,** 175-192.

BALAKRISHNAN, S., START, P. R., RAGHAVAN, D. & HUDSON, S. D. 2005. The influence of clay and elastomer concentration on the morphology and fracture energy of preformed acrylic rubber dispersed clay filled epoxy nanocomposites. *Polymer,* 46**,** 11255-11262.

BAROULAKI, I., KARAKASI, O., PAPPA, G., TARANTILI, P. A., ECONOMIDES, D. & MAGOULAS, K. 2006. Preparation and study of plastic compounds containing polyolefins and post used newspaper fibers. *Composites Part A: Applied Science and Manufacturing,* 37**,** 1613-1625.

BAX, B. & MÜSSIG, J. 2008. Impact and tensile properties of PLA/cordenka and PLA/flax composites. *Composites Science and Technology,* 68**,** 1601-1607.

BECKER, O., SIMON, G. & DUSEK, K. 2005. Epoxy layered silicate nanocomposites. *Inorganic Polymeric Nanocomposites and Membranes.* Springer Berlin Heidelberg.

BECKER, O., VARLEY, R. & SIMON, G. 2002. Morphology, thermal relaxations and mechanical properties of layered silicate nanocomposites based upon high-functionality epoxy resins. *Polymer,* 43**,** 4365-4373.

BECKER, O., VARLEY, R. J. & SIMON, G. P. 2004. Thermal stability and water uptake of high performance epoxy layered silicate nanocomposites. *European Polymer Journal,* 40**,** 187-195.

BECKWITH, S. W. 2008. Natural fibers: Nature providing technology for composites. *SAMPE Journal,* 44**,** 64-65.

BESSADOK, A., MARAIS, S., ROUDESLI, S., LIXON, C. & MÉTAYER, M. 2008. Influence of chemical modifications on water-sorption and mechanical properties of Agave fibres. *Composites Part A: Applied Science and Manufacturing,* 39**,** 29-45.

BEYER, G. 2002. Nanocomposites: a new class of flame retardants for polymers. *Plastics, Additives and Compounding,* 4**,** 22-28.

BHARADWAJ, R. K. 2001. Modeling the barrier properties of polymer-layered silicate nanocomposites. *Macromolecules,* 34**,** 9189-9192.

BIGG, D. M. 1987. Mechanical properties of particulate filled polymers. *Polymer Composites,* 8**,** 115-122.

BISMARCK, A., ARANBERRI-ASKARGORTA, I., SPRINGER, J., LAMPKE, T., WIELAGE, B., STAMBOULIS, A., SHENDEROVICH, I. & LIMBACH, H.-H. 2002. Surface characterization of flax, hemp and cellulose fibers; Surface properties and the water uptake behavior. *Polymer Composites,* 23**,** 872-894.

BISMARCK, A., MISHRA, S. & LAMPKE, T. 2005. Plant fibers as reinforcement for green composites. *In:* MOHANTY, A., MISRA, M. & DRZAL, L. (eds.) *Natural fibers, biopolymers, and biocomposites.* Boca Raton: Taylor & Francis Group.

BISWAL, M., MOHANTY, S. & NAYAK, S. K. 2012. Thermal stability and flammability of banana-fiber-reinforced polypropylene nanocomposites. *Journal of Applied Polymer Science,* 125**,** E432-E443.

BLEDZKI, A. K. & GASSAN, J. 1999. Composites reinforced with cellulose based fibres. *Progress in Polymer Science,* 24**,** 221-274.

BOGOEVA-GACEVA, G., AVELLA, M., MALINCONICO, M., BUZAROVSKA, A., GROZDANOV, A., GENTILE, G. & ERRICO, M. E. 2007. Natural fiber eco-composites. *Polymer Composites,* 28**,** 98-107.

BOS, H. L., MÜSSIG, J. & VAN DEN OEVER, M. J. A. 2006. Mechanical properties of short-flax-fibre reinforced compounds. *Composites Part A: Applied Science and Manufacturing,* 37**,** 1591-1604.

BOURMAUD, A. & BALEY, C. 2009. Rigidity analysis of polypropylene/vegetal fibre composites after recycling. *Polymer Degradation and Stability,* 94**,** 297-305.

BOZKURT, E., KAYA, E. & TANOĞLU, M. 2007. Mechanical and thermal behavior of non-crimp glass fiber reinforced layered clay/epoxy nanocomposites. *Composites Science and Technology,* 67**,** 3394-3403.

BRILL, R. P. & PALMESE, G. R. 2000. An investigation of vinyl-ester-styrene bulk copolymerization cure kinetics using Fourier transform infrared spectroscopy. *Journal of Applied Polymer Science,* 76**,** 1572-1582.

CALLISTER, W. 2003. *Materials Science and Engineering: An introduction,* Hoboken, John Wiley & Sons, Inc.

CAUVIN, L., KONDO, D., BRIEU, M. & BHATNAGAR, N. 2010. Mechanical properties of polypropylene layered silicate nanocomposites: Characterization and micro-macro modelling. *Polymer Testing,* 29**,** 245-250.

CHAKRABORTY, P., GANGULY, A., MITRA, S. & BHOWMICK, A. K. 2008. Influence of phase modifiers on morphology and properties of thermoplastic elastomers prepared from ethylene propylene diene rubber and isotactic polypropylene. *Polymer Engineering & Science,* 48**,** 477-489.

CHAN, C.-M., WU, J., LI, J.-X. & CHEUNG, Y.-K. 2002. Polypropylene/calcium carbonate nanocomposites. *Polymer,* 43**,** 2981-2992.

CHANDRADASS, J., RAMESH KUMAR, M. & VELMURUGAN, R. 2008. Effect of clay dispersion on mechanical, Ttermal and vibration properties of glass fiber-reinforced vinyl ester composites. *Journal of Reinforced Plastics and Composites,* 27**,** 1585-1601.

CHANDRAMOHAN, A., VENGATESEN, M. R., DEVARAJU, S., DINAKARAN, K. & ALAGAR, M. 2012. Organoclay Filled Vinyl Ester Monomer Toughened Epoxy – Intercrosslinked Matrix Materials. *International Journal of Polymeric Materials***,** 62, 301-308

CHANG, P. R., JIAN, R., YU, J. & MA, X. 2010. Fabrication and characterisation of chitosan nanoparticles/plasticised-starch composites. *Food Chemistry,* 120**,** 736-740.

CHANG, P. R., XIE, Y., WU, D. & MA, X. 2011. Amylose wrapped halloysite nanotubes. *Carbohydrate Polymers,* 84**,** 1426-1429.

CHAO, Y. & LIU, S. 1997. On the failure of cracks under mixed-mode loads. *International Journal of Fracture,* 87**,** 201-223.

CHEN, B. & EVANS, J. R. G. 2006. Elastic moduli of clay platelets. *Scripta Materialia,* 54**,** 1581-1585.

CHEN, B. & EVANS, J. R. G. 2008. Impact and tensile energies of fracture in polymer–clay nanocomposites. *Polymer,* 49**,** 5113-5118.

CHEN, B. & EVANS, J. R. G. 2009. Impact strength of polymer-clay nanocomposites. *Soft Matter,* 5**,** 3572-3584.

CHEN, H., MIAO, M. & DING, X. 2009. Influence of moisture absorption on the interfacial strength of bamboo/vinyl ester composites. *Composites Part A: Applied Science and Manufacturing,* 40**,** 2013-2019.

CHEUNG, H.-Y., HO, M.-P., LAU, K.-T., CARDONA, F. & HUI, D. 2009. Natural fibre-reinforced composites for bioengineering and environmental engineering applications. *Composites Part B: Engineering,* 40**,** 655-663.

CHEVRIER, P. & KLEPACZKO, J. R. 1999. Spall fracture: Mechanical and microstructural aspects. *Engineering Fracture Mechanics,* 63**,** 273-294.

CHIGWADA, G., JASH, P., JIANG, D. D. & WILKIE, C. A. 2005. Fire retardancy of vinyl ester nanocomposites: Synergy with phosphorus-based fire retardants. *Polymer Degradation and Stability,* 89**,** 85-100.

CHISHOLM, N., MAHFUZ, H., RANGARI, V. K., ASHFAQ, A. & JEELANI, S. 2005. Fabrication and mechanical characterization of carbon/SiC-epoxy nanocomposites. *Composite Structures,* 67**,** 115-124.

CHOUDALAKIS, G. & GOTSIS, A. D. 2009. Permeability of polymer/clay nanocomposites: A review. *European Polymer Journal,* 45**,** 967-984.

CHRISSAFIS, K. & BIKIARIS, D. 2011. Can nanoparticles really enhance thermal stability of polymers? Part I: An overview on thermal decomposition of addition polymers. *Thermochimica Acta,* 523**,** 1-24.

CLEMONS, C. & CAULFIELD, D. 2005. Natural fibers. *In:* XANTHOS, M. (ed.) *Functional fillers for plastics.* 2 ed. Weinheim: WILEY-VCH.

COHEN, L. J. & ISHAI, O. 1967. The elastic properties of three-phase composites. *Journal of Composite Materials,* 1**,** 390-403.

COLOM, X., CARRASCO, F., PAGÈS, P. & CAÑAVATE, J. 2003. Effects of different treatments on the interface of HDPE/lignocellulosic fiber composites. *Composites Science and Technology,* 63**,** 161-169.

CONZATTI, L., GIUNCO, F., STAGNARO, P., CAPOBIANCO, M., CASTELLANO, M. & MARSANO, E. 2012. Polyester-based biocomposites containing wool fibres. *Composites Part A: Applied Science and Manufacturing,* 43**,** 1113-1119.

CURVELO, A. A. S., DE CARVALHO, A. J. F. & AGNELLI, J. A. M. 2001. Thermoplastic starch–cellulosic fibers composites: preliminary results. *Carbohydrate Polymers,* 45**,** 183-188.

DAVTYAN, S. P., BERLIN, A., AGABEKOV, V. & LEKISHVILI, N. 2012. Synthesis, properties, and applications of polymeric nanocomposites. *Journal of Nanomaterials,* 2012**,** 3.

DE ALBUQUERQUE, A. C., JOSEPH, K., HECKER DE CARVALHO, L. & D'ALMEIDA, J. R. M. 2000. Effect of wettability and ageing conditions on the physical and mechanical properties of uniaxially oriented jute-roving-reinforced polyester composites. *Composites Science and Technology,* 60**,** 833-844.

DE LA LUZ REUS MEDINA, M. & KUMAR, V. 2007. Comparative evaluation of powder and tableting properties of low and high degree of polymerization cellulose I and cellulose II excipients. *International Journal of Pharmaceutics,* 337**,** 202-209.

DE ROSA, I. M., KENNY, J. M., MANIRUZZAMAN, M., MONIRUZZAMAN, M., MONTI, M., PUGLIA, D., SANTULLI, C. & SARASINI, F. 2011. Effect of chemical treatments on the mechanical and thermal behaviour of okra (abelmoschus esculentus) fibres. *Composites Science and Technology,* 71**,** 246-254.

DE ROSA, I. M., SANTULLI, C. & SARASINI, F. 2010. Mechanical and thermal characterization of epoxy composites reinforced with random and quasi-unidirectional untreated Phormium tenax leaf fibers. *Materials and Design,* 31**,** 2397-2405.

DENG, S., YE, L. & FRIEDRICH, K. 2007. Fracture behaviours of epoxy nanocomposites with nano-silica at low and elevated temperatures. *Journal of Materials Science,* 42**,** 2766-2774.

DENG, S., ZHANG, J. & YE, L. 2009. Halloysite–epoxy nanocomposites with improved particle dispersion through ball mill homogenisation and chemical treatments. *Composites Science and Technology,* 69**,** 2497-2505.

DENG, S., ZHANG, J., YE, L. & WU, J. 2008. Toughening epoxies with halloysite nanotubes. *Polymer,* 49**,** 5119-5127.

DHAKAL, H. N., ZHANG, Z. Y. & RICHARDSON, M. O. W. 2007. Effect of water absorption on the mechanical properties of hemp fibre reinforced

unsaturated polyester composites. *Composites Science and Technology,* 67**,** 1674-1683.

DOAN, T.-T.-L., GAO, S.-L. & MÄDER, E. 2006. Jute/polypropylene composites I. Effect of matrix modification. *Composites Science and Technology,* 66**,** 952-963.

DONG, Y., CHAUDHARY, D., PLOUMIS, C. & LAU, K.-T. 2011. Correlation of mechanical performance and morphological structures of epoxy micro/nanoparticulate composites. *Composites Part A: Applied Science and Manufacturing,* 42**,** 1483-1492.

DU, M., GUO, B. & JIA, D. 2006. Thermal stability and flame retardant effects of halloysite nanotubes on poly(propylene). *European Polymer Journal,* 42**,** 1362-1369.

DU, M., GUO, B. & JIA, D. 2010. Newly emerging applications of halloysite nanotubes: a review. *Polymer International,* 59**,** 574-582.

DU, M., GUO, B., LEI, Y., LIU, M. & JIA, D. 2008. Carboxylated butadiene–styrene rubber/halloysite nanotube nanocomposites: Interfacial interaction and performance. *Polymer,* 49**,** 4871-4876.

ESFANDIARI, A. 2008. The statistical investigation of mechanical properties of PP/natural fibers composites. *Fibers and Polymers,* 9**,** 48-54.

ESPERT, A., VILAPLANA, F. & KARLSSON, S. 2004. Comparison of water absorption in natural cellulosic fibres from wood and one-year crops in polypropylene composites and its influence on their mechanical properties. *Composites Part A: Applied Science and Manufacturing,* 35**,** 1267-1276.

FACCA, A. G., KORTSCHOT, M. T. & YAN, N. 2006. Predicting the elastic modulus of natural fibre reinforced thermoplastics. *Composites Part A: Applied Science and Manufacturing,* 37**,** 1660-1671.

FARUK, O., BLEDZKI, A. K., FINK, H.-P. & SAIN, M. 2012. Biocomposites reinforced with natural fibers: 2000–2010. *Progress in Polymer Science,* 37**,** 1552-1596.

FARUK, O. & MATUANA, L. M. 2008. Nanoclay reinforced HDPE as a matrix for wood-plastic composites. *Composites Science and Technology,* 68**,** 2073-2077.

FORNES, T. D. & PAUL, D. R. 2003. Modeling properties of nylon 6/clay nanocomposites using composite theories. *Polymer,* 44**,** 4993-5013.

FRANCO-MARQUÈS, E., MÉNDEZ, J. A., PÈLACH, M. A., VILASECA, F., BAYER, J. & MUTJÉ, P. 2011. Influence of coupling agents in the preparation of polypropylene composites reinforced with recycled fibers. *Chemical Engineering Journal,* 166**,** 1170-1178.

FU, S.-Y., FENG, X.-Q., LAUKE, B. & MAI, Y.-W. 2008. Effects of particle size, particle/matrix interface adhesion and particle loading on mechanical properties of particulate–polymer composites. *Composites Part B: Engineering,* 39**,** 933-961.

GACITUA, W., BALLERINI, A. & ZHANG, J. 2005. Polymer nanocomposites: Synthetic and natural fillers. A review. *Maderas Cienc Tecnol,* 7, 159-178.

GANTENBEIN, D., SCHOELKOPF, J., MATTHEWS, G. P. & GANE, P. A. C. 2011. Determining the size distribution-defined aspect ratio of rod-like particles. *Applied Clay Science,* 53**,** 538-543.

GAO, X. & SHIH, C. F. 1998. A Parametric Study of mixed-mode I/III ductile fracture in tough materials under small scale yielding. *Engineering Fracture Mechanics,* 60**,** 407-420.

GARKHAIL, S. K., HEIJENRATH, R. W. H. & PEIJS, T. 2000. Mechanical properties of natural-fibre-mat- reinforced thermoplastics based on Flax Fibres and Polypropylene. *Applied Composite Materials,* 7**,** 351-372.

GHOSH, R., KRISHNA, A. R., REENA G, RAJU, B. L. 2011. Effect of fibre volume fraction on the tensile strength of banana fibre reinforced vinyl ester resin composites. International journal of advanced engeneering sciences and technology 4 (1):89–91.

GIANNAKAS, A., GIANNAKAS, A. & LADAVOS, A. 2012. Preparation and characterization of polystyrene/organolaponite nanocomposites. *Polymer-Plastics Technology and Engineering,* 51**,** 1411-1415.

GLASSER, W., KAAR, W., JAIN, R. & SEALEY, J. 2000. Isolation options for non-cellulosic heteropolysaccharides (HetPS). *Cellulose,* 7**,** 299-317.

GLOAGUEN, J. M. & LEFEBVRE, J. M. 2001. Plastic deformation behaviour of thermoplastic/clay nanocomposites. *Polymer,* 42**,** 5841-5847.

GOJNY, F. H., WICHMANN, M. H. G., FIEDLER, B., BAUHOFER, W. & SCHULTE, K. 2005. Influence of nano-modification on the mechanical and electrical properties of conventional fibre-reinforced composites. *Composites Part A: Applied Science and Manufacturing,* 36**,** 1525-1535.

GORRASI, G., TORTORA, M., VITTORIA, V., POLLET, E., LEPOITTEVIN, B., ALEXANDRE, M. & DUBOIS, P. 2003. Vapor barrier properties of polycaprolactone montmorillonite nanocomposites: effect of clay dispersion. *Polymer,* 44**,** 2271-2279.

GRISHCHUK, S., CASTELLÀ, N., APOSTOLOV, A. A. & KARGER-KOCSIS, J. 2012. Structure and properties of vinyl ester resins modified with organophilic synthetic layered silicates bearing non- and co-reactive intercalants. *Journal of Composite Materials,* 46**,** 941-947.

GUILLEMINOT, J., COMAS-CARDONA, S., KONDO, D., BINETRUY, C. & KRAWCZAK, P. 2008. Multiscale modelling of the composite reinforced foam core of a 3D sandwich structure. *Composites Science and Technology,* 68**,** 1777-1786.

GUO, Z., KIM, T. Y., LEI, K., PEREIRA, T., SUGAR, J. G. & HAHN, H. T. 2008a. Strengthening and thermal stabilization of polyurethane nanocomposites with silicon carbide nanoparticles by a surface-initiated-polymerization approach. *Composites Science and Technology,* 68**,** 164-170.

GUO, Z., LEI, K., LI, Y., NG, H. W., PRIKHODKO, S. & HAHN, H. T. 2008b. Fabrication and characterization of iron oxide nanoparticles reinforced vinyl-ester resin nanocomposites. *Composites Science and Technology,* 68**,** 1513-1520.

GUO, Z., LIANG, X., PEREIRA, T., SCAFFARO, R. & THOMAS HAHN, H. 2007. CuO nanoparticle filled vinyl-ester resin nanocomposites: Fabrication, characterization and property analysis. *Composites Science and Technology,* 67**,** 2036-2044.

GURTIN, M. E. & YATOMI, C. 1979. On a Model for Two Phase Diffusion in Composite Materials. *Journal of Composite Materials,* 13**,** 126-130.

HAMIDI, Y. K., AKTAS, L. & ALTAN, M. C. 2008. Effect of nanoclay content on void morphology in resin transfer molded composites. *Journal of Thermoplastic Composite Materials,* 21**,** 141-163.

HANDGE, U. A., HEDICKE-HÖCHSTÖTTER, K. & ALTSTÄDT, V. 2010. Composites of polyamide 6 and silicate nanotubes of the mineral halloysite: Influence of molecular weight on thermal, mechanical and rheological properties. *Polymer,* 51**,** 2690-2699.

HAQ, M., BURGUEÑO, R., MOHANTY, A. K. & MISRA, M. 2008. Hybrid bio-based composites from blends of unsaturated polyester and soybean oil reinforced with nanoclay and natural fibers. *Composites Science and Technology,* 68**,** 3344-3351.

HARGITAI, H., RÁCZ, I. & ANANDJIWALA, R. D. 2008. Development of HEMP fiber reinforced polypropylene composites. *Journal of Thermoplastic Composite Materials,* 21**,** 165-174.

HARISH, S., MICHAEL, D. P., BENSELY, A., LAL, D. M. & RAJADURAI, A. 2009. Mechanical property evaluation of natural fiber coir composite. *Materials Characterization,* 60**,** 44-49.

HASHEMIFARD, S. A., ISMAIL, A. F. & MATSUURA, T. 2011. Mixed matrix membrane incorporated with large pore size halloysite nanotubes (HNTs) as filler for gas separation: Morphological diagram. *Chemical Engineering Journal,* 172**,** 581-590.

HE, A., WANG, L., LI, J., DONG, J. & HAN, C. C. 2006. Preparation of exfoliated isotactic polypropylene/alkyl-triphenylphosphonium-modified montmorillonite nanocomposites via in situ intercalative polymerization. *Polymer,* 47**,** 1767-1771.

HEDICKE-HÖCHSTÖTTER, K., LIM, G. T. & ALTSTÄDT, V. 2009. Novel polyamide nanocomposites based on silicate nanotubes of the mineral halloysite. *Composites Science and Technology,* 69**,** 330-334.

HERRERA-FRANCO, P. J. & VALADEZ-GONZÁLEZ, A. 2005. A study of the mechanical properties of short natural-fiber reinforced composites. *Composites Part B: Engineering,* 36**,** 597-608.

HOLBERY, J. & HOUSTON, D. 2006. Natural-fiber-reinforced polymer composites in automotive applications. *JOM Journal of the Minerals, Metals and Materials Society,* 58**,** 80-86.

HONG, C. K., HWANG, I., KIM, N., PARK, D. H., HWANG, B. S. & NAH, C. 2008. Mechanical properties of silanized jute–polypropylene composites. *Journal of Industrial and Engineering Chemistry,* 14**,** 71-76.

HOSSAIN, M. K., DEWAN, M. W., HOSUR, M. & JEELANI, S. 2011. Mechanical performances of surface modified jute fiber reinforced biopol nanophased green composites. *Composites Part B: Engineering,* 42**,** 1701-1707.

HOTTA, S. & PAUL, D. R. 2004. Nanocomposites formed from linear low density polyethylene and organoclays. *Polymer,* 45**,** 7639-7654.

HSIEH, T. H., KINLOCH, A. J., MASANIA, K., TAYLOR, A. C. & SPRENGER, S. 2010. The mechanisms and mechanics of the toughening of epoxy polymers modified with silica nanoparticles. *Polymer,* 51**,** 6284-6294.

HUANG, X. & NETRAVALI, A. 2007. Characterization of flax fiber reinforced soy protein resin based green composites modified with nano-clay particles. *Composites Science and Technology,* 67**,** 2005-2014.

HUDA, M. S., DRZAL, L. T., MOHANTY, A. K. & MISRA, M. 2006. Chopped glass and recycled newspaper as reinforcement fibers in injection molded poly(lactic acid) (PLA) composites: A comparative study. *Composites Science and Technology,* 66**,** 1813-1824.

HUDA, M. S., DRZAL, L. T., MOHANTY, A. K. & MISRA, M. 2007. The effect of silane treated- and untreated-talc on the mechanical and physico-mechanical properties of poly(lactic acid)/newspaper fibers/talc hybrid composites. *Composites Part B: Engineering,* 38**,** 367-379.

HUSSAIN, F., HOJJATI, M., OKAMOTO, M. & GORGA, R. E. 2006. Review article: Polymer-matrix nanocomposites, processing, manufacturing, and application: An overview. *Journal of Composite Materials,* 40**,** 1511-1575.

ISMAIL, H., PASBAKHSH, P., FAUZI, M. N. A. & ABU BAKAR, A. 2008. Morphological, thermal and tensile properties of halloysite nanotubes filled ethylene propylene diene monomer (EPDM) nanocomposites. *Polymer Testing,* 27**,** 841-850.

JAWAID, M. & ABDUL KHALIL, H. P. S. 2011. Cellulosic/synthetic fibre reinforced polymer hybrid composites: A review. *Carbohydrate Polymers,* 86**,** 1-18.

JEBRANE, M. & SÈBE, G. 2008. A new process for the esterification of wood by reaction with vinyl esters. *Carbohydrate Polymers,* 72**,** 657-663.

JI, G. & LI, G. 2008. Effects of nanoclay morphology on the mechanical, thermal, and fire-retardant properties of vinyl ester based nanocomposite. *Materials Science and Engineering: A,* 498**,** 327-334.

JINHUA, W., XIANG, Z., BING, Z., YAFEI, Z., RUI, Z., JINDUN, L. & RONGFENG, C. 2010. Rapid adsorption of Cr (VI) on modified halloysite nanotubes. *Desalination,* 259**,** 22-28.

JOHN, M. J. & THOMAS, S. 2008. Biofibres and biocomposites. *Carbohydrate Polymers,* 71**,** 343-364.

JOHNSEN, B. B., KINLOCH, A. J., MOHAMMED, R. D., TAYLOR, A. C. & SPRENGER, S. 2007. Toughening mechanisms of nanoparticle-modified epoxy polymers. *Polymer,* 48**,** 530-541.

JOSEPH, P. V., JOSEPH, K. & THOMAS, S. 1999. Effect of processing variables on the mechanical properties of sisal-fiber-reinforced polypropylene composites. *Composites Science and Technology,* 59**,** 1625-1640.

JOSEPH, P. V., JOSEPH, K., THOMAS, S., PILLAI, C. K. S., PRASAD, V. S., GROENINCKX, G. & SARKISSOVA, M. 2003. The thermal and crystallisation studies of short sisal fibre reinforced polypropylene composites. *Composites Part A: Applied Science and Manufacturing,* 34**,** 253-266.

JOSEPH, P. V., RABELLO, M. S., MATTOSO, L. H. C., JOSEPH, K. & THOMAS, S. 2002. Environmental effects on the degradation behaviour of sisal fibre reinforced polypropylene composites. *Composites Science and Technology,* 62**,** 1357-1372.

JOUSSEIN, E., PETIT, S., CHURCHMAN, J., THENG, B., RIGHI, D. & DELVAUX, B. 2005. Halloysite clay minerals: A review. *Clay Minerals,* 40**,** 383-426.

KANEKO, M. L. Q. A., ROMERO, R. B., DE PAIVA, R. E. F., FELISBERTI, M. I., GONÇALVES, M. C. & YOSHIDA, I. V. P. 2013. Improvement of toughness in polypropylene nanocomposite with the addition of organoclay/silicone copolymer masterbatch. *Polymer Composites,* 34**,** 194-203.

KARBOWIAK, T., FERRET, E., DEBEAUFORT, F., VOILLEY, A. & CAYOT, P. 2011. Investigation of water transfer across thin layer biopolymer films by infrared spectroscopy. *Journal of Membrane Science,* 370**,** 82-90.

KASHIWAGI, T., GRULKE, E., HILDING, J., HARRIS, R., AWAD, W. & DOUGLAS, J. 2002. Thermal degradation and flammability properties of poly(propylene)/carbon nanotube composites. *Macromolecular Rapid Communications,* 23**,** 761-765.

KAULLY, T., SIEGMANN, A. & SHACHAM, D. 2008. Mechanical behavior of highly filled natural $CaCO_3$ composites: Effect of particle size distribution and interface interactions. *Polymer Composites,* 29**,** 396-408.

KAUSCH, H. H., HASSELL, J. A. & JAFFEE, R. I. 1973. Deformation and fracture of high polymers. *Science,* 181**,** 961-962.

KAWAGUCHI, T. & PEARSON, R. A. 2003. The effect of particle–matrix adhesion on the mechanical behavior of glass filled epoxies: Part 1. A study on yield behavior and cohesive strength. *Polymer,* 44**,** 4229-4238.

KAWAGUCHI, T. & PEARSON, R. A. 2004. The moisture effect on the fatigue crack growth of glass particle and fiber reinforced epoxies with strong and weak bonding conditions: Part 2. A microscopic study on toughening mechanism. *Composites Science and Technology,* 64**,** 1991-2007.

KAYNAK, C., SIPAHI-SAGLAM, E. & AKOVALI, G. 2001. A fractographic study on toughening of epoxy resin using ground tyre rubber. *Polymer,* 42**,** 4393-4399.

KHOATHANE, M. C., VORSTER, O. C. & SADIKU, E. R. 2008. Hemp fiber-reinforced 1-pentene/polypropylene copolymer: The effect of fiber foading on the mechanical and thermal characteristics of the composites. *Journal of Reinforced Plastics and Composites,* 27**,** 1533-1544.

KIM, H. J. & SEO, D. W. 2006. Effect of water absorption fatigue on mechanical properties of sisal textile-reinforced composites. *International Journal of Fatigue,* 28**,** 1307-1314.

KIM, J.-K., HU, C., WOO, R. S. C. & SHAM, M.-L. 2005. Moisture barrier characteristics of organoclay–epoxy nanocomposites. *Composites Science and Technology,* 65**,** 805-813.

KINLOCH, A. J., MOHAMMED, R. D., TAYLOR, A. C., SPRENGER, S. & EGAN, D. 2006. The interlaminar toughness of carbon-fibre reinforced plastic composites using 'hybrid-toughened' matrices. *Journal of Materials Science,* 41**,** 5043-5046.

KINLOCH, A. J., MAXWELL, D. L. & YOUNG, R. J. 1985. The fracture of hybrid-particulate composites. *Journal of Materials Science,* 20**,** 4169-4184.

KITEY, R. & TIPPUR, H. V. 2005. Role of particle size and filler–matrix adhesion on dynamic fracture of glass-filled epoxy. I. Macromeasurements. *Acta Materialia,* 53**,** 1153-1165.

KLAYSOM, C., MOON, S.-H., LADEWIG, B. P., LU, G. Q. M. & WANG, L. 2011. The effects of aspect ratio of inorganic fillers on the structure and property of composite ion-exchange membranes. *Journal of Colloid and Interface Science,* 363**,** 431-439.

KOH, H. C., PARK, J. S., JEONG, M. A., HWANG, H. Y., HONG, Y. T., HA, S. Y. & NAM, S. Y. 2008. Preparation and gas permeation properties of biodegradable polymer/layered silicate nanocomposite membranes. *Desalination,* 233**,** 201-209.

KONG, M. J., LEE, S. S., LYUBOVITSKY, J. & BENT, S. F. 1996. Infrared spectroscopy of methyl groups on silicon. *Chemical Physics Letters,* 263**,** 1-7.

KOTSILKOVA, R., PETKOVA, V. & PELOVSKI, Y. 2001. Thermal analysis of polymer-silicate nanocomposites. *Journal of Thermal Analysis and Calorimetry,* 64**,** 591-598.

KU, H., CHAN, W. L., TRADA, M. & BADDELEY, D. 2007. An evaluation of fracture toughness of vinyl ester composites cured under microwave conditions. *Journal of Materials Engineering and Performance,* 16**,** 741-745.

KU, H., WANG, H., PATTARACHAIYAKOOP, N. & TRADA, M. 2011. A review on the tensile properties of natural fiber reinforced polymer composites. *Composites Part B: Engineering,* 42**,** 856-873.

KUESENG, K. & JACOB, K. I. 2006. Natural rubber nanocomposites with SiC nanoparticles and carbon nanotubes. *European Polymer Journal,* 42**,** 220-227.

KUMAR, R., YAKABU, M. K. & ANANDJIWALA, R. D. 2010. Effect of montmorillonite clay on flax fabric reinforced poly lactic acid composites with amphiphilic additives. *Composites Part A: Applied Science and Manufacturing,* 41**,** 1620-1627.

LADHARI, A., BEN DALY, H., BELHADJSALAH, H., COLE, K. C. & DENAULT, J. 2010. Investigation of water absorption in clay-reinforced polypropylene nanocomposites. *Polymer Degradation and Stability,* 95**,** 429-439.

LAMY, B. & BALEY, C. 2000. Stiffness prediction of flax fibers-epoxy composite materials. *Journal of Materials Science Letters,* 19**,** 979-980.

LANGE, F. F. 1970. The interaction of a crack front with a second-phase dispersion. *Philosophical Magazine,* 22**,** 0983-0992.

LANGE, J. & WYSER, Y. 2003. Recent innovations in barrier technologies for plastic packaging: A review. *Packaging Technology and Science,* 16**,** 149-158.

LAPLANTE, G., OURIADOV, A. V., LEE-SULLIVAN, P. & BALCOM, B. J. 2008. Anomalous moisture diffusion in an epoxy adhesive detected by magnetic resonance imaging. *Journal of Applied Polymer Science,* 109**,** 1350-1359.

LASAGABASTER, A., ABAD, M. J., BARRAL, L. & ARES, A. 2006. FTIR study on the nature of water sorbed in polypropylene (PP)/ethylene alcohol vinyl (EVOH) films. *European Polymer Journal,* 42**,** 3121-3132.

LASAGABÁSTER, A., ABAD, M. J., BARRAL, L., ARES, A. & BOUZA, R. 2009. Application of FTIR spectroscopy to determine transport properties and water–polymer interactions in polypropylene (PP)/poly(ethylene-co-vinyl alcohol) (EVOH) blend films: Effect of poly(ethylene-co-vinyl alcohol) content and water activity. *Polymer,* 50**,** 2981-2989.

LE DUIGOU, A., DAVIES, P. & BALEY, C. 2010. Interfacial bonding of flax fibre/Poly(l-lactide) bio-composites. *Composites Science and Technology,* 70**,** 231-239.

LECOUVET, B., GUTIERREZ, J. G., SCLAVONS, M. & BAILLY, C. 2011a. Structure–property relationships in polyamide 12/halloysite nanotube nanocomposites. *Polymer Degradation and Stability,* 96**,** 226-235.

LECOUVET, B., SCLAVONS, M., BOURBIGOT, S., DEVAUX, J. & BAILLY, C. 2011b. Water-assisted extrusion as a novel processing route to prepare polypropylene/halloysite nanotube nanocomposites: Structure and properties. *Polymer,* 52**,** 4284-4295.

LEE, B.-H., KIM, H.-J. & YU, W.-R. 2009. Fabrication of long and discontinuous natural fiber reinforced polypropylene biocomposites and their mechanical properties. *Fibers and Polymers,* 10**,** 83-90.

LEE, J.-H., JUNG, D., HONG, C.-E., RHEE, K. Y. & ADVANI, S. G. 2005. Properties of polyethylene-layered silicate nanocomposites prepared by melt intercalation with a PP-g-MA compatibilizer. *Composites Science and Technology,* 65**,** 1996-2002.

LEE, J. & YEE, A. F. 2001. Inorganic particle toughening II: toughening mechanisms of glass bead filled epoxies. *Polymer,* 42**,** 589-597.

LEI, Y., WU, Q., CLEMONS, C. M., YAO, F. & XU, Y. 2007. Influence of nanoclay on properties of HDPE/wood composites. *Journal of Applied Polymer Science,* 106**,** 3958-3966.

LESZCZYŃSKA, A., NJUGUNA, J., PIELICHOWSKI, K. & BANERJEE, J. R. 2007. Polymer/montmorillonite nanocomposites with improved thermal properties: Part I. Factors influencing thermal stability and mechanisms of thermal stability improvement. *Thermochimica Acta,* 453**,** 75-96.

LI, Y., MAI, Y.-W. & YE, L. 2000. Sisal fibre and its composites: a review of recent developments. *Composites Science and Technology,* 60**,** 2037-2055.

LIAO, C. Z., BAO, S. P. & TJONG, S. C. 2011. Effect of silicon carbide nanoparticle additions on microstructure and mechanical behavior of maleic anhydride compatibilized high density polyethylene composites. *Composite Interfaces,* 18**,** 107-120.

LIM, S.-H., DASARI, A., YU, Z.-Z., MAI, Y.-W., LIU, S. & YONG, M. S. 2007. Fracture toughness of nylon 6/organoclay/elastomer nanocomposites. *Composites Science and Technology,* 67**,** 2914-2923.

LIU, L., QI, Z. & ZHU, X. 1999. Studies on nylon 6/clay nanocomposites by melt-intercalation process. *Journal of Applied Polymer Science,* 71**,** 1133-1138.

LIU, M., GUO, B., DU, M., X., C. & JIA, D. 2007. Properties of halloysite nanotube–epoxy resin hybrids and the interfacial reactions in the systems. *Nanotechnology,* 18**,** 455703 (9pp).

LIU, Q. & HUGHES, M. 2008. The fracture behaviour and toughness of woven flax fibre reinforced epoxy composites. *Composites Part A: Applied Science and Manufacturing,* 39**,** 1644-1652.

LIU, S., CHAO, Y. J. & ZHU, X. 2004. Tensile-shear transition in mixed mode I/III fracture. *International Journal of Solids and Structures,* 41**,** 6147-6172.

LIU, W., HOA, S. V. & PUGH, M. 2005a. Fracture toughness and water uptake of high-performance epoxy/nanoclay nanocomposites. *Composites Science and Technology,* 65**,** 2364-2373.

LIU, W., HOA, S. V. & PUGH, M. 2005b. Organoclay-modified high performance epoxy nanocomposites. *Composites Science and Technology,* 65**,** 307-316.

LIU, W., HOA, S. V. & PUGH, M. 2008a. Water uptake of epoxy–clay nanocomposites: Experiments and model validation. *Composites Science and Technology,* 68**,** 2066-2072.

LIU, W., HOA, S. V. & PUGH, M. 2008b. Water uptake of epoxy–clay nanocomposites: Model development. *Composites Science and Technology,* 68**,** 156-163.

LIU, W., MOHANTY, A. K., DRZAL, L. T., ASKEL, P. & MISRA, M. 2004. Effects of alkali treatment on the structure, morphology and thermal properties of native grass fibers as reinforcements for polymer matrix composites. *Journal of Materials Science,* 39**,** 1051-1054.

LIU, X. & WU, Q. 2002. Polyamide 66/clay nanocomposites via melt intercalation. *Macromolecular Materials and Engineering,* 287**,** 180-186.

LOO, L. S. & GLEASON, K. K. 2004. Investigation of polymer and nanoclay orientation distribution in nylon 6/montmorillonite nanocomposite. *Polymer,* 45**,** 5933-5939.

LOW, I. M. 1990. Effects of residual stresses on the failure micromechanisms in toughened epoxy systems. *Journal of Materials Science,* 25**,** 2144-2148.

LOW, I. M., MCGRATH, M., LAWRENCE, D., SCHMIDT, P., LANE, J., LATELLA, B. A. & SIM, K. S. 2007. Mechanical and fracture properties of cellulose-fibre-reinforced epoxy laminates. *Composites Part A: Applied Science and Manufacturing,* 38**,** 963-974.

LOW, I. M., SOMERS, J., KHO, H. S., DAVIES, I. J. & LATELLA, B. A. 2009. Fabrication and properties of recycled cellulose fibre-reinforced epoxy composites. *Composite Interfaces,* 16**,** 659-669.

LU, J., ASKELAND, P. & DRZAL, L. T. 2008. Surface modification of microfibrillated cellulose for epoxy composite applications. *Polymer,* 49**,** 1285-1296.

MA, J., MO, M.-S., DU, X.-S., ROSSO, P., FRIEDRICH, K. & KUAN, H.-C. 2008. Effect of inorganic nanoparticles on mechanical property, fracture toughness and toughening mechanism of two epoxy systems. *Polymer,* 49**,** 3510-3523.

MA, X., YU, J. & KENNEDY, J. F. 2005. Studies on the properties of natural fibers-reinforced thermoplastic starch composites. *Carbohydrate Polymers,* 62**,** 19-24.

MAGARAPHAN, R., LILAYUTHALERT, W., SIRIVAT, A. & SCHWANK, J. W. 2001. Preparation, structure, properties and thermal behavior of rigid-rod polyimide/montmorillonite nanocomposites. *Composites Science and Technology,* 61**,** 1253-1264.

MAJEWSKI, P., CHOUDHURY, N. R., SPORI, D., WOHLFAHRT, E. & WOHLSCHLOEGEL, M. 2006. Synthesis and characterisation of star polymer/silicon carbide nanocomposites. *Materials Science and Engineering: A*, 434**,** 360-364.

MALLICK, P. 2007. *Fiber-reinforced composites: Materials, manufacturing, and design* New York, CRC Press: Taylor & Francis Group.

MAMMERI, F., BOURHIS, E. L., ROZES, L. & SANCHEZ, C. 2005. Mechanical properties of hybrid organic-inorganic materials. *Journal of Materials Chemistry*, 15**,** 3787-3811.

MANFREDI, L. B., RODRÍGUEZ, E. S., WLADYKA-PRZYBYLAK, M. & VÁZQUEZ, A. 2006. Thermal degradation and fire resistance of unsaturated polyester, modified acrylic resins and their composites with natural fibres. *Polymer Degradation and Stability*, 91**,** 255-261.

MARNEY, D. C. O., RUSSELL, L. J., WU, D. Y., NGUYEN, T., CRAMM, D., RIGOPOULOS, N., WRIGHT, N. & GREAVES, M. 2008. The suitability of halloysite nanotubes as a fire retardant for nylon 6. *Polymer Degradation and Stability*, 93**,** 1971-1978.

MARSH, G. 2007. Vinyl ester: The midway boat building resin. *Reinforced Plastics*, 51**,** 20-23.

MASOURAS, K., SILIKAS, N. & WATTS, D. C. 2008. Correlation of filler content and elastic properties of resin-composites. *Dental Materials*, 24**,** 932-939.

MCNALLY, T., RAYMOND MURPHY, W., LEW, C. Y., TURNER, R. J. & BRENNAN, G. P. 2003. Polyamide-12 layered silicate nanocomposites by melt blending. *Polymer*, 44**,** 2761-2772.

MENEGHETTI, P. & QUTUBUDDIN, S. 2006. Synthesis, thermal properties and applications of polymer-clay nanocomposites. *Thermochimica Acta*, 442**,** 74-77.

MENG, J. & HU, X. 2004. Synthesis and exfoliation of bismaleimide–organoclay nanocomposites. *Polymer*, 45**,** 9011-9018.

MISHRA, S., MOHANTY, A. K., DRZAL, L. T., MISRA, M., PARIJA, S., NAYAK, S. K. & TRIPATHY, S. S. 2003. Studies on mechanical performance of biofibre/glass reinforced polyester hybrid composites. *Composites Science and Technology*, 63**,** 1377-1385.

MITTAL, V. 2009. Polymer layered silicate nanocomposites: A review. *Materials,* 2**,** 992-1057.

MOHAN, T. P. & KANNY, K. 2011. Water barrier properties of nanoclay filled sisal fibre reinforced epoxy composites. *Composites Part A: Applied Science and Manufacturing,* 42**,** 385-393.

MOHANTY, A. K., MISRA, M. & DRZAL, L. T. 2005. *Natural fibers, biopolymers, and biocomposites,* CRC.

MOHANTY, A. K., WIBOWO, A., MISRA, M. & DRZAL, L. T. 2004. Effect of process engineering on the performance of natural fiber reinforced cellulose acetate biocomposites. *Composites Part A: Applied Science and Manufacturing,* 35**,** 363-370.

MOHNEN, D. 2008. Pectin structure and biosynthesis. *Current Opinion in Plant Biology,* 11**,** 266-277.

MONTEIRO, S., LOPES, F., FERREIRA, A. & NASCIMENTO, D. 2009. Natural-fiber polymer-matrix composites: Cheaper, tougher, and environmentally friendly. *JOM Journal of the Minerals, Metals and Materials Society,* 61**,** 17-22.

MORGAN, A. B. 2006. Flame retarded polymer layered silicate nanocomposites: a review of commercial and open literature systems. *Polymers for Advanced Technologies,* 17**,** 206-217.

MUÑOZ, M. A., CARMONA, C. & BALÓN, M. 2007. FTIR study of water clusters in water–triethylamine solutions. *Chemical Physics,* 335**,** 37-42.

MYLSAMY, K. & RAJENDRAN, I. 2011. The mechanical properties, deformation and thermomechanical properties of alkali treated and untreated Agave continuous fibre reinforced epoxy composites. *Materials and Design,* 32**,** 3076-3084.

NING, N.-Y., YIN, Q.-J., LUO, F., ZHANG, Q., DU, R. & FU, Q. 2007. Crystallization behavior and mechanical properties of polypropylene/halloysite composites. *Polymer,* 48**,** 7374-7384.

NORMAN, D. A. & ROBERTSON, R. E. 2003. Rigid-particle toughening of glassy polymers. *Polymer,* 44**,** 2351-2362.

OH, S. Y., YOO, D. I., SHIN, Y. & SEO, G. 2005. FTIR analysis of cellulose treated with sodium hydroxide and carbon dioxide. *Carbohydrate Research,* 340**,** 417-428.

OKAMOTO, M. 2006. Recent advances in polymer/layered silicate nanocomposites: an overview from science to technology. *Materials Science and Technology,* 22**,** 756-779.

OKSMAN, K., MATHEW, A. P., LÅNGSTRÖM, R., NYSTRÖM, B. & JOSEPH, K. 2009. The influence of fibre microstructure on fibre breakage and mechanical properties of natural fibre reinforced polypropylene. *Composites Science and Technology,* 69**,** 1847-1853.

OKUBO, K., FUJII, T. & THOSTENSON, E. T. 2009. Multi-scale hybrid biocomposite: Processing and mechanical characterization of bamboo fiber reinforced PLA with microfibrillated cellulose. *Composites Part A: Applied Science and Manufacturing,* 40**,** 469-475.

OSORIO, L., TRUJILLO, E., VAN VUURE, A. W. & VERPOEST, I. 2011. Morphological aspects and mechanical properties of single bamboo fibers and flexural characterization of bamboo/ epoxy composites. *Journal of Reinforced Plastics and Composites,* 30**,** 396-408.

PARK, J. H. & JANA, S. C. 2003. Mechanism of exfoliation of nanoclay particles in epoxy−clay nanocomposites. *Macromolecules,* 36**,** 2758-2768.

PASBAKHSH, P., ISMAIL, H., FAUZI, M. N. A. & BAKAR, A. A. 2010. EPDM/modified halloysite nanocomposites. *Applied Clay Science,* 48**,** 405-413.

PASHAEI, S., SIDDARAMAIAH & SYED, A. A. 2011. Investigation on mechanical, thermal and morphological behaviors of turmeric spent incorporated vinyl ester green composites. *Polymer-Plastics Technology and Engineering,* 50**,** 1187-1198.

PAUL, D. R. & ROBESON, L. M. 2008. Polymer nanotechnology: Nanocomposites. *Polymer,* 49**,** 3187-3204.

PAUL, M.-A., ALEXANDRE, M., DEGÉE, P., HENRIST, C., RULMONT, A. & DUBOIS, P. 2003. New nanocomposite materials based on plasticized poly(l-lactide) and organo-modified montmorillonites: thermal and morphological study. *Polymer,* 44**,** 443-450.

PAVLIDOU, S. & PAPASPYRIDES, C. D. 2008. A review on polymer–layered silicate nanocomposites. *Progress in Polymer Science,* 33**,** 1119-1198.

PÉREZ, J., MUÑOZ-DORADO, J., DE LA RUBIA, T. & MARTÍNEZ, J. 2002. Biodegradation and biological treatments of cellulose, hemicellulose and lignin: an overview. *International Microbiology,* 5**,** 53-63.

PHANG, I. Y., LIU, T., MOHAMED, A., PRAMODA, K. P., CHEN, L., SHEN, L., CHOW, S. Y., HE, C., LU, X. & HU, X. 2005. Morphology, thermal and mechanical properties of nylon 12/organoclay nanocomposites prepared by melt compounding. *Polymer International,* 54**,** 456-464.

PLATI, E. & WILLIAMS, J. G. 1975. The determination of the fracture parameters for polymers in impact. *Polymer Engineering & Science,* 15**,** 470-477.

POWELL, C. E. & BEALL, G. W. 2006. Physical properties of polymer/clay nanocomposites. *Current Opinion in Solid State and Materials Science,* 10**,** 73-80.

PRASHANTHA, K., SCHMITT, H., LACRAMPE, M. F. & KRAWCZAK, P. 2011. Mechanical behaviour and essential work of fracture of halloysite nanotubes filled polyamide 6 nanocomposites. *Composites Science and Technology,* 71**,** 1859-1866.

PUKÁNSZKY, B. & MAURER, F. H. J. 1995. Composition dependence of the fracture toughness of heterogeneous polymer systems. *Polymer,* 36**,** 1617-1625.

QI, B., ZHANG, Q. X., BANNISTER, M. & MAI, Y. W. 2006. Investigation of the mechanical properties of DGEBA-based epoxy resin with nanoclay additives. *Composite Structures,* 75**,** 514-519.

QIN, L., QIU, J., LIU, M., DING, S., SHAO, L., LÜ, S., ZHANG, G., ZHAO, Y. & FU, X. 2011. Mechanical and thermal properties of poly(lactic acid) composites with rice straw fiber modified by poly(butyl acrylate). *Chemical Engineering Journal,* 166**,** 772-778.

QINGPING GUO, CHENG, B., KORTSCHOT, M., SAIN, M., KNUDSON, R., DENG, J. & ALEMDAR, A. 2010. Performance of long Canadian natural fibers as reinforcements in polymers. *Journal of Reinforced Plastics and Composites,* 29**,** 3197-3207.

RAHMAN, N. A., HASSAN, A., YAHYA, R., LAFIA-ARAGA, R. A. & HORNSBY, P. R. 2012. Micro-structural, thermal, and mechanical properties of injection-molded glass fiber/nanoclay/polypropylene composites. *Journal of Reinforced Plastics and Composites,* 31**,** 269-281.

RAQUEZ, J. M., DELÉGLISE, M., LACRAMPE, M. F. & KRAWCZAK, P. 2010. Thermosetting (bio)materials derived from renewable resources: A critical review. *Progress in Polymer Science,* 35**,** 487-509.

RATNA-PRASAD, A. V. & MOHANA-RAO, K. 2011. Mechanical properties of natural fibre reinforced polyester composites: Jowar, sisal and bamboo. *Materials and Design,* 32**,** 4658-4663.

RATNA, D., MANOJ, N. R., VARLEY, R., SINGH RAMAN, R. K. & SIMON, G. P. 2003. Clay-reinforced epoxy nanocomposites. *Polymer International,* 52**,** 1403-1407.

REYNAUD, E., JOUEN, T., GAUTHIER, C., VIGIER, G. & VARLET, J. 2001. Nanofillers in polymeric matrix: a study on silica reinforced PA6. *Polymer,* 42**,** 8759-8768.

RIEDEL, U. & NICKEL, J. 2005. Applications of natural fiber composites for constructive parts in aerospace, automobiles, and other areas. *Biopolymers Online.* Wiley-VCH Verlag GmbH & Co. KGaA.

ROBINETTE, E. J., ZIAEE, S. & PALMESE, G. R. 2004. Toughening of vinyl ester resin using butadiene-acrylonitrile rubber modifiers. *Polymer,* 45**,** 6143-6154.

RODGERS, R. M., MAHFUZ, H., RANGARI, V. K., CHISHOLM, N. & JEELANI, S. 2005. Infusion of SiC nanoparticles into SC-15 epoxy: An investigation of thermal and mechanical response. *Macromolecular Materials and Engineering,* 290**,** 423-429.

ROOJ, S., DAS, A., THAKUR, V., MAHALING, R. N., BHOWMICK, A. K. & HEINRICH, G. 2010. Preparation and properties of natural nanocomposites based on natural rubber and naturally occurring halloysite nanotubes. *Materials and Design,* 31**,** 2151-2156.

ROSLER, J., HARDES, H. & BAKER, M. 2007. *Mechanical Behaviour of Engineering Materials Metals, Ceramics, Polymers, and Composites,* Heidelberg, Springer-Verlag.

RUDOLF, P. 2010. Nanocomposites: Industrial opportunity or challenge? *Polymer Degradation and Stability,* 95**,** 369-373.

SADDOW, S. E. 2012. Chapter 1 - Silicon carbide materials for biomedical applications. *Silicon Carbide Biotechnology.* Oxford: Elsevier.

SANCAKTAR, E. & KUZNICKI, J. 2011. Nanocomposite adhesives: Mechanical behavior with nanoclay. *International Journal of Adhesion and Adhesives,* 31**,** 286-300.

SANGTHONG, S., PONGPRAYOON, T. & YANUMET, N. 2009. Mechanical property improvement of unsaturated polyester composite reinforced with admicellar-treated sisal fibers. *Composites Part A: Applied Science and Manufacturing,* 40**,** 687-694.

SATAPATHY, A., ALOK KUMAR JHA, MANTRY, S., SINGH, S. K. & PATNAIK, A. 2010. Processing and characterization of jute-epoxy composites reinforced with SiC derived from rice husk. *Journal of Reinforced Plastics and Composites,* 29**,** 2869-2878.

SCHMIDT, D., SHAH, D. & GIANNELIS, E. P. 2002. New advances in polymer/layered silicate nanocomposites. *Current Opinion in Solid State and Materials Science,* 6**,** 205-212.

SCOTT, T. F., COOK, W. D. & FORSYTHE, J. S. 2002. Kinetics and network structure of thermally cured vinyl ester resins. *European Polymer Journal,* 38**,** 705-716.

SEE, S. C., ZHANG, Z. Y. & RICHARDSON, M. O. W. 2009. A study of water absorption characteristics of a novel nano-gelcoat for marine application. *Progress in Organic Coatings,* 65**,** 169-174.

SEYHAN, A. T., GOJNY, F. H., TANOĞLU, M. & SCHULTE, K. 2007. Rheological and dynamic-mechanical behavior of carbon nanotube/vinyl ester–polyester suspensions and their nanocomposites. *European Polymer Journal,* 43**,** 2836-2847.

SGRICCIA, N., HAWLEY, M. C. & MISRA, M. 2008. Characterization of natural fiber surfaces and natural fiber composites. *Composites Part A: Applied Science and Manufacturing,* 39**,** 1632-1637.

SHAFFER, P. 1969. A review of the structure of silicon carbide. *Acta Crystallographica Section B,* 25**,** 477-488.

SHIQIANG DENG & YOUHONG TANG 2010. Increasing load-bearing capacity of wood-plastic composites by sandwiching natural and glass fabrics. *Journal of Reinforced Plastics and Composites,* 29**,** 3133-3148.

SHOKUHFAR, A., ZARE-SHAHABADI, A., ATAI, A.-A., EBRAHIMI-NEJAD, S. & TERMEH, M. 2012. Predictive modeling of creep in polymer/layered silicate nanocomposites. *Polymer Testing,* 31**,** 345-354.

SILVA, R. V., SPINELLI, D., BOSE FILHO, W. W., CLARO NETO, S., CHIERICE, G. O. & TARPANI, J. R. 2006. Fracture toughness of natural fibers/castor oil polyurethane composites. *Composites Science and Technology,* 66**,** 1328-1335.

SINGHA, A. S. & THAKUR, V. 2008. Mechanical properties of natural fibre reinforced polymer composites. *Bulletin of Materials Science,* 31**,** 791-799.

SINHA RAY, S. & BOUSMINA, M. 2005. Biodegradable polymers and their layered silicate nanocomposites: In greening the 21st century materials world. *Progress in Materials Science,* 50**,** 962-1079.

SINHA RAY, S. & OKAMOTO, M. 2003. Polymer/layered silicate nanocomposites: a review from preparation to processing. *Progress in Polymer Science,* 28**,** 1539-1641.

SIQUEIRA, G., BRAS, J. & DUFRESNE, A. 2010. Cellulosic bionanocomposites: A review of preparation, properties and applications. *Polymers,* 2**,** 728-765.

SOMBATSOMPOP, N. & CHAOCHANCHAIKUL, K. 2004. Effect of moisture content on mechanical properties, thermal and structural stability and extrudate texture of poly(vinyl chloride)/wood sawdust composites. *Polymer International,* 53**,** 1210-1218.

SONAWANE, S. H., CHAUDHARI, P. L., GHODKE, S. A., PARANDE, M. G., BHANDARI, V. M., MISHRA, S. & KULKARNI, R. D. 2009. Ultrasound assisted synthesis of polyacrylic acid–nanoclay nanocomposite and its application in sonosorption studies of malachite green dye. *Ultrasonics Sonochemistry,* 16**,** 351-355.

SPERLING, L. H. 2005. Front Matter. *Introduction to physical polymer science.* John Wiley & Sons, Inc.

SREEKALA, M. S., GEORGE, J., KUMARAN, M. G. & THOMAS, S. 2002. The mechanical performance of hybrid phenol-formaldehyde-based composites reinforced with glass and oil palm fibres. *Composites Science and Technology,* 62**,** 339-353.

SREEKUMAR, P. A., JOSEPH, K., UNNIKRISHNAN, G. & THOMAS, S. 2007. A comparative study on mechanical properties of sisal-leaf fibre-reinforced

polyester composites prepared by resin transfer and compression moulding techniques. *Composites Science and Technology,* 67**,** 453-461.

SREENIVASAN, V. S., RAVINDRAN, D., MANIKANDAN, V. & NARAYANASAMY, R. 2011. Mechanical properties of randomly oriented short Sansevieria cylindrica fibre/polyester composites. *Materials and Design,* 32**,** 2444-2455.

STAMBOULIS, A., BAILLIE, C. A. & PEIJS, T. 2001. Effects of environmental conditions on mechanical and physical properties of flax fibers. *Composites Part A: Applied Science and Manufacturing,* 32**,** 1105-1115.

STOCCHI, A., BERNAL, C., VÁZQUEZ, A., BIAGOTTI, J. & KENNY, J. 2007. A silicone treatment compared to traditional natural fiber treatments: Effect on the mechanical and viscoelastic properties of jute-vinylester laminates. *Journal of Composite Materials,* 41**,** 2005-2024.

SUE, H. J., GAM, K. T., BESTAOUI, N., CLEARFIELD, A., MIYAMOTO, M. & MIYATAKE, N. 2004. Fracture behavior of α-zirconium phosphate-based epoxy nanocomposites. *Acta Materialia,* 52**,** 2239-2250.

SUE, H. J., GAM, K. T., BESTAOUI, N., SPURR, N. & CLEARFIELD, A. 2003. Epoxy nanocomposites based on the synthetic α-zirconium Phosphate layer structure. *Chemistry of Materials,* 16**,** 242-249.

SULTANIA, M., YADAW, S. B., RAI, J. S. P. & SRIVASTAVA, D. 2010. Laminates based on vinyl ester resin and glass fabric: A study on the thermal, mechanical and morphological characteristics. *Materials Science and Engineering: A,* 527**,** 4560-4570.

SUN, L.-H., YANG, Z.-G. & LI, X.-H. 2008a. Tensile and tribological properties of PTFE and nanoparticles modified epoxy-based polyester fabric composites. *Materials Science and Engineering: A,* 497**,** 487-494.

SUN, L., BOO, W. J., CLEARFIELD, A., SUE, H. J. & PHAM, H. Q. 2008b. Barrier properties of model epoxy nanocomposites. *Journal of Membrane Science,* 318**,** 129-136.

SUN, R. & TOMKINSON, J. 2003. Characterization of hemicelluloses isolated with tetraacetylethylenediamine activated peroxide from ultrasound irradiated and alkali pre-treated wheat straw. *European Polymer Journal,* 39**,** 751-759.

SUN, Z.-Y., HAN, H.-S. & DAI, G.-C. 2009. Mechanical properties of injection-molded natural fiber-reinforced polypropylene composites: Formulation and compounding processes. *Journal of Reinforced Plastics and Composites*.

SUPPAKARN, N. & JARUKUMJORN, K. 2009. Mechanical properties and flammability of sisal/PP composites: Effect of flame retardant type and content. *Composites Part B: Engineering,* 40**,** 613-618.

SVOBODA, P., TRIVEDI, K., SVOBODOVA, D., MOKREJS, P. & KOLOMAZNIK, K. 2012. Effect of initial melting temperature on crystallization of polypropylene/organoclay nanocomposites. *Macromolecular Research,* 20**,** 659-666.

TANG, Y., DENG, S., YE, L., YANG, C., YUAN, Q., ZHANG, J. & ZHAO, C. 2011. Effects of unfolded and intercalated halloysites on mechanical properties of halloysite–epoxy nanocomposites. *Composites Part A: Applied Science and Manufacturing,* 42**,** 345-354.

TANNIRU, M., YUAN, Q. & MISRA, R. D. K. 2006. On significant retention of impact strength in clay–reinforced high-density polyethylene (HDPE) nanocomposites. *Polymer,* 47**,** 2133-2146.

THOMASON, J. L. 2005. The influence of fibre length and concentration on the properties of glass fibre reinforced polypropylene. 6. The properties of injection moulded long fibre PP at high fibre content. *Composites Part A: Applied Science and Manufacturing,* 36**,** 995-1003.

THOMASON, J. L. & VLUG, M. A. 1996. Influence of fibre length and concentration on the properties of glass fibre-reinforced polypropylene: 1. Tensile and flexural modulus. *Composites Part A: Applied Science and Manufacturing,* 27**,** 477-484.

THOSTENSON, E. T., LI, C. & CHOU, T.-W. 2005. Nanocomposites in context. *Composites Science and Technology,* 65**,** 491-516.

THWE, M. M. & LIAO, K. 2002. Effects of environmental aging on the mechanical properties of bamboo–glass fiber reinforced polymer matrix hybrid composites. *Composites Part A: Applied Science and Manufacturing,* 33**,** 43-52.

TOHGO, K., ITOH, Y. & SHIMAMURA, Y. 2010. A constitutive model of particulate-reinforced composites taking account of particle size effects and

damage evolution. *Composites Part A: Applied Science and Manufacturing,* 41**,** 313-321.

TORTORA, M., VITTORIA, V., GALLI, G., RITROVATI, S. & CHIELLINI, E. 2002. Transport properties of modified montmorillonite-poly(ε-caprolactone) nanocomposites. *Macromolecular Materials and Engineering,* 287**,** 243-249.

TSAI, J.-L. & WU, M.-D. 2008. Organoclay effect on mechanical responses of glass/epoxy nanocomposites. *Journal of Composite Materials,* 42**,** 553-568.

TUCKER III, C. L. & LIANG, E. 1999. Stiffness predictions for unidirectional short-fiber composites: Review and evaluation. *Composites Science and Technology,* 59**,** 655-671.

VALERA-ZARAGOZA, M., RAMÍREZ-VARGAS, E., MEDELLÍN-RODRÍGUEZ, F. J. & HUERTA-MARTÍNEZ, B. M. 2006. Thermal stability and flammability properties of heterophasic PP–EP/EVA/organoclay nanocomposites. *Polymer Degradation and Stability,* 91**,** 1319-1325.

VAN VOORN, B., SMIT, H. H. G., SINKE, R. J. & DE KLERK, B. 2001. Natural fibre reinforced sheet moulding compound. *Composites Part A: Applied Science and Manufacturing,* 32**,** 1271-1279.

VENKATESHWARAN, N., ELAYAPERUMAL, A., ALAVUDEEN, A. & THIRUCHITRAMBALAM, M. 2011. Mechanical and water absorption behaviour of banana/sisal reinforced hybrid composites. *Materials and Design,* 32**,** 4017-4021.

VILAY, V., MARIATTI, M., MAT TAIB, R. & TODO, M. 2008. Effect of fiber surface treatment and fiber loading on the properties of bagasse fiber-reinforced unsaturated polyester composites. *Composites Science and Technology,* 68**,** 631-638.

VYAZOVKIN, S., DRANCA, I., FAN, X. & ADVINCULA, R. 2004. Kinetics of the thermal and thermo-oxidative degradation of a polystyrene-clay nanocomposite. *Macromolecular Rapid Communications,* 25**,** 498-503.

WAMBUA, P., IVENS, J. & VERPOEST, I. 2003. Natural fibres: can they replace glass in fibre reinforced plastics? *Composites Science and Technology,* 63**,** 1259-1264.

WAN ABDUL RAHMAN, W. A., SIN, L. T. & RAHMAT, A. R. 2008. Injection moulding simulation analysis of natural fiber composite window frame. *Journal of Materials Processing Technology,* 197**,** 22-30.

WANG, K., CHEN, L., WU, J., TOH, M. L., HE, C. & YEE, A. F. 2005. Epoxy nanocomposites with highly exfoliated clay: Mechanical properties and fracture mechanisms. *Macromolecules,* 38**,** 788-800.

WANG, W., SAIN, M. & COOPER, P. A. 2006. Study of moisture absorption in natural fiber plastic composites. *Composites Science and Technology,* 66**,** 379-386.

WANG, Y., ZHANG, B. & YE, J. 2011. Microstructures and toughening mechanisms of organoclay/polyethersulphone/epoxy hybrid nanocomposites. *Materials Science and Engineering: A,* 528**,** 7999-8005.

WETZEL, B., HAUPERT, F., FRIEDRICH, K., ZHANG, M. Q. & RONG, M. Z. 2002. Impact and wear resistance of polymer nanocomposites at low filler content. *Polymer Engineering & Science,* 42**,** 1919-1927.

WETZEL, B., HAUPERT, F. & QIU ZHANG, M. 2003. Epoxy nanocomposites with high mechanical and tribological performance. *Composites Science and Technology,* 63**,** 2055-2067.

WETZEL, B., ROSSO, P., HAUPERT, F. & FRIEDRICH, K. 2006. Epoxy nanocomposites: Fracture and toughening mechanisms. *Engineering Fracture Mechanics,* 73**,** 2375-2398.

WONG, K. J., ZAHI, S., LOW, K. O. & LIM, C. C. 2010. Fracture characterisation of short bamboo fibre reinforced polyester composites. *Materials and Design,* 31**,** 4147-4154.

WOUTERSON, E. M., BOEY, F. Y. C., WONG, S. C., CHEN, L. & HU, X. 2007. Nano-toughening versus micro-toughening of polymer syntactic foams. *Composites Science and Technology,* 67**,** 2924-2933.

WRIGHT, N. G. 2000. Silicon carbide. *Kirk-Othmer encyclopedia of chemical technology.* John Wiley & Sons, Inc.

WRIGHT, N. G. & HORSFALL, A. B. 2011. Silicon carbide: The return of an old friend. *Material Matters,* 4**,** 5.

XIE, Y., CHANG, P. R., WANG, S., YU, J. & MA, X. 2011. Preparation and properties of halloysite nanotubes/plasticized dioscorea opposita thunb starch composites. *Carbohydrate Polymers,* 83**,** 186-191.

XU, Y. & HOA, S. V. 2008. Mechanical properties of carbon fiber reinforced epoxy/clay nanocomposites. *Composites Science and Technology,* 68**,** 854-861.

YAN, W., LIN, R. J. T. & BHATTACHARYYA, D. 2006. Particulate reinforced rotationally moulded polyethylene composites: Mixing methods and mechanical properties. *Composites Science and Technology,* 66**,** 2080-2088.

YANG, H., YAN, R., CHEN, H., LEE, D. H. & ZHENG, C. 2007. Characteristics of hemicellulose, cellulose and lignin pyrolysis. *Fuel,* 86**,** 1781-1788.

YASMIN, A., LUO, J. J., ABOT, J. L. & DANIEL, I. M. 2006. Mechanical and thermal behavior of clay/epoxy nanocomposites. *Composites Science and Technology,* 66**,** 2415-2422.

YE, Y., CHEN, H., WU, J. & CHAN, C. M. 2011. Interlaminar properties of carbon fiber composites with halloysite nanotube-toughened epoxy matrix. *Composites Science and Technology,* 71**,** 717-723.

YE, Y., CHEN, H., WU, J. & YE, L. 2007. High impact strength epoxy nanocomposites with natural nanotubes. *Polymer,* 48**,** 6426-6433.

YONG, V., AAGESEN, L. K. & CHANG, R. P. H. 2008. Growth of highly ordered colloidal photonic crystals using a modeling approach. *Nanotechnology,* 19**,** 435204.

YONG, V. & HAHN, H. T. 2004. Processing and properties of SiC/vinyl ester nanocomposites *Nanotechnology* 15**,** 1338–1343.

YONG, V. & HAHN, H. T. 2006. Rheology of silicon carbide/vinyl ester nanocomposites. *Journal of Applied Polymer Science,* 102**,** 4365-4371.

YONG, V. & HAHN, T. 2009. Monodisperse SiC/vinyl ester nanocomposites: Dispersant formulation, synthesis, and characterization. *Journal of Materials Research,* 24**,** 1553-1558.

YOUNG, R. J., MAXWELL, D. L. & KINLOCH, A. J. 1986. The deformation of hybrid-particulate composites. *Journal of Materials Science,* 21**,** 380-388.

YU, T., REN, J., LI, S., YUAN, H. & LI, Y. 2010. Effect of fiber surface-treatments on the properties of poly(lactic acid)/ramie composites. *Composites Part A: Applied Science and Manufacturing,* 41**,** 499-505.

ZAINUDDIN, S., HOSUR, M. V., ZHOU, Y., NARTEH, A. T., KUMAR, A. & JEELANI, S. 2010. Experimental and numerical investigations on flexural and thermal properties of nanoclay–epoxy nanocomposites. *Materials Science and Engineering: A,* 527**,** 7920-7926.

ZAMRI, M. H., AKIL, H. M., BAKAR, A. A., ISHAK, Z. A. M. & CHENG, L. W. 2012. Effect of water absorption on pultruded jute/glass fiber-reinforced

unsaturated polyester hybrid composites. *Journal of Composite Materials,* 46**,** 51-61.

ZANETTI, M. & COSTA, L. 2004. Preparation and combustion behaviour of polymer/layered silicate nanocomposites based upon PE and EVA. *Polymer,* 45**,** 4367-4373.

ZANETTI, M., LOMAKIN, S. & CAMINO, G. 2000. Polymer layered silicate nanocomposites. *Macromolecular Materials and Engineering,* 279**,** 1-9.

ZENG, Q. H., YU, A. B., LU, G. Q. & PAUL, D. R. 2005. Clay-based polymer nanocomposites: Research and commercial development. *Journal of Nanoscience and Nanotechnology,* 5**,** 1574-1592.

ZERDA, A. S. & LESSER, A. J. 2001. Intercalated clay nanocomposites: morphology, mechanics, and fracture behavior. *Journal of Polymer Science Part B: Polymer Physics,* 39**,** 1137-1146.

ZHANG, J., DELICHATSIOS, M. A. & BOURBIGOT, S. 2009. Experimental and numerical study of the effects of nanoparticles on pyrolysis of a polyamide 6 (PA6) nanocomposite in the cone calorimeter. *Combustion and Flame,* 156**,** 2056-2062.

ZHANG, X., LI, Y., LV, G., ZUO, Y. & MU, Y. 2006. Thermal and crystallization studies of nano-hydroxyapatite reinforced polyamide 66 biocomposites. *Polymer Degradation and Stability,* 91**,** 1202-1207.

ZHANG, X. & LOO, L. S. 2009. Synthesis and thermal oxidative degradation of a novel amorphous polyamide/nanoclay nanocomposite. *Polymer,* 50**,** 2643-2654.

ZHAO, C., QIN, H., GONG, F., FENG, M., ZHANG, S. & YANG, M. 2005. Mechanical, thermal and flammability properties of polyethylene/clay nanocomposites. *Polymer Degradation and Stability,* 87**,** 183-189.

ZHAO, L.-D., ZHANG, B.-P., LI, J.-F., ZHOU, M., LIU, W.-S. & LIU, J. 2008. Thermoelectric and mechanical properties of nano-SiC-dispersed Bi_2Te_3 fabricated by mechanical alloying and spark plasma sintering. *Journal of Alloys and Compounds,* 455**,** 259-264.

ZHAO, M. & LIU, P. 2008. Halloysite nanotubes/polystyrene (HNTs/PS) nanocomposites via in situ bulk polymerization. *Journal of Thermal Analysis and Calorimetry,* 94**,** 103-107.

ZHAO, S., SCHADLER, L. S., DUNCAN, R., HILLBORG, H. & AULETTA, T. 2008b. Mechanisms leading to improved mechanical performance in nanoscale alumina filled epoxy. *Composites Science and Technology,* 68**,** 2965-2975.

ZHI-MIN, L. I., FA, L. U., XIAO-LEI, S. U., DONG-MEI, Z. H. & WAN-CHENG, Z. H. 2007. Synthesis and microwave dielectric properties of boron doped SiC powder by sol-gel method. *Trans. Nonferrous Met. Soc. China* 17**,** 656-659.

ZHOU, T., WANG, X., MINGYUAN, G. U. & LIU, X. 2008. Study of the thermal conduction mechanism of nano-SiC/DGEBA/EMI-2,4 composites. *Polymer,* 49**,** 4666-4672.

ZHU, J., UHL, F. M., MORGAN, A. B. & WILKIE, C. A. 2001. Studies on the mechanism by which the formation of nanocomposites enhances thermal stability. *Chemistry of Materials,* 13**,** 4649-4654.

ZIMMERMANN, T., PÖHLER, E. & GEIGER, T. 2004. Cellulose fibrils for polymer reinforcement. *Advanced Engineering Materials,* 6**,** 754-761.

ZUIDERDUIN, W. C. J., WESTZAAN, C., HUÉTINK, J. & GAYMANS, R. J. 2003. Toughening of polypropylene with calcium carbonate particles. *Polymer,* 44**,** 261-275.

“Every reasonable effort has been made to acknowledge the owners of copyright material. I would be pleased to hear from any copyright owner who has been omitted or incorrectly acknowledgement”

Abdullah Alhuthali

Signature: 

Date: 4th July 2013